# La limite de plaque Inde-Arabie : Evolution structurale du Crétacé supérieur à l'Actuel et aléa tsunami associe

Mathieu Rodriguez

**Thèse de doctorat de l'université Pierre et Marie Curie**

**Spécialité Géologie Marine**

# LA LIMITE DE PLAQUE INDE-ARABIE :

## *Evolution structurale du Crétacé supérieur*

## *à l'Actuel et aléa tsunami associé*

**Présentée par**

**Mathieu Rodriguez**

**Pour l'obtention du grade de**

**Docteur de l'université Pierre et Marie Curie**

Soutenue le 17/05/2013

**Devant le Jury composé de :**

| | |
|---|---|
| **Jean-Yves Royer (DR CNRS, IUEM Brest)** | **Rapporteur** |
| **Jean-Luc Schneider (Pr, Université Bordeaux 1)** | **Rapporteur** |
| **Tim Minshull (Pr, Univ. of Southampton)** | **Examinateur** |
| **Michel Sébrier (DR CNRS, iSTeP UPMC Paris VI)** | **Examinateur** |
| **Nicolas Chamot-Rooke (CR, école normale supérieure)** | **Directeur de thèse** |
| **Marc Fournier (Pr, iSTeP UPMC Paris VI)** | **Directeur de thèse** |
| **Philippe Huchon (Pr, iSTeP UPMC Paris VI)** | **Directeur de thèse** |

*Thèse préparée en collaboration avec : M. Delescluse, H. Hébert, A. Rabaute, S. Zaragosi*

**La mer secrète**

Quand nul ne la regarde,

La mer n’est plus la mer,

Elle est ce que nous sommes

Lorsque nul ne nous voit.

Elle a d’autres poissons,

D’autres vagues aussi.

C’est la mer pour la mer

Et pour ceux qui en rêvent

Comme je fais ici.

*Jules Supervielle,*

*Oublieuse mémoire, 1949,*

*Gallimard.*


*Planche I : Dessin à l'encre de Chine de la formation de Shuwayr, en discordance sur les ophiolites de Ras Madrakah (Oman).*

***Sommaire***

***Abstract-Résumé*** ***9***
***Introduction générale*** ***11***

***Chapitre 1 : Histoire géologique de la frontière de plaque Arabie-Inde*** ***17***

*1. Physiographie de la Mer d'Arabie* ***22***

*2. Âge de la frontière de plaque Inde-Arabie actuelle et localisation au cours du temps : controverses* ***35***

*3. A la recherche des frontières de plaque Inde-Arabie anté-Miocène.* **53**

*4. Synthèse : reconstitution de l'histoire géologique de la marge est-omanaise du Crétacé au Miocène* ***67***

*5. Objectifs de la thèse : évolution structurale de la frontière Inde-Arabie et aléas naturels associés* ***70***

***Chapitre 2 : Matériel et méthodes*** ***75***

***Chapitre 3 : Evolution structurale de la limite de plaque Inde-Arabie au cours du Plio-Pleistocène*** ***91***

*1. Introduction* ***91***

*2. Article 1 : "Owen Fracture Zone: the Arabia-India plate boundary unveiled"* ***95***

*3. Article 2 : "Neotectonics of the Owen Fracture Zone (NW Indian Ocean): Structural evolution of an oceanic strike-slip plate boundary"* ***101***

*4.Conclusions et perspectives de l' article "Neotectonics of the Owen Fracture Zone"* ***117***

*5.Article 3 : "Mode of opening of an oceanic pull-apart: the 20°N Basin along the Owen Fracture Zone (NW Indian Ocean)"* ***127***

*6.Conclusions et perspectives de l'article "Mode of opening of the 20°N Pull-apart Basin"* ***167***

*7. Article 4 : "Tectonics of the Dalrymple Trough and uplift of the Murray ridge (NW Indian Ocean)"* ***169***

***Chapitre 4 : La limite de plaque Inde-Arabie au cours du Miocène et le soulèvement de la Ride d'Owen*** ***199***

*1. Introduction* ***199***

*2. Article 5 : "The Owen Ridge uplift and implications on the record of Asian paleo-climate in Late Miocene marine sediments of the Arabian Sea"* ***205***

*3. Conclusions de l'article "The Owen Ridge uplift and the record of Asian paleo-climate"* ***235***

***Chapitre 5 : A la recherche de la limite de plaque Inde-Arabie au cours du Paléogène*** ***239***

*1. Introduction* ***239***

*2. Article 6 : "Tracking the India-Arabia Plate boundary since Paleocene to Early Miocene times"* ***241***

*3. Conclusions de l'article "Tracking the India-Arabia Plate boundary since Paleocene to Early Miocene times" : éléments de réflexion sur la marge omanaise à terre* ***283***

***Chapitre 6 : Aléa tsunami associé aux glissements de terrain de la Ride d'Owen*** ***291***

*1. Introduction* ***291***

*2. Article 7 : "Mass wasting processes along the Owen Ridge (Northwest Indian Ocean)"* ***301***

*3. Etude préliminaire de la stabilité des pentes au niveau de la Ride d'Owen* ***323***

*4. Article 8 : "Owen Ridge deep-water submarine landslides : implications for tsunami hazard along the Oman coast"* ***329***

***Conclusions générales et perspectives*** ***337***

***Remerciements*** ***348***

***Références bibliographiques*** ***351***

***Liste des figures*** ***371***

***Annexes*** ***382***

*1. Article 9 :"Late Quaternary megaturbidites of the Indus Fan : Origin and stratigraphic significance"*

*2. La faille du Levant : synthèse.*

*3. vulgarisation sur les tsunamis de la côte est de l'oman, paru dans la recherche du mois de Mai 2013*

***Résumé*** **:** La Zone de Fracture d'Owen (ZFO) est une faille de 800 km de long qui accommode actuellement le mouvement dextre entre l'Inde et l'Arabie. Elle s'inscrit le long d'un petit cercle qui implique un mouvement purement dextre sur la majeure partie de la faille. La couverture bathymétrique complète de la ZFO recueillie au cours de la campagne Owen-1 révèle plusieurs segments de failles séparés par des relais, dont un bassin pull-apart de 90 km de long sur 30 km de large à la latitude 20°N. Un bassin pull-apart rhomboédrique (Beautemps-Beaupré) marque la terminaison sud de l'OFZ, tandis qu'un bassin plus complexe, la fosse de Dalrymple, constitue la terminaison Nord. La ZFO recoupe la Ride d'Owen-Murray, qui forme une série d'imposants reliefs océaniques. Les décalages morphologiques de la Ride d'Owen confirment un décalage dextre d'environ 10-12 km le long de l'OFZ. En considérant constant un mouvement de 3±1 mm.a$^{-1}$ estimé à partir de données géologiques et GPS, l'âge de la ZFO est compris entre 3 et 6 Ma. De même, l'âge du bassin 20°N et de la fosse de Dalrymple sont estimés à 2-3 Ma à partir de calibration avec les forages ODP-DSDP. L'âge de ces bassins est contemporain d'une discordance majeure observée dans la plaine abyssale de l'Oman (discordance "M") associée au prisme du Makran. D'autre part, la Ride d'Owen est érodée par des systèmes complexes de glissements de terrains sous-marins, qui représentent une source potentielle d'aléa tsunami pour les côtes de l'Oman. Les données stratigraphiques indiquent que la récurrence de tels glissements (et des tsunamis associés) est faible, de l'ordre de $10^5$-$10^6$ années. Les données de sismique réflexion collectées lors de la campagne Owen-2 ont permis d'identifier les traces Miocène et Paléogène de la limite de plaque, entraînant une révision complète de son histoire géologique. Tout d'abord, l'identification de lambeaux de l'ophiolite de Masirah sur le socle du Bassin d'Owen aux abords de la marge est-omanaise indique que le socle est à cet endroit d'âge Crétacé (au minimum). Cela contraste avec l'âge Paléocène des roches forées au niveau du socle de la Ride d'Owen. Ces observations indiquent que le socle du Bassin d'Owen est d'âge mixte, et que des portions de lithosphère d'âge différent ont été mises en contact par une faille transformante majeure. Le système de zones de fracture structurant le socle du Bassin d'Owen était associé à la dorsale de Carlsberg au cours du Paléocène-Eocène. L'arrêt de son activité, associé à un épisode de transpression à la fin de l'Eocène, est marqué par le soulèvement de rides marginales et une discordance angulaire régionale. La limite de plaque Inde-Arabie est ensuite retrouvée au niveau de l'actuelle Ride d'Owen dès la fin de l'Oligocène. Cette relocalisation de la plaque Arabe a impliqué le transfert d'un vaste segment de la plaque Indienne à la plaque Arabe. Le soulèvement de la Ride d'Owen a eu lieu autour de 8.2-8.8 Ma, en réponse à un changement cinématique de la plaque Indienne, probablement en réponse à la croissance des reliefs himalayens et au début de l'étalement gravitaire de la chaîne. Cet épisode de déformation est responsable de l'inactivation de la limite de plaque Miocène, et de sa relocalisation au niveau de l'OFZ actuelle. Un changement environnemental majeur a été précédemment identifié sur le pourtour de la Mer d'Arabie dans la séquence de Siwalik au Pakistan. L'augmentation drastique des abondances de *G. Bulloides* dans la couverture sédimentaire de la Ride d'Owen, précédemment interprétée comme le résultat d'une abrupte intensification de la mousson autour de 8.5 Ma, marque en réalité un changement des conditions de préservation des foraminifères suite au soulèvement de la ride. Nous proposons que l'épisode de déformation identifié dans le Bassin d'Owen ait pu également favoriser le soulèvement de reliefs au niveau de la marge du Dhofar et du prisme d'accrétion du Makran, conduisant à une réorganisation de la circulation atmosphérique à l'origine du changement environnemental de Siwalik.

***Abstract:*** The Owen Fracture Zone (OFZ) is a 800 km-long fault system that currently accommodates the dextral strike-slip motion between India and Arabia plates. It closely follows a small circle about a rotation pole determined with GPS and seismicity data, which is consistent with a pure strike-slip motion along the entire fracture zone. As shown by the high resolution multibeam bathymetric map with full coverage (OWEN-1 cruise), it is made up of a series of fault segments separated by releasing and restraining bends, including a major pull-apart basin at latitude 20°N and two stepover basins at its terminations, the Beautemps-Beaupré Basin to the south and the Dalrymple Trough to the north. The OFZ crosscuts the Owen-Murray Ridge, a series of prominent oceanic highs. Offsets of the Owen Ridge observed on the seafloor indicate a finite dextral displacement of 10-12 km along the OFZ. Considering a steady motion of 3 ±1 mm.y$^{-1}$ estimated independently from geodetic and geological data, this implies that the present-day trace of the OFZ has been active since at least 3 to 6 Ma. Consistently, the age of opening of the 20°N Basin and the Dalrymple trough is estimated at about 2-3 Ma ago by calibration with DSDP-ODP drillings, coevally with a regional unconformity over the Oman abyssal plain (the M-unconformity). The Owen-Murray Ridge is dissected by complex systems of submarine landslides, which may represent a source of tsunami hazard for the nearby Oman coast according to numerical models. Stratigraphic studies document a recurrence in the order of $10^5$-$10^6$ yrs, indicating that such tsunamis are infrequent. The seismic dataset collected during the Owen-2 cruise provides the first identification of the Miocene and Paleogene traces of the plate boundary prior to the activation of the OFZ, and leads to a full revision of the geological history of the area. We highlight the composite age of the Owen Basin basement, made of Paleocene crust drilled on its eastern part, and composed of pre-Maastrichtian crust overlain by Upper Cretaceous ophiolites on its western side (at the edge of the Oman Margin). A major transform fault crossing the Owen Basin juxtaposed these two slivers of lithosphere of different ages. This transform system used to be associated with the Carlsberg spreading center during the Paleogene, which formed most of the Owen Basin basement. The inactivation of the transform system in Late Eocene-Early Oligocene times is marked by the uplift of marginal ridges along the Oman Margin and a regional angular unconformity. The transform system then shifted to a narrow structure located at the edge of the present-day Owen Ridge in Late Oligocene times, shortly before seafloor spreading began at the Sheba Ridge. This migration of the plate boundary involved the capture of a part of the Indian oceanic lithosphere accreted at the Carlsberg Ridge (in Paleocene-Eocene times) to the Arabian plate. The Owen Ridge uplifted much latter, in Late Miocene times (8.2-8.8 Ma), in response to a kinematic change of the Indian plate. This episode of deformation ultimately led to the inactivation of the Miocene plate boundary and the activation of the OFZ. A major environmental change is recorded over the Arabian Sea coasts in the Siwalik paleosol sequence, coevally with this episode of deformation. This environmental change was previously interpreted as the result of an intensification of the Indian Monsoon at ~8.5 Ma recorded by a drastic increase in *G. bulloides* abundance in the sedimentary cover of the Owen Ridge. In contrast, we propose that the uplift of the Owen Ridge 8-9 Ma ago induced better preservation of foraminifers. Furthermore, this episode of deformation could have also triggered continental uplift along the East Oman and the Dhofar margin, and at the Makran accretionary wedge, leading to a reorganization of the atmospheric circulation that could explain the coeval environmental change recorded in the Siwalik sequence in Pakistan.

# Introduction générale

La répartition de la sismicité mondiale permet de définir les frontières de 25 grandes plaques tectoniques (e.g., *DeMets et al., 2010*). La sismicité aux frontières de plaques est due aux forces de frottement générées par leur mouvement relatif. On distingue selon la répartition des séismes les frontières de plaques localisées et les frontières de plaque diffuses (Figure 1). Il existe trois grandes catégories de limites de plaque : les limites convergentes (zones de subduction et de collision), les limites divergentes (zones de rifting et d'ouverture océanique) et les limites coulissantes (failles transformantes). Ces dernières constituent la thématique de cette thèse.

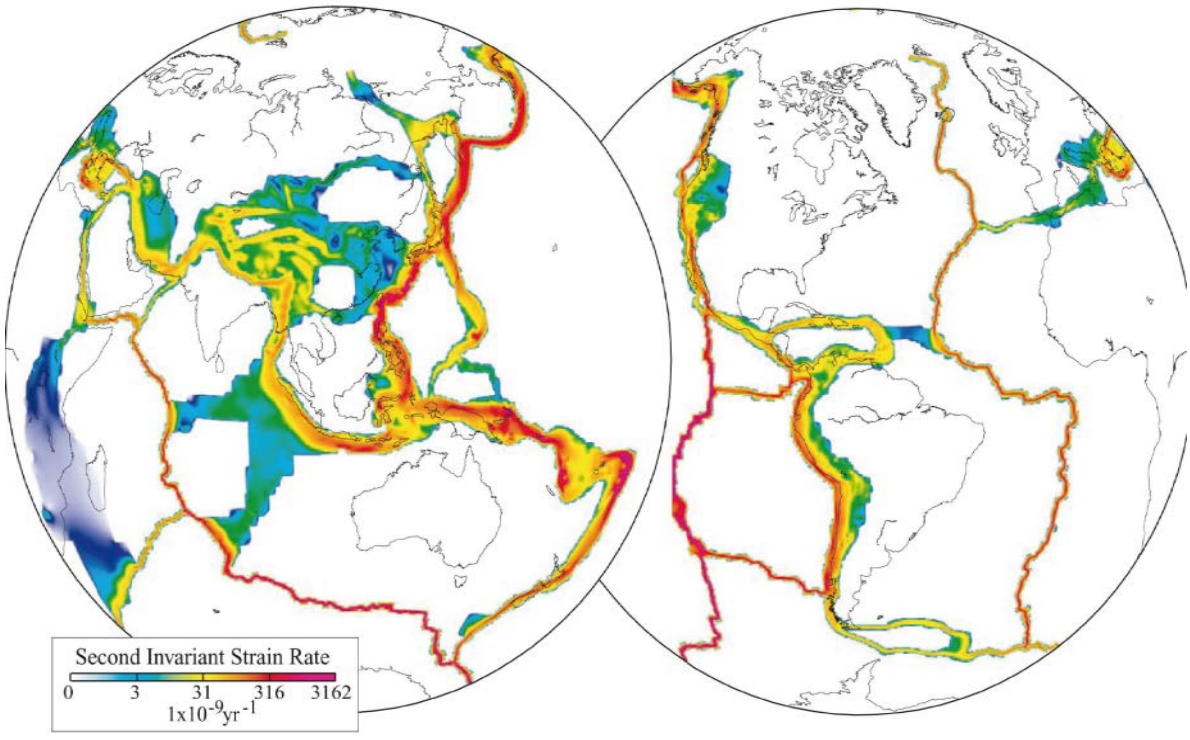


*Figure 1 : Carte du second invariant du taux de la déformation (d'après Kreemer et al., 2003)indiquant la répartition des frontières de plaque localisées et diffuses.*

Les failles transformantes sont des failles décrochantes qui transfèrent de mouvement d'une frontière de plaque à une autre (Figure 2). Par exemple, la faille du Levant *transforme* la divergence au niveau de la Mer Rouge en convergence au niveau du Zagros. La définition initiale des failles transformantes a été établie par *J.T. Wilson (1965),* qui a découvert les failles transformantes à partir des décalages horizontaux des anomalies magnétiques du plancher océanique, atteignant par endroits des centaines de kilomètres. Le tracé d'une faille transformante suit un petit cercle. Latéralement par rapport à l'axe de la dorsale, les failles transformantes océaniques deviennent inactives et les morceaux de plaque sont soudés : c'est la *zone de fracture*, vestige de l'épisode actif (une zone de fracture peut toutefois être réactivée en contexte de déformation intraplaque (*Storti et al., 2007; Delescluse et al., 2012*). La sismicité et les mécanismes au foyer sur les failles transformantes océaniques illustrent bien la localisation de l'activité tectonique entre les segments d'accrétion de la dorsale. C'est une différence majeure avec les failles décrochantes continentales, pour lesquelles la sismicité est localisée sur tout le long de la faille.

Au sens strict, une faille décrochante se définit par les stries horizontales que le mouvement relatif des blocs laisse sur le plan de faille, quelque soit le pendage de ce dernier. Cette définition est difficilement applicable au domaine marin. Nous considérons donc comme faille décrochante tout plan de faille accommodant un mouvement horizontal entre deux blocs. La plupart du temps, le plan de faille adopte un pendage sub-vertical. Les décrochements néoformés se mettent en place à la faveur d'une contrainte maximale horizontale $\sigma_1$ oblique par rapport à la direction du plan de faille. Les grands décrochements actuels (i.e. dont la longueur est de l'ordre de la centaine de kilomètres) sont souvent issus de la réactivation de grands accidents hérités de phases tectoniques antérieures. Lorsqu'un bloc est décalé vers la droite par rapport au bloc lui faisant face, le jeu de la faille est dit *"dextre"*. Lorsqu'il est décalé vers la gauche, le jeu de la faille est dit *"sénestre"* (Figure 2). Selon la façon dont le tracé de la faille dévie du petit cercle, des composantes extensives ou compressives peuvent se surimposer au mouvement décrochant, et former des relais : on parle alors de *transtension* ou de *transpression*, respectivement. Les divers mouvements décrochants sont clairement identifiables par les décalages qu'ils créent dans les paysages, ou par l'étude des mécanismes au foyer des séismes. Le jeu des failles décrochantes met en contact étroit des portions de lithosphère dont les propriétés physiques et rhéologiques sont très différentes. La faille est alors considérée comme une interface bimatérielle (*Ben Zion and Sammis, 2003*). Les contrastes les plus forts sont observés dans les cas où de la lithosphère

océanique se trouve en contact avec la lithosphère continentale, comme par exemple au niveau de Point Arena (au Nord de la faille de San Andreas).

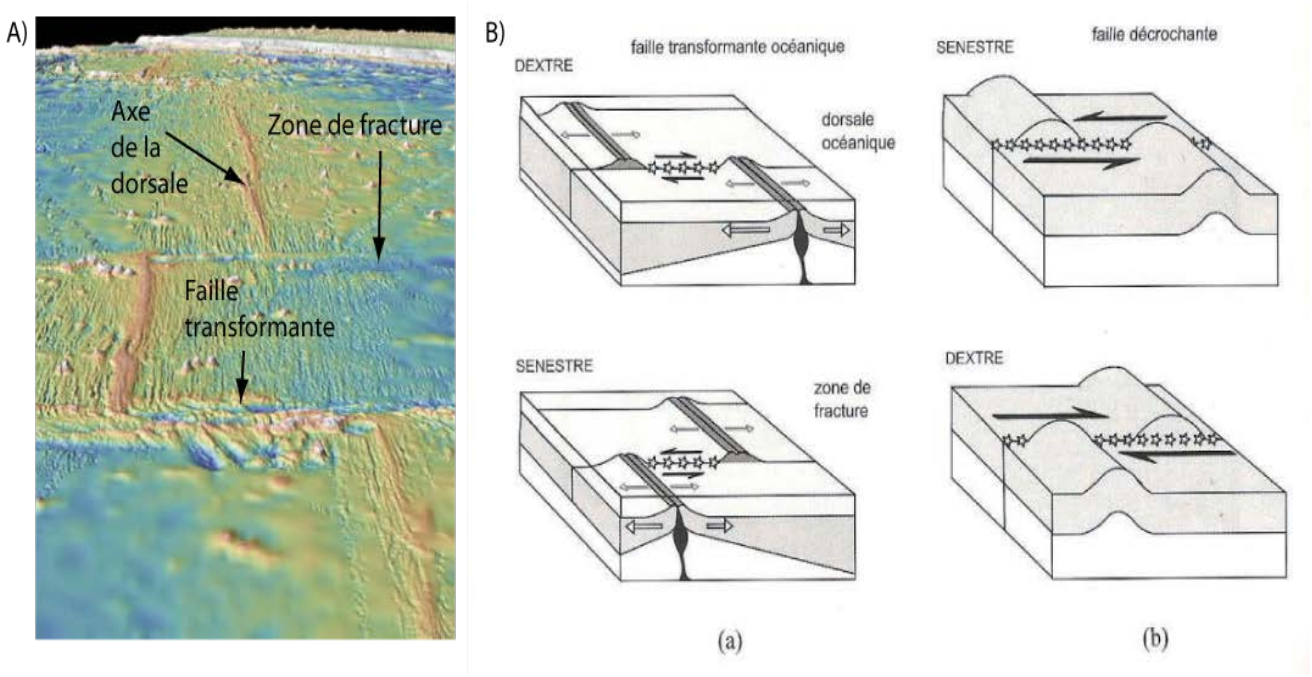


*Figure 2 : A) Bathymétrie de la transformante de l'East Pacific Rise (d'après Ryan et al., 2009). B) Les failles transformantes océaniques sont généralement sub-perpendiculaires à la direction des dorsales. Ce sont des plans verticaux qui décalent la crête des dorsales dans un sens dextre ou sénestre. La sismicité (indiquée par les étoiles) est localisée sur la partie de la faille située entre les deux crêtes de la dorsale là où les mouvements de chaque bloc sont de sens contraire; au delà des crêtes il n'y a plus de mouvement relatif le long du plan de faille, on parle alors de zone de fracture. C) Au contraire les failles décrochantes sont sismiquement actives sur toute leur longueur car l'ensemble du plan de faille est mobilisé par le mouvement (d'après Larroque et Virieux, 2001).*

Les failles décrochantes ont été identifiées dans des contextes géologiques très variés. Du fait de l'héritage structural souvent complexe d'une région, il est difficile de relier les décrochements à un régime tectonique général particulier. Les contraintes obliques nécessaires au jeu décrochant ne sont parfois que locales et liées à l'orientation favorable d'une faille alors que les contraintes régionales ne sont pas *a priori* favorables aux décrochements. Toutefois, nous considérons que les systèmes décrochants au sens large

prennent place dans cinq grands types de contextes tectoniques (*Woodcock, 1986; Mann, 2007*) (Figure 3).

1) une première catégorie est composée des failles transformantes océaniques qui segmentent les dorsales médio-océaniques (ex. transformante de Kane, de Siquieros, de Vema);

2) une seconde catégorie –à laquelle appartient la Zone de Fracture d'Owen- comprend les transformantes linéaires de plusieurs centaines de kilomètres de long marquant les limites de plaques, dont la cinématique est gouvernée sur de longues distances par un pôle eulérien (exemple de la faille de San Andreas en Californie; de la faille du Levant entre l'Arabie et la Nubie);

3) les décrochements dont le tracé peut être discontinu, qui séparent des blocs continentaux dans les zones de collision continent-continent ou arc-continent (ex. des extrusions latérales *("tectonic escape")* accommodées par la faille Nord anatolienne dans le cas du bloc anatolien, ou par les décrochements tibétains dans le cas du poinçonnement de l'Asie par l'Inde);

4) les décrochements formés à la faveur de subduction oblique et accommodant le partitionnement de la déformation, comme dans le cas de la faille de Sumatra ou des décrochements Chiliens;

5) et enfin une dernière catégorie, formée par les décrochements que l'on trouve dans les cratons continentaux, issus d'anciennes limites de plaques actives, et agissant actuellement comme des zones de concentration des contraintes à l'intérieur des plaques (exemple des zones de cisaillements armoricaines en France, ou de la faille de Pernambuco au Brésil (*Vauchez et al., 1994*)).

**Un des enjeux actuels de la tectonique est de comprendre la géométrie, la localisation et l'évolution structurale des frontières de plaques décrochantes en fonction des conditions aux limites (cinématique des plaques) et de la rhéologie de la lithosphère (continentale ou océanique).** A ce titre, le système décrochant de la limite de plaque Inde-Arabie est un objet d'étude de premier intérêt : la limite de plaque Inde-Arabie actuelle (Zone de Fracture d'Owen) est l'un des plus grands décrochements connus, avec une longueur de 800 km. Le mouvement relatif Inde-Arabie actuel est lent ($3 \pm 1 mm.an^{-1}$) et se caractérise par une sismicité de faible intensité le long de la Zone de Fracture d'Owen. Les séismes les plus

forts (Mw=5) ont été enregistrés aux extrémités de la Zone de Fracture d'Owen (Bassin Beautemps-Beaupré et fossé de Dalrymple). La Zone de Fracture d'Owen met en contact la lithosphère océanique de la plaque indienne avec la lithosphère du Bassin d'Owen, dont la nature (continentale ou océanique) est discutée (*Barton et al., 1990*). L'âge de la trace actuelle de la Zone de Fracture d'Owen actuelle est estimé entre 3 et 6 Ma (*Fournier et al., 2008 a,b*). La Zone de Fracture d'Owen constitue le dernier stade d'évolution structurale d'un système transformant dont l'initiation est estimée à 90 Ma, ce qui est fait l'un des systèmes transformants les plus anciens au monde. L'histoire géologique de la limite de plaque Inde-Arabie est mal comprise, et soumise à de nombreuses contradictions dans la littérature (*Edwards et al., 2000*). Comment l'histoire géologique de la limite de plaque Inde-Arabie a été affectée par les différents changements cinématiques associés aux orogènes Himalayen et du Zagros demeure inconnu.

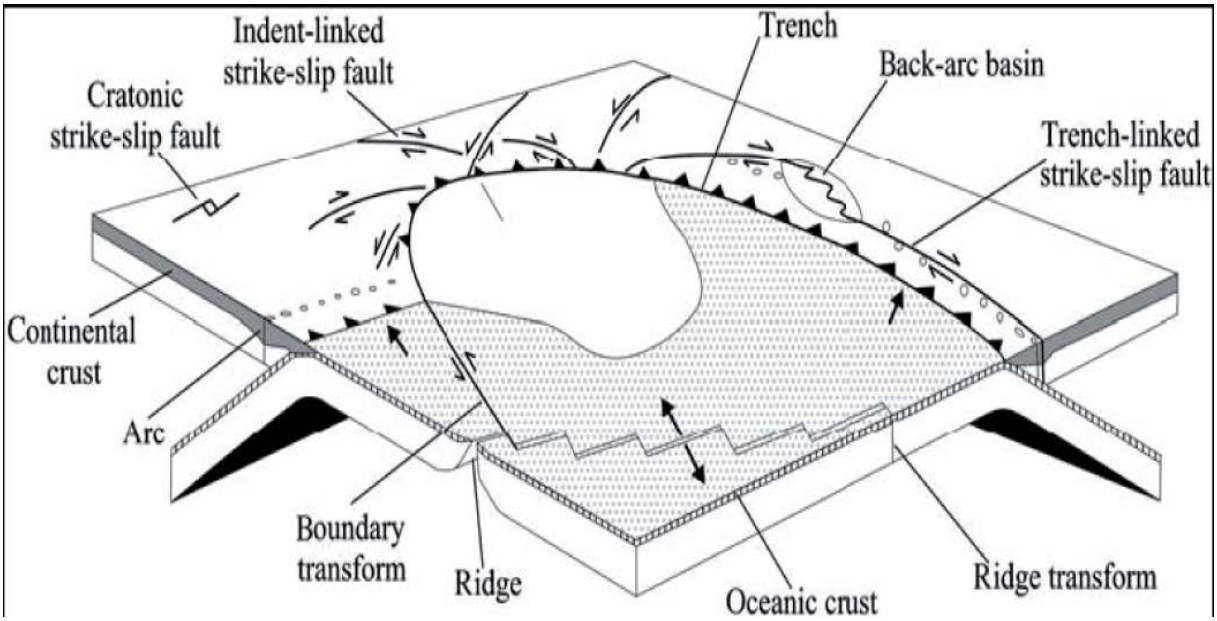


*Figure 3 : Les différents contextes tectoniques favorables aux décrochements (d'après Woodcock, 1986)*

**L'objectif principal de cette thèse est de reconstituer l'évolution structurale de la limite de plaque Inde-Arabie depuis le Crétacé supérieur, et d'établir ses localisations successives, afin de mettre en évidence le rôle des changements cinématiques sur l'évolution structurale de la limite Inde-Arabie au cours de cette période. Le second objectif est de déterminer si l'activité de ce système décrochant constitue une source potentielle d'aléa naturel pour les pays bordant la Mer d'Arabie. Un intérêt particulier a été accordé au système sédimentaire de la Ride d'Owen, relief disséqué par de**

**nombreux glissements de terrain sous-marins potentiellement tsunamigènes.** L'aléa tsunami associé aux systèmes pélagiques profonds recouvrant les rides transformantes est très peu étudié à ce jour. D'autres problématiques ont émergé aux cours de l'avancée de ces travaux, en particulier le rôle des variations relatives du niveau marin sur les apports turbiditiques au sein de l'éventail profond de l'Indus; et le rôle des évènements tectoniques de la mer d'Arabie sur l'enregistrement sédimentaire des changements paléo-environnementaux du Moyen-Orient. Ces travaux s'intègrent également dans l'optique plus générale de comprendre comment les processus de déformation associés aux décrochements sont enregistrés par les sédiments marins.

Cette thèse s'appuie essentiellement sur les données (bathymétrie, sondeur de sédiments, profils sismiques) des campagnes océanographiques OWEN 1 et 2, mais aussi sur les données des campagnes AOC, FANINDIEN et CHAMAK, dont une partie a été mise à ma disposition. Ce jeu de données a été grandement complété par les rapports des forages DSDP et ODP réalisés en Mer d'Arabie. Cette thèse a été préparée principalement au laboratoire de géologie de l'Ecole normale supérieure, mais aussi à l'institut des sciences de la Terre de Paris à l'université Pierre et Marie Curie. Le laboratoire de recherche commun (Ens-CEA) Yves Rocard a soutenu une partie de mes études sur les aléas naturels en Mer d'Arabie. Les campagnes Owen ont été financées par l'INSU/CNRS. Cette thèse a été réalisée en parallèle d'une mission d'enseignement à l'université Pierre et Marie Curie.

# Chapitre 1 : Histoire géologique de la frontière de plaque Arabie-Inde

*Introduction*

Les chaînes de montagne du Zagros et de l'Himalaya sont actuellement les chaînes de collision continentale les plus imposantes, avec les points culminants parmi les plus hauts du monde (4548 m pour le mont Zard Kuh en Iran, 8848 m pour l'Everest). Elles résultent de la convergence des plaques Arabe et Indienne avec l'Eurasie. Les différentes étapes de leur formation ont fortement conditionné la cinématique des plaques de l'Océan Indien au cours du Cénozoïque. La formation de l'Himalaya il y a environ 50-45 Ma a déclenché un ralentissement général de l'expansion des fonds océaniques, tandis que la collision du Zagros a entraîné une réorganisation générale des plaques de l'Océan Indien il y a 25 Ma. La phase de soulèvement de l'Himalaya au Miocène, serait également à l'origine de la phase de déformation intra-plaque de l'océan Indien il y a environ 8-10 Ma (*Molnar et al., 1993; Delescluse et al., 2008*). En dépit des conséquences majeures des migrations de l'Inde et de l'Arabie vers l'Eurasie sur la géologie de l'Océan Indien, la façon dont le mouvement relatif entre ces deux plaques a été accommodé tout au long du Cénozoïque demeure mal comprise.

Le mouvement relatif entre les plaques Arabie et Inde est actuellement accommodé par un grand système décrochant de plus de 800 km de long dans le nord-ouest de l'océan Indien, connu sous le nom de Zone de Fracture d'Owen (ZFO). Comme la vitesse de migration de la plaque Arabie vers l'Eurasie est supérieure à celle de la plaque Indienne, le jeu de la ZFO est dextre. Il est estimé à 3 ± 1 mm/an (*Fournier et al., 2008*), ce qui en fait l'une des frontières de plaques les plus lentes du monde. La ZFO transfère le mouvement divergent généré au niveau des dorsales de Carlsberg et de Sheba en mouvement convergent au niveau de la subduction du Makran (Figure 1). La ZFO est bordée à l'ouest par une série de hauts topographiques d'origine tectonique et volcanique, qui forment la Ride d'Owen. Elle se poursuit au nord-est par le fossé de Dalrymple et la Ride de Murray (Figure 2).

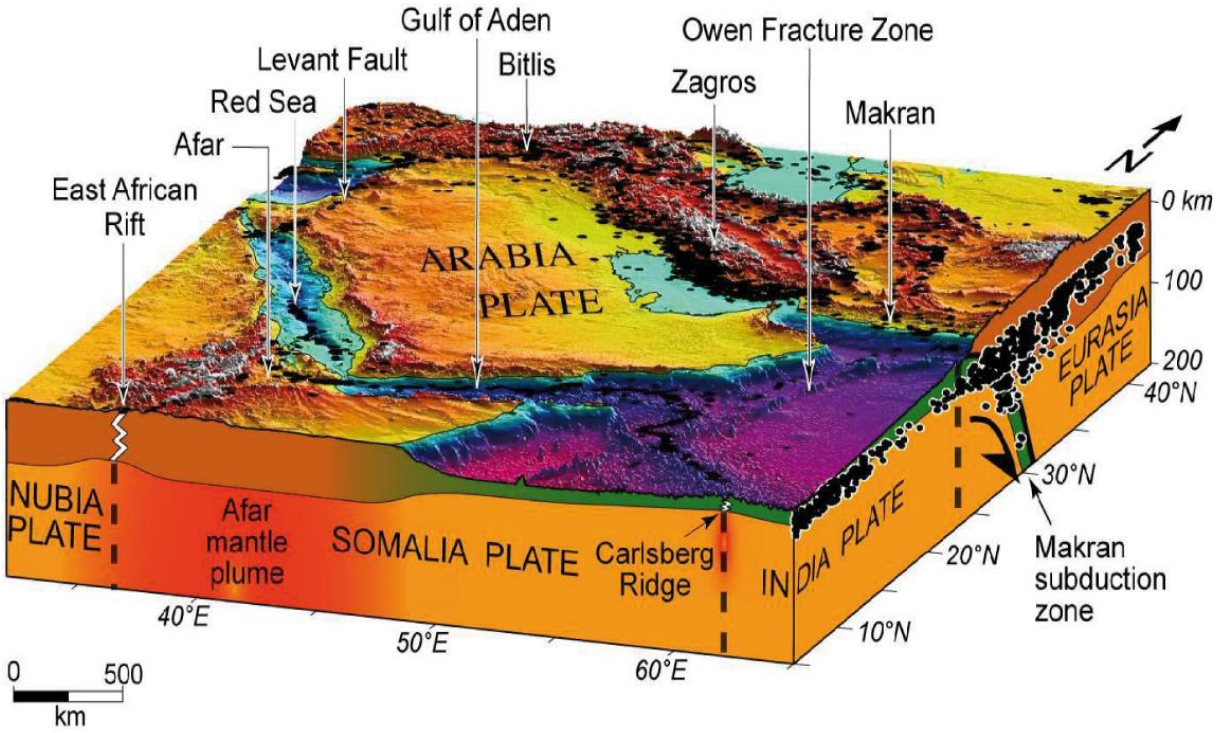


*Figure 1 : Cadre géodynamique de la plaque Arabie. Le mouvement vers le NE de l'Arabie par rapport aux plaques Nubie et Somalie est accommodé par l'expansion océanique dans la Mer Rouge et le Golfe d'Aden, qui se rejoignent au niveau du point triple des Afars. Au Nord, la plaque Arabe entre en collision avec l'Eurasie dans les régions du Bitlis et du Zagros, et plonge en subduction sous l'Eurasie au niveau du Makran. De part et d'autre de la plaque Arabe, le mouvement coulissant est accommodé par la faille du Levant à l'Ouest et la Zone de Fracture d'Owen à l'Est (Figure extraite de Fournier, 2009).*

La marge est-omanaise se situe à l'Est de la plaque Arabie et fait face à l'océan Indien et à la ZFO. Elle s'étend du Ras al'Hadd jusqu'au Ras Sharbithat (Ras signifie cap en arabe), sur une distance d'environ 600 km (Figure 2). Entre la marge est-omanaise et la Ride d'Owen s'étend le bassin d'Owen, sur une largeur variant entre 120 et 200 km selon la latitude. Ce bassin est isolé des apports sédimentaires de l'Indus par la Ride d'Owen et actuellement rempli par les sédiments provenant de la marge est-omanaise et de la Ride d'Owen. La marge est-omanaise est décrite comme une marge transformante (*Mountain et Prell, 1990*), grossièrement parallèle à la Ride d'Owen. Elle présente une suture ophiolitique, qui affleure de façon discontinue le long de la marge. Du sud au nord, nous avons : les ophiolites de Ras Madrekah, les ophiolites de l'île de Masirah et les ophiolites de Ras Jib'sch au sud du Batain (Figure 3).

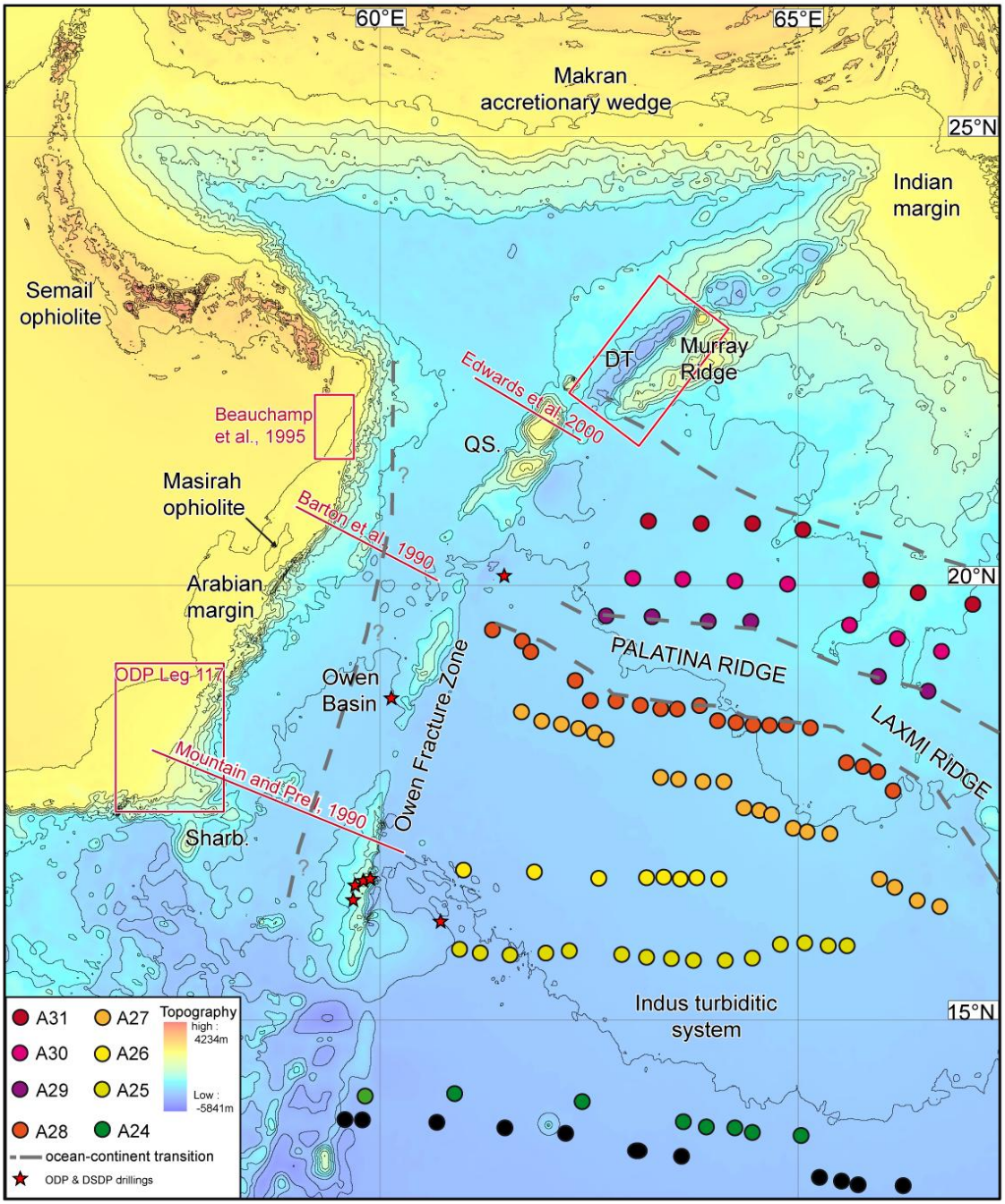


*Figure 2 : Carte physiographique de la Mer d'Arabie et des continents limitrophes, d'après Sandwell et Smith (1997). La Zone de Fracture d'Owen longe une série de reliefs, la Ride d'Owen. Le pointé des anomalies magnétiques est tiré de Royer et al. (2002). Les positions de la transition continent-océan sont d'après Calvès et al. (2011). Localisation des profils sismiques des figures 13, 29, 30 ; et localisation des données publiées dans le rapport du leg ODP 117 et dans Beauchamp et al. (1995). DT : Dalrymple Trough, QS : Qalhat Seamount, Sharb. : Ride de Sharbitat*

Le tracé actuel de la ZFO active était en 2009 encore mal identifié, et principalement déduit de la localisation des séismes. Les décalages morphologiques associés à la ZFO mesurés sur la Ride d'Owen (dont la couverture bathymétrique partielle de la pointe sud a été recueillie au cours de la campagne AOC en 2006) sont de l'ordre de la dizaine de kilomètres. À un mouvement relatif Inde-Arabie constant de 3±1 mm/an, la trace actuelle de la ZFO ne peut être plus ancienne que 6 Ma. La trace de la faille et sa localisation ont donc nécessairement évolué depuis les premiers stades de la migration de l'Inde vers l'Eurasie il y a 90 Ma.

Cette synthèse constitue l'état de l'art des résultats obtenus avant les campagnes Owen 1 et 2 (dont les caractéristiques sont décrites en chapitre 2, et les résultats exposés dans les chapitres 3 à 6), et expose le contexte géologique de la Mer d'Arabie tel qu'il était compris au début de cette thèse, avec le souci d'exposer les contradictions qui ont motivé ces travaux de thèse. A partir de l'étude de la trace active de la ZFO, nous remontons le temps à la recherche des traces fossiles pré-Pliocène potentielles. Les observations géologiques effectuées à terre sont également confrontées aux reconstitutions cinématiques basées sur les anomalies magnétiques du plancher océanique (*Royer et al., 2002; Mercuriev et al., 2006; Fournier et al., 2010*), qui sont à l'origine des principales hypothèses sur les possibles migrations de la limite de plaque Inde-Arabie et qui permettent de situer ces évènements dans le temps (à défaut d'une densité de forage suffisante).

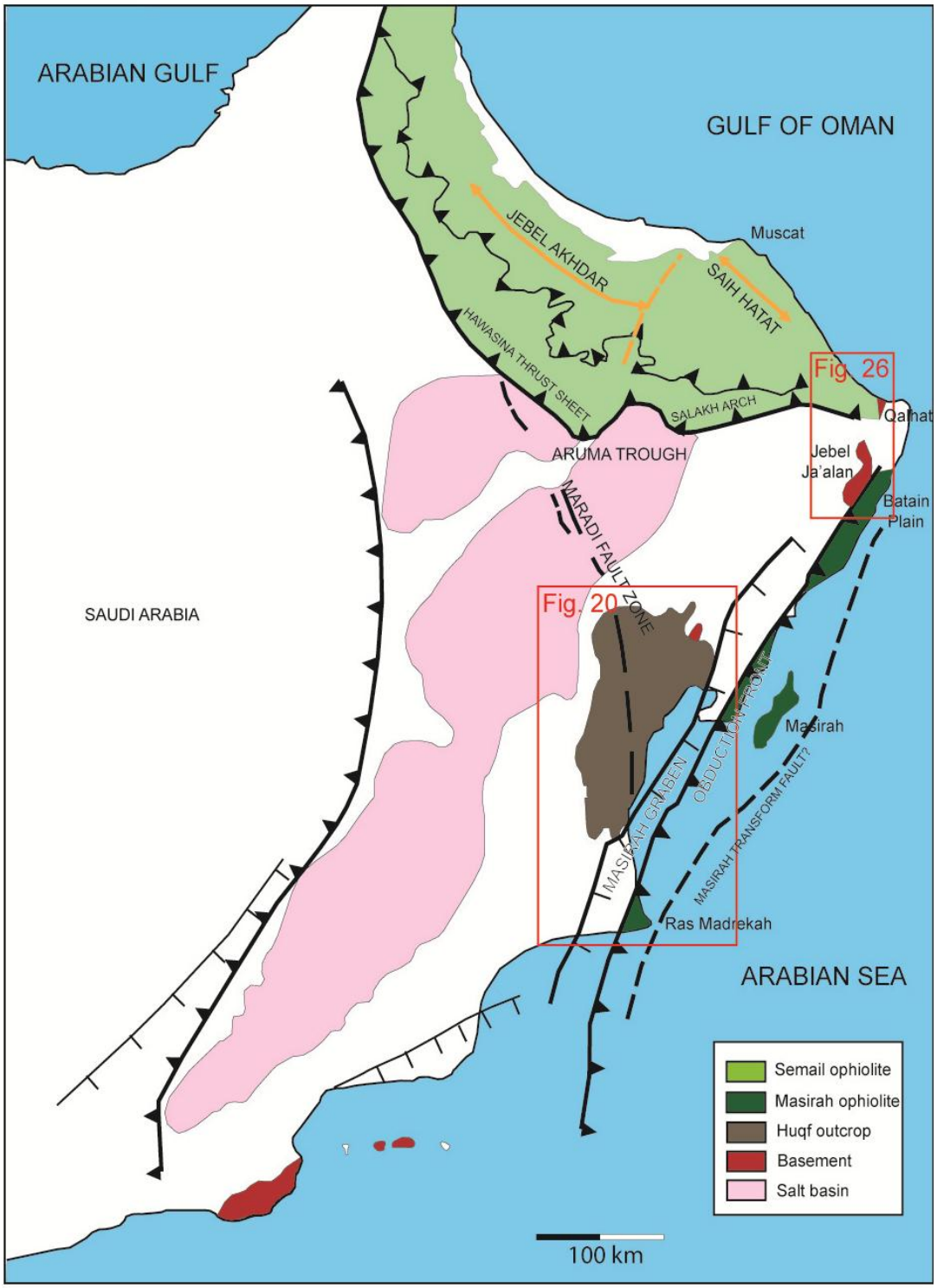


*Figure 3: Schéma structural simplifié du Sultanat d'Oman, modifié d'après Loosveld et al. (1996). La géologie de l'Oman se caractérise par ses sutures ophiolitiques. Au Nord, les ophiolites du Semail, mises en place au Santonien-Campanien, constituent les vestiges de l'Océan Téthys. A l'Est, les ophiolites de Masirah, mises en place au Maastrichtien supérieur, sont les vestiges d'un proto-océan Indien d'âge Jurassique. La marge Est-Omanaise est structurée par un système de graben.*

## *1. Physiographie de la Mer d'Arabie*

### *1.1. Reconnaissance des reliefs sous-marins de la mer d'Arabie*

L'histoire de la reconnaissance des reliefs sous-marins de la mer d'Arabie remonte au XVIIIème siècle, avec les premières cartes marines de l'océan Indien dressées par l'hydrographe britannique Alexander Dalrymple (1737-1808), dont la fosse au nord de la ZFO porte aujourd'hui le nom. Il faut attendre le XXème siècle et le mécénat du brasseur Carlsberg pour que débute réellement l'exploration des fonds sous-marins de la région. La dorsale de Carlsberg fut ainsi découverte en 1928 lors de l'expédition du Dana II (*Schmidt, 1932*). Quelques années plus tard (1933-1934) une expédition anglo-égyptienne fut menée en mer d'Arabie à bord du Mahabiss. Cette expédition fût financée grâce à des fonds laissés à sa mort par John Murray, l'un des premiers grands océanographes dont la ride localisée au large du Pakistan porte aujourd'hui le nom. On doit à cette expédition les premières cartes bathymétriques de la mer Rouge et du golfe d'Aden (*Farquharson, 1936*). Après la seconde guerre mondiale, aucune expédition océanographique notable n'a été entreprise dans l'océan Indien pendant une quinzaine d'années. Cependant, la carte de la sismicité établie par Jean-Pierre Rothé en 1954 permet déjà à Maurice Ewing de dessiner les limites de plaques dans l'Océan Indien (*Rothé, 1954 ; Ewing et Heezen, 1960*). Une expédition internationale fût ensuite menée entre 1959 et 1965. Cette expédition permit à Bruce Heezen et Mary Tharp de dresser une carte physiographique de l'océan Indien d'une précision et d'une qualité qui émerveillent encore aujourd'hui, et sur laquelle la Ride d'Owen est révélée (Figure 4). Il faudra attendre les données satellitaires de David Sandwell et Walter Smith, dans les années 90, pour obtenir une carte d'une meilleure précision (Figure 2 ; *Sandwell and Smith, 1997*). Parallèlement à ses célèbres travaux sur les anomalies magnétiques de la dorsale de Carlsberg (*Vine et Matthews, 1963*), Drummond Matthews décrit la morphologie de la Ride d'Owen et la zone de fracture associée (Figure 5) (*Matthews, 1966*). La dorsale de Sheba fût décrite par Laughton en 1966 et par Matthews, en 1967 (*Laughton, 1966 ; Matthews et al., 1967*). La Ride d'Owen est identifiée comme une série de trois reliefs d'environ 2000 m de haut par rapport au fond marin.


FIGURE 4. The Arabian Sea. A portion of the Physiographic Diagram of the Indian Ocean, published by the Geological Society of America (copyright 1964 by Bruce C. Heezen and Marie Tharp: reproduced by permission). (Depths in metres.)

*Figure 4 : Dessin de la physiographie du Nord Ouest de l'océan Indien, par Heezen et Tharp (1964). Cette carte montre le système turbiditique profond de l'Indus et le système de chenaux qui le sillonne. Le système turbiditique de l'Indus est limité au sud par la dorsale de Carlsberg et à l'Ouest par la Ride d'Owen, qui joue le rôle de barrière topographique avec le bassin d'Owen.*

Dans son article fondateur sur les failles transformantes (*Wilson, 1965*), Tuzo Wilson choisit la ZFO comme exemple type de faille transformante "dorsale-fosse", transformant le mouvement divergeant de la dorsale de Carlsberg en mouvement convergeant au niveau du système himalayen (Figure 6). La ZFO telle qu'elle était alors définie s'étendait de la transformante d'Owen actuelle jusqu'au Makran. Elle était alors considérée comme sénestre sur toute sa longueur, jusqu'à ce que les premiers mécanismes au foyer de séismes soient déterminés (*Sykes, 1968*) et suggèrent un mouvement relatif dextre à la latitude de l'actuelle ZFO. Il faut ensuite attendre les campagnes DSDP (*Deep Sea Drilling Project, 1974*) et ODP (*Ocean Drilling Project, 1989*) pour obtenir des informations complémentaires sur la physiographie de la mer d'Arabie. Ces campagnes de bathymétrie, de sismique réflexion et de forage, initialement réalisées dans le but de déterminer la stratigraphie de l'Indus et l'évolution du régime des moussons au cours des temps géologiques, ont également permis d'établir un premier cadre de l'histoire tectonique de la mer d'Arabie. Une campagne de sismique grand-angle, réalisée à bord du RSS Charles Darwin en 1986 (*Barton et al., 1990*), pointe le caractère singulier du bassin d'Owen : la croûte s'amincit jusqu'à des épaisseurs de

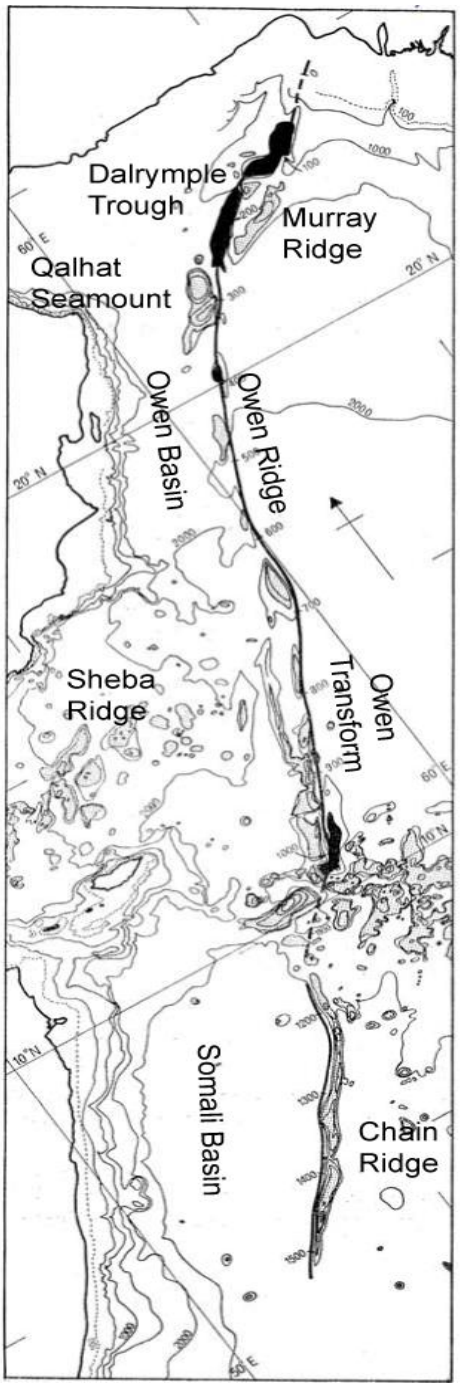


*Figure 5 : Première carte bathymétrique de la Ride d'Owen et du point triple AOC (Aden-Owen-Carlsberg) établie par Matthews (1966). Sur cette carte la Zone de Fracture d'Owen est localisée à l'Est de la Ride d'Owen est s'inscrit dans le prolongement de la faille transformante d'Owen, elle même dans le prolongement de la Ride de Chain.*

l'ordre de 6 km au niveau de la Ride d'Owen, questionnant ainsi la nature océanique ou continentale (marge ultra-étirée) de cette croûte.

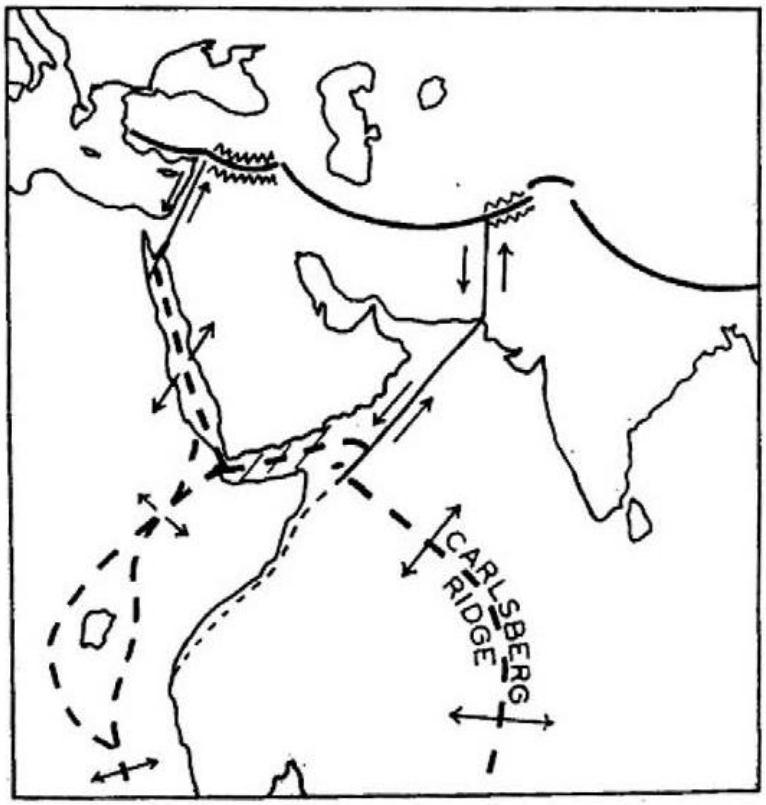


Fig. 8. Sketch illustrating the end of the Carlsberg mid-ocean ridge by a large transform fault (ridge-convex arc type) extending to the Hindu Kush, the end of the rift up the Red Sea by a similar transform fault extending into Turkey and the still younger East African rifts

*Figure 6 : La Zone de Fracture d'Owen est un des exemples choisis par Wilson (1965) pour définir les failles transformantes de type dorsale-fosse. En absence de mécanismes aux foyers et de taux d'ouvertures sur les dorsales, Wilson supposait que la faille est sénestre au niveau de l'OFZ.*

### *1.2. La zone de fracture d'Owen*

La ZFO est caractérisée par une faible sismicité (aucun séisme de magnitude Mw >5 n'a jamais été enregistré) et seuls quelques mécanismes au foyer dextre sont disponibles (Figure 7). Elle s'inscrit sur un petit cercle dont le pôle est localisé au sud de l'Inde *(Fournier et al., 2001)*. Du fait de l'importance des systèmes turbiditiques dans la région, il était a priori possible que la faille soit enfouie, et qu'aucune trace de la faille ne soit discernable sur le fond marin. La campagne AOC (2006), dont le but principal était de cartographier le point triple Aden-Owen-Carlsberg (AOC), a mis en évidence la trace de la terminaison sud de la ZFO. Le résultat fut surprenant : la trace de la ZFO est clairement visible et recoupe la Ride d'Owen,

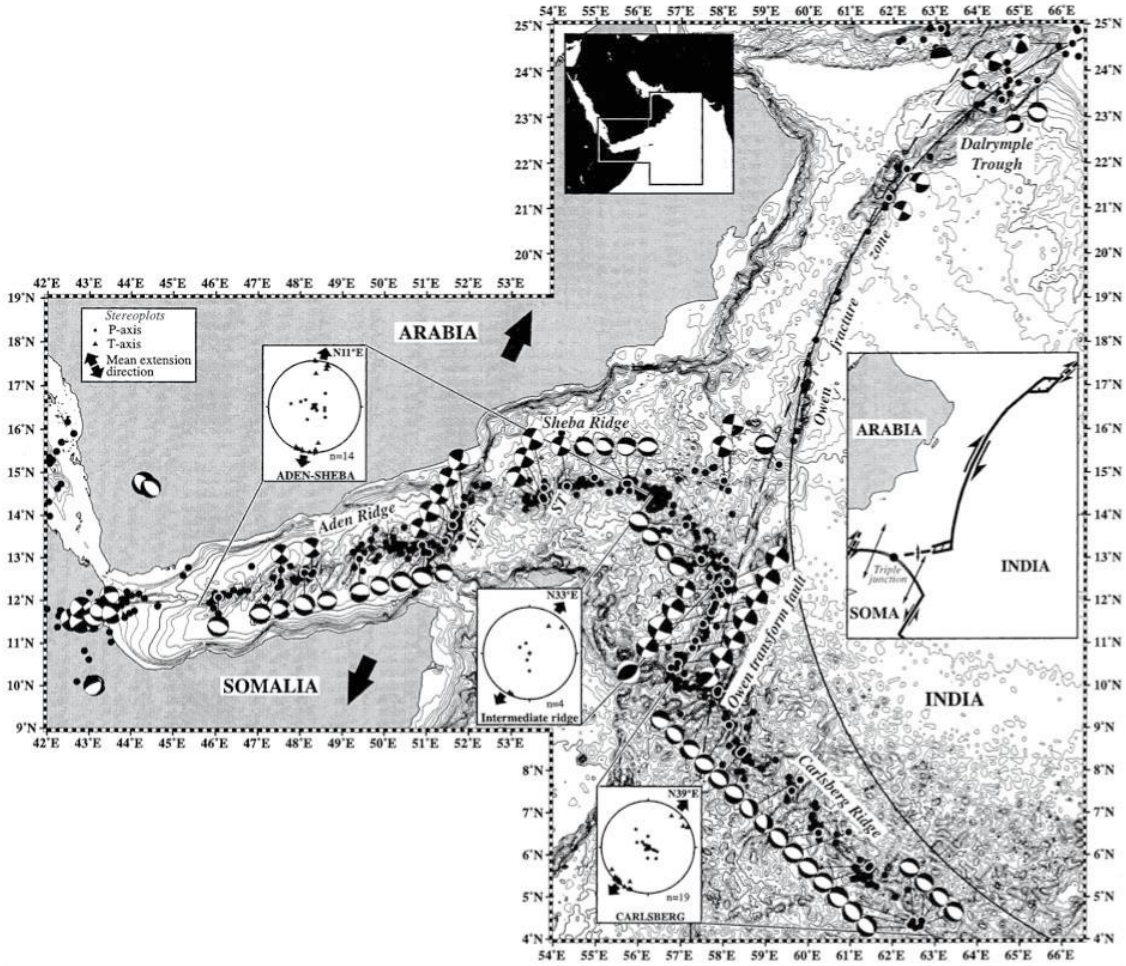


*Figure 7 : Sismicité et mécanismes au foyer des séismes dans la zone de la limite de plaque Inde-Arabie (Fournier et al., 2001). La sismicité révèle que la faille transformante d'Owen (entre les dorsales de Carlsberg et de Sheba) n'est pas connectée directement à la Zone de Fracture d'Owen, et qu'un fragment de plaque Arabe est en cours de transfert à la plaque Indienne au niveau du point triple AOC. La Zone de Fracture d'Owen s'inscrit sur un petit cercle dont le pôle est localisé au sud de L'Inde.*

qu'elle décale irréfutablement de façon dextre sur une douzaine de kilomètres (Figure 8) (*Fournier et al., 2008 a, b*).

### *1.3. Les terminaisons de la zone de fracture d'Owen.*

#### *1.3.1. Le bassin Beautemps-Beaupré, au Sud de la ZFO.*

La campagne AOC a également permis de découvrir que la ZFO se termine au Sud par un bassin en pull-apart de forme rhomboédrique, baptisé "Bassin Beautemps-Beaupré", du nom de l'hydrographe français du 19$^{ème}$ siècle et du bateau du SHOM à bord duquel s'effectuait la mission (Figure 8). Le bassin Beautemps-Beaupré mesure 50 km de large et de

120 km de long (Figure 8). Le bassin est bordé au Nord et au Sud par des failles normales orientées N70°E à N90°E. Les profils de sondeur de sédiments (3.5 kHz) à travers le bassin montrent que ses failles normales bordières présentent un décalage vertical d'environ 100 m. A l'intérieur du bassin, de nombreuses failles normales à rejet inférieur à 10 m sont localisées dans la partie sud. Le bassin présente une très forte anomalie gravimétrique à l'air libre négative de ~100 mgal par rapport à la croûte environnante. Le bassin est probablement rempli par des dépôts d'origine gravitaire et des homogénites issus de la Ride d'Owen et du système turbiditique de l'Indus. La formation du Bassin Beautemps-Beaupré marque une transition dans la configuration du point triple AOC. Avant la formation du Bassin Beautemps-Beaupré, il est probable que la ZFO se connectait directement à la faille transformante d'Owen. Le point triple était alors situé à la jonction entre la ZFO, la transformante d'Owen, et la dorsale de Sheba avec une géométrie de type Ride-Faille-Faille. Bien que cinématiquement stable en apparence depuis 10 Ma, les mécanismes au foyers indiquent que la géométrie du point triple est en train de changer. Une portion de la plaque Arabe semble en cours de transfert à la plaque Indienne (Figure 9) (*Fournier et al., 2008 a, b*). Comment un bassin pull-apart de telles dimensions peut se former le long d'une faille n'ayant accommodé qu'une dizaine de kilomètres de mouvement relatif demeure paradoxal : cela implique un fort degré de recouvrement (*overlap*) des segments de faille bordant le bassin, ainsi qu'un phénomène d'extension distribuée.

### *1.3.2. La Fosse de Dalrymple et la Ride de Murray, au Nord de la ZFO.*

Localisée au NE du Mont Qalhat, la Fosse de Dalrymple forme une dépression de 150 km de long pour 25 km de large, formée en réponse à une phase d'extension oblique localisée sur la ZFO (Figures 10, 11) (*Edwards et al., 2000, 2008*). L'épaisseur des sédiments de l'Indus est de l'ordre de 3 km dans la région. La structure de la fosse est dissymétrique, avec un réseau de failles plus dense et en-échelon sur le flanc nord-ouest, qui s'inscrit dans le prolongement de la terminaison en queue de cheval de la ZFO (Figure 10). Ceci marque soit une phase d'extension plus longue en bordure Est de la plaque Arabie, soit un comportement rhéologique différent par rapport à la plaque Indienne (*Edwards et al., 2000*). Les reliefs de la Ride de Murray atteignent plus de 2000 m par rapport au fond océanique, et constituent une barrière topographique pour les sédiments de l'Indus depuis leur surrection (*Ellouz-Zimmerman et al., 2007).* Les profils de sismique réfraction réalisés dans la zone de la Ride de Murray ont identifié une croûte continentale épaisse de 12 à 14 km (avec des vitesses Vp

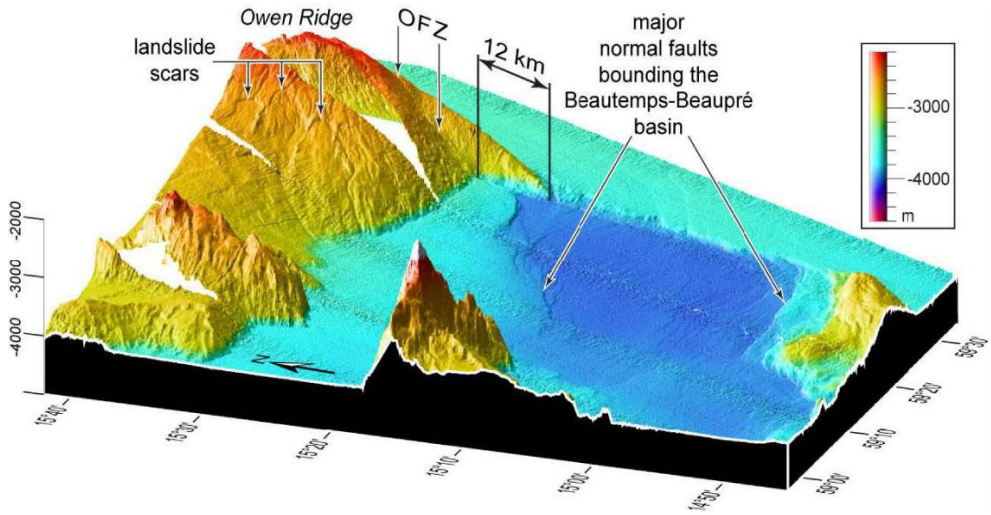


*Figure 8: Vue en perspective de l'extrémité sud de la Zone de Fracture d'Owen et de la faille active qui décale la Ride d'Owen de manière dextre sur 12 km et se termine au Sud dans le bassin en pull-apart de Beautemps-Beaupré. A un taux de déplacement de 3 ±1 mm. an$^{-1}$, l'âge de la faille active serait donc compris entre 3 et 6 Ma (Fournier et al., 2008a).*

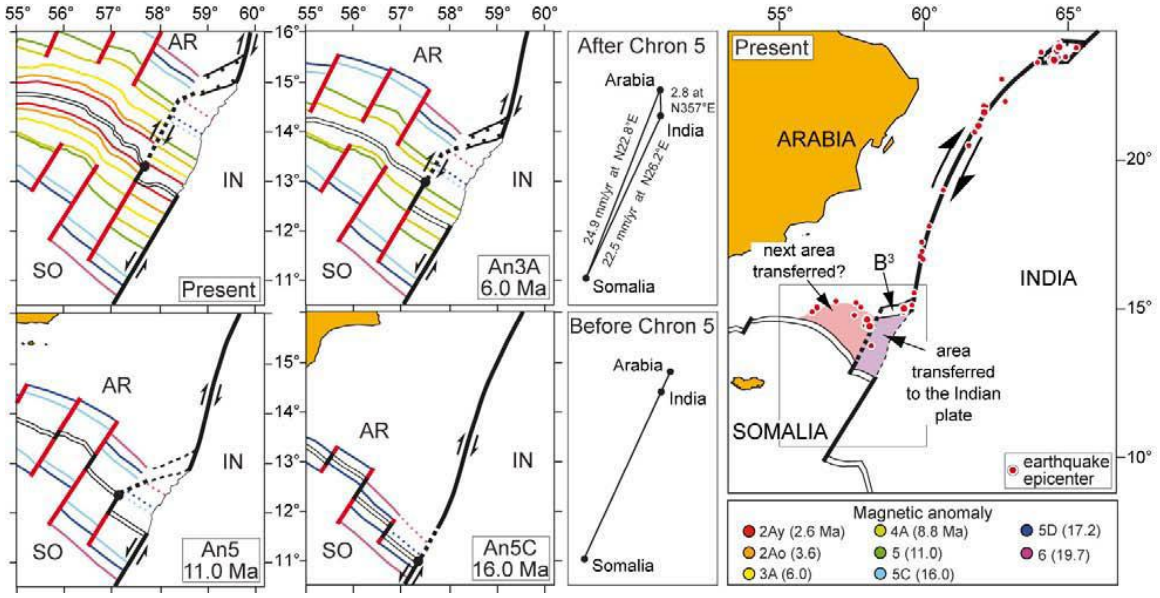


*Figure 9: Reconstitution de l'évolution du point triple AOC, aux chrons 5C, 5, 3A et actuel (Fournier et al., 2010). Le changement de configuration de la frontière Inde-Arabie et l'initiation du bassin de Beautemps-Beaupré sont synchrones d'une réorganisation cinématique régionale dans l'Océan Indien vers 10 Ma (chron 5). La configuration du point triple avant et après changement de géométrie est montrée avec le triangle de vitesse correspondant. La sismicité suggère qu'une nouvelle frontière de plaque se développe à l'Ouest du bassin de Beautemps-Beaupré. Ar : Arabie, IN : Inde, SO : Somalie.*

de 4,6-6-7 km/s) au sud-est de la fosse, au niveau de la Ride de Murray (*Edwards et al., 2008*). La fosse de Dalrymple correspond donc a une transition continent/océan abrupte, sur une largeur de 10 km. Il s'agirait d'un fragment de croûte continentale issu de la fragmentation du Gondwana au Jurassique (*Edwards et al., 2008*).

### *1.4. La transition continent-océan de la marge NW indienne*

La position de la transition continent-océan de la marge NW indienne est difficile à contraindre du fait de la complexité de l'histoire géologique de la région. La plus vieille anomalie magnétique associée à la dorsale de Carlsberg est l'anomalie A28 (~63 Ma), située à plus de 500 km du rebord de la plate-forme indienne (Figure 2). La gravimétrie et les données de sismique réflexion acquises dans la région révèlent la présence de la Ride de Laxmi enfouie sous les turbidites de l'Indus (*Calvès et al., 2011*). La nature de la Ride de Laxmi n'est pas clairement établie, mais il pourrait s'agir d'une croûte continentale (*Calvès et al., 2011*). Entre cette ride et la plate-forme indienne sont identifiées les anomalies magnétiques A29 à A31 (64.8 à 69.3 Ma) qui correspondent au Bassin de Gop (*Yateesh et al., 2009*). Le Bassin de Gop se serait formé dans les premiers stades de manifestation du panache mantellique du Deccan; tandis que la dorsale de Carlsberg se serait formée plus tardivement, alors que l'activité du panache s'était déjà atténuée (*Minshull et al., 2008*). Les données de sismique réfraction couplées à l'existence d'anomalies magnétiques dans le Bassin de Gop plaident en faveur d'une croûte océanique (*Yateesh et al., 2009*). La transition continent-océan de la marge NW Indienne est donc située à environ 300 km de la bordure de la plate-forme indienne, au niveau de l'anomalie A31 dans le Bassin de Gop.

### ***1.5. La zone de fracture d'Owen, le bassin 20°N et le système turbiditique profond de l'Indus***

Avant les campagnes AOC (2006) et OWEN (2009), les seules données disponibles sur la structure de la ZFO (issues du Leg ODP 117) ne montraient pas clairement la position de la faille, aussi cette dernière était supposée localisée au pied Est de la Ride d'Owen (*Shipboard Scientific Party, 1989*). Un pli de grande amplitude est observé à l'Est de la Ride sur des profils sismiques transverses à la Ride (Figure 12).

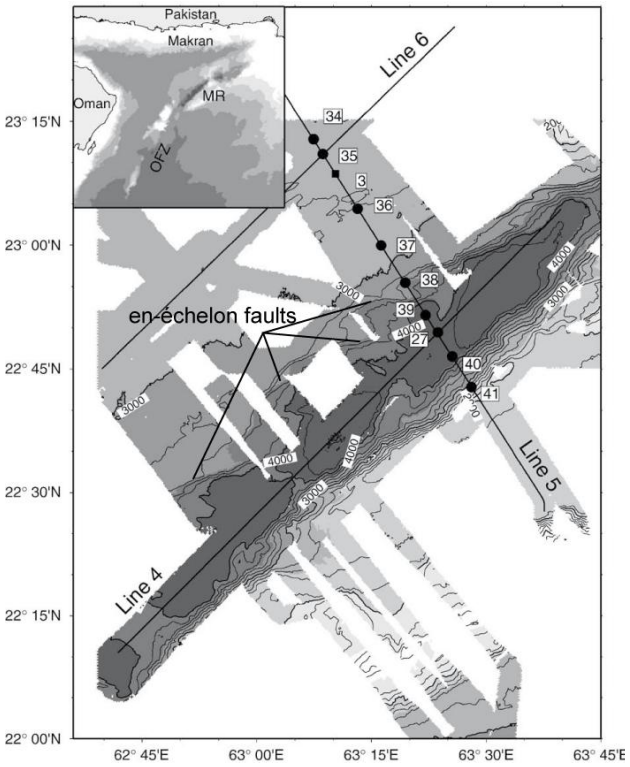


*Figure 10: Bathymétrie de la Fosse de Dalrymple (Edwards et al., 2008). Le bord Ouest de la fosse se caractérise par un système de failles en-échelon. Le bord Est est formé d'une faille normale majeure.*

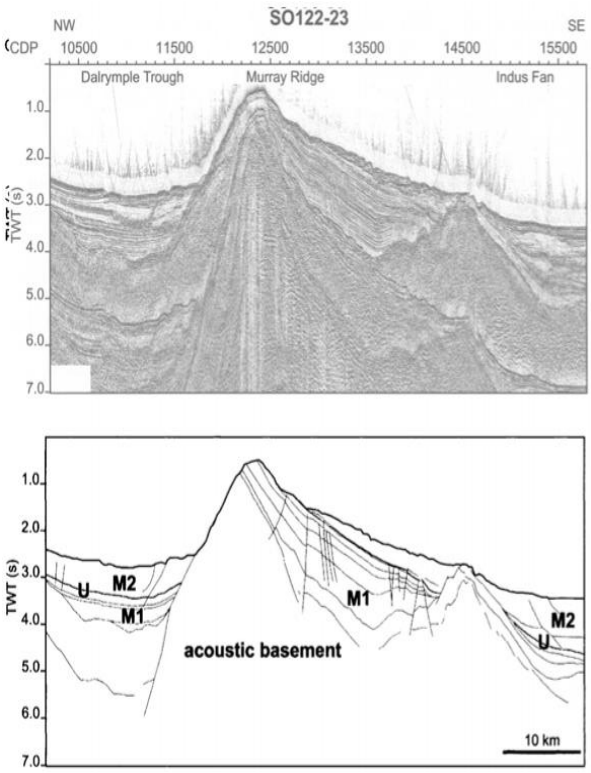


*Figure 11 : Profil sismique transverse au flanc du Fossé de Dalrymple et à la ride de Murray Sud (Gaedicke et al., 2002). Il s'agit d'un rift étroit et dissymétrique. La Ride de Murray correspond à un bloc basculé. Les discontinuités U et M sont d'âge début Miocène et début Pliocène, respectivement (voir Figure 15).*

Entre la Ride Centre et le Mont Qalhat, à l'endroit où les plaines de l'Indus et d'Owen se rejoignent, les campagnes Conrad 9 et DSDP 222 ont mis en évidence la présence d'un "fossé d'effondrement" bordé par des failles normales dont le rejet varie entre 25 et 150 m, selon le segment considéré. Les données de bathymétrie multifaisceaux collectées pendant la campagne OWEN en 2009 révèlent que ce fossé est en fait un bassin en pull-apart d'une centaine de kilomètres de long sur une trentaine de large, baptisé "bassin 20°N" en raison de sa latitude. Les auteurs du rapport DSDP notent l'absence de dépôt turbiditique majeur dans la série Pléistocène aux abords de l'OFZ, ce qui est probablement à l'origine de l'excellente préservation des structures observables sur le fond avec les données des campagnes Owen.

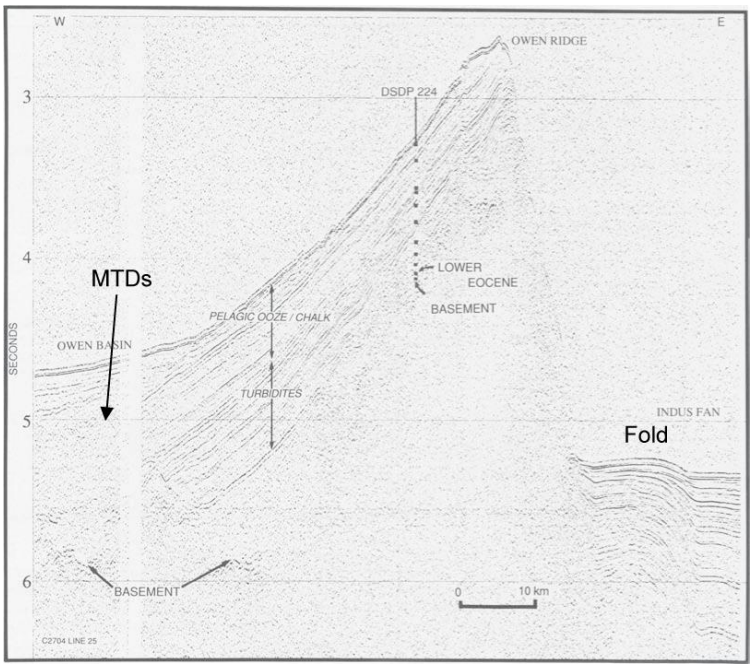


*Figure 12 : Profil sismique transverse à la Ride Sud d'Owen (Shipboard scientific party, 1989; Mountain et Prell, 1990). La couverture sédimentaire de la Ride est caractérisée par une transition (datée à 15 Ma) entre un faciès turbiditique et un faciès pélagique. Cette transition correspond à la surrection de la Ride. Les forages ont prélevé des basaltes à lamprophyres au niveau du socle. Un anticlinal est observé au pied de la Ride, à l'Est. MTDs : Mass Transport Deposits.*

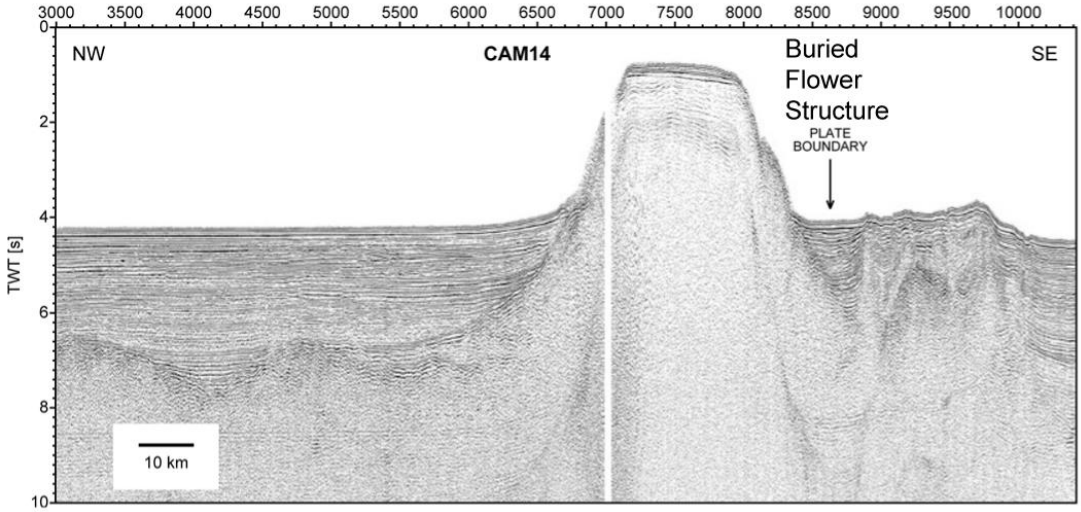


*Figure 13 : Profil sismique transverse au Mont Qalhat (Edwards et al., 2000). A l'Ouest, la sédimentation du bassin d'Owen adopte une configuration en onlap sur le guyot volcanique, indiquant un âge anté-paléocène pour ce dernier. A l'Est au contraire, la Zone de Fracture d'Owen montre une structure en fleur.*

### *1.6. La Ride d'Owen et le Mont Qalhat*

La Ride d'Owen s'étend longitudinalement sur plus de 870 km. Elle est composée de trois hauts fonds localement recoupés par l'OFZ. Les hauts fonds sont nommés selon leur position géographique (Ride Sud : de 15 à 18°N; Ride Centre : de 18 à 20°N; Ride Nord : de 20° à 22°N) (Figures 2, 5).

La Ride Sud d'Owen s'étend longitudinalement sur 330 km, pour une largeur avoisinant la centaine de kilomètres. Elle culmine à 2000 m par rapport à la plaine abyssale environnante. Elle est formée par un grand plan monoclinal basculé vers l'Ouest (pente moyenne 3-4°). La Ride Centre d'Owen s'étend elle sur 210 km de long, et plus de 50 km de large. Son altitude maximale est de 1700 m (par rapport à la plaine de l'Indus). Elle est localement formée par un plan monoclinal qui forme un plateau sous-marin. Les forages ODP réalisés sur la ride Sud (721, 722, 731) révèlent que le socle est de nature volcanique (trachybasalte à lamprophyres d'âge fini-Paléocène), bien qu'un substratum d'une autre nature puisse reposer sous les basaltes. Ces derniers sont recouverts par des dépôts turbiditiques et une série hémi-pélagique, composée principalement de vase et de boue calcaire riche en foraminifères. La couverture pélagique est disséquée par des glissements de terrain, tel qu'attesté par les forages ODP et DSDP qui révèlent des hiatus sédimentaires et des dépôts de brèches, et les profils sismiques qui montrent des faciès chaotiques (Figure 9) (*Shipboard Scientific Party, 1974, 1989*). Les dépôts turbiditiques sont issus du système turbiditique profond de l'Indus, qui recouvrait la ride avant que celle-ci ne soit soulevée. Après le soulèvement de la ride, les apports sédimentaires sont essentiellement de nature hémipélagique (Figure 12). L'âge du soulèvement de la Ride d'Owen a d'abord été établi sur la base d'une discordance angulaire entre des dépôts Oligocène et Miocène observée sur les premiers profils de sismique réflexion collectés dans la région (*Shipboard Scientific Party*, 1974). Les premiers foraminifères miocènes reposant sur la discordance sont datés à 19.7 Ma. Cet âge a ensuite servi de référence à toute la littérature, cependant faut-il garder à l'esprit qu'une discordance angulaire ne marque pas nécessairement une activité tectonique. Une transition entre turbidites et pélagites a été forée au cours du Leg ODP 117, et son âge établi biostratigraphiquement à 14-15 Ma. Les rapporteurs du Leg en concluent que cette transition de faciès correspond à l'âge du soulèvement de la Ride d'Owen (les turbidites ne pouvant pas se déposer au sommet d'une ride déjà élevée) (*Shipboard Scientific Party, 1989*). Le forage DSDP 223 atteste d'un soulèvement contemporain de la Ride Centrale. Les processus d'avulsion des chenaux turbiditiques peuvent cependant générer des faciès mixtes pélagites/

turbidite, sans qu'aucun soulèvement tectonique ne soit impliqué. L'âge du soulèvement de la Ride d'Owen est donc assez mal contraint, mais le consensus accepté au début de cette thèse plaidait en faveur d'un soulèvement au début du Miocène, peu avant l'apparition de la dorsale de Sheba. La configuration des turbidites d'âge anté-Miocène qui recouvrent partiellement la Ride Sud indiquent qu'un relief déjà important pré-existait dans les plaines de l'Indus : ce relief aurait été surélevé par la suite jusqu'à sa profondeur actuelle, entre 19 Ma et 15 Ma (Mountain et Prell, 1990). L'âge de cette paléo-Ride d'Owen est probablement le même que celui des trachybasaltes forés sur le socle de la Ride lors des Leg ODP, i.e. fini-Paléocène. Les taux de vésicules et de hyaloclastes mesurés sur les prélèvements DSDP du substratum indiquent une lave émise à des profondeurs inférieures à 1000 m (*Whitmarsh et al., 1974*) : faut-il y voir un ordre de grandeur de la profondeur initiale de la paléo- Ride d'Owen ?

La Ride Nord mesure 200 km de long, pour 70 km de large. Elle atteint des hauteurs de 2700 m par rapport à la plaine abyssale de l'Indus. La Ride Nord porte aussi le nom de Mont Qalhat, en référence à la ville éponyme du nord-est de l'Oman, située à la même latitude. Les anomalies magnétiques indiquent un substratum de nature volcanique, probablement issu de l'activité d'un point chaud (*Edwards et al., 2000; Fournier et al., 2011*). Le Mont Qalhat est tronqué en son sommet et présente une morphologie de guyot. Cette morphologie est le vestige de l'émersion, de l'érosion puis de la subsidence du Mont Qalhat. Les rares profils sismiques disponibles dans la région indiquent que les séries sédimentaires paléogènes du Bassin d'Oman ont une configuration en "onlap" sur le Mont Qalhat (Figure 13). Le relief de la Ride Nord, contrairement aux deux autres segments de la Ride dont le dernier stade de surrection est daté à 19 Ma, serait donc d'âge fini-Crétacé/début Paléogène (*Edwards et al., 2000*). Le Mont Qalhat n'est pas relié à un épisode volcanique particulier, mais son âge supposé Crétacé pourrait correspondre au volcanisme de point chaud du Deccan.

**L'éventail turbiditique de l'Indus**

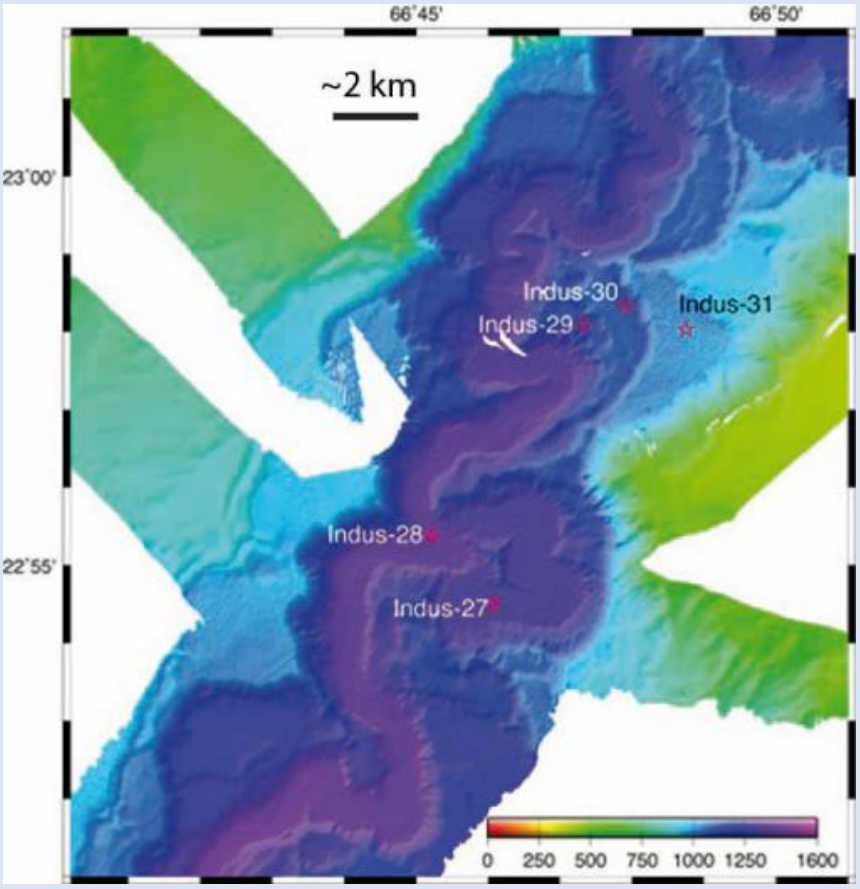


*Figure 14 : Bathymétrie multifaisceaux du canyon de l'Indus, d'après Von Rad et Tahir (1997)*

La sédimentation du système turbiditique profond de l'Indus conditionne la façon dont la déformation associée à la limite de plaque Inde-Arabie est enregistrée. Le système turbiditique de l'Indus est l'un des plus importants du monde, juste après celui du Bengale, avec une superficie de 1.1 x $10^6$ $km^2$ , et une épaisseur pouvant atteindre jusqu'à 9 km (*Clift et al., 2001*). Les plus vieux sédiments forés indiquent que la sédimentation a commencé à l'Eocène, en réponse à la formation de l'Himalaya, dont les produits d'érosion sont charriés par le fleuve Indus jusqu'en Mer d'Arabie (*Clift et al., 2001*). Le bassin versant de l'Indus draine une superficie d'environ 1 x $10^6$ $km^2$, et sa décharge annuelle avant la mise en place des barrages était de l'ordre de 450.$10^6$ T/an (*Milliman et al., 1984*). Le delta sub-aérien de l'Indus s'étend sur 750 000 km². Le système turbiditique de l'Indus est approvisionné au cours du Quaternaire par un canyon profond de 1,6 km et long de 185 km (Figure 14) (*Von Rad et Tahir, 1997*), mais aussi par les instabilités gravitaires le long de la marge ouest-

indienne (formant un système turbiditique de type "slope-apron" sensu *Reading and Richards*, *1994*). La configuration des systèmes de chenaux-levées sur l'ensemble de l'éventail est assez mal connue du fait d'une couverture multi-faisceaux très lacunaire. Des systèmes de chenaux-levées ont été toutefois identifiés au pied de la marge par *Kenyon et al. (1995), Von Rad et Tahir (1997) et Carmichael et al. (2009)*. Les systèmes de chenaux-levées au sein de l'éventail de l'Indus ne sont bien développés qu'à partir du début du Miocène, les taux de sédimentation augmentant avec la surrection de l'Himalaya (*Clift et al., 2001*). Durant le Quaternaire, la sédimentation dans l'Indus est principalement sous le contrôle des variations glacio-eustatiques (*Prins et al., 2000*). Les brefs épisodes turbiditiques sont espacés par des phases pélagiques qui dominent la sédimentation pendant le Quaternaire (*Shipboard scientific party, 1989; Govil and Naidu, 2008*). La réponse du système turbiditique de l'Indus aux variations glacio-eustatiques du Quaternaire est détaillée dans *Bourget et al*. ( 2013), joint en annexe de cette thèse.

## *2. Âge de la frontière de plaque Inde-Arabie actuelle et localisation au cours du temps : controverses*

### *2.1. L'âge de la zone de fracture d'Owen actuelle*

Les décalages morphologiques de la Ride d'Owen, convertis en temps grâce à la vitesse actuelle de la faille, suggèrent que l'âge de la ZFO actuelle serait début Pliocène (3 à 6 Ma), un âge largement postérieur à la surrection de la Ride d'Owen (19 Ma). D'autres études réalisées au niveau des terminaisons de l'OFZ apportent des contraintes complémentaires :

_ Au niveau du Bassin Beautemps-Beaupré, les pointés des anomalies magnétiques à l'Est de la dorsale de Sheba indiquent un âge possible de la ZFO autour de 8-10 Ma (chron 5), un peu plus ancien que l'âge déduit des décalages morphologiques.

_Les profils de sismique réflexion recoupant la fosse de Dalrymple, corrélés aux forages disponibles, indiquent un âge début Miocène pour un premier stade de la formation de la Fosse et de la surrection de la Ride de Murray, i.e. contemporain de la surrection de la Ride d'Owen (Figure 13) (*Gaedicke et al., 2002*). L'identification de paléo-chenaux de l'Indus à l'Ouest de la fosse de Dalrymple (*Quayrum, 1997*) confirme que la fosse n'existe pas depuis le Paléocène, comme initialement proposé par *Gaedicke et al. (2002*). Une accélération de la subsidence de la Fosse et du soulèvement de la Ride de Murray est enregistrée vers la fin du Miocène (par une discordance sédimentaire baptisée M dans la littérature (*Gaedicke et al.*,

*2002*)), et pourrait correspondre à la mise en place de la trace actuelle de la ZFO. La stratigraphie dans la région de la Ride de Murray est cependant mal contrainte du fait de l'éloignement des puits utilisés pour corréler les profils sismiques dans le temps (tous situés sur la plate-forme indienne).

Malgré les incertitudes sur son âge, la trace actuelle de la ZFO est donc bien plus récente que la surrection de la Ride d'Owen il y a 19 Ma *(Shipboard Scientific Party, 1989)*. Cependant, les reconstitutions cinématiques intégrant les anomalies magnétiques des dorsales de Sheba (*Fournier et al., 2010*) et de Carlsberg (*Mercuriev et al., 2006*) prédisent que la ZFO occupe sa place actuelle depuis environ 20 Ma (depuis l'initiation de l'accrétion océanique dans le Golfe d'Aden) (*Chamot-Rooke et al., 2009*). Un système décrochant d'environ 800 km de long et ayant valeur de limite de plaque existerait donc au pied de la Ride d'Owen depuis 20 Ma, les segments de faille inactifs ayant été enfouis sous les apports sédimentaires importants de l'Indus. Ceci semble confirmé par l'un des seuls profils sismiques recoupant la ZFO, au pied du Mont Qalhat, qui montre des sédiments affectés par un réseau complexe de failles (en structure en fleur) partiellement enfoui sous les turbidites de l'Indus (Figure 10) (*Edwards et al., 2000*). Bien que ce système de faille reste à identifier sur les segments plus méridionaux, la trace de la ZFO actuelle est probablement le dernier stade d'évolution structurale de la limite de plaque Inde-Arabie depuis environ 20 Ma (Figure 15). Aucune déformation d'origine tectonique antérieure à 20 Ma n'a été identifiée au niveau de la ZFO actuelle, mais la ZFO n'a pas été imagée par la sismique réflexion sur toute sa longueur.

Au delà de 20 Ma, l'histoire de la marge Est-Omanaise est difficile à relier aux grandes étapes de l'histoire de l'océan Indien. Les reconstitutions paléogéographiques de l'océan Indien au cours du Mésozoïque montrent que l'Inde a entamé sa migration vers l'Eurasie il y a environ 90 Ma. L'Inde était alors située à des latitudes comprises entre 40 et 60°S (Figure 16). La collision entre l'Inde et l'Eurasie est enregistrée par un brusque ralentissement du taux d'accrétion (de 15 à 5 cm/an) de la dorsale de Carlsberg daté à environ 45-50 Ma (*Patriat et Achache, 1984, Royer et al., 2002*). L'Inde a donc effectué une migration de plus de 6000 km entre 90 et 50 Ma par rapport à Madagascar. La migration de l'Inde implique l'existence d'une faille transformante, mal identifiée, de plus de 3000 km de long ayant accompagné le mouvement relatif entre l'Inde et le bloc Afrique-Arabie. De simples estimations permettent de déduire l'existence d'un système décrochant majeur au cours du Paléogène : si l'on

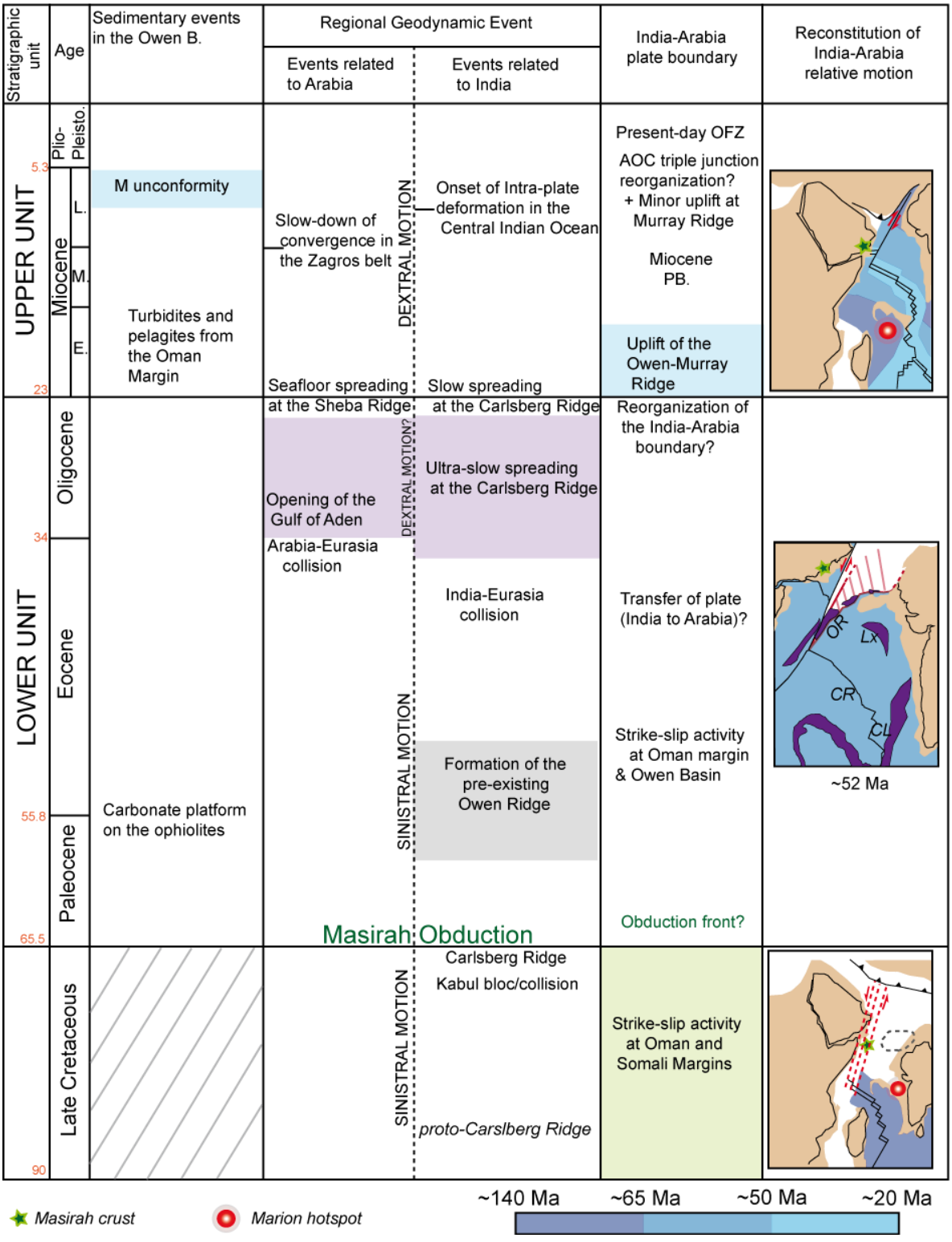


*Figure 15 : Synthèse des âges des principaux évènements géologiques associés à l'activité de la limite de plaque Inde-Arabie depuis le Crétacé supérieur (cadre géologique communément admis avant cette thèse). AOC : Aden-Owen-Carlsberg; CL : Chagos Laccadive; CR : Carlsberg Ridge; Lx : Laxmi; OR : Owen Ridge; PB : Plate Boundary.*

considère la valeur moyenne des taux d'accrétion de la dorsale de Carlsberg de l'ordre de 1 $cm.an^{-1}$ (*Mercuriev et al., 1996 ; Royer et al., 2002*) depuis 40 Ma, un mouvement relatif Inde-Arabie sénestre de l'ordre de 200 km aurait été accommodé entre 40 et 20 Ma au niveau de cette limite de plaque. Entre 30 et 20 Ma, pendant le rifting du Golfe d'Aden, le mouvement sur la limite de plaque Inde-Arabie était probablement sénestre car la vitesse d'ouverture du Golfe d'Aden était plus faible que pendant la période d'accrétion océanique. Aucune trace de cette activité n'a jusqu'à présent été identifiée au niveau de la ZFO actuelle : où peuvent avoir été localisées les traces d'activité de la limite de plaque Inde-Arabie avant 20 Ma ?

## L'histoire géologique de l'océan Indien

L'ouverture de l'océan Indien est le résultat de la dispersion du Gondwana, super continent qui regroupait à l'origine les continents Africain, Australien, Indien, Antarctique et Sud Américain. L'ouverture de l'océan Indien est associée à la subduction de l'océan Téthys. La fragmentation du Gondwana débute au *Jurassique supérieur* (Kimmeridgien/ Tithonien pour les Bassins Ouest-Somalien et Mozambique), avec l'individualisation de blocs Gondwana Ouest et Est, qui a été accompagnée par la formation de bassins (Bassin Mozambique, Bassin Ouest-Somalien) connectés par de grandes failles transformantes. *Au Crétacé inférieur* (96 Ma), Madagascar se sépare de l'Inde. La dorsale entre l'Inde et Madagascar forme le bassin des Mascareignes et reste active jusqu'au Paléocène. Un chevauchement intra-océanique reprend la dorsale téthysienne et préfigure l'obduction. *Au Campanien* se sont mises en place les ophiolites du Semail, au Nord de l'Oman. Ces ophiolites sont composées d'une portion de la Néo-Téthys, d'âge crétacé (Albien-Cénomanien). *Au Maastrichtien*, la dorsale à l'origine du Bassin Ouest Somalien a cessé son activité. La mise en place du point chaud du Deccan amorce la formation de la dorsale de Carlsberg. Un saut de dorsale contemporain de l'activité du point chaud entraîne l'abandon de la dorsale des Mascareignes (entre Madagascar et l'Inde). L'ouverture s'effectue alors plus au Nord avec la formation de la dorsale de Carlsberg entre l'Inde et les Seychelles, qui se prolonge ensuite au sud par la dorsale Centrale Indienne (A partir du chron C18). L'activité du même point chaud a formé par la suite la Ride des Chagos – Laccadive. *Au Lutétien*, la Grande Inde a migré vers le Nord, jusqu'à entrer en collision avec l'Eurasie il y a environ 50 Ma, comme indiqué par l'abrupt changement des taux d'accrétion de la dorsale de Carlsberg de 15 à 5 cm/an. Le rifting du golfe d'Aden s'est initiée il y a 35 Ma. Un changement du régime d'accrétion de la dorsale Sud Ouest Indienne vers un régime plus lent est détecté vers 25 Ma (*Patriat et al., 2008*), contemporain de la collision Arabie-Eurasie au niveau du Zagros, qui a également généré une compression orientée N-S qui a rajeuni les reliefs des montagnes du Nord de l'Oman. La limite de plaque Inde-Arabie actuelle est localisée au niveau de la ZFO depuis la formation de la dorsale de Sheba, il y a environ 20 Ma (*Fournier et al., 2010*).

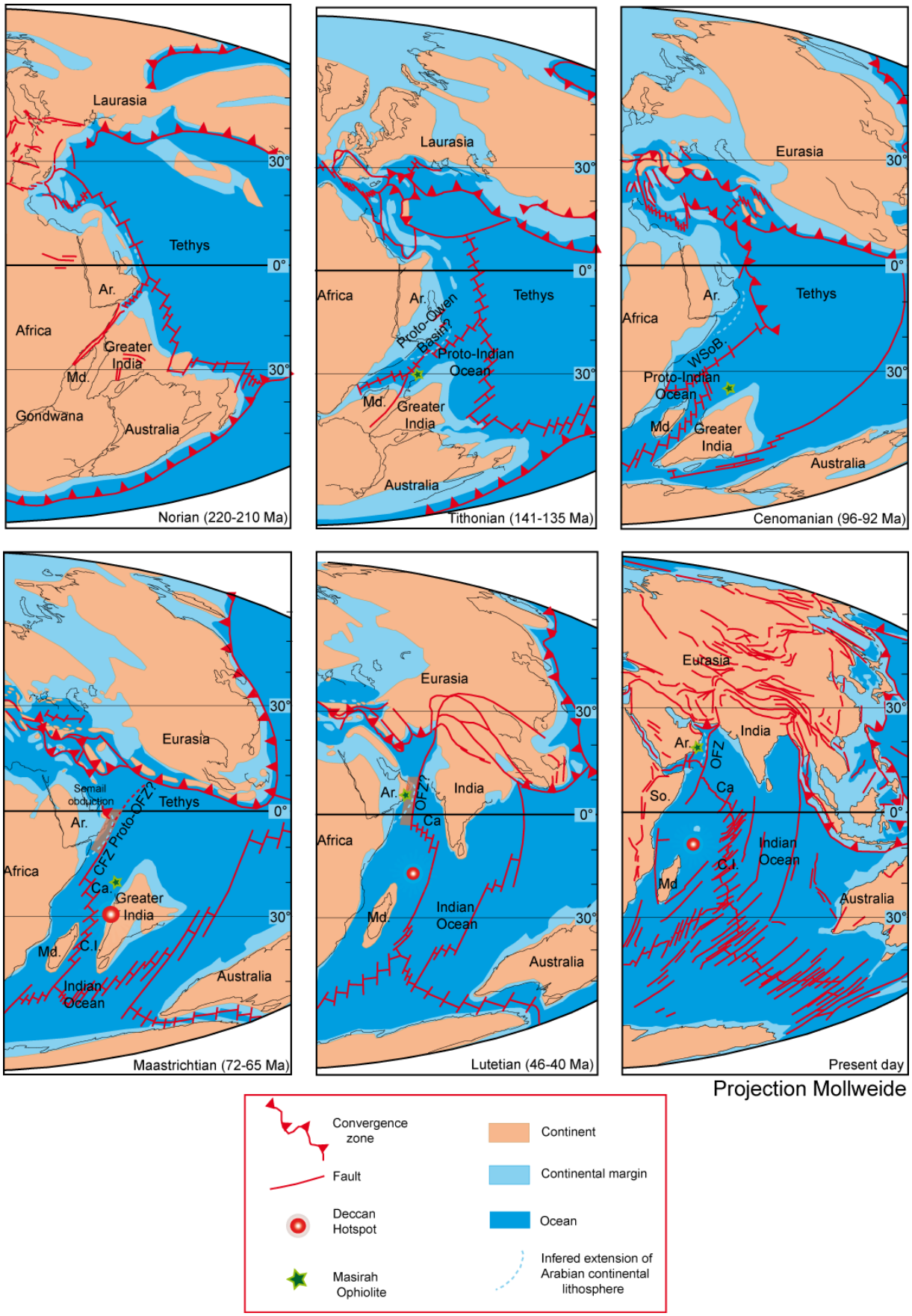


*Figure 16 : Reconstitution des principales étapes de l'ouverture de l'Océan Indien et de son évolution tectonique, modifié d'après Vrielynck, 2003.*

### *2.2. Localisation de la frontière de plaque avant le Miocène : apports de la cinématique*

La structure de la dorsale de Carlsberg et l'enregistrement des anomalies magnétiques sont d'une grande complexité entre 20 et 40 Ma, et rendent difficiles toute reconstitution pour cette période (*Mercuriev et al., 1996*). Au delà, les anomalies magnétiques 27 à 21 ont été identifiées et ont servi de base à des reconstitutions cinématiques (*Royer et al., 2002*). Les amplitudes des anomalies magnétiques mesurées dans le Bassin d'Owen suggèrent une nature océanique de la croûte, mais aucune de ces anomalies n'a pu être identifiée clairement et reliée à la charte magnéto-stratigraphique (*Whitmarsh, 1979*) ; faisant de l'âge de la croûte du Bassin d'Owen une nouvelle inconnue.

Ces reconstitutions cinématiques restent cependant difficiles à contraindre du fait de la rareté des zones de fracture dans la mer d'Arabie. Seules les zones de fracture de Chain, de Rudra et d'Owen sont clairement identifiées. A cela s'ajoutent quelques linéations dans la gravimétrie, indiquant des zones de fractures enfouies sous les sédiments. La direction des zones de fracture a changé au cours du temps, en réponse aux réorganisations de plaques successives subies par l'océan Indien, et au développement de paléo-propagateurs au niveau de la dorsale (Chaubey et al., 2002). Il n'y a pas d'anomalie magnétique clairement identifiée dans le bassin Nord Somalien délimité à l'Est par la ZF Chain, ce qui empêche de connaître le décalage absorbé par cette zone de fracture. La zone de fracture conjuguée de la ZF Chain n'est pas clairement identifiée dans la mer d'Arabie. La candidate la plus évidente paraît être la *ZFO (Whitmarsh, 1979)*. Cependant, l'orientation de la conjuguée de la ZF Chain déduite par *Royer et al. (2002) ;* Figure 17) en refermant le golfe d'Aden est oblique au bassin d'Owen, longe la marge omanaise et passe près du système de faille du Jebel Ja'alan et de Qalaht dans le NE de l'Oman (Figure 17). La conjuguée de la ZF Chain n'a jamais été observée dans le Bassin d'Owen, mais elle constitue une bonne candidate au titre d'ancienne limite de plaque Inde-Arabie anté-miocène.

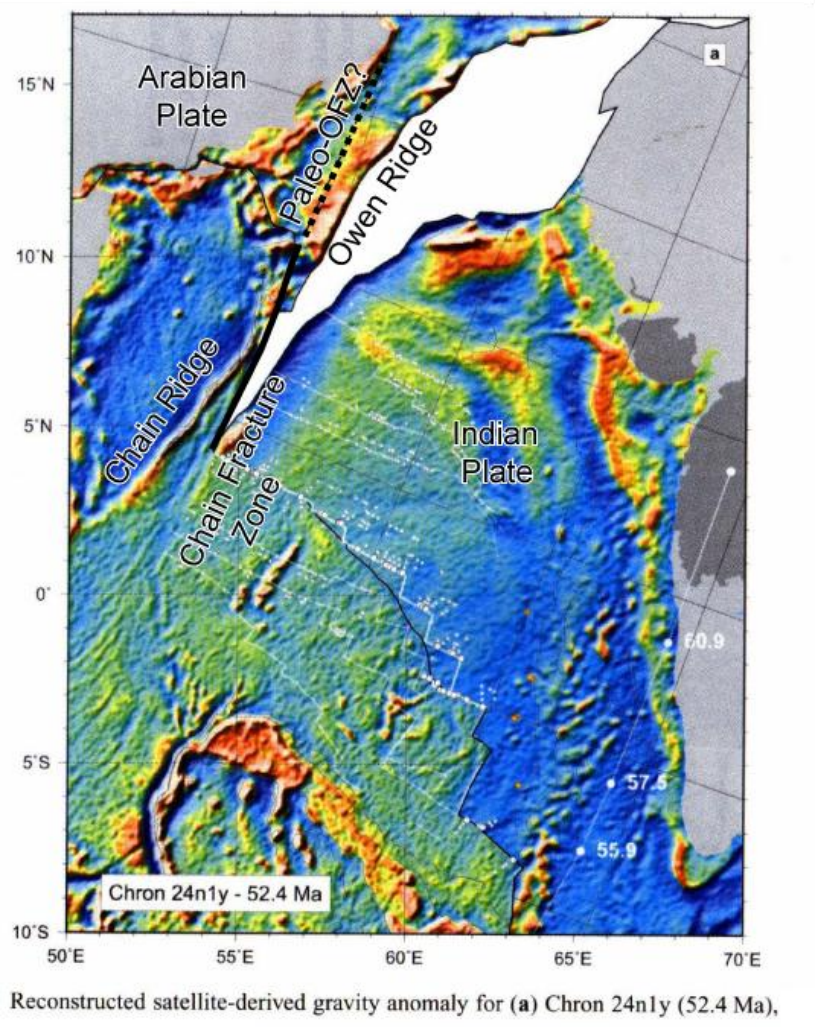


Reconstructed satellite-derived gravity anomaly for (a) Chron 24n1y (52.4 Ma),

*Figure 17 : Reconstitutions paléogéographiques de la mer d'Arabie, modifié d'après Royer et al. (2002) pour les chrons 24n1y (52.4 Ma) et 23n1y (50.8 Ma). En pointillé, la position supposée de la conjuguée de la Zone de Fracture de Chain, possible limite de plaque entre l'Inde et l'Arabie avant l'ouverture du golfe d'Aden.*

Les reconstitutions de *Royer et al. (2002)* montrent qu'il est impossible de considérer la géométrie actuelle des plaques Arabie et Indienne entre 60 et 20 Ma : combler le "vide" laissé dans les reconstitutions de *Royer et al. (2002)* impliquerait l'existence d'une zone de convergence ayant absorbé les 300 km de mouvement relatif au niveau de la Ride de Murray, ce qui n'est pas observé (Figure 18). Selon Royer et al. (2002), ceci implique un transfert d'un fragment de plaque indienne (accrétée par la dorsale de Carlsberg) à la plaque arabe autour de 20 Ma (Figure 18). Le substratum du bassin d'Owen actuel serait donc probablement d'origine mixte : la partie située à l'Ouest de la conjuguée de la Zone de Fracture de Chain est à relier à l'histoire de la plaque Arabe; la partie située à l'Est étant alors un fragment de plaque

Indienne transféré à la plaque Arabe au moment de la mise en place de la dorsale de Sheba. Cette hypothèse placerait la zone de convergence au niveau du Makran Pakistanais, et non au niveau de la Ride de Murray. De plus, les reconstitutions montrent que le plancher océanique formé à l'axe de la dorsale de Carlsberg est suffisamment vaste dès le chron 24 pour supporter les reliefs de la Ride d'Owen sur toute leur étendue, dont le substratum basaltique a été daté à la fin du Paléocène. Une origine du substratum de la Ride d'Owen sur les reliefs de la dorsale de Carlsberg (par exemple à l'aplomb d'une transformante) serait cohérent avec les taux de vésicules et de hyaloclastes mesurés sur les prélèvements DSDP du substratum, indiquant une lave émise à des profondeurs inférieures à 1000 m (*Whitmarsh et al., 1974*). L'hypothèse de Royer et al. (2002) est cohérente avec toutes les informations disponibles. Elle est nouvelle par rapport aux deux modèles préférentiellement discutés dans la littérature (*Whitmarsh, 1979; Mountain et Prell, 1990)*. Aucun de ces deux modèles ne peut aujourd'hui être considéré valide, en raison de nombreux faits géologiques découverts depuis leur formulation.

### *2.2.1. Le modèle de Whitmarsh (1979)*

*Whitmarsh (1979)* suggère que la limite de plaque Inde-Arabie est localisée au niveau de la ZFO actuelle depuis 90 Ma, date à laquelle l'Inde commence sa migration vers le Nord. Ce modèle fait de la ZFO la conjuguée de la Zone de Fracture de Chain. Dans ce cas, le substratum du bassin d'Owen serait d'âge Jurassique-début Crétacé et de nature océanique. (*Whitmarsh, 1979; Cochran, 1981, 1988; Stein et Cochran, 1985*) (Figure 19).

*Ce modèle n'est pas valide car, comme nous l'avons déjà montré, aucune structure associée à la ZFO n'est plus ancienne que 20 Ma, et la ZFO n'est pas la conjuguée de la Zone de Fracture de Chain. Cependant, elle ne peut être entièrement rejetée tant que des segments de la ZFO n'ont pas été imagés par sismique réflexion. Ces segments pourraient révéler des déformations plus anciennes que 20 Ma.*

### *2.2.2. Le modèle de Mountain et Prell (1990)*

Dans ce modèle, la limite de plaque est initialement localisée plus à l'Ouest à la fin du Crétacé, le long de la marge Est-Omanaise, pendant que la dorsale de Carlsberg se développe et que le bassin des Mascareignes s'ouvre. La limite de plaque subit un saut jusqu'à l'OFZ actuelle suite à l'ouverture du golfe d'Aden au début du Miocène. Entre le Crétacé supérieur et le début du Miocène, la limite de plaque Inde-Arabie est localisée soit au niveau de la marge Est-Omanaise, soit au niveau du bassin d'Owen. Dans ce cas, l'âge du substratum du bassin d'Owen est d'âge Crétacé supérieur-Paléocène et sa nature est océanique (Figure 19).

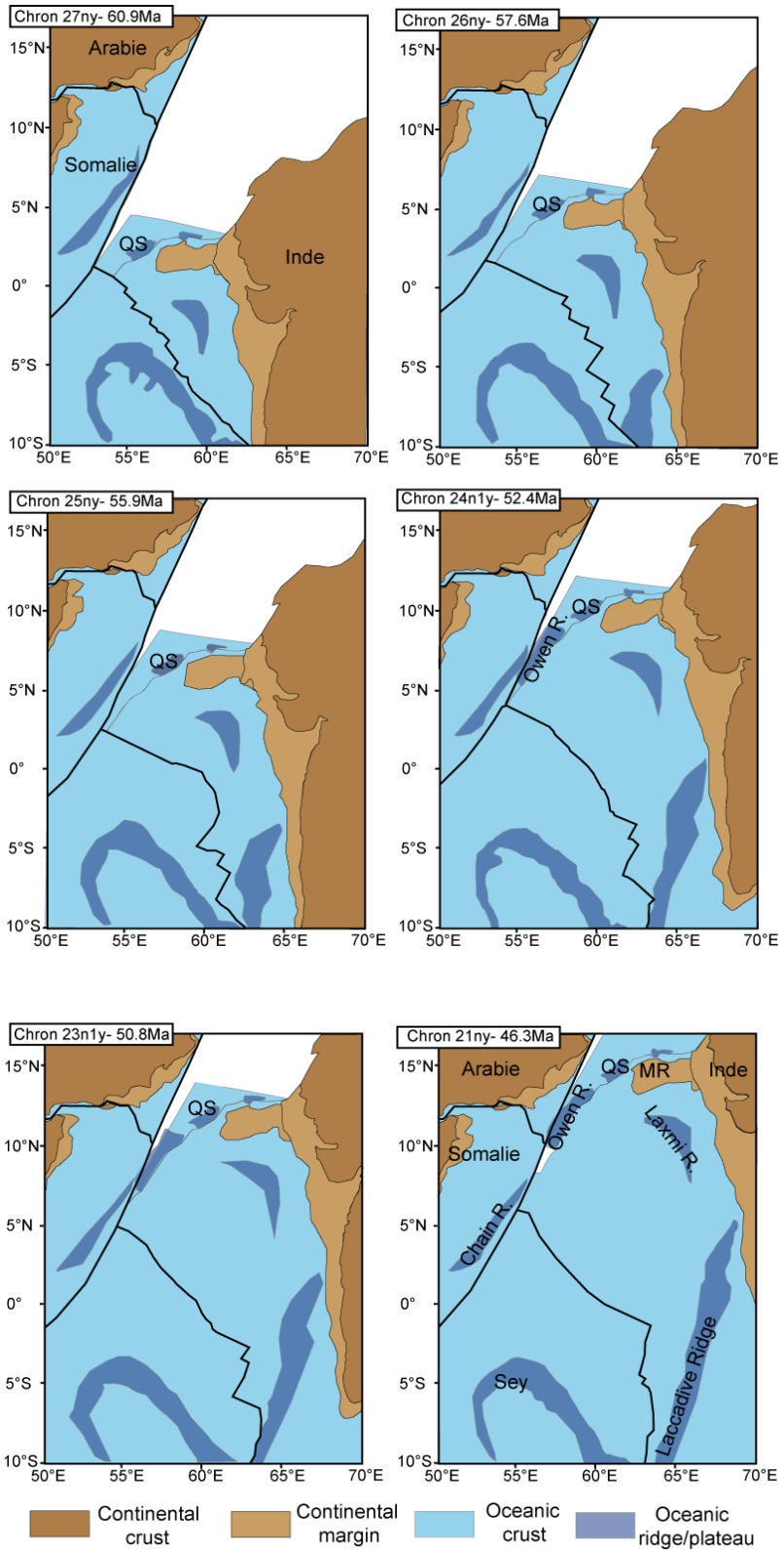


*Figure 18 : Reconstitutions paléogéographiques de la Mer d'Arabie en considérant que la conjuguée de la Zone de Fracture de Chain était la limite de plaque Inde-Arabie entre le Crétacé sup. et le début du Miocène. Modifié d'après Royer et al. (2002). QS : Qalhat Seamount ; Sey = Seychelles.*

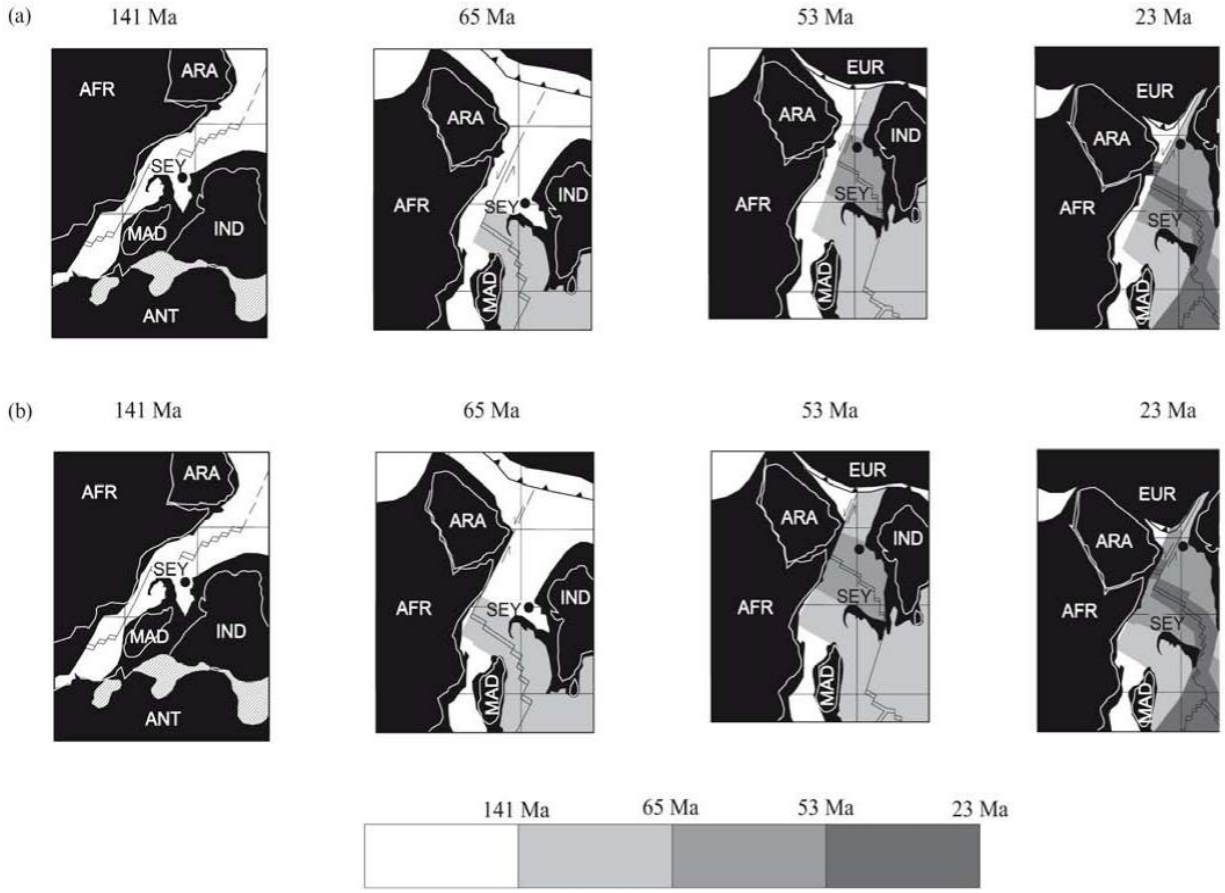


*Figure 19 : Reconstitutions paléogéographiques illustrant les deux principales hypothèses pour l'évolution tectonique de la mer d'Arabie (Edwards et al., 2000). En haut, le modèle de Whitmarsh (1979), selon lequel la frontière de plaque est localisée le long de la Zone de Fracture d'Owen depuis 90 Ma et le bassin d'Owen correspond à l'ancienne marge passive du continent Afrique-Arabie. En bas, le modèle de Mountain et Prell (1990) selon lequel la frontière de plaque saute de l'Est au début du Tertiaire depuis la marge continentale arabe jusqu'à la ZFO actuelle. La croûte du bassin d'Owen serait alors océanique et d'âge Tertiaire. Cela fait du bassin d'Owen une relique de la proto-dorsale de Carlsberg avant la formation de la dorsale de Sheba il y a 20 Ma. AFR : Plaque Afrique, ANT : Plaque Antarctique, ARA : Plaque Arabe, EUR : Plaque Eurasie Plate, IND : Plaque Indienne, MAD: Madagascar, SEY : Seycheles.*

*Mountain et Prell (1990)* proposent un âge Crétacé supérieur-Paléocène pour le bassin d'Owen, selon l'âge des sédiments les plus anciens forés au cours des Leg ODP et DSDP. Selon cette dernière interprétation, le plancher du bassin d'Owen serait de nature océanique et aurait été formé au large de la côte Sud-Est de l'Oman au niveau d'un centre d'accrétion NW-SE se terminant au niveau d'un grand couloir transformant structurant la marge Est-Omanaise sur toute sa longueur. *Mountain et Prell (1990)* postulent que c'est ce plancher d'âge fini Crétacé qui serait à l'origine des ophiolites de Masirah.

*Cependant, les travaux de paléomagnétisme de Gnos et Perrin (1997) et de Peters et Mercolli (1998), et la stratigraphie de la marge Est-Omanaise établie par Immenhauser et al. (1996) montrent que les ophiolites de Masirah sont le vestige d'un Proto-Océan Indien formé à la latitude de 40°S au Tithonien, ce qui invalide la reconstitution de Mountain et Prell (1990).*

La confrontation des modèles pré-existants et les reconstitutions cinématiques suggèrent de poursuivre nos recherches des frontières de plaque Inde-Arabie anté-Miocène à l'Ouest de la ZFO actuelle, selon les pistes suivantes :

***La marge Est-Omanaise :*** La structure de la marge Est-Omanaise est le résultat d'une histoire géologique complexe, fortement contrôlée par son héritage structural précambrien et les différentes phases d'extension qui se sont succédées du Permien à l'Actuel en réponse aux différentes phases d'ouverture de l'Océan Indien (Figure 20). La marge Est-Omanaise a également été affectée par deux phases compressives majeures, associées aux obductions des ophiolites du Semail et de Masirah (Figures 21, 22). Le mouvement relatif Inde-Arabie implique un mouvement décrochant important depuis 90 Ma. Existe-t-il des traces de ce mouvement décrochant sur la marge Est-Omanaise ? La littérature définit un accident décrochant majeur sur toute la marge Est-Omanaise, le couloir transformant de Masirah. Ce couloir comprend principalement le dôme du Huqf, les ophiolites de Masirah, ainsi que la région du Jebel Ja'alan et de la faille de Qalhat (Figure 3). Nous examinons en détail les structures décrochantes rattachées à ce système ainsi que l'âge de leurs différentes phases d'activité, afin de déterminer si ce couloir transformant est un bon candidat en tant qu'ancienne limite de plaque Inde-Arabie au Crétacé et au Tertiaire, comme proposé par *Mountain et Prell (1990)*. Il est de plus nécessaire de déterminer l'héritage structural de la

marge est-omanaise, susceptible d'avoir contrôlé la mise en place des limites de plaque Inde-Arabie successives.

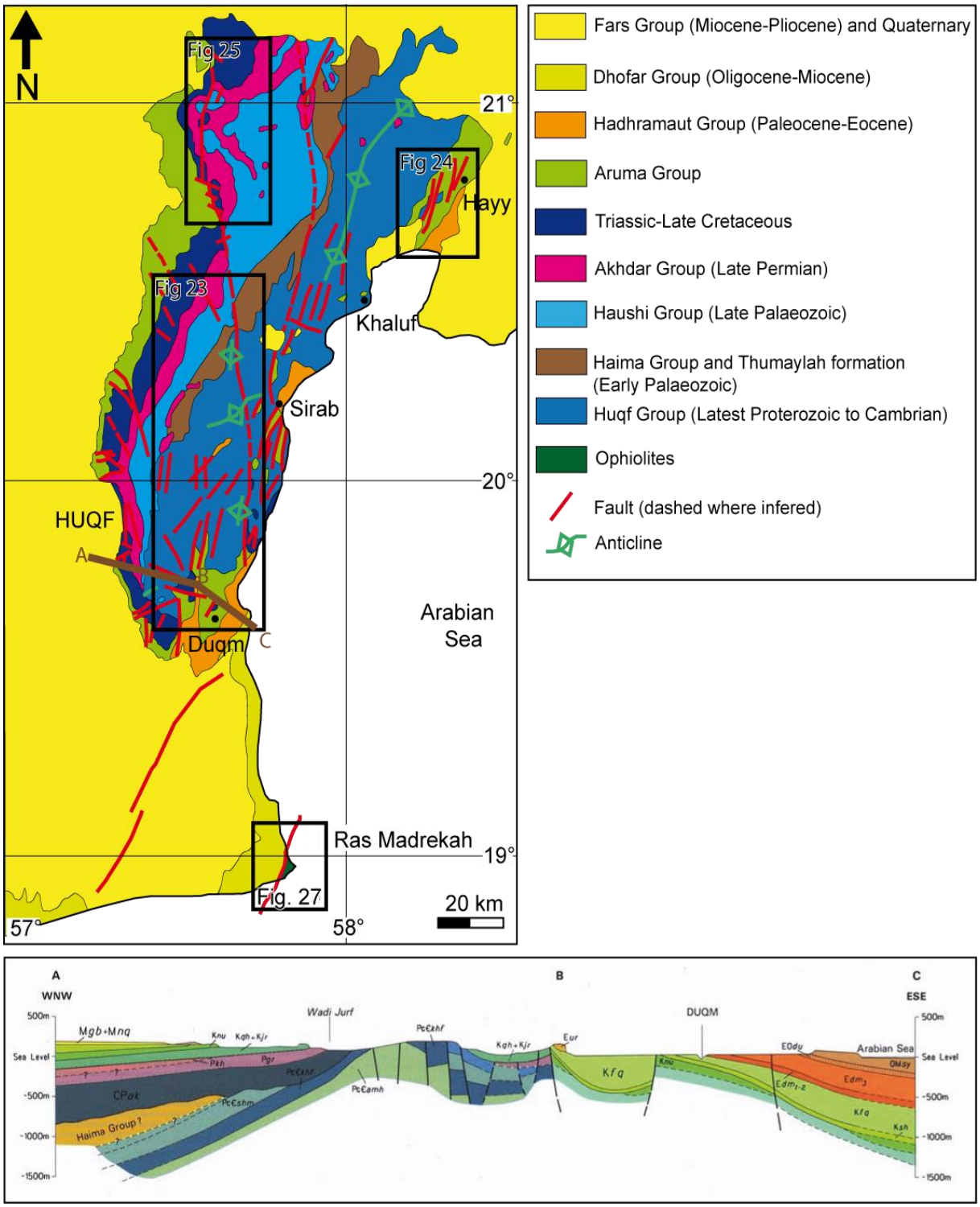


*Figure 20 : En Haut, schéma structural du Huqf, d'après la carte géologique du sultanat d'Oman au 1 : 1 000 000ème (Béchennec et al., 1993). Voir Figure 3 pour localisation. En bas, coupe géologique recoupant le Huqf (voir Figure ci-dessus pour la localisation (coupe*

*ABC)), d'après la carte au 1 : 250 000ème de Duqm et Madrekah (Platel et al., 1992). Le Huqf correspond à un système de horst et graben structuré au cours du Mésozoïque.*

***Les ophiolites de Masirah*** *:* La mise en place des ophiolites de Masirah marque l'un des évènements tectoniques majeurs de l'histoire de la marge est-omanaise, et implique que la frontière de plaque Inde-Arabie était en convergence à la fin du Crétacé (Figure 21). Certaines études affirment également que la structure des ophiolites de Masirah serait le vestige du jeu transformant du couloir de Masirah au Crétacé supérieur-Tertiaire (*Moseley et Abbotts, 1979; Abbotts, 1978; Shackelton et Ries, 1990; Smewing et al., 1991*). Si les ophiolites de Masirah se prolongent dans le Bassin d'Owen, alors cela signifie que le bassin est solidaire de la plaque Arabie depuis la mise en place des ophiolites. A contrario, l'absence d'ophiolites dans le Bassin d'Owen indiquerait la présence d'un ancien système décrochant, qui aurait déplacé les lambeaux de corps ophiolitique du bassin à des centaines de km du corps de Masirah. L'âge, l'origine, l'extension et la structure des ophiolites de Masirah sont donc des informations critiques pour localiser l'ancienne limite de plaque Inde-Arabie.

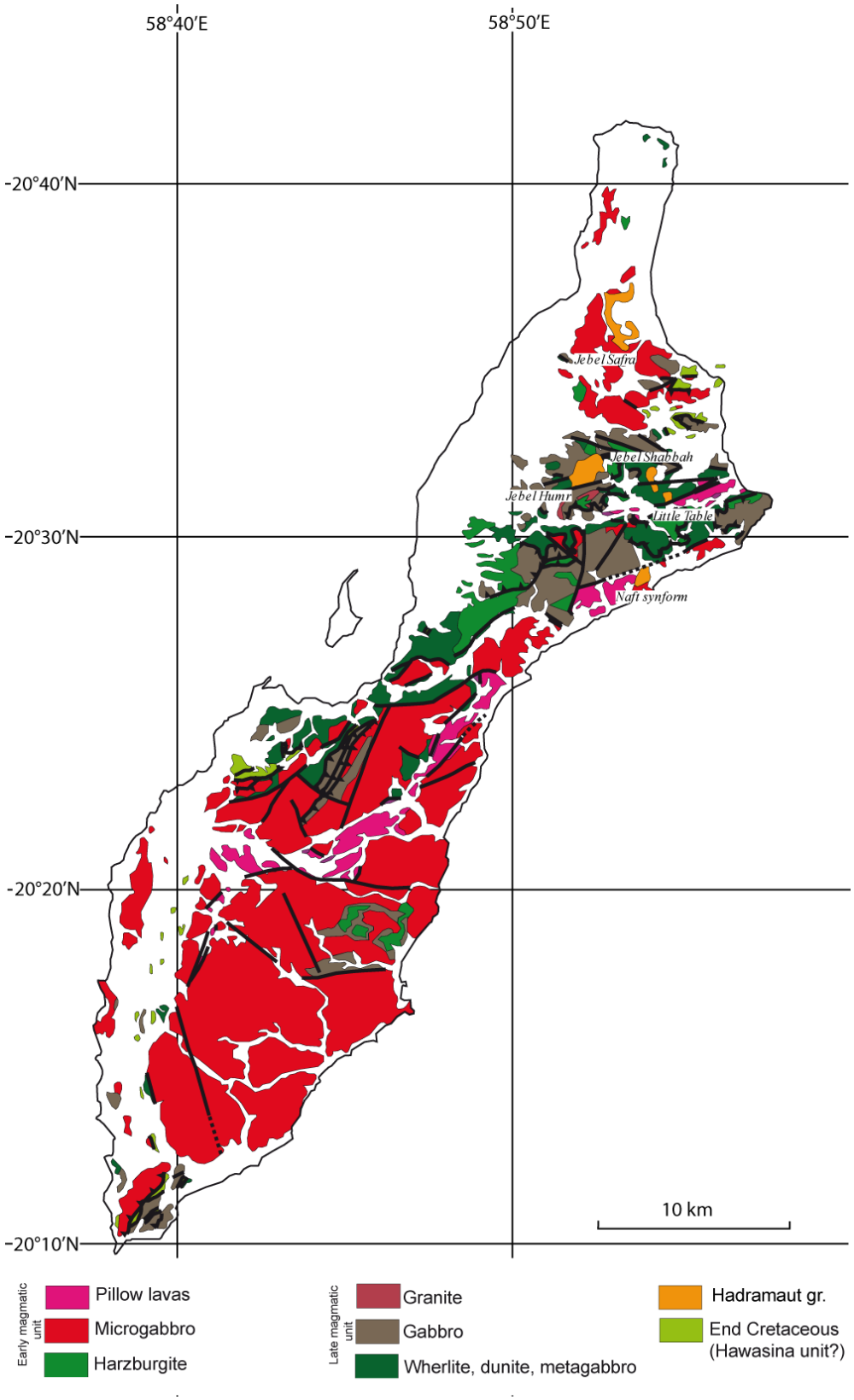


*Figure 21 : Schéma structural de l'île de Masirah (d'après LeMétour et al., 1992)*

***Le bassin d'Owen*** *:* Le bassin d'Owen est certainement l'élément le moins connu de l'histoire de la marge Est-Omanaise, comme en témoigne la confrontation des modèles de *Whitmarsh (1979)* et de *Mountain et Prell (1990),* qui prédisent des âges différents pour ce bassin. L'âge du substratum est inconnu, et sa nature discutée en dépit de la présence d'anomalies magnétiques (Figure 22). A partir des rares données disponibles dans la bibliographie, et des reconstitutions paléogéographiques, nous discutons de la présence potentielle des anciennes limites de plaque Inde-Arabie dans ce secteur (Figure 22). La stratigraphie de la marge est-omanaise est également susceptible d'avoir enregistré des évènements tectoniques potentiellement associés à la création du bassin d'Owen. Une question sous-jacente à la recherche des anciennes limites de plaque Inde-Arabie est de savoir si celles-ci étaient localisées, comme la ZFO actuelle, ou diffuses.

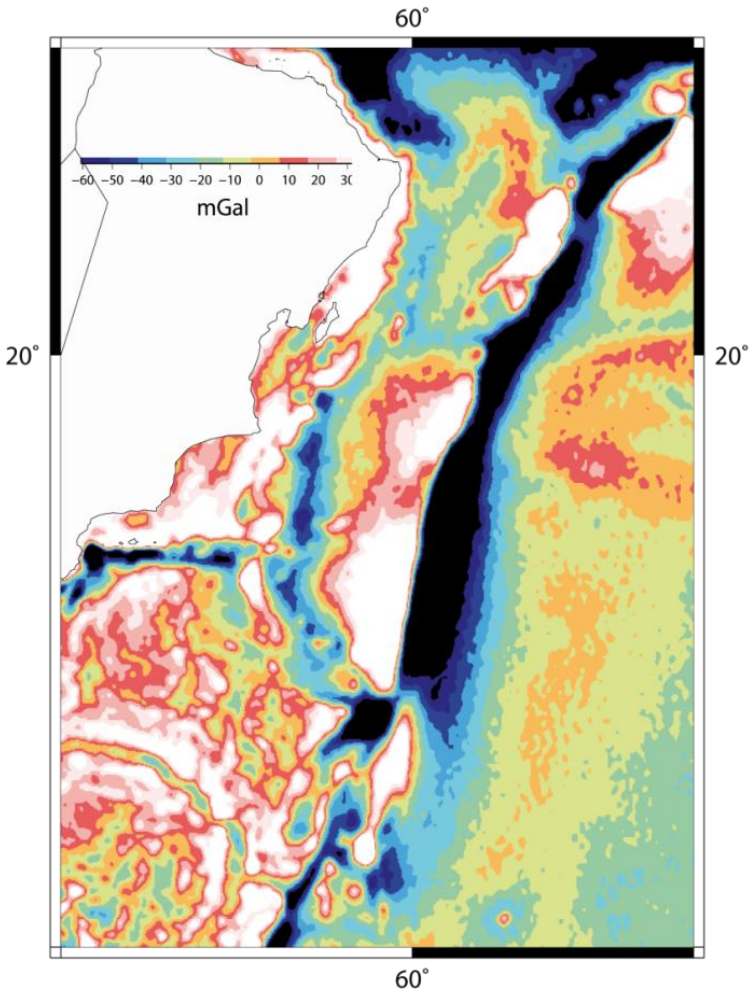


*Figure 22 a : Carte des anomalies à l'air libre du Bassin d'Owen (Delescluse, pers.com.). Les fortes anomalies négatives au niveau de l'OFZ actuelle traduisent l'effet flexural de la lithosphère indienne aux abords de l'OFZ (Weissel et al., 1992). Aucun linéament particulier, indicateur d'une potentielle limite de plaque fossile, n'est révélé dans le bassin d'Owen.*

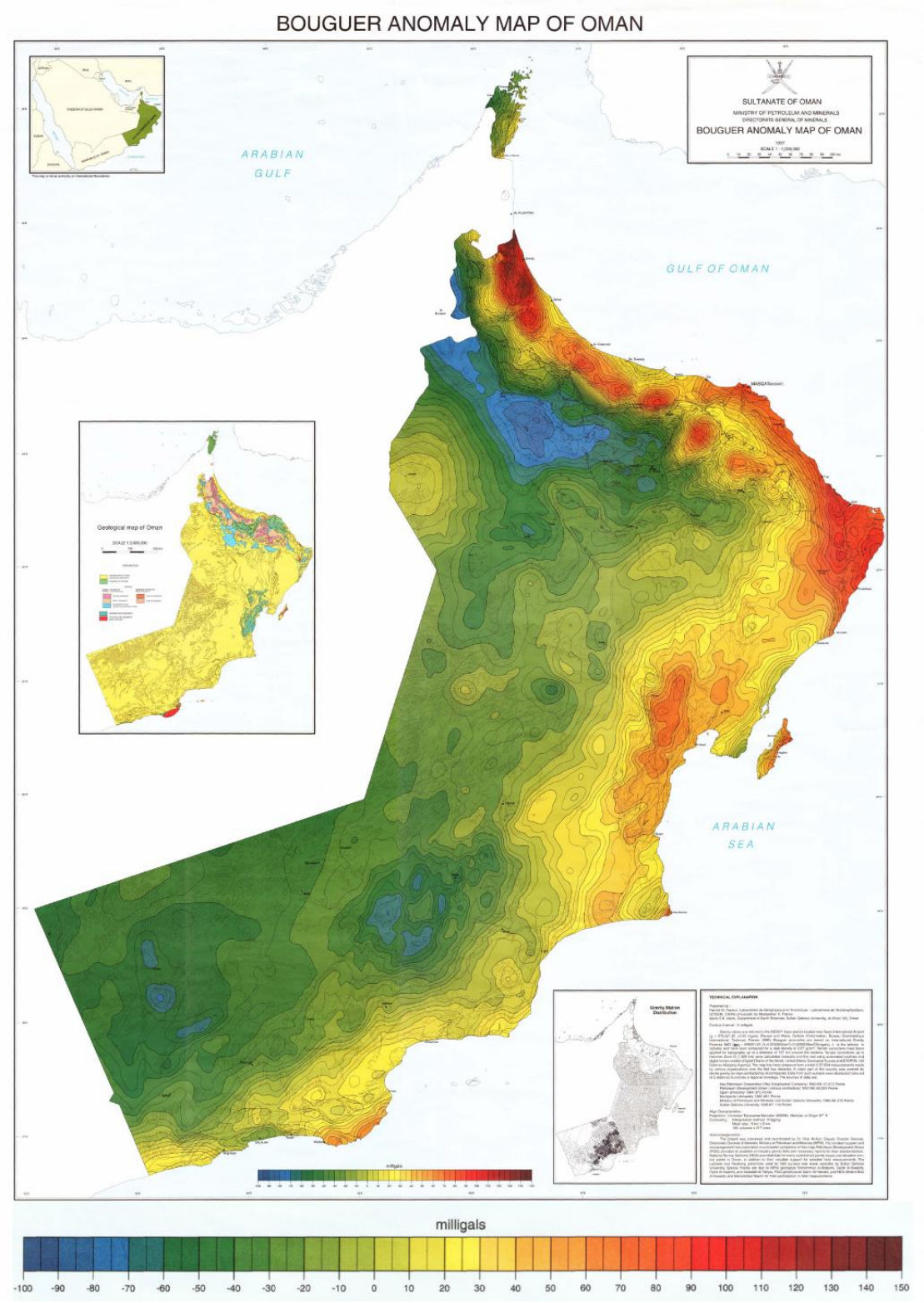


*Figure 22 b : Carte des anomalies de Bouguer de l'Oman. La marge est caractérisée par une forte anomalie positive, qui correspond aux corps protérozoïques. Les lambeaux d'ophiolites (Semail & Masirah) sont aussi marqués par une anomalie positive.*

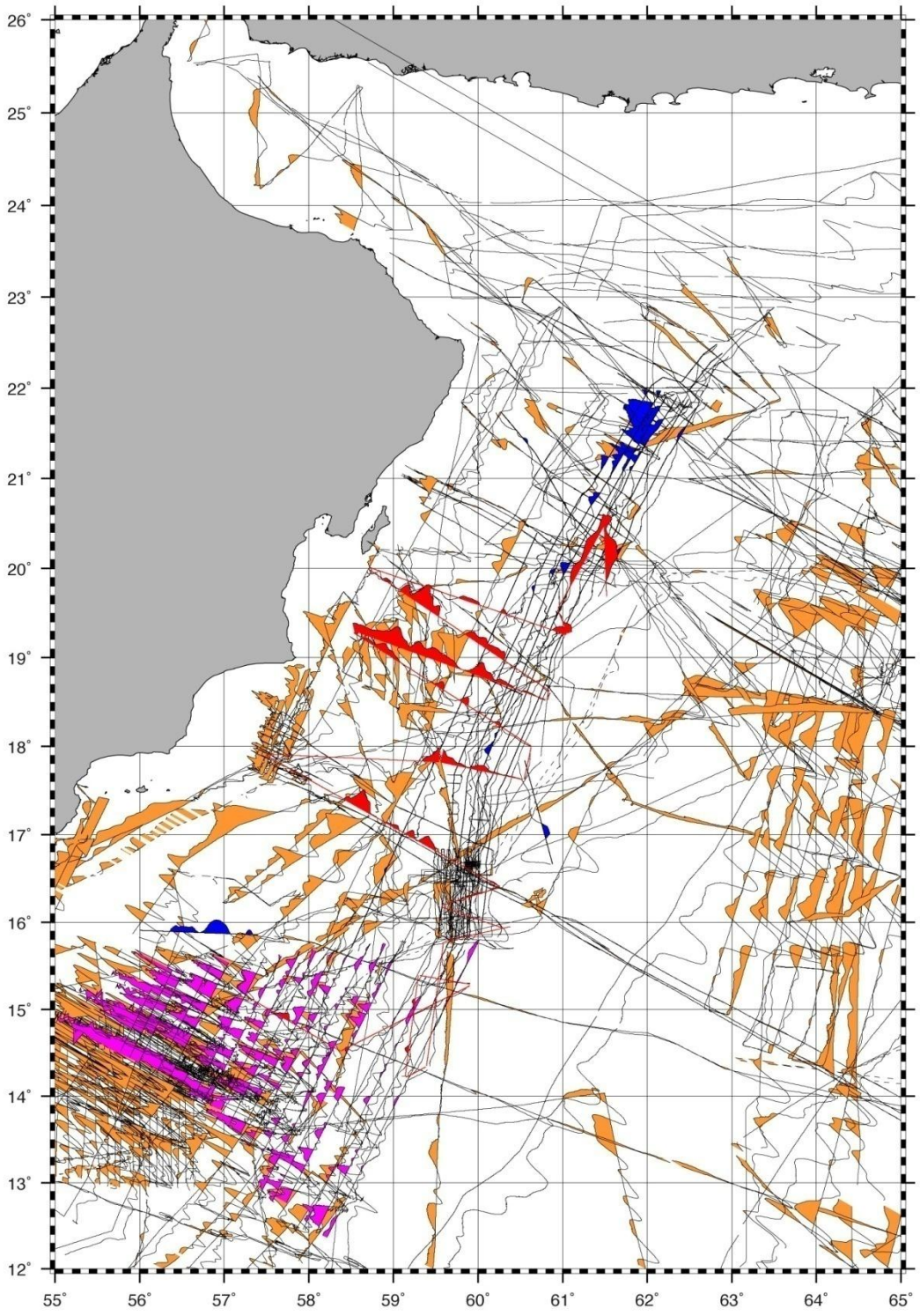


*Figure 22c : Compilation des mesures du champ magnétique dans la région du Bassin d'Owen (Fournier, com. pers.). Le bassin d'Owen est riche en anomalies magnétiques, ce qui indique une nature océanique. Il demeure toutefois difficile d'identifier les anomalies dans ce bassin.*

## *3. A la recherche des frontières de plaque Inde-Arabie anté-Miocène*

### *3.1. Les décrochements du Huqf*

Plusieurs structures identifiées sur la marge est-omanaise constituent les vestiges d'une ou plusieurs phases d'activité décrochante. Cependant, la répartition éparse des séries sédimentaires mésozoïques et cénozoïques sur le Huqf (Figure 23) ne fournit pas l'enregistrement nécessaire pour dater de façon précise l'activité de l'ensemble des décrochements identifiés dans la région. Il faut néanmoins composer avec cette lacune importante, et se contenter des observations sur les structures suivantes :

- *Le système de failles de Saiwan-Nafun*, orienté N-S, dont l'origine remonte au Paléozoïque (Figures 23, 24, 25; *Shackeleton and Ries, 1990*). Cette déformation distribuée produit localement des décalages de l'ordre du kilomètre. La quantité de mouvement total absorbée par l'ensemble de ces structures est indéterminée (*Ries et al., 1984).*

- *Le système de failles de Jebel Ja'alan / Qalhat* : situé au nord-est de l'Oman, ce système comporte l'unique décalage important (plusieurs dizaines de km) observé : le socle paléozoïque affleurant au niveau du Jebel Ja'alan est retrouvé plus au Nord, près de la ville de Qalhat. Le décalage entre ces deux portions de socle impliquerait un mouvement décrochant d'environ 40 km, bien que ce dernier soit difficile à expliquer avec la cartographie (Figure 26 ; *Filbrandt et al., 1990*). L'âge du décalage observé au niveau de Qalhat est inconnu.

Deux phases d'activité de ces décrochements sont déterminées :

La première phase est globalement d'âge Santonien-Campanien (*Ries et al., 1984*) et concerne le système de faille de Saiwan-Nafun. La deuxième phase est d'âge Oligo-Miocène, et réactive le système de Saiwan-Nafun : les plis de Khufai, Shuram et Anquau y sont décalés de façon sénestre à l'Oligo-Miocène, suite à une seconde réactivation du système de faille (Figure 23) (*Salel et Breton, pers.com.*). Les mêmes décalages sénestres ont été observés dans la région de Mahatta Humaid, à l'est du Huqf (*Pilcher et al., 1996*). Des études microtectoniques réalisées sur les formations tertiaires de Shuwayr et Warak discordantes sur les ophiolites de Ras Madrekah montrent, quant à elles, l'existence de jeux décrochants dextres (*Fournier et al., 2004*), probablement liés à une inversion du mouvement relatif Inde-Arabie vers l'Oligocène (de façon contemporaine au rifting d'Aden).

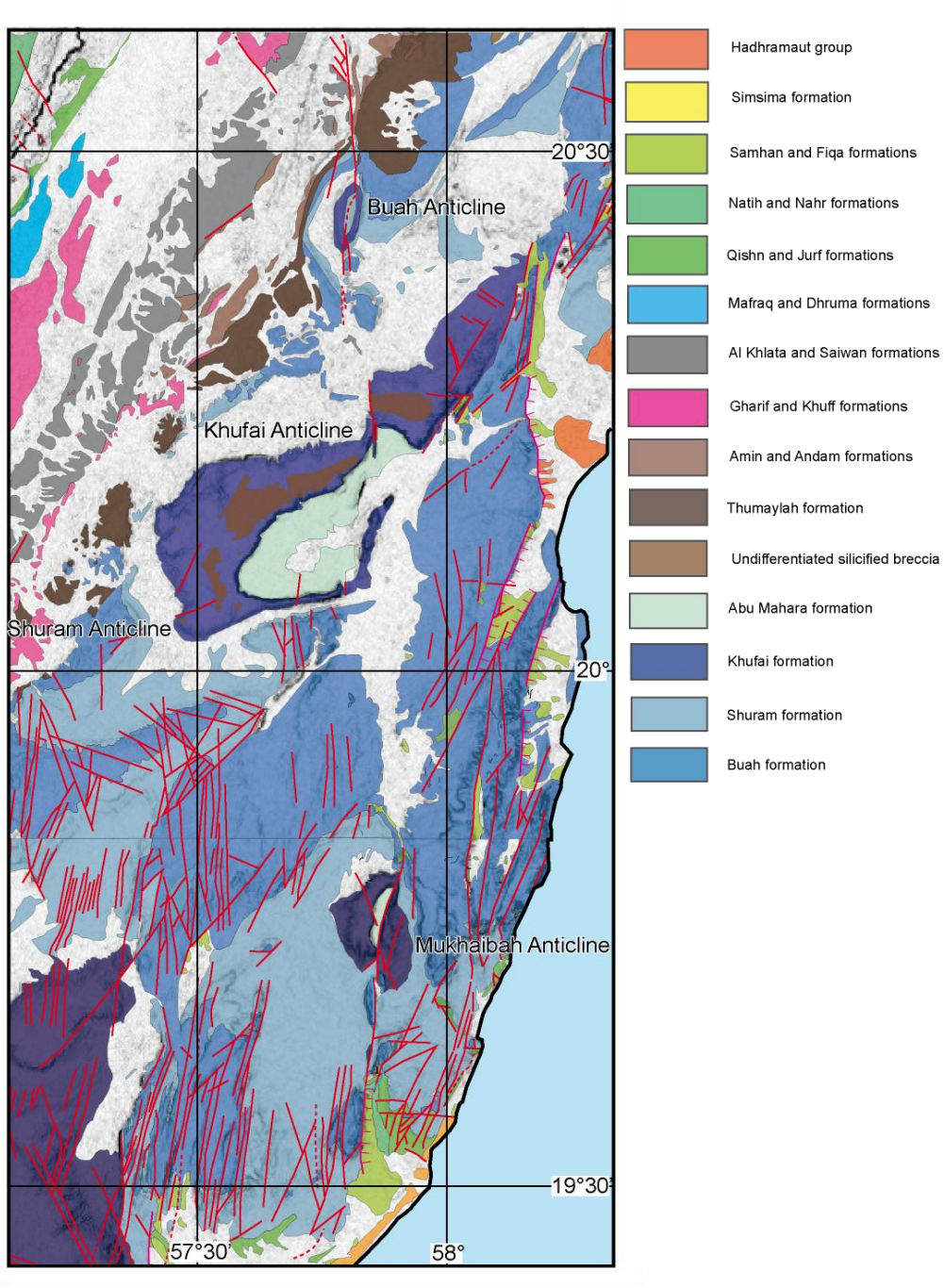


*Figure 23 : Schéma structural du système décrochant de Haushi-Nafun (au centre du Huqf) plaqué sur la topographie SRTM 3 sec. (d'après les cartes géologiques au 1 : 250 000ème de Duqm et Madreka et de Khalouf, Platel et al., 1992). Les plis précambriens de Buah, de Mukhaibah, et de Khufai sont décalés de façon sénestre par un réseau de failles verticales orientées N-S. Les décalages mesurés sont de l'ordre du kilomètre. L'activité du système décrochant est daté du Santonien au Campanien, principalement (Shakleton et Ries, 1990). La quantité totale de déplacement accommodée par ce système décrochant distribué est inconnue. Voir Figure 20 pour localisation.*

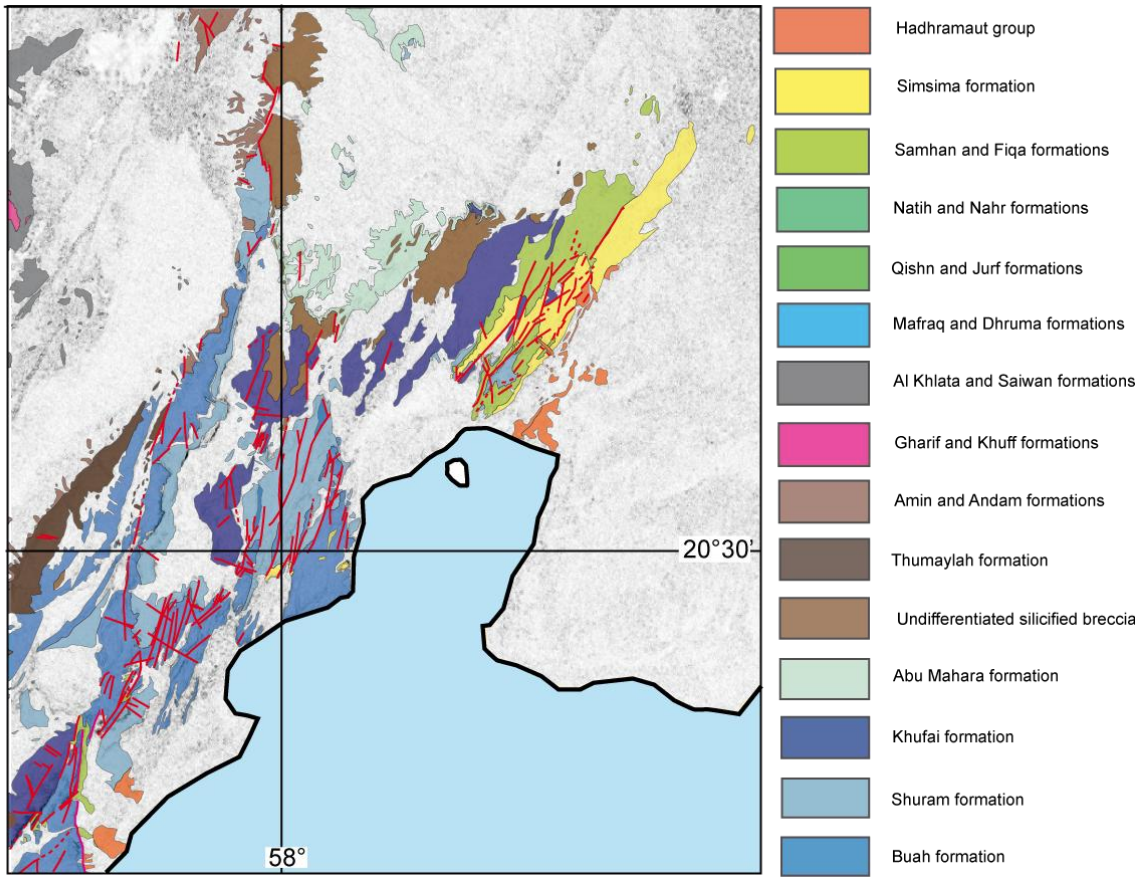


*Figure 24 : Schéma structural du système décrochant du dôme de Haushi (au NW du Huqf) plaqué sur la topographie SRTM 3 sec. (d'après la carte géologique au 1 : 250 000ème de Khalouf, Platel et al., 1992). Les décalages mesurés sont de l'ordre du kilomètre. L'activité du système décrochant est daté du Santonien au Campanien, principalement (Shakleton et Ries, 1990). Voir Figure 20 pour localisation.*

- *La transformante de Masirah* : Le front de chevauchement des ophiolites de Masirah est décrit comme ayant un pendage très abrupt (*Schreurs et Immenhauser, 1999*). Ceci pourrait suggérer qu'à l'origine, cette faille devait être une faille transformante (*Schreurs et Immenhauser, 1999*). *Schakleton et Ries (1990)* proposent qu'il s'agit de la faille transformante majeure entre l'Inde et l'Arabie dans les premiers stades de leur mouvement relatif (vers 90 Ma), et qu'elle aurait été remobilisée lors de l'obduction des ophiolites de Masirah. Cependant, ce n'est pas parce que le pendage de la faille est important qu'il s'agit d'un décrochement. Cette faille dont la localisation est ailleurs déduite de l'alignement des ophiolites sur la marge Est-Omanaise, est en grande partie sous-marine.

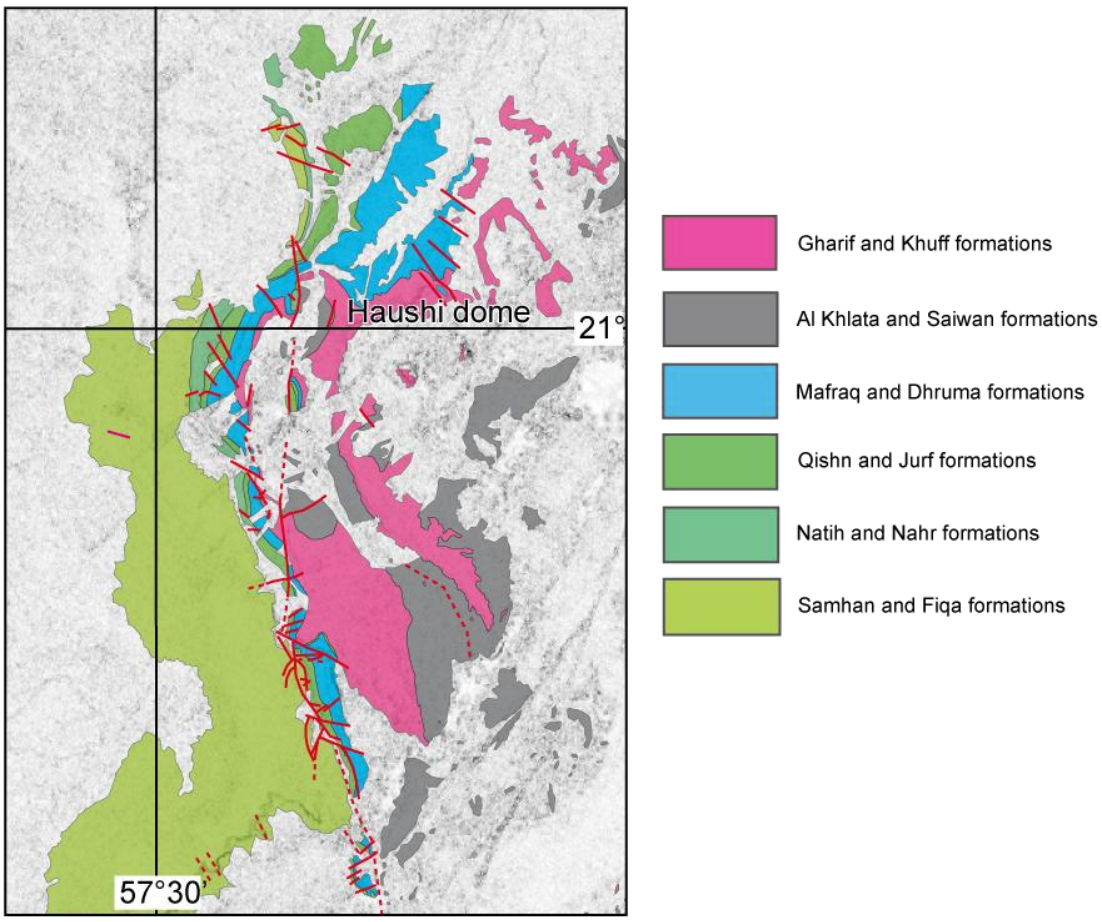


*Figure 25 : Schéma structural du système décrochant du Huqf NE plaqué sur la topographie SRTM 3 sec. (d'après la carte géologique au 1 : 250 000ème de Khalouf, Platel et al., 1992). Voir Figure20 pour localisation.*

De fait, la quantité de mouvement décrochant accommodé par cette faille n'est pas estimée. Une faille décrochante dextre observée sur le terrain au niveau de Ras Madrekah pourrait correspondre à cette transformante (les stries sur le miroir de la faille indiquent irréfutablement un mouvement décrochant ; Figure 27). *Loosveld et al. (1996)* positionnent cette faille de Masirah plus au large, au niveau de la bordure de la plate-forme Omanaise. Il semblerait que cela s'appuie sur les résultats des études en mer exposés par *Mountain et Prell (1990)* : les profils sismiques enregistrés lors du Leg ODP 117 au large de Ras Sharbitat (dans la baie de Siquirah) révèlent par endroits, selon *Mountain et Prell (1990)* des structures en fleur négatives recoupant la couverture sédimentaire tertiaire (Figure 28).

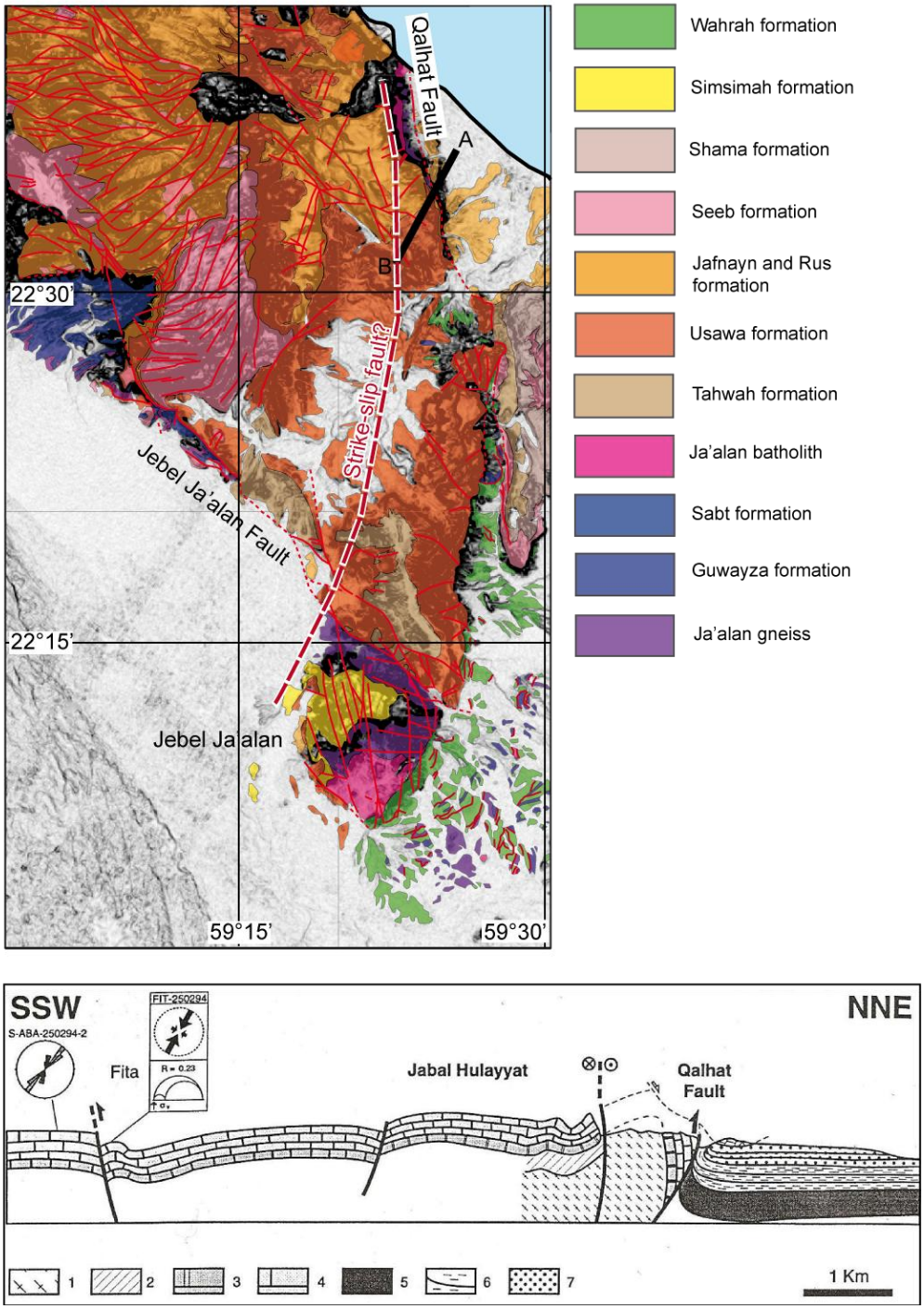


*Figure 26 : Schéma structural du secteur de la faille de Qalhat et du Jebel Ja'alan (haut) et coupe schématique entre Fita et la faille de Qalhat (bas) (d'après Carbon, 1996). Légende de la coupe : 1 : socle cristallin, 2 : Hawasina, 3 : sédiments post-nappe d'âge Fini-Crétacé, 4 : calcaires marneux éocène des formations de Jafnayn et de Abat, 5 : formation de Thawah (Oligocène à Aquitanien), 6 : formation de Sur (Miocène Moyen), 7 : formation de Salmiyah (Miocène supérieur). Voir Figure 3 pour localisation.*

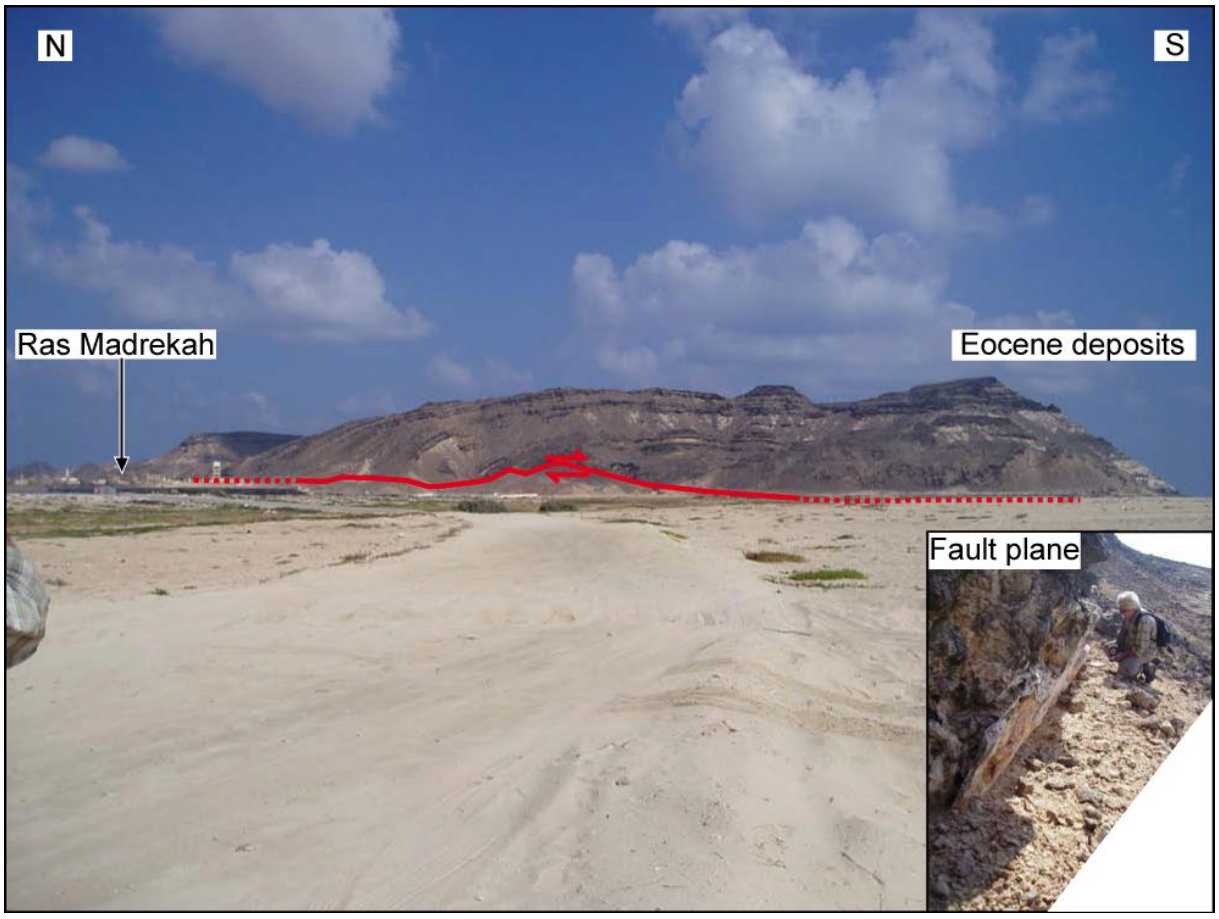


*Figure 27 : Photographies de la faille décrochante dextre bordant les formations éocènes de Ras Madrekah. L'encart montre le plan de faille. Il pourrait s'agir d'une réactivation tertiaire de la faille de Masirah. Voir Figure 20 pour localisation.*

En fait de structures en fleurs, il s'agit clairement de canyons turbiditiques comblés par des dépôts contouritiques, qui, du fait de l'exagération verticale importante de la sismique réflexion, apparaissent comme des failles (nous sommes revenus sur cette région au cours de la campagne OWEN 2 pour confirmer cette interprétation). Il n'y a donc pas de traces de déformation décrochante connue à ce jour sur le plateau continental de la marge Est-Omanaise.

### *3.2. Les ophiolites de Masirah*

Ces ophiolites affleurent dans les localités de Ras Madrekah, de Jib'sch et sur l'île de Masirah (Figure 3). L'étendue sous-marine de ces ophiolites (au niveau de la plate-forme et du bassin d'Owen) est inconnue. Parmi ces localités, les ophiolites de l'île de Masirah sont les plus étudiées (Figure 21). L'île de Masirah s'étend sur ~ 700 km². Ces ophiolites sont de type harzburgitique, comme celles du Semail dans le Nord de l'Oman. La séquence ophiolitique de

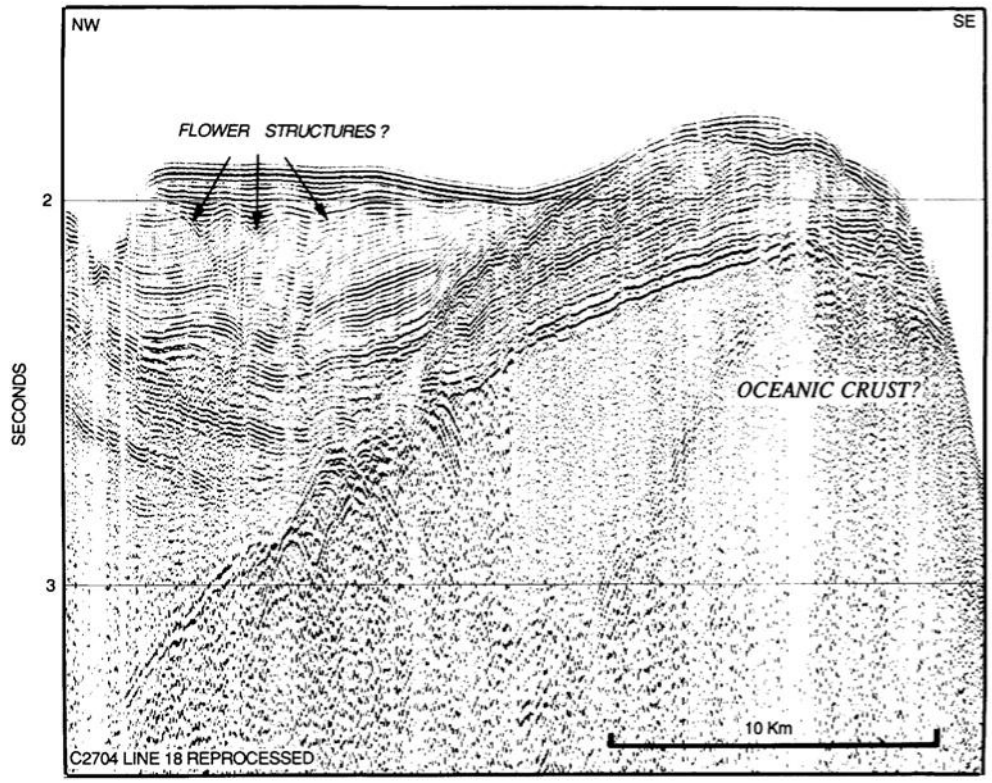


*Figure 28 : Profil sismique montrant des structures en fleur dans la couverture sédimentaire de la marge Est-Omanaise selon Mountain et Prell, (1990), indiquant un possible mouvement décrochant au Tertiaire. Il s'agit en fait de canyons turbiditiques fossiles.*

Masirah est composée par, de la base au sommet : des harzburgites, des gabbros à olivine avec intrusions de wehrlites et de dunites à plagioclase ; puis des gabbros foliés, avec intrusions de dykes, et enfin des sédiments. Représentant une série océanique épaisse de 2 km seulement, elles sont entaillées et segmentées par un réseau de failles complexes (Figure 21). La faible épaisseur de ces ophiolites, paradoxale pour des ophiolites de type HOT, suggère que nous avons ici la croûte ayant résisté à l'écaillage, et non la série complète. Elles représentent par ailleurs un objet d'intérêt pour les pétrographes, car elles permettent d'étudier la mise en place d'une série ophiolitique complète extrêmement mince *(Peters et Mercolli, 1998)*. Les ophiolites de Masirah ont longtemps été considérées sur la base de la ressemblance de leur séquence (de type HOT) comme un diverticule des ophiolites du Semail, décalé de ces dernières par un accident dextre (*Morton, 1959; Moseley, 1969; Stoneley, 1974*), faisant d'elles un vestige de la Néo-Téthys. L'étude de l'âge de l'obduction de Masirah et de l'origine du plancher océanique qui la compose montre toutefois une réalité différente.

L'âge de l'obduction est principalement établi selon des critères stratigraphiques. De façon générale, les déformations maastrichtiennes enregistrées dans la plaine du Batain, et la

discordance des formations calcaires éocènes sur les ophiolites de Masirah, l'âge Coniacien-Santonien de la formation de Fayah, permettent d'estimer l'âge de l'obduction entre le Maastrichtien et le Paléocène supérieur. Une surface d'érosion majeure, potentiellement associée à l'obduction Masirah, est identifiée dans les formations maastrichtiennes sur l'ensemble de l'Oman : elle aurait érodé jusqu'à 200 m de sédiments dans le Nord de l'Oman (formation de Simsima) (*Nolan et al., 1990*). L'obduction Masirah serait responsable de la phase de compression "laramide" reportée dans les notices des cartes géologiques (*Roger et al., 1991; Rabu et al., 1993*).

Les datations radiochronologiques et les mesures des anomalies paléomagnétiques réalisées sur les ophiolites de Masirah permettent d'affirmer que la croûte océanique qui les compose a été formée au Tithonien, à la latitude de 40°S (*Peters et Mercolli, 1998*). Les ophiolites de Masirah correspondent donc clairement à un proto-océan Indien, alors que les ophiolites du Semail correspondent à l'océan Téthysien.

L'âge de l'obduction Masirah à la limite Crétacé-Paléocène est clairement différent de l'obduction du Semail, à 85-90 Ma. Les ophiolites de Masirah ne sont donc pas la preuve de l'existence d'un système de faille dextre qui les relierait aux ophiolites du Semail… et ne sont donc pas la preuve d'une ancienne limite de plaque décrochante d'âge Crétacé.

**L'île de Masirah**

La structure de l'île de Masirah est complexe et controversée. Des portions d'ophiolites de séquence différente sont en contact abrupt par endroits, et l'île dans son ensemble est intensément fracturée. De fait, les ophiolites de Masirah ont longtemps été considérées comme un mélange résultant du jeu des failles d'un grand système décrochant, le couloir de Masirah (*Mosely et Abbotts, 1979; Abbotts, 1981; Shackelton et Ries, 1990; Smewing et al., 1991*). Cependant, plusieurs coupes géologiques réalisées par l'équipe responsable de la cartographie au 1:50.000ème (Peters et al. 1995) montrent des basaltes en coussins, ou encore des radiolarites, surmontés par des harzburgites. Il y aurait donc sur l'île des endroits où la superposition de deux nappes ophiolitiques serait observée. Dans ces zones de contact, des traces de déformation ductile et cassante ont été observées. Ces traces sont réparties selon des bandes étroites sub-horizontales. Les directions des linéations principales ont été mesurées (*Marquer et al., 1995*) et semblent en accord avec un chevauchement intra-océanique vers le

Nord (toutefois les linéations observées dans les péridotites peuvent correspondre à la foliation lors de l'accrétion océanique). L'existence de deux nappes ophiolitiques mises en contact par un chevauchement impliquerait un chevauchement intra-océanique initiant l'obduction du corps de Masirah. *Peters et Mercolli (1998)* proposent que la mise en place de ce chevauchement serait contemporaine de la formation de la dorsale de Carlsberg et du volcanisme du Deccan, et de la rotation de l'Inde qui s'en suivit (*Royer et al., 1992*). Il est cependant impossible de démontrer l'étendue régionale d'un tel chevauchement simplement à partir de l'étude de l'île de Masirah. Ce chevauchement peut très bien être un accident local mis en place au cours de l'obduction. De plus, ce chevauchement est difficilement identifiable en de nombreux endroits où il a été cartographié par les auteurs de la carte au 1:50 000ème. Par exemple, la formation sédimentaire de Fayah (turbiditique, âge Coniacien-Santonien) est décrite sur l'île de Masirah par *Marquer et al. (1995)* et *Immenhauser (1996)* comme comprise entre les deux nappes ophiolitiques et scellant la nappe inférieure : elle serait antérieure au chevauchement intra-océanique proposé par ces auteurs, et profondément déformée par l'obduction. Cependant, nos observations réalisées sur le terrain montrent que la formation de Fayah n'est pas chevauchée par une nappe ophiolitique, et aucune déformation n'est observée dans cette formation. Ainsi, si l'existence des deux nappes ophiolitiques d'épaisseur et de séquence différentes semble démontrée par les analyses pétrologiques et géochimiques de *Peters et Mercolli (1998)*, la nature du contact tectonique entre ces nappes (faille décrochante, ou chevauchement, voire détachement (core complex?)) mérite d'être clarifiée par une étude des conditions de fabrique des minéraux situés dans le plan de contact entre les deux séquences d'ophiolite.

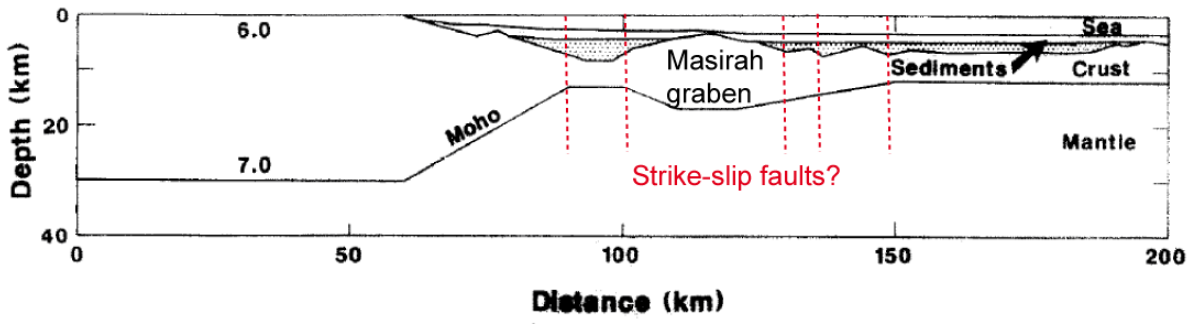


*Figure 29 : Structure crustale du Bassin d'Owen d'après l'interprétation des données OBS de Barton et al. (1990). La croûte du bassin d'Owen s'amincit vers l'Est jusqu'à atteindre une épaisseur de 6 km. Les blocs identifiés à l'Ouest pourraient être le résultat du jeu décrochant d'anciennes limites de plaque Inde- Arabie. Les irrégularités du substratum du bassin d'Owen pourraient aussi être liées aux ophiolites de Masirah.*

## *3.3. Le bassin d'Owen et les anciennes limites de plaque Inde-Arabie*

### *3.3.1. Description générale du Bassin d'Owen*

Actuellement, le bassin d'Owen s'étend de la marge Est-Omanaise jusqu'à la Ride d'Owen sans présenter d'obstacle topographique majeur. Il est délimité au sud par la Ride de Sharbitat, un alignement de monts sous-marins qui le sépare de la croûte océanique formée par la dorsale de Sheba (Figure 2). La marge transformante Est-Omanaise présente une pente continentale abrupte et étroite (entre 10 et 40 km de large). La pente moyenne de la marge est comprise entre 4 et 6°. Les données recueillies lors du Leg ODP 117 révèlent que la plate-forme continentale de la marge Est-Omanaise est recouverte par une faible épaisseur de sédiments (marge maigre ; *Mountain et Prell, 1990*). Localement, des bassins atteignant 1 km d'épaisseur sont formés par des structures interprétées comme des blocs basculés de la marge (*Barton et al., 1990 ;* Figure 29).

### ***3.3.2. Nature et structure du substratum du bassin d'Owen***

Les interprétations des vitesses des ondes sismiques (enregistrées à bord du RSS Charles Darwin en 1986) ne permettent pas de discriminer entre un substratum de nature océanique (mis en place par un ancien centre d'accrétion), un substratum de nature ophiolitique (mis en place par obduction, dans le prolongement du corps de l'île de Masirah), et un substratum de nature continentale (*Barton et al., 1990 ;* Figure 29). La sismique réfraction révèle que la structure du bassin au large de la plate-forme, enfouie sous les sédiments, est plus accidentée. A environ 30 km au large de la côte, un premier bassin sédimentaire profond (Bassin de Masirah ; *Minshull et al., 1992*) repose sur une croûte continentale très amincie (5 km). Il est séparé d'un second bassin, qui se prolonge jusqu'à la Ride d'Owen, par une structure interprétée en blocs basculés (Ride de Masirah). La croûte, épaisse de 14 km à l'aplomb du bloc principal de la Ride de Masirah, s'amincit progressivement vers l'Est, pour atteindre l'épaisseur de 6 km à 40 km à l'Ouest de la Ride d'Owen (*Barton et al., 1990*). Une telle diminution d'épaisseur suggère la présence d'une croûte océanique à l'aplomb de la Ride d'Owen, tout comme le montrent les basaltes recueillis dans les forages ODP sur la Ride d'Owen.

La marge Est-Omanaise a été forée au cours du Leg ODP 117, mais le substratum n'a pas été atteint. Comme proposé par *Peters et Mercolli (1997*), les nappes ophiolitiques émergées au niveau de l'île de Masirah, peu épaisses (2 km au maximum), pourraient reposer sur de la croûte continentale extrêmement amincie. Cela supposerait un bassin d'Owen

solidaire de la plaque Arabie depuis l'obduction Masirah. Cependant, aucune anomalie gravimétrique caractéristique d'un corps ophiolitique n'est observée sur le bassin d'Owen... comment distinguer sur la gravimétrie un corps ophiolitique de 2km d'épaisseur maximale si le substratum du bassin est océanique?

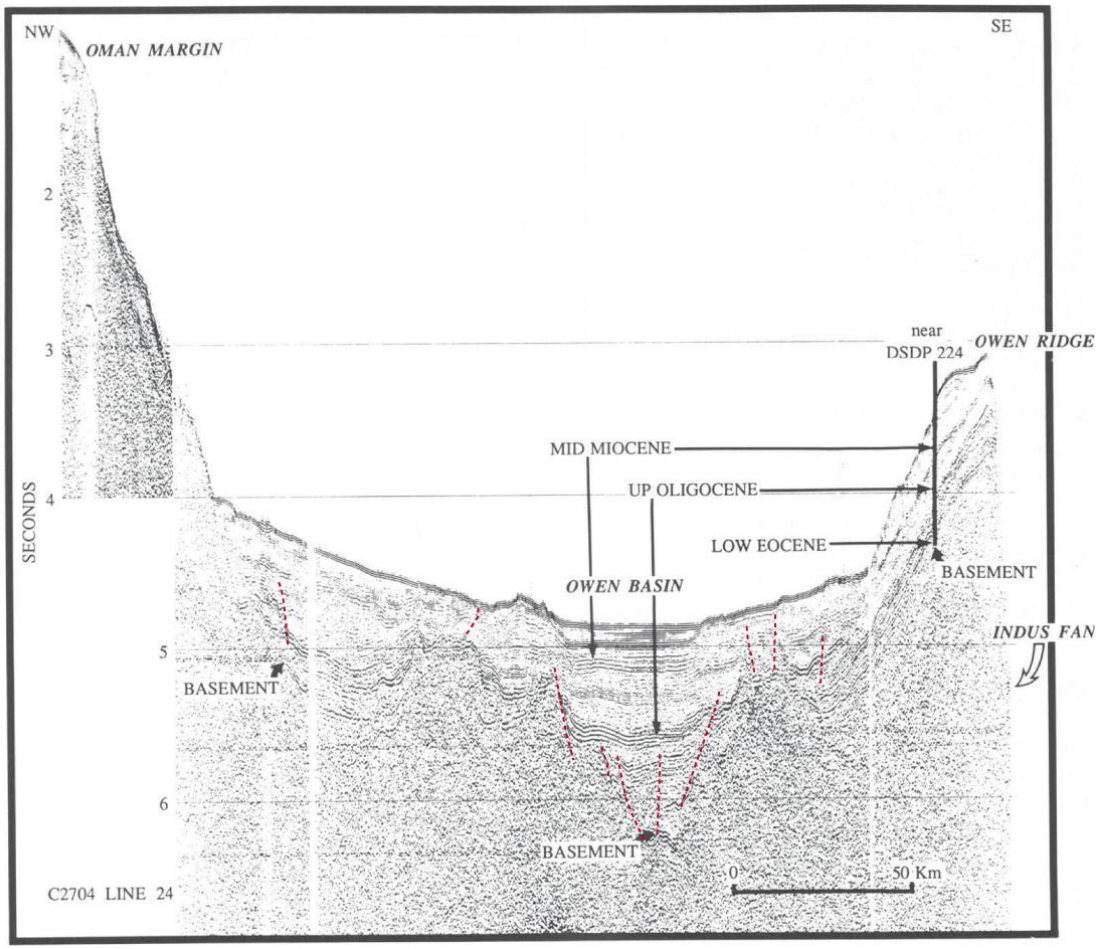


*Figure 30 : Profil sismique transverse au bassin d'Owen (Mountain et Prell, 1990). La couverture sédimentaire a une épaisseur de l'ordre de 2 km. La structure du socle, à l'Est du Bassin, est probablement le résultat d'une activité tectonique liée à d'anciennes limites de plaque Inde-Arabie. Cette activité tectonique n'est pas retrouvée au Nord sur le profil de la Figure 10.*

Un argument décisif repose dans l'étude des anomalies magnétiques du bassin d'Owen (Figure 22) : si les quelques anomalies mesurées n'ont pas été identifiées, leur distribution au sein du bassin et leur intensité suggèrent fortement une nature océanique du substratum. Les directions des anomalies magnétiques mesurées lors des campagnes DSDP et ODP sont compatibles avec les directions des anomalies des premiers stades d'accrétion de la dorsale de Carlsberg (Chron 25 – 26), ce qui confirmerait l'hypothèse inspirée de *Royer et al. (2002)* d'un transfert de plaque Inde à la plaque Arabie. La couverture des anomalies magnétiques du Bassin d'Owen reste cependant à densifier pour autoriser la validation de cette hypothèse.

### *3.3.3. Âge du Bassin d'Owen*

L'âge du Bassin d'Owen demeure inconnu. Certes, les plus anciens sédiments ont été forés et leur âge estimé au Paléocène. Cependant, les forages ODP et DSDP sont localisés sur la Ride d'Owen ou sur ses flancs, c'est-à-dire à des endroits où le substratum du bassin est surélevé. Il peut donc y avoir des sédiments plus vieux que le Paléocène dans les régions plus profondes du Bassin d'Owen. Il peut aussi s'agir de sédiments recouvrant les ophiolites de Masirah, et non le substratum original du bassin. L'histoire du Bassin d'Owen a été un premier temps déduite d'après une comparaison avec le Bassin Ouest-Somalien (*Whitmarsh, 1979*), où de la croûte océanique est formée dans le Bassin Somalien entre l'anomalie M25 (153 Ma ; *Rabinowitz et al., 1983*) ou M22 (150 Ma ; *Ségoufin et Patriat, 1980)* et M0 (120 Ma). Si le substratum du Bassin d'Owen est effectivement d'âge Crétacé (*Whitmarsh, 1979*), l'absence d'anomalie magnétique clairement identifiée dans ce dernier peut s'expliquer par la période de calme entre 80 et 110 Ma, au cours de laquelle aucune inversion n'eut lieu (mais aussi par une couverture insuffisante des anomalies magnétiques du Bassin d'Owen !). Cependant, le profil sismique transverse au Bassin d'Owen présenté par *Mountain et Prell (1990)* montre que l'épaisseur de la couverture sédimentaire du Bassin d'Owen n'est que de 2 km au maximum, là où celle du Bassin de Somalie atteint 8 km, ce qui suggère une histoire plus ancienne que le Bassin d'Owen. Le substratum du Bassin d'Owen est aussi beaucoup moins profond que celui du Bassin de Somalie. Le Bassin d'Owen semble donc avoir eu une histoire différente de celle du bassin somalien, et ne peut être considéré comme son conjugué. En revanche, le bassin Nord-Somalien n'a jamais été étudié avec les moyens modernes de la géophysique, et pourrait être le conjugué du Bassin d'Owen.

L'enregistrement stratigraphique de la marge est-omanaise met en évidence plusieurs phases extensives qui pourraient être associées à la formation du Bassin d'Owen, ou du moins à une phase de son évolution.

- Une première phase, d'âge fini-jurassique/début Crétacé, correspond à l'ouverture océanique entre les blocs Gondwana Est et Ouest. L'ouverture océanique aurait généré un recul de la ligne de rivage sur plus de 250 km, enregistré par une discordance sur le Huqf. Ces évènements sont enregistrés dans les formations sédimentaires de la plaine du Batain et du bassin de l'Hawasina (Figure 3 ; *Immenhauser et al., 2000 et références inclues*).

- Une seconde phase, d'âge Crétacé supérieur et correspondant à l'activité du graben de Masirah, probablement contemporaine de la phase d'extension campanienne à maastrichtienne enregistrée au niveau du Jebel Ja'alan à terre (*Filbrandt et al., 1990; Beauchamp et al., 1995*), ou d'une phase antérieure.

***Le graben de Masirah***

*Le graben de Masirah s'étend sur la totalité de la marge Est-Omanaise, du Ras Madrekah au Ras al'Hadd, et constitue la structure majeure de la marge (Figure 3). Sa trace est révélée par la gravimétrie (Figure 22). Sa bordure Ouest est délimitée par le Huqf. Sa frontière Est est marquée par le front de chevauchement des ophiolites de Masirah, et, au Nord, par celui des ophiolites du Semail. Les données de sismique réflexion disponibles, couplées à celles des forages industriels, montrent l'existence d'un graben sous les ophiolites (Beauchamp et al., 1995). Le graben de Masirah serait une structure héritée de la séparation de la Pangée et de l'ouverture de l'Océan Indien (Beauchamp et al., 1995). Sa formation a été contrôlée par l'héritage structural du Huqf (Figure 20). La plaine du Batain, qui s'étend sur 4000 km$^2$ au Nord Est du graben de Masirah, au Sud ouest de la ville de Sur, face aux nappes de l'Hawasina, au front Sud des montagnes du Semail. est en partie comblée par les dépôts liés à l'érosion des montagnes du Semail. La série sédimentaire complexe du Batain a été déformée dans sa totalité pendant l'obduction de Masirah sur environ deux kilomètres d'épaisseur (Schreurs et Immenhauser, 1999). Sous les ophiolites, la sismique révèle une structure en bloc basculé -interprétée comme le graben de Masirah- recouverte par une série sédimentaire de 4 km d'épaisseur, peu déformée, provenant de l'érosion du Huqf (Beauchamp et al., 1995). Une grande partie de l'histoire extensive de la marge Est-Omanaise est donc probablement enfouie sous les ophiolites.*

### *3.3.4. Les évènements tectoniques susceptibles d'avoir affecté le Bassin d'Owen*

La convergence entre les plaques Arabie, Inde et l'Eurasie est responsable des grands réarrangements tectoniques de la mer d'Arabie et de l'océan Indien au Tertiaire *(Patriat et al.,*

*2008)*, dont la (les) migration(s) de la limite de plaque Inde-Arabie (Figure 19) fait (font) probablement partie. Un examen des évènements tectoniques enregistrés à terre sur la marge Est-Omanaise permet d'identifier les évènements ayant potentiellement affecté l'histoire du Bassin d'Owen depuis le Paléocène.

Tout d'abord, le rifting du golfe d'Aden à l'Oligocène (dont l'initiation remonte possiblement jusqu'à 35 Ma) a généré une déformation extensive sur l'ensemble de la plaque Arabe, identifiée jusque dans les formations sédimentaires des montagnes du Nord de l'Oman (*Fournier et al., 2004, 2006*). Cette extension est responsable des failles normales tertiaires qui segmentent les ophiolites de Masirah, et de la réactivation du graben de Masirah. Les études microtectoniques de *Fournier et al. (2004)* montrent également l'influence d'une compression néogène N-S dans les sédiments de l'Est de l'Oman, qui correspond probablement à la déformation en champ lointain liée à la formation du Zagros et au rajeunissement des reliefs du Nord de l'Oman (Semail). D'autres études ont mis en évidence une série de déformations compressives, orientées E-W à NNW-SSE, d'âge Oligocène (*Filbrandt et al., 1990; Carbon, 1996; Schreus and Immenhauser, 1999; Fournier et al., 2004)*. Les traces à terre de compression Oligocène pourraient être reliées à la surrection de la Ride d'Owen il y a 20 Ma et au dernier épisode de relocalisation de la limite de plaque Inde-Arabie.

### *3.3.5. Quelles traces de structures décrochantes dans le Bassin d'Owen ?*

L'ensemble de ces évènements ont-ils laissé une trace dans la structure du bassin d'Owen ? Les variations abruptes d'épaisseur de la croûte mises en évidences par *Barton et al. (1990)* sont interprétées comme le résultat du jeu d'un réseau de grands décrochements crustaux, qui auraient favorisé la juxtaposition de blocs dont l'épaisseur et l'état de compensation isostatique diffèrent (Figure 29). S'agit-il là des véritables vestiges des anciennes limites de plaque Inde-Arabie que nous recherchons ? Seul un profil sismique transverse au Bassin d'Owen est disponible dans la bibliographie (*Mountain et Prell, 1990*) (Figure 30). Certaines déformations pourraient être assimilables à des structures en fleur, mais la faible qualité du profil, son importante exagération verticale (x 30) et le manque de données complémentaires empêchent de pousser plus loin nos interprétations.

### *4. Synthèse : reconstitution de l'histoire géologique de la marge Est-Omanaise du Crétacé au Miocène*

Dans ce chapitre, nous récapitulons, à la lumière des informations disponibles dans la bibliographie, les grandes interrogations liées à chaque étape de cette histoire, qui guideront l'exploitation des données des campagnes OWEN 1 & 2 dans la suite de cette thèse. Un résumé de l'histoire de l'Océan Indien est présenté en Figure 31, afin d'aider à l'intégration de l'histoire de la marge Est-Omanaise dans son contexte global.

*Au Crétacé supérieur*

Avant l'obduction Masirah, la marge est structurée par une série de blocs basculés hérités de phases d'extension au Mésozoïque. Les décalages kilométriques observés sur la marge Est-Omanaise sont certes les témoins d'une activité tectonique, mais sont-ils suffisants pour définir une limite de plaque? Les décalages mesurés sont -au maximum- de l'ordre de quelques kilomètres seulement, ce qui semble incohérent avec un mouvement de l'ampleur de la migration de l'Inde depuis 90 Ma. A moins de considérer un système distribué, ou relocalisé au cours du temps (on fait bien de la ZFO actuelle une limite de plaque avec 12 km de rejet seulement (*Fournier et al., 2008*)). Il se peut que la trace principale de la limite de plaque Inde - Arabie au Crétacé ait été localisée au niveau du front de chevauchement des ophiolites de Masirah, mais qu'elle soit aujourd'hui difficilement identifiable en raison de sa remobilisation lors de l'obduction Masirah. Il est également impossible d'estimer la quantité de mouvement et pendant combien de temps ce système de faille décrochant a été actif.

*A la limite K/T*

L'obduction des ophiolites de Masirah est contemporaine de la formation de la dorsale de Carlsberg et de la mise en place de l'activité du point chaud du Deccan. L'étendue sous-marine des ophiolites de Masirah sur l'ensemble du Bassin d'Owen est inconnue. Aussi l'interprétation de la topographie du substratum du Bassin d'Owen est difficile : les irrégularités sont-elles formées par les ophiolites ?

Ou sont-elles liées aux blocs basculés de la marge omanaise ? La topographie du substratum suggérant des blocs mis en contact par des failles transformantes étroites (*Barton et al., 1990*) peut aussi bien être formée par des fragments d'ophiolite chevauchés les uns sur les autres (Figure 29).

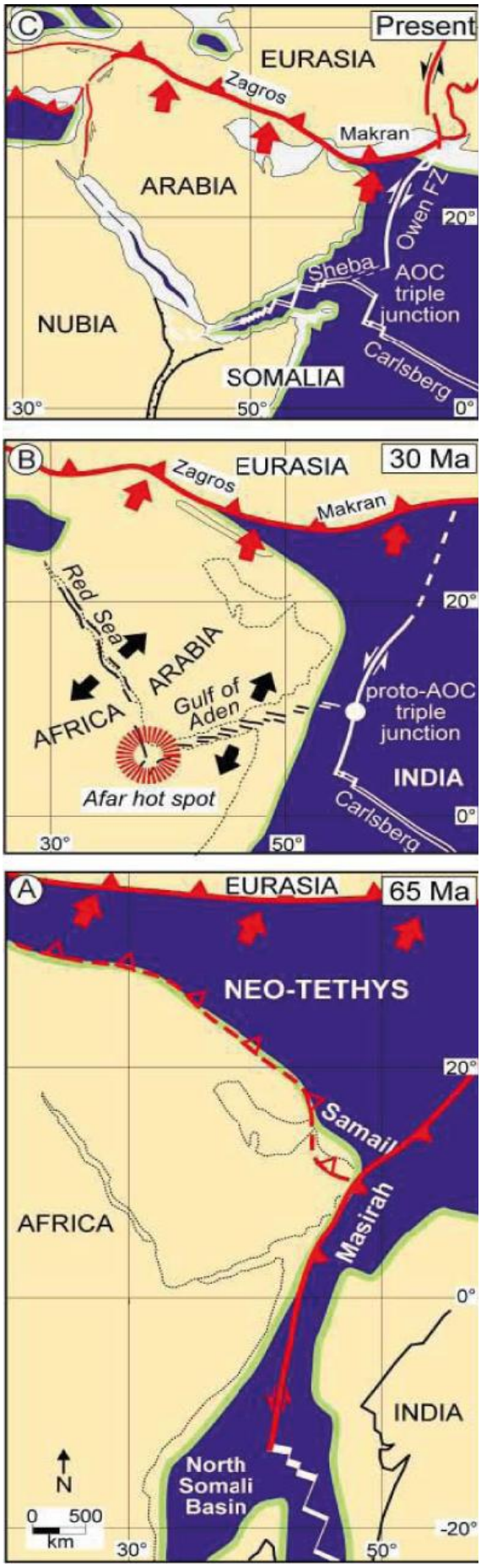


*Figure 31 : Reconstitution paléogéographique de la Mer d'Arabie et de la marge Est-Omanaise du Crétacé à l'actuel, d'après Fournier, 2009.*

*Du Paléogène à l'Oligocène*

La localisation de la limite de plaque Inde-Arabie est inconnue durant toute cette période. Les décalages observés sur la marge Est-Omanaise sont trop faibles pour correspondre au décrochement principal, qui devait être localisé dans le Bassin d'Owen. La localisation précise du décrochement principal est inconnue. Nous ne savons pas si le décrochement principal actif à ce moment-là est le même que celui actif au Crétacé. Il aurait pu être réactivé suite à l'obduction et segmenter les ophiolites. Les structures associées à ce paléo-décrochement sont inconnues, tout au plus peut-on en deviner sur l'unique profil sismique recoupant le Bassin d'Owen.

La conjuguée de la ZF Chain (qui reste à identifier) est probablement localisée dans le Bassin d'Owen (*Royer et al., 2002*) et aurait pu faire office de limite de plaque avant l'ouverture du Golfe d'Aden. La structure de la marge et la quantité de sédiments délivrés à cette époque ne sont pas connues, tout comme la position exacte de la transition continent-océan.

*A l'Oligocène supérieur-Miocène inférieur*

La surrection de la Ride d'Owen, contemporaine de l'ouverture du golfe d'Aden, marque la dernière relocalisation de la limite de plaque Inde-Arabie. Cet accident sépare la lithosphère océanique indienne du substratum du Bassin d'Owen dont la nature est inconnue. Les modalités de cette migration de la limite de plaque Inde-Arabie sont inconnues : s'agit-il d'une migration abrupte, avec un saut de frontière de plaque de plusieurs dizaines de kilomètres? Ou est-ce que la migration s'est faite de façon progressive, avec l'activation alternée de plusieurs décrochements vers l'Est? S'agit-il d'un ancien système distribué, qui aurait fini par se localiser sur un système de faille bien déterminé ? Comment ses migrations s'inscrivent-elles dans le contexte de la compression Oligocène identifiée sur la marge Est-Omanaise et de l'ouverture du Golfe d'Aden?

*5. Objectifs de la thèse : évolution structurale de la frontière Inde-Arabie et aléas naturels associés*

Cette thèse s'organise sous la forme d'un voyage dans le temps : à partir de l'étude de la limite de plaque Inde-Arabie actuelle, nous allons peu à peu découvrir ses traces plus anciennes, enquête qui nous conduira jusqu'au Crétacé supérieur. Un bref descriptif des principes d'acquisition des données et de leur localisation est fourni en **chapitre 2**.

La Zone de Fracture d'Owen est avec ces 800 km de long l'une des failles décrochantes actives les moins connues à l'heure actuelle. La couverture bathymétrique complète de la faille recueillie au cours de la campagne Owen 1 révèle sa localisation précise et permet d'établir le premier schéma structural détaillé de la faille. La cartographie fine de la ZFO permet d'en préciser la cinématique actuelle. La présence à proximité de la faille de forages profonds (DSDP-ODP) permet de contraindre dans le temps les grandes étapes de l'évolution structurale de ce système décrochant. La ZFO a favorisé la mise en place de bassins pull-apart majeurs, dont le mode de mise en place demeure inconnu (bassin 20°N) ou contradictoire (Fosse de Dalrymple). L'évolution structurale au Plio-Pléistocène de la ZFO permet de discuter de l'existence d'éventuels changements cinématiques au Plio-Pléistocène entre l'Inde et l'Arabie. Ces questions sont discutées dans le **chapitre 3**.

Selon le cadre géologique communément accepté, la Ride d'Owen se soulève en réponse à la migration de la limite de plaque Inde-Arabie de la marge omanaise vers sa position actuelle. Comment l'évolution structurale de la limite de plaque Inde-Arabie est associée au soulèvement de la Ride d'Owen est donc une question fondamentale pour la validation des différentes reconstitutions cinématiques proposées. Du fait de sa localisation sur le passage de la Zone de Convergence Inter-Tropicale, la Ride d'Owen a été au cours des dernières décennies le lieu d'étude privilégié de la mousson asiatique du Miocène à nos jours. Comment l'activité de la limite de plaque a pu contrôler le soulèvement de la ride, et ainsi modifier les conditions de l'enregistrement sédimentaire des paléo-climats du Moyen-Orient, sont des questions capitales. Ces thèmes sont abordés dans le **chapitre 4**.

Le **chapitre 5** porte sur la question de la localisation de la frontière de plaque Inde-Arabie avant l'activation de l'OFZ. Les reconstitutions cinématiques à partir des anomalies magnétiques des dorsales de Carlsberg et de Sheba suggèrent que la frontière était localisée proche de sa position actuelle depuis la formation de la dorsale de Sheba il y a 20 Ma, mais aucune observation n'a permis de confirmer cette hypothèse à l'heure actuelle. La localisation

de la frontière de plaque avant le Miocène est inconnue, et les hypothèses proposées jusqu'à présent contradictoires (*Whitmarsh, 1979 ; Mountain and Prell, 1990 ; Edwards et al., 2000*).

La couverture multi-faisceaux de la Ride d'Owen révèle les cicatrices laissées par des glissements de terrain sous-marins parfois imposants (plusieurs $km^3$ de volume mobilisé). La découverte de glissements de terrain dans un contexte pélagique ouvre une perspective nouvelle par rapport aux glissements ayant lieu sur les marges passives et actives, en contexte terrigène, et fait l'objet du **chapitre 6**. Les études de sédimentologie réalisées sur les marges passives montrent que les forts taux de sédimentation sont des conditions nécessaires à la déstabilisation des sédiments. De façon surprenante, nos données montrent des glissements de terrain importants dans un contexte pélagique, dominé par de faibles taux de sédimentation. Les originalités du système sédimentaire de la Ride d'Owen sont discutées, sur une période s'étendant du début du Miocène à nos jours. Contrairement aux marges passives où de nombreux facteurs peuvent déclencher les glissements de terrain (*Hampton, 1996*), seuls les séismes sont susceptibles d'agir dans le contexte de la Ride d'Owen. Le système sédimentaire de la Ride d'Owen est donc un cas naturel privilégié pour étudier le rôle des séismes dans le déclenchement des glissements de terrain. Ces glissements sous-marins représentent une source d'aléa tsunami potentielle, dont il convient de déterminer le comportement au cours des temps géologiques. L'aléa tsunami associé aux sources gravitaires profondes (>2000 m) est encore peu étudié.

Ces grands thèmes sont traités par la suite en chapitre distincts, principalement articulés autour d'articles publiés ou en préparation. Les publications sont à considérer comme une photographie de l'état de la compréhension de la limite de plaque Inde-Arabie au moment de leur parution. Cependant, ma réflexion ayant évolué au fil des articles et de l'acquisition de données nouvelles, le lecteur pourra être gêné par certaines incohérences. Afin de pallier ce défaut inhérent aux thèses sur article, chaque chapitre est complété d'une auto-critique des résultats, dont le lecteur trouvera une synthèse en conclusion de cette thèse. Ces résultats sont confrontés aux études réalisées sur les autres décrochements, continentaux ou océaniques, afin de mettre en avant les particularités de la limite de plaque Inde-Arabie. Les comparaisons sont enrichies d'encarts hors-texte, présentant de façon synthétique les principales caractéristiques des failles.

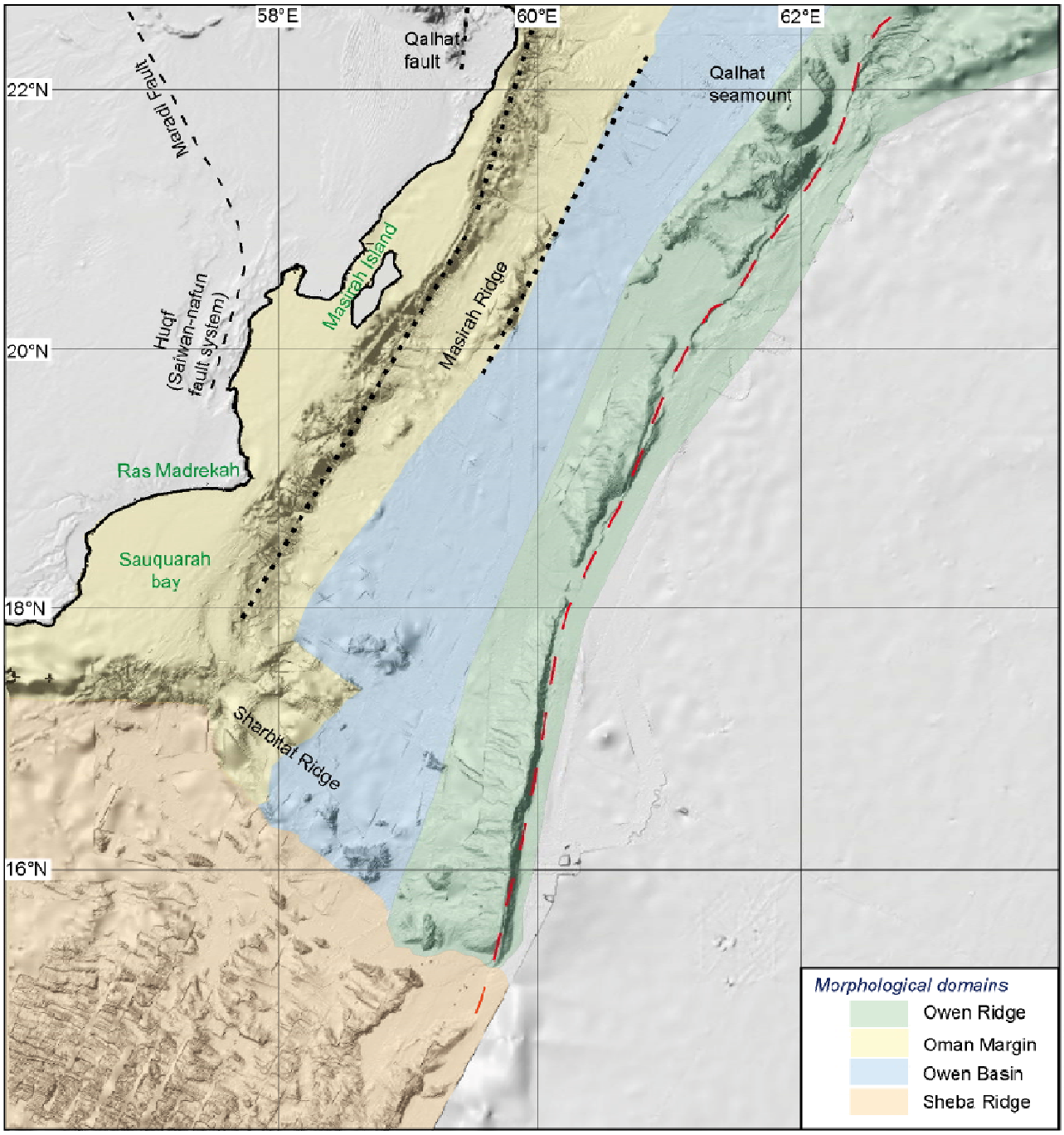


Figure 32 : Carte des principaux domaines géologiques du bassin d'Owen, représentant les localisations potentielles des limites de plaque Inde-Arabie fossiles.


*Planche II : Dessin à l'encre de Chine des formations calcaires en discordance sur les ophiolites de l'île de Masirah, Oman*

# Chapitre 2 : Matériel et méthodes


*Figure 1 : Photo du Beautemps-Beaupré, le navire du SHOM (Cliché : M. Fournier).*

Les campagnes océanographiques Owen 1 et Owen 2 se sont déroulé du 1er au 16 mars 2009 entre Djibouti et Salalah (Sultanat d'Oman), et du 15 mars au 1° Avril 2012 entre Salalah (Sultanat d'Oman) et Abu Dhabi (Emirats Arabes Unis), respectivement. Ces campagnes ont été menées sur le bâtiment hydrographique et océanographique *BHO Beautemps-Beaupré* de la Marine nationale, dans le cadre de la coopération entre le SHOM et l'IFREMER (Figure 1). Etudier la géologie de la Mer d'Arabie est aujourd'hui difficile du fait des nombreux actes de piraterie répertoriés dans la région. Les campagnes géophysiques nécessitent la protection de l'armée, et le choix des outils est déterminé par les capacités du *Beautemps-Beaupré*. L'objectif d'Owen 1 était de reconnaître la frontière de plaque entre l'Arabie et l'Inde dans le nord-ouest de l'Océan Indien. La stratégie adoptée pour cette campagne a consisté à cartographier la frontière de plaque active par sondeur multi-faisceaux. Des profils de sondeurs de sédiments ont été acquis en parallèle pour établir la structure de sub-surface de la ZFO (Figure 2). L'objectif d'Owen 2 était d'imager la structure profonde de la ZFO et du Bassin d'Owen, afin de déterminer l'évolution structurale et cinématique de ce système décrochant depuis le Crétacé supérieur. Dans ce cas, la stratégie a consisté en l'acquisition de profils de sismique réflexion multi-traces, pour imager les structures affectant la pile sédimentaire jusqu'au socle (Figure 3). La couverture bathymétrique du Bassin d'Owen a été complétée au cours de cette mission. Au cours de ces deux campagnes, des relevés magnétométriques ont également été récoltés. En raison d'une panne du gravimètre, le champ gravimétrique n'a pas pu être mesuré lors d'Owen 2. Les données gravimétriques n'ont pas été exploitées (couverture trop faible) et ne seront pas détaillées par la suite.

La campagne Owen 1 a été réalisée par *M. Fournier (Chef de mission), N. Chamot-Rooke, P. Huchon, C. Petit, M.O. Beslier, et B. Hazar*. La campagne Owen 2 a été réalisée par *N. Chamot-Rooke (Chef de mission), M. Fournier, P. Huchon, M. Rodriguez et M. Delescluse*. Les travaux ont été menés à bien grâce aux moyens fiables et performants du BHO Beautemps-Beaupré mis en oeuvre par les hydrographes du Groupe Océanographique de l'Atlantique (GOA) du SHOM sous la conduite des ingénieurs *Vincent Lamarre, Daniel Levieuge* et de l'ingénieur *Yves-Marie Tanguy* pour la logistique, et grâce au concours des commandants du bâtiment, successivement le capitaine de frégate *Geoffroy de Kersauson*, et le capitaine *Rémy de Monteville*. Je tiens à exprimer ma gratitude pour leur accueil ainsi que pour le travail effectué par leurs officiers et leur équipage. La préparation des campagnes et le traitement des données ont bénéficié de l'aide *d'A. Rabaute*.

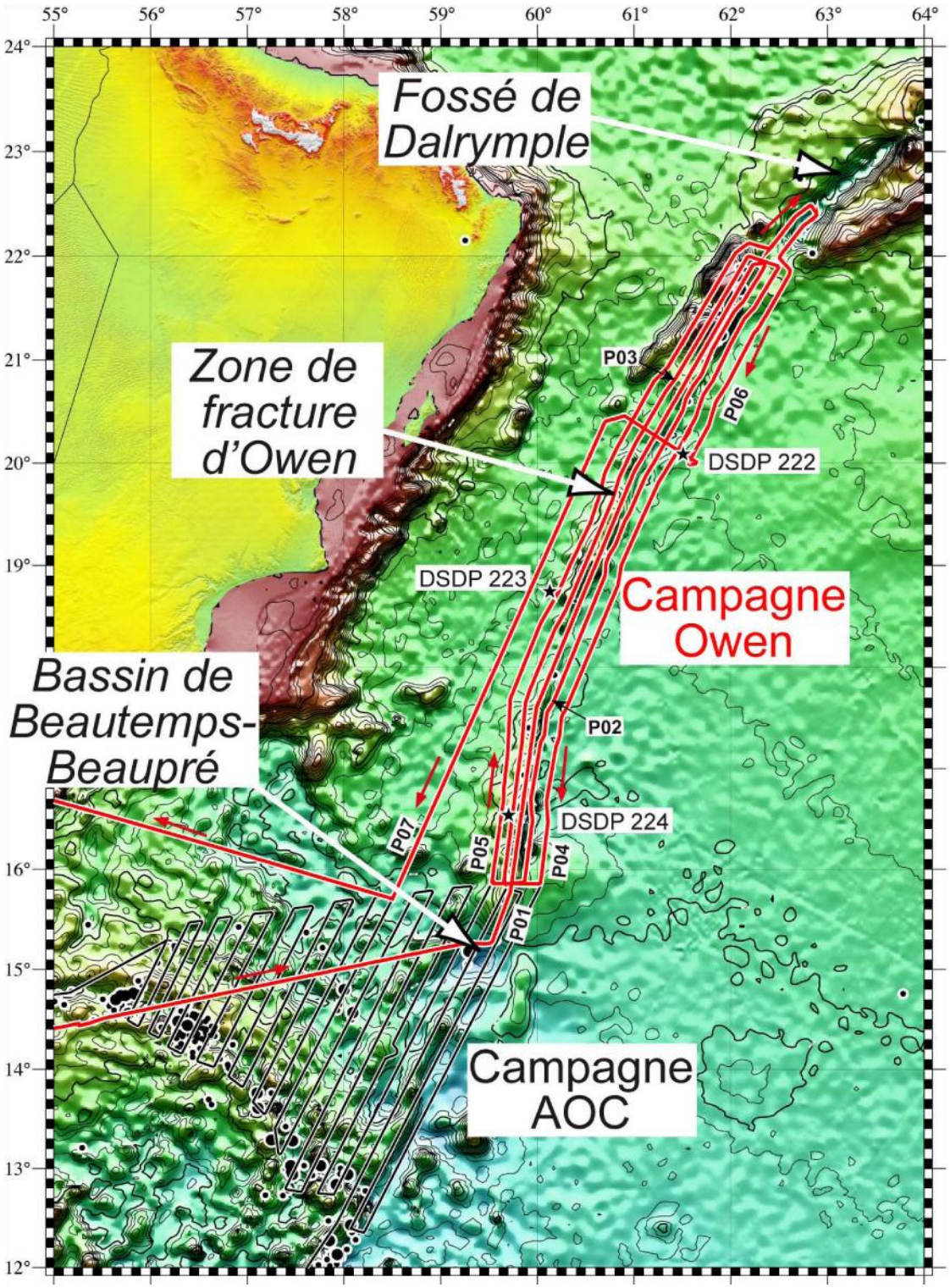


*Figure 2 : Plan de position de la campagne Owen 1*

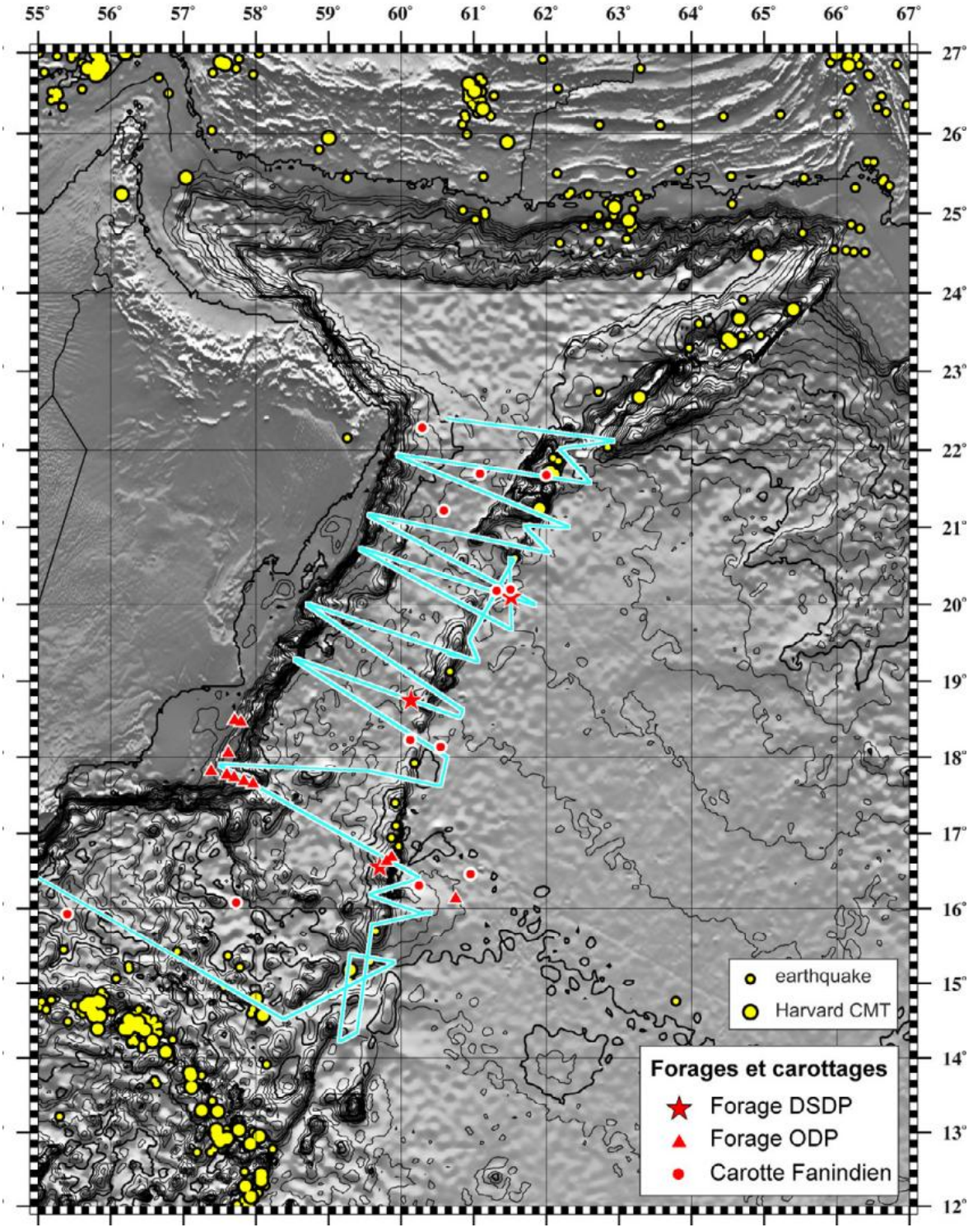


*Figure 3 : Plan de position de la campagne Owen 2*

*Bathymétrie multi-faisceaux*

Le sondeur multifaisceaux permet l'acquisition rapide et précise des relevés topographiques des reliefs sous-marins (bathymétrie) et des images sonar présentant la réflectivité locale du fond. Le sondeur génère une onde acoustique qui se propage dans l'eau, se reflète sur le fond de la mer et est réceptionnée au retour par un capteur. Le temps mis par l'onde pour effectuer le trajet est converti en profondeur, dans la mesure où l'on connait la vitesse de propagation de l'onde dans l'eau de mer (environ 1500 $m.s^{-1}$, mais des variations existent en fonction de la stratification des eaux (Température & salinité)). Cette technique utilise plusieurs sources sonores et des dispositifs d'écoute répartis sur la gondole du navire (Figure 4). A intervalles réguliers de quelques secondes, les sources sonores émettent des ultrasons qui atteignent une mince bande du fond, perpendiculaire à la trajectoire du navire. Ainsi, les ultrasons captés par le navire proviennent des intersections entre la bande des sons émis et les couloirs d'écoute. L'ouverture angulaire latérale maximale est de 150°, ce qui permet de couvrir une superficie au sol dont la largeur équivaut à 6 à 7 fois la hauteur d'eau. Les échos sont enregistrés à des intervalles réguliers de quelques secondes pendant que le navire avance, et l'accumulation des données autorise la reconstruction du relief le long de la trajectoire du navire. Les caractéristiques morpho-sédimentaires d'un secteur peuvent donc être rapidement obtenues avec ce type de systèmes embarqués.

Le sondeur du BHO Beautemps-Beaupré (Kongsberg/Simrad EM-120) est un sondeur de « seconde génération », basé sur la technique de la gondole sous coque. La résolution verticale du sondeur multi-faisceaux du Beautemps-Beaupré est inférieure à 10 m. La spécificité du BHO Beautemps-Beaupré est la présence d'une équipe d'hydrographes du SHOM (GOA – Groupe Océanographique de l'Atlantique) qui assure non seulement les quarts acquisition, mais également le traitement de la sonde. Des grilles de la ZFO et de la Ride d'Owen au pas de 80 m ont été obtenues au cours des campagnes Owen 1 & 2 (Figure 5).


*Figure 4:* Gondole sous-coque du *BHO Beautemps-Beaupré (sondeur EM 120)*

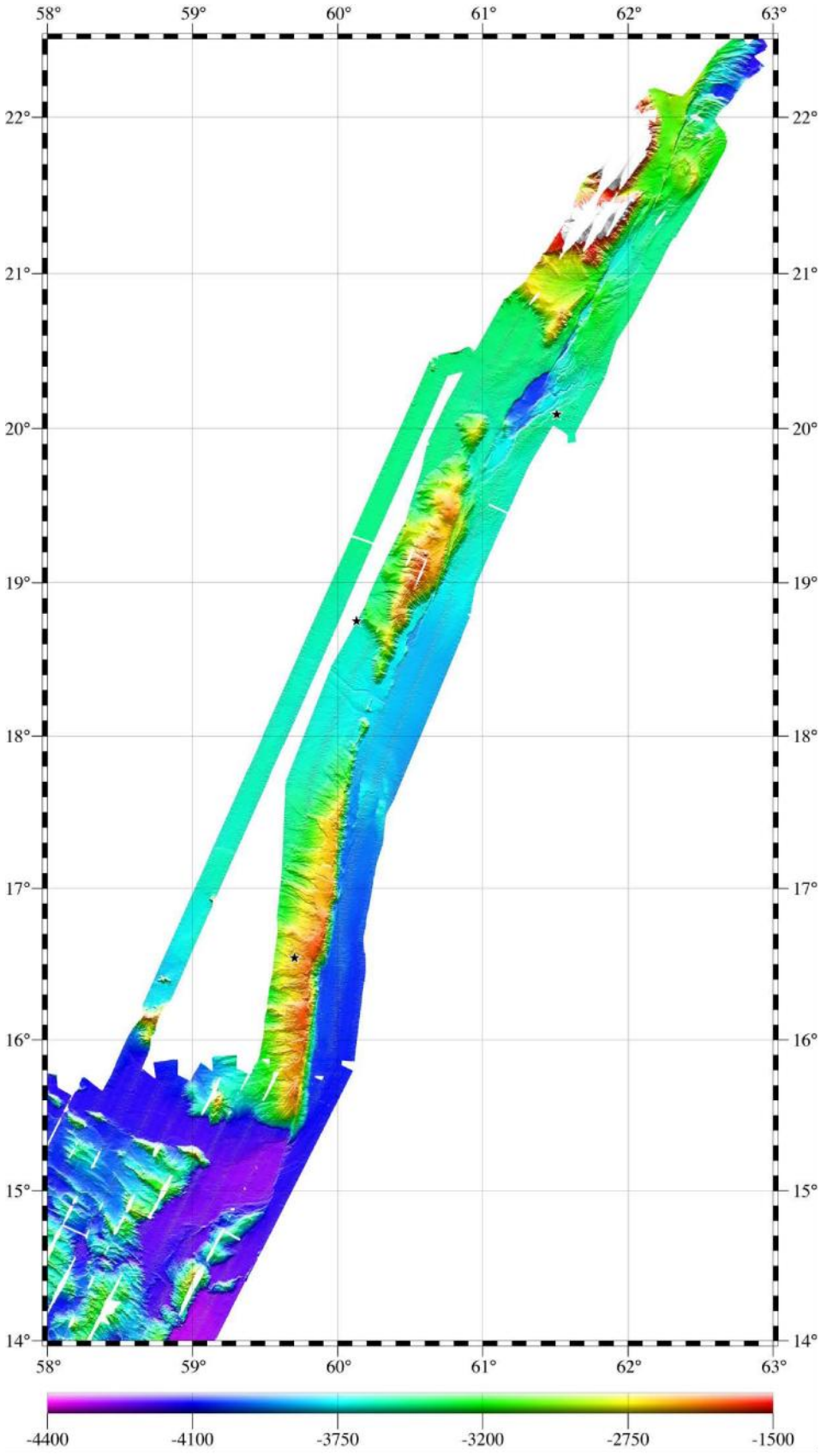


*Figure 5 : bathymétrie multi-faisceaux recueillie lors de la campagne Owen 1*

*Les systèmes d'informations géographiques (SIG)*

Les données bathymétriques et la réflectivité ont été intégrées dans des logiciels appelés systèmes d'informations géographiques. Ces logiciels permettent de réaliser des cartes bathymétriques, des cartes des pentes. Ils permettent d'utiliser de nombreuses projections géographiques en fonction des besoins de l'étude. Les figures présentes dans cette thèse ont été réalisées à partir d'ArcGis 9.3 (ESRI), Global mapper, GMT, et Fledermaus. L'extension MapPublisher du logiciel Adobe illustrator a également été utilisée pour la réalisation de certaines cartes et figures, en particulier les schémas structuraux de l'Oman et de la ZFO.

*Réflectivité acoustique*

Les enregistrements des sondeurs multi-faisceaux fournissent également une appréciation de la nature du fond en fonction de la texture des images et du degré de réflectance codé en niveaux de gris des faciès acoustiques. L'amplitude du signal réfléchi au voisinage de la verticale est très élevée. En outre, le signal s'atténue en fonction de la distance parcourue, donc du temps. Afin d'éviter une saturation des amplificateurs, et pour garder un niveau de signal le plus régulier possible, une loi de *time varying gain* (TVG) est appliquée au signal reçu. Une fois cette compensation établie, l'amplitude du signal reçu est appelée réflectivité. Les mosaïques obtenues sont comparées aux données de prélèvement ou d'observation du fond pour être ensuite calibrées et interprétées sous la forme de faciès sédimentaires. Dans certains cas des fonds de nature différente peuvent présenter une réflectivité acoustique équivalente. Une calibration par prélèvements est donc indispensable avant toute interprétation. Dans cette thèse, la calibration est basée sur les travaux de *Bourget (2009)* et sur les forages ODP et DSDP réalisés dans la région.

*Sondeur de sédiments (d'après Pacault et al., 2004)*

Les sondeurs de sédiments sont des instruments acoustiques utilisés pour visualiser les strates sédimentaires enfouies sous le fond de l'eau jusqu'à plusieurs dizaines de mètres de profondeur. Ces sondeurs permettent d'insonifier le fond avec un faisceau dont l'ouverture est typiquement comprise entre 10° et 40°. Ces sondeurs fonctionnent à des fréquences de quelques kHz (généralement de 2kHz à 8kHz) de façon à obtenir une pénétration suffisante tout en conservant des dimensions acceptables. Le signal émis peut être un signal large bande (plusieurs kHz), modulé en fréquence (chirp). Le signal reçu correspond à une série temporelle d'échos réfléchis sur les discontinuités du sous-sol. Un traitement cohérent est

appliqué sur ce signal, ce qui permet d'augmenter le rapport signal/bruit. L'approche adoptée pour le sondeur de sédiment de nouvelle génération SBP120 développé par Kongsberg-Maritime et installé à bord du BHO Beautemps-Beaupré s'appuie sur une technologie multifaisceaux. Elle repose sur la mise en oeuvre de deux antennes de plus de 7 m de long. Une antenne, fixée dans le sens de la longueur du bateau, est utilisée pour l'émission du signal; l'autre, montée perpendiculairement à l'antenne d'émission, est utilisée pour la réception. Ce dispositif permet de former des faisceaux étroits (largeur 3° x 3° à 4 kHz). Les antennes d'émission et de réception du SBP120 sont installées dans une gondole fixée sous la partie avant du bateau. Cette antenne est utilisée à la fois pour la réception des données du sondeur multifaisceaux EM120, et pour les données du sondeur de sédiments SBP120. Les différentes données sont séparées par filtrage après réception (bande passante SBP120 : 2,5 –7 kHz (3.4 kHz dans notre cas), bande passante EM120 : 11 – 13 kHz). La résolution verticale du sondeur est de l'ordre de 1/B, où B correspond à la largeur de la bande passante. Pour une modulation de fréquence linéaire de 2,5 kHz à 7 kHz, on a donc une résolution verticale de l'ordre de 0.2 ms (temps aller-retour TWT), ce qui correspond à une distance inférieure à 0.2 m (pour une vitesse de propagation de 1500 m/s). La pénétration des ondes acoustiques est dépendante de leur coefficient d'atténuation. Dans la bande passante utilisée, il est possible de considérer que le coefficient d'atténuation des ondes de compression varie linéairement en fonction de la fréquence *(Hamilton, 1980)*. Les hautes fréquences sont atténuées beaucoup plus rapidement que les basses fréquences. Cette diminution de la fréquence centrale et de la largeur de la bande passante effective en fonction de la profondeur s'accompagne donc d'une diminution de la résolution intrinsèque. Seuls les premiers mètres de sédiments sont investigués. La fenêtre temporelle d'enregistrement est de 200 ms temps double (TWT), correspondant à environ 150 m, mais les couches sont visibles sur environ 70 m de profondeur (une vingtaine de mètres pour les zones sableuses). En général, les zones de forte pente ne donnent aucun signal utilisable, en raison d'importants échos latéraux. Ces résolutions verticales et ces profondeurs de pénétration font du SBP un outil privilégié pour étudier l'architecture des corps sédimentaires peu profonds et la tectonique de surface de ZFO. Les faciès acoustiques obtenus sur les profils SBP renseignent sur la nature des dépôts sédimentaires (Figure 6), lorsque calibrés avec des forages (ODP et DSDP) ou des carottages (de type Küllenberg dans notre cas).

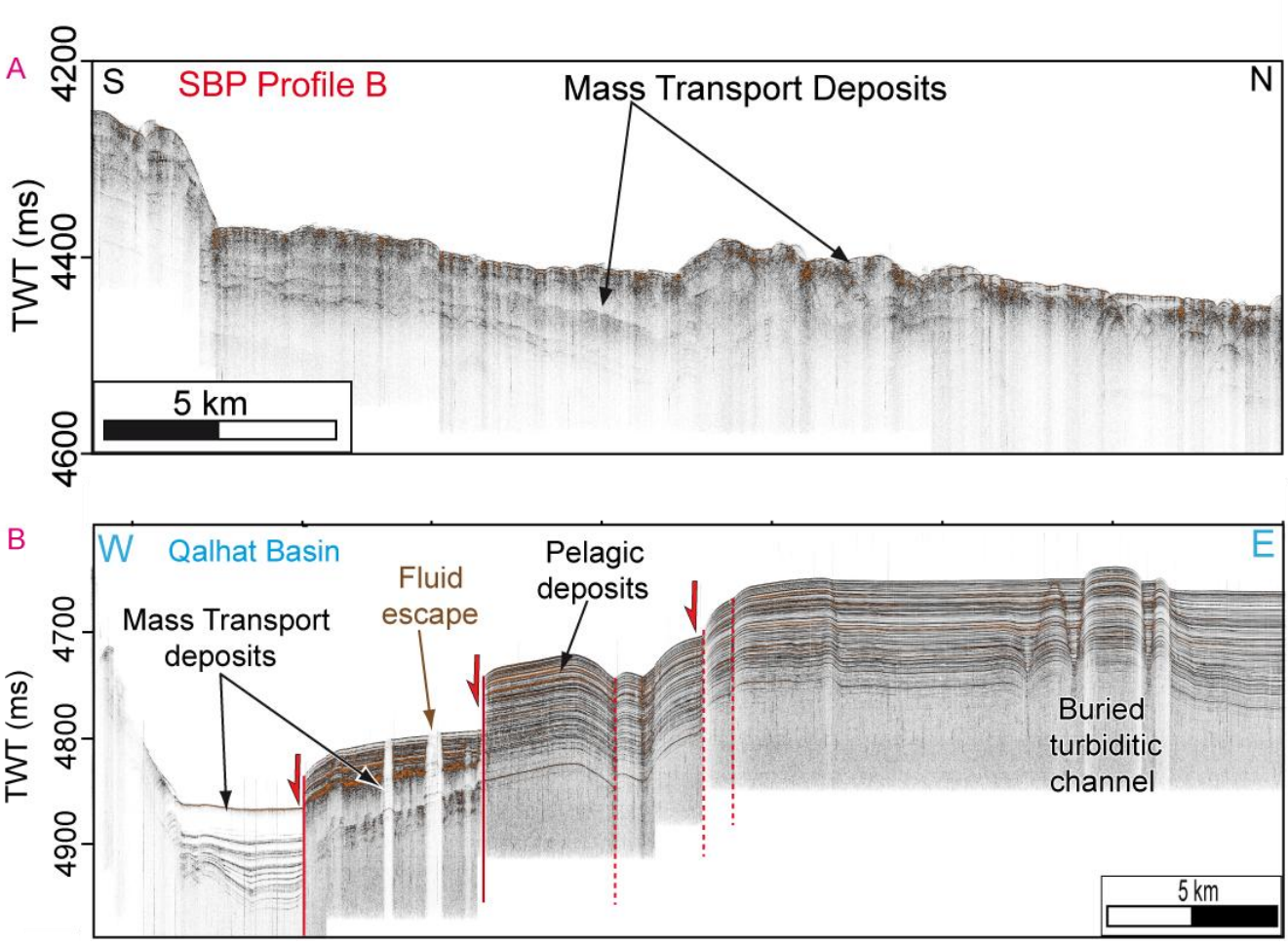


*Figure 6 : Exemples de profils de sondeur de sédiments. Le profil en haut recoupe les glissements de terrain de la Ride d'Owen, caractérisés par un faciès chaotique. Le profil en bas recoupe le bassin de Qalhat (découvert lors de cette thèse), montrant des failles bien marquées. Le bassin est rempli par des glissements de terrain et des dépôts pélagiques, en alternance. Des figurés d'échappements de fluides sont observés sur l'un des blocs basculés du bassin. Un chenal turbiditique fossile (drapé par des pélagites) est visible à l'Est du profil.*

*Sismique réflexion SISRAP*

La reconnaissance sismique est basée sur la mesure des temps de propagation, dans les couches du sous-sol, d'ondes acoustiques générées artificiellement par une source. Les ondes émises sont réfléchies ou réfractées par l'interface eau-sédiment (selon la loi de Snell-Descartes) et par les surfaces de discontinuité entre les différentes couches du sous-sol. Les ondes se propagent à une vitesse qui dépend de la nature des couches traversées. En fonction des variations de lithologie, et des variations des propriétés physiques des roches avec la profondeur (densité, porosité, température), les couches géologiques se caractérisent par des

contrastes d'impédance acoustique, qui déterminent les discontinuités marquées par les réflecteurs. Les temps de propagation des ondes entre la source et les récepteurs permettent de déterminer la géométrie, la structure et la configuration des couches géologiques.

Les équipements nécessaires à la mesure sismique sont de trois types : les émetteurs (ou sources), les récepteurs et les systèmes d'acquisition. Le rôle de la source est d'émettre une onde acoustique dont on connaît les caractéristiques (fréquences, durée, amplitude du signal) dans le milieu liquide. Le principe des récepteurs est de convertir les variations de pression liées à la propagation de l'onde acoustique en tension électrique. En sismique réflexion, pour capter le signal acoustique, on utilisera principalement une flûte (ou streamer) constituée d'un ensemble d'hydrophones alignés montés électriquement en série ou en parallèle.

Il existe différents types de sismique réflexion selon les objectifs scientifiques à remplir. Plus le signal est à basse fréquence (ex. 10 Hz), plus la pénétration est grande (elle peut atteindre plusieurs dizaines de kilomètres). En contre partie, la résolution est faible. A l'opposé, avec l'utilisation d'une source de plus haute fréquence (> 200 Hz), on peut imager des couches sédimentaires avec une très bonne résolution (<1m) mais avec une pénétration limitée (quelques dizaines de mètres). L'objectif principal de cette thèse -l'identification des structures associées au mouvement relatif Inde-Arabie depuis le Paléocène- nécessite d'imager la couverture sédimentaire du Bassin d'Owen et de la Mer d'Arabie. L'usage d'une sismique à forte pénétration mais basse résolution est donc recommandé. Compte tenu des contraintes liées au piratage en Mer d'Arabie, nous avons utilisé la sismique rapide SISRAP de l'IFREMER, qui a été transféré sur le Beautemps-Beaupré pour l'occasion. Les caractéristiques de cette sismique sont détaillées sur le site suivant (http://flotte.ifremer.fr/flotte/Presentation-de-la-flotte/Equipements/Equipements-de-sismique/Sismique-rapide-numerique-SISRAP) (Figure 7). La fréquence est de 50 à 55 Hz, et garantit une résolution verticale d'environ 5 m. Cette sismique peut pénétrer plusieurs centaines de mètres en fonction de la nature des sédiments, du type de source, de la profondeur de l'eau, de la géométrie d'acquisition, et de la qualité des traitements d'imagerie. Le traitement de la sismique d'Owen 2 (Stack, Normal Move Out, Filtrage & Gain) a été réalisé à l'aide du logiciel de traitement GEOCLUSTER (CGG Veritas) (Figure 8).

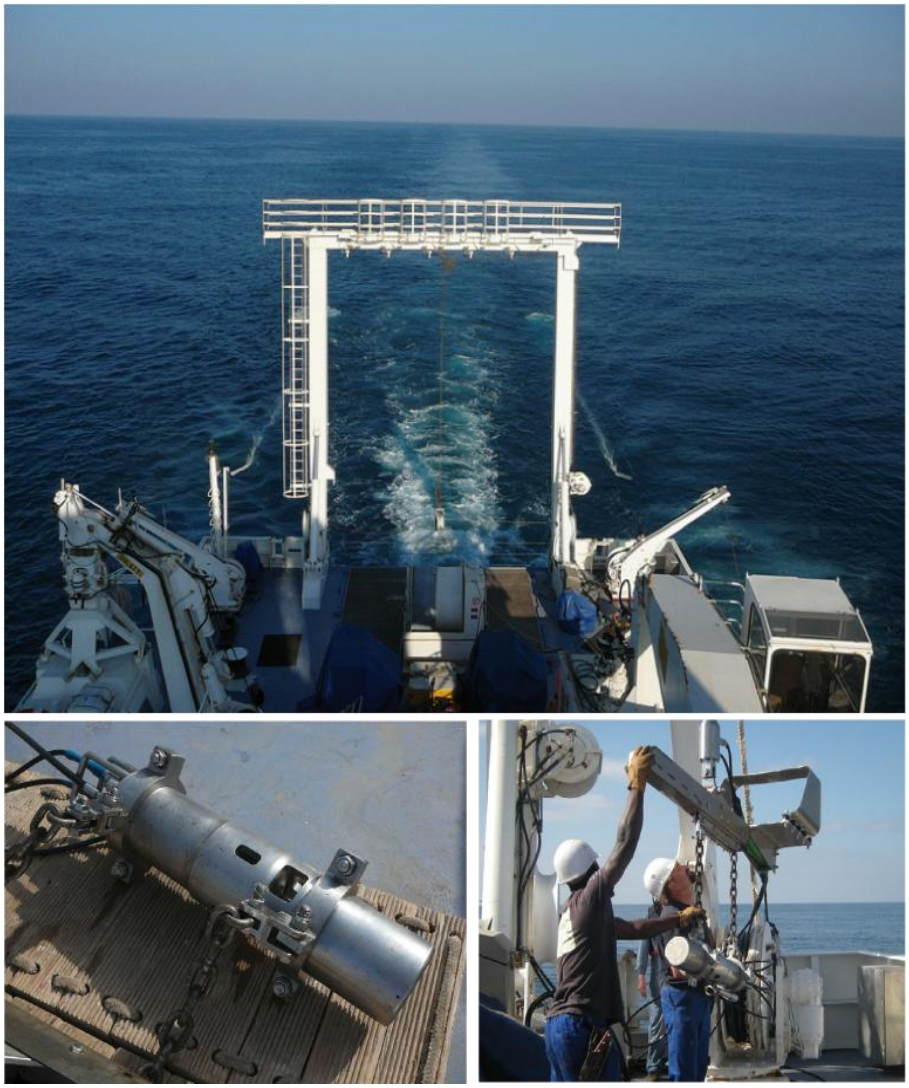

*Figure 7 : Haut : Dispositif SISRAP à l'arrière du Beautemps Beaupré. Bas Gauche : Canon Sodera GI, source de la sismique. Bas droite : Mise à l'eau des canons Sodera GI.*

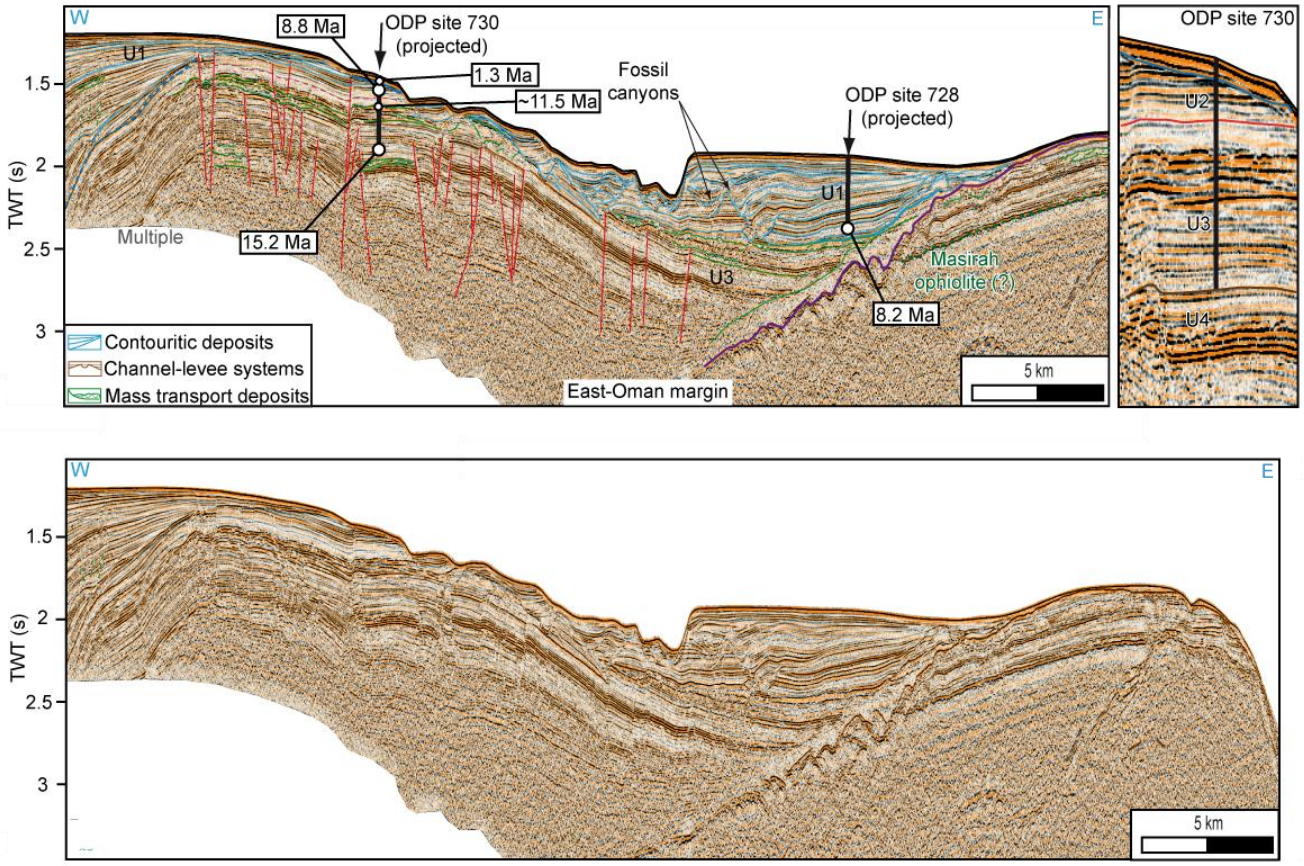


*Figure 8 : exemple de profil SISRAP enregistré au cours de la campagne Owen 2, recoupant la marge omanaise et montrant une grande diversité de dépôts sédimentaires et de structures tectoniques. En haut le profil interprété, en bas le profil brut.*

*Magnétométrie*

Le magnétomètre utilisé à bord du Beautemps-Beaupré est le magnétomètre Thomson Sintra SMM II de type scalaire à effet Overhauser, équipé d'un capteur omnidirectionnel (Figure 9). La cadence de mesure de ce magnétomètre est de 1 Hz avec une résolution de 0,01 nT. Compte tenu du niveau de bruit généré par le bâtiment et les mouvements du capteur, la résolution est de l'ordre de 0,1 nT. Les mesures aberrantes sont peu nombreuses. Le traitement des données à bord avec le logiciel TIMICA du SHOM a été entièrement assuré par l'équipe du SHOM, qui nous a fourni les valeurs de l'anomalie magnétique au pas de temps initial de l'acquisition (1 seconde), après suppression des valeurs aberrantes, calcul de la position du capteur en tenant compte du déport à l'antenne GPS (270 m) et soustraction du champ de référence (IGRF 2005). La carte des anomalies magnétiques nouvellement collectées est fournie en figure 10.

*Figure 9 : magnétomètre de queue de flûte sismique utilisé à bord du BHO Beautemps-Beaupré*

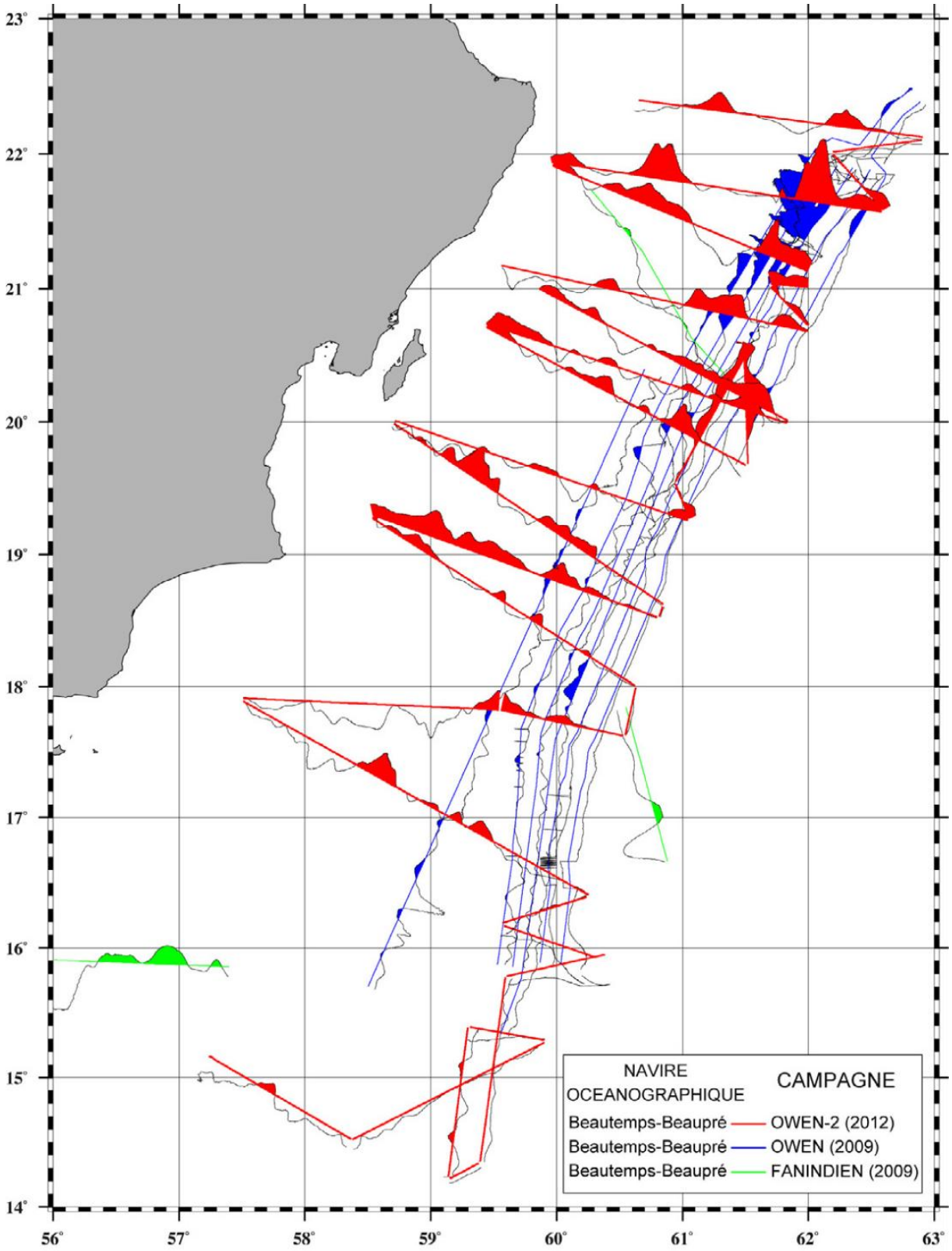


*Figure 10 : Carte des anomalies magnétiques recueillies lors des campagnes Owen et fanindien*

# Chapitre 3 : Evolution structurale de la limite de plaque Inde-Arabie au cours du Plio-Pleistocène : apports à la compréhension du mouvement Inde-Arabie.

Ce chapitre s'articule autour de 4 articles, publiés, soumis ou en préparation.

Le premier article est publié à la revue *Earth and Planetary Science Letters*, sous la référence suivante :

*Fournier, M., N. Chamot-Rooke, M. Rodriguez, P. Huchon, C. Petit, M.-O. Beslier, and S. Zaragosi (2011), Owen Fracture Zone: the Arabia-India plate boundary unveiled, Earth Planet. Sci. Lett., 302, 247-252, doi:10.1016/j.epsl.2010.12.027*

Il a pour but de présenter de façon générale la Zone de Fracture d'Owen. Cet article présente les données de bathymétrie multi-faisecaux recueillies au cours de la campagne Owen 1, et identifie la position précise et les caractéristiques structurales majeures de la ZFO, à savoir la présence d'un bassin pull-apart de dimensions comparables à celles de la Mer Morte situé à la latitude 20°N, et d'une terminaison en structure dite « en queue de cheval » à l'entrée de la fosse de Dalrymple. La couverture multifaisceaux révèle également des décalages morphologiques de la Ride d'Owen de l'ordre de la dizaine de kilomètres par la ZFO, ce qui permet de confirmer, considérant un mouvement relatif à ~3 mm/an, l'âge Pliocene de la ZFO. La cartographie fine de la faille permet de localiser avec précision la position du petit cercle sur lequel s'inscrit la ZFO. En accord avec les quelques mécanismes au foyer calculés dans la région, le tracé de la faille et la position du petit cercle décrivent une faille purement dextre. Ceci est en contradiction avec le modèle MORVEL, qui prédit de la transtension sur la ZFO au nord de la latitude 18°N, latitude à partir de laquelle les bassins en pull-apart semble se développer. Cet article présente aussi, de façon sommaire, les glissements de terrain identifiés sur la Ride d'Owen, détaillés en dernière partie de cette thèse.

Le deuxième article est publié à la revue *Geophysics Geochemistry Geosystems*, sous la référence suivante :

*Rodriguez, M., M. Fournier, N. Chamot-Rooke, P. Huchon, J. Bourget, M. Sorbier, S. Zaragosi, and A. Rabaute (2011), Neotectonics of the Owen Fracture Zone (NW Indian Ocean): Structural evolution of an oceanic strike-slip plate boundary, Geochem. Geophys. Geosyst., 12, Q12006, doi:10.1029/2011GC003731*

Il propose une analyse détaillée de la structure de l'OFZ à partir des données de bathymétrie multi-faisceaux et de sondeur de sédiments recueillies au cours de la campagne Owen 1. Il propose une première estimation des âges des structures identifiées le long de ZFO, et un premier cadre conceptuel concernant son évolution structurale. Etablir l'évolution structurale d'un système décrochant à partir de simples profils de sondeurs de sédiments, dont la pénétration est très limitée, est un exercice périlleux, les interprétations étant en partie limitées et imposées par l'échelle d'observation. Nombre des résultats de cet article ont donc été précisés ou invalidés par la suite, à la lumière des données recueillies au cours de la campagne Owen 2 (qui avait été déprogrammée du fait de la recrudescence des actes de piraterie au moment de la rédaction de cet article). Cet article propose une description de la couverture sédimentaire aux abords de la faille, un premier modèle d'ouverture du bassin pull-apart situé à la latitude de 20°N, et un premier modèle de l'évolution structurale du système de faille entre 20 et 22°N. Cet article décrit un bassin jusqu'alors inconnu, baptisé le bassin de Qalhat en référence à la ville située à la même latitude en Oman, et au mont sous-marin adjacent. Au vu de ces premiers résultats, il semblait que l'évolution structurale de la ZFO était commandée par la simple évolution mécanique du système, les structures et les segments de faille semblant s'activer au gré de la distribution des contraintes au cours du temps, et ne correspondant à aucun changement cinématique connu.

Les deux articles suivants sont basés sur les données de sismique réflexion acquises lors de la campagne Owen 2, et ont pour objectif de caractériser la structure de la couverture sédimentaire au niveau des structures majeures de la ZFO, i. e. le bassin 20°N et la fosse de Dalrymple.

Le troisième article de ce chapitre, intitulé *"Mode of opening of an intra-oceanic pull-apart: the 20°N Basin along the Owen Fracture Zone (NW Indian Ocean)"*, a été soumis en Janvier 2013 à la revue Tectonics et se trouve en cours d'évaluation. Cet article détaille le mode d'ouverture du bassin 20°N, et critique les hypothèses de l'article publié à G3. La proximité du site DSDP 222 permet de relativement bien contraindre le cadre stratigraphique de la région, ainsi que de dater les principales étapes de l'ouverture du bassin 20°N. L'âge d'ouverture du bassin est d'environ 2-3 Ma, ce qui est étonnant au vu de ces dimensions (90 x 35 km). Il semblerait qu'une réorganisation structurale de la ZFO aurait individualisé un bloc d'environ 40 km de long, dont la subsidence aurait contrôlé l'évolution de la déformation aux abords du bassin. Cette étude ouvre des perspectives sur la compréhension du mode

d'ouverture de la Mer Morte et montre que de nombreuses similitudes avec le bassin 20°N en dépit de contextes rhéologiques opposés.

Le dernier article de ce chapitre, intitulé : " *Tectonics of the Dalrymple Trough and the horsetail termination of the Owen Fracture Zone (NW Indian Ocean)"*, est un article en préparation pour la revue Tectonophysics. Il propose une révision complète du cadre stratigraphique de la déformation au niveau de la fosse de Dalrymple et de la Ride de Murray. L'âge de l'ouverture de la fosse de Dalrymple, et du soulèvement principal de la Ride de Murray, est évalué autour de 2-3 Ma, contrairement à l'âge de 20 Ma proposé dans les études précédentes. Une phase de déformation fini-Miocene est également observée et sera pleinement discutée dans le chapitre suivant.

L'ouverture quasi-simultanée du bassin 20°N et de la fosse de Dalrymple suggère un potentiel changement cinématique au niveau de l'OFZ autour de 2-3 Ma, dont les origines possibles sont discutées en conclusion de ce chapitre. Les conclusions de *Fournier et al., 2011* sont discutées à la lumière de ces récents résultats.

Earth and Planetary Science Letters 302 (2011) 247–252

Contents lists available at ScienceDirect

Earth and Planetary Science Letters

journal homepage: www.elsevier.com/locate/epsl

# Owen Fracture Zone: The Arabia–India plate boundary unveiled

M. Fournier [a,b,c,*], N. Chamot-Rooke [c], M. Rodriguez [a,b,c], P. Huchon [a,b], C. Petit [d], M.O. Beslier [d], S. Zaragosi [e]

[a] iSTeP, UMR 7193, UPMC Université Paris 6, Case 129, 4 place Jussieu, F-75005 Paris, France
[b] iSTeP, UMR 7193, CNRS, F-75005 Paris, France
[c] Laboratoire de Géologie, CNRS UMR 8538, Ecole normale supérieure, 24 rue Lhomond, F-75005 Paris, France
[d] Géosciences Azur, CNRS UMR 6526, Observatoire océanologique, BP48, 06235 Villefranche-sur-mer, France
[e] EPOC, CNRS UMR 5805, Université Bordeaux 1, Avenue des Facultés, 33405 Talence, France

ARTICLE INFO

*Article history:*
Received 16 June 2010
Received in revised form 6 December 2010
Accepted 10 December 2010
Available online 3 January 2011

Editor: R.D. van der Hilst

*Keywords:*
plate kinematics
strike-slip faults
pull-apart basins
Arabia–India plate boundary
Owen Fracture Zone

ABSTRACT

We surveyed the Owen Fracture Zone at the boundary between the Arabia and India plates in the NW Indian Ocean using a high-resolution multibeam echo-sounder (Owen cruise, 2009) for search of active faults. Bathymetric data reveal a previously unrecognized submarine fault scarp system running for over 800 km between the Sheba Ridge in the Gulf of Aden and the Makran subduction zone. The primary plate boundary structure is not the bathymetrically high Owen Ridge, but is instead a series of clearly delineated strike-slip fault segments separated by several releasing and restraining bends. Despite an abundant sedimentary supply by the Indus River flowing from the Himalaya, fault scarps are not obscured by recent deposits and can be followed over hundreds of kilometres, pointing to very active tectonics. The total strike-slip displacement of the fault system is 10-12 km, indicating that it has been active for the past ~3 to 6 Ma if its current rate of motion of $3 \pm 1$ mm yr$^{-1}$ has remained stable. We describe the geometry of this recent fault system, including a major pull-apart basin at the latitude 20°N, and we show that it closely follows an arc of small circle centred on the Arabia–India pole of rotation, as expected for a transform plate boundary.


## 1. Introduction

The Arabia–India plate motion is currently accommodated along the Owen Fracture Zone (OFZ) in the NW Indian Ocean (Gordon and DeMets, 1989; Matthews, 1966; Whitmarsh, 1979; Wilson, 1965). The OFZ belongs to the large strike-slip plate boundaries like the San Andreas, Dead Sea, North Anatolian and Alpine faults in the continental domain, and the Macquarie Ridge in the oceanic domain (Le Pichon et al., 2005; Lebrun et al., 2003; Mann, 2007; Massell et al., 2000; Stein et al., 1997; Weber et al., 2009). The OFZ is marked by a moderate seismicity and by a prominent bathymetric ridge, the Owen Ridge, up to 2000-m high with respect to the surrounding seafloor (Fig. 1). The Owen Ridge acts as a barrier to turbidites of the Indus deep-sea Fan and prevents their sedimentation towards the west into the Owen Basin (Clift et al., 2001; Mountain and Prell, 1990). As indicated by dextral strike-slip focal mechanisms of earthquakes along the OFZ (Fournier et al., 2001; Gordon and DeMets, 1989; Quittmeyer and Kafka, 1984), the Arabian plate moves northwards slightly faster than the Indian plate at a differential rate of 2 to 4 mm yr$^{-1}$ estimated independently from geodetic (Fournier et al., 2008a) and geological (DeMets et al., 1990, 1994, 2010) data. We recently surveyed the OFZ onboard the *R/V Beautemps-Beaupré* (Owen cruise, 2009) using a high-resolution deep-water multibeam echo-sounder and a 3.5 kHz sub-bottom seismic profiler to identify surficial traces of active faults and characterize the geometry of the fault system in relation with its kinematics. Magnetic and gravity measurements were also routinely acquired.

## 2. Geometry of the plate boundary

Multibeam bathymetric data reveal an outstanding active submarine fault system between the Beautemps-Beaupré Basin to the south (Fig. 1; Fournier et al., 2008b) and the Dalrymple Trough to the north (Edwards et al., 2008). The fault scarps are well preserved on the seafloor and run at the base of the east-facing escarpment of the Owen Ridge, except at its southern extremity and in its central part where the faults crosscut the ridge (Fig. 1). The fault system is remarkably linear and focused on a single strand along much of its length. Six main fault segments can be identified, apparently uninterrupted over lengths between 60 and 180 km (Fig. 2). The overall geometry of the fault system hereafter described, including releasing and restraining bends, pull-apart basins localized on releasing bends, and basins ending the fault system, is consistent with a dextral strike-slip motion.

We used an oblique Mercator projection with the Arabia–India pole of rotation as pole of projection to test if the trace of the OFZ follows a small circle of the Arabia–India motion (Fig. 2a). In this coordinate system, transform faults should be horizontal straight lines if they strictly follow small circles. The trace of the OFZ is generally

* Corresponding author. iSTeP, UMR 7193, CNRS, F-75005 Paris, France.
*E-mail address:* marc.fournier@upmc.fr (M. Fournier).

0012-821X/$ – see front matter © 2010 Elsevier B.V. All rights reserved.
doi:10.1016/j.epsl.2010.12.027

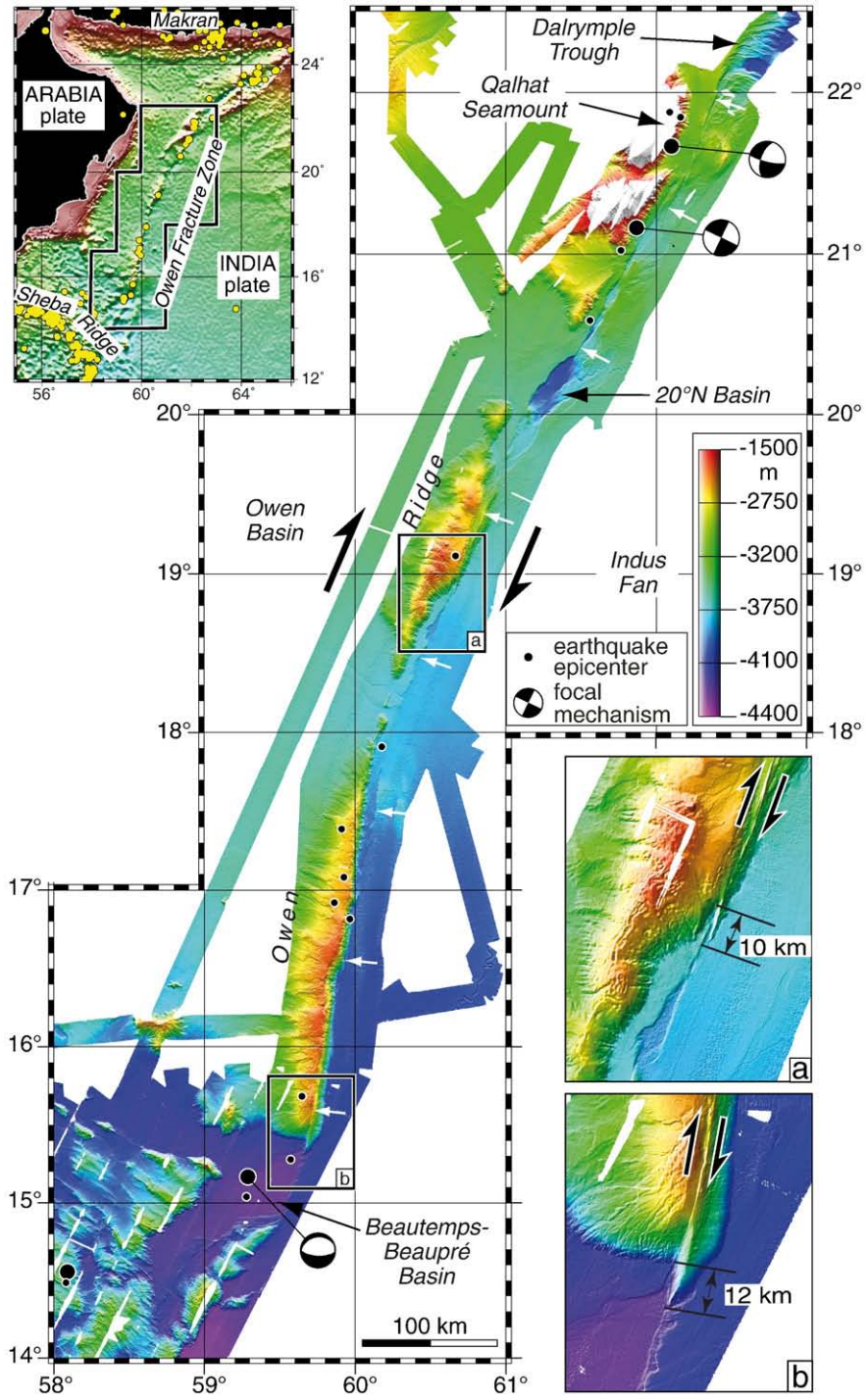


**Fig. 1.** Active fault scarps of the OFZ mapped with a multibeam echo-sounder can be followed over 800 km from the Beautemps–Beaupré Basin to the Dalrymple Trough (white arrows). The OFZ is bounded to the east by the Indian plate oceanic floor of Paleocene age formed at the Carlsberg Ridge (Chaubey et al., 2002; Royer et al., 2002), overlain by thick deposits (up to 12 km) of the Indus Fan (the second largest deep-sea fan), and to the west by the Owen Basin floored with oceanic crust of poorly constrained age between Late Jurassic and Eocene (Edwards et al., 2000; Mountain and Prell, 1990; Whitmarsh, 1979). The Owen Ridge is made up of three distinct portions separated by two thresholds at 18.2°N and 20°N. The southern ridge is asymmetric with a steep east-facing scarp and a gentle western flank, whereas the central ridge displays a dome morphology elongated in the direction of the Owen fracture zone. The southern and central ridges do not bear any magnetic signal. In contrast, the northern ridge, which rises ~2500 m above the surrounding seafloor and is topped by a flat platform at depths of 400 m below present sea level, is characterized by high amplitude magnetic anomalies attesting to a volcanic origin. It corresponds to the Qalhat Seamount, a volcanic guyot of probable Cretaceous age like the Little Murray Ridge in the Oman Basin (Edwards et al., 2000; Ellouz-Zimmermann et al., 2007; Gaedicke et al., 2002). a) and b) Strike-slip geomorphologic offsets of the active faults reach 10 to 12 km.

parallel to a small circle and is diverted from it between 16.5°N and 20.3°N, where a system of adjacent releasing and restraining bends constituting a paired bend (Mann, 2007) is observed. The releasing bend is made up of two pull-apart basins, a small rhomboidal basin at 18.6°N (see Fig. 1a) and a larger basin at a change in trend of the OFZ at 20°N (see Section 4). Between 16.5°N and 18°N, the fault trace slightly deviates from the direction of the interplate slip vector, leading to the development of a gentle restraining bend. Minor

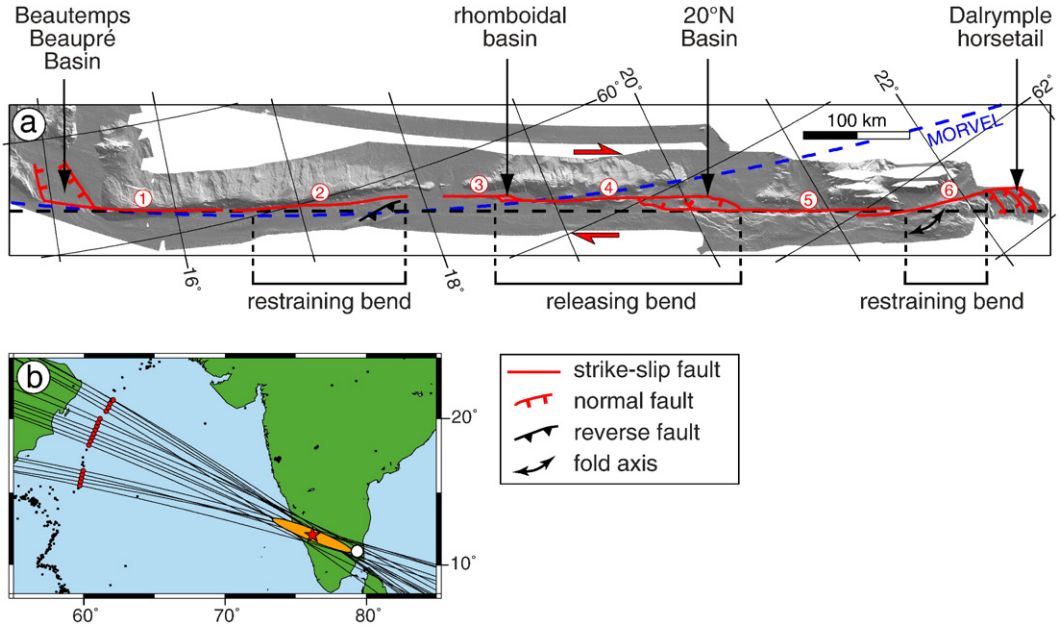


**Fig. 2.** Two graphical tests confirm that the OFZ is a transform fault. a) On an oblique Mercator map where the pole of projection has been shifted to the Arabia–India rotation pole (12.1°N, 76.2°E; Fournier et al., 2008a), the OFZ is aligned with Eulerian parallels (black dashed line), as expected for a transform fault. Between 16.5°N and 20.3°N, the fault trace is deviated from the horizontal reference line by a paired bend, but returns to it once the bend is passed. A small circle about the closure-enforced MORVEL Arabia–India rotation pole (blue dashed line; DeMets et al., 2010) is parallel to a horizontal straight line south of 18.5°N and diverge increasingly from it north of 18.5°N. Six apparently uninterrupted fault segments are labelled from 1 to 6. b) Great circles perpendicular to the fault trace intersect near the Arabia–India rotation pole (12.1°N, 76.2°E) shown by a red star with its 95% confidence ellipse. The best-fitting MORVEL Arabia–India pole is shown by an open circle (DeMets et al., 2010). The closure-enforced MORVEL Arabia–India pole (−3.2°N, 116.6°E) and the GPS-based Arabia–India pole of Reilinger et al. (2006; 17.7°N, 110.9°E) are located more than 30° toward the east.

compressional structures adjacent to the restraining bend are deduced from the seafloor morphology east of the fault and from the observation of folds and reverse faults in the recent deposits on 3.5 kHz profiles. At the northern end of the OFZ, a second restraining bend associated with folds on the Indian plate side is observed.

To further test the transform motion of the OFZ, we determined the location of the Arabia–India pole from the great circles perpendicular to the fault. As shown in Fig. 2b, the great circles perpendicular to the fault strike, measured out of releasing or restraining bends, intersect close to the rotation pole independently determined from GPS and seismicity data (Fournier et al., 2008a), and close to the best-fitting Arabia–India pole determined from geological data (fault azimuths; DeMets et al., 2010). The closure-enforced MORVEL Arabia–India rotation pole (DeMets et al., 2010), which is located much farther to the east (3.2°S, 116.6°E), predicts right-lateral slip parallel to the OFZ between 15°N and 18.5°N, becoming more and more extensional north of 18.5°N (Fig. 2a). Thus, recent kinematic models agree that the present-day OFZ is a pure strike-slip plate boundary over ~400 km between 15°N and 18.5°N and that, north of 18.5°N, the motion is dominantly strike-slip, but a small component of boundary-normal extensional motion cannot be excluded. MORVEL solution requires a partitioning mechanism north of 18.5°N to accommodate the predicted extensional component of boundary-normal motion, since segments 4 and 5 are pure strike-slip (Fig. 2a). On the other hand, MORVEL prediction is pure strike-slip along segment 6, at the entrance of the Dalrymple horsetail, whereas our model would imply a small component of compression. Non strike-slip components, either extensional or compressional, are expected to be so small that, if distributed over a wide area, they may be difficult to recognize.

## 3. Age of the active fault system

The active fault system crosscuts the Owen Ridge and offsets it dextrally. The total displacement is well constrained between 10 and 12 km by two strike-slip offsets of morphologic features (Fig. 1a and b). A long-term extrapolation of the GPS-derived slip rate of the OFZ ($3\pm1$ mm yr$^{-1}$) would restore the observed offset in ~3 to 6 Ma. The small finite offset therefore testifies that the present-day fault system initiated recently, most probably during the Pliocene.

The reconstruction of the Arabia–India plate motion from the Somalia-Arabia and Somalia-India plate motion models (Fournier et al., 2010; Merkouriev and DeMets, 2006), indicates that the OFZ rate of motion remained nearly stable since oceanic spreading initiated in the Gulf of Aden 20 Ma ago (Chamot-Rooke et al., 2009). This result implies that, before the development of the present-day fault system, the Arabia–India motion was accommodated by an older fault system, or 'paleo OFZ', inactive since ~3–6 Ma.

The development of the present-day fault system postdates the uplift of the southern and central parts of the Owen Ridge. The onset of uplift of the southern Owen Ridge, related to vertical motions on the paleo OFZ (Weissel et al., 1992), is recorded by the transition from turbidites to pelagic sediments and is precisely dated by drilling of the Early Miocene (19 Ma; Shipboard Scientific Party, 1989; Whitmarsh et al., 1974). The onset of uplift of the Owen Ridge is synchronous of the initiation of seafloor spreading in the Gulf of Aden, constrained by the age of the oldest magnetic anomaly identified (An 6, 19.7 Ma; Fournier et al., 2010).

## 4. Tectonic record in the 20°N pull-apart basin

The main releasing bend along the OFZ is marked by a 90-km-long pull-apart basin at the latitude of 20°N (Fig. 3). The 20°N-Basin corresponds to a right step-over of 12 km between two master strike-slip faults trending N25°E south of the basin and N30°E north of it. The dimensions of the 20°N-Basin ($90\times12$ km) are of the same order than those of the Dead Sea pull-apart basin ($132\times16$ km; Ten Brink et al., 1993) along the Dead Sea strike-slip fault on the western side of the Arabian plate. The 20°N-Basin becomes wider (25 km) and deeper

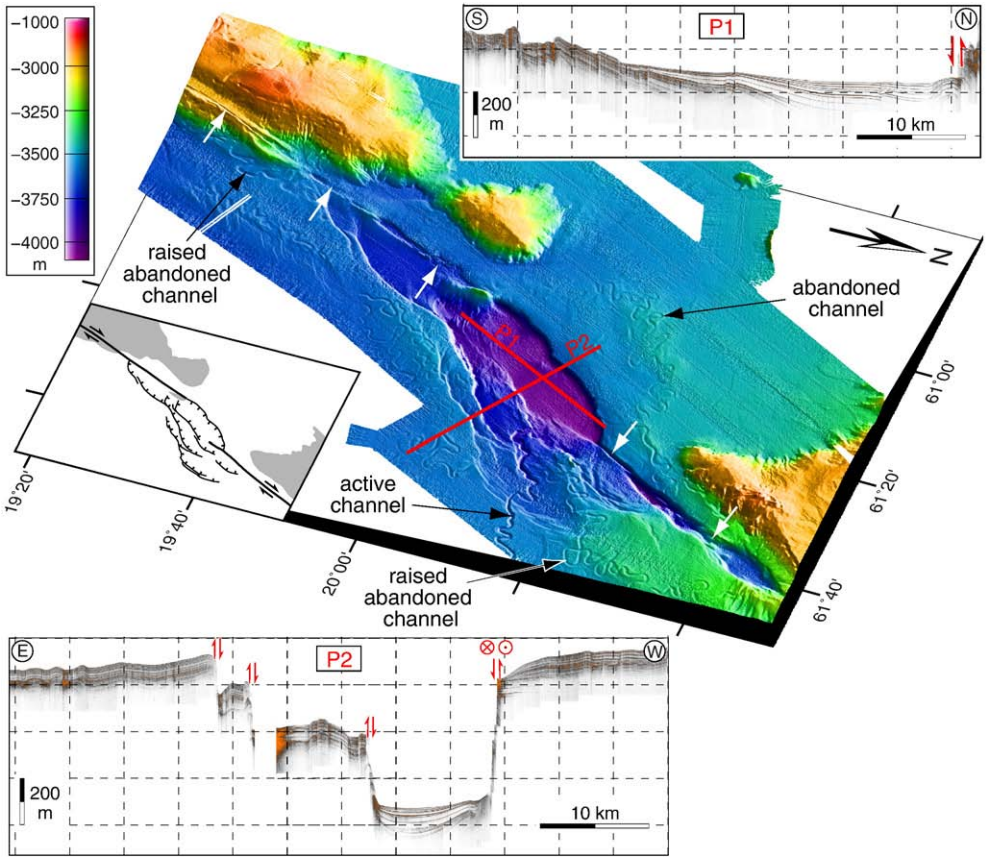


**Fig. 3.** The 20°N pull-apart basin is located at the main threshold of the Owen Ridge, south of the Qalhat Seamount. The basin is directly supplied in turbiditic deposits by an active channel of the Indus Fan. Two sub-bottom seismic profiles across the basin, along (P1) and perpendicular (P2) to its great axis, show that the turbiditic deposits, characterized on profiles by an alternation of thin highly reflective levels and thick transparent layers, are tilted towards the north due to motion of the border normal fault. White arrows indicate the master strike-slip faults.

(4050 m) to the north, where it is bounded to the west by a master normal fault scarp with a vertical throw of 500 m, and to the east by three normal fault scarps with throws between 100 and 300 m stepping down towards the basin axis (profile P2 in Fig. 3).

The spindle shape of the 20°N-Basin can be compared to pull-apart basins of sandbox analogue models formed in pure strike-slip or transtensional setting (Smit et al., 2008; Wu et al., 2009). The overall geometry of the 20°N-Basin compares closely with pull-aparts developed in a pure strike-slip regime (Wu et al., 2009). In particular, the 20°N-Basin does not exhibit margins of en-echelon oblique-extensional faults, typical of transtensional basins. This observation further confirms that the OFZ is a pure strike-slip feature.

The 20°N-Basin is directly supplied in turbidity–current deposits by an active channel of the Indus Fan (the mouth of the Indus river is 800 km away towards the northeast), which deeply incises the recent deposits (Fig. 3). The channel displays a moderate sinuosity, compared with nearby highly meandering abandoned channels, which attests to a resumption of erosion on a steeper gradient. Similar changes in gradient are evidenced by abandoned channels, raised and tilted in the vicinity of the active faults (Fig. 3), indicating local tectonic uplift provoked by the fault motion. The trace of the active faults bounding the 20°N-Basin is not obscured by turbiditic deposits despite the slow rate of slip of the OFZ. The preservation of normal fault scarps bounding the basin indicates that the rate of vertical (dip-slip) motion along the faults has exceeded the rate of deposition and burial by the sediments of the Indus Fan. The tectonic process is therefore dominant over deposition.

Sub-bottom seismic profiles (3.5 kHz) across the 20°N-Basin show that the basin is asymmetric with a turbidite sequence that becomes thicker towards the north, where the present-day depocentre of the basin is located (profile P1 in Fig. 3). Turbiditic currents feeding the 20°N-Basin could be related to the regional seismicity and/or to the activity of the Indus River in relation with sea-level variations. The basin could thus preserve a record of the seismic activity of the OFZ in its sediments, and possibly of the seismicity of the Makran subduction zone.

## 5. Terminations of the Owen Fracture Zone

At its both tips, the OFZ terminates into extensional structures associated with basins. To the north, the OFZ ends into the Dalrymple Trough by a system of regularly spaced normal faults that branch from the master strike-slip fault and form a spectacular 30-km-wide horsetail splay (Fig. 4a). The normal faults delineate a series of deep basins (up to 4000 m deep), which constitute the southern part of the Dalrymple Trough. The horsetail splay is indicative of slip dying out gradually towards the northern tip of the OFZ. To the south in contrast, the OFZ terminates abruptly into the Beautemps–Beaupré Basin, a 50-km-wide and 120-km-long basin bounded by two N70-N90°E-trending conjugate master normal faults (Fig. 4b; Fournier et al., 2008b). The basin is characterized by a strong negative gravity anomaly in relation with a thick sedimentary infill of at least 3–4 km. Recent works on the Arabia–India–Somalia triple junction showed that the Arabia–India motion was transferred to the west of the Beautemps–Beaupré Basin along a dextral shear zone, which joins southward the Sheba Ridge axis (Fournier et al., 2010). Numerous landslide scars are observed on the slopes of the Beautemps–Beaupré Basin and the southern Owen Ridge (Fig. 4b and c). Giant landslides, probably triggered by earthquakes along the active fault system, massively impinge the western flank of the Owen Ridge and were evacuated westward in the Owen Basin. Because of their huge volume,

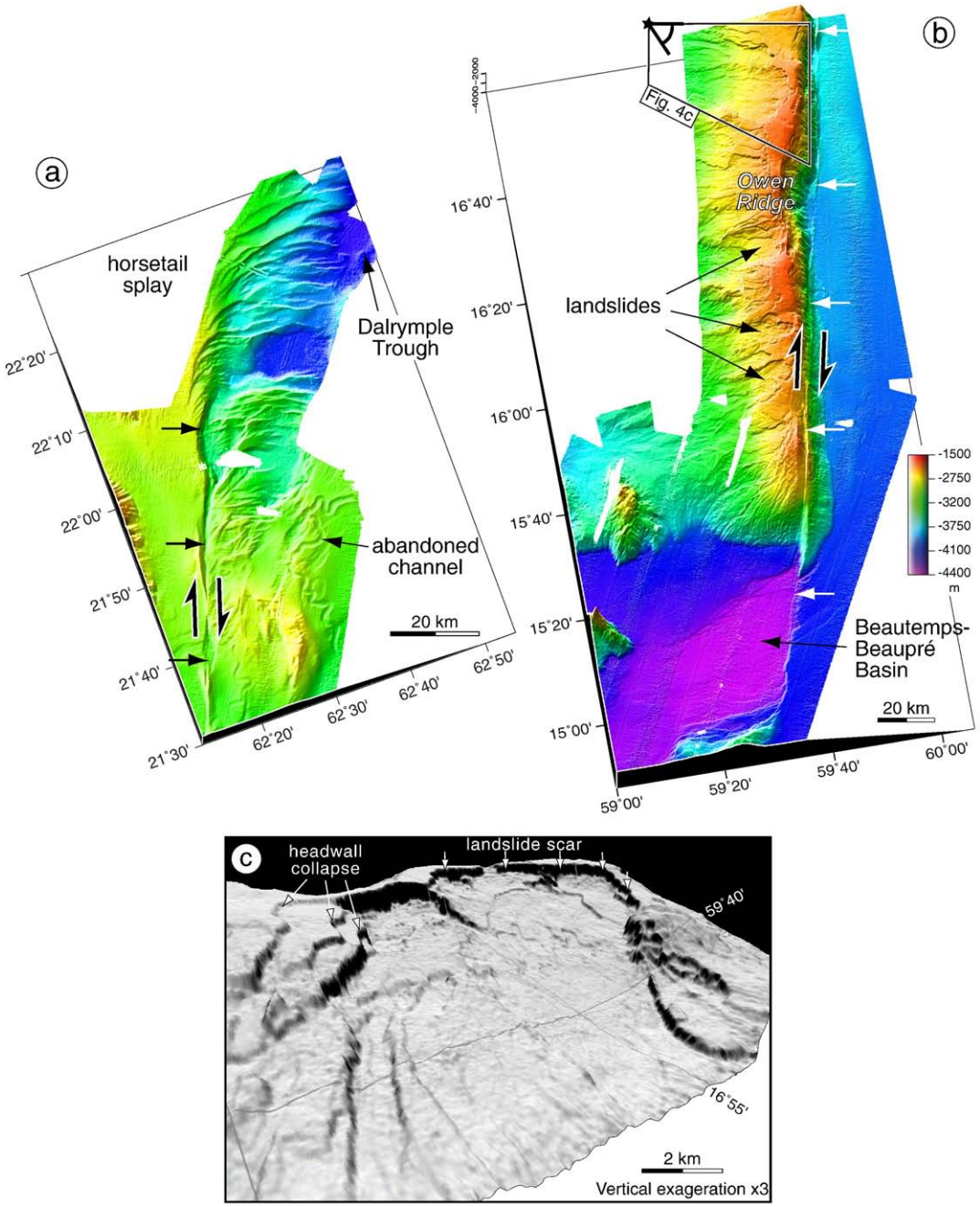


**Fig. 4.** a) The horsetail splay of the Dalrymple Trough developed in the northern tip-damage zone of the OFZ. Normal faults branch from the master strike-slip fault at low angles, curve progressively and become parallel to the maximum horizontal stress. b) Giant submarine landslides, probably due to strong ground motions from earthquakes of nearby active faults, occurred on western flank of the Owen Ridge and are suspected to have generated tsunami (Heidarzadeh et al., 2008b). c) Perspective view from the northwest of a multi-events generated landslide and related headwall collapses. This landslide removed up to 14 $km^3$ of material from the pelagic cover of the Owen Ridge (Rodriguez et al., 2010). Location in Figure 4b.

these mass failures represent a potential source of tsunami for the nearby coasts of Oman (Donato et al., 2009; Okal et al., 2006).

## 6. Conclusion

Our work sheds light on a previously unknown 800-km-long active fault system associated with giant landslides at the Arabia–India plate boundary. These results will motivate a reappraisal of the seismic and tsunami hazard assessment in the NW Indian Ocean (Heidarzadeh et al., 2008a; Okal and Synolakis, 2008). We show that the OFZ is a pure strike-slip boundary between the Arabian and Indian plates. The geometry of the active fault system is probably controlled both by the pre-existing faults of the paleo OFZ and by the topography of the Owen Ridge since the 20°N-Basin is located at the main threshold of the ridge. Extrapolating the present-day slip rate of the OFZ for 3–6 Ma accounts for its total displacement. The initiation of strike-slip motion along the present-day fault system does not coincide with any tectonic event recorded on land in Oman (Fournier et al., 2004, 2006; Lepvrier et al., 2002), but is coeval with a major tectonic reorganization of the Arabia–Eurasia collision from western Turkey to Iran between 3 and 7 Ma (Allen et al., 2004; Axen et al., 2001; Shabanian et al., 2009) deduced from the extrapolation of short-term deformation rates. It is also synchronous with the initiation of extrusion of Anatolia ca. 5 Ma (Armijo et al., 1999) and the onset of seafloor spreading in the Red Sea 4–5 Ma ago (Cochran and Karner,

2007). The lateral transport of the Anatolian lithosphere out of the collision zone could be at the origin of this widespread reorganization, including initiation of the present-day fault system at the Arabia–India plate boundary.

## Acknowledgements

We are indebted to the Captain Geoffroy de Kersauson, officers, and crew members of the *BHO Beautemps-Beaupré*, and to the French Navy hydrographers Vincent Lamarre and Yves-Marie Tanguy, and the hydrographic team of the 'Groupe Océanographique de l'Atlantique', for their assistance in data acquisition. We acknowledge the support of SHOM, IFREMER, and INSU-CNRS for the Owen cruise. We thank Thierry Garlan from SHOM for making available bathymetric data of the Fanindien survey. We also thank C. DeMets his insightful review.

## References

Allen, M., Jackson, J., Walker, R., 2004. Late Cenozoic reorganization of the Arabia–Eurasia collision and the comparison of short-term and long-term deformation rates. Tectonics 23, TC2008, doi:10.1029/2003TC00153.

Armijo, R., Meyer, B., Hubert-Ferrari, A., Barka, A.A., 1999. Propagation of the North Anatolian fault into the northern Aegean: timing and kinematics. Geology 27, 267–270.

Axen, G.J., Lam, P.S., Grove, M., Stockli, D.F., Hassanzadeh, J., 2001. Exhumation of the west-central Alborz Mountains, Iran, Caspian subsidence, and collision-related tectonics. Geology 29 (6), 559–562.

Chamot-Rooke, N., Fournier, M., Scientific Team of AOC and OWEN cruises, 2009. Tracking Arabia–India motion from Miocene to Present. American Geophysical Union, Fall Meeting 2009.

Chaubey, A.K., Dyment, J., Bhattacharya, G.C., Royer, J.-Y., Srinivas, K., Yatheesh, V., 2002. Paleogene magnetic isochrons and paleo-propagators in the Arabian and Eastern Somali basins, Northwest Indian Ocean. In: Clift, P., Kroon, D., Gaedicke, C., Craig, J. (Eds.), The Tectonic and Climatic Evolution of the Arabian Sea Region: Geological Society Special Publication, 195, pp. 71–85.

Clift, P.D., Shimizu, N., Layne, G.D., Blusztain, J.S., Gaedicke, C., Schluter, H.U., Clark, M.K., Amjad, S., 2001. Development of the Indus Fan and its significance for the erosional history of the Western Himalaya and Karakoram. Geol. Soc. Am. Bull. 113 (8), 1039–1051.

Cochran, J.R., Karner, G.D., 2007. Constraints on the deformation and rupturing of continental lithosphere of the Red Sea: the transition from rifting to drifting. In: James, K.H., Lorente, M.A., Pindell, J.L. (Eds.), The Origin and Evolution of the Caribbean Plate: Geol. Soc. Spec. Pub., 282, pp. 265–289, doi:10.1144/SP282.13.

DeMets, C., Gordon, R.G., Argus, D.F., Stein, S., 1990. Current plate motions. Geophys. J. Int. 101, 425–478.

DeMets, C., Gordon, R.G., Argus, D.F., Stein, S., 1994. Effect of recent revisions of the geomagnetic reversal time scale on estimates of current plate motions. Geophys. Res. Lett. 21, 2191–2194.

DeMets, C., Gordon, R.G., Argus, D.F., 2010. Geologically current plate motions. Geophys. J. Int. 181, 1–80, doi:10.1111/j.1365-246X.2009.04491.x.

Donato, S.V., Reinhardt, E.G., Boyce, J.I., Pilarczyk, J.E., Jupp, B.P., 2009. Particle-size distribution of inferred tsunami deposits in Sur Lagoon, Sultanate of Oman. Mar. Geol. 257, 54–64.

Edwards, R.A., Minshull, T.A., White, R.S., 2000. Extension across the Indian–Arabian plate boundary: the Murray Ridge. Geophys. J. Int. 142, 461–477.

Edwards, R.A., Minshull, T.A., Flueh, E.R., Kopp, C., 2008. Dalrymple Trough: an active oblique-slip ocean-continent boundary in the northwest Indian Ocean. Earth Planet. Sci. Lett. 272, 437–445.

Ellouz-Zimmermann, N., et al., 2007. Offshore frontal part of the Makran Accretionary prism: the Chamak survey (Pakistan). In: Lacombe, O., Lavé, J., Roure, F., Vergés, J. (Eds.), Thrust Belts and Foreland Basins - From Fold Kinematics to Hydrocarbon System, Frontiers in Earth Science Series. Springer Berlin Heidelberg, pp. 351–366.

Fournier, M., Patriat, P., Leroy, S., 2001. Reappraisal of the Arabia–India–Somalia triple junction kinematics. Earth Planet. Sci. Lett. 189, 103–114.

Fournier, M., Bellahsen, N., Fabbri, O., Gunnell, Y., 2004. Oblique rifting and segmentation of the NE Gulf of Aden passive margin. Geochem. Geophys. Geosyst. 5, Q11005, doi:10.1029/2004GC000731.

Fournier, M., Lepvrier, C., Razin, P., Jolivet, L., 2006. Late Cretaceous to Paleogene post-obduction extension and subsequent Neogene compression in the Oman Mountains. GeoArabia 11, 17–40.

Fournier, M., Chamot-Rooke, N., Petit, C., Fabbri, O., Huchon, P., Maillot, B., Lepvrier, C., 2008a. In-situ evidence for dextral active motion at the Arabia–India plate boundary. Nat. Geosci. 1, 54–58, doi:10.1038/ngeo.2007.24.

Fournier, M., Petit, C., Chamot-Rooke, N., Fabbri, O., Huchon, P., Maillot, B., Lepvrier, C., 2008b. Do ridge-ridge-fault triple junctions exist on Earth? Evidence from the Aden–Owen–Carlsberg junction in the NW Indian Ocean. Basin Res. 20, 575–590, doi:10.1111/j.1365-2117.2008.00356.x.

Fournier, M., Chamot-Rooke, N., Petit, C., Huchon, P., Al-Kathiri, A., Audin, L., Beslier, M.O., d'Acremont, E., Fabbri, O., Fleury, J.M., Khanbari, K., Lepvrier, C., Leroy, S., Maillot, B., Merkouriev, S., 2010. Arabia–Somalia plate kinematics, evolution of the Aden–Owen–Carlsberg triple junction, and opening of the Gulf of Aden. J. Geophys. Res. 115, B04102, doi:10.1029/2008JB006257.

Gaedicke, C., Prexl, A., Schlüter, H.U., Meyer, H., Roeser, H., Clift, P., 2002. Seismic stratigraphy and correlation of major regional unconformities in the northern Arabian Sea. In: Clift, P.D., Kroon, D., Gaedicke, C., Craig, J. (Eds.), The Tectonic and Climatic Evolution of the Arabian Sea Region: Geological Society, London, Special Publications, 195, pp. 25–36.

Gordon, R.G., DeMets, C., 1989. Present-day motion along the Owen fracture zone and Dalrymple trough in the Arabian Sea. J. Geophys. Res. 94, 5560–5570.

Heidarzadeh, M., Pirooz, M.D., Zaker, N.H., Yalciner, A.C., 2008a. Preliminary estimation of the tsunami hazards associated with the Makran subduction zone at the northwestern Indian Ocean. Nat. Hazards, doi:10.1007/s11069-008-9259-x.

Heidarzadeh, M., Pirooz, M.D., Zaker, N.H., Yalciner, A.C., Mokhtari, M., Esmaeily, A., 2008b. Historical tsunami in the Makran Subduction Zone off the southern coasts of Iran and Pakistan and results of numerical modeling. Ocean Eng. 35, 774–786.

Le Pichon, X., Kreemer, C., Chamot-Rooke, N., 2005. Asymmetry in elastic properties and the evolution of large continental strike-slip faults. J. Geophys. Res. 110, B03405, doi:10.1029/2004JB003343.

Lebrun, J.-F., Lamarche, G., Collot, J.-Y., 2003. Subduction initiation at a strike-slip plate boundary: the Cenozoic Pacific–Australian plate boundary, south of New Zealand. J. Geophys. Res. 108 (B9), 2453, doi:10.1029/2002JB002041.

Lepvrier, C., Fournier, M., Bérard, T., Roger, J., 2002. Cenozoic extension in coastal Dhofar (southern Oman): implications on the oblique rifting of the gulf of Aden. Tectonophysics 357, 279–293.

Mann, P., 2007. Global catalogue, classification and tectonic origins of restraining- and releasing bends on active and ancient strike-slip fault systems. Geol. Soc. London Spec. Pub., 290, pp. 13–142.

Massell, C., Coffin, M.F., Mann, P., Mosher, S., Frohlich, C., Schuur, C.L., Karner, G.D., Ramsay, D., Lebrun, J.F., 2000. Neotectonics of the Macquarie ridge complex, Australia–Pacific plate boundary. J. Geophys. Res. 105, 13457–13480.

Matthews, D.H., 1966. The Owen fracture zone and the northern end of the Carlsberg Ridge. Phil. Trans. R. Soc. A 259, 172–186.

Merkouriev, S., DeMets, C., 2006. Constraints on Indian plate motion since 20 Ma from dense Russian magnetic data: implications for Indian plate dynamics. Geochem. Geophys. Geosyst. 7, Q02002, doi:10.1029/2005GC001079.

Mountain, G.S., Prell, W.L., 1990. A multiphase plate tectonic history of the southeast continental margin of Oman. In: Robertson, A.H.F., Searle, M.P., Ries, A.C. (Eds.), The Geology and Tectonics of the Oman Region: Geol. Soc. London Spec. Pub., 49, pp. 725–743.

Okal, E.A., Synolakis, C.E., 2008. Far-field tsunami hazard from mega-thrust earthquakes in the Indian Ocean. Geophys. J. Int. 172, 995–1015.

Okal, E.A., Fritz, H.M., Raad, P.E., Synolakis, C.E., Al-Shijbi, Y., Al-Saifi, M., 2006. Oman field survey after the December 2004 Indian Ocean tsunami. Earthquake Spectra 22 (S3), S203–S218.

Quittmeyer, R.C., Kafka, A.L., 1984. Constraints on plate motions in southern Pakistan and the northern Arabian Sea from the focal mechanisms of small earthquakes. J. Geophys. Res. 89, 2444–2458.

Reilinger, R., et al., 2006. GPS constraints on continental deformation in the Africa–Arabia–Eurasia continental collision zone and implications for the dynamics of plate interactions. J. Geophys. Res. 111, B05411, doi:10.1029/2005JB004051.

Rodriguez, M., Fournier, M., Chamot-Rooke, N., Huchon,P., 2010. Mass wasting processes and giant landslides along the Owen fracture zone (Northwest Indian Ocean), American Geophysical Union, Fall Meeting 2010.

Royer, J.-Y., Chaubey, A.K., Dyment, J., Bhattacharya, G.C., Srinivas, K., Yatheesh, V., Ramprasad, T., 2002. Paleogene plate tectonic evolution of the Arabian and Eastern Somali basins. In: Clift, P., Kroon, D., Gaedicke, C., Craig, J. (Eds.), The Tectonic and Climatic Evolution of the Arabian Sea Region: Geol. Soc. Spec. Pub., 195, pp. 7–23.

Shabanian, E., Siame, L., Bellier, O., Benedetti, L., Abbassi, M.R., 2009. Quaternary slip rates along the northeastern boundary of the Arabia–Eurasia collision zone (Kopeh Dagh Mountains, Northeast Iran). Geophys. J. Int. 178, 1055–1077, doi:10.1111/j.1365-246X.2009.04183.x.

Shipboard Scientific Party, 1989. Site 731. In: Prell, W.L., Niitsuma, N., et al. (Eds.), Proc. ODP, Init. Repts., 117: College Station, TX (Ocean Drilling Program), pp. 585–652.

Smit, J., Brun, J.P., Cloetingh, S., Ben-Avraham, Z., 2008. Pull-apart basin formation and development in narrow transform zones with application to the Dead Sea Basin. Tectonics 27, doi:10.1029/2007TC002119.

Stein, R.S., Barka, A.A., Dieterich, J.H., 1997. Progressive failure of the North Anatolian Fault since 1939 by earthquake stress triggering. Geophys. J. Int. 128, 594–604, doi:10.1111/j.1365-246X.1997.tb05321.x.

Ten Brink, U.S., Ben-Avraham, Z., Bell, R.E., Hassouneh, M., Coleman, D.F., Andreasen, G., Tibor, G., Coakley, B., 1993. Structure of the Dead Sea pull-apart basin from gravity analyses. J. Geophys. Res. 98 (B12), 21,877–21,894, doi:10.1029/93JB02025.

Weber, M., et al., 2009. Anatomy of the Dead Sea Transform from lithospheric to microscopic scale. Rev. Geophys. 47, RG2002, doi:10.1029/2008RG000264.

Weissel, J.K., Childers, V.A., Karner, G.D., 1992. Extensional and Compressional Deformation of the Lithosphere in the Light of ODP Drilling in the Indian Ocean. Synthesis of Results from Scientific Drilling in the Indian Ocean, Geophysical Monography 70, American Geophysical Union.

Whitmarsh, R.B., 1979. The Owen Basin off the south-east margin of Arabia and the evolution of the Owen Fracture Zone. Geophys. J. R. Astron. Soc. 58, 441–470.

Whitmarsh, R.B., Weser, O.E., Ross, D.A., 1974. Initial report DSDP, v. 23. U.S. Government Printing Office, Washington, D.C, p. 1180.

Wilson, T.J., 1965. A new class of faults and their bearing on continental drift. Nature 207, 343–347.

Wu, J.E., McClay, K., Whitehouse, P., Dooley, T., 2009. 4D analogue modelling of transtensional pull-apart basins. Mar. Pet. Geol. 26, 1608–1623.

Geochemistry Geophysics Geosystems G3

*Article*
Volume 12, Number 12
17 December 2011
Q12006, doi:10.1029/2011GC003731
ISSN: 1525-2027

Published by AGU and the Geochemical Society

# Neotectonics of the Owen Fracture Zone (NW Indian Ocean): Structural evolution of an oceanic strike-slip plate boundary

**M. Rodriguez**
*Institut des Sciences de la Terre de Paris, UMR 7193, Université Pierre et Marie Curie, CNRS, Case 129, 4 place Jussieu, F-75252 Paris CEDEX 05, France*

*Laboratoire de Géologie, UMR 8538, Ecole Normale Supérieure, 24 rue Lhomond, F-75231 Paris CEDEX 05, France (rodriguez@geologie.ens.fr)*

**M. Fournier**
*Institut des Sciences de la Terre de Paris, UMR 7193, Université Pierre et Marie Curie, CNRS, Case 129, 4 place Jussieu, F-75252 Paris CEDEX 05, France*

**N. Chamot-Rooke**
*Laboratoire de Géologie, UMR 8538, Ecole Normale Supérieure, 24 rue Lhomond, F-75231 Paris CEDEX 05, France*

**P. Huchon**
*Institut des Sciences de la Terre de Paris, UMR 7193, Université Pierre et Marie Curie, CNRS, Case 129, 4 place Jussieu, F-75252 Paris CEDEX 05, France*

**J. Bourget**
*Université Bordeaux 1, UMR 5805 EPOC, Avenue des Facultés, F-33405 Talence CEDEX, France*

**M. Sorbier**
*Laboratoire de Géologie, UMR 8538, Ecole Normale Supérieure, 24 rue Lhomond, F-75231 Paris CEDEX 05, France*

**S. Zaragosi**
*Université Bordeaux 1, UMR 5805 EPOC, Avenue des Facultés, F-33405 Talence CEDEX, France*

**A. Rabaute**
*Institut des Sciences de la Terre de Paris, UMR 7193, Université Pierre et Marie Curie, CNRS, Case 129, 4 place Jussieu, F-75252 Paris CEDEX 05, France*

[1] The Owen Fracture Zone is a 800 km-long fault system that accommodates the dextral strike-slip motion between India and Arabia plates. Because of slow pelagic sedimentation rates that preserve the seafloor expression of the fault since the Early Pliocene, the fault is clearly observed on bathymetric data. It is made up of a series of fault segments separated by releasing and restraining bends, including a major pull-apart basin at latitude 20°N. Some distal turbiditic channels from the Indus deep-sea fan overlap the fault system and are disturbed by its activity, thus providing landmarks to date successive stages of fault activity and structural evolution of the Owen Fracture Zone from Pliocene to Present. We determine the durability of relay structures and the timing of their evolution along the principal displacement zone, from their inception

Geochemistry Geophysics Geosystems G3



10.1029/2011GC003731

to their extinction. We observe subsidence migration in the 20°N basin, and alternate activation of fault splays in the vicinity of the Qalhat seamount. The present-day Owen Fracture Zone is the latest stage of structural evolution of the 20-Myr-old strike-slip fault system buried under Indus turbiditic deposits whose activity started at the eastern foot of the Owen Ridge when the Gulf of Aden opened. The evolution of the Owen Fracture Zone since 3–6 Myr reflects a steady state plate motion between Arabia and India, such as inferred by kinematics for the last 20 Myr period. The structural evolution of the Owen Fracture Zone since 20 Myr, including fault segments propagation and migration, pull-apart basin opening and extinction, seems to be characterized by a progressive reorganization of the fault system, and does not require any major kinematics change.

**Components:** 11,900 words, 15 figures.

**Keywords:** Indian Ocean; Owen Fracture Zone; pull-apart; transform fault.

**Index Terms:** 3039 Marine Geology and Geophysics: Oceanic transform and fracture zone processes; 8150 Tectonophysics: Plate boundary: general (3040); 8158 Tectonophysics: Plate motions: present and recent (3040).

**Received** 27 May 2011; **Revised** 12 October 2011; **Accepted** 18 October 2011; **Published** 17 December 2011.

Rodriguez, M., M. Fournier, N. Chamot-Rooke, P. Huchon, J. Bourget, M. Sorbier, S. Zaragosi, and A. Rabaute (2011), Neotectonics of the Owen Fracture Zone (NW Indian Ocean): Structural evolution of an oceanic strike-slip plate boundary, *Geochem. Geophys. Geosyst.*, *12*, Q12006, doi:10.1029/2011GC003731.

## 1. Introduction

[2] Large strike-slip faults in continental or oceanic domains display a variety of geological features that received considerable attention from researchers (see *Mann* [2007] for a synthesis). Of particular interest are structures transverse to the main strike-slip fault that take place in areas where the layout of the principal displacement zone is discontinuous or curved. These relay structures accommodate the transfer of slip between adjacent fault segments on both sides of the stepover region. Depending on fault geometry and local stress field, these discontinuities may undergo compression or extension, leading to the formation of a positive relief or a basin, forming a restraining bend or a releasing bend, respectively [*Sylvester*, 1988; *Cunningham and Mann*, 2007]. Strike-slip stepover regions are often considered as progressively increasing in structural relief (subsidence or uplift) with increasing slip along the principal displacement zone [*Aydin and Nur*, 1982; *Mann et al.*, 1983].

[3] In contrast, recent studies of the San Andreas fault system (*Wakabayashi et al.* [2004] and *Wakabayashi* [2007]) showed that some stepover regions may migrate along the main strike-slip fault. Further evidence of migration is found in the narrow, elongated Dead Sea pull-apart basin along the Levant fault [*Kashai and Croker*, 1987; *ten Brink and Ben-Avraham*, 1989; *Garfunkel and Ben-Avraham*, 1996; *ten Brink and Rybakov*, 1999; *Smit et al.*, 2008]. In both cases, little structural relieves are generated as compared to what would be expected from the progressive growth model. Basin migration is in contrast to prior observations that, within stepover basins, mature strike-slip systems tend to develop simple throughgoing faults that accommodate the relative motion [*Zhang et al.*, 1989; *Le Pichon et al.*, 2001; *Rangin and Le Pichon*, 2004; *Ben-Zion and Sammis*, 2003; *Wesnousky*, 2005; *Schattner and Weinberger*, 2008; *Wu et al.*, 2009; *Schattner*, 2010; *Garcia Moreno et al.*, 2011]. These works thus raise the question of the durability of relay structures and the timing of their evolution along the principal displacement zone, from their inception to their extinction.

[4] We recently surveyed a major strike-slip feature in the Northwest Indian Ocean, which forms the present-day India-Arabia plate boundary: the Owen Fracture Zone (OFZ hereafter) [*Matthews*, 1966; *Whitmarsh*, 1979; *Gordon and DeMets*, 1989; *Fournier et al.*, 2008b, 2011]. The OFZ is a 800 km-long dextral strike-slip fault which connects the Makran subduction zone to the north and the Aden-Owen-Carlsberg triple junction to the south (Figure 1). New bathymetry data collected during the Owen and FanIndien 2009 cruises reveal that fault scarps are well preserved on the seafloor and can be followed continuously over hundreds of kilometers, pointing to very active tectonics [*Fournier et al.*, 2011]. Although the overall geometry of the OFZ follows a small circle

Geochemistry Geophysics Geosystems G3



10.1029/2011GC003731

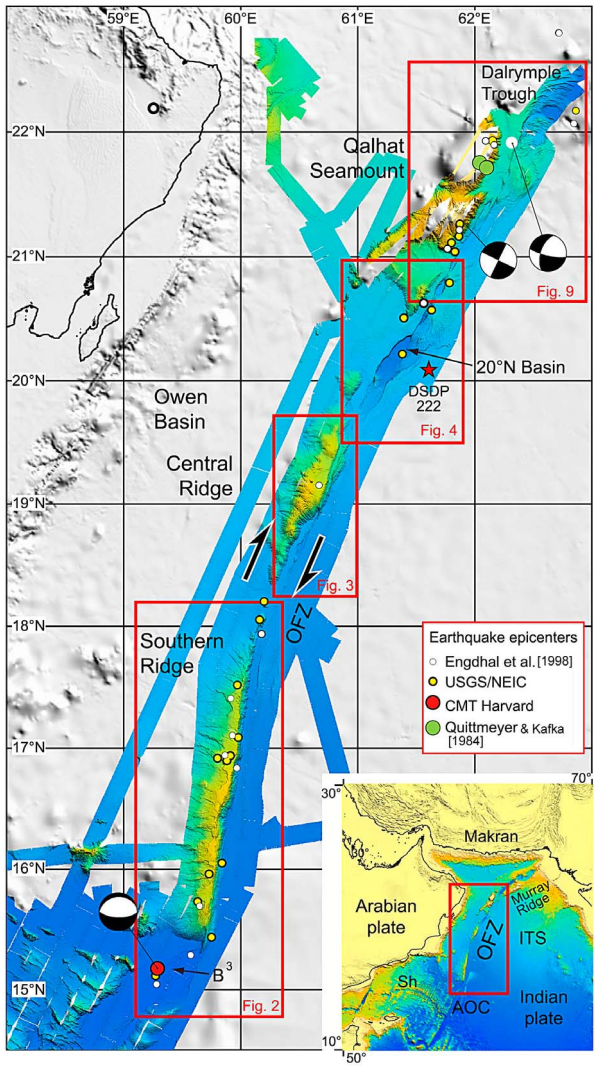


**Figure 1.** Multibeam bathymetric map of the Owen Fracture Zone acquired during the Owen and Fanindien cruises, with location of Figures 2 to 5. Shallow seismicity since 1973 (focal depth < 50 km, magnitude > 2), from USGS/NEIC database (yellow dots), *Engdahl et al.* [1998] (white dots), CMT Harvard database (red dots), and *Quittmeyer and Kafka* [1984] (green dots), and earthquake focal mechanisms for the Owen Fracture Zone. The seismicity along the OFZ is moderate, the maximum magnitude recorded to date being a Mw 5.8 earthquake. However, infrequent but large earthquake may be expected as at other slow boundaries. Inset shows the regional tectonic setting of the India-Arabia plate boundary. AOC: Aden-Owen-Carlsberg triple junction; $B^3$: Beautemps-Beaupré basin; ITS: Indus turbiditic system; OFZ: Owen Fracture Zone; Sh: Sheba Ridge.

about the India-Arabia pole of rotation (i.e., is a pure transform fault), the fault system displays a succession of releasing and restraining bends, with related tectonic features such as the 20°N pull-apart basin (Figure 1). South and North, the OFZ terminates into the Beautemps-Beaupré rhomboidal pull-apart basin and the Dalrymple Trough, respectively (Figure 1) [*Fournier et al.*, 2008a, 2011; *Edwards et al.*, 2008]. The objective of this paper is to constrain the timing of the structural evolution of the OFZ over the Plio-Pleistocene period. Since the OFZ is located at the western end of the Indus turbiditic system, distal turbiditic channels are strongly disturbed by neotectonics of this fault system and provide good landmarks to date the successive stages of fault activation and structural evolution of the OFZ. In some areas, transition from mass transport to pelagic deposition mode can also be related to tectonic events and constrain their dating.

## 2. Tectonic and Kinematic Setting

### 2.1. Main Structural Features of the Owen Fracture Zone and Present-Day Kinematics

[5] The overall shape of the OFZ is curved (Figure 1): the fracture zone azimuth increases progressively from N10°E at latitude 15°30′N (Beautemps-Beaupré Basin) to N31°E at the entrance of the Dalrymple Trough at 22°N. The OFZ closely follows a small circle about the rotation pole determined with GPS and seismicity data, which is consistent with a pure strike-slip motion along the entire fracture zone [*Fournier et al.*, 2011], in contrast with the increasing transtension north of 18°N predicted by the MORVEL closure-enforced pole [*DeMets et al.*, 2010]. The OFZ is made up of six apparently uninterrupted fault segments, ranging in length from 60 to 180 km [*Fournier et al.*, 2011]. The fault system is associated with a major morphological feature, the Owen Ridge, which rises up to 2000 m with respect to the surrounding seafloor. The Owen Ridge is disrupted by two morphological thresholds at 18°10′N and 20°N. The entire plate boundary can be divided into five geographic segments, starting from the Beautemps-Beaupré Basin (Figure 1): the southern ridge (300 km long), the central ridge (220 km long), the 20°N pull-apart basin (100 km long), the Qalhat seamount, and the Murray Ridge (which is not covered by our data set). As indicated by dextral strike-slip focal mechanisms of earthquakes along the OFZ (Figure 1) [*Quittmeyer and Kafka*, 1984; *Gordon and DeMets*, 1989; *Fournier et al.*, 2001], the Arabian plate moves northward slightly faster than the Indian plate with a relative motion of $3 \pm 1$ mm $yr^{-1}$ estimated independently from geodetic [*Reilinger et al.*, 2006; *Fournier et al.*, 2008b]

and geological [*DeMets et al.*, 1990, 1994, 2010] data.

### 2.2. History and Origin of the Owen Ridge and the Owen Fracture Zone

[6] Offsets on the seafloor imply a finite dextral displacement of 10–12 km along the OFZ (Figures 2 and 3) [*Fournier et al.*, 2008b, 2011]. Considering a steady motion of 3 ± 1 mm $yr^{-1}$, this indicates that the present-day trace of the OFZ has been active since 3–6 Myr. The reconstruction of the India-Arabia motion based on magnetic anomalies suggests that the rate of dextral strike-slip motion remained stable along the OFZ since the first stages of seafloor spreading in the Gulf of Aden [*Merkouriev and DeMets*, 2006; *Chamot-Rooke and Fournier*, 2009; *Fournier et al.*, 2010]. This would imply the existence of an at least ~20-Myr-old strike-slip fault system accommodating the Arabia-India motion at the Eastern foot of the Owen Ridge. The trace of the OFZ observed on the seafloor is the latest stage of this strike-slip activity. The southern and central segments of the Owen Ridge were uplifted along this ~20-Myr-old OFZ 19 Myr ago, as attested by the rapid transition from turbiditic to pelagic deposits in DSDP and ODP cores [*Whitmarsh et al.*, 1974; *Shipboard Scientific Party*, 1989; *Weissel et al.*, 1992]. *Patriat et al.* [2008] identify a kinematic change in seafloor spreading on the Southwest Indian Ridge at 24 Ma, and hypothesizes that the collision between Arabia and Eurasia induced a major plate reorganization phase at the scale of the Western Indian Ocean. The uplift and the initiation of seafloor spreading in the Gulf of Aden (dated at 19.7 Myr (Chron 6) [*Whitmarsh*, 1979; *Fournier et al.*, 2010]) most probably occurred in response to this plate reorganization event. The Dalrymple Trough at the northern end of the OFZ is of Early Miocene age too, with an increase in subsidence observed since the Late Miocene [*Edwards et al.*, 2000; *Gaedicke et al.*, 2002]. OBS data suggest that the trough developed along a small piece of continental crust, probably inherited from the fragmentation of the Gondwanaland [*Edwards et al.*, 2000, 2008; *Gaedicke et al.*, 2002]. At the northern end of the OFZ, the history of the Qalhat Seamount is not clearly established. The nature of the underlying basement remains unknown, as it has never been directly sampled, but the presence of the Little Murray Ridge volcanic seamounts buried under the Oman basin [*Gaedicke et al.*, 2002; *Mouchot*, 2009], coupled with the existence of a strong magnetic anomaly in the vicinity of the seamount and a typical flat top morphology, strongly suggest that the Qalhat Seamount is a volcanic guyot [*Edwards et al.*, 2000; *Fournier et al.*, 2011]. Onlap of Paleocene sediments onto the Qalhat seamount [*Edwards et al.*, 2000, 2008; *Gaedicke et al.*, 2002] demonstrates that the seamount is older than Paleocene.

### 2.3. The Owen Ridge and the Indus Fan

[7] The Owen Ridge acts as a topographic barrier for the Indus turbiditic system and isolates the Owen Basin, located west of the Owen Ridge, from any sediment supply from the east [*Whitmarsh*, 1979; *Mountain and Prell*, 1989]. The Indus turbiditic system covers 1.1 × $10^6$ $km^2$, stretching 1500 km into the Indian Ocean from the present delta front [*Clift et al.*, 2001]. The oldest sediments drilled suggest a Paleogene age for the emplacement of this sedimentary system [*Whitmarsh et al.*, 1974; *Shipboard Scientific Party*, 1989; *Weedon and McCave*, 1991; *Qayyum et al.*, 1997; *Ellouz-Zimmermann et al.*, 2007]. At its thickest part the fan is more than 9 km thick, but its thickness decreases westward when approaching the Owen and Murray Ridges (DSDP site 222 [*Shipboard Scientific Party*, 1974; *Clift et al.*, 2001; *Calvès*, 2008]). Seismic stratigraphy revealed that channel and levee complexes are most pronounced after the Early Miocene, coincident with a sharp increase in sedimentation rates related to the uplift of the Himalaya [*Clift et al.*, 2001]. ODP site 720 located at the southern extremity of the fan documents an alternation of pelagic and short turbiditic episodes over the entire Pleistocene sequence, in response to shifts in the loci of Indus Fan deposition [*Shipboard Scientific Party*, 1989; *Govil and Naidu*, 2008].

## 3. Methods and Data Set

### 3.1. Identification of the Structure of the Owen Fracture Zone

[8] Bathymetry and acoustic imagery were collected using a Kongsberg-Simrad EM 120 echosounder on board the R/V Beautemps-Beaupré operated by the French navy during the Owen and FanIndien 2009 surveys. A DEM at 80 m grid interval was produced as well as mosaics of the acoustic imagery (bottom reflectivity). In addition to bathymetry and reflectivity, the SBP120 subbottom profiler coupled with the EM120 provided a set of high frequency (3.5 kHz), high resolution profiles with penetration down to 100 m in fine grained sediments and about 25 m in sand rich

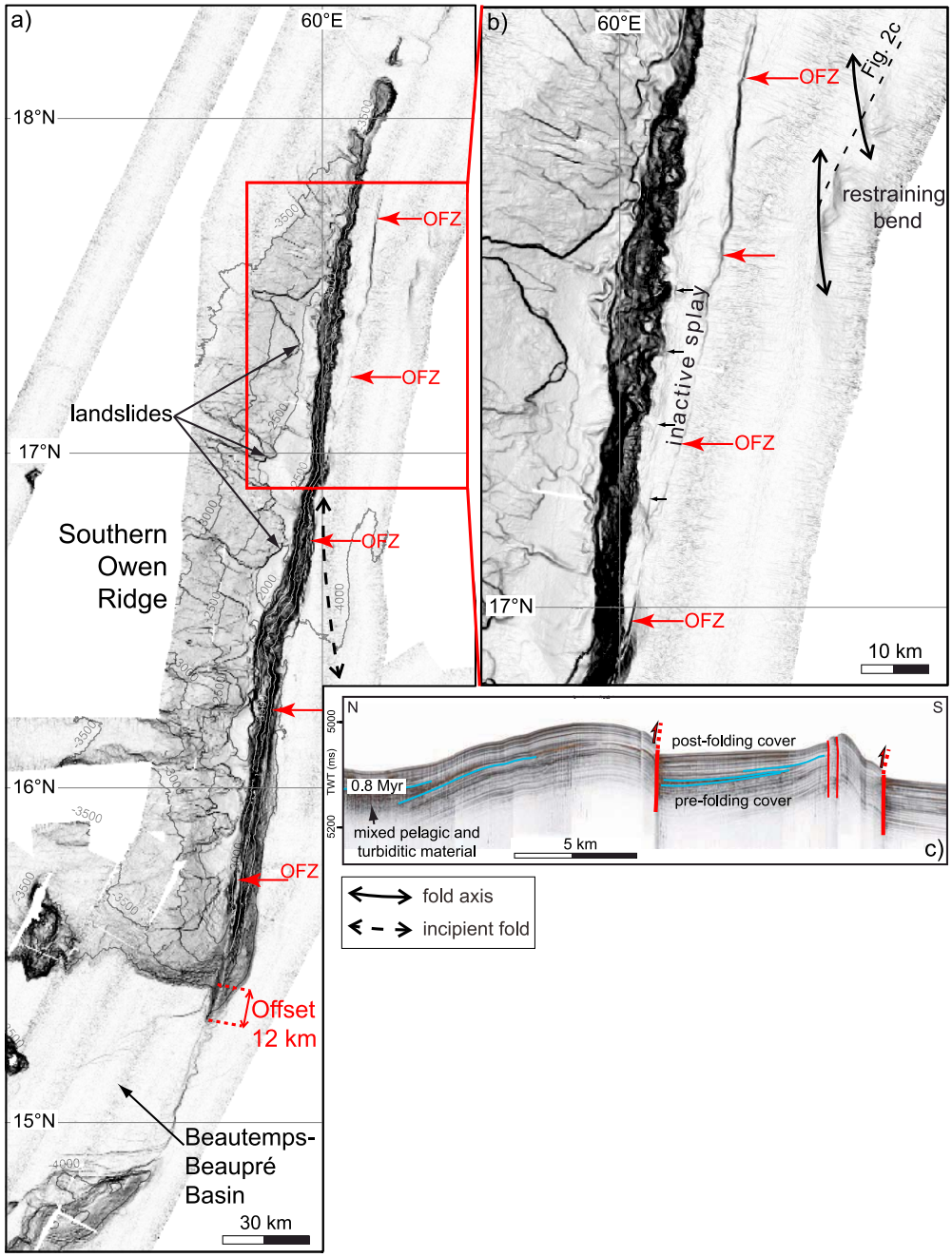


**Figure 2.** (a) Slope map of the OFZ along the southern Owen Ridge. (b) Inset shows the restraining bend which initiates where the trend of the linear segment of the OFZ slightly deviates and divides into two splays. The inactive splay is buried under mass transport deposits from the southern ridge. The maximal vertical throw of the OFZ is associated to the maximal vertical throw of the restraining bend. (c) 3.5 kHz profile running through the restraining bend (see Figure 2b for location). A slight and abrupt increase in folding is observed at ~0.8 Myr (see text).

floor. Only a AGC has been applied. Because of slow pelagic sedimentation rates along the OFZ since the Early Pliocene [*Shipboard Scientific Party*, 1974], the trace of the fault is well preserved on the seafloor. The fault traces observed on both bathymetric data and SBP120 profiles were mapped. Active faults are expected to be identified by a scarp at the seafloor. However, for some of these faults, it is difficult to assess whether they are active or not. Indeed, in areas dominated by pelagic deposition, the pelagic cover takes the exact shape of the underlying morphology and preserves fault

Geochemistry Geophysics Geosystems G3



10.1029/2011GC003731

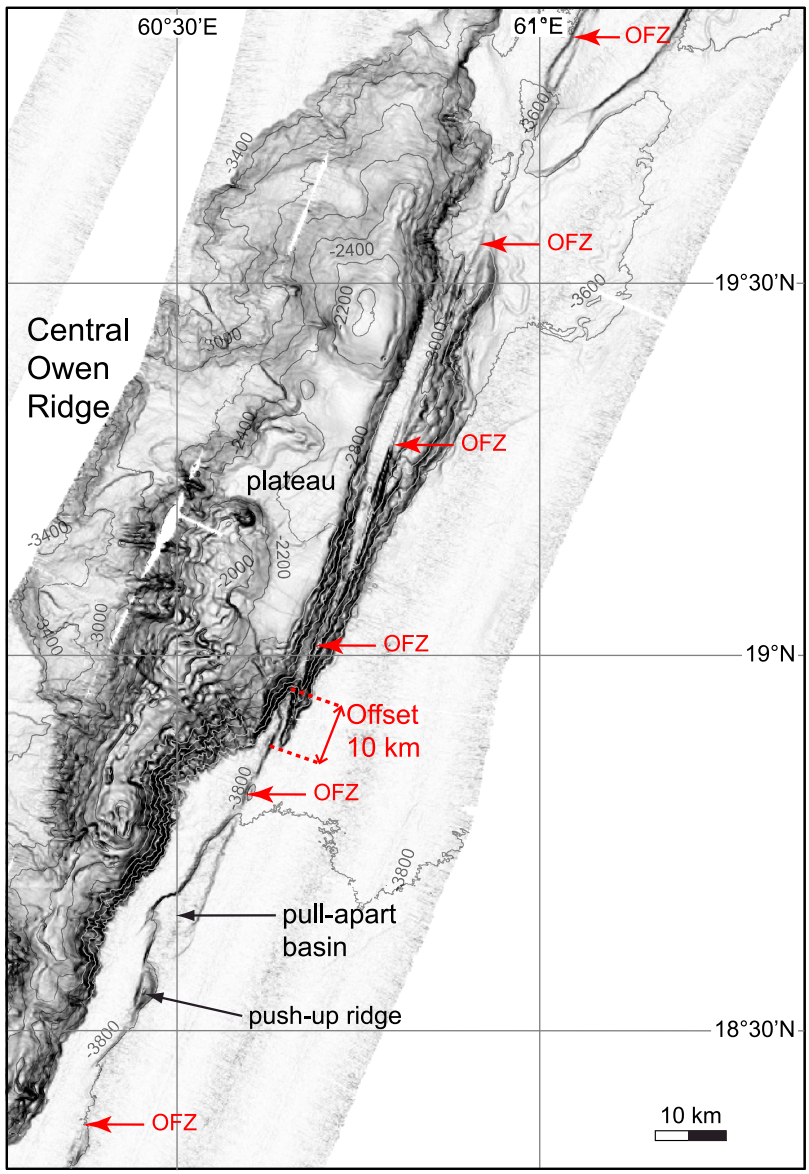


**Figure 3.** Slope map of the OFZ along the central Owen Ridge. A pull-apart basin is observed at 18°40′N. The OFZ offset dextrally the Owen Ridge over 10 km.

offsets through times. Thus the detection of offsets at the seafloor is not by itself an indicator of the present-day activity of the fault. On the other hand, active faults are well observed in areas dominated by turbiditic processes, since their frequency allows a good record of the progressive offset of growth-faults and associated sedimentary tilting.

## 3.2. Interpretation of Sedimentary Deposits on SBP120 (3.5 kHz) Profiles

[9] We recognize pelagic and turbiditic deposits in the sub-bottom high resolution profiles based on their seismic characters. Where SBP120 profiles display well stratified, continuous and conformable horizons, the deposits are interpreted as pelagic in origin. This interpretation is supported by correlation with DSDP site 222 drill hole (see Figure 1 for location), and by the analysis of a Küllenberg core (J. Bourget et al., Late Quaternary megaturbidites of the Indus Fan: Origin and stratigraphic significance, manuscript in preparation, 2011). Where SBP120 profiles display well-stratified horizons with successions of high and low amplitude reflections, or thick transparent horizons in pull-apart areas, the deposits are interpreted as turbiditic in origin. This interpretation is also supported by the analysis of a Küllenberg core (see Figure 4 for

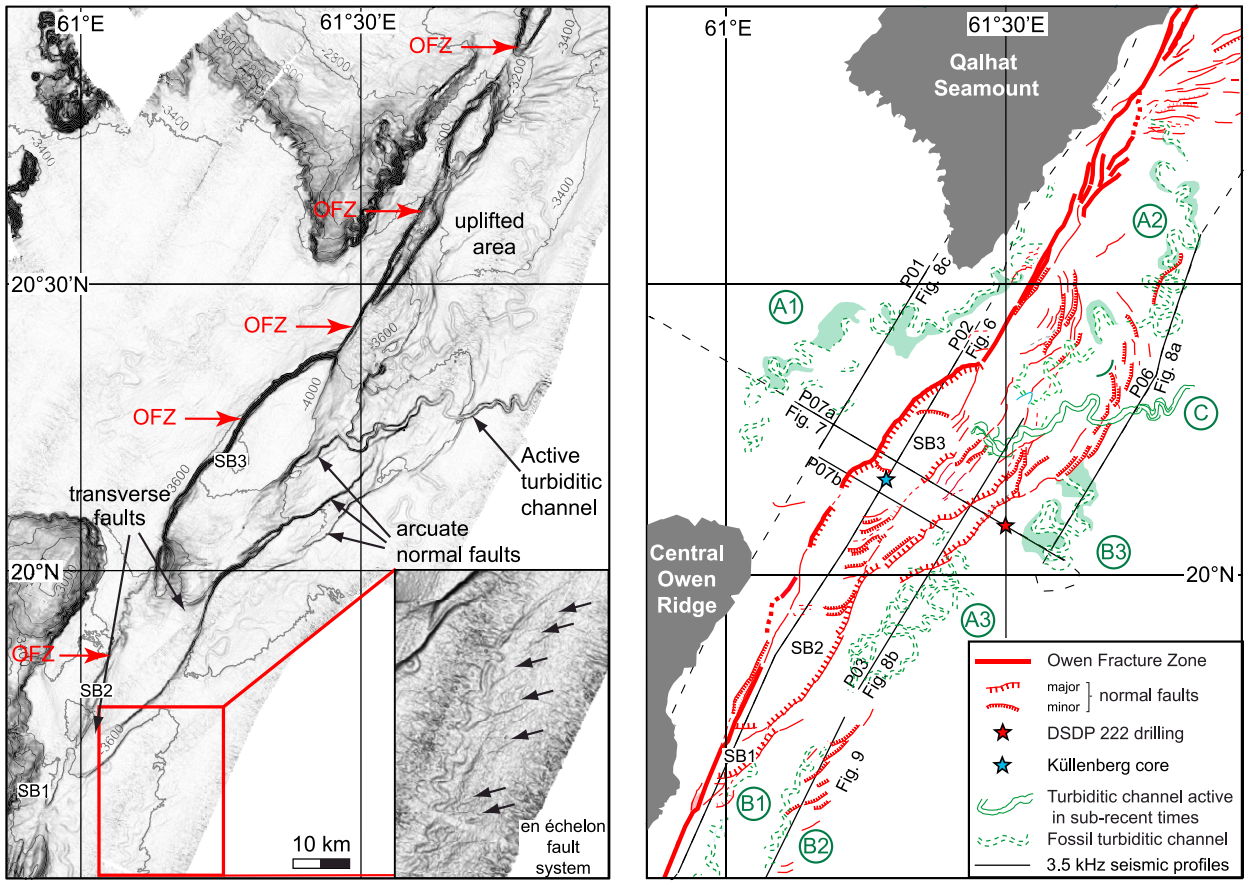


**Figure 4.** Slope map of the asymmetric 20°N pull-apart basin, and interpretative structural scheme. SB: sub-basin; A, B, C: channels. Inset shows the en-échelon fault system located to the southeast.

location) (Bourget et al., manuscript in preparation, 2011).

## 3.3. Age Estimates

[10] Several DSDP and ODP drillings are available in our studied area. Estimated sedimentation rates for the Pliocene pelagic interval are used to date the tectonic and sedimentary events we observe on SBP profiles. All pelagic sedimentation rates estimated at different drilling sites range between ~30 and ~50 m.Myr$^{-1}$ [*Shipboard Scientific Party*, 1974, 1989]. There is little spatial variation of Plio-Pleistocene pelagic sedimentation rates along the Owen Ridge, allowing large scale interpolation of these values. In this study, we use sedimentation rates estimated at site DSDP 222, because of its proximity to the OFZ. Sedimentation rates at site DSDP 222 quoted between 43 and 53 m.Myr$^{-1}$ for the last 2 Myr interval [*Shipboard Scientific Party*, 1974]. Two-way travel time to seismic reflectors was converted to depth using a P wave velocity of 1500 m.s$^{-1}$.

[11] A different approach based on the analysis of Küllenberg cores is used to estimate the age of turbiditic deposits in the 20°N pull-apart basin. Küllenberg cores were sampled in areas where turbiditic deposits are the thinnest in order to sample the highest number of turbiditic events. The high resolution of SBP 120 profiles allows correlation of turbiditic reflectors with turbiditic deposits identified on Küllenberg cores. Turbiditic deposits are dated using the $^{14}$C method on planctonic foraminifera sampled in undisturbed layers of the core. $^{14}$C ages obtained for the first turbiditic events are extrapolated to deeper horizons using the constant tilting rate of turbiditic horizons in the 20°N Basin. The method and the role of relative sea level variations in the turbiditic infill of the 20°N Basin are detailed in (Bourget et al., manuscript in preparation, 2011).

## 4. Results

[12] In this section, we describe the different segments of the OFZ fault system. We first focus

on the dominantly strike-slip portions, and then describe stepover areas. Each description focuses on the geomorphic expression of the OFZ, in relation with the turbiditic channels from the Indus Fan where present. We describe channels whose activity can be used as a time indicator for the relative and/or absolute age of the deformation in stepover areas. The depth of pull-apart basins is given with respect to the surrounding seafloor.

### 4.1. Dominantly Strike-Slip Segments: The South and Central Owen Ridge

[13] The southern Owen Ridge consists in a 300 km-long, 50 km-wide, and 2000 m-high, asymmetric relief, with a steep east-facing scarp associated with the OFZ and a gentle western slope dissected by numerous landslides (M. Rodriguez et al., Mass wasting processes along the Owen Ridge (NW Indian Ocean), submitted to *Marine Geology*, 2011) (Figure 2). To the south, the OFZ offsets the southern ridge dextrally over 12 km (Figure 2) [*Fournier et al.*, 2008b]. The area shows no evidence of vertical motion on the bathymetric data, suggesting dominantly pure strike-slip motion along this segment.

[14] Northward, a minor restraining bend is observed on the Indian plate side at the northern end of the southern ridge (Figure 2). The restraining bend corresponds to a series of gentle folds related to the slight deviation of the OFZ trend between 17°N and 18°N. At the same latitude, the vertical throw of the OFZ is maximum. The folds generate a relief up to 120-m-high (Figure 2). A similar gentle fold has been observed on ODP seismic profiles [*Shipboard Scientific Party*, 1989], which appears to have been active during the entire Pleistocene, accommodating about 150 m of vertical motion. Thus a small component of fault-normal compressional motion can be inferred in this area.

[15] The central Owen Ridge is a 220-km-long, 50-km-wide, and up to 1700-m-high relief (Figure 3). The central ridge displays an irregular morphology, with a 1300 m-high plateau spreading over 485 km$^2$ and seamounts dissected by complex networks of gullies and landslides (Rodriguez et al., submitted manuscript, 2011). The OFZ crosscuts the central ridge between 18°50′N and 19°35′N and offsets it dextrally over 10 km (Figure 3). Southeast of the central ridge (at latitude 18°40′N), a 7-km-wide stepover between two segments of the OFZ gives birth to a releasing bend associated with a small 25-km-long and 90-m-deep pull-apart basin.

### 4.2. The 20°N Pull-Apart Basin Releasing Bend

[16] The 20°N Basin is a 90-km-long and up to 35-km-wide pull-apart basin (Figure 4). The basin developed in a 12-km-wide stepover between two major strike-slip faults trending N25°E south of the basin and N30°E north of it. The overall structure of the basin is asymmetric, with the OFZ as a steep master fault on the western side, and a single normal fault dividing northward into several arcuate splays on the eastern side. The throw of arcuate normal faults clusters between 100 m and 300 m, and the associated topographic uplift decreases northward as the number of faults increases, suggesting partitioning of local extensional deformation. To the southeast of the 20°N basin, a system of en-échelon faults, oriented 25° clockwise with respect to the OFZ is observed between 19°18′N and 19°45′N (Figure 4).

[17] The bathymetric map shows three distinct sub-basins (labeled SB1, SB2, and SB3 in Figure 4). SB1 and SB2 extend over 70 km$^2$ and 340 km$^2$, respectively. SB3 extends over 590 km$^2$. E-W-trending transverse normal faults separate the sub-basins. The 20°N basin deepens abruptly northward, as sub-basins 1, 2, 3 form terraces respectively 60, 100, and 360 m deep with respect to the surrounding seafloor (Figure 5). Pelagic deposits blanket SB1 and SB2, as well as the half grabens of the eastern hanging wall, whereas recent turbiditic deposits filled in SB3 (Bourget et al., manuscript in preparation, 2011). In SB3, Indus turbiditic deposits adopt vertically a fanning configuration on the longitudinal SBP120 profile (Figure 5). The turbiditic infill forms a subtle and asymmetric syncline on transverse SBP120 profiles (Figure 6). A change of sense of asymmetry occurs along strike within SB3, where horizons within the southern part of the basin dip toward the west (profile P07b), whereas in the northern section, horizons dip to the east (profile P07a).

[18] Although SBP120 profiles do not reach the substratum of the 20°N basin, they give some insights about its deep structure. Turbiditic horizons onlap tilted blocks at the southern end of the 20°N basin (Figure 5). Turbiditic reflectors are slightly disturbed in the northern part of the 20°N basin, as a series of small buried benches, probably related to the activity of a minor normal fault (Figure 5).

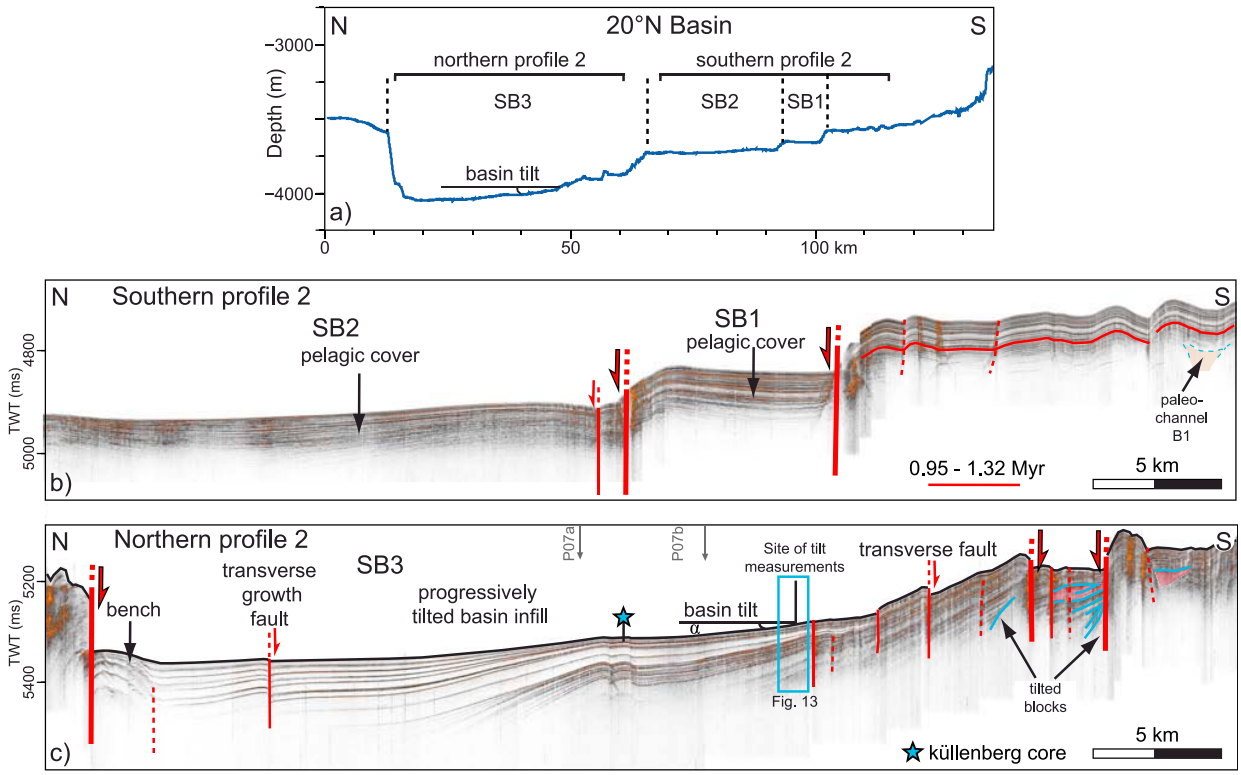


**Figure 5.** (a) Topography of the 20°N Basin. SB1 and SB2 are flat, whereas SB3 is gently tilted. 3.5 kHz profiles oriented longitudinally along the 20°N basin (b) across the inactive sub-basin SB1 and SB2 and (c) across the active sub-basin SB3 (see Figure 4 for location). Major transverse faults are observed at the seafloor (Figure 4) whereas minor transverse faults show only on SBP120 profiles since vertical deformation is erased by rapid deposition. The pelagic blanket of SB1 and SB2 was gently and progressively folded by flexural deformation.

## 4.3. Age of the Indus Turbiditic Channels Affected by the Opening of the 20°N Basin

[19] The opening of the 20°N basin affected the evolution of seven turbiditic channels belonging to three distinct generations labeled A, B, and C in younging order (Figures 5 and 7). These channels are located 600 km away from the Indus canyon and are part of the distal Indus fan.

### 4.3.1. Channel A: Generation Before the Onset of the Owen Fracture Zone (>3–6 Myr Old)

[20] The oldest channel (A1) is located in the Owen Basin and is now disconnected from the Indus fan. This highly meandering channel is now abandoned and covered by a thick (>100 m) pelagic drape (Figures 4 and 7). No trace of activity of this channel is observed on SBP120 profiles. Thus, the channel is older than the oldest sub-bottom reflector, the age of which is estimated at 3 Myr based on sedimentation rates at DSDP site 222. It is the minimum age for this channel, which could be older. The presence of channel A1 in the Owen Basin indicates that no significant relief acting as a topographic barrier for sediments coming from the Indus existed during its activity. This channel thus pre-dates the onset of the present-day trace of the OFZ.

[21] The meandering channel A2 is supposed to be of the same generation, since no trace of channel activity is observed on SBP120 data (Figure 7). Arcuate normal faults of the 20°N basin crosscut channel A2, the channel being now located on an uplifted area. We thus infer that the uplift post-dates the channel activity.

[22] Other channels (group A3) that do not display any trace of activity at the depth of SBP120 penetration are located in the Indus abyssal plain (Figure 4). This group of channels was subjected to avulsion. As normal faults dissected the bifurcation point, it is difficult to discriminate which channel predates the other. Channel avulsion is known to be an autocyclic process that spans thousands of years [*Babonneau et al.*, 2002], but it can be driven by tectonics processes related to the tectonic evolution of the 20°N basin which spans millions years. For that reason, we cannot use the occurrence of

Geochemistry Geophysics Geosystems G3



10.1029/2011GC003731

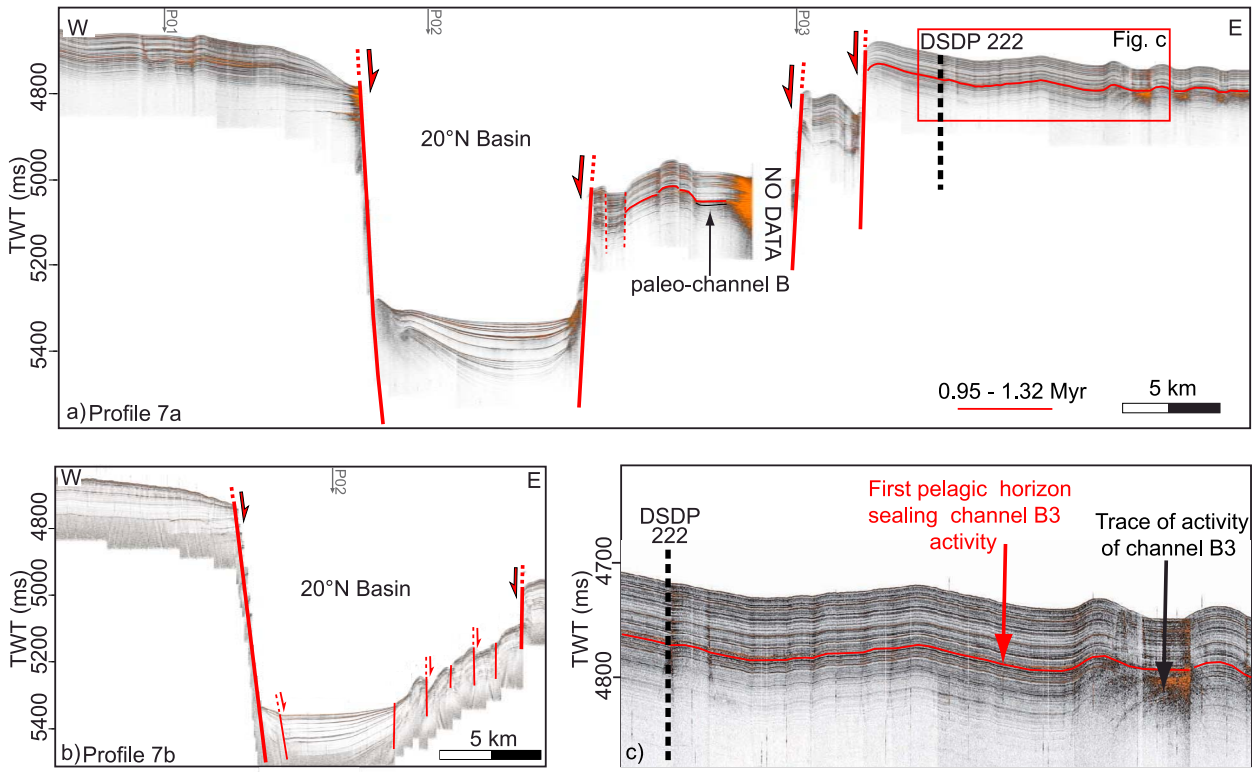


**Figure 6.** 3.5 kHz profiles oriented transverse to the 20°N basin (see Figure 4 for location). (a) This profile runs across the sub-basin SB3 and the DSDP 222 site, allowing correlations of the ages deduced from sedimentation rates. (b) This profile runs across sub-basin SB3. (c) Zoom of Figure 6a showing the location of DSDP site 222 and the picking of the pelagic reflector that seals the activity of turbiditic channel B3. The pelagic drape is imaged by conformable reflectors and is composed of detrital clay nanno-ooze to nanno-rich detrital carbonate silty clay (DSDP site 222 [*Shipboard Scientific Party*, 1974]). The trace of activity of the turbiditic channel is imaged by a chaotic and rough facies. The age of 0.95–1.32 Myr is deduced from pelagic sedimentation rates calculated at site DSDP 222.

avulsion as a tectonic indicator. The channels run parallel to the OFZ and do not seem to have been "attracted" by the presence of any topographic depression during their activity. A normal fault of the 20°N Basin dissects the eastern channel A3. Thus the channel activity seems to pre-date the opening of the basin, and is probably coeval with the channel A1. We infer that the group of channels A3 could be the southward prolongation of channel A2.

### 4.3.2. Channel B: Generation and the Opening of the Southern Sub-basins of the 20°N Basin

[23] The generation B is composed of three channels. The paleo-activity of these channels is marked by a lens-shaped, rough and chaotic facies on SBP120 profiles (Figure 7). Two of them (B1 and B2) are located at the southernmost part of the 20°N basin (Figures 4 and 5). The normal fault bounding the southernmost sub-basins 1 and 2 dissects channel B1, which is also incised by the system of en-échelon faults to the east (Figures 4 and 8). The complex arcuate normal fault system that borders the eastern side of the 20°N basin strongly dissects channel B3. Small relics of channel B3 are also observed close to the currently active channel on bathymetry. A thick pelagic drape covers lens-shaped features since 1.32 to 0.95 Myr according to sedimentation rates at DSDP site 222.

### 4.3.3. Channel C: Generation and the Filling of the Present-Day 20°N Basin

[24] The currently active channel of the 20°N basin (generation C) is recognizable on the seafloor morphology because of its deep incision through the complex normal fault system and its highly meandering sinuosity (Figures 4 and 7). It displays a U-shape in cross section. The incision becomes wider at the mouth of the channel. A transparent body is observed on both sides of the channel, and is interpreted as a HARP (high amplitude reflections package) incised by the channel (Figure 8).

Geochemistry Geophysics Geosystems G3



10.1029/2011GC003731

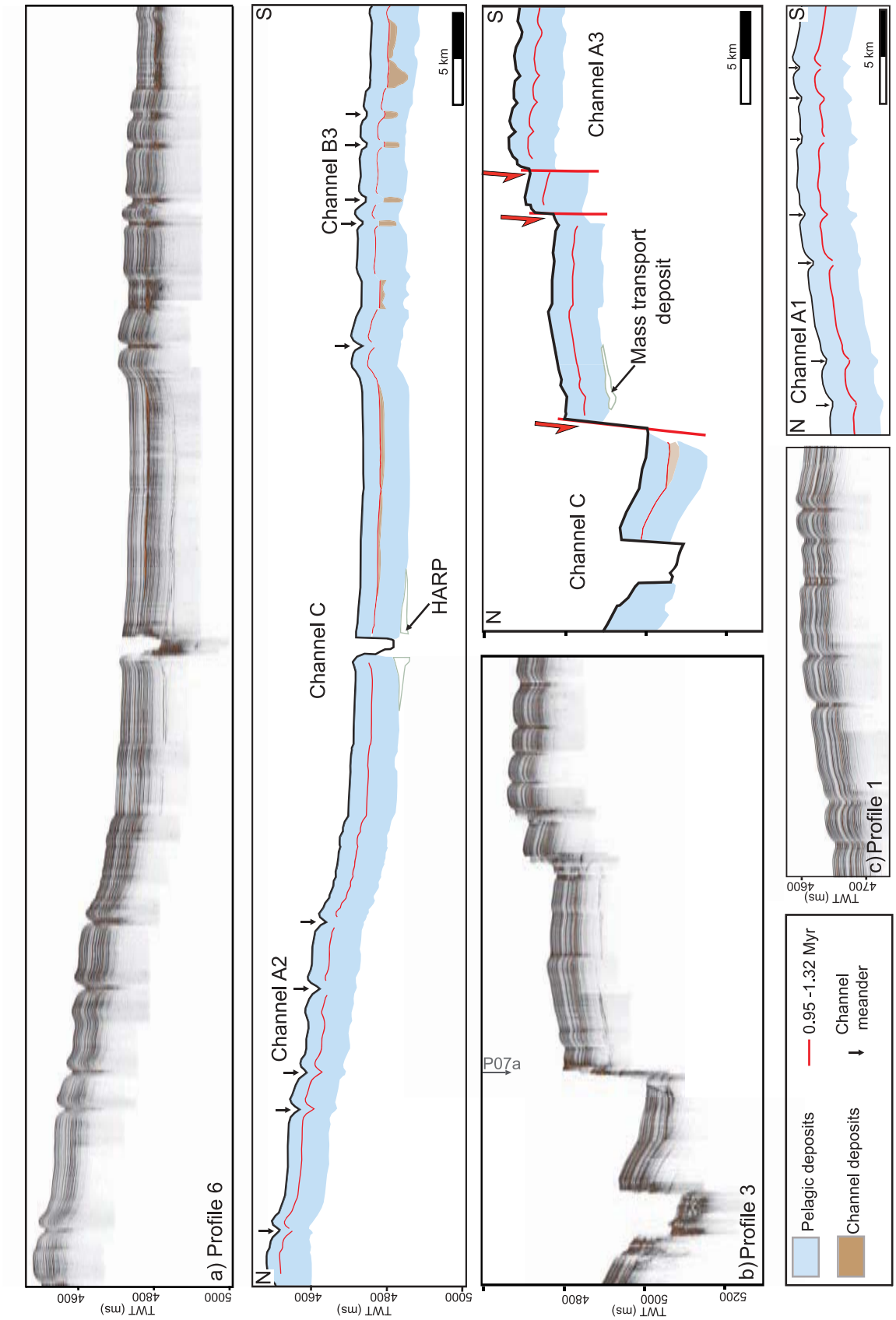


**Figure 7.** 3.5 kHz profiles across the turbiditic channels affected by the opening of the 20°N basin (see Figure 4 for location). Channel activity is imaged by a rough and chaotic facies on SBP profile.

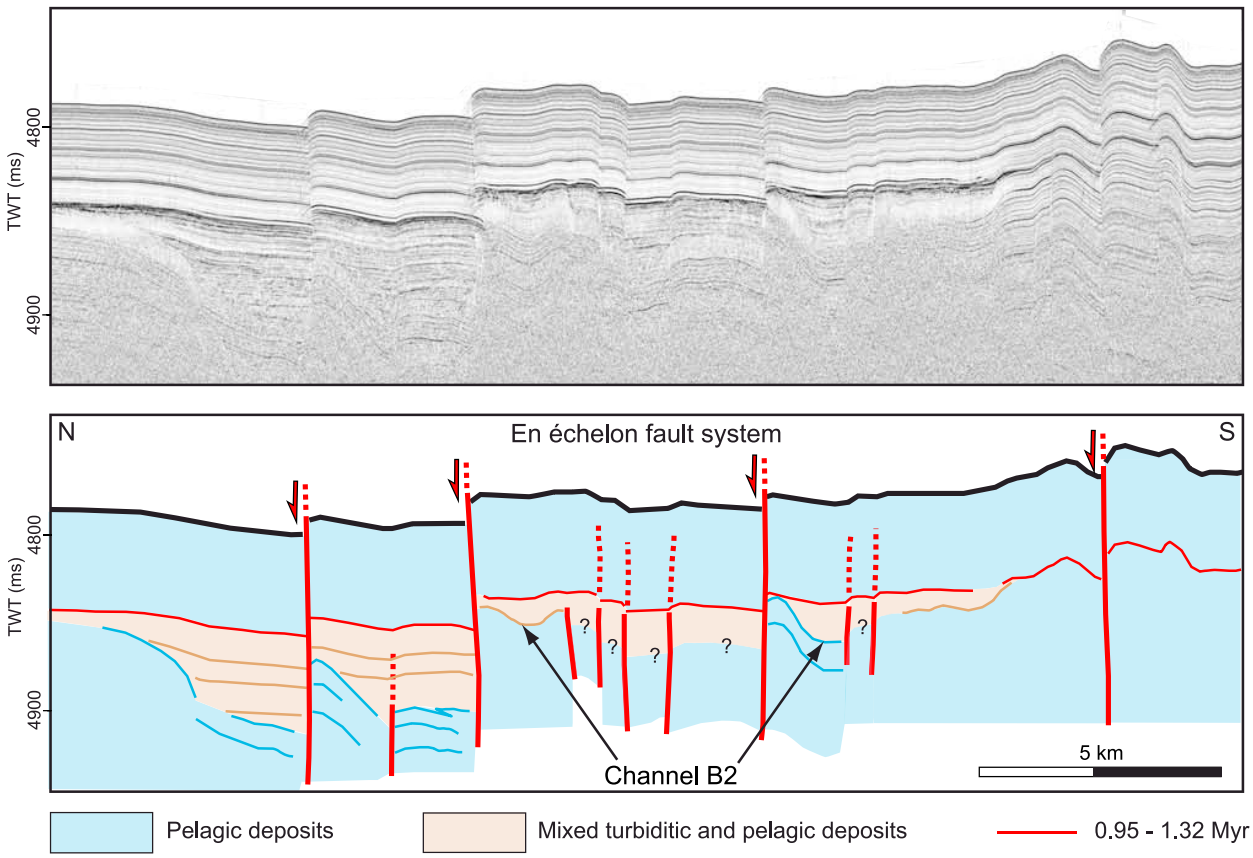


**Figure 8.** 3.5 kHz profile across the "en-échelon" fault system located at the southern end of the 20°N basin (see Figure 4 for location). The sedimentary filling that onlaps tilted blocks must be the result of fast deposition related to channel B2, as it lies between two concordant layers of pelagic deposits on the southern part of the SBP profile. It is therefore interpreted as mixed turbiditic and pelagic deposits.

The path of channel C was probably imposed by the growing topography formed by normal faults footwalls.

## 4.4. Present-Day Deformation East of the Qalhat Seamount

[25] The northern Owen Ridge, or Qalhat Seamount, is a volcanic guyot that extends between 20°30′N and 22°10′N (Figure 9). It is a 210-km-long, more than 55-km-wide, and up to 2700-m-high relief, characterized by a flat and 400-m-deep top. It is eroded by complex networks of mass wasting features (Rodriguez et al., submitted manuscript, 2011). The OFZ runs on the eastern side of the Qalhat Seamount, where it is divided into three major splays. The principal splay (labeled 1 in Figure 9) trends N 30E° and bends to N20E° at latitude 21°30′N. A second splay (labeled 2 in Figure 9), located west of the first one, also trends N30E°. Those two splays (1 and 2) delimitate a 160-m-deep, 45-km-long and up to 20-km-wide pull-apart basin. We propose the name of "Qalhat Basin" for this still-unnamed feature. The third splay (labeled 3 in Figure 9) is composed of an en-échelon fault system, which trends 14° to the east with respect to the main OFZ (splay 1). At latitude 21°35′N, a 700-m-high and arcuate relief interrupts the en-échelon fault system, which merges northward with the Dalrymple Trough.

[26] The deep structure of this portion of the OFZ has been partly imaged by seismic lines collected by the RSS Charles Darwin (Figure 10) [*Edwards et al.*, 2000, 2008]. As suggested by strong magnetic anomalies, seismic lines confirm that an eastward prolongation of the Qalhat Seamount buried under Indus turbiditic deposits underlies the OFZ. Thus, the arcuate relief that disrupts the en-échelon fault system (labeled 3 in Figure 9) is volcanic in origin. The OFZ forms a flower-structure in this area, with several sub-parallel vertical splays imaged on seismic profile (Figure 10). The currently active fracture zone is one of the several splays of the flower structure.

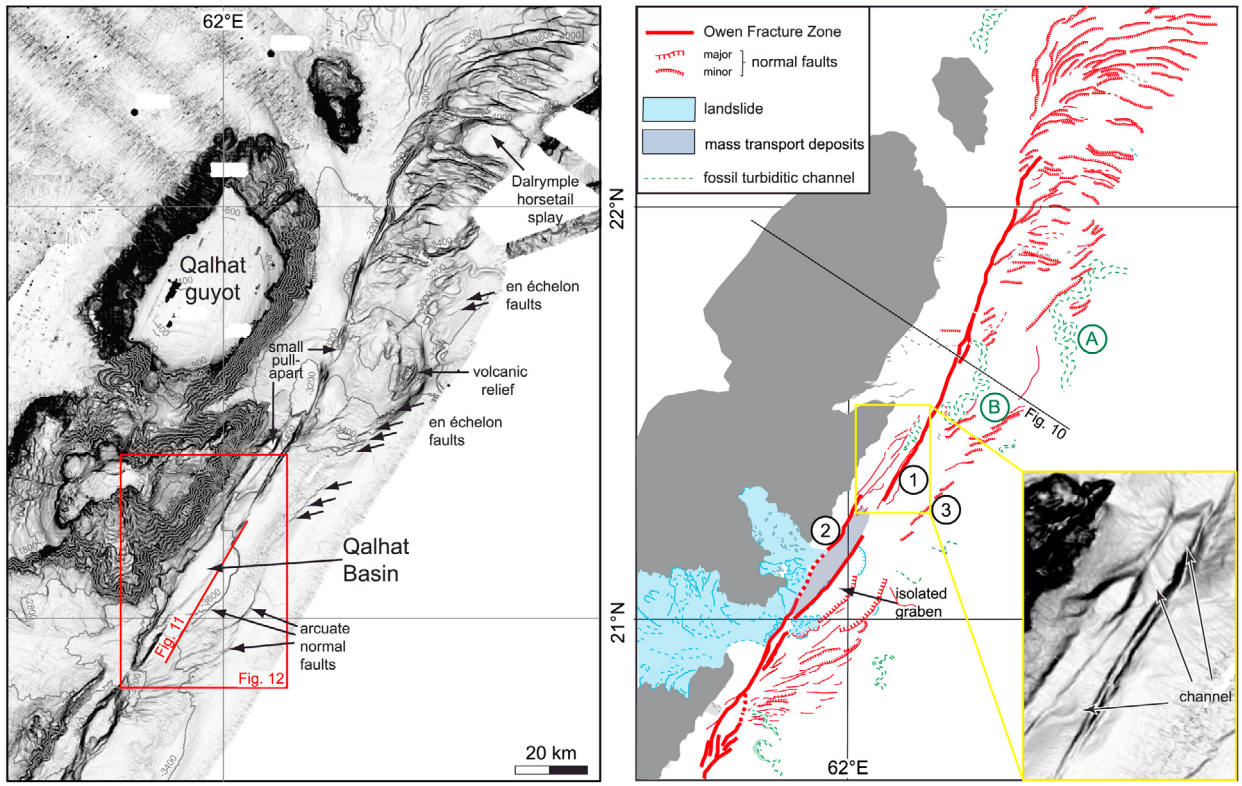


**Figure 9.** Slope map of the OFZ along the Qalhat Seamount, and interpretative structural scheme. 1, 2, 3: splays of the OFZ; A, B: channels. Inset shows a turbiditic channel dissected by the splays of the OFZ. A part of the slope gradient map is derived from data published in the work by *Bourget et al.* [2010].

[27] The Qalhat Basin is the most conspicuous tectonic feature in this area. It displays a needle geometry, with a very elongated depocenter. Arcuate normal faults with vertical throws of 20 to 70 m delimitate two half grabens on the eastern side of the basin. The active OFZ crosses the basin and has accommodated 30 m of vertical slip since its onset, suggesting a negligible extensional component to the strike-slip motion in this area. Complex slope failures are observed on both sides of the Qalhat Basin, which is a catchment for mass transport deposits. Two distinct seismic facies observed on the SBP120 profile that crosses the half graben allow to distinguish two modes of sedimentary deposition in this basin (Figure 11). The transparent and thick body at the bottom is interpreted as the result of mass transport, whereas the covering well-stratified facies is interpreted as pelagic deposits. The currently active depocenter displays a low reflectivity facies, whereas half-grabens display a highly reflective facies (Figure 12). This indicates that the active depocenter is filled in by mass transports deposits from the Qalhat Seamount, whereas the elevated graben is now isolated from such supply and mainly filled in by pelagic deposits, which imprint their signature on seafloor reflectivity.

[28] Two turbiditic channels belonging to the Indus system are of particular interest with regards to the tectonic activity of the OFZ. The first channel (labeled A on Figure 9) is dissected by an en-échelon fault system. No trace of its activity is observed on SBP120 profiles, suggesting an age older than 3 Myr. The second channel (labeled B on Figure 9) is dissected by the two splays of the OFZ (labeled 1 and 2 in Figure 10) that border the current depocenter of the Qalhat Basin. The western splay of the OFZ (labeled 2 in Figure 9) crosscuts some of the meanders of channel B. It indicates that the channel used to pass west of the splay 2. Thus, the channel predates the onset of the OFZ in this area. These turbiditic channels could possibly be coeval with turbiditic channels identified West of the Dalrymple Trough and at the top of the Murray Ridge [*Ellouz-Zimmermann et al.*, 2007; *Mouchot*, 2009].

[29] Since Indus turbiditic channels on the northwestern side of the Dalrymple Trough all pre-date the onset of the trough [*Ellouz-Zimmermann et al.*,

Geochemistry Geophysics Geosystems G3



10.1029/2011GC003731

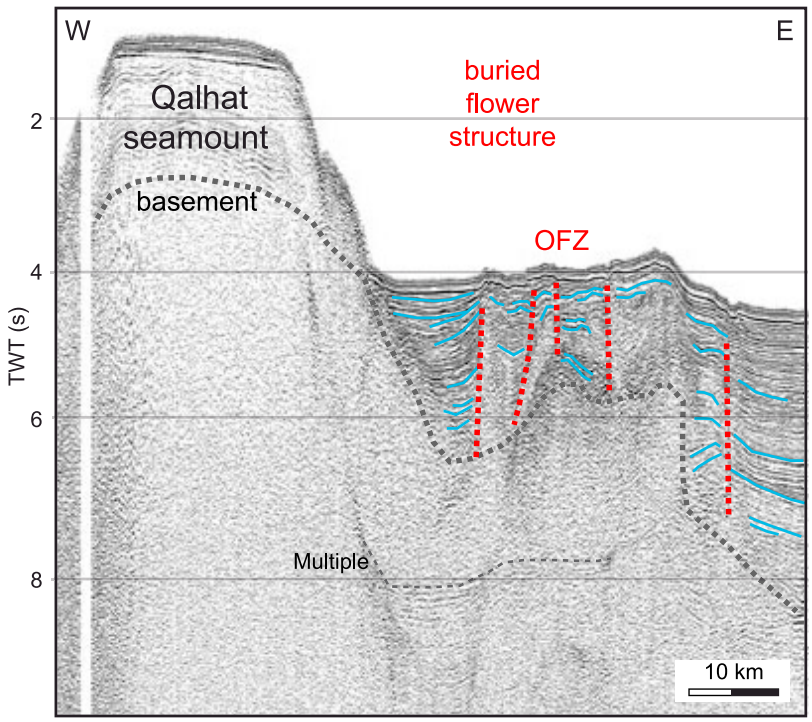


**Figure 10.** Seismic profile modified from *Edwards et al.* [2000], showing a negative flower structure buried under turbiditic deposits at the eastern foot of the Qalhat Seamount (see Figure 9 for location).

2007; *Mouchot*, 2009] and since the turbiditic system of the Makran accretionary wedge does not form any channel [*Bourget*, 2009; *Bourget et al.*, 2010], they cannot be used as time indicators for the propagation of the deformation toward the Dalrymple horsetail structure.

## 5. Summary of the Constraints on the Age of the Deformation Along the Owen Fracture Zone

[30] In this section we discuss the age and relative chronology of deformation along the different segments of the OFZ. In areas where different scenarios are possible, we decipher which one is the most likely in order to propose a detailed history of the structural evolution of the OFZ since the Early Pliocene.

### 5.1. Age of Deformation in the Restraining Bend (Southern Owen Ridge)

[31] The fold observed on ODP seismic line [*Shipboard Scientific Party*, 1989] along the main restraining bend of the southern Owen Ridge offers a good opportunity to follow the deformation rate through time. The fold has been active during the entire Pleistocene. The most recent episode of folding is observed on SBP profile that crosses the

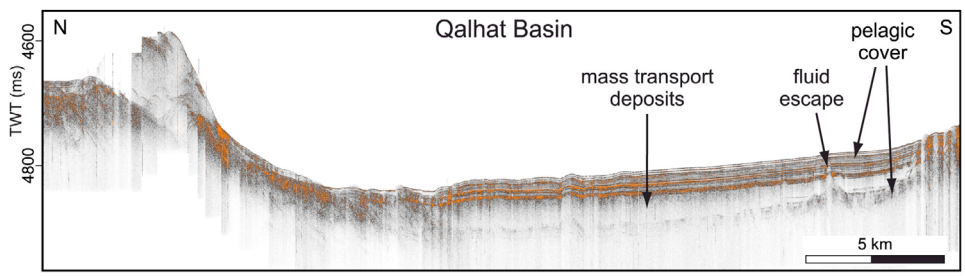


**Figure 11.** 3.5 kHz profile across the elevated graben of the Qalhat Basin (see Figures 9 and 12 for location). Mass Transport Deposits (MTD) are observed beneath the pelagic cover. The graben used to be a catchment for MTD but it is now isolated because of the onset of the main OFZ that crosscuts the Qalhat Basin.

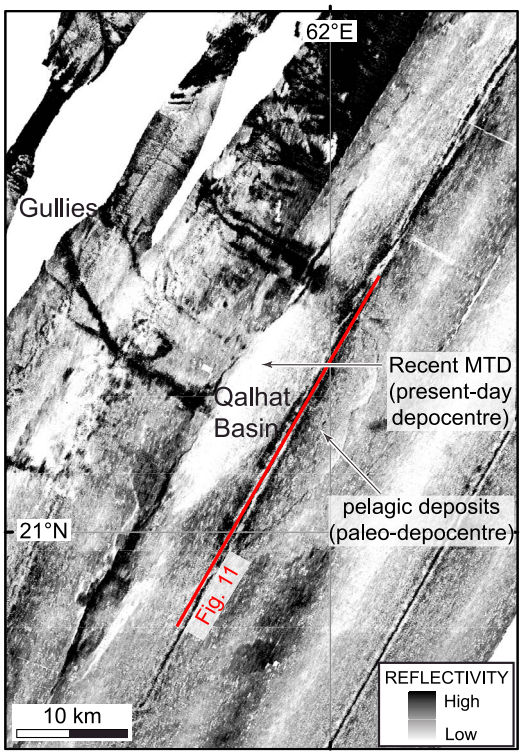


**Figure 12.** Reflectivity map of the Qalhat Basin (see Figure 9 for location). The low reflectivity area indicates that the present-day depocenter is still a catchment for Mass Transport Deposits (MTD), whereas the high reflectivity facies of the graben indicates that it is not supplied by MTDs anymore.

restraining bend located between 17°N and 18°N (Figure 3). The restraining bend consists in two folds. A quantitative analysis of the folding rate using sedimentation rates estimated at site ODP 720 (32 m.Myr$^{-1}$) suggests an increase around 0.8 Myr followed by a smooth and constant deformation.

## 5.2. Age of Deformation in the Vicinity of the 20°N Basin

[32] The best chronological record comes from the 20°N pull-apart basin. The onset of the OFZ and the opening of the 20°N basin clearly post-date the activity of channels of the generation A (Figures 4 and 7). The first stage of deformation is an uplift associated with normal fault activity. The uplift is recorded at 1.8–1.5 Myr at DSDP site 222, and marks the transition from turbiditic to pelagic deposits [*Shipboard Scientific Party*, 1974]. This could be a local uplift associated with the local formation of a new fault. However, no trace of channel activity of the B generation is observed either on seafloor bathymetry or on SBP120 profiles in the Owen Basin, west to the 20°N Basin. These could be proofs of an incipient 20°N basin where channels of the B generation used to discharge turbiditic material. The second stage of extensional deformation corresponds to the development of a series of half grabens bounded by the system of en-échelon normal faults between 19°18′N and 19°45′N (Figures 4 and 8). The onset of normal faults seems to be responsible for the channel deactivation, as all the channels of the B generation are faulted. Thus, dating the deactivation of channels, i.e., the base of the pelagic blanket that covers lens-shaped features, gives the age of the deformation. If faulting is not responsible of channel deactivation, then faults emplaced latter than the age of the base of the pelagic blanket that covers lens-shaped features, which is therefore the maximal age of faults. The age of the base of the pelagic blanket that seals traces of channel activity is estimated at 1.32 to 0.95 Myr using sedimentation rates calculated at DSDP site 222 (Figures 7 and 8). Arcuate normal faults on the hanging wall of the 20°N Basin and the en-échelon fault system must be the latter stage of the normal fault system that started to develop at 1.8–1.5 Myr. With regards to the sub-basin SB3, the extrapolation of the ages of turbiditic deposits measured on Küllenberg core samples gives an age of 420 kyr for the deepest sub-bottom reflector imaged (Figure 13) (Bourget et al., manuscript in preparation, 2011). Thus, the sub-basin SB3 is at least 400 kyr old.

## 5.3. Age of Deformation in the Vicinity of the Qalhat Seamount

[33] All the turbiditic channels in this area pre-date the onset of the present OFZ and the opening of the Qalhat basin (Figures 9 and 14). We could not assess with field evidences the age of the en-échelon fault system labeled "3" in Figure 9. Field evidences are compatible with two different scenarios. On one hand, the en-échelon fault system could be the very early stage of the present-day OFZ. The alternative is that it is the location of the future OFZ.

[34] In the first case (Figure 14), the horsetail termination develops in the continuity of the present-day OFZ and not along the en échelon-fault system, suggesting that the formation of the en-échelon fault system predates the formation of the horsetail structure. This scenario is consistent with several analog modeling works [*Aydin and Nur*, 1982; *Rahe et al.*, 1998; *Basile and Brun*, 1999; *Schlische et al.*, 2002; *Wu et al.*, 2009] which show that

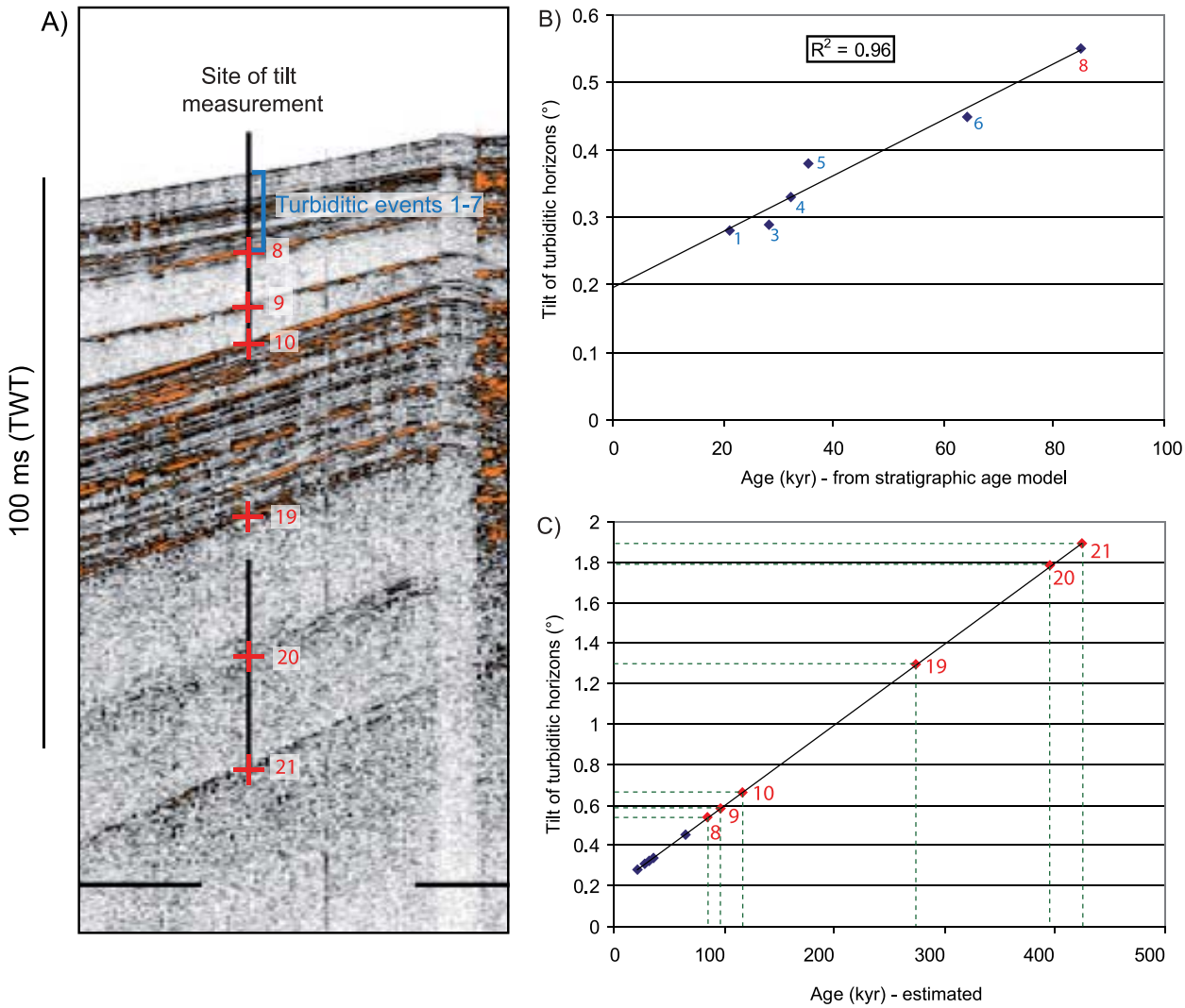


**Figure 13.** (a) Blow-up of 3.5 kHz profile 2 (see Figure 5) showing the location of the site of tilt measurement. The first ten meters have been sampled by Küllenberg cores. (b) Relation between the tilt of turbiditic deposits and their age. The tilt of turbiditic horizons in sub-basin 3 is measured on SBP profiles (see Figure 5 for location) and corrected from vertical exaggeration $^{14}C$ ages are available for turbiditic events 1 to 8 [*Bourget et al.*, 2011]. The relation between the tilt of turbiditic horizons and $^{14}C$ ages is fairly linear, suggesting a constant rate of tilting through times. (c) The measurement of the tilt of turbiditic horizons can be used as a time indicator for deeper horizons unsampled by Küllenberg cores according to the relation obtained in Figure 13b. The deepest turbiditic deposit we could date is 420 kyr old.

en-échelon fault systems are usually emplaced at the very early stage of strike-slip deformation. In the second case, the direction of the en-échelon fault system is more consistent with the small-circle predicted for a pure-strike-slip motion than the direction of the present-day OFZ [*Fournier et al.*, 2011]. In this latter case, the en-échelon fault system is considered as the incipient stage of the future OFZ. If confirmed, this scenario would lead to a reorganization of the horsetail termination.

[35] The study of the sedimentary infill of the Qalhat Basin can be used to decipher the relative chronology of the deformation in this area. Indeed, the presence of turbiditic or mass transport deposits sealed by a pelagic cover on the graben of the Qalhat Basin (Figure 12) indicates that the graben used to be a part of the Qalhat Basin depocenter, and has been subsequently slightly uplifted (by about 30 m). Thus, the Qalhat Basin used to be wider, and has been restrained by the onset of the currently main arm of the fracture zone which crosscuts diagonally the basin (Figures 9 and 11). We assume that the onset of the diagonal fault is responsible of the graben isolation from mass

Geochemistry Geophysics Geosystems G3



10.1029/2011GC003731

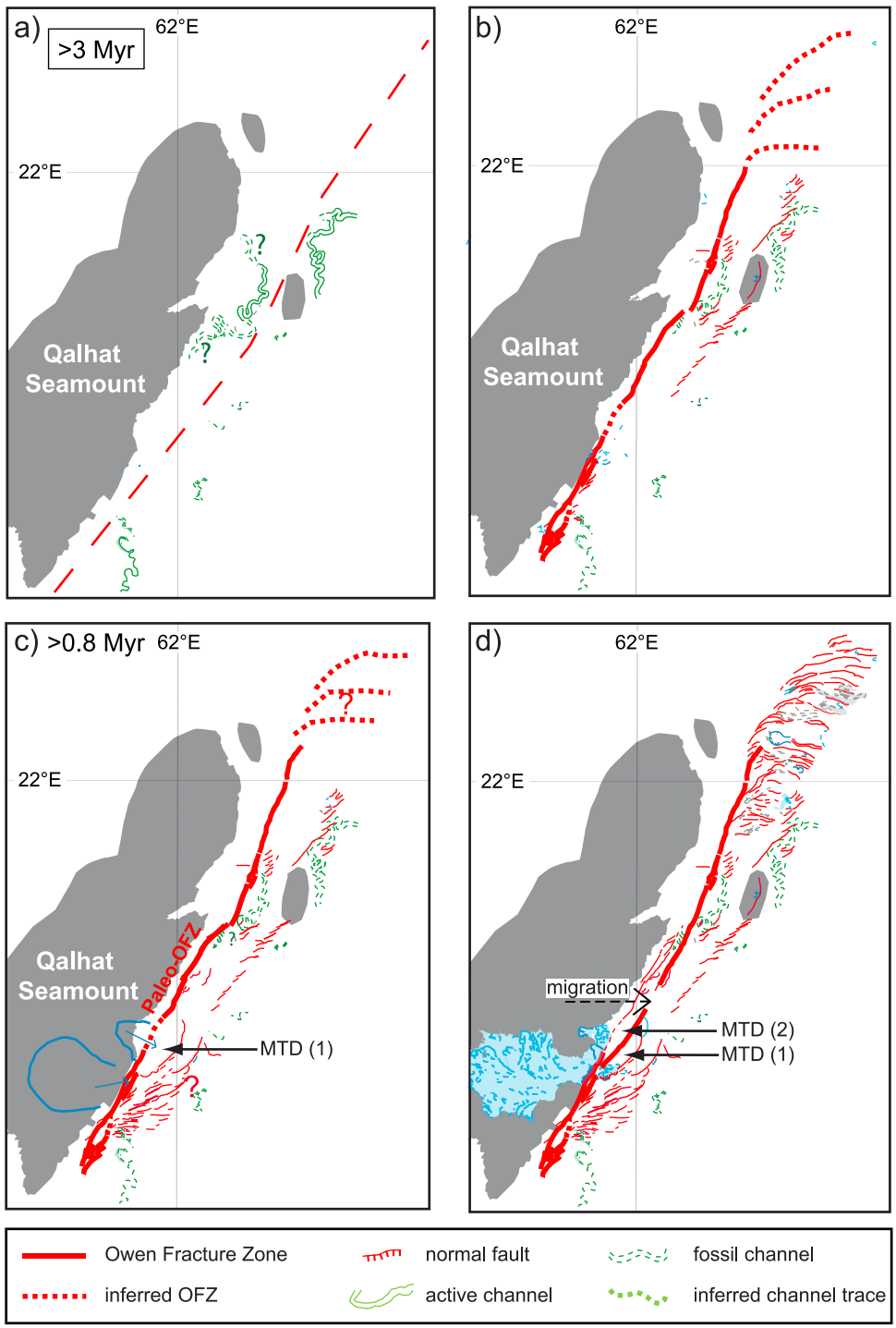


**Figure 14.** Chronology of the evolution of the Owen Fracture Zone (OFZ) in the vicinity of the Qalhat Seamount. (a–d) Stages are younger from Figures 14a to 14d, although they cannot be precisely dated. Figure 15 shows the structural evolution of the OFZ in the case where the en-échelon fault system pre-dates the onset of the horsetail termination. The identification of mass transport deposits (MTD) on the 3.5 kHz profile of Figure 12 indicates that the Qalhat Basin used to be wider (Figure 14c) before being crosscut by the present-day main OFZ 0.8 to 0.7 Myr ago (Figure 14d) An alternative interpretation is that the en-échelon fault system developed recently and could be the incipient future OFZ.

transport deposits. The age of the base of the isolated graben pelagic cover, and thus the age of the Qalhat Basin extinction, occurred 0.7 to 0.6 Myr ago assuming pelagic sedimentation rates close to the ones estimated at DSDP site 222 [*Shipboard Scientific Party*, 1974] (Figures 11 and 14).

[36] The uplift observed at the southern end of the Qalhat Basin is likely to post-date the opening of the Qalhat Basin, as the related normal faults are uplifted too. The age of the extinction of the Qalhat Basin is nearly coeval with the onset of the increase in folding observed at the restraining bend along the southern ridge. The uplift could be due to local compression along the OFZ, which could be responsible for the basin extinction too.

### 5.4. Summary of the History of the Owen Fracture Zone for the Last 3–6 Myr

[37] Although the present trace of the OFZ on the seafloor is only 3–6 Myr old, kinematic studies suggest that the relative motion between India and Arabia plates is located along the Owen Ridge since the opening of the Gulf of Aden 20 Myr ago [*Chamot-Rooke and Fournier*, 2009; *Fournier et al.*, 2010, 2011]. Thus the present-day OFZ is the exposed part of a strike-slip corridor which is partly buried under the Indus deep-sea fan. The following chronology focuses on the structural evolution of the exposed part of the OFZ whose activity spans the Plio-Pleistocene period.

[38] 1. The Present-day trace of the OFZ emplaced about 3 to 6 Myr ago, as deduced from finite offsets on the seafloor [*Fournier et al.*, 2011]. It runs at the foot of the eastern flanks of the southern and the central ridges since this time (Figures 2 and 3). A horsetail termination (Figure 9) and a rhomboidal pull-apart basin (Figure 2) began to develop at the northern and southern ends of the fracture zone, respectively [*Edwards et al.*, 2000; *Fournier et al.*, 2008a]. The onset of the horsetail termination could be related to the increase in subsidence of the Dalrymple Trough observed at ~ 5 Myr by *Gaedicke et al.* [2002].

[39] 2. 1.8 to 1.5 Myr ago, a tectonic activity possibly related to the first stages of formation of the 20°N Basin is observed on DSDP drilling [*Shipboard Scientific Party*, 1974].

[40] 3. An en-échelon fault system and asymmetric transform basins were emplaced 1.3 to 0.95 Myr ago at 20°N (Figures 4, 8, and 15).

[41] 4. A small shortening phase is recorded at the northern extremity of the southern ridge 0.8 Myr ago. It could be associated to a slight deviation of the OFZ from its previous trace. It is the last step of a more regional shortening, which started in the Early Pleistocene [*Shipboard Scientific Party*, 1989].

[42] 5. It is still unclear when the Qalhat Basin opened, and when the uplift to the south of it occurred. However, it was intersected by the master OFZ fault 0.7 to 0.6 Myr ago (Figure 9). The uplift south of the Qalhat Basin could be coeval with the shortening phase identified on the southern ridge.

[43] 6. Since its opening, the subsidence of the 20°N basin has been relocated in different sub-basins. The currently active sub-basin is at least ~400 kyr old (Figures 4, 5, and 13).

[44] Uncertainties remain in the dating exposed above. The age of the en-échelon fault system to the east of the Qalhat Basin, and the age of the uplift south of it, are not assessed by clear field evidences, and the timing of 20°N sub-basins migration needs to be further constrained. This summary must be considered as the most likely relative ages with regards to the general tectonics of the OFZ.

## 6. Discussion

### 6.1. Does the Structure of the Owen Fracture Zone Reflect a Steady State India-Arabia Relative Plate Motion?

[45] The structures that we describe above are those formed along a dextral strike-slip boundary since at least 3 Ma. The relative motion between India and Arabia is small (3 ± 1 mm/yr), and consequently very sensitive to any change of plate velocities. Indeed, a slight decrease of the northward motion of Arabia would have inverted the motion along the OFZ from dextral to sinistral, which is not observed. We thus conclude that the relative motion has been stable during the Pliocene, which is further supported by the agreement between geodetic and geologic kinematic modeling [*Fournier et al.*, 2008b; *DeMets et al.*, 2010]. The finite offset itself (10 to 12 km) is compatible with a constant shear rate during the same period of time (about 3 mm/yr). Taken all together, this confirms that the major structures that we observe along the OFZ, and in particular the pull-apart basins, are younger than 3–6 Myr.

Geochemistry Geophysics Geosystems G3



10.1029/2011GC003731

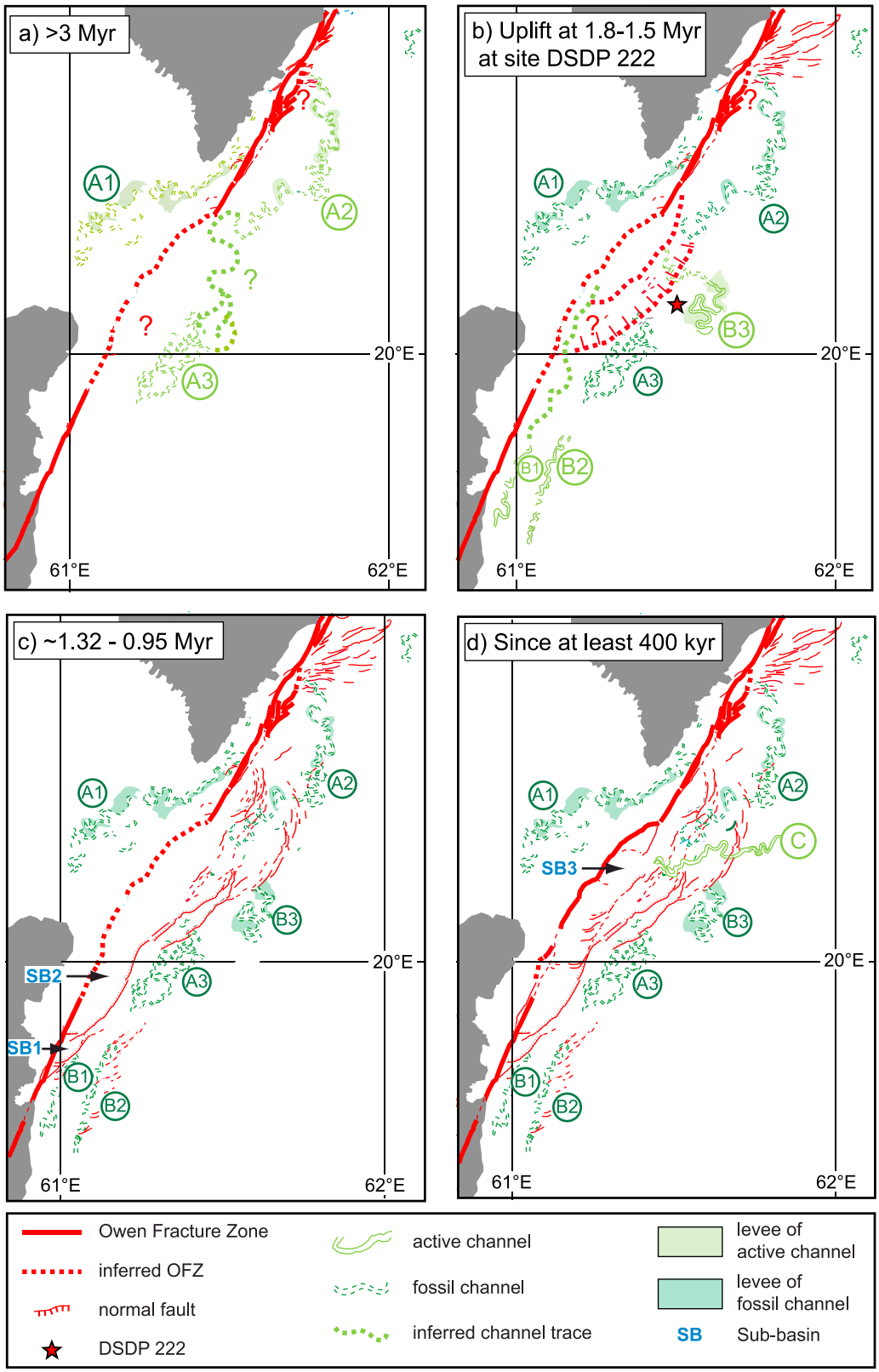


**Figure 15**

[46] On the other hand, several observations suggest that the dextral strike-slip motion started much earlier, probably when oceanic accretion initiated in the Gulf of Aden. This is supported by kinematics reconstructions [*Chamot-Rooke and Fournier*, 2009] that suggest an initiation of the dextral motion around 17 Ma or slightly earlier, and a finite differential motion between Arabia and India of the order of 80 km. Furthermore, the amount of horizontal extension at both ends of the OFZ seems to be larger than the 10–12 km offsets. Indeed, 10–12 km of offset are not sufficient to create the subsidence calculated at the Beautemps-Beaupré Basin [*Fournier et al.*, 2008a]. The Dalrymple Trough itself may have been active as an oblique rifting as early as the Early Miocene, based on stratigraphic studies [*Gaedicke et al.*, 2002]. There is thus an apparent mismatch between the present-day active trace of the fault and the inferred age of initiation of strike-slip motion along the Owen Ridge. This consequently raises the question of the location of the OFZ prior to the Pliocene. One possibility is that the old fault system is located in the same area as the present-day fault system, but is buried under Indus turbiditic deposits, as shown by one seismic profile across the northern OFZ (Figure 10). This profile clearly shows more splays than active fault traces at the surface. Acceleration of the turbiditic sedimentation rate between 15 Ma and 5 Ma [*Shipboard Scientific Party*, 1974, 1989; *Clift et al.*, 2001], in relation with the uplift of the Tibet and the correlative increase in the erosional rates, may have favored such a burial. Considering that the trace of the fault system on seafloor morphology is the result of the competition between the fault activity and sedimentation rates, the presence of the turbiditic channel A1 in the Owen Basin can be explained by a period where sedimentation rates were high enough to entirely cover the active trace of the OFZ fault system.

[47] The initiation of the present-day fault trace is synchronous with an increase of the subsidence rate in the Dalrymple Trough and of the uplift of the Murray Ridge around 4–5 Myr [*Gaedicke et al.*, 2002]. However, this Pliocene change does not correlate with any known plate-scale regional kinematic changes or major regional tectonic events [*Lepvrier et al.*, 2002; *Delescluse and Chamot-Rooke*, 2007; *Fournier et al.*, 2004, 2006, 2011]. Therefore, the structural evolution of the OFZ since 20 Myr and the onset of the present-day trace of the OFZ 3–6 Myr ago both fit into the scheme of a continuum of deformation and a gradual reorganization of the OFZ fault system unrelated to any major kinematics change.

## 6.2. Main Characteristics of the Structural Evolution of the Owen Fracture Zone

[48] In this section, we emphasize the main characteristics of the last structural reorganization of the OFZ since 3–6 Myr through a comparison with other transform plate boundaries, mainly the Levant Fault [*Aydin and Nur*, 1982; *ten Brink and Ben-Avraham*, 1989; *Lazar et al.*, 2006], the San Andreas Fault [*Wakabayashi et al.*, 2004; *Wakabayashi*, 2007], and a large continental strike-slip fault: the Hayuan fault in China [*Zhang et al.*, 1989].

### 6.2.1. Role of Structural Inheritance in the Structural Evolution of the Owen Fracture Zone

[49] Several observations suggest a control of structural inheritance in the reorganization of the OFZ fault system. First, the topographic relief of the Owen Ridge does not seem to affect the location of the OFZ, which runs alternatively across the slope or at the eastern foot of the Owen Ridge (Figures 2 and 3). This conspicuous configuration could be the result of the reactivation of a buried splay of the OFZ. Second, the activation of the 0.7–0.6 Myr old segment of the OFZ in the area of the Qalhat Basin could be the result of the reactivation of a buried splay of the flower structure identified

**Figure 15.** Chronology of the opening and the evolution of the 20°N basin. (a) Schematic reconstruction of the OFZ at 20°N before 3 Myr. Channels of the generation A are active. The location of channel A1 west of the OFZ could indicate that the active trace of the fault system was probably buried under turbiditic deposits at those times. (b) Schematic reconstruction of the OFZ at 20°N at 1.8–1.5 Myr. Transition of sedimentary facies recorded at DSDP site 222 indicates fault activity at those times, which could be related to incipient stages of formation of the 20°N pull-apart basin. Turbiditic channels of generation B were probably active and could have canalized turbiditic deposits to the incipient 20°N Basin. (c) Schematic reconstruction of the OFZ at 20°N at 1.32–0.95 Myr. Turbiditic channels of the generation B are inactive, probably because of the opening of the 20°N Basin. The active depocenter was wider than it is today. (d) Schematic reconstruction of the OFZ at 20°N since at least 400 kyr. Between 1.32 and 0.95 Myr and 400 kyr, the 20°N Basin has undergone subsidence delocalization in the smaller but deeper sub-basin 3. Turbiditic channel C activated and filled in the sub-basin 3.

in this area (Figures 9, 10, and 14). Basin inception and extinction thus seem to be related to the alternate activation of fault segments in the fracture zone. This situation is very similar to the one observed at the Dayinshui Basin located along the Haiyuan Fault in China [*Zhang et al.*, 1989]. Even if the OFZ accommodated only 10–12 km of relative motion [*Fournier et al.*, 2011], the structural evolution of the OFZ in the area of the Qalhat Basin could possibly show a transition from a diffuse to a more localized deformation pattern with increasing maturity of strike-slip motion, as observed elsewhere [*Le Pichon et al.*, 2001; *Ben-Zion and Sammis*, 2003; *Wesnousky*, 2005; *Schattner and Weinberger*, 2008; *Wu et al.*, 2009; *Garcia Moreno et al.*, 2011]. The deformation tends to localize on pre-existing major fault segments with time.

### 6.2.2. Asymmetry and Inception of Pull-Apart Basins Along the Owen Fracture Zone

[50] All pull-apart basins developed along the OFZ are asymmetric (18°40′N, 20°N, Qalhat Basin). Asymmetric basins are commonly observed along strike-slip faults [*Ben-Avraham and Zoback*, 1992; *Brothers et al.*, 2009; *Seeber et al.*, 2010] and interpreted as the result of transform normal extension. Asymmetry exists even at the scale of the sub-basin SB3 of the 20°N Basin (Figure 6), which compares closely with the Zofar Basin along the Levant fault because of the reversal of its asymmetry [*Frieslander*, 2000].

[51] The activity of pull-apart basins along the OFZ spans over different time-scales. The opening of pull-apart basins at 20°N 1.8 to 1.5 Myr ago is not coeval with the activation of the present-day OFZ 3–6 Myr ago. (Figure 15). When the main releasing bend formed at 20°N 1.8 to 1.5 Myr ago, the OFZ was already emplaced since 20 Myr. This is similar to the timing of emplacement of the Dead Sea Basin 3 to 5 Myr ago along the 17 to 11.5 Myr old Levant Fault [*Le Pichon and Gaulier*, 1988; *Garfunkel and Ben-Avraham*, 2001] in response to a small gradual change in relative plate kinematics [*Garfunkel*, 1981]. It may also be compared to the emplacement of the Olema Creek formation 110 to 185 kyr ago along the 18 Myr old San Andreas Fault [*Wakabayashi*, 2007].

### 6.2.3. Migrating Subsidence Along the Owen Fracture Zone

[52] Several observations suggest that subsidence migration is one of the main characteristics of the OFZ fault system reorganization since 3–6 Myr. The 20°N basin displays a series of three sub-basins (Figure 4). Sub-basin 2 is 40 m deeper than sub-basin 1, and sub-basin 3 is 260 m deeper than sub-basin 2. Sub-basins 1 and 2 were topographically isolated from the turbiditic supply of the currently active channel since its inception in this area and are sealed by a pelagic blanket. The topography of sub-basins 1 and 2 is flat, whereas the topography of sub-basin 3 is gently tilted, so as the corresponding turbiditic layers (Figure 5). These observations indicate that subsidence is currently inactive in sub-basin 1 and 2, and is localized in sub-basin 3. Subsidence initiated to the south of the 20°N Basin, and migrated northward, creating deeper and younger sub-basins bounded by transverse faults.

[53] This situation is very close to what is observed in the case of the Dead Sea pull-apart basin [*Aydin and Nur*, 1982; *ten Brink and Ben-Avraham*, 1989; *Lazar et al.*, 2006] and the San Andreas Fault system [*Wakabayashi et al.*, 2004; *Wakabayashi*, 2007] where episodes of migration of subsidence are documented [*Kashai and Croker*, 1987; *Garfunkel and Ben-Avraham*, 1996]. The active Dead Sea Basin is indeed divided in two sub-basins separated by a transverse fault, the northern one being 350 m deeper than the southern one. However, subsidence migration in the Dead Sea is still a matter of debate, and alternate interpretations have been proposed [*Ben-Avraham and Schubert*, 2006; *Lazar et al.*, 2006; *Ben-Avraham et al.*, 2008].

[54] Sandbox laboratory experiments performed by *Smit et al.* [2008] show that migration of sub-basins occurs where the ratio between the strike-slip faults spacing and the thickness of the deforming layer is $< 1$. *Smit et al.* [2008] conclude that this ratio determines not only the basin width, but also its geometry and the migration of subsidence. In these models simulating the migration of subsidence, the intrabasinal transverse faults appear during basin migration, and do not result from the reactivation of previous faults dividing the basin, consistently with observations of *Kashai and Croker* [1987] on the Dead Sea Basin.

[55] In the case of the 20°N Basin, the subsidence migrated much faster than the displacement accommodated along the OFZ during the last million years (more than 60 km of displacement for the depocenter, versus less than 10 km of displacement along the master fault). Following the nomenclature proposed by *Wakabayashi* [2007], sub-basins SB1 and SB2 are interpreted as the "wake" of the active

depocenter (Figure 4). In the light of the model of *Smit et al.* [2008], the active transverse syn-subsidence faults observed in the active sub-basin 3 (Figure 5) could be incipient stages of future transverse faults that isolate and concentrate the subsidence. If verified, this would confirm the tendency of subsidence to localize in a smaller but deeper sub-basin, without increasing the overall size of the releasing bend with increasing offset along the master fault.

## 7. Conclusions and Perspectives

[56] The present-day trace of the OFZ emplaced 3 to 6 Myr ago. The structural evolution of the OFZ was principally marked by the development of a major releasing bend at 20°N ~1.8–1.5 Myr ago and subsequent subsidence migration, local compression at 17°30′N and 20°30′N ~0.8 Myr ago, and the extinction of the Qalhat Basin 0.7 Myr ago. The structural evolution of the OFZ since the Pliocene suggests a continuous adjustment to a steady state relative plate motion between the Arabian and Indian plates. The present-day OFZ strike-slip system is the latest stage of the evolution of the India-Arabia plate boundary. Older stages of evolution need to be further constrained by deeper seismic lines. Indeed, the structure of the inferred 20-Myr-old buried strike-slip system that accommodated the motion between India and Arabia since the opening of the Gulf of Aden has not been clearly observed. The location of the India-Arabia plate boundary for the Paleogene-Early Miocene interval is far less known. Kinematics modeling [*Royer et al.*, 2002] and geological studies [*Edwards et al.*, 2000] postulate that the OFZ was located in the Owen Basin at those times, but there is no structural evidence for this hypothesis.

## Acknowledgments

[57] We are indebted to the Captain Geoffroy de Kersauson, officers, and crew members of the *BHO Beautemps-Beaupré* and to the French Navy hydrographers Vincent Lamarre and Yves-Marie Tanguy and the hydrographic team of the 'Groupe Océanographique de l'Atlantique' for their assistance in data acquisition. We thank Thierry Garlan for the supply of the Fanindien and the Marabie cruises data and the support of ARTEMIS for the use of $^{14}C$ ages measured on the cores collected during the Fanindien cruise. We greatly acknowledge Tim Minshull, an anonymous reviewer, and G3 editors for their constructive comments. We thank Baptiste Mulot, Pierpaolo Dubernet, and Matthias Delescluse for their technical assistance. We acknowledge the support of SHOM, IFREMER, CEA (LRC Yves-Rocard), and INSU-CNRS for the Owen and the Fanindien 2009 cruises and their support of M. Rodriguez's thesis.

## References

Aydin, A., and A. Nur (1982), Evolution of pull-apart basins and their scale independence, *Tectonics*, *1*(1), 91–105, doi:10.1029/TC001i001p00091.

Babonneau, N., B. Savoye, M. Cremer, and B. Klein (2002), Morphology and architecture of the present canyon and channel system of the Zaire deep-sea fan, *Mar. Pet. Geol.*, *19*, 445–467, doi:10.1016/S0264-8172(02)00009-0.

Basile, C., and J. P. Brun (1999), Transtensional faulting patterns ranging from pull-apart basins to transform continental margins: An experimental investigation, *J. Struct. Geol.*, *21*, 23–37, doi:10.1016/S0191-8141(98)00094-7.

Ben-Avraham, Z., and G. Schubert (2006), Deep "drop down "basin in the southern Dead Sea, *Earth Planet. Sci. Lett.*, *251*, 254–263, doi:10.1016/j.epsl.2006.09.008.

Ben-Avraham, Z., and M. D. Zoback (1992), Transform normal extension and Asymmetric basins: An alternative to pull-apart models, *Geology*, *20*, 423–426, doi:10.1130/0091-7613(1992)020<0423:TNEAAB>2.3.CO;2.

Ben-Avraham, Z., Z. Garfunkel, and M. Lazar (2008), Geology and evolution of the southern Dead Sea Fault with emphasis on subsurface structure, *Annu. Rev. Earth Planet. Sci.*, *36*, 357–387, doi:10.1146/annurev.earth.36.031207.124201.

Ben-Zion, Y., and C. G. Sammis (2003), Characterization of fault zones, *Pure Appl. Geophys.*, *160*, 677–715.

Bourget, J. (2009) Les systèmes turbiditiques du golfe d'Oman et de la marge Est-africaine: Architecture, évolution des apports au quaternaire terminal, et impact de la distribution sédimentaire sur les propriétés géoacoustiques des fonds, Ph.D. thesis, 404 pp., Univ. Bordeaux 1, Talence, France.

Bourget, J., S. Zaragosi, T. Mulder, J.-L. Schneider, T. Garlan, A. Van Toer, V. Mas, and N. Ellouz-Zimmermann (2010), Hyperpycnal-fed turbidite lobe architecture and recent sedimentary processes: A case study, *Sediment. Geol.*, *229*, 144–159, doi:10.1016/j.sedgeo.2009.03.009.

Bourget, J., S. Zaragosi, N. Ellouz-Zimermann, N. Mouchot, T. Garlan, J.-L. Schneider, V. Lanfumey, and S. Lallemant (2011), Turbidite system architecture and sedimentary processes along topographically complex slopes: The Makran convergent margin, *Sedimentology*, *58*, 376–406, doi:10.1111/j.1365-3091.2010.01168.x.

Brothers, D. S., N. W. Driscoll, G. M. Kent, A. J. Harding, J. M. Babcock, and R. L. Baskin (2009), Tectonic evolution of the Salton Sea inferred from seismic reflection data, *Nat. Geosci.*, *2*, 581–584, doi:10.1038/ngeo590.

Calvès, G. (2008), Tectonostratigraphic and climatic record of the NE Arabian Sea, Ph.D. thesis, 305 pp., Univ. of Aberdeen, Aberdeen U. K.

Chamot-Rooke, N., and M. Fournier (2009), Tracking Arabia-India motion from Miocene to Present, *Eos Trans. AGU*, *90*(52), Fall Meet. Suppl., Abstract T53G-01.

Clift, P. D., N. Shimizu, G. D. Layne, J. S. Blusztain, C. Gaedicke, H. U. Schluter, M. K. Clark, and S. Amjad (2001), Development of the Indus Fan and its significance for the erosional history of the Western Himalaya and Karakoram, *Geol. Soc. Am. Bull.*, *113*, 1039–1051, doi:10.1130/0016-7606(2001)113<1039:DOTIFA>2.0.CO;2.

Cunningham, W. D., and P. Mann (2007), Tectonics of strike-slip restraining and releasing bends, in *Tectonics of Strike-*

*Slip Restraining and Releasing Bends*, edited by W. D. Cunningham and P. Mann, *Geol. Soc. Spec. Publ.*, *290*, 1–12.

Delescluse, M., and N. Chamot-Rooke (2007), Instantaneous deformation and kinematics of the India-Australia Plate, *Geophys. J. Int.*, *168*, 818–842, doi:10.1111/j.1365-246X.2006.03181.x.

DeMets, C., R. G. Gordon, D. F. Argus, and S. Stein (1990), Current plate motions, *Geophys. J. Int.*, *101*, 425–478, doi:10.1111/j.1365-246X.1990.tb06579.x.

DeMets, C., R. G. Gordon, D. F. Argus, and S. Stein (1994), Effect of recent revisions of the geomagnetic reversal time scale on estimates of current plate motions, *Geophys. Res. Lett.*, *21*, 2191–2194, doi:10.1029/94GL02118.

DeMets, C., R. G. Gordon, and D. F. Argus (2010), Geologically current plate motions, *Geophys. J. Int.*, *181*, 1–80, doi:10.1111/j.1365-246X.2009.04491.x.

Edwards, R. A., T. A. Minshull, and R. S. White (2000), Extension across the Indian–Arabian plate boundary: The Murray Ridge, *Geophys. J. Int.*, *142*, 461–477, doi:10.1046/j.1365-246x.2000.00163.x.

Edwards, R. A., T. A. Minshull, E. R. Flueh, and C. Kopp (2008), Dalrymple Trough: An active oblique-slip ocean-continent boundary in the northwest Indian Ocean, *Earth Planet. Sci. Lett.*, *272*, 437–445, doi:10.1016/j.epsl.2008.05.007.

Ellouz-Zimmermann, N., et al. (2007), Offshore frontal part of the Makran accretionary prism (Pakistan) the Chamak Survey, in *Thrust Belts and Foreland Basins: From Fold Kinematics to Hydrocarbon Systems*, edited by O. L. Lacombe et al., pp. 349–364, Springer, Berlin.

Engdahl, E. R., R. van der Hilst, and R. Buland (1998), Global teleseismic earthquake relocation with improved travel times and procedures for depth determination, *Bull. Seismol. Soc. Am.*, *88*, 722–743.

Fournier, M., P. Patriat, and S. Leroy (2001), Reappraisal of the Arabia-India-Somalia triple junction kinematics, *Earth Planet. Sci. Lett.*, *189*, 103–114, doi:10.1016/S0012-821X(01)00371-5.

Fournier, M., N. Bellahsen, O. Fabbri, and Y. Gunnell (2004), Oblique rifting and segmentation of the NE Gulf of Aden passive margin, *Geochem. Geophys. Geosyst.*, *5*, Q11005, doi:10.1029/2004GC000731.

Fournier, M., C. Lepvrier, P. Razin, and L. Jolivet (2006), Late Cretaceous to Paleogene post-obduction extension and subsequent Neogene compression in the Oman Mountains, *GeoArabia*, *11*, 17–40.

Fournier, M., C. Petit, N. Chamot-Rooke, O. Fabbri, P. Huchon, B. Maillot, and C. Lepvrier (2008a), Do ridge-ridge-fault triple junctions exist on Earth? Evidence from the Aden-Owen-Carlsberg junction in the NW Indian Ocean, *Basin Res.*, *20*, 575–590, doi:10.1111/j.1365-2117.2008.00356.x.

Fournier, M., N. Chamot-Rooke, C. Petit, O. Fabbri, P. Huchon, B. Maillot, and C. Lepvrier (2008b), In-situ evidence for dextral active motion at the Arabia-India plate boundary, *Nat. Geosci.*, *1*, 54–58, doi:10.1038/ngeo.2007.24.

Fournier, M., et al. (2010), Arabia-Somalia plate kinematics, evolution of the Aden-Owen-Carlsberg triple junction, and opening of the Gulf of Aden, *J. Geophys. Res.*, *115*, B04102, doi:10.1029/2008JB006257.

Fournier, M., N. Chamot-Rooke, M. Rodriguez, P. Huchon, C. Petit, M.-O. Beslier, and S. Zaragosi (2011), Owen Fracture Zone: The Arabia-India plate boundary unveiled, *Earth Planet. Sci. Lett.*, *302*, 247–252, doi:10.1016/j.epsl.2010.12.027.

Frieslander, U. (2000), The structure of the Dead Sea transform emphasizing the Arava using new geophysical data, Ph.D. thesis, 204 pp., Hebrew Univ. of Jerusalem, Jerusalem.

Gaedicke, C., A. Prexl, H. U. Schlüter, H. Roeser, and P. Clift (2002), Seismic stratigraphy and correlation of major regional unconformities in the northern Arabia Sea, in *The Tectonic and Climatic Evolution of the Arabian Sea Region*, edited by P. Clift et al., *Geol. Soc. Spec. Publ.*, *195*, 25–36.

Garcia Moreno, D., A. Hubert Ferrari, J. Moernaut, J. G. Fraser, X. Boes, M. Van Daele, U. Avsar, N. Cagatay, and M. De Batist (2011), Structure and recent evolution of the Hazar Basin: A strike slip basin on the East Anatolian Fault, Eastern Turkey, *Basin Res.*, *23*, 191–207, doi:10.1111/j.1365-2117.2010.00476.x.

Garfunkel, Z. (1981), Internal structure of the Dead Sea leaky transform (Rift) in relation to plate kinematics, *Tectonophysics*, *80*, 81–108, doi:10.1016/0040-1951(81)90143-8.

Garfunkel, Z., and Z. Ben-Avraham (1996), The structure of the Dead Sea basin, *Tectonophysics*, *266*, 155–176, doi:10.1016/S0040-1951(96)00188-6.

Garfunkel, Z., and Z. Ben-Avraham (2001), Basins along the Dead Sea transform, in *Peri-Tethys Memoir 6: Peri-Tethyan Rift/Wrench Basins and Passive Margins*, edited by P. A. Ziegler et al., *Mem. Mus. Natl. Hist. Nat.*, *186*, 607–627.

Gordon, R. G., and C. DeMets (1989), Present-day motion along the Owen Fracture Zone and Dalrymple trough in the Arabian Sea, *J. Geophys. Res.*, *94*, 5560–5570, doi:10.1029/JB094iB05p05560.

Govil, P., and P. D. Naidu (2008), Late Quaternary changes in depositional processes along the western margin of the Indus Fan, *Geo Mar. Lett.*, *28*, 1–6, doi:10.1007/s00367-007-0083-1.

Kashai, E. L., and P. F. Croker (1987), Structural geometry and evolution of the Dead Sea-Jordan rift system as deduced from new subsurface data, *Tectonophysics*, *141*, 33–60, doi:10.1016/0040-1951(87)90173-9.

Lazar, M., Z. Ben-Avraham, and U. Schattner (2006), Formation of sequential basins along a strike-slip fault: Geophysical observations from the Dead Sea basin, *Tectonophysics*, *421*, 53–69, doi:10.1016/j.tecto.2006.04.007.

Le Pichon, X., and J. M. Gaulier (1988), The rotation of Arabia and the Levant fault system, *Tectonophysics*, *153*, 271–294, doi:10.1016/0040-1951(88)90020-0.

Le Pichon, X., et al. (2001), The active main Marmara fault, *Earth Planet. Sci. Lett.*, *192*, 595–616, doi:10.1016/S0012-821X(01)00449-6.

Lepvrier, C., M. Fournier, T. Bérard, and J. Roger (2002), Cenozoic extension in coastal Dhofar (southern Oman): Implications on the oblique rifting of the Gulf of Aden, *Tectonophysics*, *357*, 279–293, doi:10.1016/S0040-1951(02)00372-4.

Mann, P. (2007), Global catalogue, classification and tectonic origins of restraining- and releasing bends on active and ancient strike-slip fault systems, in *Tectonics of Strike-Slip Restraining and Releasing Bends*, edited by W. D. Cunningham and P. Mann, *Geol. Soc. Spec. Publ.*, *290*, 13–142, doi:10.1144/SP290.2.

Mann, P., M. R. Hempton, D. C. Badley, and K. Burke (1983), Development of pull-apart basins, *J. Geol.*, *91*, 529–554, doi:10.1086/628803.

Matthews D. H. (1966), The Owen Fracture Zone and the northern end of the Carlsberg Ridge, *Philos. Trans. R. Soc. London A*, *259*, 172–186.

Merkouriev, S., and C. DeMets (2006), Constraints on Indian plate motion since 20 Ma from dense Russian magnetic data: Implications for Indian plate dynamics, *Geochem. Geophys. Geosyst.*, *7*, Q02002, doi:10.1029/2005GC001079.

Mouchot, N. (2009), Tectonique et sédimentation sur le complexe de subduction du Makran pakistanais, Ph.D. thesis, 364 pp., Univ. de Cergy-Pontoise, Cergy-Pontoise, France.

Mountain, G. S., and W. L. Prell (1989), Geophysical Reconnaissance Survey for ODP Leg 117 in the Northwest Indian Ocean, *Proc. Ocean Drill. Program Initial Rep.*, *117*, 51–64.

Patriat, P., H. Sloan, and D. Sauter (2008), From slow to ultra-slow: A previously undetected event at the Southwest Indian Ridge at ca. 24 Ma, *Geology*, *36*, 207–210, doi:10.1130/G24270A.1.

Qayyum, M., R. A. Lawrence, and A. R. Niem (1997), Molasse-Delta-Flysch continuum of the Himalayan orogeny and closure of the Paleogene Katawaz remnant ocean, Pakistan, *Int. Geol. Rev.*, *39*, 861–875, doi:10.1080/00206819709465306.

Quittmeyer, R. C., and A. L. Kafka (1984), Constraints on plate motions in southern Pakistan and the northern Arabian Sea from the focal mechanisms of small earthquakes, *J. Geophys. Res.*, *89*, 2444–2458, doi:10.1029/JB089iB04p02444.

Rahe, B., D. Ferrill, and A. Morris (1998), Physical analog modeling of pull-apart basin evolution, *Tectonophysics*, *285*, 21–40, doi:10.1016/S0040-1951(97)00193-5.

Rangin, C., and X. Le Pichon (2004), Strain localization in the Sea of Marmara: Propagation of the North Anatolian Fault in a now inactive pull-apart, *Tectonics*, *23*, TC2014, doi:10.1029/2002TC001437.

Reilinger, R., et al. (2006), GPS constraints on continental deformation in the Africa–Arabia–Eurasia continental collision zone and implications for the dynamics of plate interactions, *J. Geophys. Res.*, *111*, B05411, doi:10.1029/2005JB004051.

Royer, J. Y., A. K. Chaubey, J. Dyment, G. C. Bhattacharya, K. Srinivas, V. Yateesh, and T. Ramprasad (2002), Paelogene plate tectonic evolution of the Arabian and Eastern Somali basins, in *The Tectonic and Climatic Evolution of the Arabian Sea Region*, edited by P. Clift et al., *Geol. Soc. Spec. Publ.*, *195*, 7–23.

Schattner, U. (2010), What triggered the early to-mid Pleistocene tectonic transition across the entire eastern Mediterranean?, *Earth Planet. Sci. Lett.*, *289*, 539–548, doi:10.1016/j.epsl.2009.11.048.

Schattner, U., and R. Weinberger (2008), A mid-Pleistocene deformation transition in the Hula basin, northern Israel: Implications for the tectonic evolution of the Dead Sea Fault, *Geochem. Geophys. Geosyst.*, *9*, Q07009, doi:10.1029/2007GC001937.

Schlische, R. W., M. O. Withjack, and G. Eisenstadt (2002), An experimental study of the secondary deformation produced by oblique slip normal faulting, *AAPG Bull.*, *86*(5), 885–906.

Seeber, L., C. Sorlien, M. Steckler, and M.-H. Cormier (2010), Continental transform basins: Why are they asymmetric?, *Eos Trans. AGU*, *91*(4), 29–30, doi:10.1029/2010EO040001.

Shipboard Scientific Party (1974), Site 222, *Initial Rep. Deep Sea Drill. Proj.*, *23*, 211–289, doi:10.2973/dsdp.proc.23.106.

Shipboard Scientific Party (1989), Site 731, *Proc. Ocean Drill. Program Initial Rep.*, *117*, 585–652.

Smit, J., J. P. Brun, S. Cloetingh, and Z. Ben-Avraham (2008), Pull-apart basin formation and development in narrow transform zones with application to the Dead Sea Basin, *Tectonics*, *27*, TC6018, doi:10.1029/2007TC002119.

Sylvester, A. G. (1988), Strike-slip faults, *Geol. Soc. Am. Bull.*, *100*, 1666–1703, doi:10.1130/0016-7606(1988)100<1666:SSF>2.3.CO;2.

ten Brink, U. S., and Z. Ben-Avraham (1989), The anatomy of a pull-apart basin: Seismic reflection observations of the Dead Sea, *Tectonics*, *8*, 333–350, doi:10.1029/TC008i002p00333.

ten Brink, U. S., and M. Rybakov (1999), Anatomy of the Dead Sea transform: Does it reflect continuous changes in plate motion?, *Geology*, *27*, 887–890, doi:10.1130/0091-7613(1999)027<0887:AOTDST>2.3.CO;2.

Wakabayashi, J. (2007), Stepovers that migrate with respect to affected deposits: Field characteristics and speculation on some details of their evolution, in *Tectonics of Strike-Slip Restraining and Releasing Bends*, edited by W. D. Cunningham and P. Mann, *Geol. Soc. Spec. Publ.*, *290*, 169–188.

Wakabayashi, J., J. V. Hengesh, and T. L. Sawyer (2004), Four-dimensional transform fault processes: Progressive evolution of step-overs and bends, *Tectonophysics*, *392*, 279–301, doi:10.1016/j.tecto.2004.04.013.

Weedon, G. P., and I. N. McCave (1991), Mud turbidites from the Oligocene and Miocene Indus Fan at sites 722 and 731 on the Owen Ridge, *Proc. Ocean Drill. Program Sci. Results*, *116*, 215–220.

Weissel, J. K., V. A. Childers, and G. D. Karner (1992), Extensional and compressional deformation of the lithosphere in the light of ODP drilling in the Indian Ocean, in *Synthesis of Results From Scientific Drilling in the Indian Ocean*, *Geophys. Monogr. Ser.*, vol. 70, edited by R. A. Duncan et al., pp. 127–156, AGU, Washington, D. C., doi:10.1029/GM070p0127.

Wesnousky, S. G. (2005), The San Andreas and Walker Lane fault systems, western North America: Transpression, transtension, cumulative slip and the structural evolution of a major transform plate boundary, *J. Struct. Geol.*, *27*, 1505–1512, doi:10.1016/j.jsg.2005.01.015.

Whitmarsh, R. B. (1979), The Owen Basin off the south-east margin of Arabia and the evolution of the Owen Fracture Zone, *Geophys. J. R. Astron. Soc.*, *58*, 441–470.

Whitmarsh, R. B., O. E. Weser, and D. A. Ross (1974), *Initial Reports of Deep Sea Drilling Project*, vol. 23, 1180 pp., U.S. Gov. Print. Off., Washington, D. C.

Wu, J. E., K. McClay, P. Whitehouse, and T. Dooley (2009), 4D analogue modelling of transtensional pull-apart basins, *Mar. Pet. Geol.*, *26*, 1608–1623, doi:10.1016/j.marpetgeo.2008.06.007.

Zhang, P.-Z., B. C. Burchfiel, S. Chen, and Q. Deng (1989), Extinction of pull-apart basins, *Geology*, *17*, 814–817, doi:10.1130/0091-7613(1989)017<0814:EOPAB>2.3.CO;2.

## Conclusions et perspectives de l' article "Neotectonics of the Owen Fracture Zone"

*Critique des principaux résultats de Rodriguez et al. 2011*

Du fait de la profondeur de pénétration limitée du sondeur de sédiment (SBP), une importante erreur d'interprétation a été commise dans cet article : Les dépôts turbiditiques sur la base desquels la génération B des chenaux (à l'Est du bassin 20°N) a été identifiée sur les figures 6 et 7 de l'article ne sont pas des dépôts formés par l'activité du chenal carté "B", mais par le débordement de panaches turbiditiques canalisés par des chenaux situés ~20 km plus à l'Est. Les chenaux identifiés comme appartenant à la génération B sont en fait des chenaux de la génération A qui ont été partiellement recouverts par un épisode turbiditique il y a environ 1 Ma. Les dépôts turbiditiques âgés d'un million d'années ne marquent donc pas le dernier épisode d'activité turbiditique avant l'ouverture du bassin. Les données de la campagne Owen 2 ont permis de ré-évaluer de façon plus fiable l'âge du bassin 20°N : ces travaux sont détaillés dans l'article 3 *"Mode of opening of an intra-oceanic pull-apart: the 20°N Basin along the Owen Fracture Zone (NW Indian Ocean)"* soumis à Tectonics.

*Eléments de comparaison avec l'évolution structurale d'autres décrochements*

L'article précédent tente en dépit de fortes incertitudes de décrire la naissance, la croissance, l'évolution structurale, et l'inactivation des bassins pull-apart le long de la ZFO. Les résultats et les mécanismes sont similaires à de nombreux cas d'étude dans le monde, dont voici un bref tour d'horizon. Une brève revue de l'âge d'ouverture des grands bassins pull-apart, confrontée à l'âge du système décrochant auquel ils sont rattachés, montrent qu'ils peuvent se former à des moments divers dans l'histoire du décrochement. Par exemple, de nombreux bassins pull-apart sont contemporains de la mise en place de leur décrochement au niveau de San Andreas (*Wesnousky, 2005*), alors que d'autres sont plus tardifs (*Wakabayashi, 2007*). Le bassin de la Mer Morte a 5 Ma, alors que l'âge de la faille du Levant est estimé autour de 15 Ma. D'autre part, les bassins pull-apart se développent sur des durées de temps variables, principalement en fonction du taux de décrochement, mais aussi en fonction de la structure du système décrochant, des propriétés mécaniques du système de faille, et des changements tectoniques régionaux. Des relais de courte durée de vie et de dimensions restreintes ont été identifiés sur plusieurs décrochements (bassins de Dagg et de Hammer le long de la faille alpine de Nouvelle Zélande *; Barnes et al., 2001*). Ces relais prennent place sur des structures en fleur négatives. Leur durée de vie est estimée entre $10^5$ et $10^6$ Ma (ces durées étant bien sûr dépendantes du taux de décrochement). Ces structures sont les témoins

de réarrangements locaux du décrochement principal au cours de son évolution. D'autres bassins, de plus grandes dimensions, peuvent être en place depuis plusieurs millions d'années (ex. le bassin de la mer Morte). Le long d'un même décrochement peuvent donc co-exister des bassins de taille et d'âge variables. Avec l'activation alternative de fragments de faille, un bassin peut être abandonné simplement parce que le segment sur lequel il se développait a été abandonné. De la même façon, un bassin peut naître en conséquence de l'activation d'un nouveau segment de faille. Les travaux de *Wenousky (1988)*, basés sur les failles Nord Anatolienne et de San Andreas, montrent que les décrochements ayant accommodé un plus grand décalage sont ceux qui affichent le moins de relais, et dont le tracé est le plus rectiligne. La durée de vie des relais est donc associée à la maturation du couloir décrochant, au sein duquel la déformation tend à se localiser sur des segments bien précis avec le temps. Sur un grand décrochement, l'évolution structurale du réseau de faille et de la subsidence peut mener à l'extinction de bassins pull-apart. Ce phénomène a été pour la première fois décrit sur le réseau de faille de Haiyuan en Chine (Figure 1 ; *Zhang et al., 1989*). Le mode d'extinction le plus courant semble être le développement d'une nouvelle faille décrochante le long d'une des failles normales ayant accommodé la subsidence du bassin, ou la mise en place d'une faille qui recoupe le bassin sur sa diagonale et fait disparaître le relais en joignant ses extrémités. Les failles normales bordant le bassin peuvent fusionner et connecter les segments décrochants. La migration du décrochement principal vers le centre du bassin peut aussi mener à son extinction (Figure 1 ; ex. bassin Hazar (NAF) *(Garcia Moreno et al., 2010;* bassin de Hula (faille du Levant ; *Schattner and Weinberger, 2008*); Mer de Marmara (*LePichon et al., 2001; 2003*; discuté par *Armijo et al., 2002; 2005*).

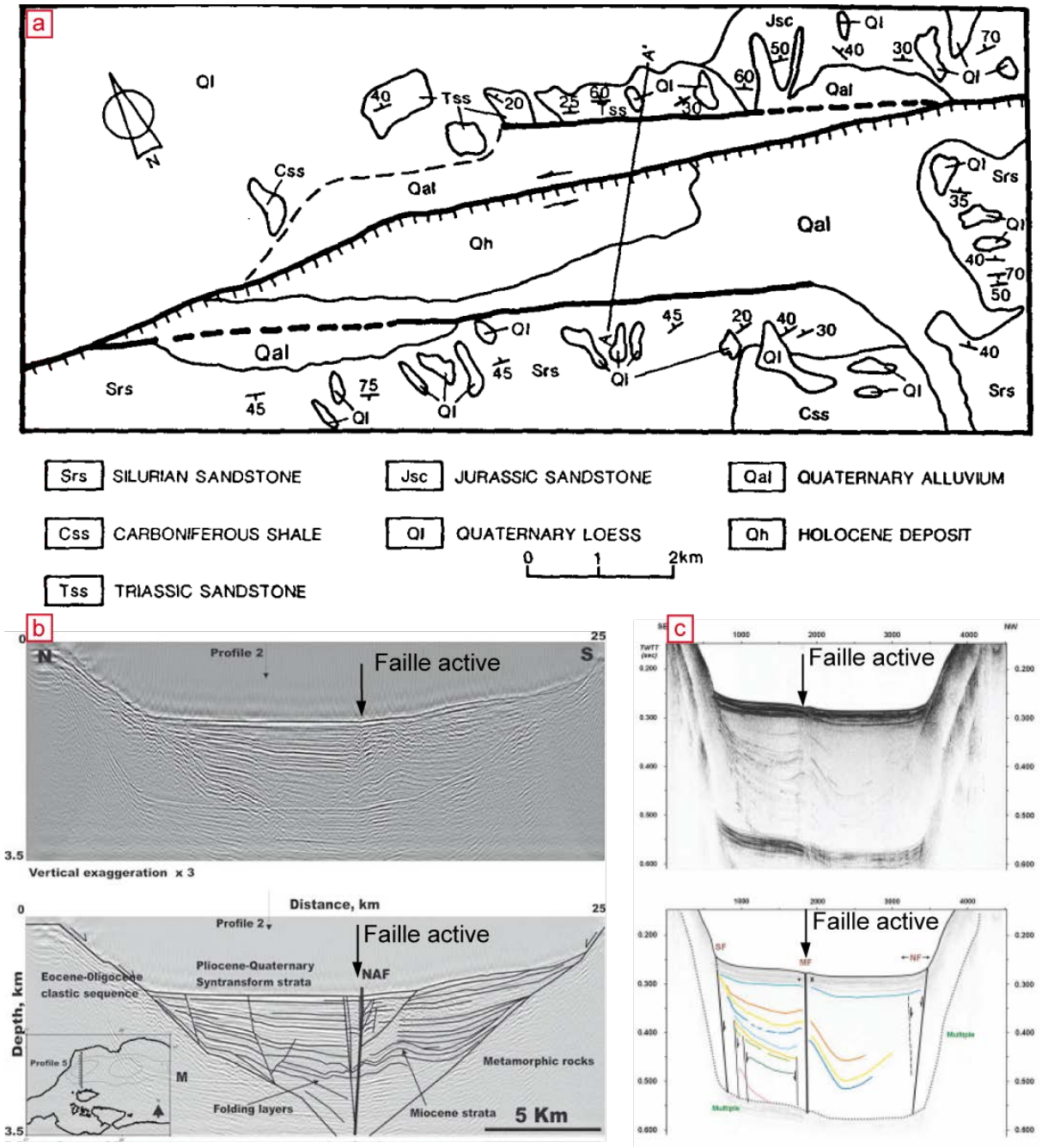


*Figure 1 : a) Schéma structural du Danshui sur la faille de Haiyuan en Chine (d'après Zang et al., 1989). Une faille diagonale recoupe le bassin et relie ses extrémités.La configuration de ce bassin est similaire au bassin de Qalaht le long de l'OFZ. b) Profil sismique transverse au bassin de Terkidag (Mer de Marmara ; d'après Kanbur et al., 2007). c) Profil sismique transverse au bassin de Hazar, sur la Faille Est-Anatolienne (d'après Garcia-Moreno et al., 2010) Dans les deux cas (b & c), les bassins sont recoupés par la faille active du système décrochant. Une telle faille n'est pas observée au niveau du bassin 20°N le long de l'OFZ, indiquant un stade de maturation structurale moins avancé.*

Au vu de la gamme d'âge possible pour l'OFZ (3 à 6 Ma), il est difficile de dire si les bassins sont nés en même temps que l'activation de l'OFZ. Le bassin de Qalhat semble avoir été inactivé par la relocalisation de la ZFO, ce dernier mécanisme étant encore à confirmer avec les données de sismique réflexion acquises au cours d'Owen 2. Comme nous le montrerons plus tard, la trace Miocène de la limite de plaque Inde-Arabie est localisée proche de la ZFO actuelle, mais enfouie sous les turbidites. Comme pour la mise en place de la Mer Morte, la mise en place du bassin 20°N et de la fosse de Dalrymple pourrait être l'effet de la réorganisation structurale de la ZFO, sans grande migration de la limite de plaque Inde-Arabie. La quantité de mouvement accommodée par la ZFO semble cependant encore trop faible pour mener à l'abandon de ses principaux bassins pull-apart.

*La migration de la subsidence au sein des bassins pull-apart : comparaison avec la Faille du Levant et la Faille de San Andreas*

L'une des hypothèses principales discutée dans *Rodriguez et al. 2011* est que le bassin 20°N aurait subi des épisodes de migration de la subsidence, impliquant le développement de failles transverses entre les sub-bassins. Cette hypothèse est basée sur la ressemblance structurale du bassin 20°N avec les bassins pour lesquels le processus de migration de la subsidence et des relais a été pour la première fois proposé. Afin de faciliter la compréhension de la comparaison qui suit, un encart synthétisant les caractéristiques principales de la Faille du Levant est fourni en fin de thèse (annexes).

Le premier cas d'école est la formation du ruisseau d'Olema le long de la faille de San Andreas *(Wakabayashi, 2007)*. Cette formation, composée de dépôts détritiques, est âgée de 110 à 185 ka et affleure sur environ 2 $km^2$ à proximité de la faille de San Andreas. Cette formation est récente par rapport à l'âge de la faille de San Andreas dans la région, estimé à 18 Ma. Depuis 100 ka, la faille de San Andreas a accumulé près de 5 km de déplacement, ce qui est bien supérieur aux 3,5 km de long estimés pour le paléo-bassin. Cette formation a subi une inversion tectonique, et forme aujourd'hui un relief de 70 m. Aucun changement tectonique régional n'a été identifié pour les derniers 100 ka. *Wakabayashi (2007)* propose que le dépôt centre a migré vers le nord, laissant la formation d'Olema dans son sillage, susceptible d'être reprise par un soulèvement très localisé le long du décrochement.

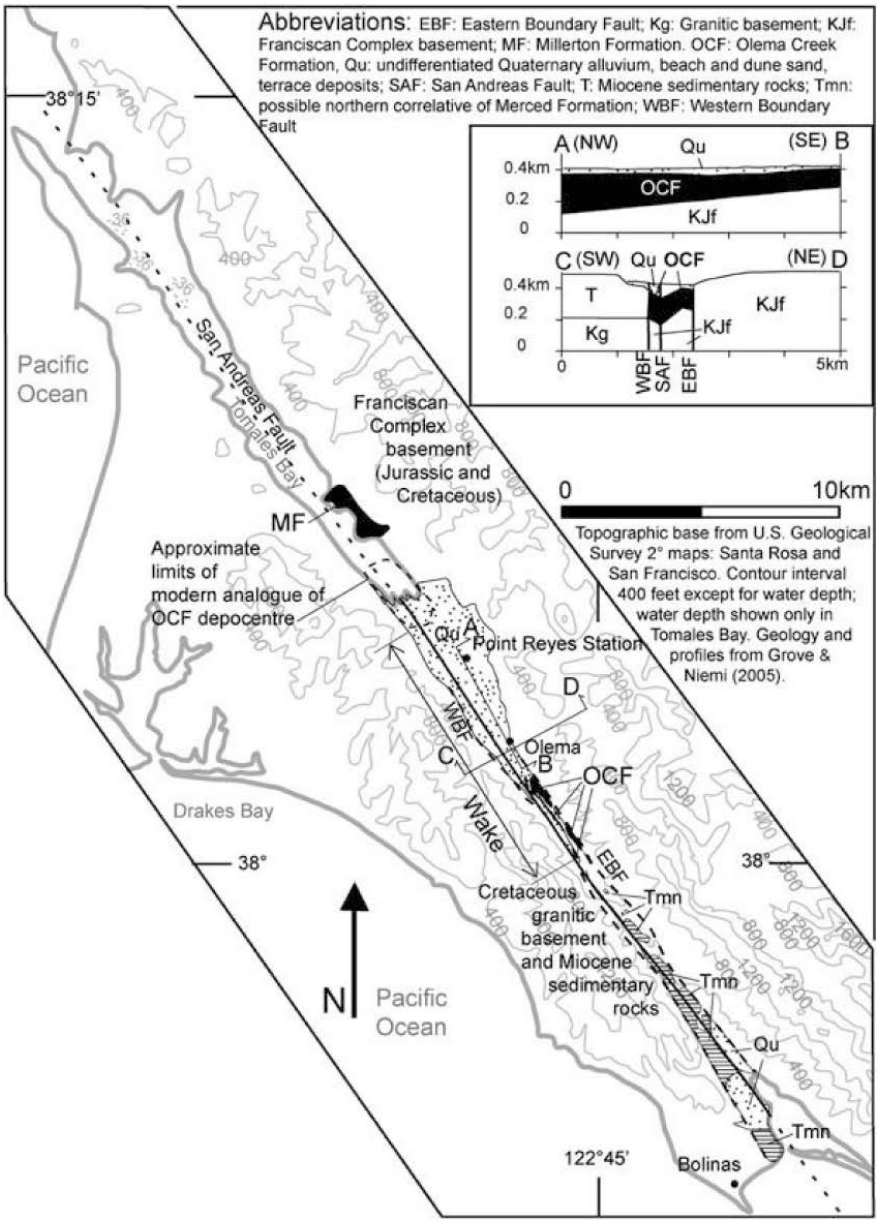


*Figure 2 : Schéma structural de la faille de San Andreas dans la région de la formation d'Olema's Creek (d'après Wakabayashi, 2007).*

La migration des dépôts centres au sein d'un même relais transtensif est une hypothèse également évoquée pour le bassin de la Mer Morte sur la faille du Levant, mais soumise à de nombreuses discussions (*Aydin and Nur, 1982; Ten Brink and Ben Avraham, 1989; Lazar et al., 2006*). La Mer Morte présente elle aussi de nombreux indices morphologiques, stratigraphiques et structuraux suggérant que des migrations de dépôt centres ont eu lieu : A) le bassin sud est sub-aérien, alors que le bassin nord est profond de 350 m, suggérant un abandon de la subsidence au Sud, relocalisée au Nord; B) de nombreuses failles transverses, rarement identifiées sur les relais de San Andreas, séparent différents dépôts centre *(Ce sont*

*les failles de Iddan, Amazyahu et Ein Gedi)*; C) l'analyse de la stratigraphie à partir des profils sismiques collectés dans la région montre que le mouvement en rollover de la faille listrique d'Amazyahu n'a commencé qu'au milieu du Pleistocène, alors que le bassin de la Mer Morte a près de 5 Ma (Pliocène ; *Ten Brink and Ben-Avraham, 1989).* La migration de la subsidence semble donc avoir eu lieu deux fois : tout d'abord lorsque le segment Miocène de la vallée d'Arava est devenu inactif, et ensuite lorsque la subsidence a migré du bassin sud vers le bassin nord de la Mer Morte actuelle *(Kashaï et Croker, 1988).*

A partir des observations ci-dessus, et en accord avec la synthèse de *Wakabayashi (2007),* nous pouvons conclure qu'il y a migration de relais lorsque : A) les dimensions des reliefs (positifs ou négatifs) formés par les relais sont bien inférieures à ce qui est attendu pour la quantité de glissement estimée le long du décrochement ; B) des phénomènes d'inversion tectonique de bassins pull-apart apparemment déconnectés des changements tectoniques régionaux ont eu lieu; C) des dépôts de bassin aujourd'hui inactifs sont retrouvés le long du décrochement principal, mais situés à proximité de bassins actifs.

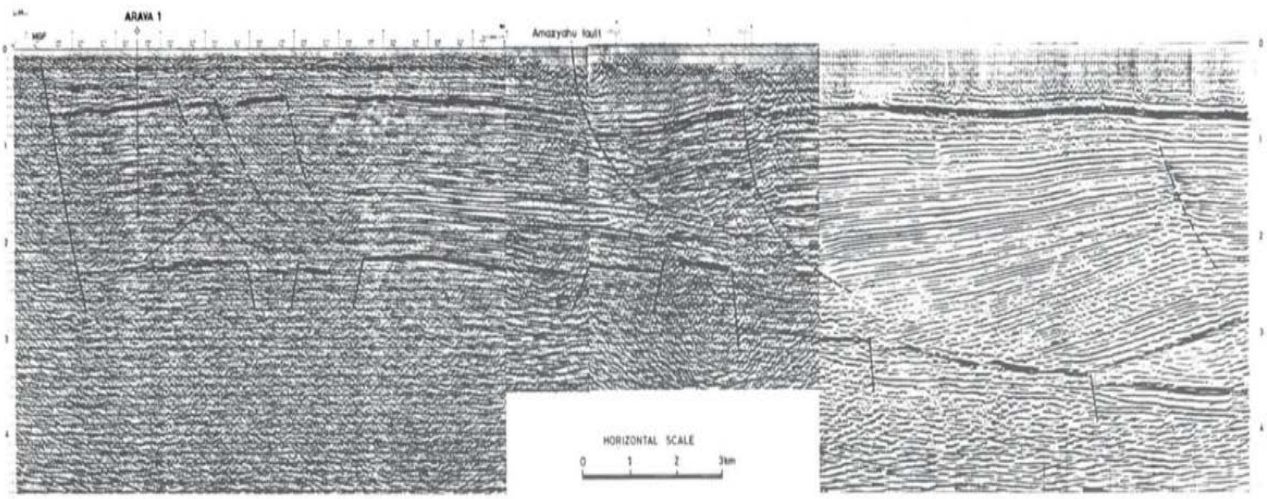


*Figure 3 : Profil sismique S-N recoupant la Mer Morte longitudinalement (d'après Kashaï et Croker, 1988). Les failles transverses délimitent des blocs basculés et leur pendage s'amortit en profondeur. Les failles transverses ne sont pas des structures de socle ré-activées.*

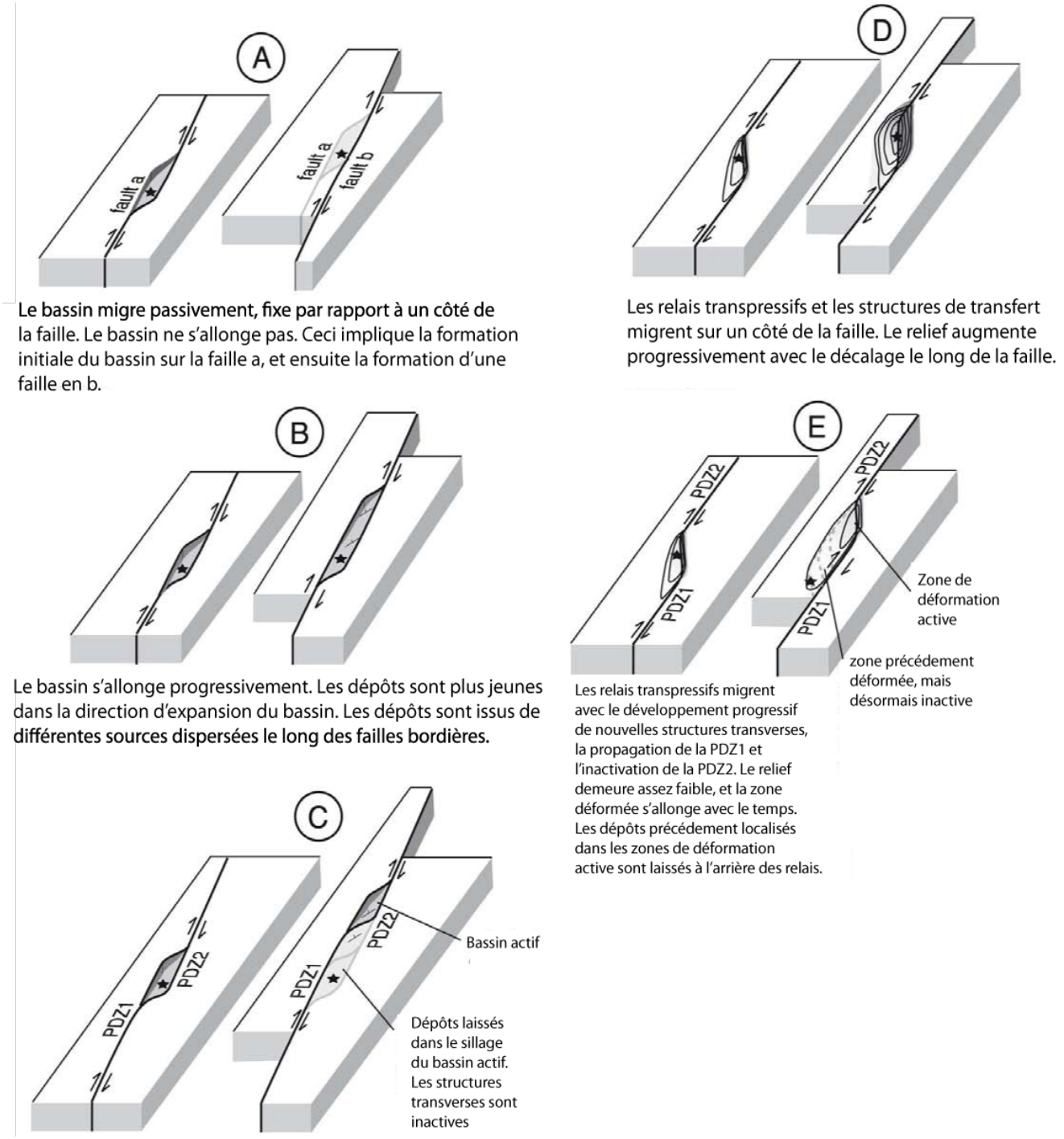


*Figure 4 : Blocs diagrammes synthétisant les différents scénarios possibles pour l'évolution structurale des relais le long d'un décrochement (d'après Wakabayashi, 2007).*

Quels mécanismes peuvent expliquer la migration de la subsidence et le développement de failles transverses? Comment ces mécanismes ont-ils lieu au cours du temps? *Smit et al. (2008)* ont testé, par le biais de modèles analogiques, le rôle des variations du rapport entre la largeur du relais et l'épaisseur de la couche déformée dans l'évolution des bassins pull-apart. Lorsque le relais est moins large que l'épaisseur de la couche déformée, les modèles réussissent à recréer la migration des dépôts centres au sein d'un bassin pull-apart. Les résultats obtenus ressemblent fortement à la structure du bassin de la Mer Morte. Ce modèle permet de comprendre comment se forment les failles transverses au cours de la migration des dépôts centres. Quand les failles transverses apparaissent, elles se connectent aux bordures du bassin et localisent la subsidence au nord de la faille, tandis que le bassin au sud devient inactif ; reproduisant ainsi la migration vers le nord de la subsidence observée dans le cas de la mer morte. Ceci implique que le socle du bassin repose sur toute sa longueur sur le décrochement du Levant, qui contrôle la géométrie du bassin et ses migrations. Cela implique aussi que la rhéologie de la lithosphère, ainsi que le rapport entre la largeur du relais et l'épaisseur de la croûte sont des facteurs de contrôle importants de la déformation au sein des couloirs transformants. Le sel dans la Mer Morte peut aussi jouer un rôle important (niveau de décollement) dans la formation de ces failles transverses et la migration des bassins.

Dans ces modèles, les failles transverses se forment progressivement dans la direction de la migration. Il est important de considérer ces failles comme des structures néo-formées en lien avec la migration des relais (comme suggéré par les modèles de *Smit et al. (2008)*), et non comme des failles pré-existantes soumises à une migration. Car si tel était le cas, le matériel délimité par ces failles migrerait lui aussi, et les relais se seraient agrandis. Les relais ne semblent migrer qu'une fois une certaine taille acquise, et abandonnent dans leur sillage les failles ayant délimité leur stades antérieurs *(Wakabayshi, 2007; Ten Brink et al., 1989)*. Ceci est une différence fondamentale par rapport aux modèles d'ouverture continue de *Mann (1983)*, impliquant que la croissance s'effectue toujours dans le même espace, en mobilisant toujours les mêmes accidents transverses. La migration des relais transtensifs suggère également que la faille bordant le pull-apart d'un côté se propage dans la direction de la migration du relais, laissant à l'arrière et condamnant à l'inactivité la faille qui borde l'autre côté du bassin. Une autre implication de la migration des relais est qu'ils se déplacent à une vitesse supérieure à celle du déplacement accommodé par le décrochement principal. Par exemple, le dépôt centre de la formation d'Olema a migré de 10 km par rapport à sa position initiale. S'il avait migré à la vitesse du déplacement de la faille de San Andreas, il ne serait

qu'à environ 5 km de sa position initiale. Des systèmes intermédiaires se mettent toutefois en place, où la vitesse de migration du relais est inférieure à la vitesse du décrochement principal. Enfin, concernant les inversions tectoniques des dépôts de bassin qui ne sont reliées à aucune phase de déformation régionale, *Wakabayash*i (2007) propose qu'elles soient le fait de la migration de relais transpressifs, dont la course rejoint la position précédemment occupée par un bassin actif. Le processus de migration des bassins peut alors être considéré comme une autre façon de répartir les contraintes au sein d'un couloir décrochant (prédominance de facteurs internes), indépendamment de tout changement cinématique.

Du fait de sa structure, le bassin 20°N est un cas d'étude privilégié pour questionner les processus de migration de la subsidence et de formation des failles transverses au sein d'un bassin pull-apart. Les données de sismique réflexion de la campagne Owen 2 ont permis de mieux contraindre la structure du bassin 20°N, et de comprendre son évolution structurale, détaillée dans l'article suivant (Rodriguez et al., accepté à Tectonics). De façon surprenante, aucun épisode de migration de subsidence n'est mis en évidence dans cette étude, ce qui m'a conduit à proposer un nouveau mode d'ouverture des bassins pull-apart.

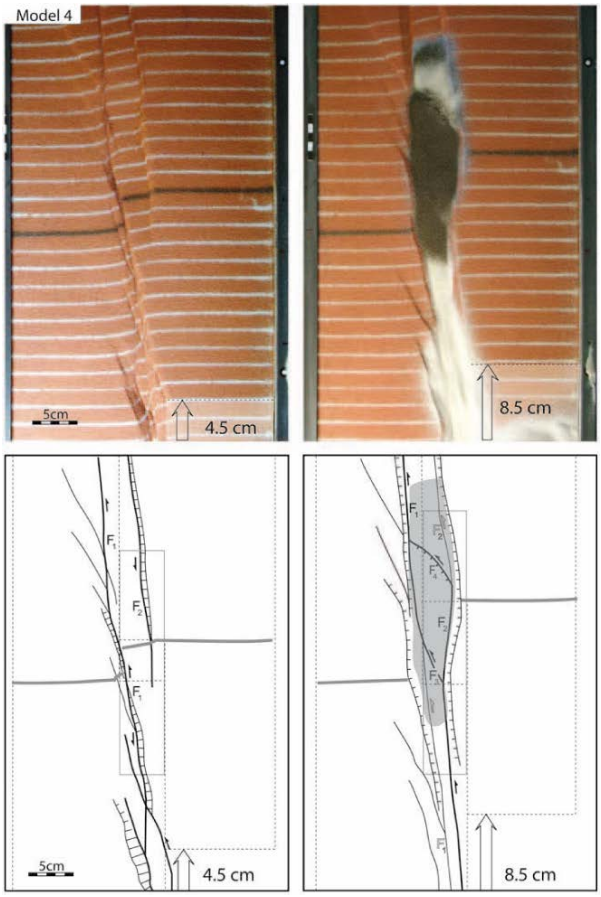


*Figure 5 : Résultat des modèles analogiques de Smit et al. (2008), montrant la formation des failles transverses et la migration de la subsidence au fur et à mesure que le décalage accommodé par le décrochement devient important (de 4.5 à 8.5 cm).*

Comparaison des modèles proposés pour l'ouverture et le développement du Bassin de la Mer Morte (d'après Lazar et al., 2006)

| | Bassins sur zone de relais (Aydin et Nur, 1982) | Propagation de bassins (Ten Brink et Ben Avraham, 1989) | Etirement des bassins (Garfunkel et Ben Avraham, 1996) | Bassins séquentiels (Lazar et al.,2006) |
|---|---|---|---|---|
| Nature des sub-bassins | Des bassins séparés sont formés entre une série de failles en échelon. Ces bassins finissent par fusionner pour former un grand bassin | Des sub-bassins de taille fixe fusionnent. Les sub-bassins se forment entre les extrémités des segments en échelon du décroche--ment principal | Allongement du bassin principal le long de l'axe du décrochement principal | Sub-bassins séparés, devenant de moins en moins profonds et de plus en plus étroits |
| Nombre de sub-bassins actifs à un instant donné | Une série de bassins actifs fusionnent | Un | Un | Plusieurs sub-bassins actifs |
| Localisation du dépôt centre actif | Non spécifié | Migre dans une direction le long de la faille principale. Les vieux bassins cessent d'être actifs. | Fixe au centre du bassin le plus large. Les sub-bassins sont inactifs | Chaque sub-bassin peut être actif |
| Failles transverses | Reliques des enjambements entre les branches du décrochement | Equidistantes, transfèrant le mouvement d'un segment à l'autre | Déterminées par le pull-apart initial. Les sub-bassins sont étirés lorsque les failles s'éloignent. | Délimitent et séparent les sub-bassins. La distance entre les failles varie. |
| Délimitation du système de bassin | Non spécifié | Non spécifié | Non spécifié | Les failles bordières se rapprochent. |

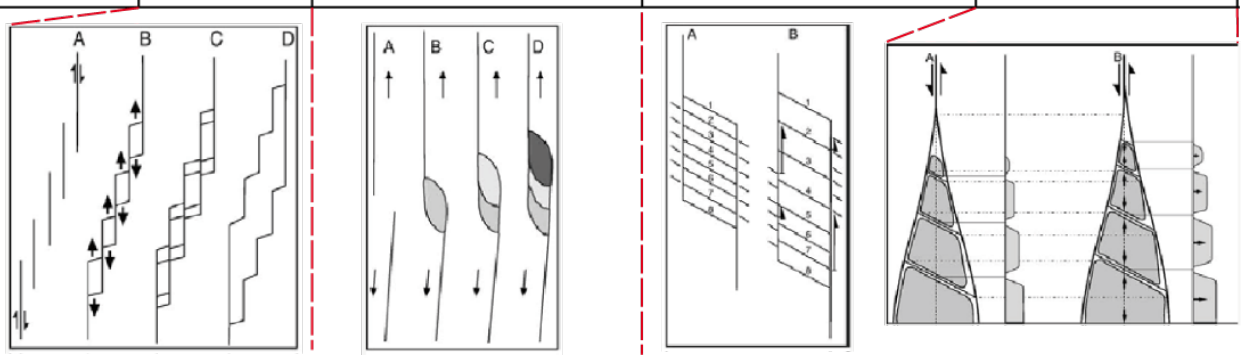


*Figure 6 : Synthèse des modes d'ouverture proposés pour le bassin de la mer Morte (faille du Levant).*

**Mode of opening of an oceanic pull-apart: the 20°N Basin along the Owen Fracture Zone (NW Indian Ocean)**

Mathieu Rodriguez[1,2,3*], Nicolas Chamot-Rooke[1], Marc Fournier[2,3], Philippe Huchon[2,3], Matthias Delescluse[1].

(1) Laboratoire de Géologie de l'Ecole normale supérieure, CNRS UMR 8538, 24 rue Lhomond, 75005 Paris, France

(2) Institut des Sciences de la Terre de Paris, CNRS UMR 7193, Université Pierre & Marie Curie, case 129, 4 place Jussieu, 75005 Paris, France

(3) iSTeP, UMR 7193, CNRS, F-75005 Paris, France

*Corresponding author: rodriguez@geologie.ens.fr

**Abstract**

**Pull-apart basins are common features observed at releasing bends along major strike-slip faults. The formation and structural evolution of such basins have mostly been investigated in the continental domain and by sandbox laboratory experiments or numerical models. Here we present recently acquired multibeam bathymetry, 3.5 kHz echo-sounder and seismic profiles across the 20°N pull-apart Basin along the India-Arabia transform boundary, known as the Owen Fracture Zone (OFZ). Using nearby oceanic drilling (DSDP 222) we constrain the structural evolution of the basin since opening some 3 Myrs ago. The 20°N Basin is large (90-km-long, and 35-km-wide) despite limited transcurrent motion (~10-km). The first stage involved the formation of a stepover along the OFZ and the subsequent isolation of a subsiding half-graben. Extension and subsidence were further partitioned over three distinct sub-basins separated by complex sets of transverse faults. The size of the basin was enhanced by gravity-driven collapse. The 20°N Basin has been a catchment for Indus turbidites since its opening, which provide a good record of syn-sedimentary deformation. The deformation related to the subsidence of the half graben mimics rollover structures commonly encountered in salt tectonics, suggesting that subsidence was accommodated by one or several décollement layers at depth. Despite a different rheological context, the sub-surface structure of the nascent oceanic 20°N Basin is very similar to the more mature continental Dead Sea Basin along the Levant Fault, which also displays sub-basins separated by transverse faults.**

## 1. Introduction

Pull-apart basins are topographic depressions commonly observed along strike-slip faults (see *Cunningham and Mann* [2007] for a synthesis). They occur in stepover-releasing bend areas, either in transtensional or pure strike-slip contexts [*Wu et al.*, 2010]. Pull-apart basins accommodate the transfer of slip between adjacent fault segments on both sides of the stepover region, generating higher subsidence rates with respect to other types of basin [*Christie-Blick and Biddle*, 1985]. First studies on the Dead Sea Basin proposed a progressive size increase of the basin with increasing finite strike-slip [*Aydin and Nur*, 1982; *Mann et al.*, 1983]. Subsequent works showed that the growth of the basin is accommodated by the coalescence of distinct sub-basins driven by a gravity process together with subsidence localization through times [*Ten Brink and Ben Avraham*, 1989; *Ten Brink et al.*, 1993]. More recent studies of the San Andreas Fault System show that stepover regions migrate along the main strike-slip fault [*Wakabayashi et al.*, 2004; *Wakabayashi*, 2007]. Either subsidence re-localization or migrating stepovers involve the formation of transverse faults orthogonal or oblique to the main strike-slip direction. Although progressive structure development within pull-apart basins has been the focus of many analog modelling works [*Rahe et al.*, 1998; *Basile and Brun*, 1999; *Smit et al.*, 2008; *Wu et al.*, 2010], few field examples constrain the precise age or the relative chronology of such structure emplacement [*Ten Brink and Ben Avraham*, 1989; *Carton et al.*, 2007; *Brothers et al*., 2009].

The 20°N pull-apart basin, named after its latitude, is situated in the Arabian Sea along the Owen Fracture Zone (hereafter OFZ), which is the currently active, pure strike-slip India-Arabia plate boundary (Figure 1) [*Fournier et al.*, 2011]. The 800-km-long dextral strike-slip system connects the Makran subduction zone to the north to the Aden-Owen-Carlsberg triple junction to the south (Figure 1; *Fournier et al.*[2008a]). The OFZ closely follows a small circle about the Arabia-India rotation pole determined with GPS and seismicity data, which predicts pure strike-slip motion along the entire fracture zone [*Fournier et al*., 2011], in contrast with the increasing transtension north of 18°N predicted by the MORVEL closure-enforced pole [*DeMets et al*., 2010]. As indicated by dextral strike-slip focal mechanisms of earthquakes, the Arabian plate moves northward slightly faster than the Indian plate with a relative motion of $3 \pm 1$ mm.y$^{-1}$ estimated independently from geodetic [*Reilinger et al.*, 2006; *Fournier et al.*, 2008b] and geological data [*DeMets et al.*, 1990, 1994, 2010]. The OFZ cuts through the Owen Ridge, a prominent relief affected by numerous submarine landslides [*Rodriguez et al.*, 2012; 2013]. Offsets of the Owen Ridge observed on the seafloor imply a finite dextral displacement of 10-12 km along the OFZ [*Fournier et al.*, 2008b; 2011]. Considering a steady motion of $3 \pm 1$ mm.y$^{-1}$, this indicates that the present-day trace of the OFZ has been active since at least 3-6 Ma.

The mean depth of the surrounding seafloor indicates that the 20°N basin cuts into thin crust, either oceanic or highly stretched continental. West, the substratum of the Owen Basin is a 6-km-thick oceanic crust [*Barton et al*., 1990] of Paleocene age according to deep-sea drillings [*Shipboard*

*Scientific Party*, 1974; 1989]. East, magnetic anomaly A28 (63 Ma), formed at the onset of seafloor spreading at the Carlsberg Ridge, is identified up to 19°N [*Dyment*, 1998*; Royer et al.*, 2002; *Chaubey et al.*, 2002]. North of anomaly A28, magnetic anomalies have been tentatively identified as the oceanic lineations of the Gop Basin (A31 or A29 to A25, 69/64 to 56 Ma, *Yateesh et al.* [2009]). The nature of the crust between the Arabian oceanic lithosphere and the Gop oceanic basin remains uncertain. It may correspond to the Laxmi-Palatina Ridge, which is interpreted as a continental remnant separated from the Seychelles Bank during its break-up from India ~65 Ma ago [*Minshull et al.*, 2008; *Yateesh et al.*, 2009; *Calvès et al.*, 2011]. The connection between these elements and the OFZ remains unstudied.

*Fournier et al.* [2011] and *Rodriguez et al.* [2011] used multibeam bathymetry and 3.5 kHz echosounder profiles to map the sub-surface structure of the 20°N Basin. The 20°N Basin is a 90-km-long and up to 35-km-wide pull-apart basin, which developed in a 12-km-wide stepover between two major segments of the OFZ (Figure 1). The overall structure of the basin is asymmetric, with the OFZ as a steep master fault on the western side, and a complex system of arcuate normal faults on the eastern sidewall. The 20°N Basin is divided in three distinct sub-basins (labelled SB1, SB2 and SB3 in Figure 1) limited by transverse faults. Sub-basins 1, 2, and 3 extend over 70 km², 340 km², and 590 km², respectively. The 20°N Basin deepens abruptly northward, as sub-basins 1, 2, and 3 form relatively flat areas respectively 60, 100, and 360 m deep with respect to the non depressed surrounding seafloor. A system of *en-échelon* faults is observed on its southeastern side. An active turbiditic channel cuts through the arcuate fault system and feeds SB3, which has recorded the Indus deep-sea fan activity since the opening of the basin [*Rodriguez et al*., 2011].

The structural characteristics of the 20°N Basin raises several questions about the mode of pull-apart basin opening in an oceanic setting. First, the dimension of the 20°N Basin is much larger than the relative motion accommodated by the OFZ since its inception by almost one order of magnitude, thus invalidating some models [*Aydin and Nur*, 1982; *Petrunin and Sobolev*, 2006]. This raises the question of how extensional deformation is distributed in a stepover basin, and what mechanism is responsible for the high amount of subsidence. Second, it remains unclear whether sub-basins are still all active or not [*Rodriguez et al.*, 2011]. The origin of transverse faults within pull-apart basins, together with subsidence localization processes through times, are key processes in the structural evolution of pull-apart basins [*Ten Brink and Ben Avraham*, 1989; *Ben Avraham and Ten Brink*, 1989; *Smit et al.*, 2008a,b].

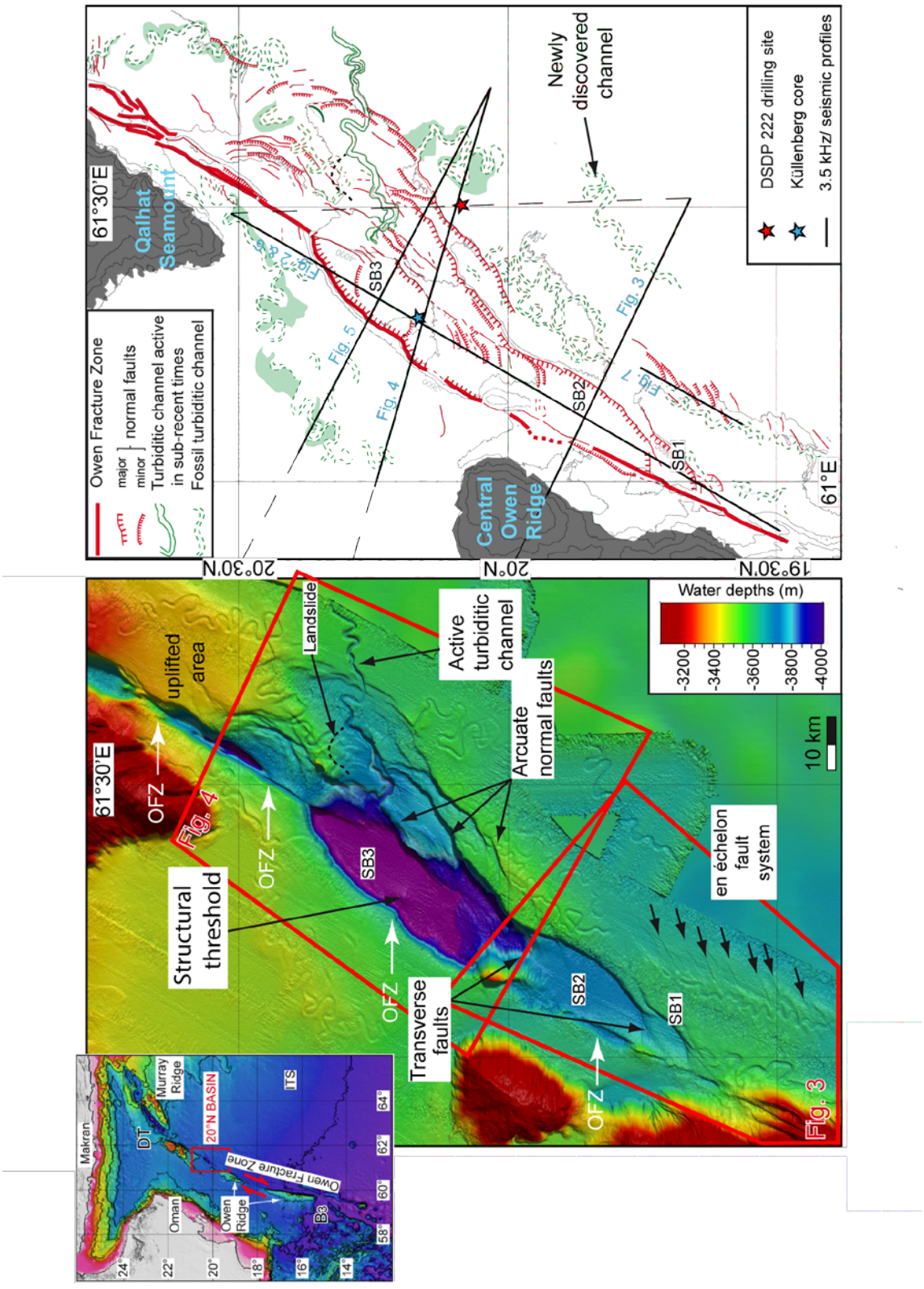


***Figure 1 :*** *Multibeam map of the 20°N pull-apart basin and interpretative structural scheme, together with the location of seismic profiles, cores and drilling available in the study area. Inset on the left hand corner shows the regional framework of the 20°N Basin. B3: Beautemps-Beaupré Basin, DT : Dalrymple Trough, ITS: Indus Turbiditic System, OFZ: Owen Fracture Zone, SB: sub-basin.*

The aim of this study is to constrain the structural evolution of the 20°N Basin since its inception, through the analysis of newly acquired seismic lines. The close location of DSDP site 222, together with Küllenberg cores from *Bourget et al.*[2013], provide a good stratigraphic control on seismic lines (Figure 1). Seismic profiles document the nature of sedimentary deposits (in particular, pelagites versus turbidites), which are essential to the understanding of the active deformation in marine environments (e.g., [*Barnes and Pondard,* 2010; *Pondard and Barnes,* 2010]). The tectonic activity and related topographic changes strongly influenced the course of distal Indus turbiditic channels as well as the emplacement of bottom-current. Turbiditic and contouritic deposits provide good dated landmarks of the opening of the 20°N Basin. The structure of the 20°N Basin is compared with other pull-apart basins (with a particular emphasis over the Dead Sea Basin) and analog modeling studies [*Smit et al.*, 2008 a,b; *Brun and Mauduit*, 2008; *Dooley and Schreurs*, 2012].

## 2. Structure of the 20°N pull-apart basin

### 2. 1. Seismic dataset

Here we present a dataset composed of four seismic lines (located on Figure 1), complementary documented by 3.5 kHz profiles collected during the OWEN (2009) and OWEN-2 (2012) cruises on board the R/V *Beautemps-Beaupré*. Seismic reflection profiles were shot using two GI air guns and a short 600 m-long streamer allowing high-speed acquisition (10 knots) and a penetration of the order of ~2s TWT. The processing consisted in geometry setting, water-velocity normal move-out, stacking, water-velocity F-K domain post-stack time migration, band pass filtering (8-80 Hz) and automatic gain control. All profiles are displayed with a vertical exaggeration of 8 at the seafloor. Two-way travel times in the sediments were converted to depth using 1530 and 1730 m. $s^{-1}$ lower and upper bounds for the P-wave velocity. This range of values covers safely the measurements performed in the same type of pelagic sediments at others ODP and DSDP sites in the area [*Shipboard Scientific Party*, 1974; 1989]. Depth values are given with respect to the surrounding seafloor. In the following, sedimentary series before the opening of the 20°N Basin are referred to as the “substratum” of the 20°N Basin , which is employed in the sense of “pre-rift” series, in order to avoid the confusion with the oceanic basement of the Owen Ridge observed on several profiles. The reflectors picked on seismic profiles have been selected upon the base of seismic discontinuities that either reflect lithological changes, stratigraphic hiatuses or tectonic deformation.

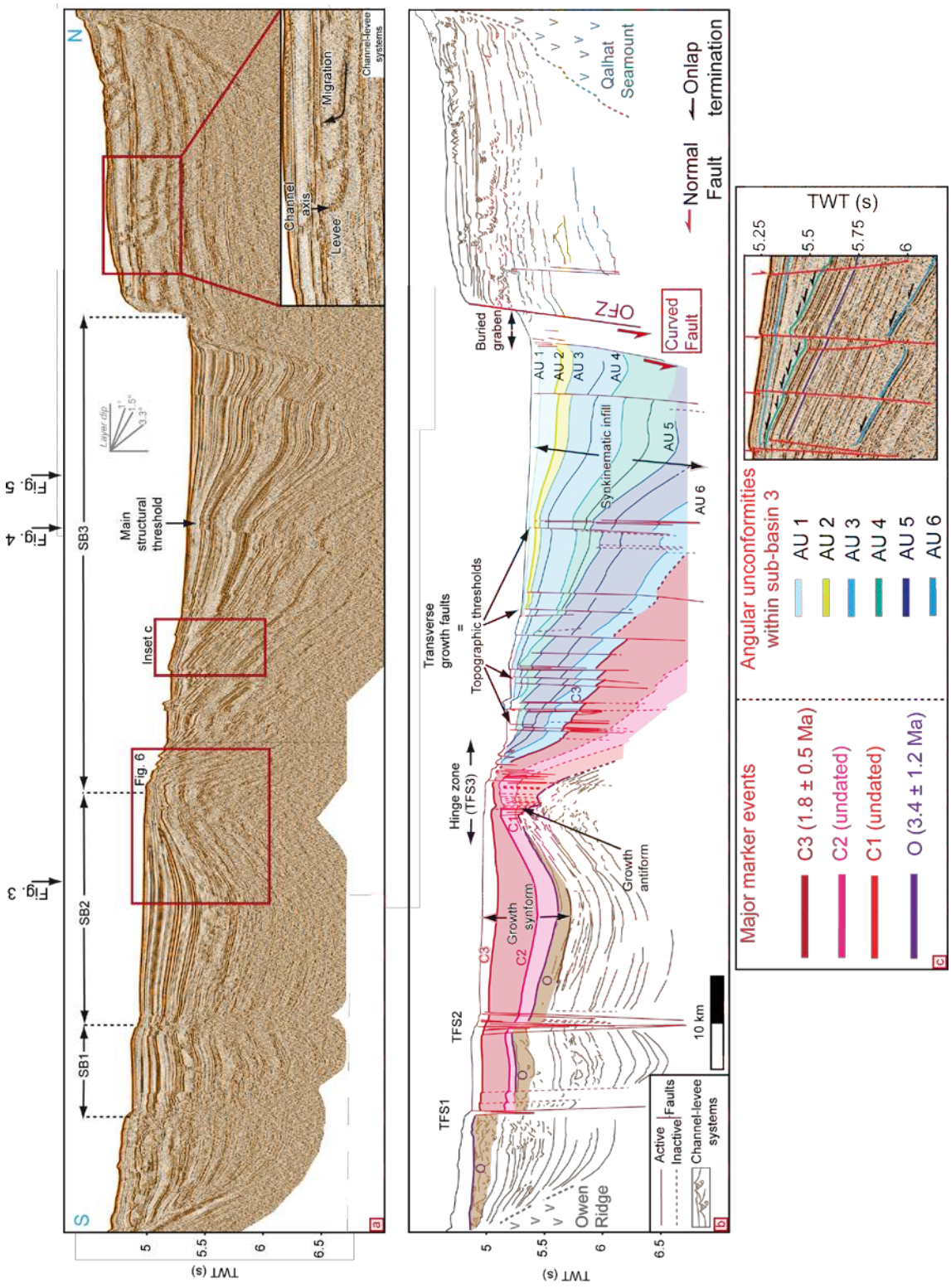


***Figure 2:*** *Longitudinal seismic line crossing the 20°N Basin (see Figure 1 for location). Inset shows a close-view of migrating turbiditic channels. Inset c) presents the horizons mapped in seismic section across the 20°N Basin and their stratigraphic significance. The 20°N Basin is composed of three sub-basins labeled SB1, SB2, and SB3 from south to north. The sub-basins are separated by Transverse Fault Systems (TFS).*

### 2. 2. Architecture of the 20°N Basin

A NNE-SSW-trending longitudinal profile crosses the three sub-basins (SB1, SB2, SB3) and provides a general picture of the 20°N Basin (Figure 2). The three sub-basins are asymmetric and bounded by non-equidistant transverse faults systems (Figure 1). Three additional ESE-WNW seismic profiles (Figures 3, 4, 5) cut these transverse structures, allowing discussing their main structural characteristics and their relation with the eastern arcuate fault system. In the following we describe the longitudinal structure of the 20°N Basin from south (SB1) to north (SB3), as well as the transverse structures of SB2 and SB3.

The deep longitudinal structure of the 11-km-long SB1 in Figure 2 shows reflectors tilted to the south below 5.3 s (TWT), which contrasts with the flat reflectors above. At the seafloor one single oblique normal fault bounds SB1 southward, but the longitudinal profile reveals additional normal growth faults buried below 5 s (TWT) (Figure 2).

A set of transverse normal faults, clearly expressed at the seafloor, makes the junction with SB2. Although flat topped, SB2 displays a syncline structure at depth both on the longitudinal (Figure 2) and the transverse (Figure 3) profiles. The symmetry of SB2 indicates that west and east bounding faults accommodate nearly the same rate of subsidence (Figure 3). On the longitudinal profile, the tilt of the northern limb of SB2 is more pronounced than the southern limb, which is nearly flat (Figure 2). The increase of seismic horizons dip with depth on both transverse and longitudinal sections suggests that SB2 is a growth structure (i.e. the structure grows while simultaneously covered by sediments). Minor normal faulting is observed below 5.5 s (TWT) on the transverse profile (Figure 3). An anticline separates SB2 from SB3 (Figures 1, 2), forming a hinge zone characterized by the progressive tilting of sedimentary layers on both of its limbs. Numerous non-equidistant transverse growth faults, characterized by the increase of their throw with depth, cut through the hinge zone. There, numerous faults observed at depth below 5.2 s (TWT) are not expressed at the seafloor (Figure 2), suggesting that they are inactive.

SB3 is the largest of the three sub-basins. It forms a half-graben on the longitudinal section, and a syncline on the transverse ones (Figures 4, 5). This half-graben is bounded to the north by the OFZ with a strong normal component there. The longitudinal fanning configuration of the turbiditic deposits in SB3 reflects its strong structural asymmetry, indicating that most of the subsidence is accommodated by the OFZ (Figure 2). The configuration of SB3 deposits is typical of a rollover anticline [*Cloos*, 1968; *Brun and Mauduit*, 2008]. At the hanging wall of the OFZ, 20°N Basin deposits have progressively buried a 4-km wide graben composed of Indus fan sediments, which is bounded by a transverse fault slightly expressed at the seafloor (Figures 1, 2). Subsidence within SB3 is controlled by a set of numerous transverse growth faults that show a subtle expression at the seafloor (Figures 1,

2). The growth fault activity is associated with the increasing tilt of the sedimentary layers. The rate of displacement of the transverse growth fault located at the latitude of 20°10'N is larger than the surrounding faults, which formed the main structural threshold within SB3 (Figure 2).

The last main structural characteristic of SB3 is the dense network of arcuate faults on the eastern side of the basin (Figures 1, 4, 5). The density of normal faults decreases towards the Indus plain. The offset of sedimentary layers cut by arcuate faults is roughly constant at depth. The entire arcuate normal fault system has accommodated over 500 m of distributed subsidence.

## 3. Stratigraphic framework

Correlation of seismic horizons documents the timing of faulting and folding through dating based upon sedimentation rates or relative chronology dating. The correlation of 20°N Basin deposits also documents periods of connection between sub-basins controlled by the competition between sedimentation and structure growth. The dataset partially images the depth of the substratum of the 20°N Basin, i.e. the depth of the last Indus channel-levee system deposited before its opening (Figure 2). The stratigraphic ages of major chronologic markers are summarized in Figure 2 (inset c) and Table 1.

### 3. 1. Identification of sedimentary deposits

The identification of sedimentary deposits in the 3.5 kHz and seismic profiles is based on their seismic characters and correlation with DSDP site 222 [*Shipboard Scientific party*, 1974] and Küllenberg cores from *Bourget et al.* [2013] (see Figure 1 for location). Turbiditic deposits are observed in all seismic profiles crossing the Owen and Indus abyssal plains, in agreement with DSDP site 222 [*Shipboard Scientific party*, 1974]. Indus Fan sedimentation started during the Middle Eocene as the result of the onset of the India-Eurasia collision and accelerated since the Early Miocene until Pleistocene in the area of the 20°N Basin [*Clift et al.*, 2001; *Clift*, 2002].

The arcuate fault system east of SB3 affects a complex sequence of channel-levee systems. They display well-stratified horizons with successions of high and low amplitude reflections on 3.5 kHz and seismic profiles (Figures 2, 3, 4, 5). Turbiditic processes commonly form channel-levee systems that are easily detectable (inset in Figure 2a). Channel axes are characterized by a typical lens-like architecture with a concave-up lower boundary, and discontinuous, high amplitude reflections. The associated levees display a wedge shape, high amplitude, and transparent seismic facies. Migration of the channel axis is indicated by lateral shifts of the channel infill facies. In the area of the 20°N Basin, a Pleistocene pelagic drape overlies fossil turbiditic channels observed in the Indus and Owen abyssal

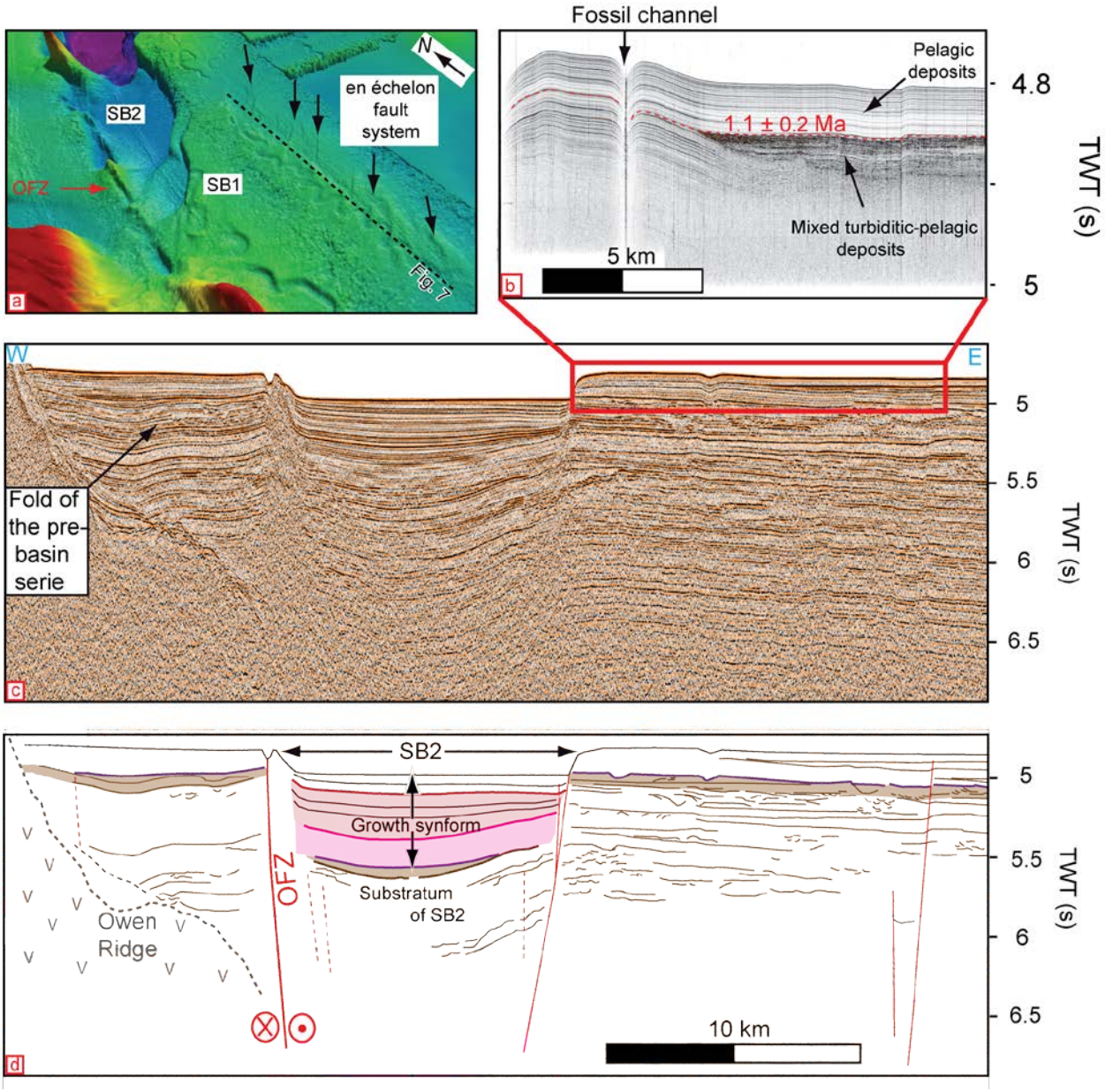


***Figure 3:*** *a) 3D bathymetric view of the en-échelon fault system near SB1 and SB2. b) 3.5 kHz profiles crossing the channel dissected by 20° Basin faults. 1.1 ±0.2 Ma-old turbiditic deposits overlying this channel come from an adjacent, unfaulted channel. c) Seismic profile transverse to SB2 and d) the related interpretation. See Figure 1 for location and Figure 2c for stratigraphic captions. OFZ: Owen Fracture Zone, SB: sub-Basin.*

plains. The pelagic drape has preserved their morphology over millions of years (Figures 2, 3, 4, 5) [*Shipboard Scientific Party,* 1974*; Rodriguez et al.,* 2011]. Pelagic deposits display well-stratified, continuous and conformable horizons on 3.5 kHz profiles (Figures 3, 4, 5), which sometimes mimic the turbiditic facies. The pelagic drape is composed of detrital clay nanno-ooze to nanno-rich detrital carbonate silty clay [DSDP site 222, *Shipboard scientific party,* 1974]. A pelagic facies is also observed in the uppermost section of the SB1 and 2. Additionally, some mass transport deposits are occasionally observed at the edge of some faults of the arcuate system (Figure 4). They display a typical chaotic to transparent facies on both 3.5 kHz and seismic data.

Deep-sea currents disturbed by the topography of the 20°N Basin influenced the architecture of the pelagic cover at the edges of the 20°N Basin. Deep-sea currents typically induce significant lateral thickness variations related to lateral gradients of current velocity, and geometric discontinuities related to variations of current activity through time. Typical sigmoid geometries composed of reflectors non-parallel to the accumulation surface [*Faugères et al*., 1999; *Faugères and Mulder,* 2011]. were observed on the western edge of the 20°N Basin (Figure 5) and over some of the arcuate normal faults to the east (Figure 4).

Sub-basin 3 displays particularly thick and transparent sedimentary layers on seismic profiles, with strong lateral thickness variations (Figures 2, 4, 5). This facies corresponds to turbiditic deposits according to Küllenberg core analysis [*Bourget et al,* 2013]. Ponded turbidites are commonly observed in pull-apart basins [e.g. pull-apart basins in the Marmara Sea, *McHugh et al*., 2006; *Beck et al.*, 2007] since they represent very restricted areas of deposition in comparison to abyssal plains. The volume of the turbiditic plume, usually spread over large surfaces, is thus confined and the plume material is submitted to oscillations, leading to strong sediment sorting. Coarser grains are deposited at the bottom of the sequence and favour high amplitude reflection, whereas the muddy part of the flow concentrates and produces the observed thick, transparent facies on seismic profiles. A typical characteristic of such deposits is that they can smooth and flatten the pre-existing topography if voluminous enough (Figure 2).

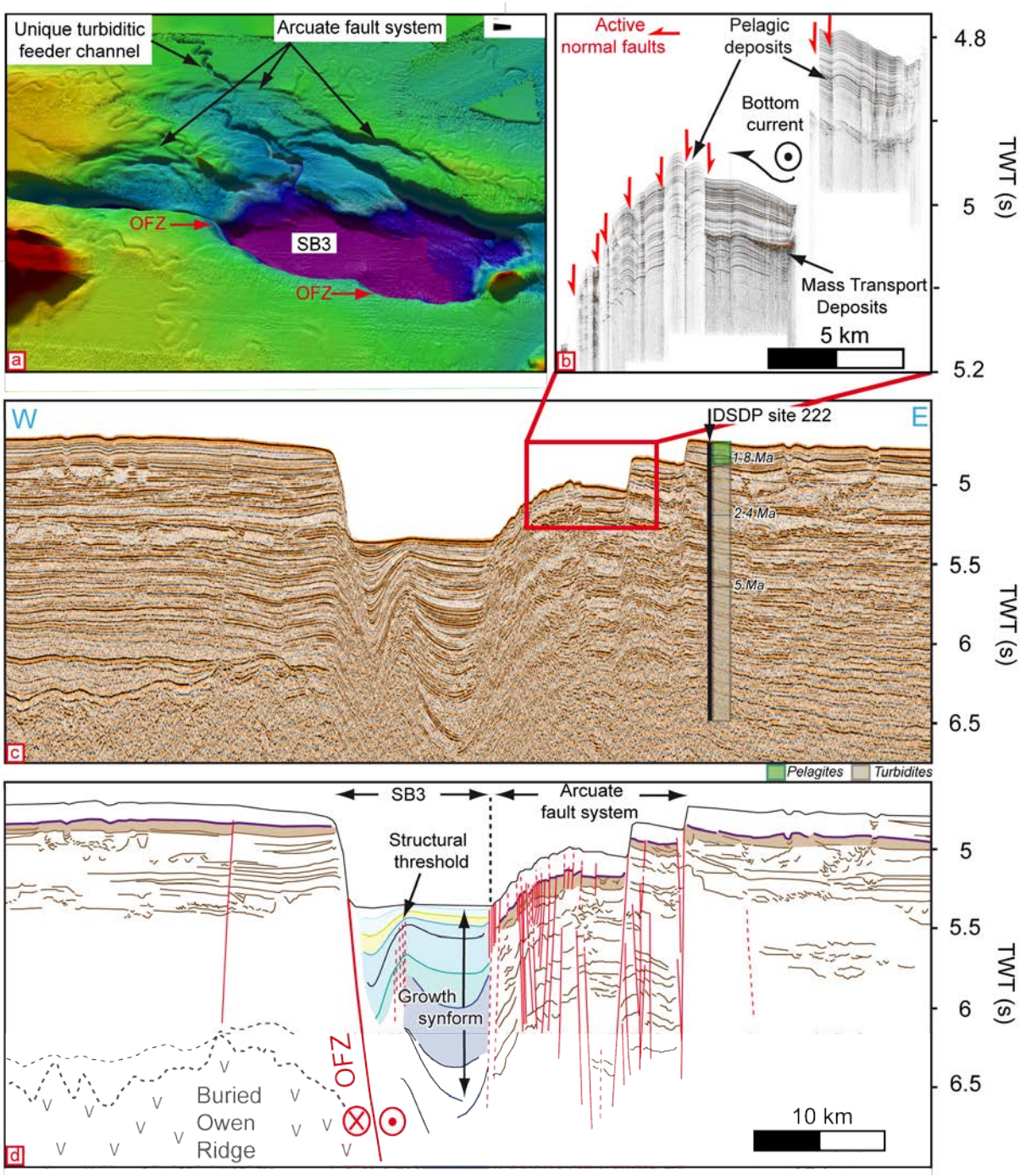


***Figure 4:*** *a) 3D bathymetric view of SB3 and its arcuate normal fault system. b) 3.5 kHz profile crossing the arcuate normal fault system. c) Seismic line transverse to SB3 and d) the related interpretation. DSDP site 222 documents a Pleistocene pelagic cover overlying Pliocene and Miocene turbidites from the Indus Fan [Shipboard Scientific Party, 1974]. See Figure 1 for location and Figure 2 for stratigraphic captions. OFZ: Owen Fracture Zone, SB: sub-Basin.*

### 3. 2. Age of the 20°N Basin

Several fossil turbiditic channels coming from the Indus fan [*Rodriguez et al*., 2011] are observed at the seafloor on both sides of the 20°N Basin (i.e. west and east, Figure 1). Assuming they were travelling in the abyssal plain, traces of their activity should predate the opening of the 20°N Basin and therefore give its maximal age. Consistently, the last folded layer on the western side of SB2 (Figure 3) is formed by a channel-levee system. Seismic reflection profiles show that faulted fossil channel-levee systems located both on the western and eastern side of the 20°N Basin are covered by a 0.14-0.16 s (TWT)-thick pelagic drape (corresponding to 105-140m) (Figures 4, 5). DSDP site 222 and ODP site 722 sedimentation rates [*Shipboard scientific party*, 1974, 1989] range between 30 and 46 m. $Ma^{-1}$ for the Pleistocene interval, which gives a ~3.4±1.2 Ma age of deactivation of the channels (Table 1). Traces of late activity of the turbiditic channels found east of the 20°N basin (Figure 3) can be dated at 1.1 ± 0.2 Ma using the same method. The important clue is that these turbidites are not found on the opposite (western) side of the basin, the depression acting as a topographic barrier.

The sigmoid pattern in the pelagic sediments at 4.8 s (TWT) on the western edge of the OFZ (Figure 5) probably indicates a local reorganization of the deep-sea currents at the onset of the drastic subsidence at SB3. Thus, the age of opening of the 20°N Basin, i.e., the age of a well developed topographic step along the OFZ, can be estimated independently by dating the last pelagic layer unaffected by bottom current at 4.8 s (TWT). Trough seismic correlation (Figure 5a), we measured the pelagic thickness overlying the 4.8 s (TWT) reflector in an area unaffected by bottom currents further west in the Owen Basin. The 0.09-0.12 s (TWT)-thick cover measured on the western side of the basin (Figure 5a) indicates an age of 2.5 ± 1.0 Ma according to DSDP-ODP sedimentation rates (Table 1). Using the age of cessation of activity of the channels and the age of initiation of the contouritic deposits, we conclude that the opening of the 20°N Basin started around ~3 Ma.

### 3. 3. Identification of the substratum of the 20°N Basin

The identification of a buried channel-levee system within the 20°N Basin gives the maximal depth of the substratum. The assumed depth of the substratum (i.e. pre-opening strata) is labelled "O" (which stands for Opening) and picked in purple on seismic lines. The age of the substratum is assumed to be the same as the age of the opening of the basin, i.e. ~3 Ma. In the area of SB1, a channel-levee system from the Indus fan is identified at ~5.3 s (TWT), which must be considered as the maximal depth of the substratum of SB1. The last active channel-levee system identified west of SB2 (Figure 3) can be confidently correlated within the basin. Its top marks the maximal depth of the substratum. Below this key O-reflector, the dip of the reflectors is rather constant, local and limited lateral thicknesses variations are due to fossil channel-levee systems of the Indus fan. This contrasts with the growth fold con-

figuration observed above the O-reflector (Figures 2, 6), which indicates active and long-lived subsidence.

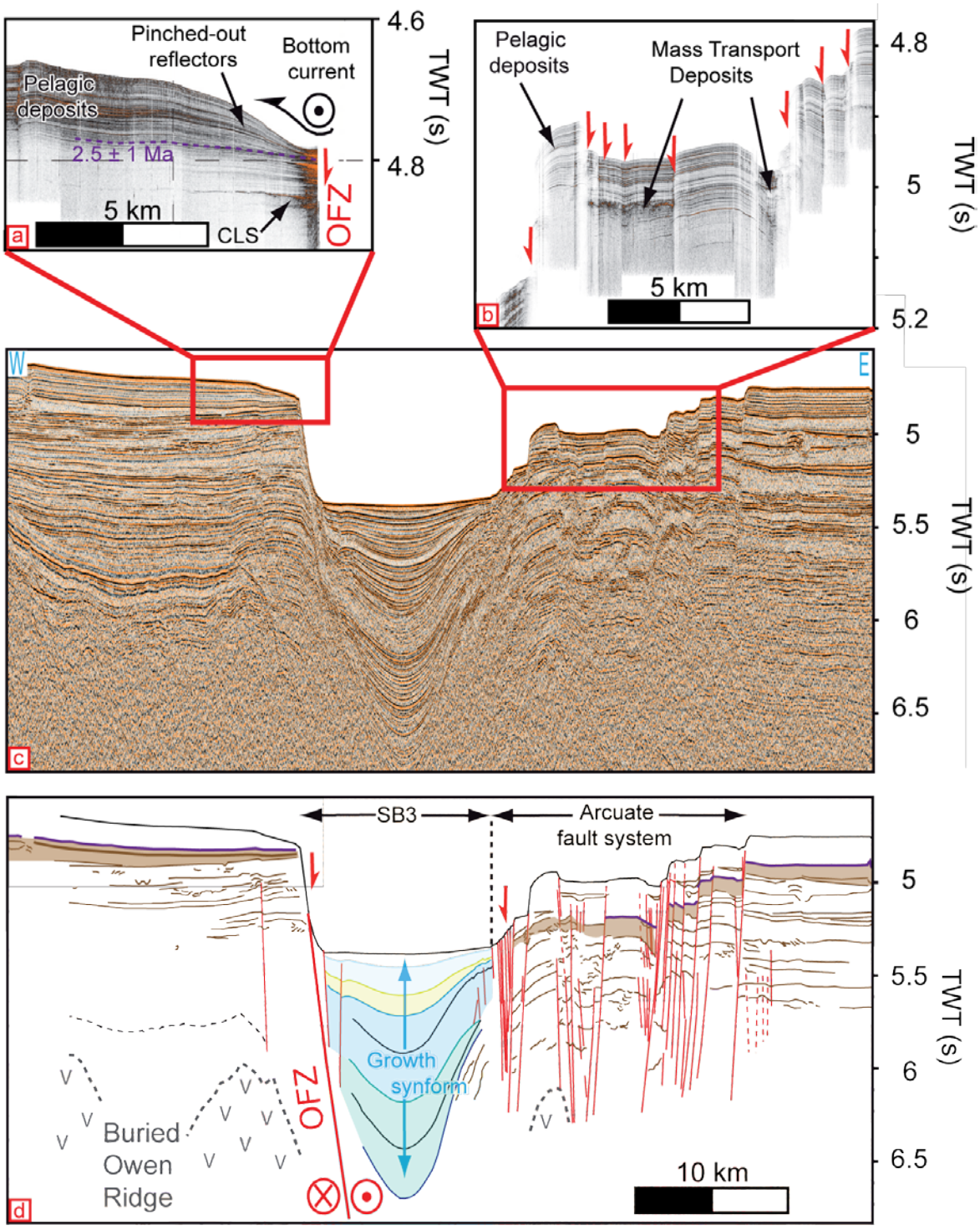


***Figure 5:*** *a) 3.5 kHz profile showing the influence of bottom-current on sediment architecture on the western edge of the 20°N Basin. b) 3.5 kHz profile crossing the arcuate normal fault system. c) Seismic line transverse to SB3 and d) the related interpretation. See Figure 1 for location and Figure 2 for stratigraphic captions. OFZ: Owen Fracture Zone, SB: sub-Basin.*

The substratum of SB3 was not reached. An angular unconformity is observed between 5.3 and 5.7 s (TWT) in the area of the transverse fault system between SB2 and SB3 (Figures 2, 6). This surface is evidenced by toplap terminations of the underlying deposits (Figure 6). The overlying deposits adopt an onlap configuration over the unconformity (Figures 2, 3, 6). Although difficult to pick because of the density of faulting, this unconformity seems to correlate fairly well with the substratum of SB2. It indicates that the unconformity marks the onset of subsidence of SB2 and SB3 together with the beginning of growth folding along the hinge zone between SB2 and SB3.

### 3. 4. The sedimentary infill of the 20°N Basin

The present-day feeder channel of the 20°N Basin incises the arcuate fault system to the east (Figures 1, 4). Closeby channel-levee systems are all inactive since the opening of the basin, which implies that the present-day feeder has been the only turbiditic route to the basin. The depth of the thalweg has preserved the feeder-channel from major avulsion during the last million years. The longitudinal seismic profile across the 20°N Basin (Figure 2) shows that recent turbiditic deposits are confined in the northern part of SB3 (which is the depocenter), and that the southern part of SB3, and SB2 and SB1 are currently isolated from turbiditic deposits since the reflector picked in yellow (named AU2 in Figure 2). This reflector is about 120 ka-old according to the correlation with a Küllenberg core collected within SB3 [*Bourget et al.*, 2013]. The overlying reflectors display a pinched-out configuration towards the south and end abruptly on the tilted topography created by a transverse growth fault (Figure 2). In sub-recent times, the topography accumulated by this growth fault activity has exceeded the sedimentary supply, leading to the disconnection of the southernmost part of SB3 (Figure 2). Because of the progressive tilting of the sedimentary layers through times in each sub-basin, one should consider that the deepest tilted horizons in the present-day configuration were nearly flat when deposited.

At least 7 angular unconformities are identified within SB3 (labeled AU1 to 6 and C3, Figures 2, 4, 5) and indicate periods of turbiditic starving, promoting disconnection within SB3 compartments. Similarly, the growth of the hinge zone between SB2 and SB3 promoted the disconnection of these sub-basins, currently blanketed by pelagic deposits [*Rodriguez et al.*, 2011]. The thickness of deposits above the substratum of SB1 and SB2 (reflector "O") is much larger than what would be expected with pelagic processes alone (0.1 s (TWT) corresponds to 1.4-1.7 Ma according to DSDP site 222 sedimentation rates). This suggests periods of turbiditic deposition in SB1 and SB2, i.e. connection with SB3. Four sedimentary units can be distinguished within SB2 since the opening of the basin, and interpreted in term of episodes of connection or disconnection with SB3.

1- The first unit is delineated by the discontinuity “O” on the bottom and the red reflector (labeled C1) on the top (Figure 2).

2- The second unit (between reflectors C1 and C2) shows a constant thickness, and can be correlated toward the SB3.

3- The third unit is delineated by the pink reflector (labeled C2) on the bottom and the dark red reflector on the top (labeled C3) (Figure 2).

4- The fourth unit is defined by the reflector C3 at the bottom and the topography.

In the deepest part of the hinge zone, sediments belonging to SB3 onlap the unconformity "O" (referred to as the substratum of the 20°N Basin) and end abruptly on a fault belonging to the hinge zone (Figures 2, 6). In the hinge zone, the fault delineated by the abrupt termination of sediments might have acted as a topographic barrier and favoured sub-basin disconnection in the first stages of opening. The second unit is likely to mark the first episode of connection between SB2 and 3. The correlation shows that an episode of connection between SB1 and SB2-3 occurred before the reflector C3. Unfortunately, we cannot precisely date when the connection between SB1 and SB2 established. SB1 may have been in an elevated position with respect to SB2 until the time of reflector C2, and isolated from deposits coming from the feeder channel. The geometry of the third units is characterized by large lateral variations of layer thickness, and pinched-out configuration of reflectors on the hinge zone (Figures 2, 6) and the bounding faults (Figure 3). This configuration is very similar to what is observed on transverse growth structures in SB3 (Figure 2), and indicates a change in the sedimentation/ topography growth balance. The seismic correlation of the longitudinal profile shows that the definitive disconnection between SB2 and SB3 occurred at the time corresponding to reflector C3 (at 5 s TWT) (Figure 2). According to the ~68 m thick overlying pelagic cover measured in SB1, this disconnection occurred ~1.8 ± 0.5 Ma ago.

**4. Activity of structures in the 20°N Basin**

Turbiditic processes provide frequent snapshots of fault activity by erasing the topography. In contrast, slow pelagic sedimentation rates do not exceed the rate of fault activity, which results in a permanent fault scarp [*Barnes and Pondard*, 2010]. In seismic, it may be difficult to recognize a fresh fault scarp (active fault) from a pelagic drape of an inactive scarp. The arcuate fault system on the eastern sidewall is dominantly covered by pelagic deposits, as shown by both 3.5 kHz and seismic profiles (Figures 4, 5) [*Rodriguez et al.*, 2011]. However, mass transport deposits are observed at the edge of some fault scarps on multibeam, 3.5 kHz and seismic data (Figure 5), whereas there are absent in the older sequences This strongly suggests that fault activity is responsible for mass failures. These mass transport deposits are about 1.2 ± 0.3 s (TWT) Ma old according to the thickness of the overlying pelagic cover, which indicates a minimal age of activity of the arcuate fault system. Further, the topographic profile running through the

axis of the feeder channel displays several major knick-points, which indicates that the arcuate fault system is still active [*Bourget et al.*, 2013]. The turbiditic infill of SB3 provides a good record of the activity of the numerous transverse growth faults. Only a few faults are inactive (dotted lines in Figure 2). The signification of angular unconformities within the SB3 remains ambiguous. They could either indicate coeval periods of abrupt increase in fault activity, or period of sediment starving. In the latter case, deformation is still accumulating on each fault during periods of non-deposition, but the record is discontinuous.

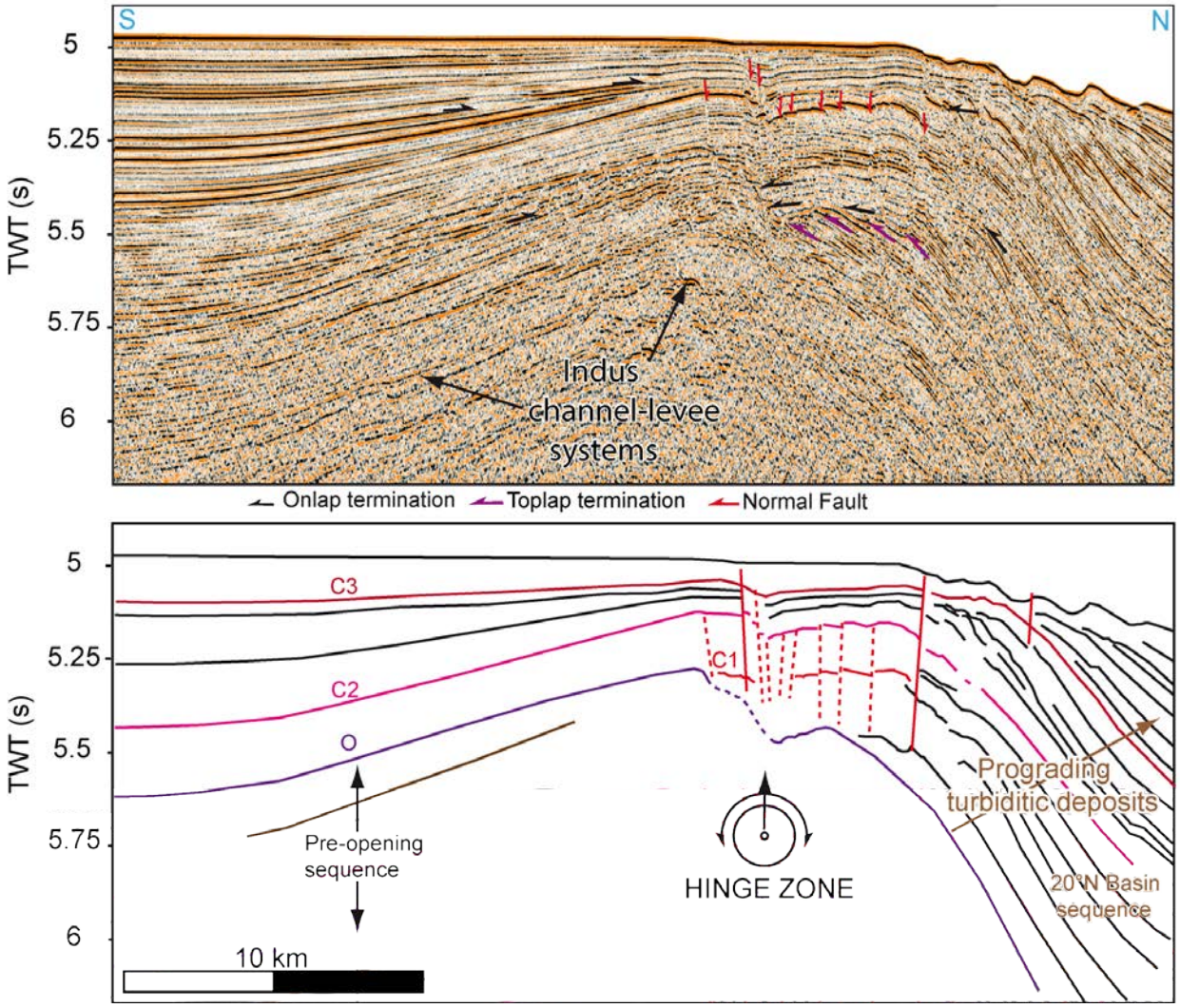


***Figure 6*** *: Close-view of the longitudinal seismic profile crossing the hinge zone between SB2 and SB3. See Figure 2 for location and for stratigraphic captions.*

The record of deformation in SB1 and 2 is dependent upon episodes of connection with SB3. An undeformed pelagic cover seals the buried growth faults identified south of SB1 since the time of reflector C3 (~1.8 ± 0.5 Ma), i.e. the time of disconnection with SB3 (Figure 2). We cannot assess if the southernmost normal fault is active or if the fault scarp is simply preserved by the pelagic sedimentation. The latter observations cast doubts on the activity of subsidence in SB1 since the reflector C3. The growth fold geometry of SB2 is observed in the sub-surface reflectors, which indicates that subsidence is still active in SB2, although at a very slow rate. The reflector C2 crossing the hinge zone marks an episode of deactivation of most of the faults between SB2 and 3 (Figures 2, 6). Only one major fault is still active in this area, indicating that subsidence is mostly accommodated by transverse growth faults within SB3 (Figures 2, 6). The en-échelon fault system located to the southeast of the 20°N Basin is also covered by a 1.1 ± 0.2 Ma-old pelagic drape (Figure 8) [*Rodriguez et al.*, 2011]. However, the en-échelon fault system offsets the last turbiditic deposits, indicating that faulting was active after 1.1 ± 0.2 Ma. Turbiditic deposits at ~1.1 Ma have partly smoothed the numerous half-graben isolated by en-échelon strands, but faults remained active after this episode.

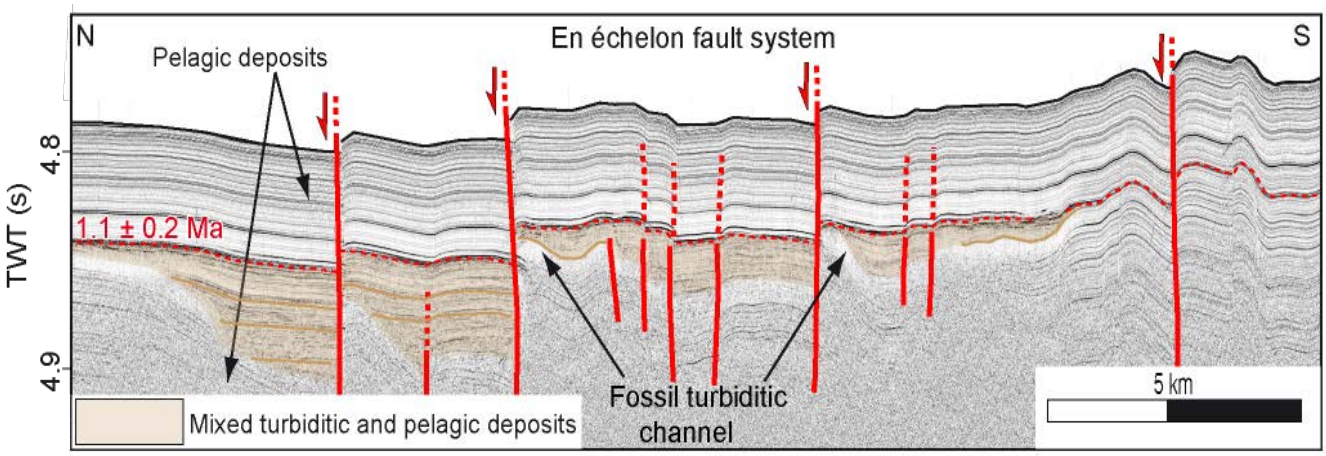


***Figure 7:*** *3.5 kHz profile crossing the en-échelon fault system. See Figures 1 and 3 for location.*

## 5. Discussion

### 5. 1. History of the 20°N pull-apart basin

We propose a first order chronology of the most probable structural evolution of the 20°N Basin and its sedimentary filling (Figure 8).

1) The study of channel-levee systems activity and bottom-current deposits indicates that the 20°N Basin is at the most 3.4 ± 1.2 Ma old. The observation of contouritic deposits indicates that the topography related to the subsidence of the SB3 was already significant at 2.5 ± 1.0 Ma. Reflector C2 documents that all sub-basins were already well formed at a time that cannot be strictly estimated, but prior to 1.8 ± 0.5 Ma (age of reflector C3). Abrupt folding in SB2 sealed by the O discontinuity, together with progressive tilt of the overlying deposits, indicates that the hinge zone between SB2 and SB3 has been active since the very early stage of opening of the basin (Figure 6). It remains unclear whether SB1 stood as an elevated graben since the very early stage of opening, or was formed subsequently. The length of the 20°N Basin was already close to the present-day one (i.e. ~80-km-long) after less than one million years of development only. The precise age of activation of the en-échelon fault system to the south remains unknown, but 3.5 kHz data show evidences for activity before 1 Ma. Analog models [*Tchalenko*, 1970; *Schlische et al.*, 2002] suggest that en-échelon fault systems take place in the first stages of structural evolution of strike-slip fault systems. Thus, the activation of the en-échelon fault system might be synchronous or even earlier than the 20°N Basin inception.

2) During the first stage of basin infill, SB1 and SB2 were disconnected from SB3 by a topographic barrier formed by the transverse fault system between SB2 and 3 (labeled TFS3 in Figure 2). The first deposits of SB3 steeply terminate on this topographic barrier (Figure 6). The unit deposited between C1 and C2 marks the first episode of sedimentary connection between SB2 and SB3. The reflector C2 (between ~3.3 and ~1.8 Ma) marks several geological changes. First, numerous faults of the hinge zone were deactivated at that time (Figures 2, 6). Second, the overlying sedimentary unit displays a fanning configuration, which might indicate a period of sub-basin disconnection or sediment starving at the time corresponding to reflector C2. Third, it appears that connection between SB1 and SB2 occurred shortly before C2.

3) Reflector C3, which is 1.8 ± 0.5Ma old, corresponds to the definitive disconnection between SB1-2 and SB3 (Figure 6). It also coincides with fault deactivation in the southernmost part of SB1. Since 1.8 ± 0.5 Ma, SB1 and SB2 are blanketed by pelagic deposits only.

4) Growth faults within SB3 seem to have been active before 1.8 ± 0.5 Ma, although we cannot assess the precise time of their activation, neither their connection to the substratum. Only a few of them were deactivated at the time corresponding to reflector AU5. Several episodes of isolation of the

southernmost part of SB3 from turbiditic deposits occurred. The present-day depocenter is restricted to the northern part of SB3 since ~120 ka according to calibration with a Küllenberg core [*Bourget et al.*, 2013], but it used to cover a greater part of the SB3 before. In the present-day configuration, growth faults within SB3, the arcuate fault system, and the transverse fault systems between SB1-2 and SB2-3 show evidences of activity.

Despite some remaining uncertainties with regard to the present-day state of activity of some of the faults (the fault bounding the southern extremity of the SB1 and the en-échelon fault-system), the precise depth of the substratum in SB3 and the precise age of some sedimentary discontinuities, the summary exposed above must be considered as the most likely structural evolution of the 20°N Basin.

| Sedimentation rates (ODP 722) | | 46 m/Ma | | | 30 m/Ma | | |
|---|---|---|---|---|---|---|---|
| P wave velocity (m/s) | | 1530 | 1630 | 1730 | 1530 | 1630 | 1730 |
| Thickness of pelagic deposits overlying the last active CLS | 0.14 s (TWT) | 2.33 | 2.48 | 2.63 | 3.57 | 3.80 | 4.04 |
| | 0.16 s | 2.66 | 2.83 | 3.01 | 4.08 | 4.35 | 4.61 |
| Thickness of pelagic deposits corresponding to the onset of contouritic deposits | 0.09 s (TWT) | 1.56 | 1.67 | 1.77 | 2.4 | 2.55 | 2.71 |
| | 0.12 s | 2.02 | 2.16 | 2.29 | 3.11 | 3.31 | 3.52 |
| Thickness of pelagic deposits overlying the C3 reflector | 0.08 s (TWT) | 1.38 | 1.47 | 1.56 | 2.12 | 2.25 | 2.39 |

***Table 1**: Conversion of the thickness of pelagic deposits into time.*

### 5.2. The Indus turbiditic system and the sedimentary filling of the 20°N Basin

The 20°N Basin has been dominantly filled-in by turbiditic deposits from the present-day active channel since the first stage of opening, other surrounding channels being deactivated shortly before the opening. This highlights the exceptional longevity of this turbiditic channel (at least ~1.8 Ma and most probably ~3 Ma), whose deep incision has precluded major avulsion processes through times. The filling of the 20°N Basin is ruled by the competition between tectonic activity and sedimentation rates. Episodes of sub-basins disconnection document periods of time during which the topography accumulated by the transverse growth structures exceeds the rate of sedimentation. Conversely, episodes of connection evidence periods where the rate of sedimentation exceeds the accumulated topography. Several sequence stratigraphy works document glacio-eustatic sea-level changes and subsequent positions of the deltaic shoreline as the main control factors of the Indus fan sedimentation during the Pleistocene, turbiditic sedimentation being enhanced during sea-level lowstands, and reduced during highstands [*Posamentier et al*., 1989; *Kenyon et al.*, 1995; *von Rad and Tahir*, 1997; *Prins et al*., 2000; *Prins and Postma*, 2000*;Posamentier and Kolla*, 2003; *Catuneanu et al.*, 2009; *Bourget et al.*, 2010; 2013].

Angular unconformities observed within SB2 and SB3 might indicate either an abrupt and episodic increase in faulting/folding rate linked to irregularities in the subsidence rate, or a hiatus in the sedimentary record of deformation. Sandbox experiments show that the evolution of rollover structures similar to SB3 does not produce abrupt and cyclic episodes of increased deformation, although the deformation may not be steady state [*Mauduit and Brun*, 1998]. The apparent cyclic and periodic pattern of angular unconformities observed in SB3 might rather correspond to glacio-eustatic episodes of sediment starving related to sea-level highstands. The upward decrease of the apparent thickness of sedimentary layers within sequences delineated by angular unconformities is in good agreement with the progressive reduction of the quantity of sediment available on the Indian continental shelf as expected during sea-level lowstand periods [*Catuneanu et al.*, 2009].

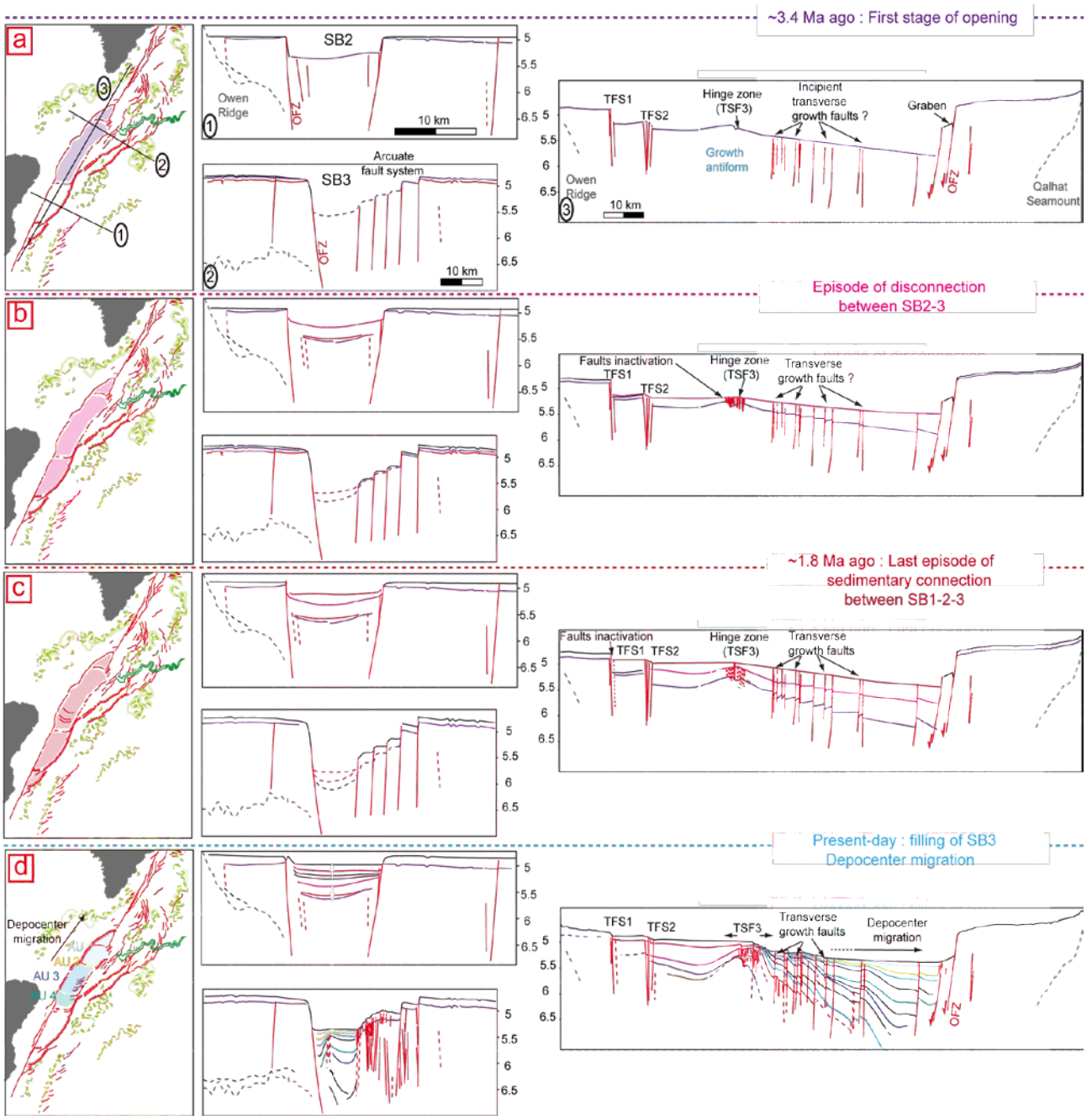


***Figure 8:*** *Synthesis of the structural evolution of the 20°N Basin. See discussion for details.*

### 5. 3. Mode of opening of the 20°N pull-apart basin

Since the first stage of opening of the 20°N Basin ~3 Ma ago, the OFZ has accommodated only 10-12 km of relative motion between India and Arabia [*Fournier et al.*, 2011]. This amount of relative motion drastically contrasts with the dimensions of the 20°N Basin, which questions the relationship linking the size of a pull-apart basin to the relative motion along the main strike-slip fault [*Aydin and Nur*, 1982; *Mann et al.*, 1983]. The opening of the 20°N Basin is characterised by the synchronous formation of three distinct sub-basins since the very first stage of opening, which indicates that the dimension of the 20°N Basin did not significantly change with increasing slip along the OFZ. It implies that the amount of opening (i.e. the distance between the basin-bounding faults) is not equal to the amount of displacement along the OFZ. The formation of a stepover area might have isolated a subsiding graben (corresponding to SB3, i.e. the main locus of subsidence), which subsequently underwent 10-12 km of distributed extension.

Asymmetric subsidence accommodated by the OFZ formed a rollover structure in SB3 (Figure 2). Elsewhere, transverse profiles (Figures 4, 5) do not show significant structural asymmetry, consistently with pure strike-slip motion along the OFZ [*Fournier et al.*, 2011]. The hinge zone between SB2 and SB3 is the major structure decoupling the subsidence between the sub-basins, similarly to what is observed in the Salton Sea along the San Andreas Fault [*Brothers et al.*, 2009].

Where connection with the substratum is observed (SB1 and SB2), transverse faults do not seem to be inherited structures, but new structures formed during the early stages of the 20°N Basin opening. Only one major episode of transverse fault abandonment is evidenced in the hinge zone, but a few of them are still active. The activity of transverse growth faults may have last at least since ~$1.8 \pm 0.5$ Myrs, as observed in SB3, indicating long-lived structures at the scale of the basin history. Most of the 10-12 km divergence was thus distributed over transverse fault systems, with a shift of their activity in SB3 as the hinge zone grew up. The huge amount of subsidence in SB3 has enhanced gravity-driven deformation over SB1 and SB2, as well as along the arcuate fault system (Figure 9).

### 5. 4. Comparison with analogue modeling experiments

The structures developed during the first stages of the stepover formation are not well preserved for the 20°N Basin. However, analog models [*Dooley and Schreurs*, 2012] illustrate how a subsiding block can be isolated by the development of faults oblique to the main strike-slip direction connecting the two strike-slip segments bounding the stepover area. The size and the shape of the isolated graben are dependent upon the distance between the two bounding strike-slip segments and their degree of overlap. The definitive isolation of the graben may mark the initiation of the rapid subsidence characteristic of pull-apart basins.

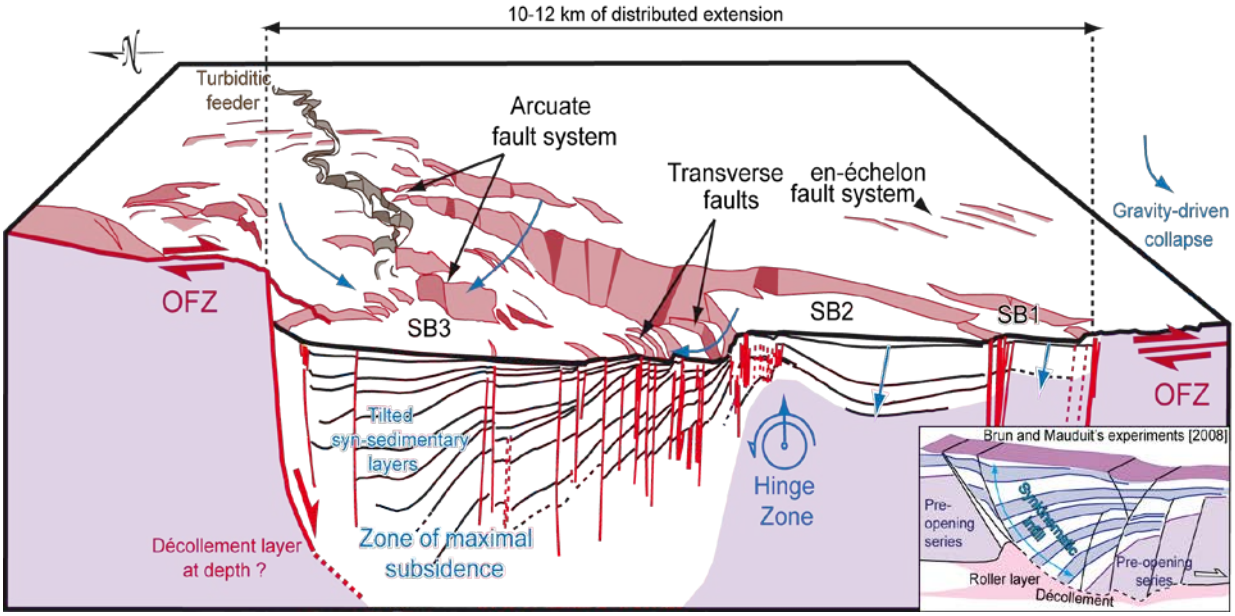


***Figure 9**: Schematic diagram showing subsidence in the 20°N Basin along the OFZ, and the progressive tilting of sediments accommodated by a hinge zone. Arcuate normal faults, sub-basins 1 and 2, transverse faults are the result of gravity-driven deformation in response to the high amount of subsidence accommodated by a rollover zone in sub-basin 3. Inset on the right hand corner shows results from sand box experiments performed by Brun and Mauduit [2008].*

The architecture of SB3 shows strong similarities with sandbox models simulating the development of rollover structures in salt tectonics [*Brun and Mauduit*, 2008]. According to these experiments, the development of a rollover structure requires a three blocks system, i.e. two blocks that separate from each other on top of an extending décollement layer, isolating in-between a third subsiding block [*Brun and Mauduit*, 2008]. Their experimental setup corresponding to a small amount of extension strikingly reproduces most of the structure of the 20°N Basin (see inset in Figure 10). The fanning configuration of deposits within SB3 and the upward curved-geometry of the fault observed to the north of SB3 suggest it connects to a décollement layer at depth. Numerous clay-layers drilled in the Indus deep-sea fan [*Shipboard Scientific Party*, 1974; 1989] represent potential décollement layers at depth, whose thickness can control the subsidence of the basin. The growth of the 20°N Basin may thus result from gravity-driven deformation accommodated by a décollement layer at depth, and enhanced by distributed extension in the area.

On the other hand, results from experiments performed by *Smit et al.* [2008a] show that migration of sub-basins and transverse fault initiation occur where the ratio between the stepover wideness and the thickness of the deforming layer is <1. *Smit et al.* [2008] conclude that this ratio determines not only the basin width, but also its geometry and the migration of subsidence. In these models, the intra-basin transverse faults appear during basin migration, and do not result from the reactivation of inherited

faults dividing the basin. In this framework, the migration of subsidence accounts for the growth of the pull-apart basin with increasing motion along the principal strike-slip fault. Although the experimental setup of models by *Smit et al.* [2008] applies well to the 20°N Basin, our proposed structural evolution does not show any evidence for sub-basin or subsidence migration through times. Sub-basins are delineated by newly formed transverse faults since the first stages of opening of the basin. The location of these transverse fault systems remained fixed and they formed growing structural barriers that delineated areas of differential subsidence, the highest subsidence rates being recorded in SB3. Some of these faults may have become deactivated (for instance between SB2 and SB3), thus transferring larger amount of extension onto other pre-existing transverse faults. *Ben Avraham and Ten Brink* [1989] showed that transverse faults within the Dead Sea formed as normal faults accommodating subsidence, subsequently submitted to strike-slip regime. A too important strike-slip component could lead to the deactivation of the normal offset at transverse faults, but it could not be evidenced in the 20°N Basin.

### 5. 6. Comparison with other pull-apart basins

Intra-oceanic pull-apart basins commonly occur along leaky-transforms (e.g. the Siquieros transform fault in the Pacific [*Fornari et al*., 1989], or the Andrews-Bain transform fault in the Indian Ocean [*Sclater et al*., 2005]). Their size and their shape gradually evolve with increasing slip along the transform segments, ultimately giving birth to a spreading center that fill-in the hole created by the pull-apart configuration (e.g. the Caïman Trough in Caribbean [*Leroy et al*., 1996; *Hayman et al*., 2011]). This mode of opening is referred to as the "continuum model" [*Mann et al*., 1983; *Mann*, 2007]. Direct comparison with the 20°N Basin is difficult because the stepover is much more limited, and the basin is nascent. The surprise is to see how closely the intra-oceanic 20°N Basin compares with the continental Dead Sea Basin.

Indeed, the dimension of the 20°N Basin is of the same order than that of the Dead Sea Basin (132-km-long, 16-km-wide). The Dead Sea Basin is also characterized by transverse faults delineating distinct sub-basins of different depths [*Kashai and Croker*, 1987]. The major subsidence phase within the Dead Sea Basin started about 2-5 Ma ago, which would correspond to about 15-45 km of relative motion along the Dead Sea Fault [*Ginat et al.*, 1998; *Garfunkel and Ben Avraham*, 2001; *Le Béon et al.*, 2008]. Finite motion along the OFZ since the opening of the 20°N Basin is less than the thickness of the deforming layer (oceanic crust plus sediments), which makes the 20°N Basin a nascent pull-apart basin, whereas the Dead Sea Basin is more mature [*Smit et al.*, 2008a]. This is related to the faster velocity along the Levant Fault, which is about twice that of the OFZ. Numerous conflicting modes of opening have been proposed [*Ten Brink and Ben Avraham*, 1989; *Lazar et al*., 2006], but the role of gravity-driven deformation in pull-apart growth has been previously invoked by *Ten Brink et al.* [1989] for the Dead Sea Basin. The latter also displays a longitudinal rollover structure formed by an upward-concave fault (the Amazyahu Fault) rooting at depth on the salt layer of the Seldom formation

acting as a décollement layer [*Kashai and Croker*, 1987]. Seismic profiles [*Larsen et al.*, 2002] and analog modelling experiments [*Smit et al*., 2008b] highlighted that the salt layer in the Dead Sea (Sedom fm.) mechanically decoupled the sedimentary infill from the basement structure. If the presence of a décollement layer in the 20°N Basin is confirmed, then the surface structure of the basin simply reflects gravity-driven deformation of the sedimentary cover in a narrow stepover area (similarly to the Dea Sea), and does not reflect the pattern of the basement tectonics. Considering that the surface structures of the Dead Sea and the 20°N basins result from cover-tectonics would explain why they compare so closely in spite of a different rheological setting.

### 5. 6. Origin of the 20°N Basin

The OFZ is associated with two large stepover basins at its terminations, the Dalrymple Through to the North (150 km-long; 30 km-wide) [*Edwards et al*., 2000] and the Beautemps-Beaupré Basin to the South (120 km-long; 50 km-wide) [*Fournier et al.*, 2008a,b]. As for the 20°N Basin, their large dimensions contrast with the estimated motion along the OFZ. However, the structural style of the OFZ terminations differs from the 20°N Basin. The OFZ forms a horsetail termination at the entrance of the Dalrymple Trough (characterized by a complex set of transverse faults) [*Fournier et al*., 2011*; Rodriguez et al*., 2011], whereas the Beautemps-Beaupré Basin displays a rhomboedric shape.

The structural complexity of the OFZ between 20°N and 22°30'N contrasts with the "single-strand" pattern observed south of the 20°N Basin [*Fournier et al*., 2011; *Rodriguez et al*., 2011]. The 20°N Basin lies in the region of transition from the Arabian oceanic basin to the continental Laxmi-Palatina Ridge and the oceanic Gop Basin [*Minshull et al*., 2008; *Calvès et al*., 2011]. The increasing degree of complexity of the OFZ to the north may thus reflect the complexity of the nature and the properties of the adjoining lithospheres. The alternative is that the extensional component along the OFZ is gradually increasing to the north, as proposed in *DeMets et al.* [2010].

Whether the opening of the 20°N Basin and the widening of the horsetail basins are coeval needs to be further investigated. Stepover basins do not necessarily date the inception of strike-slip motion, since they were shown to develop a few million years after the initiation of the San Andreas Fault (e.g. *Wakabayashi et al*. [2007]) and the Levant Fault (*Garfunkel and Ben Avraham* [2001]). An intriguing point is that the major episode of opening of the Dead Sea Basin along the Levant Fault is coeval with the structural reorganization of the OFZ [*Ten Brink and Flores*, 2012]. Similarly to the OFZ, it remains unclear whether the opening of the Dead Sea reflects the mechanical evolution of the Levant fault or a kinematic change [*Schattner and Weinberger*, 2008; *Schattner*, 2010]. The coeval structural reorganization of both the Levant Fault and the OFZ may reflect a poorly constrained Pleistocene kinematic change of the Arabian plate [*Allen et al*., 2004].

## 6. Conclusions

The 20°N Basin is a young asymmetric pull-apart basin initiated about 3 Ma ago along the slow India-Arabia transform plate boundary. The dimensions of this pull-apart (90 km-long, 35 km-wide) are strikingly large with regards to the 10-12 km of finite motion accommodated since its inception.The sub-surface structural evolution of the 20°N Basin may be assimilated to a rollover structure developing onto a décollement layer at depth in a narrow stepover. Our understanding of the accommodation of the deformation in the deeper layers is still limited by the lack of gravity and deep-seismic data. In spite of their different rheological setting, oceanic versus continental, the 20°N Basin may represent a good analogue of the incipient stages of formation of the Dead Sea Basin. The presence of a décollement at depth, responsible for sub-surface gravity driven deformation decoupled from the crust, may explain the strong similarities between the superficial structure of the oceanic 20°N Basin and the continental Dead Sea Basin. The way the crust thins to accommodate the subsidence at the 20°N Basin remains enigmatic. *Ten Brink and Flores* [2012] recently emphasized that increased fluid flux in the continental crust beneath the Dead Sea might have enhanced the Pleistocene subsidence. An alternative is that the increase in subsidence resulted from a kinematic change along the Levant Fault [*Schattner and Weinberger*, 2008]. Kinematic changes drive stepover reorganization along strike-slip boundaries. The local geometry of the stepover is probably controlled by inherited rheological heterogeneities, determining *in fine* the dimensions of pull-apart basins. The rough synchronicity between the onset of both the 20°N and the Dead Sea basins suggests as a working hypothesis that the OFZ and the Levant faults recorded a Pleistocene change in the Arabian plate motion.

***Acknowledgements***

We are grateful to Captain Rémi De Monteville, officers and crew members of the *BHO Beautemps-Beaupré*, GENAVIR team and hydrographer D. Levieuge for their help in data acquisition. Processing of the Owen-2 dataset was carried out using Geocluster 5000 software developed by CGG Veritas. Bathymetric views were performed with the Fledermaus software. We thank J. Smit and A. Boutoux for interesting discussions about the mode of pull-apart opening, and P. Dubernet and N. Bacha for technical assistance. Tim Minshull and associate editor Claudio Faccenna provided useful comments that helped us to improve the manuscript. This study was supported by SHOM, IFREMER, INSU-CNRS, and CEA (LRC Yves-Rocard).

## References

Allen, M., J. Jackson, and R. Walker (2004), Late Cenozoic reorganization of the Arabia-Eurasia collision and the comparison of short term and long term deformation rates, *Tectonics*, 23, TC2008, doi:10.1029/2003TC001530.

Aydin, A., and A. Nur (1982), Evolution of pull-apart basins and their scale independence, *Tectonics*, *1*, 91-105, doi:1029/TC001i001p00091.

Basile, C., and J.P. Brun (1999), Transtensional faulting patterns ranging from pull-apart basins to transform continental margins: an experimental investigation, *J. Struct. Geol.*, *21*, 23-37.

Barnes, P., and N. Pondard (2010), Derivation of direct on-fault submarine paleoearthquake records from high-resolution seismic reflection profiles: Example from the Wairau Fault, New Zealand, *Geochem. Geophys. Geosyst.*,*11*, Q11013, doi:10.1029/2010GC003254.

Barton, P.J., T.R.E. Owen, and R.S. White (1990), The deep structure of the east Oman continental margin : preliminary result and interpretation, *Tectonophysics*, 173, 319-331

Beck, C., et al. (2007), Late Quaternary co-seismic sedimentation in the Sea of Marmara's deep basins, *Sediment. Geol.*, *199*, 65-89.

Ben Avraham, Z. and U. S. Ten Brink (1989), Transverse faults and segmentation of basins within the Dead Sea Rift, *J. African Earth Sci.*, *8*, 603-616.

Ben-Zion, Y., and C. G. Sammis (2003), Characterization of fault zones, *Pure Appl. Geophys.*,*160*, 677–715.

Bourget, J., S. Zaragosi, M. Rodriguez, M. Fournier, T. Garland, and N. Chamot-Rooke (2013), Late quaternary megaturbidites from the Indus fan : origin and stratigraphic significance, *Mar. Geol.*, 336, 10-23,doi: 10.1016/j.margeo.2012.11.011

Brothers D. S., N. W. Driscoll, G. M. Kent, A. J. Harding, J. M. Babcock, and R. L. Baskin (2009), Tectonic evolution of the Salton Sea inferred from seismic reflection data, *Nat. Geosci.*,*2*, 581-584, doi: 10.1038/ngeo590.

Brun, J.-P., and O. Mauduit (2008), Rollovers in salt tectonics: the inadequacy of the listric fault model, *Tectonophysics*, *457*, 1-11.

Calvès, G., A. M. Schwab, M. Huuse, P. D. Clift, C. Gaina, D. Jolley, A. R. Tabrez, and A. Inam (2011), Seismicvolcanostratigraphy of the western Indian rifted margin: The pre-Deccan igneous province, *J. Geophys. Res.*, 116, B01101,doi:10.1029/2010JB000862.

Carton, H., et al. (2007), Seismic imaging of the three-dimensional architecture of the Cinarcık Basin along the North Anatolian Fault, *J. Geophys. Res.*, *112*, B06101, doi:10.1029/2006JB004548.

Catuneanu, O., et al. (2009), Towards the standardization of sequence stratigraphy, *Earth-Sci Rev*, 92, 1-33.

Chaubey, A. K., J. Dyment, G. C. Bhatthacharya, J-Y. Royer, K. Srinivas, and V. Yateesh (2002),

Paleogene magnetic isochrons and palaeo -propagators in the Arabian and Eastern Somali Basins, NW Indian Ocean, in The Tectonic and Climatic Evolution of the Arabian Sea Region, edited by P. D. Clift et al., *Geol. Soc. Spec. Publ.*, 195,71-85.

Christie-Blick, N., and K.T. Biddle (1985), Deformation and basin formation along strike-slip faults, in *Strike-slip Deformation, Basin Formation, and Sedimentation*, edited by K. T. Biddle and N. Christie-Blick, Society of Economic Paleontologists and Mineralogists, Spec. Publ., *37*, 1–35

Clift, P. D., N. Shimizu, G. D. Layne, J. S. Blusztain, C. Gaedicke, H. U. Schluter, M. K. Clark, and S. Amjad (2001), Development of the Indus Fan and its significance for the erosional history of the Western Himalaya and Karakoram, *Geol. Soc. Am. Bull.,113(8)*, 1039–1051.

Cloos, E. (1998), Experimental analysis of Gulf Coast fracture patterns. Am. Assoc. Pet. Geol. Bull., 52, 420-444.

Cunningham, W. D., and P. Mann, (2007), Tectonics of strike-slip restraining and releasing bends, in *Tectonics of Strike-Slip Restraining and Releasing Bends*, edited by W. D. Cunningham and P. Mann, *Geol. Soc. Spec. Publ., 290*, 1-12

Delescluse, M. and N. Chamot-Rooke (2007), Instantaneous deformation and kinematics of the India-Australia Plate, *Geophys. J. Int*., 168, 818-842, doi: 10.1111/j.1365-246X.2006.03181.x

DeMets, C., R.G. Gordon, D.F. Argus, and S. Stein (1990), Current plate motions, *Geophys. J. Int. 101*, 425-478.

DeMets, C., R.G. Gordon, D.F. Argus, and S. Stein (1994), Effect of recent revisions of the geomagnetic reversal time scale on estimates of current plate motions, *Geophys. Res. Lett.21,* 2191-2194.

DeMets C., R. G. Gordon, D.F. Argus (2010), Geologically current plate motions, *Geophys. J. Int.,181*, 1-80, doi: 10.1111/j.1365-246X.2009.04491.x

Dooley, T. and G. Schreurs (2012), Analogue modelling of intraplate strike-slip tectonics: a review and new experimental results, *Tectonophysics*, 574-575, 1-71.

Dyment, J. (1998), Evolution of the Carlsberg Ridge between 60 and 45 Ma: Ridge propagation, spreading asymmetry, and the Deccan-Reunion hotspot, *J. Geophys. Res.*, 103, 24067–24084 DOI: 10.1029/98JB01759.

Edwards R.A., T. A. Minshull, and R. S. White (2000), Extension across the Indian–Arabian plate boundary: the Murray Ridge, *Geophys. J. Int., 142*, 461–477

Edwards, R. A., T. A. Minshull, E. R. Flueh and C. Kopp (2008), Dalrymple Trough: An active oblique-slip ocean-continent boundary in the northwest Indian Ocean, *Earth Planet. Sci. Lett., 272*, 437-445.

Faugères, J.C., D.A.V. Stow, P. Imbert, and A. Viana (1999), Seismic features diagnostic of contourite drifts, *Mar. Geol., 162*, 1-38.

Faugeres J.C., and T. Mulder (2011), Contour Currents and Contourite Drifts, *In: HeikoHuneke and*

*Thierry Mulder, Editor(s), Developments in Sedimentology, Elsevier, 2011, Volume 63, Deep-Sea Sediments*, 149-214.

Fornari, D., D. Gallo, M. H. Edwards, J. A. Madsen, M. R. Perfit, and A. N. Shor (1989), Structure and topography of the Siquieros Transform Fault System: evidence for the development of intra-transform spreading centers, *Mar. Geophys. Res.*, 11, 263-299.

Fournier, M., C. Petit, N. Chamot-Rooke, O. Fabbri, P. Huchon, B. Maillot, and C. Lepvrier (2008a), Do ridge-ridge-fault triple junctions exist on Earth? Evidence from the Aden-Owen-Carlsberg junction in the NW Indian Ocean, *Basin Research, 20,* 575-590, doi: 10.1111/j.1365-2117.2008.00356.x

Fournier, M., N. Chamot-Rooke, C. Petit, O. Fabbri, P. Huchon, B. Maillot, and C. Lepvrier (2008b), In-situ evidence for dextral active motion at the Arabia-India plate boundary, *Nat. Geosci., 1*, 54-58, doi:10.1038/ngeo.2007.24.

Fournier, M., N. Chamot-Rooke, C. Petit, P. Huchon, A. Al-Kathiri, L. Audin, M.-O. Beslier, E. d'Acremont, O. Fabbri, J.-M. Fleury, K. Khanbari, C. Lepvrier, S. Leroy, B. Maillot, and S. Merkouriev (2010), Arabia-Somalia plate kinematics, evolution of the Aden-Owen-Carlsberg triple junction, and opening of the Gulf of Aden, *J. Geophys. Res., 115*, B04102, doi:10.1029/2008JB006257.

Fournier, M., N. Chamot-Rooke, M. Rodriguez, P. Huchon, C. Petit, M.-O. Beslier, and S. Zaragosi (2011), Owen Fracture Zone: the Arabia-India plate boundary unveiled, *Earth Planet. Sci. Lett., 302,* 247-252, doi:10.1016/j.epsl.2010.12.027

Garfunkel, Z. and Z. Ben-Avraham (2001), Basins along the Dead Sea transform, in *Peri-Tethys Memoir 6: Peri-Tethyan Rift/Wrench Basins and Passive Margins,* edited by P.A. Ziegler, W. Cavazza, A.H.F. Robertson, and S. Crasquin-Soleau, Mémoires Museum National d'Histoire Naturelle de Paris, 186, 607–627.

Ginat, H., Y. Enzel, and Y. Avni (1998), Translocated Plio-Pleistocene drainage systems along the Arava fault of the Dead Sea transform, *Tectonophysics*, 284, 151-160.

Hayman, N., N. Grindlay, M. Perfit, P. Mann, S. Leroy, and B. Mercier de Lépinay (2011), Oceanic core complex development at the Mid-Cayman spreading centre, *Geochem., Geophys., Geosyst.* 12, Q0AG02, doi:10.1029/2010GC003240.

Kashai E.L., and P. F. Croker (1987), Structural geometry and evolution of the Dead Sea-Jordan rift system as deduced from new subsurface data, *Tectonophysics*, *141*, 33-60.

Kenyon, N.H., A. Amir, and A. Cramp (1995), Geometry of the younger sediment bodies of the Indus Fan, in *Atlas of deep water environments: architectural style in turbidite systems,* edited by Pickering, K.T., Hiscott, R.N., Kenyon, N.H., Ricci Lucchi, F., Smith, R.D.A., Chapman & Hall, London, pp. 89-90.

Larsen, B. D., Z. Ben-Avraham, and H. Shulman (2002), Fault and salt tectonics in the southern Dead Sea Basin, *Tectonophysics*, 346, 71-90.

Lazar, M., Z. Ben-Avraham, Z., and U. Schattner (2006), Formation of sequential basins along a strike-slip fault – geophysical observations from the Dead Sea basin. *Tectonophysics, 421*, 53–69.

Le Beon, M., Y. Klinger, A. Q. Amrat, A. Agnon, L. Dorbath, G. Baer, J.-C. Ruegg, O. Charade, and O. Mayyas (2008), Slip rate and locking depth from GPS profiles across the southern Dead Sea Transform, *J. Geophys. Res*., 113, B11403, doi:10.1029/2007JB005280.

Leroy S., B. Mercier de Lépinay, A. Mauffret, and M. Pubellier (1996), Structure and Tectonic Evolution of the Eastern Cayman Trough (Caribbean Sea) from seismic reflection data, *Am. Ass. Petrol. Geol. Bull*, 80, 222-247.

Mann, P., M. R. Hempton, D.C. Badley, and K. Burke (1983), Development of pull-apart basins.*J. Geol.*, *91*, 529–554.Mann, P. (2007), Global catalogue, classification and tectonic origins of restraining- and releasing bends on active and ancient strike-slip fault systems, *Geol. Soc. London Spec. Pub*.,*290*, 13-142.

Mauduit, T., and J.-P. Brun (1998), Development of growth fault/ rollover systems, *J. Geophys. Res*., 103, 18119-18130

McHugh, C.M.G., L. Seeber, M-H. Cormier, J., Dutton, N., Cagatay, A., Polonia, A., W.B.F. Ryan, and N. Gorur (2006), Submarine earthquake geology along the North Anatolia Fault in the Marmara Sea, Turkey: A model for transform basin sedimentation, *Earth Planet. Sci*. *Lett*.,*248*, 661-684, doi:10.1016/j.epsl.2006.05.038

Minshull, T., C. Lane, J. S. Collier, and R. Whitmarsh (2008), The relationship between rifting and magmatism in the northeastern Arabian Sea, *Nat. Geosci*., 1, 463-467, doi:10.1038/ngeo228.

Petrunin, A. and S. Sobolev (2006), What controls thickness of sediments and lithospheric deformation at a pull-apart basin?, *Geology, 34,* 389-392. doi: 10.1130/G22158.1

Pondard, N., and P. M. Barnes (2010), Structure and paleoearthquake records of active submarine faults, Cook Strait, New Zealand: Implications for fault interactions, stress loading, and seismic hazard, *J. Geophys. Res*., *115*, B12320, doi:10.1029/2010JB007781.

Posamentier, H.W., M.T. Jervey, and P.R. Vail (1989), Eustatic controls on clastic deposition I - conceptual framework, in: Wilgus, al., e. (Eds.), Sea-level changes: an integrated approach. SEPM Special Publication, Tulsa, pp. 110-124.

Posamentier, H.W., and V. Kolla (2003), Seismic Geomorphology and Stratigraphy of Depositional Elements in Deep-Water Settings, *J. Sediment. Res*., *73*, 367-388.

Prins, M.A., and G. Postma (2000), Effects of climate, sea level, and tectonics unraveled for last deglaciation turbidite records of the Arabian Sea, *Geology*, 375-378.

Prins, M.A., G. Postma, J. Cleveringa, A. Cramp, and N.H. Kenyon (2000), Controls on terrigenous sediment supply to the Arabian Sea during the late Quaternary: the Indus Fan, *Mar. Geol.*,*169*, 327-

349.

Rahe, B., D. Ferrill, and A. Morris (1998), Physical analog modeling of pull-apart basin evolution, *Tectonophysics*, *285*, 21-40, doi:10.1016/S0040-1951(97)00193-5.

Reading, H.G., and M. Richards (1994), Turbidites systems in deep-water basin margins classified by grain size and feeder system, *Am. Assoc. Petrol. Geol. Bull*., 792-822.

Reilinger, R., et al. (2006), GPS constraints on continental deformation in the Africa – Arabia – Eurasia continental collision zone and implications for the dynamics of plate interactions, *J. Geophys. Res.*, *111*, B05411, doi:10.1029/2005JB004051

Rodriguez, M., M. Fournier, N. Chamot-Rooke, P. Huchon, J. Bourget, M. Sorbier, S. Zaragosi, and A. Rabaute (2011), Neotectonics of the Owen Fracture Zone (NW Indian Ocean): Structural evolution of an oceanic strike-slip plate boundary, *Geochem. Geophys. Geosyst*.,*12*, Q12006, doi:10.1029/2011GC003731

Rodriguez, M., M. Fournier, N. Chamot-Rooke, P. Huchon, S. Zaragosi, and A. Rabaute (2012), Mass wasting processes along the Owen Ridge (Northwest Indian Ocean), *Mar. Geol., 326-328,* 80-100, doi: 10.1016/j.margeo.2012.08.008.

Rodriguez, M., N. Chamot-Rooke, H. Hébert , M. Fournier, P. Huchon (2013), Owen Ridge deep-water submarine landslides : implications for tsunami hazard along the Oman coast, *NHESS*,13, 417-424.

Royer, J. Y., A. K. Chaubey, J. Dyment, G. C. Bhattacharya, K. Srinivas, V. Yateesh, and T. Ramprasad (2002), Paeleogene plate tectonic evolution of the Arabian and Eastern Somali basins, in The Tectonic and Climatic Evolution of the Arabian Sea Region, edited by P. D. Clift et al., *Geol. Soc. Spec. Publ.*, *195*, 7-23

Schattner, U. and R. Weinberger (2008), A mid-Pleistocene deformation transition in the Hula basin, northern Israel: Implications for the tectonic evolution of the Dead Sea Fault, *Geochem. Geophys. Geosyst.*,9, Q07009, doi:10.1029/2007GC001937.

Schattner, U. (2010), What triggered the early-to-mid Pleistocene tectonic transition across the entire eastern Meditterranean? *Earth Planet. Sci. Lett*., *289*, 539-548.

Schlische, R. W., M. O. Withjack, and G. Eisenstadt (2002), An experimental study of the secondary deformation produced by oblique slip normal faulting, *Am. Assoc. Petrol. Geol. Bull., 86(5),* 885-906.

Sclater, J. G., N. R. Grindlay, J. A. Madsen, and C. Rommevaux-Jestin (2005), Tectonic interpretation of the Andrew Baintransform fault: Southwest Indian Ocean, *Geochem. Geophys. Geosyst*., 6, Q09K10, doi:10.1029/2005GC000951.

Shipboard Scientific Party, Site 222 (1974), In R.B. Whitmarsh, O.E. Weser, and D.A. Ross, DSDP Init. Repts, 23, doi:10.2973/dsdp.proc.23.106.

Smit J., J.-P Brun, S. Cloetingh, and Z. Ben-Avraham (2008), Pull-apart basin formation and devel-

opment in narrow transform zones with application to the Dead Sea Basin, *Tectonics, 27*, TC6018, doi:10.1029/2007TC002119

Smit, J., J.-P. Brun, X. Fort, S. Cloething, and Z. Ben-Avraham (2008b), Salt tectonics in pull-apart basins with application to the Dead Sea Basin, *Tectonophysics*, 449, 1-16.

Tchalenko, J. S. (1970), Similarities between shear zones of different magnitudes, *Geol. Soc. Am. Bull.,81*, 1625-1640.

ten Brink, U. S., and Z. Ben-Avraham (1989), The anatomy of a pull-apart basin: seismic reflection observations of the Dead Sea, *Tectonics, 8*, 333-350.

ten Brink, U.S., Z. Ben-Avraham, R.E. Bell, M. Hassouneh, D.F. Coleman, G. Andreasen, G. Tibor, and B. Coakley (1993), Structure of the Dead Sea pull-apart basin from gravity analyses, *J. Geophys. Res.*, *98*, 877-21,894.

ten Brink, U. S., and C. H. Flores (2012), Geometry and subsidence history of the Dead Sea basin: A case for fluid induced mid-crustal shear zone?, *J. Geophys. Res., 117*, B01406, doi:10.1029/2011JB008711.

von Rad, U., and M. Tahir (1997), Late Quaternary sedimentation on the outer Indus shelf and slope (Pakistan): evidence from high-resolution seismic data and coring, *Mar. Geol.,138*, 193-236.

Yatheesh, V., G. C. Bhattacharya, and J. Dyment (2009), Early oceanic opening off Western India-Pakistan margin : the Gop Basin revisited, *Earth. Planet. Sci. Lett.*, 284, 399-408.

Wakabayashi, J., J. V. Hengesh, and T. L. Sawyer (2004), Four-dimensional transform fault processes: progressive evolution of step-overs and bends, *Tectonophysics*, *392*, 279-301.

Wakabayashi, J. (2007), Stepovers that migrate with respect to affected deposits: field characteristics and speculation on some details of their evolution, in CUNNINGHAM, W. D. & MANN, P. (eds) *Tectonics of Strike-Slip Restraining and Releasing Bends*, edited by W. D. Cunningham and P. Mann, *Geol. Soc.Spec. Publ.*, *290*, 169-188.

Wu, J. E., K. McClay, P. Whitehouse, and T. Dooley (2010), 4D analogue modelling of transtensional pull-apart basins, *Mar. Petr. Geol.*, *26*, 1608-1623.

## Conclusions et perspectives de l'article "Mode of opening of the 20°N Pull-apart Basin"

Le cadre structural de l'ouverture du bassin 20°N établit dans l'article précédent montre que ce bassin a été le réceptacle des dépôts turbiditiques de l'Indus depuis environ 3 Ma. Considérant que le chenal déversant actuellement les turbidites dans le bassin 20°N est le seul chenal actif à s'être déversé dans le bassin 20°N depuis son ouverture, cela implique que ce chenal est actif depuis au moins ~1.8 Ma (réflecteur C3), et probablement davantage (jusqu'à 3 Ma). Cette longévité est exceptionnelle au regard de la durée d'activité communément admise pour un chenal turbiditique, de l'ordre de la dizaine de milliers d'années au maximum (*Babonneau et al., 2002*). Entre les latitudes de 20°-22°N, une couverture pélagique drape la trace de la ZFO, mais aussi les anciens systèmes de chenaux-levées depuis plus de 2 Ma. La dominance des pélagites à ces latitudes est probablement liée à l'inactivation de l'ancien canyon de l'Indus, dont les traces sont encore visibles en bathymétrie (*Kolla and Coumes, 1987*). Le canyon actuel déverse les turbidites plus au sud (en deça de la latitude 20°N ) (*Prins et al., 2000*). Comme développé dans l'article *Bourget et al. 2013* joint en annexe de cette thèse, le bassin 20°N a donc probablement été rempli par les turbidites formées au niveau des anciens canyons de l'Indus, dont l'âge précis d'inactivation demeure inconnu. Cependant, les carottages réalisés au sein du bassin montrent que les dernières turbidites ont environ vingt mille ans, ce qui indiquerait que les anciens canyons de l'Indus sont encore épisodiquement actifs, alors que le canyon de l'Indus actuel est actif depuis au moins le dernier cycle glaciaire-interglaciaire (soit ~120 000 ans) (Von Rad and Tahir, 1997). L'exceptionnelle longévité du chenal remplissant le bassin 20°N peut s'expliquer d'une part par la dominance des dépôts pélagiques qui drapent et préservent la morphologie du chenal au lieu de l'enfouir; et d'autre part par l'activité épisodique de ce chenal, lorsqu'il arrive qu'un glissement de terrain s'initie sur les flancs d'un canyon fossile. Dans ce contexte, le passage du panache turbiditique entaillerait davantage le thalweg du chenal et construirait ses levées au lieu de l'enfouir, favorisant sa stabilité au cours du temps. La quantité de sédiments disponibles sur la plate- forme aux abords des canyons fossiles varie selon les oscillations du niveau marin relatif; ainsi le volume des turbidites arrivant jusqu'au bassin 20°N est-il lui aussi dépendant de ces variations (comme confirmé au premier ordre par Bourget et al., 2013). La faible fréquence des courants de turbidité charriés par le chenal du bassin 20°N est certainement un facteur important dans la préservation du chenal au cours du temps.

Le bassin 20°N représente donc un enregistrement confiné du flux sédimentaire du système de l'Indus au cours des 3 derniers Ma, et, au premier ordre, un enregistrement des

variations du niveau marin relatif. La configuration en éventail des dépôts dans le sub-bassin 3 en fait un site idéal pour un forage, qui permettrait de calibrer la stratigraphie des dépôts et de fournir un calendrier des variations du niveau marin relatif sur la marge indienne. Un tel calage stratigraphique des dépôts permettrait, via la corrélation des réflecteurs, d'estimer le taux de rejet au niveau de chacune des failles transverses du bassin, ainsi que le taux de croissance de la structure en rollover formant le sub-bassin 3; ce qui apporterait des contraintes naturelles inédites aux modèles analogiques de *Brun et Mauduit (2008)*. En dépit de ces perspectives de premier plan, la planification prochaine d'une campagne de forage au niveau du bassin 20°N semble peu probable du fait des nombreux actes de piraterie dans la région, qui interdisent à tout bateau de rester immobile le temps d'un forage. Le navire Beautemps Beaupré permet cependant de réaliser des carottages Küllenberg, qui pénètrent la première dizaine de mètres de sédiments. Du fait de la configuration en éventail des dépôts du SB3, les dépôts affleurant dans la partie sud du bassin sont plus anciens que ceux de la partie Nord. En dépit du risque de ne recueillir que des dépôts pélagiques, une forte densité de carottages Küllenberg, stratégiquement placés, permettrait d'apporter des réponses préliminaires aux questions exposées ci-dessus, sans immobiliser le bateau trop longtemps pour faire face à la menace pirate.


*Planche III : Dessin à l'encre de chine d'une ruelle de Salalah au sud de l'Oman, peu avant l'embarquement sur le Beautemps-Beaupré pour la campagne Owen 2*

**Tectonics of the Dalrymple Trough and uplift of the Murray Ridge (NW Indian Ocean)**

Mathieu Rodriguez[1*],Nicolas Chamot-Rooke[1], Philippe Huchon[2,3], Marc Fournier[2,3], Siegfried Lallemant[4], Sébastien Zaragosi[5], Matthias Delescluse[1], Nicolas Mouchot[6]

(1) Laboratoire de Géologie de l'Ecole Normale Supérieure, CNRS UMR 8538, 24 rue Lhomond, 75005 Paris, France

(2) Institut des Sciences de la Terre de Paris, UMR 7193, Université Pierre & Marie Curie, case 129, 4 place Jussieu, 75005 Paris, France

(3) iSTeP, UMR 7193, CNRS, F-75005 Paris, France

(4) Département Géosciences Environnement, Université de Cergy-Pontoise, 5 mail Gay-Lussac, Neuville/Oise, 95031 Cergy-Pontoise, France

(5) EPOC Université Bordeaux1, UMR 5805, avenue des facultés, 33405 Talence, France

(6) Projets Nouveaux, TOTAL, Paris, France

*Corresponding author: rodriguez@geologie.ens.fr

Tel. +33 1 44 27 59 43

*in prep. For Tectonophysics*

## ABSTRACT

**The Dalrymple Trough is a 150-km-long, 30-km-wide basin that takes place at the termination of the present-day India-Arabia plate boundary in the Arabian Sea, known as the Owen Fracture Zone (OFZ). The Dalrymple Trough is closely associated with the Murray Ridge, a complex of prominent bathymetric highs located on its western flank. The recent multibeam mapping of the connection of the Dalrymple Trough with the OFZ reveals a horsetail structure, suggesting a close relationship between geological histories of both structures. The 3-6 Ma-old age of the OFZ drastically contrasts with the commonly accepted early miocene age of emplacement of the Dalrymple Trough. New seismic lines were acquired during the OWEN-2 cruise in 2012 to investigate the role of the emplacement of the OFZ over the structural history of the Dalrymple Trough. Here we propose a new tectonic history of the Dalrymple Trough, involving two major episodes of deformation along the India-Arabia plate boundary at ~8-9 Ma and ~2Ma. The first 8-9 Ma episode is marked by a system of folds associated to the main uplift of the southern Murray Ridge and the first uplift of the northern Murray Ridge. This episode may be related to the change in India's kinematics related to the Late Miocene growth of Himalayas. The Dalrymple Trough opened~2-3 Ma ago as a stepover basin formed subsequently to a structural reorganization of the India-Arabia plate boundary, coeval with the regional M-unconformity in the Oman abyssal plain, and the last uplift of the northern Murray Ridge.**

## 1. Introduction

The Dalrymple Trough is a part of the Murray Ridge complex, which links the Owen Fracture Zone (OFZ hereafter) in the south to the Ornach-Nal Fault Zone in Pakistan (Fig. 1; McKenzie and Sclater, 1971; Minshull et al., 1992).The Dalrymple Trough is located southeast of the Makran accretionary wedge, which absorbs the convergence between the Arabian and Eurasian plates and produced strong earthquakes ($M_w$=8.1 for the 1945 event). The southern part of the Dalrymple Trough (between 22-23°N) is a150-km-long, 30-km-wide, down to 4200-m-deep basin, which takes place on the western side of the ~400-m deep southern Murray Ridge (Fig. 1, 2). The southern part of the Dalrymple Trough abruptly ends at the Jinnah Seamount at ~23°N (Burgath et al., 2002). The northern Murray Ridge (between 23°N and 23°40'N) has a more subtle topographic expression (about 1000-m with respect to the surrounding seafloor). The substratum of the Murray Ridge, although never sampled, is interpreted as continental in origin according to seismic refraction data (Edwards et al., 2008). The Dalrymple Trough represents a very narrow ocean-continent transition, with abrupt crust thickness variations (from a ~14 km-thick continental crust to a 6 km-thick oceanic crust in the Oman abyssal plain, Edwards et al., 2008).A set of volcanic reliefs, namely the Qalhat Seamount and the Little Murray Ridge, are located west of the trough (Fig. 1, 2) (Edwards et al., 2000; Fournier et al., 2011). Although the seismicity along the OFZ is low and scattered, the strongest magnitude event ($M_w$=5.8) has been recorded in the Dalrymple Trough, indicating it is still an active area (Fig. 2) (Quittmeyer and Kafka, 1984; Gordon and DeMets, 1989; Fournier et al., 2001).

Recently acquired multibeam bathymetry revealed the southern part of the Dalrymple Trough as a rare case of oceanic horsetail termination marking the end of the OFZ (Fig. 1, 2) (Fournier et al., 2011). There, the horsetail structure displays characteristic sets of faults oblique to the main strike-slip direction that isolate several sedimentary basins. Although the deep structure of the Dalrymple Trough has been well characterized by previous seismic studies (Edwards et al., 2000, 2008; Gaedicke et al., 2002a,b), the way it connects to the OFZ and it relates to its tectonic history remains unknown.

New seismic lines acquired during the OWEN 2 cruise in 2012, together with previously acquired multibeam bathymetry and published works (Edwards et al., 2000; Gaedicke et al., 2002; Ellouz-Zimmermann et al., 2007), allows us to reassess the stratigraphic framework of the area and to propose a new tectonic history of the Dalrymple Trough and the Murray Ridge in close association with structural reorganizations of the India-Arabia plate boundary at ~8-9 Ma and ~2.1 ± 0.5 Ma. The objectives of this study are to understand how rifting took place at the Dalrymple Trough, and subsequently evolved into a large and complex stepover basin; and to unravel the complex, poly-phased history of the Murray Ridge uplift.

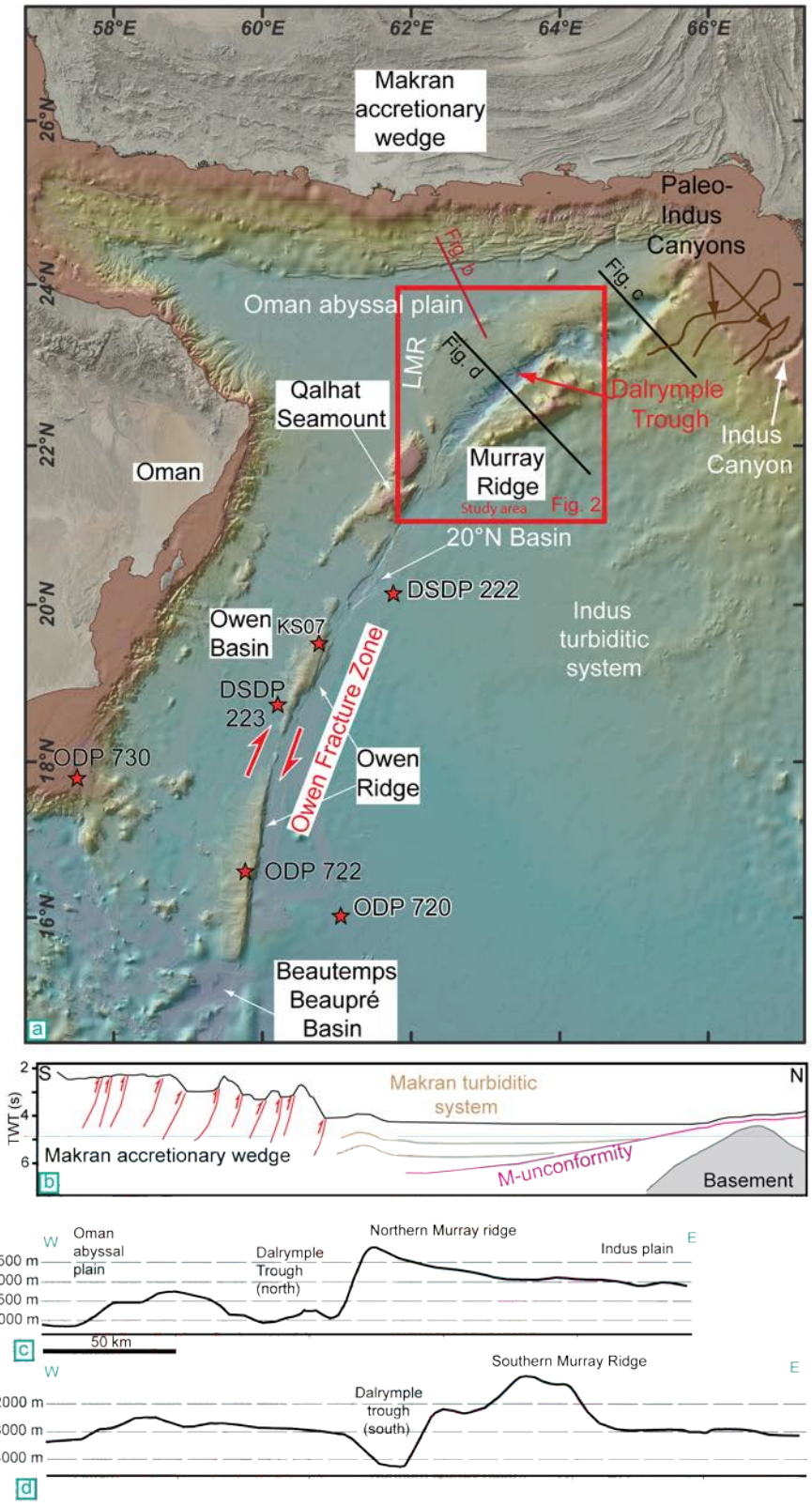


***Figure 1 :*** *a) Regional framework of the India-Arabia plate boundary. LMR : Little Murray Ridge. b) Simplified cross section of the Oman abyssal plain, modified from White and Klitgord (1976) (see a) for location). c) and d) : topographic profiles running transverse to the northern and southern Murray Ridge.*

## 2. Geological and kinematic background of the India-Arabia plate boundary

### *2.1. Present-day kinematics*

The OFZ is an 800 km-long dextral strike-slip fault system that currently accommodates the relative plate motion between India and Arabia (Whitmarsh, 1979; Gordon and DeMets, 1989; Fournier et al., 2008a). It closely follows a small circle about a rotation pole determined with GPS and seismicity data, which is consistent with a pure strike-slip motion along the entire fracture zone (Fig. 2) (Fournier et al., 2011), in contrast with the increasing transtension north of 18°N predicted by the MORVEL closure-enforced pole (DeMets et al., 2010). However, the latter is in better agreement with transtensional focal mechanisms calculated in the Dalrymple Trough (Fournier et al., 2001), and better predicts the direction of the segment of the OFZ connecting the entrance of the Dalrymple Trough (Fig. 2).

### *2.2. Geological history*

South of the Dalrymple Trough, the OFZ cuts through the Owen Ridge, a prominent oceanic ridge located east of the OFZ. Offsets of the Owen Ridge observed on the seafloor indicate a finite dextral displacement of 10-12 km along the OFZ (Fournier et al., 2008; 2011). Considering a steady motion of 3 ±1 $mm.y^{-1}$ estimated independently from geodetic (Reilinger et al., 2006; Fournier et al., 2008a) and geological data (DeMets et al., 1990, 1994, 2010), this implies that the present-day trace of the OFZ has been active since at least 3 to 6 Ma. Older locations of the India-Arabia plate boundary remain debated (Whitmarsh et al., 1979; Mountain and Prell, 1990; Edwards et al., 2000; Royer et al., 2002), but most reconstitutions agree that the boundary was located close to the present-day Owen Ridge since the Early Miocene, fossil traces being buried under the Indus turbiditic sedimentation (Rodriguez et al., 2011).

As attested by Paleogene hemipelagites recognized on its top (Gaedicke et al., 2002a,b), the Murray Ridge used to be a part of a series of reliefs formed in Paleocene-Early Eocene times (Fig.1, 3) and subsequently rejuvenated during Neogene times. Previous works of Edwards et al. (2000) and Gaedicke et al. (2002b) proposed two phases of uplift of the Murray Ridge related to two coeval phases of subsidence in the Dalrymple Trough, in the Early and the upper Late Miocene. The Early Miocene age is an extrapolation of the 20-Ma age of uplift inferred for the Owen Ridge upon the base of an angular unconformity, labeled “U” in the literature (Whitmarsh et al., 1979; Mountain and Prell, 1990; Gaedicke et al., 2002). The upper Late Miocene age is assumed from an angular unconformity revealed by seismic profiles crossing the Oman abyssal plain (White and Klitgord, 1976; Ross et al., 1986). It is referred as the M-unconformity in the literature (Fig. 1b) (where M stands for Makran, Gaedicke et al., 2002b; Schlüter et al., 2002; Ellouz-Zimmermann et al., 2007).

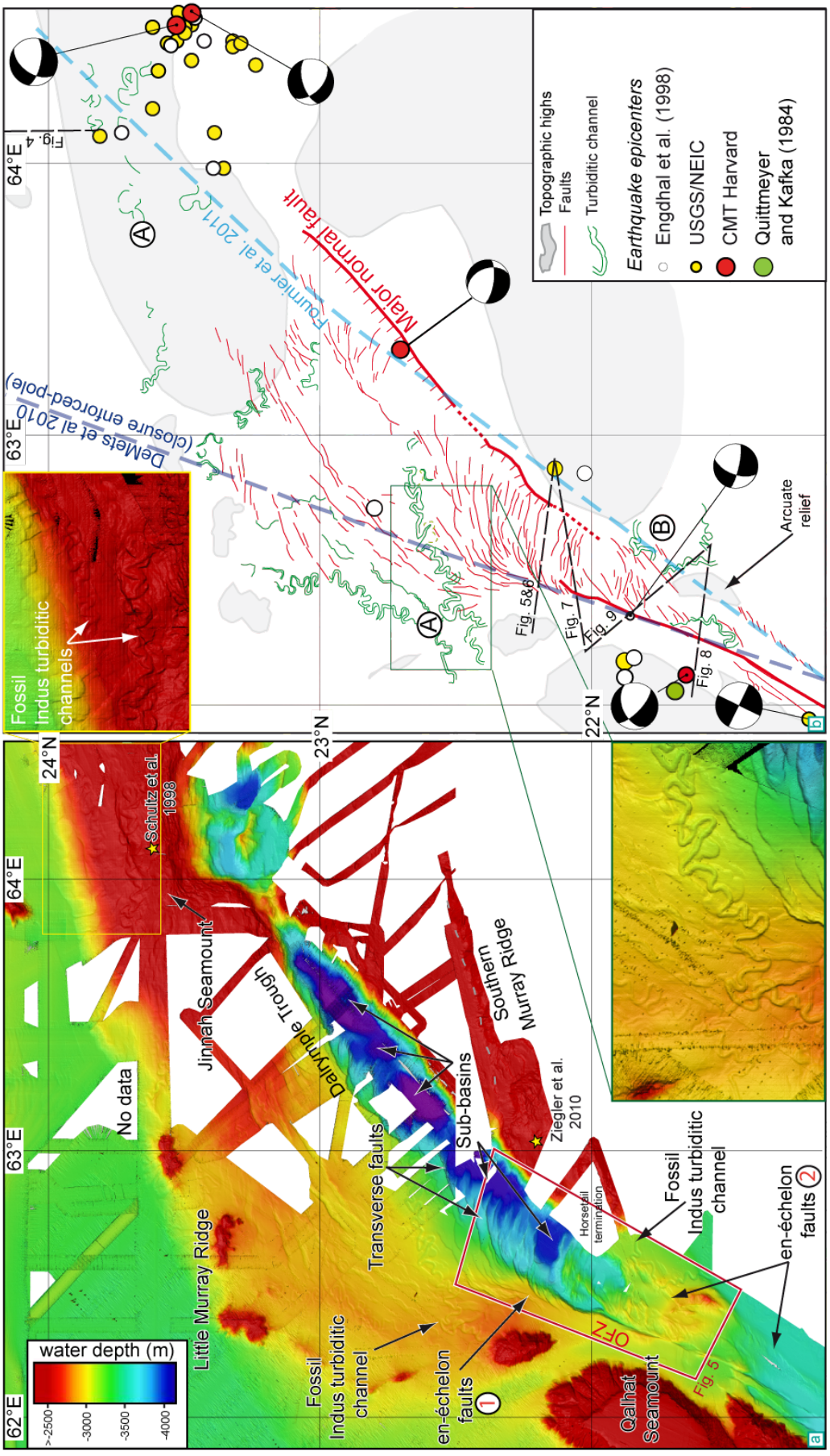
62°E
63°E
64°E
24°N
23°N
22°N
water depth (m)
>-2500
-3000
-3500
-4000
No data
Schultz et al. 1998
Jinnah Seamount
Little Murray Ridge
Dalrymple Trough
Transverse faults
Sub-basins
Southern Murray Ridge
Ziegler et al. 2010
Fossil Indus turbiditic channel
en-échelon faults ①
Horsetail termination
OFZ
Fossil Indus turbiditic channel
en-échelon faults ②
Qalhat Seamount
Fig. 5
a
Fig. 4
Fournier et al. 2011
DeMets et al 2010 (closure enforced-pole)
Major normal fault
Topographic highs
Faults
Turbiditic channel
Earthquake epicenters
Engdhal et al. (1998)
USGS/NEIC
CMT Harvard
Quittmeyer and Kafka (1984)
Fig. 5&6
Fig. 7
Fig. 9
Fig. 8
Arcuate relief
b

***Figure 2** : Multibeam imagery of the Dalrymple Trough (a), and interpretative morpho-structural scheme (b), with local crustal seismicity since 1973 (focal depth < 50 km, magnitude Mw > 2) from the different databases available. The small circle about the closure-enforced MORVEL Arabia–India rotation pole(dark blue dashed line; DeMets et al., 2010) is parallel to the trend of the OFZ at the entrance of the trough, whereas the small circle determined from the active trace of the OFZ (light blue dashed line, Fournier et al., 2011) is parallel to the trace of the OFZ up to 21°30°N and to the en-échelon fault system 2. Location of seismic profiles is indicated in black dashedlines. Insets show close-views of the turbiditic channels observed in the area, labeled A and B according to their age of activity(A : older channel, 6 ±1.5 Ma, B : younger channel, 3.7 ±0.9 Ma.*

### *2.3. Regional unconformities in the Arabian Sea*

*U-unconformity and the uplift of the Owen-Murray Ridge*

The U-unconformity is recognized overall the Owen Basin and the Oman abyssal plain (Shipboard Scientific Party, 1974; Whitmarsh et al., 1974; 1979). The U-unconformity marks a highly diachronous transition between Late Oligocene-Early Miocene pelagic chalk and Late Oligocene-Early Miocene turbidites drilled at DSDP sites along the Owen Ridge. As emphasized by ODP reporters of Leg 117, the U-unconformity does not have a tectonic origin, and simply reflects the transition from oligocene pelagites to lower miocene turbidites as the substratum of the Owen Ridge gets progressively buried under the Indus deep-sea fan (Mountain and Prell, 1990). The last turbidite drilled at the top of the Owen Ridge is 14-15 Ma-old, and is overlaid by a ~500-m-thick pelagic cover (Shipboard Scientific Party, 1989).The transition from turbiditic to pelagic deposits was supposed to mark the time at which the ridge was uplifted above the level of turbiditic deposition (Mountain and Prell, 1990). However, thick pelagic sequences (several hundred meters) developed within the Indus turbiditic system, in response to shifts in the locus of turbiditic lobes (Shipboard Scientific Party, 1989). The 14-15 Ma-old transition from turbidites to pelagites thus cannot be used as a proxy for the Owen Ridge uplift, casting doubts about the Early Miocene age assumed for the uplift of the Owen-Murray Ridge. The angular unconformity effectively marking the uplift of the southern Murray Ridge is not the U-unconformity, but a younger unconformity of Late Miocene age according to calibration with an industrial drilling located in the Indus fan (Calvès, 2008) (Fig. 3). The latter unconformity is formed by 8-9 Ma-old channel-levee system adopting an onlap configuration over a pre-10 Ma-old tilted series of channel-levee systems (Kolla and Coumes, 1987; Calvès, 2008).

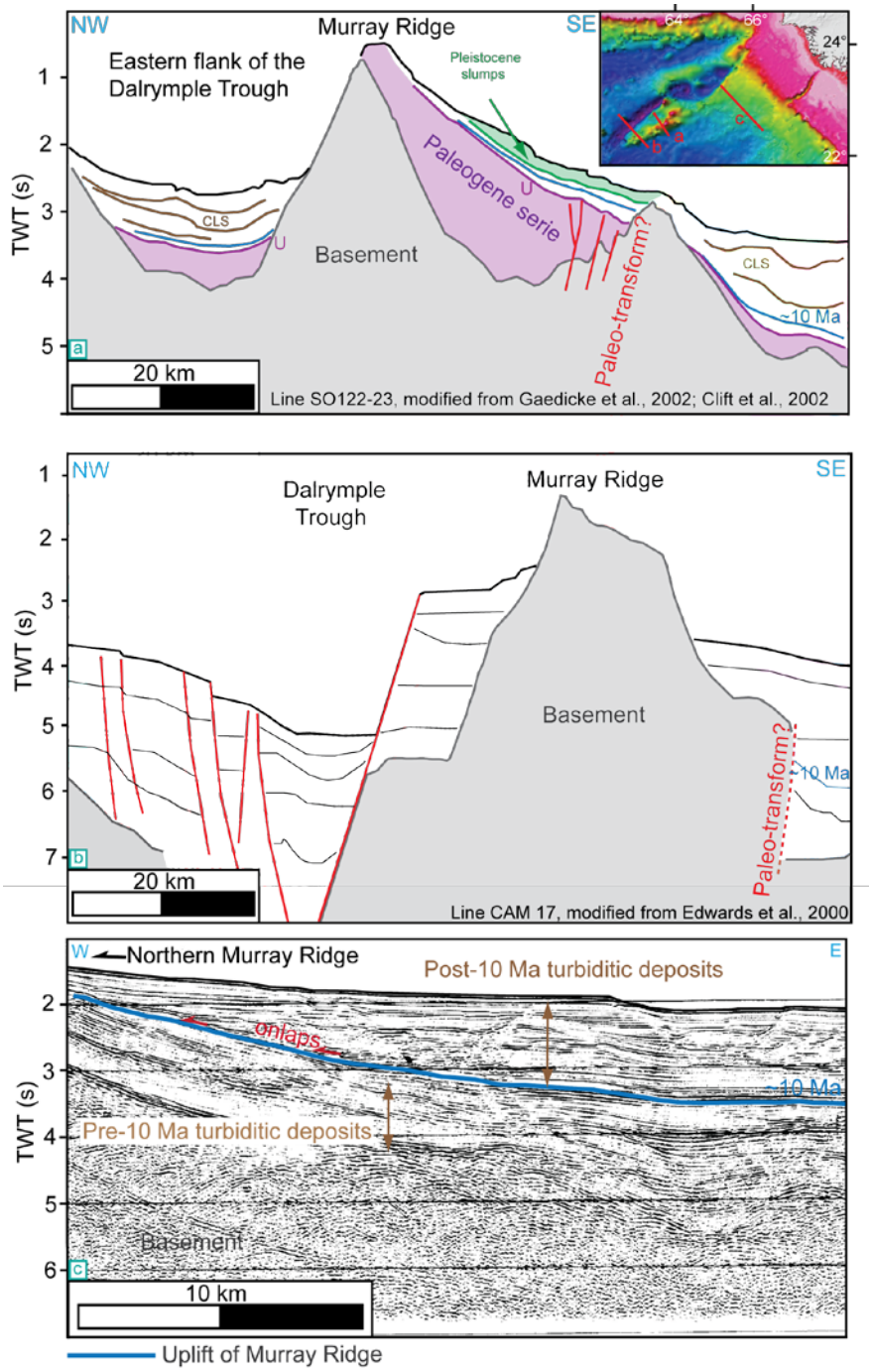


***Figure 3 :****Line drawing of seismic profiles previously published in the Dalrymple Trough-Murray Ridge area(see the inset in the upper right hand corner for location).a) Line drawing of a seismic profile crossing the southern Murray Ridge, modified after Gaedicke et al., 2002b. b) Line drawing of a seismic profile crossing the Dalrymple Trough and the southern Murray Ridge, modified after Edwards et al., 2000. c) Seismic profile modified from Kolla and Coumes (1987) showing an angular unconformity on the eastern side of the Murray Ridge. The angular unconformity was dated at 8-10 Ma by calibration with an industrial drilling located in the Indus deep-sea fan (Calvès et al., 2008).CLS= Channel-Levee Systems.*

*M-unconformity*

The M-unconformity in the Oman abyssal plain marks both an episode of subsidence in the Dalrymple Trough, and an abrupt tilt of Indus channel-levee systems lying on the subducting plate (Fig. 4) (Gaedicke et al., 2002). Turbiditic deposits coming from the Makran adopts an onlap configuration on the M-unconformity (Fig. 4). The latter is probably coeval with the last stage of uplift of the Murray Ridge.This unconformity has never been drilled, which results in strong uncertainties in its age (Schlüter et al., 2002). First related to a Messinian uplift event in the Zagros Mountain (Ross et al., 1986), it has been also related to the onset of seafloor spreading in the Gulf of Aden (Schlüter et al., 2002), estimated at 13 Ma when these studies were published (Cochran, 1981). The latter age cannot be considered valid anymore according to recent magnetic anomalies studies that document the onset of seafloor spreading in the Gulf of Aden ~20 Ma ago (Fournier et al., 2010). Extrapolations of deformation rates suggest a 3-7 Ma-old kinematic change related to the Arabia-Eurasia collision (Allen et al., 2004; Mouthereau et al., 2012) that may account for the M-unconformity, but such a kinematic change remains a matter of debate (Hatzfeld and Molnar, 2010).

### *2.4. The Indus deep-sea fan*

Tectonic deformation along the India-Arabia plate-boundary is well recorded by sediments belonging to the Indus turbiditic system. At its thickest part the fan is more than 9-km thick, but its thickness decreases when approaching the Owen-Murray Ridge (Fig. 3c) (Coumes and Kolla, 1984; Clift et al., 2001). It forms a typical mud-rich, “passive margin fan” (*sensu* Reading and Richards, 1994), with numerous inter-bedded pelagic layers (Shipboard Scientific Party, 1989).Indus Fan sedimentation started during the Middle Eocene as the result of the onset of the India-Eurasia collision and accelerated since the Early Miocene, coincident with a sharp increase in sedimentation rates related to the uplift of the Himalaya and the onset of the Asian monsoon (Clift et al., 2001; Clift and Gaedicke, 2002). Seismic lines collected in the Indus deep-sea fan document the apparition of important channel-levee complexes since the Middle Miocene (Clift et al., 2001; Calvès, 2008). In the Early Pleistocene, the Indus canyon underwent a southeast migration, leading to a major episode of avulsion and concentration of Indus deposits on the southeastern part of the fan (fossil Indus canyons are mapped in Figure 1) (Kolla and Coumes, 1987). The latter resulted in dominantly pelagic deposits along the OFZ, allowing a good preservation of the fault scarps on the seafloor (Shipboard Scientific Party, 1974; Rodriguez et al., 2011).

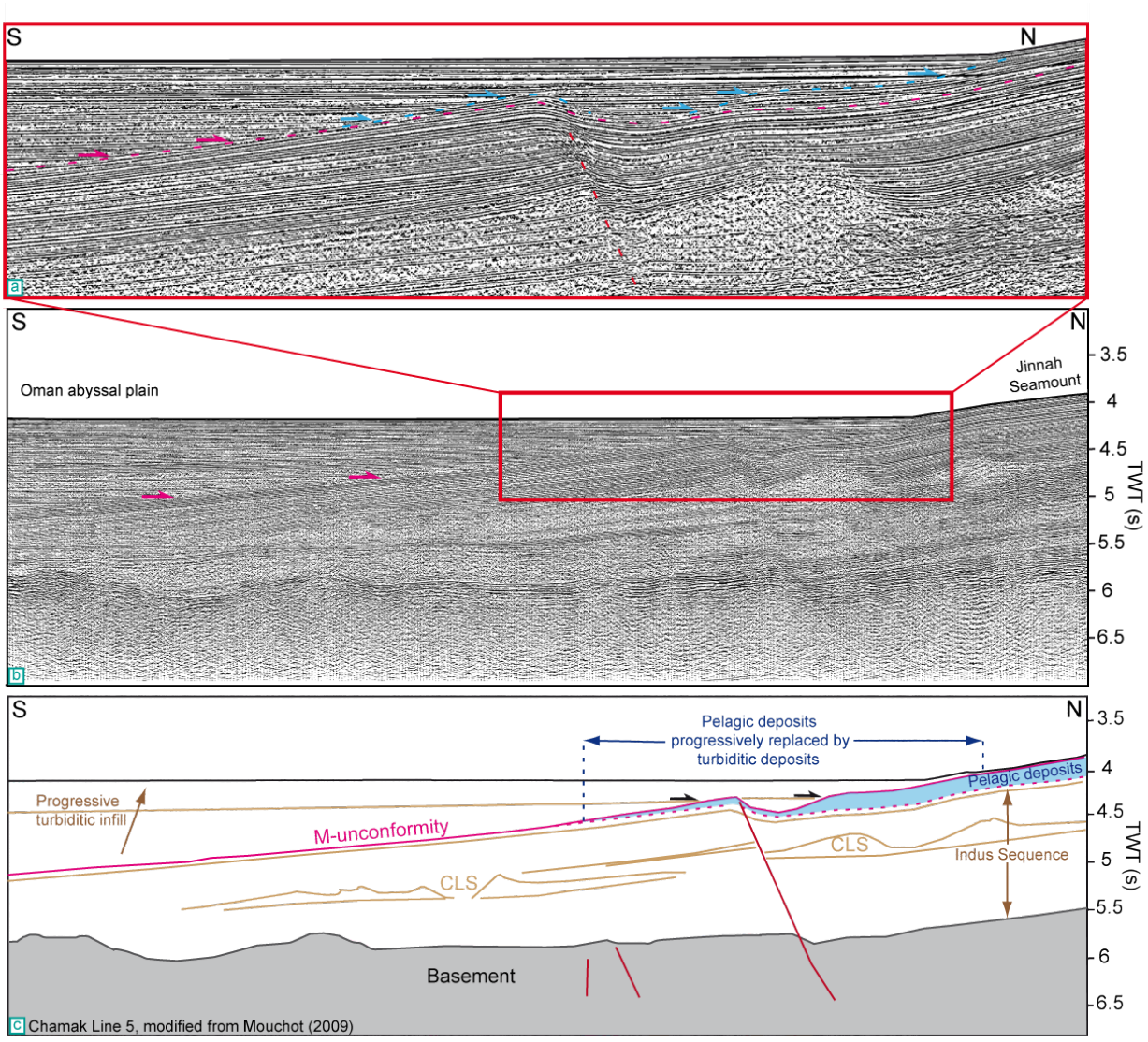


***Figure 4 :*** *Seismic profile from the Chamak cruise (Ellouz-Zimmerman et al., 2007; Mouchot, 2009) crossing the Jinnah seamount, showing the M-unconformity (see figure 2 for location).a) close view of the M-unconformity in the area of the Jinnah Seamount; b) Seismic profile showing the M-unconformity and c) the related line drawing. CLS = channel-levee system.*

## 3. Material and Methods

The new dataset presented in this study was during the OWEN-2 survey acquired onboard the R/V *Beautemps-Beaupré*. The OWEN-2 seismic reflection profiles were shot using two GI air-guns and a 600 m-long streamer allowing high-speed acquisition (10 knots) and a penetration of the order of ~2s TWT. The processing consisted in geometry setting, water-velocity normal move-out, stacking, water-velocity F-K domain post-stack time migration, bandpass filtering (8-80 Hz), and automatic gain control. All the profiles are displayed with a vertical exaggeration of 8 at the seafloor. Two-way travel time to seismic reflectors was converted to depth using a P-wave velocity between1530 and 1730 m. s $^{-1}$ lower and upper bounds for the P-wave velocity. This range of values covers safely the

measurements performed in the area in the same pelagic sediments (Shipboard Scientific Party, 1974, 1989). An extreme P-wave velocity of 1950 $m.s^{-1}$ has been measured in the Pliocene turbidites underneath the pelagic cover (White and Klitgord, 1976; Kolla and Coumes, 1987). Depth values are given with respect to the surrounding seafloor. The reflectors picked on seismic profiles have been selected upon the base of seismic discontinuities that either reflect lithological changes, stratigraphic hiatuses or tectonic deformation. In the following, sedimentary series before the opening of the Dalrymple Trough are referred to as the "substratum" of the Dalrymple Trough, which is employed in the sense of "pre-rift" series, in order to avoid the confusion with the continental basement of the Murray Ridge observed on several profiles. The multibeam bathymetry coverage is a combination of previously published data acquired during the MARABIE, CHAMAK, and OWEN-1 cruises. Multibeam bathymetry and seismic facies analysis help to decipher the nature of the sedimentary deposits and their mode of deposition, and hence, the way the deformation has been recorded.

## 4. Structure of the Dalrymple Trough

The Dalrymple Trough is an asymmetric structure comparable to a half-graben oriented N50°E bordered by a single normal fault to the southeast, and a complex set of antithetic faults to the west (Fig. 1) (Edwards et al., 2000). The Dalrymple Trough displays a syncline structure on previously published seismic lines, with longitudinal changes in dip according to the sub-basin (Fig. 3) (Edwards et al., 2000; Gaedicke et al., 2002 a,b). Similarly, the southernmost subsiding sub-basin formed at the entrance of the Dalrymple Trough is characterized by an isopach synclinorium structure (Fig. 5). A series of angular unconformities is observed within the synclinorium structure, indicating that a growing topography was located in this area prior to the formation of the synclinorium (Fig. 5, 6).

The southern Murray Ridge follows a N60°E trend, and displays an asymmetric shape on seismic sections, with a flat southeastern flank, and a steep north western flank facing the Dalrymple Trough (Fig. 3) (Edwards et al., 2000). The angular unconformity marking the uplift of the southern Murray Ridge (picked in blue) is well identified on its eastern side (Fig. 3) (Edwards et al., 2000; Clift et al., 2001; Gaedicke et al., 2002 a,b) and on its western side (Fig.7b and c). Abrupt and sharp vertical fault offsets buried under the Indus fan and previously observed on the eastern side of the Southern Murray Ridge (Edwards et al., 2000) might indicate the location of an extinct transform fault (Fig. 3). To the north, the tilt of Indus deposits at the origin of the M-unconformity forms the Jinnah seamount.

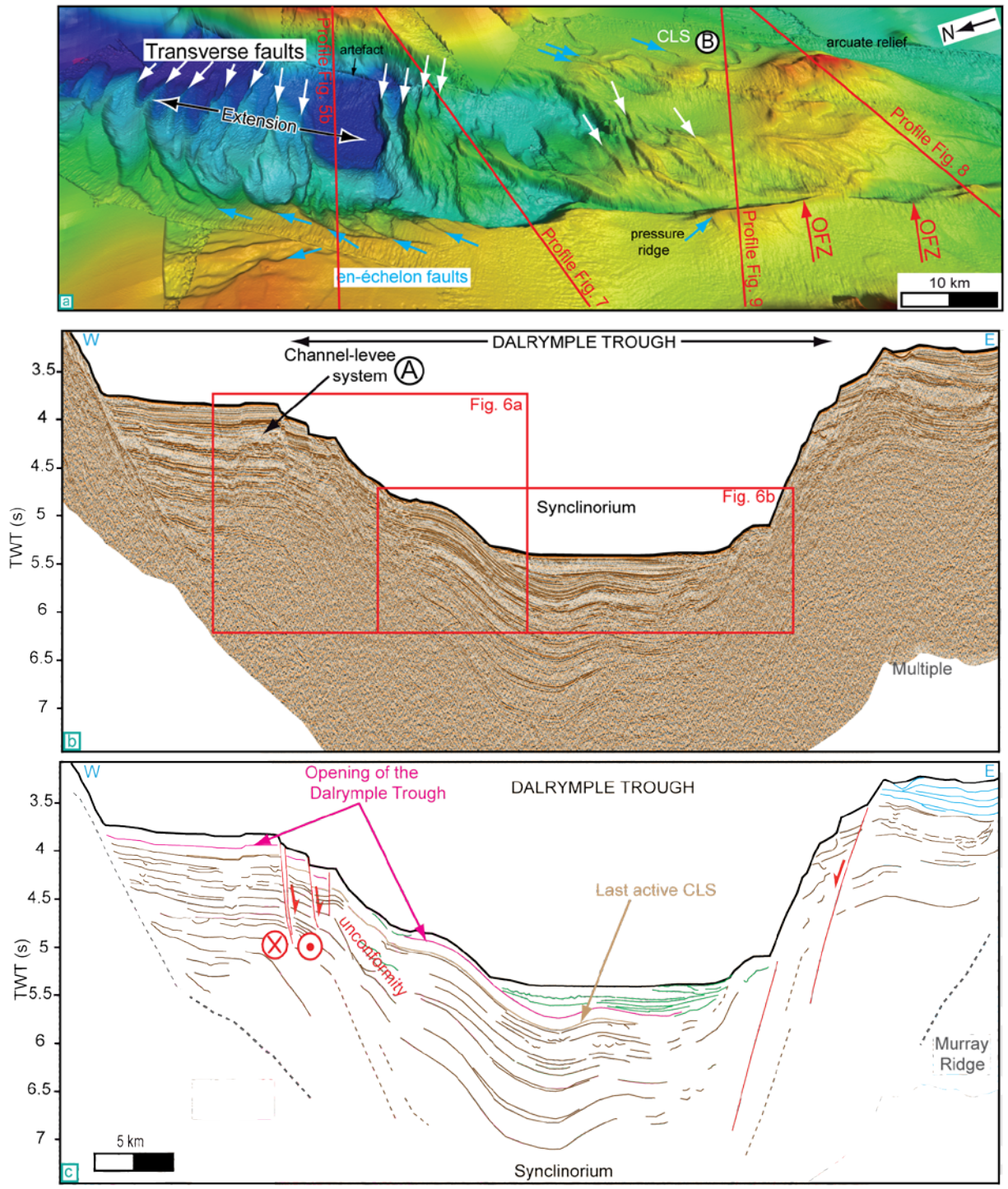


***Figure 5** : a) Bird eye view of the connection between the Owen Fracture Zone (OFZ) and the Dalrymple Trough, showing en-échelon faults evolving laterally into transverse faults within the trough. b) Seismic profile transverse to the Dalrymple Trough (see Fig. 2 and 5 for location) and c) related interpretation. MTD = mass transport deposits. CLS = channel-levee system.*

The connection between the OFZ and the Dalrymple Trough forms a complex horsetail structure (Fig. 2). The horsetail structure is composed of several transverse faults in the continuation of a dense network of right-stepping, en-échelon faults on the northwestern side (labelled 1 on Fig. 2). Transverse faults delineate subsiding sub-basins within the trough, whose lengths range between 10 and 20 km (Fig. 2). In the area of connection with the trough, the OFZ is oriented N20°E, and forms a positive flower structure on seismic profiles, expressed by a pressure ridge on the bathymetry (Fig. 8, 9).

The OFZ is accompanied to the east by a set of N38°E en-échelon faults (labelled 2 on Fig. 2), which merges northwards with the single normal fault at the eastern side of the trough. This en-échelon fault system (2) is interrupted by a 700-m high arcuate relief at the latitude of 21°35'N, which corresponds to a buried system of folds evidenced on seismic profile (Fig. 8). The tilt of sedimentary layers on the eastern side of the arcuate relief indicates that some compression is still active in this area (Fig. 8) and may represent an analog of the successive unconformities observed within the synclinorium structure of the Dalrymple Trough (Fig.5). A syncline structure is also observed on the western side of the OFZ (Fig. 8, 9). The amplitude of the fold-system ranges between 1s (TWT) (Fig. 9) and 2s (TWT) (Fig. 8), indicating that reliefs formed by these folds were about 700-1500 m-high before the emplacement of their turbiditic cover.

The seismic profile displayed in Fig. 9 highlights a contrast in the deformation pattern on both sides of the OFZ, the syncline structure being observed solely on its western side. The latter results from the right-lateral offset of the fold system, which moved the fold initially located at the latitude of profile 9 to the latitude of profile 8.

## 5. Stratigraphic framework

### *5.1. Identification of sedimentary deposits*

Turbiditic channels are characterized on seismic profiles by a typical lens-like architecture with a concave-up lower boundary, and discontinuous, high amplitude reflection. The associated levees display a wedge shape, with high amplitude, transparent seismic facies. Mass transport deposits display the same chaotic to transparent seismic facies, but their geometry is more irregular. On the other hand, pelagic deposits display well-stratified, continuous and conformable horizons on seismic profiles. It is sometimes difficult to discriminate between turbiditic and pelagic deposits on seismic profiles. Bottom-currents may influence the geometry of pelagic deposits, leading to typical pinched-out, sigmoid geometries referred as contouritic drifts (Faugères et al., 1999).

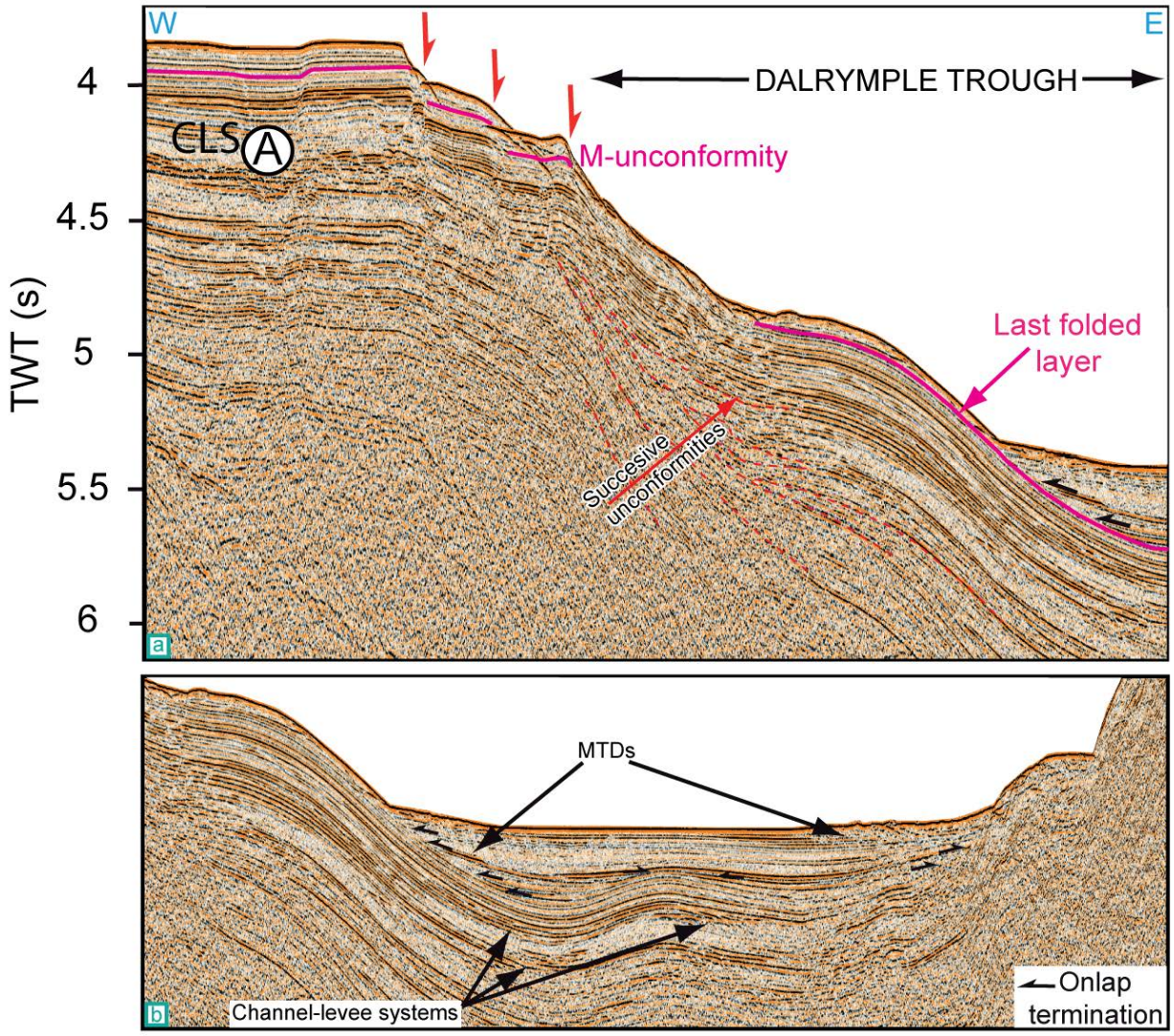


***Figure 6*** *: a) Close view of the seismic profile displayed in fig. 6, showing the stratigraphic correlation of the last deformed layer within the trough. b) close view of the synclinorium structure identified within the Dalrymple Trough.*

Previously published multibeam-bathymetry data reveal the presence of fossil meandering turbiditic channels on the top of the Murray Ridge (Fig. 2), on the Jinnah Seamount (Ellouz-Zimmermann et al., 2007, Mouchot, 2009; Mouchot et al., 2008, 2010).Turbiditic channels are identified below ~4.1 s (TWT) in the vicinity of the OFZ (Fig. 8, 9) and on the western flank of the Dalrymple Trough (Fig. 5, 6). Perched turbiditic channels are also observed on the eastern flank of the trough (Fig. 5, 7). The synclinorium structure within the trough displays a seismic facies typical of a turbiditic and pelagic layers succession (Fig. 5, 6). It further indicates that the turbiditic sequence identified on both sides of the trough used to be connected before its opening (Fig. 5, 6). The turbiditic series deformed by the synclinorium thus corresponds to the substratum of the Dalrymple Trough, the top of which corresponds to the last sedimentary layer deposited before its opening.

The synclinorium structure within the trough is sealed by a ponded sedimentary sequence, mainly composed of mass transport deposits (Fig. 6). The contouritic drifts identified at the edge of the Qalhat Seamount and at the edge of the pressure ridges of the OFZ (Fig. 7, 9) mark the transition from turbiditic to pelagic processes possibly related to a major avulsion episode of the Indus deep-sea fan (Kolla and Coumes, 1987; Bourget et al., 2013), and do not reflect any tectonic change.

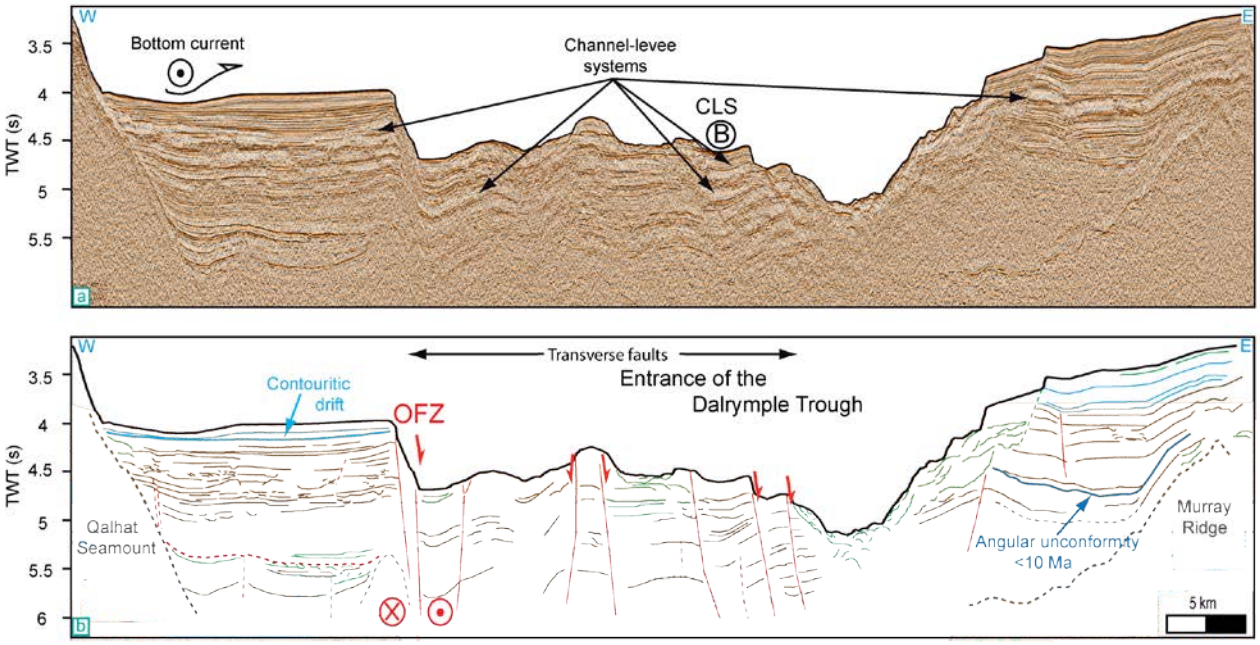


***Figure 7** : a) seismic profile crossing the transverse fault system and b) the related interpretation.*

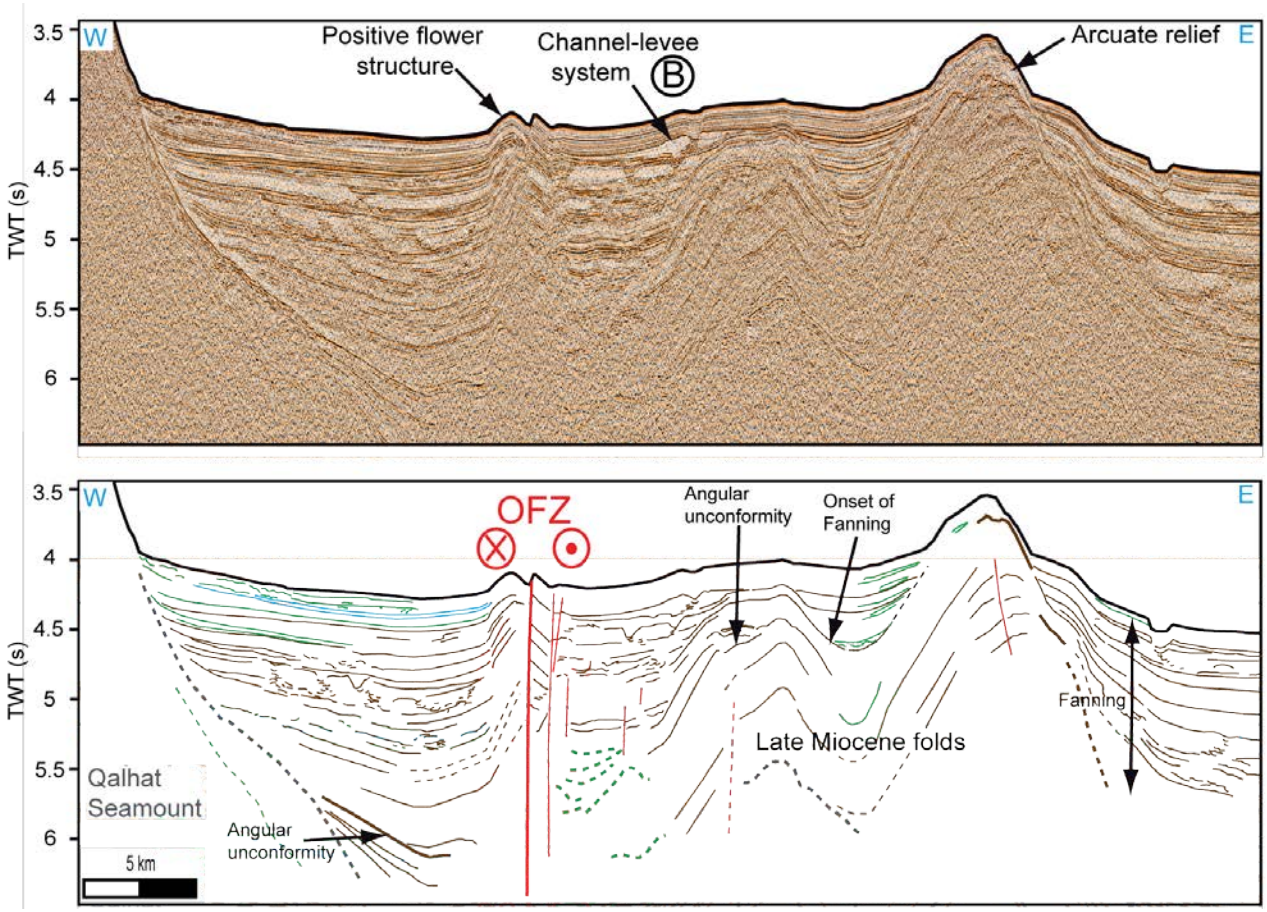


***Figure 8 :*** *a) seismic profile crossing the Owen fracture Zone at the entrance of the Dalrymple Trough (see Fig. 2 and 5 for location) and b) the related interpretation.*

### *5.2. Sedimentation rates*

During their activity (Late Miocene-Pliocene), the sedimentation rates ranged between 350 and 600 m $Ma^{-1}$ according to estimations at DSDP site 222 located at the edge of the OFZ (Fig. 1; latitude ~20°N) (Shipboard Scientific Party, 1974). Turbiditic channels are sealed by a Pleistocene pelagic drape according to calibration with DSDP site 222 (Shipboard scientific party, 1974; Rodriguez et al., 2011).Several DSDP and ODP drillings are available along the Owen Ridge (Shipboard Scientific Party, 1974; 1989), but the complete sedimentary sequence of the Murray Ridge has never been drilled down to the basement (Schulz et al., 1998; Ziegler et al., 2010). All average Pleistocene pelagic sedimentation rates estimated at different drilling sites along the Owen-Murray Ridge range between 30 and 50 m $Ma^{-1}$(Shipboard scientific party, 1974, 1989), with the exception of rates calculated from core MD 04873 (Ziegler et al., 2010), which indicates rates in the order of 100 m $Ma^{-1}$(Table 1). However, the nearby core S090-93KL (Schulz et al., 1998) (located only 40 km away from the core MD 04873) (Fig. 2a) documents rates in the order of 50 m $Ma^{-1}$, which suggests that core MD 04873 has undergone core overpull. There is consequently little spatial variation of Pleistocene pelagic sedimentation rates along the Owen Ridge, allowing large-scale interpolation of these values in areas exclusively covered by pelagic deposits. These values cannot be extrapolated in areas where bottom-

currents seem to have interacted with pelagic processes, as observed in the vicinity of the pressure ridges formed by the OFZ and at the edge of the Qalhat Seamount (Fig. 8, 9).

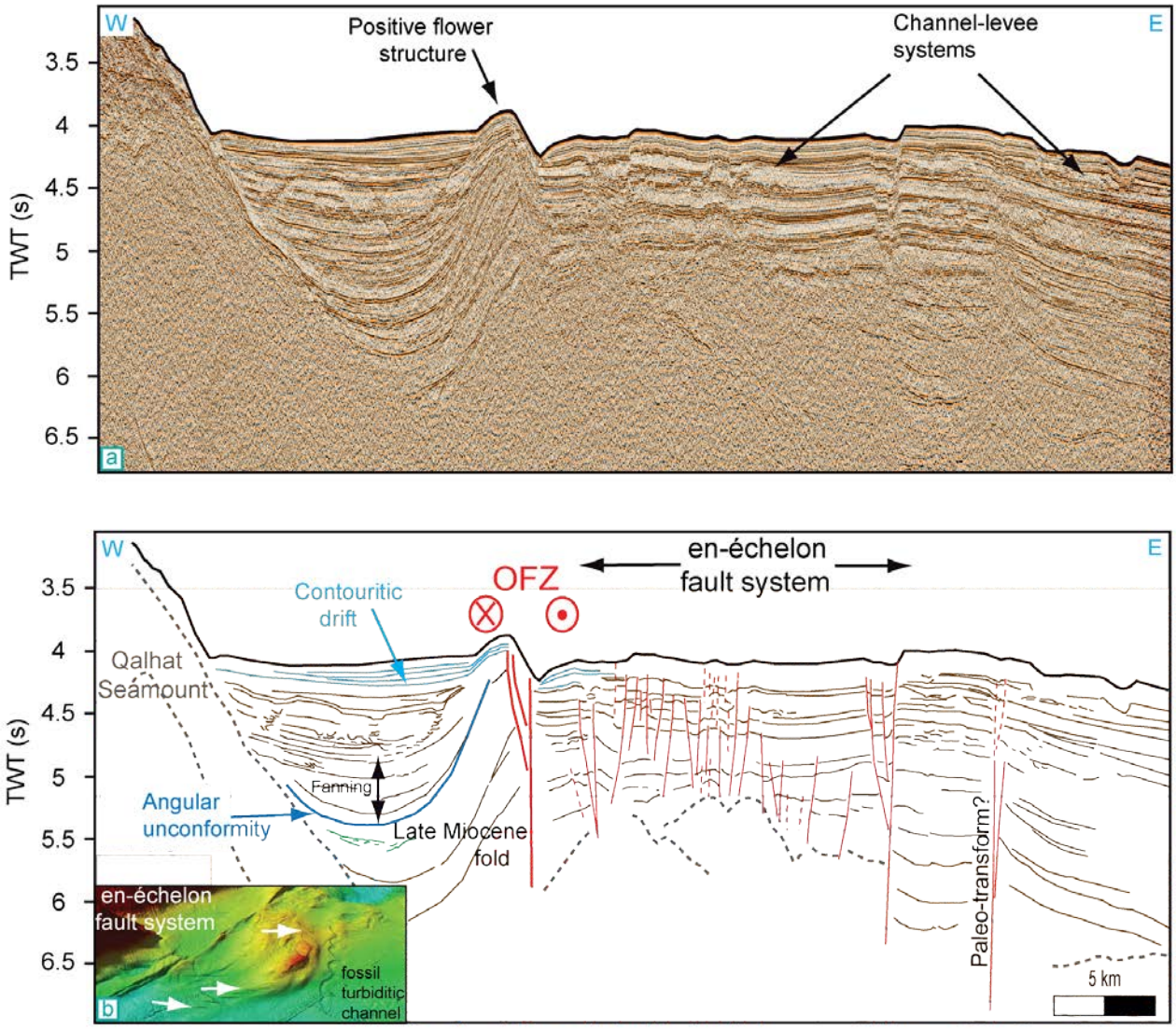


***Figure 9 :*** *a)Seismic profile crossing the Owen Fracture Zone (OFZ) and the en-échelon fault system 2 (see Fig. 2 and 5 for location) and b) the related interpretation. Inset shows a bird eye view of the en-échelon fault system 2, with a particular emphasis over its relationship with fossil Indus turbiditic channels.*

### *5.3. Age estimates of the deformation*

*Opening of the Dalrymple Trough, Northern Murray Ridge uplift, and M-unconformity*

Although the morphology of turbiditic channels is well expressed on the seafloor (Ellouz-Zimmermann et al., 2007; Rodriguez et al., 2011), none of them are active anymore in the vicinity of the trough. Because of the steep slopes created by the active thrusts of the Makran wedge, the turbiditic canyons cutting through the wedge do not form any turbiditic channel at their mouth (Bourget et al., 2011). North of the Dalrymple Trough, the Jinnah seamount acts as a topographic barrier for the turbiditic deposits coming from the Makran (Fig. 4). The origin of the turbiditic sequence observed on both sides of the Dalrymple Trough and below the M-unconformity is thus the Indus deep-sea fan, in agreement with previous interpretations (Gaedicke et al., 2002a,b; Ellouz-Zimmermann et al., 2007). Therefore, the last generation of channel-levee system in the area pre-dates the opening of the Dalrymple Trough and the formation of the M-unconformity, and gives their maximal age. The age of inactivation of the last active channel-levee is estimated by the thickness of the overlying pelagic cover, converted into time using uniform pelagic sedimentation rates in the area (in the order of 30-50 m $Ma^{-1}$).

Channel-levee systems (labelled A) observed both on the top of the Jinnah Seamount (Ellouz-Zimmerman et al., 2007) and west of the Dalrymple Trough (Fig. 5) are covered by ~0.3 s (TWT) of pelagic deposits and are therefore ~6 ±1.5 Ma old. On the other hand, the channel-levee system (labelled B on Figures 5 and 7) observed on the west side of the connection between the OFZ and the Dalrymple Trough is covered by a ~0.18 s TWT-thick pelagic cover, making this channel the most recent in the area. This pelagic thickness indicates that turbiditic sedimentation is inactive in the area since at least 3.7± 0.9 Ma. This channel-levee system is dissected by the transverse faults at the entrance of the trough, indicating it predates this episode of deformation (Fig. 7). The maximal age of the Dalrymple Trough emplacement is therefore 3.7± 0.9 Ma.

The age of opening of the Dalrymple Trough can be precised by seismic correlations performed on the profile transverse to the trough (Fig. 5, 6). The uppermost pelagic reflector of the synclinorium structure (marking the last sedimentary layer deposed before the opening) (Fig. 5, 6) correlates fairly well with the sedimentary sequence west of the Trough, where it is overlaid by a 0.1 s (TWT)-thick pelagic cover corresponding to 2.1 ± 0.5 Ma**.**

On the other hand, the M-unconformity observed on Figure 4 can be correlated up to the Jinnah Seamount. Although indicating a tectonic tilt of the Indus channel-levee systems in the Oman abyssal plain, the dip of the unconformity slightly changes at the approach of the Jinnah Seamount. This change in dip is due to the progressive transition from pelagic to turbiditic deposits as the M-unconformity gets progressively buried by the Makran turbiditic system. The thickness of pelagic deposits covering the M-unconformity in the area uncovered by Makran turbidites is about 0.1 s (TWT), which gives an age of about ~2.1 ± 0.5Ma too. The formation of the Dalrymple Trough is thus coeval with the M-unconformity. About 1200-m of subsidence has been accommodated by the trough

since 2.1 ± 0.5 Ma (which corresponds to a mean-rate in the order of 480-800 m.Ma$^{-1}$, i.e. ~five times less than the present-day subsidence rate in the Dead Sea Basin (ten Brink and Flores, 2011)).

Topographic profiles running transverse to the southern and northern Murray Ridge (Fig. 1) show uplifted flanks (elevation in the order of 1000 m over an area encompassing ~30 km around the trough), which corresponds to the flexural effect of the lithosphere associated to the opening of the trough. Consistently, Kolla and Coumes (1987) previously noticed the southeastward shift of Pleistocene Indus channel-levee systems that could be related to a tectonic tilt of the area. On the other hand, the southern Murray Ridge is outside the area affected by the flexural uplift of the flanks of the Dalrymple Trough, and has probably been little affected by this uplift phase.

*Late Miocene Murray Ridge uplift and buried folds*

The use of the distribution of turbiditic channels as a marker of the evolution of the topography of the Murray Ridge is more problematic. The profile displayed in Fig. 3c shows that before its 2-3 Ma-old uplift, the northern Murray Ridge was almost totally buried by Indus turbidites. The paleo-location of the Indus canyon in the northwestern extremity of the Indian margin prior to the Pleistocene (Fig.1, Kolla and Coumes, 1987) implies that turbiditic channels might have simply bypassed the southern Murray Ridge. However, assuming that they were emplaced in a roughly flat abyssal plain, the tilt of turbiditic deposits indicates the creation of topography.

According to a recent industrial drilling located in the Indus abyssal plain, the unconformity marking the first uplift of the Murray Ridge is ~8-10 Ma-old (Fig. 3) (Calvès, 2008). The southern Murray Ridge was thus a prominent relief since 8-10 Ma ago, but did not act as a major barrier for the Indus turbidites due to the paleo-location of the canyon. The buried folds identified on Figures 8 and 9 cannot be precisely dated because of the large range of Late Miocene-Pliocene Indus sedimentation rates (Kolla and Coumes, 1987; Clift et al., 2001; Calvès, 2008). The system of folds shows an isopach deformation at depth, followed by a fanning configuration upward (Fig. 9). The isopach deformation at depth suggests an abrupt onset of deformation, whereas the fanning configuration represents a period of time during which the sedimentation rates slightly exceeded the growth of the topography. The formation of the isopach folds is probably coeval with the main uplift episode of the southern Murray Ridge, which would imply that the latter resulted from a compressive episode. As evidenced by the tilt of channel-levee systems (Fig. 8), the fanning configuration of turbiditic deposits (Fig. 9) and by the successive angular unconformities identified within the synclinorium in the Dalrymple Trough (Fig. 6), compressive deformation was still active in the area since the main episode of deformation 8-10 Ma ago. Considering the axis of the arcuate relief at ~21°35°N oriented N-S implies a roughly E-W compression.

*Owen Fracture Zone emplacement and en-échelon fault systems*

The right-lateral offset of the folds observed on Fig. 8 and 9 indicates that the OFZ emplaced after 8-10 Ma, consistently with its assumed 3-6 Ma-old age (Fournier et al., 2011). The arcuate relief at ~21°35°N and the pressure ridge at ~21°50°N (Fig. 9) could represent morphologic traces of the 8-10 Ma-old folds. Although the low density of seismic lines available in the area precludes any precise estimation of the offset, the latter seems to be in the order of 10-15 km, consistently with the 10-12 km morphological offsets measured elsewhere along the Owen Ridge (Fournier et al., 2011).

The age of emplacement of the en-échelon fault system (labeled 2 on Fig. 2) observed east of the OFZ between 21-22°N is ambiguous (Fig. 2). The en-échelon faults (2) crosscut a turbiditic channel inactive since at least 3.7± 0.9 Ma according to the overlying 140-m-thick pelagic cover. At first sight, this would indicate the emplacement of the en-échelon fault system postdates the last active turbiditic channel in the area. However, the en-échelon fault system (2) displays at depth stronger vertical offsets, and juxtaposes on both sides sedimentary layers with strong contrasts in dip (Figure 9). It is possible that the Late Miocene-Pliocene turbiditic sedimentation rates largely exceeded the topography formed by this system of fault during this time interval.The latter interpretation is consistent with analog models (Basile and Brun, 1999; Schlische et al., 2002; Dooley and Schreurs, 2012) that suggest that en-échelon fault systems take place in the first stages of structural evolution of strike-slip fault systems, and subsequently merge in a continuous fault. The en-échelon fault system (2) may thus mark the incipient stage of the segment of the OFZ in the area (Rodriguez et al., 2011).

| | | Owen Ridge | | | | | | Murray Ridge | | | |
|---|---|---|---|---|---|---|---|---|---|---|---|
| **CORES** | | ODP 722 shipboard sci. party, 1989 | | | | KS07 Bourget et al., 2013 | | MD-2881 Ziegler et al., 2007 | | S090-93KL Schultz et al., 1998 | |
| Time sampled | | ~15 Ma | | | | ~160 ka | | ~750 ka | | ~110 ka | |
| Average sedimentation rates | | 30 m/Ma (Plio-Pleistocene rates) | | 46 m/Ma | | 54 m/Ma | | 40 m/Ma | | 55 m/Ma | |
| P wave velocity(m/s) | | 1530 | 1730 | 1530 | 1730 | 1530 | 1730 | 1530 | 1730 | 1530 | 1730 |
| Thickness of pelagic deposits overlying the last active CLS (OFZ-Dalrymple connection) | (TWT) 0.18s | 4.6 | 5.2 | 3 | 3.4 | 2.55 | 2.9 | 3.4 | 3.9 | 2.5 | 2.8 |
| Thickness of pelagic deposits overlying the last active CLS (Top of Murray R.) | 0.3s | 7.7 | 8.7 | 5 | 5.6 | 4.25 | 4.8 | 5.7 | 6.5 | 4.2 | 4.7 |
| Thickness of pelagic deposits sealing the 'M' unconformity | 0.1s | 2.55 | 2.9 | 1.7 | 1.9 | 1.4 | 1.6 | 1.9 | 2.2 | 1.4 | 1.6 |

***Table 1 :*** *Age estimations of the different markers used in this study, from sedimentation rates calculated at the different drilling/coring sites available. See fig. 1 and 2 for sites locations.*

## 5. Discussion

The results above document at least three episodes of deformation: a first one (8-10 Ma-old) related to the folds observed on the sides of the OFZ (Fig. 8, 9) and the uplift of the Murray Ridge (Fig. 9) (Kolla and Coumes, 1988; Calvès, 2008); a second one corresponding to the emplacement of the OFZ about 3-6 Ma ago, and a third one (2-3 Ma-old) related to the subsidence of the Dalrymple Trough and the uplift of its flanks, and the formation of the M-unconformity in the Oman plain (Fig. 5, 6).Compressive deformation was still active in the area since 8-10 Ma. This framework, summarized in Figure 10, contrasts with the two stages history (Early and Late Miocene episodes) previously assessed (Gaedicke et al., 2002), and suggests a new geodynamic interpretative scheme of the Dalrymple Trough-Murray Ridge system.

### *5.1. Tectonic history of the Dalrymple Trough-Murray Ridge system*

*Origin of the ~8-10 Ma-old episode of deformation*

A 8-9 Ma-old compressive deformation episode is also evidenced at the East Oman Margin (ODP site 730, Shipboard Scientific Party, 1989) and throughout the Owen Basin (Rodriguez et al., in prep. for EPSL), pointing out a regional episode of deformation. The 8-10 Ma deformation episode coincides in time with the abrupt decrease of the deceleration of seafloor spreading rates at 8-11Ma recorded by magnetic anomalies at the Carlsberg Ridge (DeMets et al., 2005; Mercuriev and DeMets, 2006), expressed by intra-plate deformation in the Central Indian Ocean (Wiens et al., 1985; Chamot-Rooke et al., 1993; Henstock et al., 2004; DeMets et al., 2005; Mercuriev and DeMets, 2006; Delescluse and Chamot-Rooke, 2007; Delescluse et al., 2008).

On the other hand, the India-Eurasia boundary in Pakistan is marked by the Late Miocene uplift of the Kirthar-Sulaiman ranges (evidenced by a major avulsion of the Indus River, Waheed and Wells, 1990; 1992). A major structural reorganisation of the Makran accretionnary wedge also occurred in Tortonian, as attested by the development of large folds (up to 2-km high) (McCall, 1997; Ellouz-zimmerman et al., 2007a) and huge olistostromes (>40 000 $km^3$) (Burg et al., 2008; Smit et al., 2010).

These coeval events may be tentatively interpreted as a side effect of the increase in stress applied by the Late Miocene growth of the Himalayas on the Indian plate (Molnar et al., 1993).

*Origin of the ~2-3 Ma-old episode of deformation*

The origin of the 2.1 ± 0.5 Ma-old episode is more enigmatic. The onset of subsidence at the Dalrymple Trough is roughly coeval with the onset of a major pull-apart basin 2.6 ± 0.5 Ma ago at the latitude of 20°N along the OFZ (Rodriguez et al., 2013). The synchronicity between the opening of the Dalrymple Trough and the M-unconformity, which is only observed on the Arabian Plate, suggests a causal relationship with the Makran subduction zone. Although the modern wedge emplaced in Late Miocene (McCall, 1997), the age of emplacement of the present-day frontal thrust of the wedge is

unknown. The southward migration of the frontal thrust some 2-3 Ma ago may be at the origin of the M-unconformity, and a structural reorganization of the India-Arabia plate boundary. The Dalrymple Trough emplaced in the flexural bulge of the subducting plate. An abrupt release of elastic stresses subsequently to a structural reorganization of the India-Arabia plate-boundary might have enhanced the tilt of the Indus series below the M-unconformity and the flexural uplift at the Dalrymple Trough flanks, responsible of the present-day elevation of the northern Murray Ridge.
The coeval opening of the Dalrymple Trough and the 20°N Basin is striking and suggests the inception of the OFZ some 2-3 Ma ago. However, stepover basins were shown to develop a few million years after the initiation of the San Andreas Fault (e.g. *Wakabayashi et al*. [2007]) and the Levant Fault (*Garfunkel and Ben Avraham* [2001]). This raises the question of the location of the plate-boundary between ~8 Ma (uplift of the Owen-southern Murray Ridge) and ~3 Ma (emplacement of the OFZ). It is possible that the fossil transform segment identified on the eastern flank of the southern Murray Ridge (Fig. 3) (Edwards et al., 2000) acted as the plate boundary for this time span. The sharp continental-oceanic interface west of the Murray Ridge (Edwards et al., 2008) may have controlled the location of the OFZ during its migration.

Additionally, the linear plate velocity differences between MORVEL estimations (averaged over 3.16 Ma (chron 2A)) and GPS studies are in the order of 8 $mm.a^{-1}$ for both the India-Eurasia and the Arabia-Eurasia convergences (DeMets et al., 2010). It suggests a kinematic change occurred during the Plio-Pleistocene, after 3.16 Ma. Such a kinematic change could also explained the discrepancy between the direction of the OFZ predicted by MORVEL (DeMets et al., 2010) and the direction effectively observed on multibeam bathymetry (Fournier et al., 2011). By extrapolating present-day slip rates determined by GPS or field analysis, Allen et al. (2004) showed that the total shortening or strike-slip offset on most of the active faults in the Arabia-Eurasia collision zone can be accommodated in only 3-7 Ma, consistently with the age estimates of the OFZ (Fournier et al., 2011). The opening of the Dead Sea Basin along the Levant Fault is roughly coeval with the opening of both the Dalrymple Trough and the 20°N Basin (TenBrink et al., 1989; Rodriguez et al., 2013). The coeval opening of major pull-apart basins along both strike-slip boundaries of the Arabian plate may reflect this poorly constrained kinematic change.

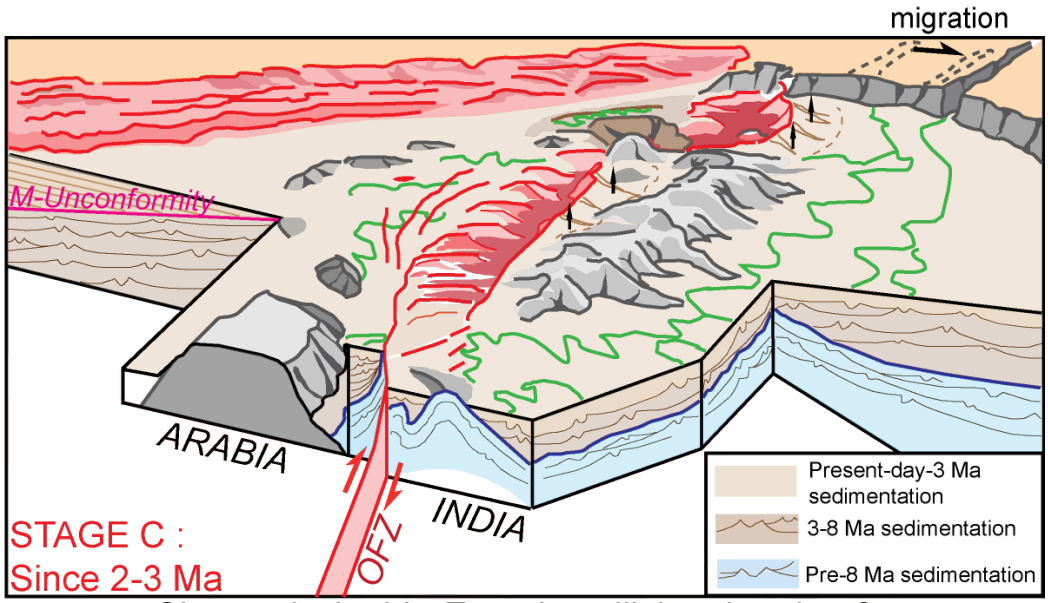


Change in Arabia-Eurasia collisional regime?

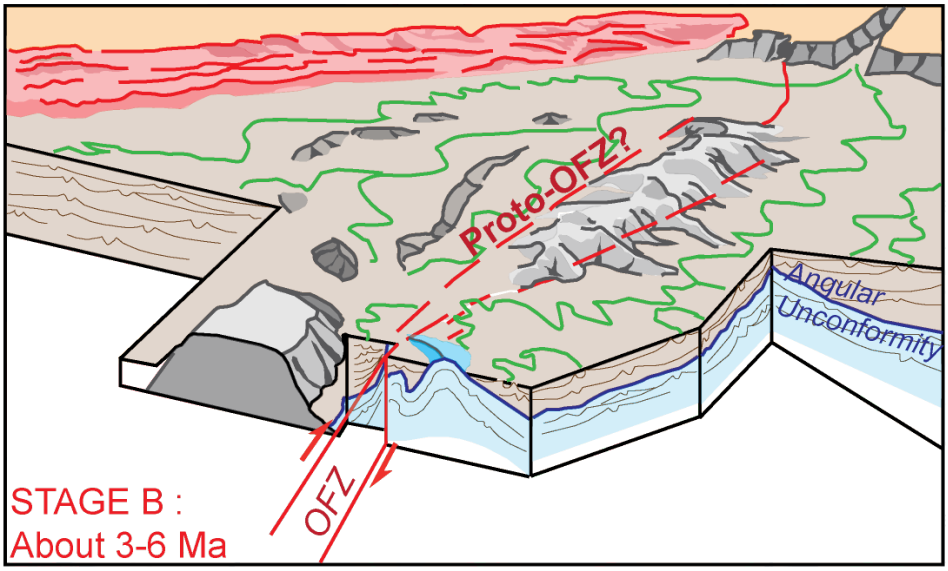


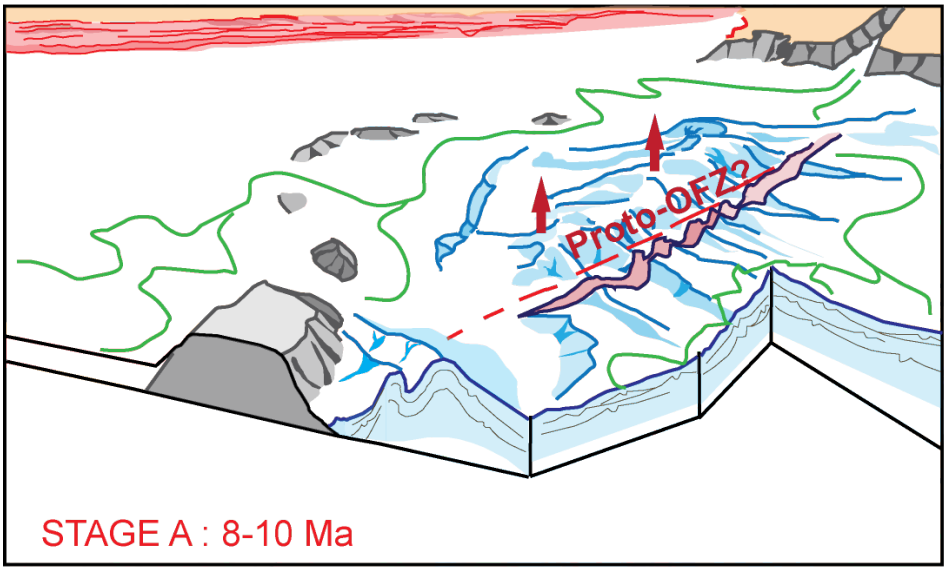

***Figure 10 :*** *Sketches of the geological history of the Dalrymple Trough and the Murray Ridge.OFZ : Owen Fracture Zone, PB : Plate-Boundary. Stage A : A Late Miocene episode of compression along the India-Arabia plate boundary triggered the main uplift of the Murray Ridge. The plate boundary was probably located on the eastern side of the Murray Ridge. Stage B : The OFZ emplaced between 3-6 Ma ago, and started to offset dextrally the Late Miocene folds, the latter being progressively buried under Indus turbidites. Stage C: The Dalrymple Trough opened, and provoked a new episode of uplift of the northern Murray Ridge. It is related to the formation of the M-unconformity in the Oman abyssal plain. At the same time, the Indus canyon began its migration towards the south-east.*

### *5.2. Mode of opening of the Dalrymple Trough and uplift of the Murray Ridge*

Since the beginning of the rifting of the Dalrymple Trough ~2.1 ± 0.5 Ma ago, the OFZ has accommodated only ~4-8 km of relative motion between India and Arabia. This amount of relative motion drastically contrasts with the dimensions of the Dalrymple Trough (150-km-long, 30-km-wide), which questions the relationship linking the size of a pull-apart basin to the relative motion along the main strike-slip fault (Aydin and Nur, 1982).The isopach synclinorium structure identified within the trough (Fig. 5) indicates an abrupt deformation phase at its first stage of opening. It is consistent with an abrupt structural reorganization of the strike-slip fault system corresponding to the formation of a stepover. The formation of the stepover might have isolated a subsiding half graben of dimensions close to the present-day Dalrymple Trough. The numerous transverse faults observed throughout the trough might have subsequently individualized several sub-basins, accommodated distributed extension and subsidence corresponding to the 4-8 km of India-Arabia relative motion. The direction of extension is orthogonal to the transverse faults, i.e. parallel to the direction of the OFZ in the area (Fig. 2, 7).

Faults inherited from the 8-10 Ma deformation phase, together with the complex rheological pattern of the area (presence of an Ocean-Continent Transition, i.e. abrupt crust thickness variations) (Edwards et al., 2008), might have controlled the stepover localization. Sand-box experiments of Basile and Brun (1999) highlighted the role of Ocean-Continent Transition in favouring the development of horsetail structures.

Transverse faults are common structures within narrow (<15-km-wide) stepover basins such as the Dead Sea Basin (Kashai and Croker, 1987; Ben Avraham and ten Brink, 1989; Lazar et al., 2006) or the 20°N Basin along the OFZ (Rodriguez et al., 2011, 2013). They probably result from the partitioning of the strike-slip deformation in stepover areas. Results from sand-box experiments (Smit et al., 2008) show that transverse fault initiation occurs where the ratio between the stepover wideness and the thickness of the deforming layer is <1. It is not the case for the Dalrymple Trough, where the crustal thickness is about 15 km (Edwards et al., 2008), leading to a stepover wideness/crustal thickness ratio equal to 2. The occurrence of transverse faults within the Dalrymple Trough is thus

conspicuous. A tempting hypothesis would be to consider that sharp rheological contrasts at Ocean-Continent Transition favor the formation of transverse faults.

The uplift of the northern Murray Ridge is related to the emplacement of the Dalrymple Trough. The topographic expression of extension and compression within the oceanic lithosphere is mainly controlled by the lithospheric strength, which is a function of the thermal state -and therefore the age- of the lithosphere (Weissel et al., 1992). Consequently, even a local reorganization related to the formation of a stepover area can modify the local distribution of stress and generate prominent reliefs of flexural origin such as the northern Murray Ridge and the western part of the southern Murray Ridge.

## 6. Conclusions

The Dalrymple Trough is a major, 2.1 ± 0.5 Ma-old stepover basin located between the OFZ and the Ornach-Nal Fault in Pakistan. The Dalrymple horsetail area marks a transition between the strike-slip motion along the OFZ and the extension within the trough. A very similar horsetail structure is described in the Andaman Sea (Northeast Indian Ocean) (Cattin et al., 2009), and along the Ghana Margin in the Atlantic Ocean (Basile et al., 1993) in a context of Ocean-Continent transition, that seems to favor the formation of horsetail-type stepover basins. The reassessment of the age of opening of the Dalrymple Trough and the M-unconformity at 2.1 ± 0.5 Ma points out interesting perspectives for the Indus turbiditic system and the Makran accretionnary wedge.

First, the uplift of the northern Murray Ridge since ~2 Ma might account for the Pleistocene southwestward migration of the Indus canyon on the Indian Margin (Kolla and Coumes, 1987). A precise dating of the episodes of migration of the canyon, together with reconstitutions of the evolution of the topography fossilized by channel-levee systems, would highlight the complex interaction between tectonic and sedimentary processes.

Second, the younger age of the M-unconformity indicates that the erosion rates of the Makran accretionnary wedge have been strong during the Pleistocene, probably in the same order as current rates (>2 $mm.yr^{-1}$, Bourget et al., 2011). Sedimentation rates control the temperature at the deformation front, high sedimentation rates favoring shallow seismogenic rupture along megathrusts (Smith et al., 2012; 2013). The opening of the Dalrymple Trough isolated the Makran from Indus deposits, the only source remaining Makran sands. How this transition in the sedimentation regime affected the seismogenic potential of the Makran wedge is poorly understood.

Finally, the Late Miocene episode of deformation at the origin of the southern Murray Ridge suggests that the India-Arabia plate boundary reacted to the kinematic change at the origin of intra-plate deformation in the Indian Ocean (Chamot-Rooke et al., 1993). This kinematic change could have also influenced the rise of the Owen Ridge, controlled the location of the India-Arabia plate-boundary (Rodriguez et al., 2011) and deformation overall the Owen Basin (Rodriguez et al., in prep for EPSL).

Deep-sea drillings would be useful to decipher the precise timing of the deformation in the area, and the way it reacted to kinematic changes.

**Acknowledgements**

We are grateful to Captain Rémi De Monteville, officers and crew of the BHO Beautemps-Beaupré. We thank the GENAVIR team and the hydrographer D. Levieuge for their help in data acquisition. Processing of the OWEN-2 dataset was carried out using the Geocluster 5000 software from CGGVeritas. We thank P. Dubernet and N. Bacha for technical assistance. This study was supported by SHOM, IFREMER, INSU-CNRS, and CEA (LRC Yves-Rocard).

**References**

Allen, M., Jackson, J., Walker, R., 2004. Late Cenozoic reorganization of the Arabia-Eurasia collision and the comparison of short term and long term deformation rates. Tectonics 23, TC2008, doi:10.1029/2003TC001530.

Aydin, A., Nur, A., 1982. Evolution of pull-apart basins and their scale independence. Tectonics 1, 91–105, doi:1029/TC001i001p00091.

Barnes, P., Pondard, N., 2010. Derivation of direct on-fault submarine paleoearthquake records from high-resolution seismic reflection profiles: Example from the Wairau Fault, New Zealand, Geochemistry, Geophysics, Geosystems 11, Q11013, doi:10.1029/2010GC003254.

Basile , C., Mascle, J., Popoff, M., Bouillin, J.P., Mascle, G., 1993. The Ivory Coast-Ghana transform margin: a marginal ridge structure deduced from seismic data. Tectonophysics 222, 1-19.

Basile, C., Brun, J.P., 1999. Transtensional faulting patterns ranging from pull-apart basins to transform continental margins: an experimental investigation. Journal of Structural Geology 21, 23–37.

Ben Avraham, Z., Ten Brink, U. S., 1989. Transverse faults and segmentation of basins within the Dead Sea Rift. Journal of African Earth Science 8, 603-616.

Bourget, J., Zaragosi, S., Ellouz-Zimermann, N., Mouchot, N., Garlan, T., Schneider, J.-L., Lanfumey, V., Lallemant,S., 2011.Turbidite system architecture and sedimentary processes along topographically complex slopes: The Makranconvergent margin. Sedimentology 58, 376–406, doi:10.1111/j.1365-3091.2010.01168.x

Bourget, J., Zaragosi, S., Rodriguez, M., Fournier, M., Garlan, T., Chamot-Rooke, N., 2013. Late Quaternary megaturbidites of the Indus Fan: Origin and stratigraphic significance. Marine Geology 336, 10-23, http://dx.doi.org/10.1016/j.margeo.2012.11.011.

Burg, J.P., Bernoulli, D., Smit, J., Dolati, A., Bahroudi, A., 2008. A giant catastrophic mud-and-debris flow in the Miocene Makran. Terra Nova 20, 188–193, doi: 10.1111/j.1365-3121.2008.00804.x

Burgath, K. P., Von Rad, U., Van der Linden, W., Block, M., Ali Khan, A., Roeser, H. A., Weiss, W., 2002. Basalt and peridotites from Murray Ridge: are they of supra-subduction origin? in The Tectonic and Climatic Evolution of the Arabian Sea Region, edited by P. D. Clift et al., Geological Society Special Publication, 195, 117-135

Cattin, R., Chamot-Rooke, N., Pubellier, M., Rabaute, A.,Delescluse, M., Vigny, C., Fleitout, L., Dubernet, P., 2009.Stress change and effective friction coefficient along the Sumatra-Andaman-Sagaing fault system after the 26 December 2004 (Mw=9.2) and the 28 March 2005 (Mw=8.7) earthquakes. Geochemistry, Geophysics, Geosystems 10, doi:10.1029/2008GC002167.

Calvès, G., 2008.Tectonostratigraphic and climatic recordof the NE Arabian Sea, Ph.D. thesis, 305 pp., Univ. ofAberdeen, Aberdeen U. K.

Chamot-Rooke, N., Jestin, F., DeVoogd, B., 1993.Intraplate shortening in the central Indian-ocean determined from a 2100-km-long north-south deep seismic-reflection profile. Geology 21, 1043–1046.

Clift, P. D., Shimizu, N., Layne, G. D., Blusztain, J. S., Gaedicke, C., Schluter, H.-U., Clark,M. K., Amjad, S., 2001. Development of the Indus Fan and its significance for the erosionalhistory of the Western Himalaya and Karakoram. Geological Society of America Bulletin 113(8), 1039–1051.

Clift, P. D., Gaedicke, C, 2002. Accelerated mass flux to the Arabian Sea during the middle to late Miocene.Geology 30, 207-210.doi:10.1130/0091-13

Cochran, J. R., 1981. The Gulf of Aden: structure and evolution of a young ocean basin and continental margin. Journal of Geophysical Research 86, 263-287.

Coumes, F., Kolla, V., 1984. Indus Fan: seismic structure, channel migration and sediment thickness in the upper fan. in: Haq, B.U., J.D., M. (Eds.), Marine Geology and Oceanography of Arabian Sea and coastal Pakistan. Van Nostrand Reinhold Comp., New York, pp. 101-110.

Delescluse, M., Chamot-Rooke, N., 2007.Instantaneous deformation and kinematics of the India-Australia Plate. Geophysical Journal International 168, 818-842, doi: 10.1111/j.1365-246X.2006.03181.x

Delescluse, M., Montési, L. G. J, Chamot-Rooke, N., 2008. Fault reactivation and selective abandonment in the oceanic lithosphere. Geophysical Research Letters 35, L16312 doi:10.1029/2008GL035066

DeMets, C., Gordon, R., Royer, J-Y., 2005. Motion between the Indian, Capricorn and Somalian plates since 20 Ma: implications for the timing and magnitude of distributed lithospheric deformation in the equatorial Indian Ocean. Geophysical Journal International 161, 445-468, doi: 10.1111/j.1365-246X.2005.02598.x

DeMets, C., Gordon, R.G., Argus, D.F., Stein, S., 1990. Current plate motions. Geophysical Journal International 101, 425-478.

DeMets, C., Gordon, R.G., Argus, D.F., Stein S., 1994. Effect of recent revisions of the geomagnetic reversal time scale on estimates of current plate motions. Geophysical Research Letters 21, 2191-2194.

DeMets C., Gordon R. G., Argus, D.F., 2010.Geologically current plate motions, Geophysical Journal International 181, 1-80. doi: 10.1111/j.1365-246X.2009.04491.x.

Dooley, T. , Schreurs, G., 2012. Analogue modelling of intraplate strike-slip tectonics: a review and new experimental results. Tectonophysics 574-575, 1-71.

Edwards R.A., Minshull,T. A., White, R. S., 2000. Extension across the Indian–Arabian plate boundary: the Murray Ridge. Geophysical Journal International 142, 461-477.

Edwards, R. A., Minshull, T. A., Flueh, E. R., Kopp, C., 2008. Dalrymple Trough: An active oblique-slip ocean-continent boundary in the northwest Indian Ocean. Earth and Planetary Science Letters 272, 437-445.

Ellouz Zimmermann, N., Deville, E., Müller, C., Lallemant, S., Subhani, A. B., Tabreez, A. R., 2007. Impact of sedimentation on convergent margin tectonics : example of the Makran Accretionary prism (Pakistan). Thrust Belts and Foreland Basins: From Fold Kinematics to Hydrocarbon Systems, edited by O. L. Lacombe et al., pp. 327–350, Springer, Berlin.

Ellouz-Zimmermann, N. et al., 2007.Offshore frontal part of the Makranaccretionary prism (Pakistan) the ChamakSurvey.inThrust Belts and Foreland Basins: From Fold Kinematics to Hydrocarbon Systems, edited by O. L. Lacombe et al., pp. 349–364, Springer, Berlin.

Faugères, J.C., Stow, D.A.V., Imbert P., Viana, A. 1999. Seismic features diagnostic of contourite drifts, Marine Geology 162, 1-38.

Fournier, M., Patriat, P., Leroy, S., 2001. Reappraisal of the Arabia–India–Somalia triple junction kinematics. Earth and Planetary Science Letters 189, 103–114.

Fournier, M., Chamot-Rooke, N., Petit, C., Fabbri, O., Huchon, P., Maillot, B., Lepvrier, C., 2008a.In-situ evidence for dextral active motion at the Arabia–India plate boundary. Nature Geoscience 1, 54–58 http://dx.doi.org/10.1038/ngeo.2007.24.

Fournier, M., Petit, C., Chamot-Rooke, N., Fabbri, O., Huchon, P., Maillot, B., Lepvrier, C., 2008b. Do ridge-ridge-fault triple junctions exist on Earth? Evidence from the Aden–Owen–Carlsberg junction in the NW Indian Ocean. Basin Research 20, 575–590 http://dx.doi.org/10.1111/j.1365-2117.2008.00356.x.

Fournier, M., Chamot-Rooke, N., Petit, C., Huchon, P., Al-Kathiri, A., Audin, L., Beslier,M.-O., d'Acremont, E., Fabbri, O., Fleury, J.-M., Khanbari, K., Lepvrier, C., Leroy, S., Maillot, B., Merkouriev, S., 2010. Arabia–Somalia plate kinematics, evolution of the Aden–Owen–Carlsberg triple junction, and opening of the Gulf of Aden. Journal of Geophysical Research 115, B04102 http://dx.doi.org/10.1029/2008JB006257.

Fournier, M., Chamot-Rooke, N., Rodriguez, M., Huchon, P., Petit, C., Beslier, M.-O., Zaragosi, S., 2011. Owen Fracture Zone: the Arabia–India plate boundary unveiled. Earth and Planetary Science Letters 302, 247–252 http://dx.doi.org/10.1016/j.epsl.2010.12.027.

Gordon, R.G.,DeMets, C., 1989. Present-day motion along the Owen fracture zone and Dalrympletrough in the Arabian Sea. Journal of Geophysical Research 94, 5560-5570.

Gaedicke, C.,Schlüter, H. U., Roeser, H. A., Prexl, A.,Schreckenberger, B., Meyer, H., Reichert, C., Clift, P.,Amjad, S., 2002. Origin of the northern Indus Fan and Murray Ridge, Northern Arabian Sea: interpretation from seismic and magnetic imaging. Tectonophysics, 355,127–143, http://dx.doi.org/10.1016/S0040-1951(02)00137-3

Gaedicke, C., Prexl, A., Schlüter, H.-U., Roeser, H., Clift, P., 2002. Seismic stratigraphy and correlation of major regional unconformities in the northern Arabina Sea. In: The Tectonic and Climatic Evolution of the Arabian Sea Region (Eds P. Clift, D. Kroon, C. Gaedicke and J. Craig), Geological Society of London, Special Publication, 195, 25-36.

Hatzfeld, D., Molnar, P., 2010. Comparisons of the kinematics and deep structures of the Zagros and Himalaya and of the Iranian and Tibetan plateaus and geodynamic implications. Review of Geophysics 48, RG2005, doi:10.1029/2009RG000304.

Henstock, T. J., Minshull, T. A., 2004. Localized rifting at Chagos bank in the India-Capricorn plate boundary zone. Geology 32, 237–240.

Kashai, E. L., Croker, P. F., 1987. Structural geometry and evolution of the Dead Sea-Jordan rift system as deduced from new subsurface data. Tectonophysics 141, 33-60.

Kolla, V., Coumes, F., 1987. Morphology, internal structure, seismic stratigraphy, and sedimentation of Indus Fan, The American Association of Petroleum Geologists Bulletin, pp. 650-677

Lazar, M., Ben-Avraham, Z., Schattner, U., 2006.Formation of sequential basins along a strike-slip fault – geophysical observations from the Dead Sea basin. Tectonophysics 421, 53–69.

Mann, P., 2007.Global catalogue, classification and tectonic origins of restraining- and releasing bends on active and ancient strike-slip fault systems. Geological Society Special Publications 290, 13-142.

McCall, G.J.H., 1997. The geotectonic history of the Makran and adjacent areas of southern Iran. Journal of Asian Earth Science 15, 517-531.

McKenzie, D. P., Sclater, J. G., 1971. The evolution of the Indian Ocean since the Late Cretaceous, Geophysical Journal of Royal Astronomy Society 25, 437–528.

Merkouriev, S., DeMets, C., 2006.Constraints on Indianplate motion since 20 Ma from dense Russian magnetic data:Implications for Indian plate dynamics. Geochemistry, Geophysics, Geosystems 7, Q02002, doi:10.1029/2005GC001079.

Minshull, T. A., White, R. S., Barton, P. J., Collier, J. S., 1992. Deformation at plate boundaries around the Gulf of Oman, Mar. Geol., 104, 265–277, doi:10.1016/0025-3227(92)90101-M.

Mouchot, N., 2009. Tectonique et sédimentation sur le complexe de subduction du Makran pakistanais. PhD thesis, 364 pp., Univ. Cergy-Pontoise, France.

Mouchot, N, Lallemant, S., Loncke, L., Leturmy, P., Mahieux, G., Chanier, F., Ellouz-Zimmermann, N., 2008. Vertical movements and recent sedimentary processes on the Makranaccretionary prism off Pakistan, EGU General Assembly, Vienna.

Mouchot, N, Loncke, L., Mahieux, G., Bourget, J., Lallemant, S., Ellouz-Zimmermann, N., Leturmy, P., 2010. Recent sedimentary processes along the Makran trench (Makran active margin, off Pakistan), Marine Geology, 271, 17-31.

Mountain, G. S., Prell, W.L. 1990.A multiphase plate tectonic history of the southeast continental margin of Oman. In: Robertson, A. H. F., Searle, M. P. and Ries, A. C. (eds) the Geology and Tectonics of the Oman Region, Geological Society of London Special Publications, 49, 725-743.

Mouthereau, F., Lacombe, O., Vergés, J., 2012.Building the Zagros collisional orogen: Timing, strain distribution and the dynamics of Arabia/Eurasia plate convergence. Tectonophysics 532–535, 27–60.

Quittmeyer R. C., Kafka,A. L., 1984. Constraints on plate motions in southern Pakistan and the northern Arabian Sea from the focal mechanisms of small earthquakes. Journal of Geophysical Research 89, 2444-2458.

Reading, H.G., Richards, M., 1994. Turbidites systems in deep-water basin margins classified by grain size and feeder system. American Association of Petroleum Geology Bulletin, 792-822.

Reilinger, R., et al., 2006.GPS constraints on continental deformation in the Africa – Arabia – Eurasia continental collision zone and implications for the dynamics of plate interactions. Journal of Geophysical Research 111, B05411, doi:10.1029/2005JB004051

Rodriguez, M., Fournier, M., Chamot-Rooke, N., Huchon, P., Bourget, J., Sorbier,M., Zaragosi, S., Rabaute, A., 2011. Neotectonics of the Owen Fracture Zone (NW Indian Ocean): structural evolution of an oceanic strike–slip plate boundary (2011). Geochemistry, Geophysics, Geosystems 12, Q12006 http://dx.doi.org/10.1029/2011GC003731.

Rodriguez, M., M. Fournier, N. Chamot-Rooke, P. Huchon, S. Zaragosi, and A. Rabaute (2012), Mass wasting processes along the Owen Ridge (Northwest Indian Ocean), Marine Geology 326-328, 80-100, 10.1016/j.margeo.2012.08.008

Ross, D. A., Uchupi, E., White, R., 1986. The geology of the Persian-Gulf of Oman Region : a synthesis. Reviews of Geophysics 24, 537-556.

Royer, J. Y., Chaubey, A. K., Dyment, J., Bhattacharya, G. C., Srinivas, K., Yateesh, V., Ramprasad,T., 2002.Paelogene plate tectonic evolution of the Arabian and Eastern Somali basins. in The Tectonic and Climatic Evolution of the Arabian Sea Region, edited by P. D. Clift et al., Geological Society Special Publications 195, 7–23

Schlische, R. W., Withjack M. O.,Eisenstadt, G., 2002.An experimental study of the secondary deformation produced by oblique slip normal faulting. American Association of Petroleum Geology Bulletin 86, 885–906.

Schlüter, H. U., Prexl, A., Gaedicke, C., Roeser, H., Reichert, C., Meyer, H., von Daniels C., 2002.The Makranaccretionary wedge: sediment thicknesses and ages and the origin of mud volcanoes. Marine geology 185, 219-232

Schulz, H., von Rad, U.,Erlenkeuser, H., 1998. Correlation between Arabian Sea and Greenland climate oscillations of the past 110 000 years. Nature, 393, 54-57.

Shipboard Scientific Party,1989.Site 731. InPrell, W.L., Niitsuma, N., et al., Proc. ODP, Init.Repts., 117: College Station, TX (Ocean Drilling Program), 585-652.

Smit J., Brun J. P, Cloetingh, S., Ben-Avraham, Z., 2008.Pull-apart basin formation and development in narrow transform zones with application to the Dead Sea Basin. Tectonics 27, TC6018, doi:10.1029/2007TC002119

Smit J, Burg J-P, Dolati A, Sokoutis D (2010) Effects of mass waste events on thrust wedges: analogue experiments and application to the Makran accretionary wedge. Tectonics 29: TC3003

Smith, G., McNeill, L. Henstock, T. J., Bull, J., 2012. The structure and fault activity of the Makran accretionary Prism. Journal of Geophysical Research 117, B07407, doi:10.1029/2012JB009312.

Smith, G. L., McNeill, L. C., Wang, K. He, J., Henstock, T.J., 2013. Thermal structure and megathrust seismogenic potential of the Makran subduction zone. Geophysical Research Letters 40, 1528–1533, doi:10.1002/grl.50374.

ten Brink, U. S., Flores, C. H., 2012. Geometry and subsidence history of the Dead Sea basin: A case for fluidinduced mid-crustal shear zone? Journal of Geophysical Research 117, B01406, doi:10.1029/2011JB008711.

Vigny C., Huchon P., Ruegg J.C., Khanbari K., Asfaw L.M., 2006. Confirmation of Arabia plate slow motion by new GPS data in Yemen, Journal of Geophysical Research 111, B02402, doi:10.1029/2004JB003229

Weissel, J.K., Childers, V.A., Karner, G.D., 1992. Extensional and Compressional Deformationof the Lithosphere in the Light of ODP Drilling in the Indian Ocean.Synthesisof Results from Scientific Drilling in the Indian Ocean. : Geophysical Monography70, American Geophysical Union.

White, R. S., Klitgord, K., 1976. Sediment deformation and plate tectonics in the Gulf of Oman. Earth and Planetary Science Letters 32, 199-209.

Whitmarsh, R.B., 1979. The Owen Basin off the south-east margin of Arabia and the evolution of the Owen Fracture Zone. Geophysical Journal of the Royal Astronomical Society 58, 441-470.

Wiens, D. A., Demets, C., Gordon, R. G., Stein, S., Argus, D., Engeln, J. F., Lundgren, P., Quible, D., Stein, C.,Weinstein, S., Woods, D. F., 1985. A diffuse plate boundary model for Indian ocean tectonics. Geophysical Research Letters 12, 429–432.

Wu, J. E., McClay, K., Whitehouse, P., Dooley, T., 2010.4D analogue modelling of transtensional pull-apart basins. Marine and Petroleum Geology 26, 1608-1623.

Ziegler, M., Lourens, L. J., Tuenter, E., Hilgen, F., Reichart, G-J., Weber, N. Precession phasing offset between Indian summer monsoon and Arabian Sea productivity linked to changes in Atlantic overturning circulation. Paleoceanography 25, PA3213 (2010)doi:10.1029/2009PA001884.

# Chapitre 4 : La limite de plaque Inde-Arabie au cours du Miocène et le soulèvement de la Ride d'Owen

Dans l'article précédent, " *Tectonics of the Dalrymple Trough and uplift of the Murray Ridge (NW Indian Ocean) "*, nous montrons que le relief du segment sud de la Ride de Murray est probablement le résultat d'une phase de compression tortonienne associée au même changement cinématique que celui à l'origine de la déformation intra-plaque dans l'océan Indien Central. Cette découverte nous conduit naturellement à l'hypothèse selon laquelle le soulèvement de la Ride d'Owen pourrait être lui aussi d'âge Tortonien (8-10 Ma), et non Burdigalien (~20 Ma) comme initialement proposé.

Ce chapitre s'articule principalement autour d'un article intitulé "*The Owen Ridge uplift and implications on the record of Asian paleo-climate in Late Miocene marine sediments of the Arabian Sea"*, rédigé en vue d'une soumission prochaine à la revue *Earth and Planetary Science Letters.*

Cet article met en évidence, à partir des données de sismique réflexion de la campagne Owen 2, une phase de déformation fini-Miocène jusqu'alors mal contrainte sur l'ensemble du Bassin d'Owen (incluant la Ride d'Owen et la marge omanaise). Une surface d'érosion identifiée sur la marge omanaise indique qu'une topographie aérienne a été formée par cette déformation. Cette phase de déformation pourrait aussi expliquer le soulèvement post-rift de la marge du Dhofar, dont l'origine est soumise à controverses. D'autre part, des indices dans la littérature suggèrent une brusque augmentation de la topographie au niveau du Makran autour du Tortonien, potentiellement associé à cette phase de déformation. La discordance régionale Miocène inférieur identifiée par *Whitmarsh (1979)* dans le Bassin d'Owen, et le faciès de transition turbidite-pélagite à 15 Ma identifié par *Mountain et Prell (1990)* ne constituent plus des preuves du soulèvement de la ride au début du Miocène.

Bien que plusieurs évènements géodynamiques aient pu être à l'origine de cette phase de déformation, l'hypothèse la plus probable en terme de chronologie est que la plaque Arabie ait réagi au changement cinématique à l'origine de la déformation intra-plaque dans l'Océan Indien. L'Océan Indien Central est en effet le siège d'une vaste zone de déformation diffuse, initiée il y a environ 9 Ma (voire 20 Ma pour les premiers stades selon les travaux de J-Y Royer), et marquant la naissance probable d'une nouvelle frontière de plaque entre l'Australie, l'Inde, et la plaque Capricorne. L'origine de cette phase de déformation intra-plaque serait la brusque accélération de la croissance des reliefs Himalayens autour de 10 Ma, qui aurait engendré une redistribution des forces au niveau de la plaque Inde (*Molnar et al., 1993*).

Cependant, ce brusque épisode de croissance de l'Himalaya est de plus en plus discuté, et aurait démarré plusieurs millions d'années avant la mise en place de la déformation intra-plaque dans l'océan Central Indien. Il se peut que la déformation intra-plaque marque le passage d'une valeur "seuil" dans la topographie himalayenne, suffisante pour déformer l'ensemble de la plaque Indienne. D'autres moteurs sont proposés (voir la thèse de *M. Delescluse, 2008*). Des études cinématiques (*Mercuriev et DeMets*, 2005) basées sur les anomalies magnétiques formées par la dorsale de Carlsberg (entre 20 Ma et l'Actuel) montrent que la décélération des taux d'accrétion enregistrée depuis 20 Ma s'arrête autour de 10 Ma. A partir de cette date, les taux d'accrétion sont constants (Figure 1).

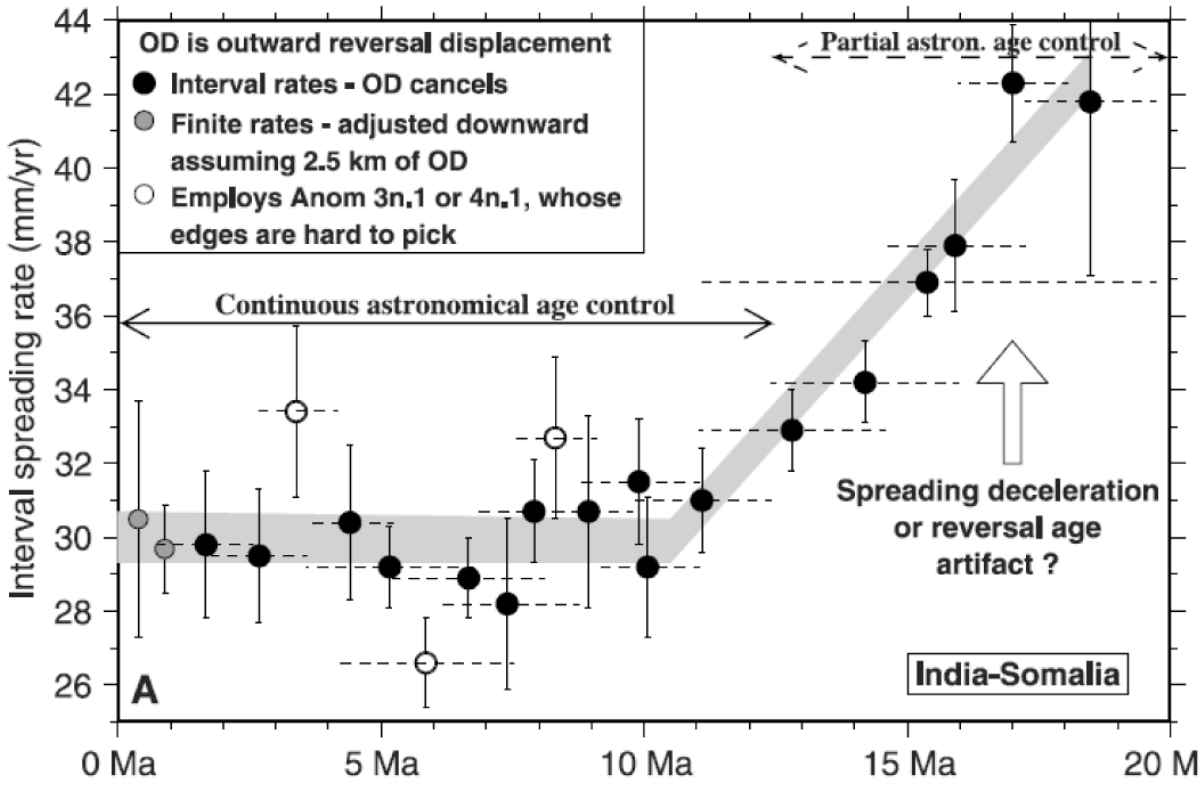


*Figure 1 : Evolution des taux d'ouverture au niveau de la dorsale de Carlsberg au cours des 20 derniers Ma (Mercuriev et DeMets, 2005).La décélération des taux d'ouverture s'arrête vers 10 Ma, de façon contemporaine avec la mise en place de la déformation intra-plaque dans l'Océan Central Indien. Il est possible que la limite de plaque Inde-Arabie ait réagi à ce changement cinématique, entraînant le soulèvement de la Ride d'Owen*

Cet épisode de déformation semble s'être répercuté sur la plaque Arabie au niveau des interfaces rhéologiques (limite de plaque Inde-Arabie, Marge Omanaise, transformantes du Golfe d'Aden) , qui ont favorisé un effet flexural de la lithosphère. Le comportement flexural de la lithosphère permet de former des reliefs importants (plusieurs centaines de mètres) en absence de contraintes importantes. Le soulèvement de la Ride ne s'est certainement pas fait de façon abrupte à 8.5 Ma, et a probablement commencé à 11 Ma au moment de l'initiation du changement cinématique supposé à son origine. Cependant, du fait de dépôts essentiellement pélagiques sur la ride à ce moment là, il est difficile de fournir des observations permettant de contraindre précisément le début de la croissance de ce relief. Une discordance angulaire légèrement exprimée est datée à 10.4 Ma sur la ride d'Owen, et pourrait correspondre au début du soulèvement (Figure 2). A partir de données de sismique réflexion, Matthias Delescluse a démontré dans sa thèse que la croissance des reliefs dans la zone de déformation diffuse de l'Océan Central Indien s'est faîte en deux temps (Figure 3) : une première étape de déformation autour de 9 Ma, marquée par une première discordance, aurait donné naissance à des reliefs relativement modestes (quelques centaines de mètres); une deuxième étape, autour de 8 Ma, marque la brusque croissance de ces reliefs (avec une discordance angulaire beaucoup plus marquée), qui atteignent des altitudes de l'ordre du millier de mètres. Il est possible que la première étape de croissance des reliefs mise en évidence par *Delescluse (2008)* dans l'océan Indien Central n'ait pas été bien enregistrée au niveau du Bassin d'Owen, ou alors qu'il y ait un diachronisme spatial de la déformation.

L'âge du soulèvement de la Ride d'Owen est ré-évalué à 8-9 Ma au lieu de 20 Ma. Ceci a une importance sur la compréhension de l'histoire de la mousson asiatique au Miocène. Les forages réalisés sur la Ride d'Owen ont permis dans les années 90 l'identification d'un brusque épisode d'augmentation des abondances des faunes de *G. Bulloïdes*, interprété comme un épisode d'intensification de la mousson à 8.5 Ma. Cet épisode n'est pas expliqué par l'évolution des paramètres astronomiques de Milankovitch et sa réalité a été récemment mise en cause (*Huang et al., 2007*). Il a longtemps été supposé à l'origine de l'épisode de croissance fini-Miocène de l'Himalaya (alimentant un débat passionnant sur les interactions reliefs-climats), et d'un changement paléo-environnemental majeur au niveau du Pakistan et des alentours. Ce dernier a certainement contrôlé l'évolution et les migrations des faunes et flores du Miocène terminal dans la région.

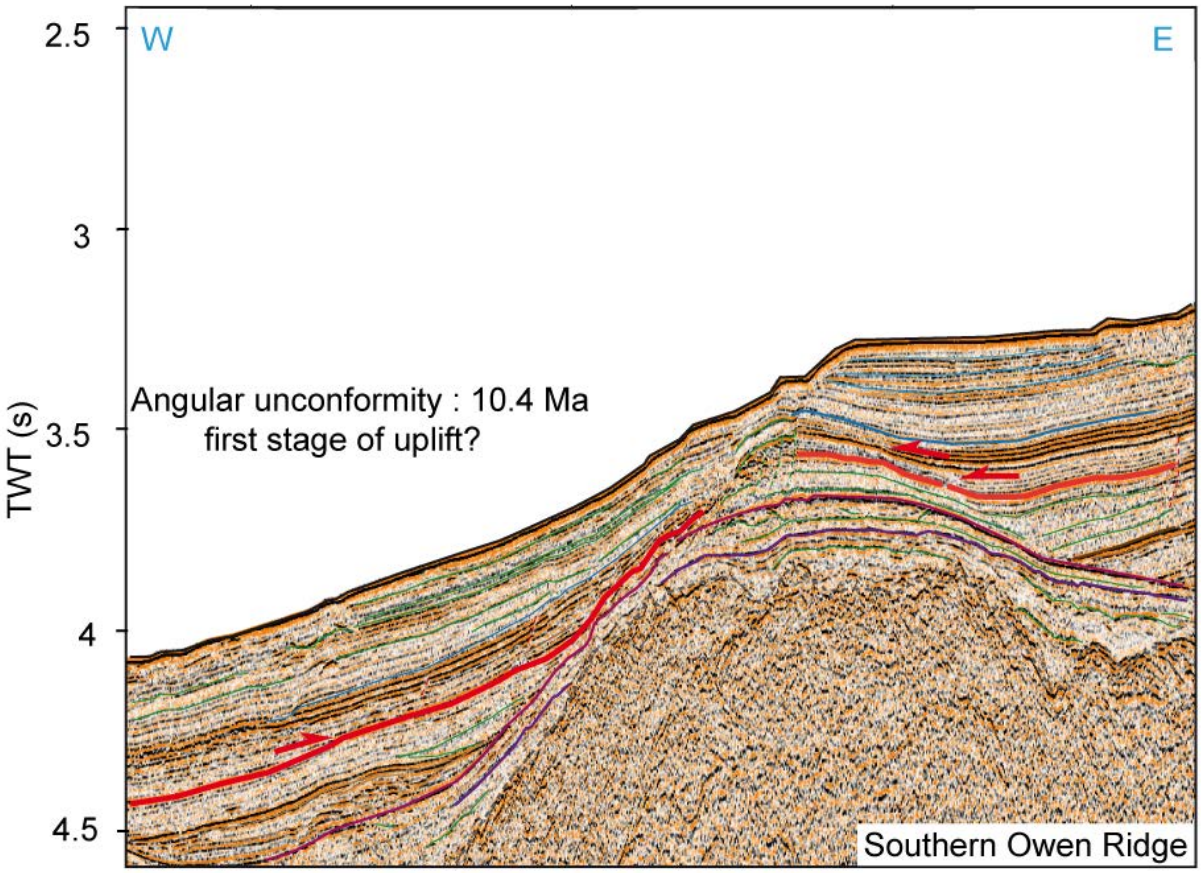


*Figure 2 : profil sismique recoupant le segment sud de la Ride d'Owen. Une discordance angulaire observée à 10.4 Ma (en rouge vif sur le profil) pourrait correspondre au début du soulèvement de la ride. La topographie de l'ordre de 2000 m semble cependant avoir été créée plus tard entre 8 et 9 Ma.*

La ré-évaluation de l'âge du soulèvement de la Ride d'Owen résout les contradictions précédemment discutées. Il semblerait que la brusque augmentation de *G. bulloides* à 8.5 Ma marque simplement de meilleures conditions de préservation de ces microfossiles associées à la surrection de la ride. Un soulèvement rapide de la Ride d'Owen de plus de 2000 m implique que la tranche d'eau traversée par les microfossiles avant leur dépôt est plus faible. Les microfossiles subissent moins longtemps la dissolution par les eaux acides (riches en $CO_2$) des océans avant leur dépôt. Ceci est en accord avec les études géochimiques de *Huang et al. (2007)* qui suggèrent que le pic de *G. bulloides* autour de 8.5 Ma observé par *Kroon et al (1991)* correspond en fait à un changement des conditions de dissolution des foraminifères, et non à un bloom planctonique a cet époque. Ainsi, l'augmentation des abondances de *G. bulloides* ne date pas un changement climatique mais le changement cinématique à l'origine

des reliefs et de la Ride d'Owen, et des reliefs de l'océan Indien Central. Les changements topographiques engendrés au niveau des côtes de la mer d'Arabie par cet épisode de déformation pourrait expliquer le changement environnemental observé au niveau du Pakistan. Les implications potentielles de cette phase de déformation sur l'évolution structurale de la limite de plaque Inde-Arabie et sur la réorganisation de la circulation océanique profonde sont discutées en fin de chapitre. Concernant l'interaction entre la mousson et la croissance de l'Himalaya, il se pourrait donc que ce soit l'intensification de la mousson dès 15 Ma qui ait accentué la croissance des reliefs, mais ceci reste à démontrer.

*Figure 3 : Profils sismiques recoupant la zone de déformation diffuse de l'Océan Central Indien (extraits de Delescluse (2008)). Des discordances angulaires marquent deux épisodes de surrection des reliefs (en vert : ~9 Ma; en rouge : ~8 Ma).Le profil du haut montre les structures actuelles. Les deux autres profils ont été corrigés de la déformation à l'origine des discordances angulaires.*

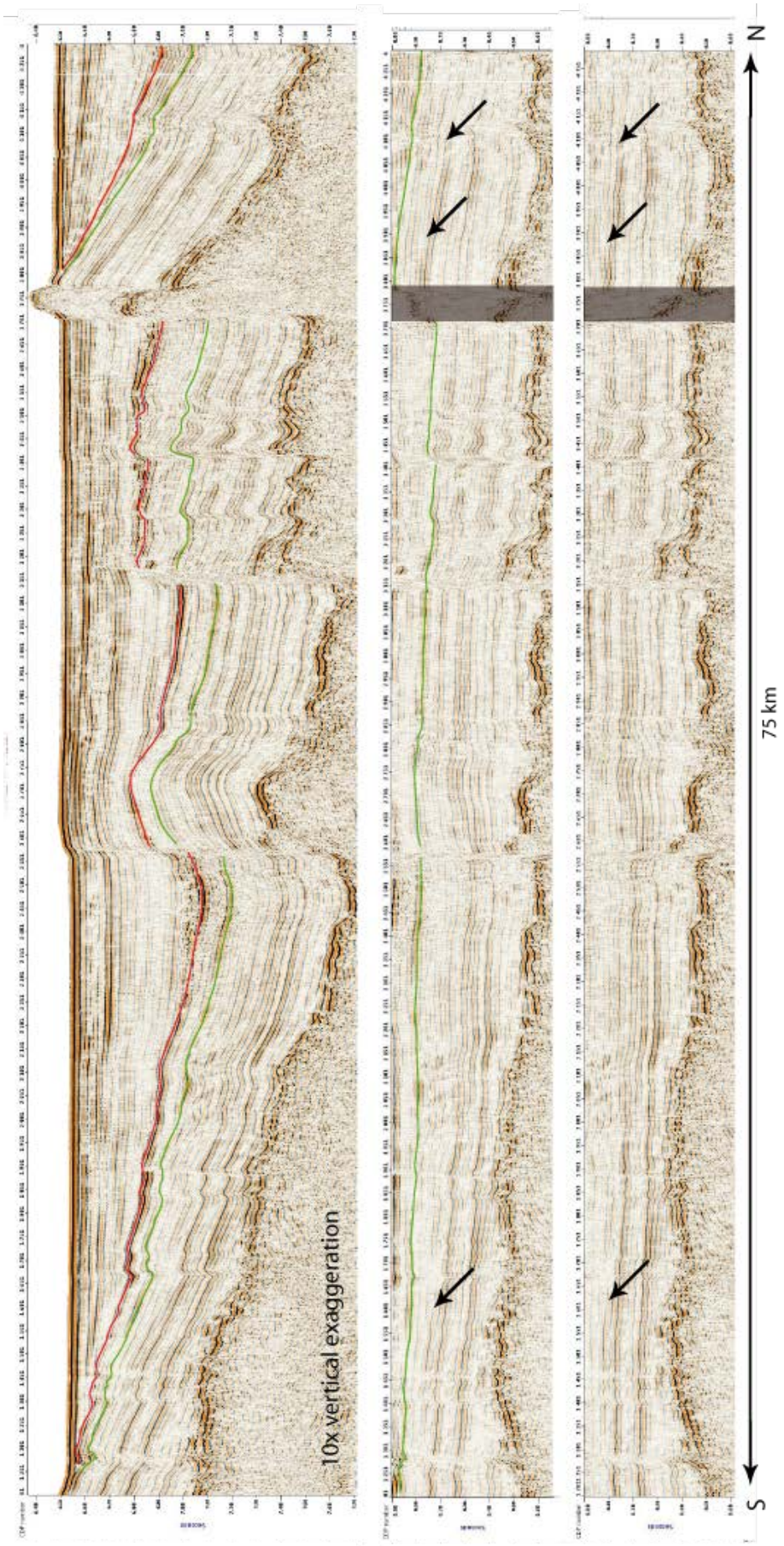
10x vertical exaggeration
N
S
75 km

**The Owen Ridge uplift in the Arabian Sea: implications on the sedimentary record of Indian monsoon in Late Miocene**

Mathieu Rodriguez[1*], Nicolas Chamot-Rooke[1], Philippe Huchon[2,3], Marc Fournier[2,3], Matthias Delescluse[1]

(1) Laboratoire de Géologie de l'Ecole normale supérieure de Paris; CNRS UMR 8538, 24 rue Lhomond, 75005 Paris, France

(2) Institut des Sciences de la Terre de Paris, CNRS UMR 7193, Université Pierre & Marie Curie, case 129, 4 place Jussieu, 75005 Paris, France

(3) iSTeP, UMR 7193, CNRS, F-75005 Paris, France

*Corresponding author: rodriguez@geologie.ens.fr

*in prep. forEPSL*

**Abstract**

**The Indian monsoon may have influenced continental erosion, relief uplift and the environment over the Arabian Sea. Most paleoclimatic reconstitutions based on deep-sea drillings collected on the Owen Ridge in the Arabian Sea document an increase in *G. bulloides* abundance interpreted as the result of an intensification of the Indian Monsoon at ~8.5 Ma. Such a climatic change cannot be explained by astronomic parameters alone, leading some authors to consider it might be an artifact of the marine sediments record. We use recently acquired seismic reflection data to document Late Miocene deformation at the India-Arabia plate boundary and along the Oman margin. The age of the main uplift of the Owen Ridge is assessed at ~8.5 Ma, which contrasts with the age of ~15-20 Ma previously inferred. The rise of the Owen Ridge at ~8.5 Ma accounts for the better preservation of *G. bulloides* population. This Late Miocene episode of deformation is also recognized along the Dhofar and the East Oman margins, where it favored the deposition of contourite drifts. It relates in time with reliefs rise at the Makran accretionary wedge and along the India-Eurasia boundary, which could have lead to a reorganization of the atmospheric circulation at the origin of the coeval environmental change recorded in the Siwalik sequence in Pakistan. This Late Miocene regional episode of deformation is coeval with the formation of reliefs related to intra-plate deformation in the Central Indian Ocean, triggered by the Late Miocene growth of the Himalayas.**

## 1. Introduction

The Arabian Sea is located on the path of the migration of the Inter Tropical Convergence Zone, which drives the seasonality of the Asian monsoon. The Owen Ridge, the Qalhat Seamount, and the Murray Ridge (hereafter referred as the Owen-Murray ridge system) consist in a series of prominent oceanic highs dividing the Arabian Sea (Fig. 1). Today, the Owen-Murray ridge system acts as a

barrier for bottom waters circulation between the Arabian Sea and the Owen Basin, thus controlling the upwelling zone off the Sultanate of Oman. The pelagic cover of the Owen-Murray ridge system has been intensively studied (Shipboard Scientific Party, 1974, 1989) in order to understand the monsoon evolution during the Cenozoic. Marine sediments drilled on the flank of the southern Owen Ridge document an increase at ~8.5 Ma in the abundance of *Globigerina bulloides* (Kroon et al., 1991), a planktonic foraminifera commonly used as a proxy for monsoon-driven upwelling. The latter observation leads Kroon et al. (1991) to consider a ~8.5 Ma monsoon intensification event as the origin of a coeval environmental change recorded in the Siwalik paleosol sequence in Pakistan, India, and Nepal (Quade et al., 1989). This environmental change is characterized by a shift from $C_3$ to $C_4$ vegetation and the associated change in mammal faunas (Quade et al., 1989; Cerling et al., 1997; Molnar, 2005). However, an intensification of the monsoon at ~8.5 Ma cannot be explained by the evolution of astronomic parameters alone (Molnar et al., 1993; Molnar, 2005; Wang et al., 2005), suggesting the action of an internal forcing over the climatic system.

Based upon their apparent synchronicity, it has been assumed in the early 90's that the rise of the Himalayan-Tibetan Plateau estimated at ~8 Ma at that time (Harrison et al., 1992) was at the origin of the monsoon intensification through a reorganisation of the atmospheric circulation (Ann et al., 2001).

Conversely, the Late Miocene intensification of the Indian monsoon might have influenced continental erosion, and relief uplift through isostatic compensation (Molnar et al., 1993), highlighting retroaction processes between relief building and climate evolution (Molnar and England, 1990; Molnar, 2005). Subsequent works challenged this hypothesis, and reveal that most of the areas of the Himalayan-Tibetan Plateau successively reached their maximal elevations several millions years before the ~8.5 Ma monsoon intensification (Molnar, 2005; Dupont-Nivet et al., 2008; Wang et al., 2012), thus ruling out the uplift as a potential forcing factor of the ~8.5 Ma monsoon intensification.

A recent analysis of marine sediments drilled at the Owen Ridge has questioned the reality of the monsoon intensification at ~8.5 Ma (Huang et al., 2007). To make abstraction of the effect of variations in carbonate dissolution in the record of Foraminifera abundances, Huang et al. (2007) selected Foraminifera of large size and document only a minor change in the fraction of *G. bulloides* near 10 Ma. Moreover, their study of sea surface temperature evolution based on the $U^{K'}_{37}$alkenone index does not show the decrease expected for the emplacement of a monsoon-driven upwelling off Oman between 10 and 5 Ma. The latter is consistent with the absence of any Late Miocene change in sedimentation rates in the Indus fan (Clift et al., 2001; 2003; 2008; Clift and Gaedicke, 2002; Clift, 2002). Consequently, the origin of the environmental change recorded in the Siwalik sequence remains unknown (Molnar et al., 2010).

The timing of oceanic reliefs rise in the Indian Ocean is critical to the understanding of the sedimentary record of climate evolution over the Cenozoic. The commonly accepted tectonic framework of the Arabian Sea is that the uplift of the Owen-Murray ridge system was coeval with the beginning of accretion at the Sheba Ridge in the Gulf of Aden 15-20 Ma ago (Fig. 1) (Whitmarsh,

1979) and, possibly, with a structural reorganisation of the India-Arabia plate-boundary (Mountain and Prell, 1990). Here we present evidences of a Late Miocene tectonic uplift in the Owen Basin throughout the analysis of a new seismic reflection dataset. The main objective of this study is to highlight the tectonic processes at the origin of this uplift, and to discuss their impact on the record of climatic and deep-sea circulation changes in the Owen Basin sediments, leading to a new hypothesis for the origin of the Late Miocene environmental change observed in Pakistan.

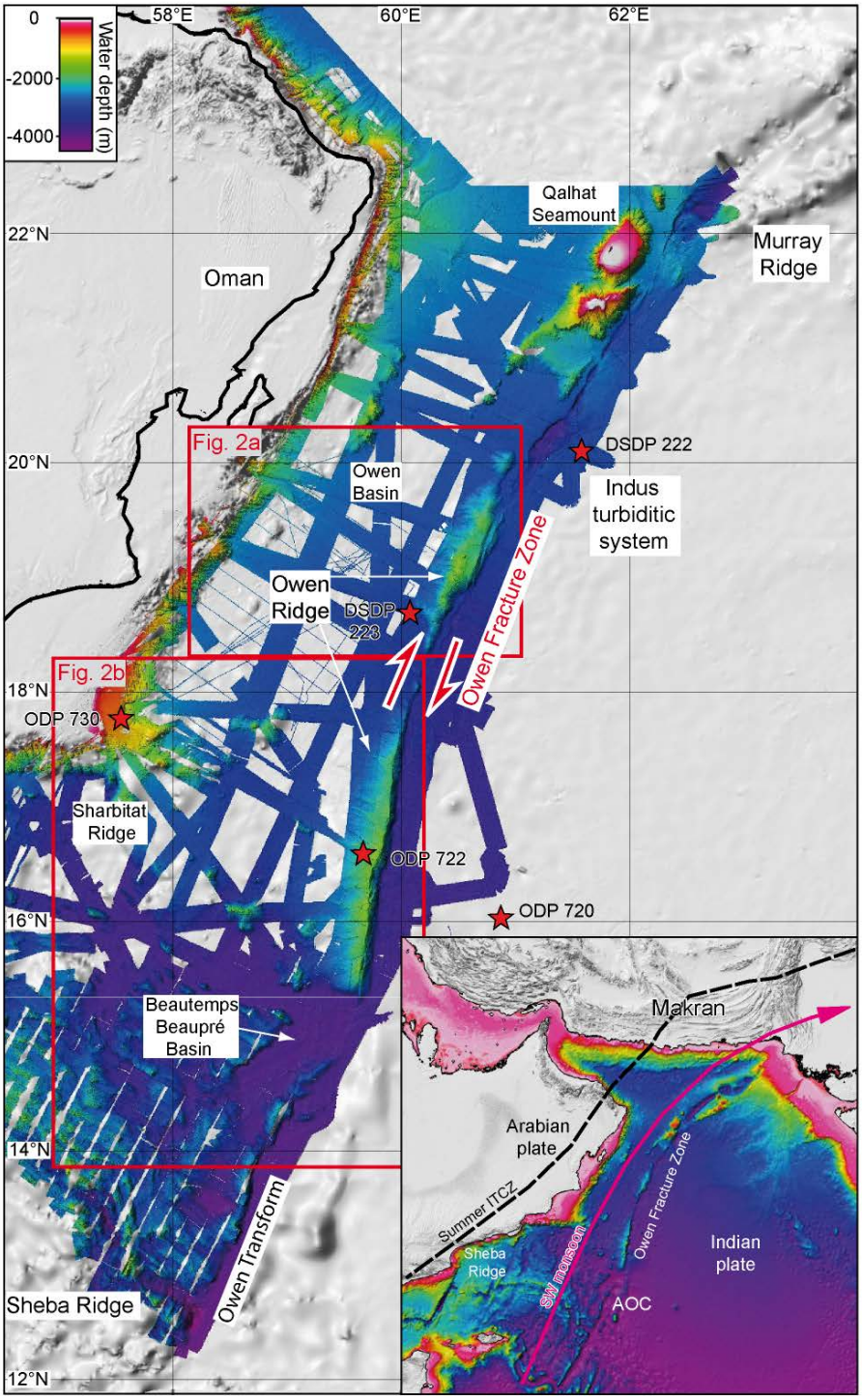

***Figure 1*** *: Bathymetric map of the Arabian Sea, with location of ODP and DSDP drilling sites. The multibeam bathymetric coverage is draped over SRTM 30" topography. Inset shows the regional tectonic setting of the India-Arabia plate boundary, and the position of the summer Inter-Tropical Convergence Zone (ITCZ). AOC : Aden-Owen-Carlsberg triple junction.*

## 2. Geological framework of the Arabian Sea and the Owen-Murray Ridge

### 2.1. *Present-day morphology of the Arabian Sea*

The Owen-Murray Ridge system runs along the present-day India-Arabia plate boundary, which is an 800-km-long strike-slip fault system known as the Owen Fracture Zone (OFZ hereafter) (Fig. 1). Morphological offsets of the Owen Ridge revealed by multibeam mapping document a dextral displacement of 10 to 12 km along the OFZ (Fig. 2). Extrapolating the present-day relative motion of 3 ±1 mm $yr^{-1}$ to the recent past would indicate that the modern morphological trace of the OFZ and the related structures formed during the last 3 to 6 Ma (Fournier et al., 2008; Fournier et al., 2011; Rodriguez et al., 2011).

The southern Owen Ridge is a 300 km-long, 50-km wide, up to 2000 m-high relief that appears as a large-scale tilted and relatively flat slab (Fig. 2b). It contrasts with the uneven topography of the 220 km-long, 50 km-wide, and up to 1700 m-high central ridge (Fig. 2a). The Qalhat seamount is a 210 km-long, more than 55 km-wide, and up to 2700 m-high relief, with a flat-top typical of a guyot morphology (Fig. 1). At the northern end of the OFZ, the Murray Ridge is divided in two 200-km and 150-km-long segments, reaching elevations up to 2000 m with respect to the surrounding seafloor.

### 2.2. *Substratum of the Owen-Murray ridge system*

Several seismic lines run as pre-site surveys for DSDP and ODP reached the basement of the southern and the central ridges. They show an uneven substratum subsequently buried by Indus turbidites. The substratum, drilled at DSDP sites 223 and 224 (Fig. 2), is basaltic in composition and of Late Paleocene age (Shipboard Scientific Party, 1974; 1989). These 50-55 Ma-old reliefs might either be tilted slivers of oceanic crust or volcanic highs (Fig. 3b), and are hereafter referred as the "pre-Owen Ridge". Both the southern and the central ridges may have stand as positive basement features being progressively buried under turbiditic deposits from the Indus fan, as suggested by the Oligocene and Early to Middle Miocene turbiditic deposits drilled at site DSDP 224 between two basement highs on the southern ridge (Fig. 2) (Shipboard Scientific Party, 1989; Clift et al., 2001). The progressive burial of the pre-Owen Ridge is marked by a diachronous angular unconformity, biostratigraphically dated at 19.6 Ma and ~14 Ma at the southern (Fig. 3b) and central (Fig. 3c) Owen Ridge, respectively (Shipboard Scientific Party, 1974). The history of the Murray Ridge is not clearly established, as none of these reliefs have been drilled down to their basement. Based upon seismic refraction data, the Murray Ridge has been interpreted as a small piece of continental crust inherited from Gondwana break-up (Edwards et al., 2008).

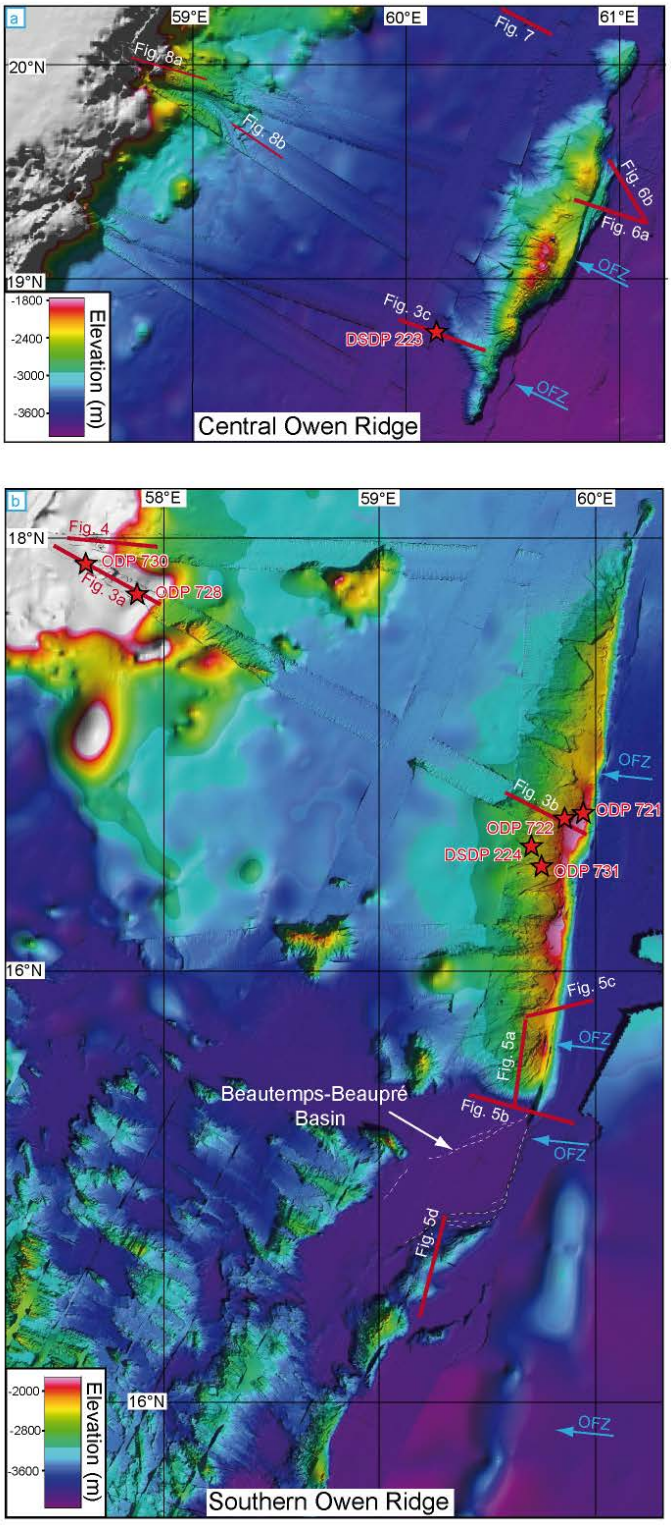


***Figure 2*** *: Bathymetric maps of the central (a) and southern (b) portions of the Owen Basin, and location of the seismic lines. See Fig. 1 for location. The bathymetry shows the offset of the Owen Ridge by the Owen Fracture Zone (OFZ). DSDP and ODP sites are shown by red stars. Supp. a and b : location of seismic profiles provided in supplementary material.*

2.3. *Uplift of the Owen Ridge*

In its present-day configuration, the Owen Ridge is formed at its top by early miocene turbidites coming from the Indus deep-sea fan and the subsequent pelagic cover (Fig. 3b) (Shipboard Scientific Party, 1974; 1989). This indicates that the present-day Owen Ridge is the result of an uplift episode, rejuvenating the topography related to the pre-Owen Ridge and the Indus fan.

The uplift of the Owen Ridge was first related to the angular unconformity between the oligocene pelagic cover of the pre-Owen Ridge and lower miocene turbidites (Whitmarsh et al., 1974; 1979), but the latter simply marks the progressive burial of the pre-Owen Ridge under Indus turbidites.

Conversely, the transition from Indus turbidites to pelagic deposits drilled at DSDP site 224 and ODP sites 721, 722, 731 (top of Unit 4, Fig. 3) has been considered as an indicator of the uplift of the Southern Owen Ridge. The transition is marked by a mixed pelagic-turbiditic sequence, composed of thin detrital particles, interpreted as the uppermost part of the turbiditic plume being deposited during the first stages of ridge uplift. The first pelagic sediment overlying this transitional unit is biostratigraphically dated at 14-15 Ma, and is supposed to mark the time at which the ridge was uplifted above the level of turbiditic deposition (Mountain and Prell, 1990). Following the identification of the anomaly 5 (11 Ma) in the Gulf of Aden (Cochran, 1981), the uplift of the Owen Ridge has been correlated with the beginning of oceanic accretion at the Sheba Ridge. By extrapolation of these results, the main uplift of the Murray Ridge and the first stage of formation of the Dalrymple Trough have also been assessed to an early miocene age (Edwards et al., 2000; Gaedicke et al., 2002). However, recent works show that seafloor spreading started 19.7 Ma ago at the Sheba Ridge (Fournier et al., 2010), leading to a 5-Ma stratigraphic misfit with the inferred 14-15 Ma age of uplift of the Owen Ridge.

2.4. *Tectonics of the India-Arabia plate-boundary*

Past locations of the India-Arabia plate boundary prior to the present-day OFZ are currently unknown. First paleogeographic reconstitutions by Whitmarsh (1979) suggests that the India-Arabia plate boundary was already at its present-day location when India started to move northwards at ~90 Ma. A second paleogeographic reconstitution postulates that the India-Arabia plate-boundary initially laid along the Oman margin, while the Mascarene Basin opened and the Carlsberg Ridge developed (Mountain and Prell, 1990). The India-Arabia plate-boundary then jumped to its present-day position in the early Miocene, when seafloor spreading started at the Sheba Ridge (Mountain and Prell, 1990). In the latter framework, this inferred jump of the India-Arabia plate-boundary marks the inactivation of strike-slip motion along the Oman margin and the uplift of the Owen-Murray Ridge ~20 Ma ago is supposed to mark a migration of the India-Arabia plate-boundary. A Paleogene location of the India-Arabia plate-boundary in the Owen Basin is also supported by paleo-geographic reconstitutions based upon the record of magnetic anomalies over the Arabian Sea (Royer et al., 2002).

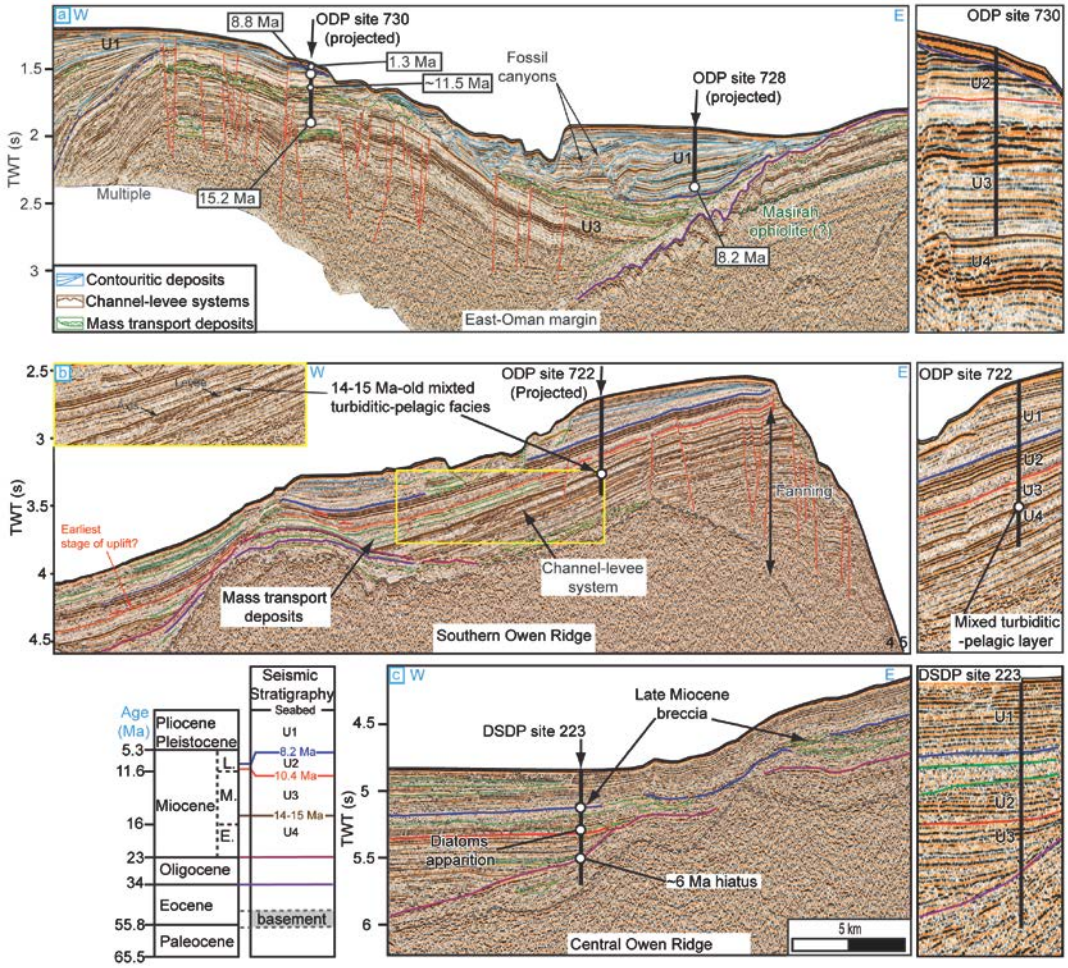


***Figure 3*** *: Seismic profiles crossing a) the Oman continental margin, b) the Southern Owen Ridge, c) the Central Owen Ridge (see Fig. 2 for location). Insets show close-views of the seismic profiles in the area of deep-sea drilling (ODP and DSDP) locations. The stratigraphic framework is summarized on the lower left hand corner. Profile a) displays a major anticline structure affecting chalk-rich turbiditic deposits that is overlapped by a 8 Ma-old contouritic drift, composed of pelagic ooze with inserted MTDs. Older events, including an upper-Eocene unconformity, and the obduction of Masirah Ophiolites, are not discussed in this study. Profile b) shows a W-E seismic profile crossing the Southern Owen Ridge at the location of ODP site 722. The basement, drilled at site DSDP 224, consists of 50-55 Ma-old basaltic lamprophyres. A major unconformity is observed on the western side of the ridge, where Early Miocene turbiditic deposits (Unit 4) onlap Oligocene deposits drilled at DSDP site 224. Unit 3 corresponds to a pelagic layer and ends at 10.4 Ma. The overlying Unit 2 is composed of radiolarian rich pelagic chalk and ends at 8.2 Ma. Unit 1 is composed of pelagic ooze and chalk, and dissected by landslide failures. c) shows an W-E seismic profile crossing the Central Owen Ridge. A major unconformity, corresponding to a hiatus of 6 Myr, has been drilled at DSDP site 223, together with Late Miocene mass transport deposits. The overlying cover is mainly composed of pelagic chalk and ooze, with a detrital component in the Owen Basin. Late Miocene breccias, correlated with an unconformity on the central ridge, have been drilled at site 223.*

## 3. Materials and Methods

The dataset presented in this study was acquired onboard the French Navy oceanographic vessel *Beautemps-Beaupré* during the Owen (2009 and 2012) surveys. Multibeam bathymetry was collected using a Kongsberg-Simrad EM 120. Areas not surveyed are filled-in by the SRTM 30" bathymetry. Seismic reflection profiles were acquired using two GI air-guns and a 24-channels, 600 m-long streamer. The common mid-point (CDP) spacing was 6.25 m. The high speed acquisition has a limited subsurface penetration of ~2s TWT. The processing consisted in geometry setting, water-velocity normal move-out, stacking, water-velocity F-K domain post-stack time migration, bandpass filtering and automatic gain control (AGC). All the profiles are displayed with a vertical exaggeration of 8 at the seafloor. The seismic dataset is calibrated to the DSDP and ODP drillings available in the Arabian Sea (Shipboard Scientific Party, 1974; 1989) to provide the stratigraphic framework (Fig. 3, inset). The reflectors picked on seismic profiles have been selected upon the base of seismic discontinuities that either reflect lithological changes, stratigraphic hiatuses or tectonic deformation.

## 4. Results

### 4.1. *Late Miocene deformation on the East-Oman margin*

Seismic profiles crossing the edge of the continental platform reveal a large, ~20-km-wide anticline affecting lower to upper miocene sediments according to calibration with the nearby ODP sites (units U2 and U3, Fig. 3a and 4) (Shipboard Scientific Party, 1989). A dense network of faults affects the anticline and is sealed by upper miocene to plio-pleistocene contouritic deposits (unit U1, Fig. 3a and 4). The offset of sedimentary layers at individual faults does not increase significantly with depth. This pattern of deformation does not indicate long-lived structures, but rather faults formed synchronously with the anticline (Fig. 3a). The folded unit is composed of transparent to high amplitude concordant horizons, which correspond to calcareous turbidites according to ODP site 730. The folded unit contains planctonic faunas typical of a deep-sea environment (Shipboard Scientific Party, 1989). An erosive surface sealing the top of the anticline is observed on seismic profiles (Fig. 3a and 4) and drilled at ODP site 730, indicating local emersion of the platform after the folding episode. At the location of the ODP site 730, the fold then subsided down the sea-level in early Pleistocene times, as indicated by the age of the first overlying sediments (1.3 Ma). Thick chaotic bodies interpreted as Mass Transport Deposits (MTD hereafter) on Fig. 3a and 4 are observed down the eastern flank of the fold, which may also indicate sudden slope over-steepening related to the formation of the fold. The youngest calcareous turbidites affected by the deformation are ~8.8 Ma old according to correlations with ODP site 730. The fold is overlaid by ~8.2 Ma-old undeformed sediments according to ODP site 728 (Shipboard Scientific Party, 1989). This set of evidences documents a major uplift episode along the Oman margin around 8.5 Ma.

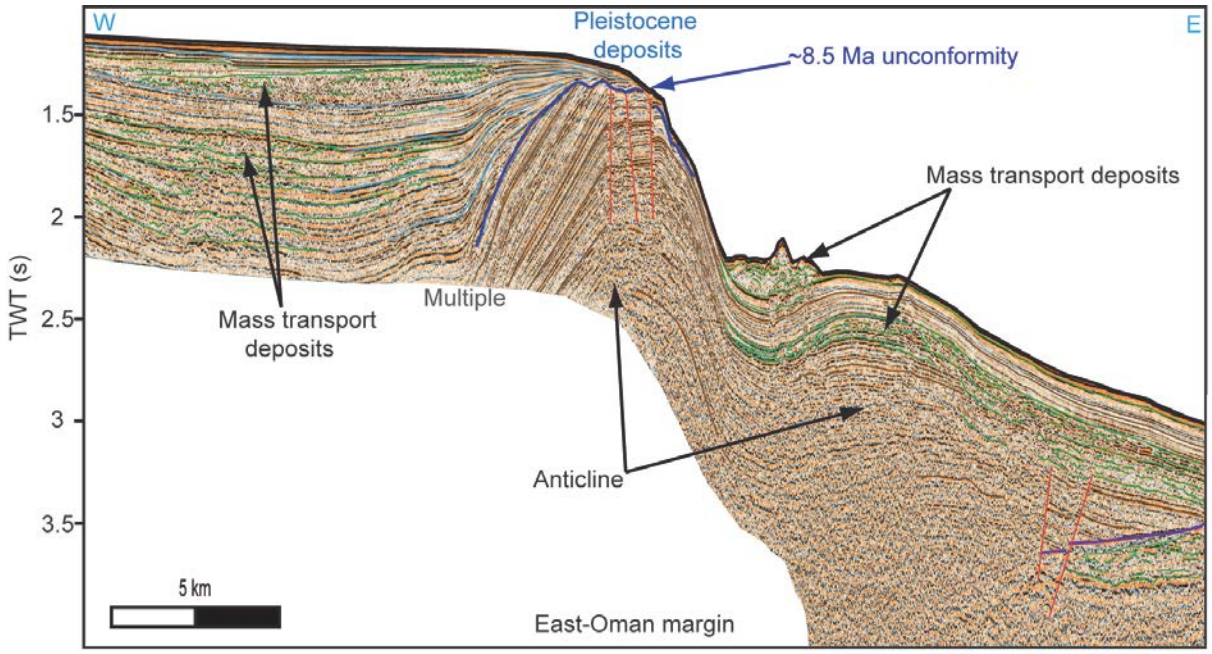


***Figure 4*** *: Seismic profile crossing the Oman margin, showing a major anticline affecting Miocene sediments. See fig. 2 for location. See fig. 3 for stratigraphic legend.*

4. 2. *Late Miocene deformation at the Southern Owen Ridge*

An E-W seismic line was acquired close to site ODP 722 on the Southern Owen Ridge, where the most complete sequence has been drilled (Fig. 3b). Ages of reflectors and the lithology of sedimentary units are established by correlation with ODP site 722. The sedimentary sequence at the top of the Owen Ridge is faulted throughout its entire thickness up to Unit 2, i.e. 8.2 Ma (Fig. 3b and 5a). It is unclear whether offsets of the uppermost layers of Unit 2 are the result of faulting or the result of pelagic deposits covering the fault scarps, suggesting the deformation could have stopped shortly before 8.2 Ma. Similarly to what is observed on the Oman margin, the offset of sedimentary layers at individual fault does not increase significantly with depth, indicating a short-lived deformation event (Fig. 3b and 5a). A fanning configuration characterizes the lower miocene turbidites on top of the Owen Ridge (Fig. 3b). The seismic profile crossing ODP site 722 (Fig. 3b) shows that the 14-15 Ma-old turbiditic-pelagic facies has been drilled on the levee of a fossil channel-levee system. The channel axis, ~40-m-deep, is identified by a typical lens-like architecture and discontinuous, high-amplitude reflections. The associated levees display a characteristic wedge shape with high-amplitude, transparent seismic facies (Fig. 3b).

The sedimentary cover overlying the last turbiditic channel (units U3 to U1) is composed of pelagic deposits (Fig. 3, 5). The pelagic Unit 3 displays slight lateral thicknesses variations (<0.1 s TWT), which results from MTDs coming from the pre-existing Owen Ridge that has still stood above the seafloor before the uplift (see supplementary material Fig. a, b). The transition between Unit 3 and 2 is marked by an increase of the sedimentation rates (from 15 to 54 $m.Ma^{-1}$) (Shipboard Scientific Party, 1989).The Unit 2 is marked by the apparition of submarine failures at ~8.5Ma according to the nearby

ODP sites 721 and 731 (Fig. 2, 3, 5). The age of ~8.5 Ma corresponds to the age of the Foraminifera (*Discoaster hamatus*) immediately overlying the sedimentary hiatus (formed by the submarine failure) drilled at site 721, but submarine failures could have removed older pelagic sediments depending on the depth of the failure plane. The configuration of submarine failures observed in the uppermost part of the pelagic section clearly shows that the sediment were failed and transported in direction of the Owen Basin. Thus, the southern segment of the Owen Ridge was already uplifted at 8.5 Ma.

Several folds are observed at the eastern foot of the southern Owen Ridge, and south of the Beautemps-Beaupré Basin (Fig. 5). The seismic profile in Fig. 5b clearly shows the sedimentary layers composing the Owen Ridge as a folded structure composed of Indus turbidites. A sharp and vertical fault plane, interpreted as a fossil fracture zone, crosscuts the eastern side of the Owen Ridge at depth (Fig. 5b, 5c). As revealed by the growth anticline displayed in Fig. 5c, the OFZ is still undergoing deformation at the edge of the Southern Owen Ridge (Rodriguez et al., 2011). Such a deformation is not recorded by the pelagic sediments on the top of the ridge (U1) (Fig. 3, 5).

The series of folds deforming Indus deposits observed south of the Beautemps-Beaupré Basin (Fig. 5d) display an isopach pattern at depth. The overlying deposits show angular unconformities indicating several discontinuities in episodes of folding. Unfortunately, the penetration of the nearby ODP site 720 (location on Fig. 1) is too shallow to provide a confident dating of the initiation of this compressive episode. These folds could correspond either to the Owen Ridge uplift or to the emplacement of the OFZ.

***Figure 5** : Seismic profiles crossing the Southern Owen Ridge. Profile a) shows a N-S section that displays the Late Miocene faults affecting the pelagic cover. Profile b) shows a transverse section of the southernmost extremity of the southern ridge. It shows that the ridge is formed by folded Indus sediments, crosscut to the east by an inactive vertical fault, interpreted as a fossil transform fault possibly corresponding to the India-Arabia plate boundary. The present-day OFZ is evidenced on the western side of the ridge, where it is associated with the Beautemps-Beaupré basin. Profile c) shows a fossil transform at the eastern foot of the southern ridge, and compressive deformation in the overlying sediments. Profile d) shows a series of folds located south of the Beautemps-Beaupré Basin. See Fig. 2 for location and Fig. 3 for stratigraphic legend.*

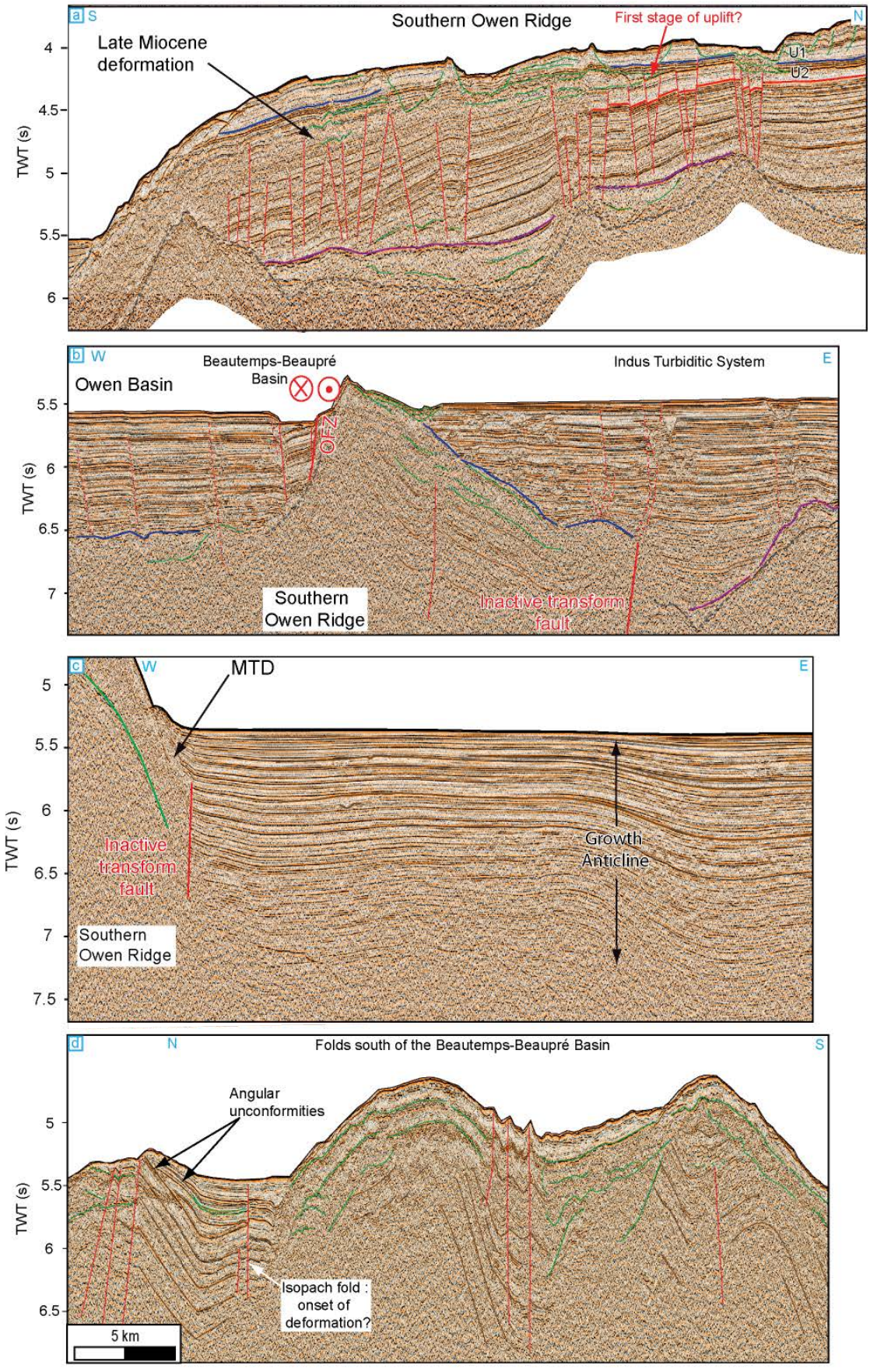
a S
Southern Owen Ridge
First stage of uplift?
N
Late Miocene deformation
U1
U2
TWT (s)
4
4.5
5
5.5
6
b W
Beautemps-Beaupré Basin
Indus Turbiditic System
E
Owen Basin
OFZ
TWT (s)
5.5
6
6.5
7
Southern Owen Ridge
Inactive transform fault
c
W
MTD
E
TWT (s)
5
5.5
6
6.5
7
7.5
Inactive transform fault
Growth Anticline
Southern Owen Ridge
d
N
Folds south of the Beautemps-Beaupré Basin
S
Angular unconformities
TWT (s)
5
5.5
6
6.5
Isopach fold : onset of deformation?
5 km

4.3. *Late Miocene deformation at the Central Owen Ridge and mass transport deposits*

Seismic profiles crossing the eastern side of the Central Owen Ridge reveal an angular unconformity (in blue in Fig. 6) within the Indus deep-sea fan. The angular unconformity becomes laterally concordant with the overlying sediments from the Indus fan. This key reflector is about 1 s TWT deep in the undeformed area, which corresponds to a Late Miocene age according to the nearby DSDP site 222. Similarly to what is observed at the southern ridge, an inactive vertical fault, interpreted as a fracture zone, is identified at the eastern edge of the ridge (Fig. 6a). These observations suggest that the present-day topography of the Central Owen Ridge is the result of a Late Miocene phase of deformation.

The site DSDP 223 is located west of the central segment of the Owen Ridge, where the early miocene unconformity was first evidenced (Shipboard Scientific Party, 1974; Whitmarsh, 1979). A second, more recent unconformity is observed both at the top of the central Owen Ridge and in the Owen Basin, where it is underlined by MTDs composed of upper miocene sediments (Fig. 3c) overlying diatoms-rich sediments dated at 10 Ma (Shipboard Scientific Party, 1974). The reflector corresponding to the top of the MTDs is correlated with sediments at the top of the Owen Ridge. The thickness of the overlying pelagic layer is 0.3 s (TWT) at the top of the central ridge, where it is devoid of MTDs. The thickness of 0.3 s (TWT) is the same as the Unit 1 on the Southern Owen Ridge in areas undisturbed by submarine failures (Fig. 3). Assuming pelagic sedimentation rates similar to the one estimated at the southern ridge (Bourget et al., 2013) implies a Late Miocene age of the unconformity (~8 Ma), consistently with the MTDs drilled downslope at DSDP site 223. A similar unconformity sealed by 0.3s (TWT) of pelagic sediments is observed at the top of most of the reliefs buried by the Indus fan and sediments from the Oman margin in the Owen Basin (see supplementary material fig. c). This suggests a regional phenomenon at the origin of this ~8 Ma-old unconformity.

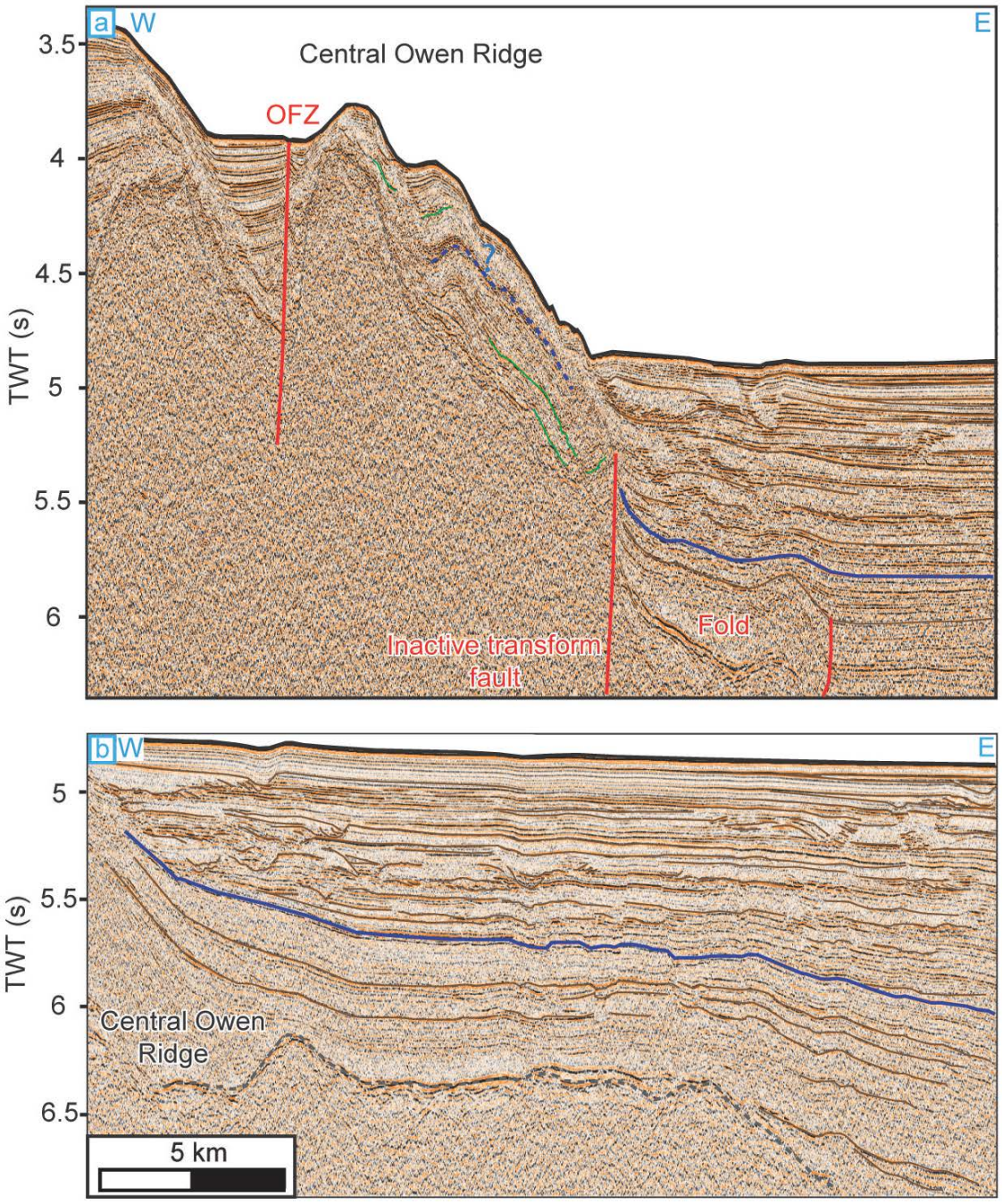


***Figure 6*** *: Seismic profiles crossing the eastern side of the Central Owen Ridge. Profile a) shows an angular unconformity sealed by Late Miocene turbidites according to the nearby site DSDP 222. An extinct transform fault is evidenced at the eastern foot of the ridge, the present-day active boundary being localized at the mid-slope of the ridge. Profile b) shows the Late Miocene angular unconformity formed during the uplift of the Owen Ridge. See fig.2b for location and fig. 3 for stratigraphic legend.*

4.4. *Late Miocene contourites*

Influences of deep-sea currents on sediment architecture appear in several places in the Owen Basin after ~8.5 Ma according to calibration with ODP site 728 (Fig. 3), with strong variations in the architecture of the deposits related to the margin morphology.

The most conspicuous evidence is provided at the latitude of the Sharbitat Ridge (Fig. 3a), where a complicated set of imbricated, sigmoid to undulated geometries, all non-parallel to the accumulation surface, overlies the anticline structure. Additionally, truncated reflectors reveal slope incision by canyons, being progressively filled-in by sigmoid sedimentary bodies. As canyons incision diminished progressively in response to the deposition of contouritic deposits, the sigmoid bodies preferentially moved up-slope and landward, also indicating bottom current influence rather than the action of gravity forces alone. This description corresponds to a confined drift according to the classification of Faugères et al. (1999), and is very similar to what is observed on the Algarve Margin (Portugal) (Marchès et al., 2010) or the Brasilian margin (Faugères et al., 1999). A confined drift is also observed on the western side of the anticline, where Plio-Pleistocene MTDs from the continent are trapped (Fig. 4). Northwards, the Oman margin is dissected by numerous canyons (Bourget et al., 2009), which also display evidences of bottom current influence on the sediment architecture. For instance, the canyon identified at the latitude of 20°N displays sigmoid bodies in its uppermost part, whereas a typical plastered drift architecture (sensu Faugères et al., 1999) with frequent inter-fingered MTDs is identified downslope (Fig. 7).

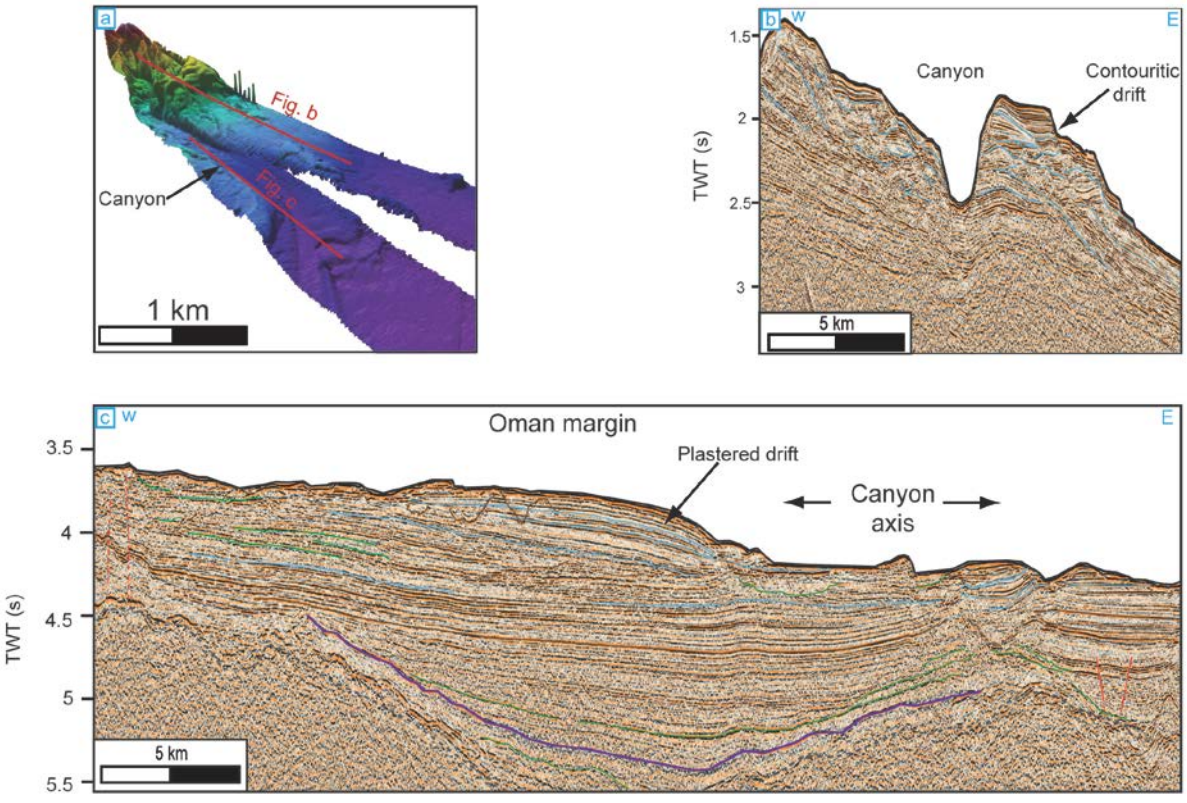

***Figure 7** : Anatomy of a canyon dissecting the Oman margin, with special emphasis over bottom-current deposits. a) Bird eye view of the canyon. b) Seismic profile crossing the uppermost flanks of the canyons, showing imbricated sigmoid bodies typical of contouritic drifts. c) Downslope seismic section of the canyon, showing typical plastered drifts sensu Faugères et al. (1999). See Fig. 2b for location.*

## 5. Discussion

### 5. 1. *Age of uplift of the Owen Ridge and Late Miocene deformation in the Owen Basin*

The observations above suggest a regional tectonic event in the Owen Basin around 8-9 Ma, consistently with the age of an angular unconformity marking the uplift of the Murray Ridge estimated by calibration with an industrial drilling in the Indus fan (Clift et al., 2001; Calvès, 2008). This Late Miocene episode of deformation contrasts with the 15-20 Ma-old age previously assessed for the uplift of the Owen Ridge (Whitmarsh, 1979; Mountain and Prell, 1990). First, the angular unconformity evidenced by Whitmarsh (1979) has a depositional and not a tectonic origin, and simply reflects the transition from oligocene pelagites to lower miocene turbidites as the "pre-Owen Ridge" gets progressively buried under the Indus deep-sea fan (Mountain and Prell, 1990). The age of the first turbidite overlying the unconformity marks the time at which the turbiditic system was developed enough to bury the pre-existing Owen Ridge at the site of drilling. The 6-Ma misfit between the age of the first turbidite at site DSDP 223 and DSDP 224 indicates that site DSDP 223 used to be shallower than site DSDP 224. In this framework, the upper oligocene-lower miocene MTDs drilled at DSDP sites 223-224 probably originated from the pre-Owen Ridge. The second argument in favour of a 15-20 Ma-old uplift of the Owen Ridge was the 14-15 Ma-old mixed turbiditic-pelagic facies drilled at ODP sites (Mountain and Prell, 1990). Because of its location on a turbiditic levee (Fig. 3), the 14-15 Ma-old mixed facies cannot be interpreted by itself as the first stage of the southern ridge uplift. During their deposition along turbiditic channels, turbiditic plumes frequently undergo flow-stripping or overspilling processes (Piper and Normark, 1983; Hiscott et al., 1997). These processes imply that the uppermost part of the turbiditic plume, composed of the thinner detritic particules, overflows throughout the channel axis, leading to the deposition of mixed turbiditic-pelagic sequence on turbiditic levees similar to the one described at site ODP 722. The axis of the last turbiditic channel of the Unit 4 is ~40-m-deep, which may have favored either flow-stripping or overspilling. The significance of the overlying pelagic deposits (Units 2-3) is ambiguous with regards to the age of the Owen Ridge uplift. Thick pelagic layers are common features of the present-day Indus fan. For instance, a ~100-m-thick pelagic sequence has been drilled at site DSDP 222 (Shipboard Scientific Party, 1974). Thicker pelagic intervals are observed in the vicinity of site ODP 720 in the Indus deep-sea fan, where the alternation of turbidites within pelagic sequences is controlled by avulsion processes, and not by any uplift of relief. On the other hand, slight lateral thickness variations of Unit 3 (less than 0.1 s (TWT) are observed (see supplementary material and Fig. 3), together with a slightly

expressed angular unconformity recognized on figures 3b and 5a at the transition between Unit 2 and 3 (10.4 Ma). The lysocline depth is currently at ~4000 m in the area (Kolla et al., 1976), making difficult to discriminate whether fluctuations in the conditions of microfossils preservation throughout Unit 3 reflect the first stage of uplift of the Owen Ridge or oscillations in the lysocline depth. Consequently, we do not evidence any indicator of a prominent topography (in the order of ~1000m) during the deposition of Units 2 and 3.

The Late Miocene apparition of major submarine failures is a striking feature of both the southern and the central Owen Ridges. Submarine failures and their related deposits clearly sealed the 8-9 Ma-old deformation at the southern ridge. The large expansion of the erosive surface created by failure planes over both segment, together with the erosive surface observed at the top of buried reliefs in the Owen Basin and the synchronicity with the formation of anticlines along the Oman margin, strongly suggest a regional tectonic uplift as the most likely triggering process. Consequenty, the uplift of the Owen Ridge at ~8.5 Ma would have significantly raised the seafloor above the lysocline, inducing the apparent dominance of *G. bulloides* since 8.5 Ma (Shipboard Scientific Party, 1989; Kroon et al., 1991) without any marked climatic change (Huang et al., 2007). The Late Miocene change in Foraminifera abundances therefore likely reflect a change in their conditions of preservation rather than a climatic change, consistently with the general increase of carbonate accumulation since ~10 Ma in the Indian Ocean (Peterson et al., 1992). The ~8 Ma-old environmental change in the Siwalik may thus not be related to a change in the Indian monsoon.

### 5. 2. *Uplift of the Owen Ridge*

Based on free-air gravimetry and seismic profiles analysis, Weissel et al. (1992) showed that the uplift of the Owen Ridge occurred as a flexural response to either an extensional or a compressive event, making the tectonic interpretation of the ridge ambiguous. The topographic expression of deformation processes within the oceanic lithosphere is mainly controlled by the lithospheric strength and the elastic thickness, which is a direct function of the thermal state -and therefore the age- of the lithosphere (Weissel et al., 1992). Consequently, even a low deformation rate (less than 5%) can generate prominent reliefs (>1000 m), as observed in the Central Indian Ocean (Chamot-Rooke et al., 1993; Delescluse et al., 2008), the Central Atlantic Ocean (Pichot et al., 2012) or along the Romanche (Bonatti et al., 1994) and the Vema Transforms (Bonatti et al., 2005) in the Atlantic Ocean. A slight change in the India-Arabia relative motion could have generated flexural deformation in areas of strong rheological contrasts (i.e. the India-Arabia plate-boundary and the Oman margin), leading to the uplift of the Owen Ridge and deformation over the Owen Basin.

The inactive transform segments observed at the eastern edge of the Owen Ridge (Fig. 5, 6) might correspond to the fossil India-Arabia plate-boundary in Miocene times. This Miocene plate-boundary might have localized the stress that lead to the uplift of the ridge. The offset along the fracture zone might have changed the stress field around it, leading to the formation of a nearby new boundary while

the initial one became extinct, similarly to what inferred for normal faults dynamics (Buck et al., 1993). The Miocene plate boundary might have been very weak to allow the uplift of the Owen Ridge. This scheme is consistent with the 3-6 Ma age inferred for the present-day OFZ (Fournier et al., 2008a, b; 2011), which could result from a 5-10 km migration of the plate-boundary subsequently to the uplift of the Owen Ridge (Fig. 5). This migration of the India-Arabia plate-boundary results from the stress field evolution within the plate boundary, but does not involve any significant change in the direction of the India-Arabia relative motion, consistently with kinematics reconstitutions of Chamot-Rooke et al. (2009).

5. 3. *Origin of the Late Miocene deformation in the Owen Basin*

Our dating of the deformation in the Owen Basin (uplift of the Oman margin at 8.2-8.8 Ma) coincides in time with the rise of prominent reliefs in the central Indian Ocean (Wiens et al., 1985; Chamot-Rooke et al., 1993; Henstock et al., 2004; Delescluse and Chamot-Rooke, 2007; Delescluse et al., 2008; Krishna et al., 2009; Bull et al., 2010), suggesting that both events recorded at opposite extremities of the Indian Plate reacted to the same kinematic change, most probably caused by the increase in stress applied by the Late Miocene growth of the Himalayas on the Indian plate (Molnar et al., 1993; Molnar and Stock, 2009). In the Arabian Sea, the magnetic anomalies record over the Carlsberg (Somalia-India motion) and the Sheba Ridges (Somalia-Arabia motion) documents a deceleration of seafloor spreading rates between 20 and 10 Ma, then followed by nearly constant spreading rates after 8-10 Ma (DeMets et al., 2005; Merkouriev and DeMets, 2006; Fournier at al., 2010). A two-phases growth of reliefs is recognized in the Central Indian Ocean, the first and minor one being dated at 13.9-15.4 Ma, and the second, major one, at 8-9 Ma (Delescluse et al., 2008; Krishna et al., 2009; Bull et al., 2010). Evidences of initiation of compression around 13.9-15.4 Ma at the Owen Ridge are scarce, only slight lateral thickness variations of Unit 3 (less than 0.1 s (TWT) being observed (see supplementary material and Fig. 3). Thus, the main uplift of the Owen Ridge may have started around 10 Ma (as suggested by the slight 10.4 Ma-old unconformity (Fig. 3b)), followed by an abrupt acceleration around 8.5 Ma. Considering the uplift of the Owen Ridge involved a vertical motion of about ~2000m would imply an average uplift rate of ~1 mm. $yr^{-1}$ between 8.5 and 10.4 Ma. Considering most of the uplift occurred between 8.2 and 8.8 Ma implies an uplift rate in the order of 3-4 $mm.yr^{-1}$, in the same range than estimated values for the uplift of transverse ridges in the Atlantic Ocean (Bonatti et al., 2005).

5. 4. *Surface uplift along the Arabian Sea coasts*

The Late Miocene deformation episode in the Owen Basin is coeval with several geological events around the Arabian Sea coasts. The Dhofar margin in the Gulf of Aden recorded a Tortonian post-rift uplift episode evidenced on land (Platel and Roger, 1989) and in marine sediments (Bache et al.,

2010). Additionally, the folds identified at the Oman margin (Fig. 3, 4) used to form emerged reliefs subsequently eroded and submerged some 1.3 Ma ago (erosive surface observed on Fig. 3, 4).

Several local processes have been invoked for the uplift episode in the Dhofar (Bache et al., 2010; Leroy et al., 2010), but the Late Miocene episode of deformation identified in the Owen Basin could better account for this uplift as rifted areas are prone to be reactivated by intra-plate deformation (Cloething et al., 2008). Monsoon and relative sea-level variations could have enhanced the uplift through the isostatic compensation induced by erosional unloading (Petit et al., 2007).

A Late Miocene episode of uplift also occurred in Pakistan. Tortonian folds reaching altitudes of 1000-2000 m according to cross-sections (Ellouz Zimmerman et al., 2007) developed over a décollement layer at the front of the aerial part of the Makran accretionary wedge. Prior to the Late Miocene, no significant topography was associated to the wedge (McCall, 1997). The formation of these anticlines was followed by huge submarine olistostromes (~42 000 $km^3$), pointing out abrupt topographic changes in Pakistan (Burg et al., 2008), and associated to the migration of the frontal thrust to its present-day position (McCall, 1997). The Late Miocene in Pakistan marks the definitive deviation of the paleo-Indus river system identified by Qayyum (1997), highlighted by the vanishing of channel-levee systems in the Parkini Fm. (Ellouz Zimmerman et al., 2007) and the disappearance of deltaic environments evidenced by isotopic reconstructions of mammals habitats (Nelson, 2006). The Tortonian avulsion of the meandering section of the Indus river (over ~400 km) was triggered by surface uplift along the Kirthar-Sulaiman ranges (Waheed and Wells, 1990; 1992). Similarly to the India-Arabia boundary, the India-Eurasia boundary seems to have also reacted to the Late Miocene growth of the Himalayas.

### 5. 5. *Late Miocene environmental changes over the Arabian Sea*

Tectonic processes involved in relief uplift act at a different time-scale and are less precisely dated than ecological and climatic changes, making any relationship based on synchronicity difficult to assess. However, the coincidence in time between tectonic-induced physiographic changes, the deposition of contouritic drifts, and the environmental change in the Siwalik sequence is striking (Fig. 8). At first sight, the apparition of contouritic drifts may be related to a sudden change in bottom water circulation caused by the Late Miocene deformation in the Owen Basin, which could have restricted and localized the pathway of the deep-sea currents. However, the re-interpretation of the sedimentary sequence of the Owen Ridge by Huang et al. (2007) does not evidence any climatic change nor upwelling intensification (and the related decrease in the sea surface temperature) between 10 and 5.5 Ma, consistently with the deep thermocline ~10 Ma ago (Philander and Fedorov, 2003). An alternative interpretation of the Late Miocene contouritic drift would be to consider that middle-water depth currents pre-existed in the area (as suggested by Gourlan et al., 2008), but were not recorded in absence of significant reliefs to support contouritic drifts. The Late Miocene environmental change is thus unlikely to be the result of a reorganization of the oceanic circulation.

According to Huang et al. (2007), the record of eolian deposits in the sedimentary sequence of the Owen Ridge documents a 45% increase in the $C_4$ plant cover from 10 Ma to 8.4 Ma, before a 15% decrease from 8.4 to 7.9 Ma, subsequently followed by a major increase of $C_4$ plants. This record contrasts with the Siwalik paleosoil sequence in Pakistan, which does not show the 15% decrease in $C_4$ coverage between 8.4 and 7.9 Ma. Huang et al. (2007) postulated that a change in the eolian transport paths from continent to ocean may have contributed to the apparent decrease of the $C_4$ plant coverage recorded at ODP site 722. An uplift of the Oman and Pakistan continental margins at ~8.5 Ma would have formed topographic barriers for the eolian transport to the Arabian Sea, explaining the 15% decrease in $C_4$ plants recorded at the Owen Ridge. It would also have induced a reorganization of the atmospheric circulation, reducing monsoon precipitation coming from the ocean over the Pakistan and Oman climate, without affecting the seasonality (consistently with environment reconstitutions of Nelson, 2006). This framework leads to increased seasonal aridity, with a greater fraction of precipitation coming from continental sources in the Siwalik area (Huang et al. 2007), consistently with the record of the development of $C_4$ vegetation (Quade et al., 1989).

The development of $C_4$ plants started at ~10 Ma in the Pakistan (Huang et al., 2007), coevally with recent estimates of monsoon intensification at ~10.5 Ma over India (Clift et al., 2008; Prasanta and Sinha, 2010) and Africa (Sakai et al., 2010) and the global decrease in $CO_2$ concentration in the atmosphere (Cerling et al., 1997). However, $C_4$ plants remained in tight competition with $C_3$ plants until 8 Ma in Pakistan (Nelson, 2006; Huang et al., 2007), and the estimated decrease in annual precipitation (~120 mm) and increase in annual temperature (+3°C) cannot account for the ecological transition alone (Nelson, 2006). By driving the deviation of the Indus delta and isolating the Pakistan climate of its oceanic influence, the Tortonian continental uplift may explain the hydrological change (Huang et al., 2007) and may have forced the shift from $C_3$ to $C_4$ vegetation. The major increase in $C_4$ plants proxies at the Owen Ridge since 7.9 Ma ago could correspond either to the re-establishment of the eolian pathway between the continent and the sea subsequently to a significant erosion of Late Miocene reliefs, or –more likely- to the expansion of $C_4$ plants over India.

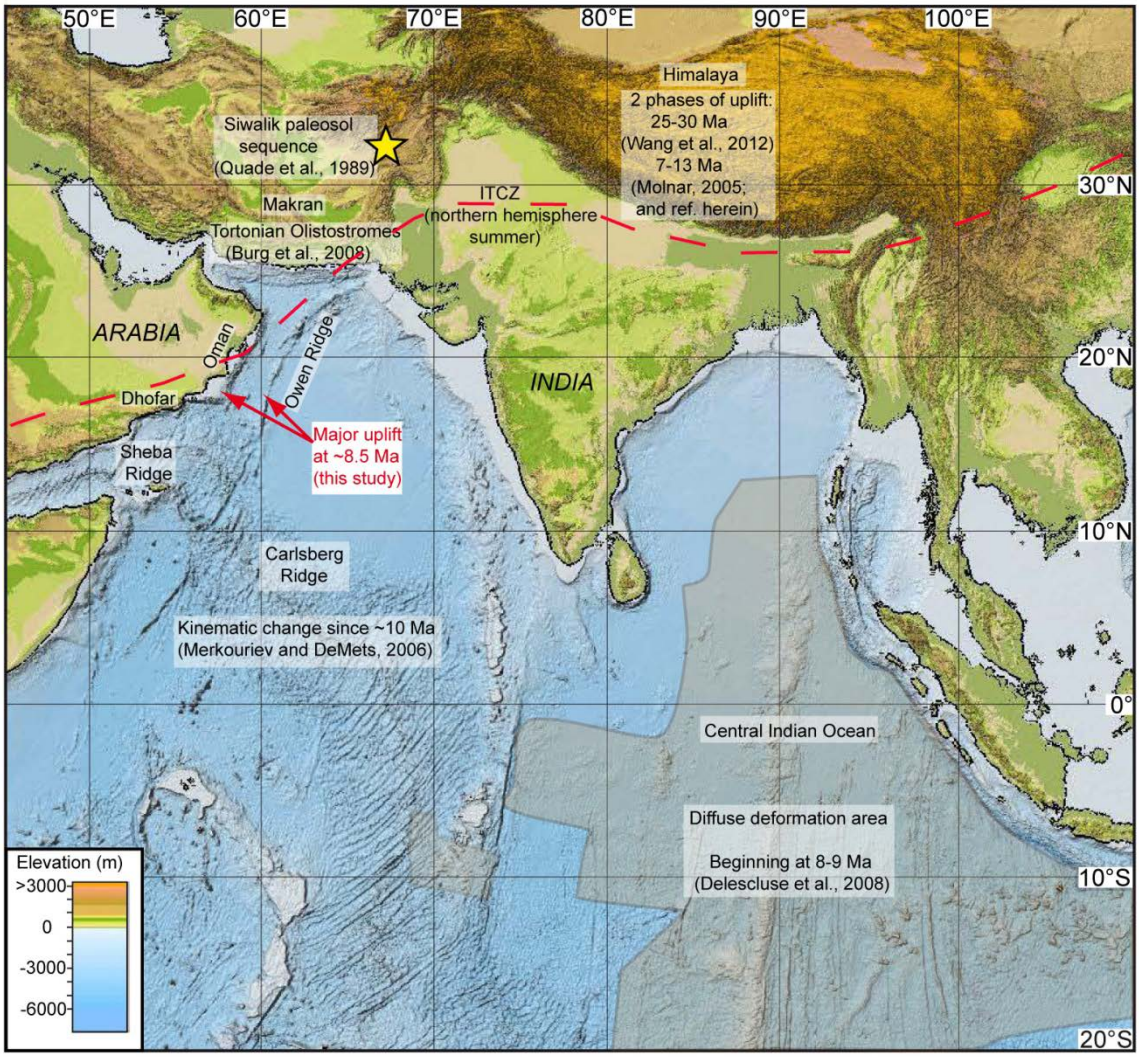


***Figure 8 :*** *Map of the Indian Ocean compiling the different deformation areas related to the Late Miocene motion of the Indian Plate. ITCZ : Inter Tropical Convergence Zone.*

## 6. Conclusions

The Owen margin, basin and ridge have undergone an important episode of deformation previously undocumented in the Late Miocene, leading to the uplift of the east Oman margin and the Owen Ridge. Whether the triggering of olistostromes on the Makran wedge and the uplift of the Dhofar margin were related to the Late Miocene deformation in the Owen Basin needs a better dating to be confirmed. The best-dated deformation is the anticline structure on the Oman margin, bracketed between 8.2 and 8.8 Ma. The Late Miocene episode of deformation could coincide with a reorganization of the India-Arabia plate-boundary resulting from the 8-9 Ma kinematic change linked to the onset of intraplate deformation in the Central Indian Ocean. The rise of the Owen Ridge induced changes in the condition of preservation of Foraminifera, which confirms that the apparent increase in

*G. Bulloides* at 8.5 Ma is not related to a climatic change. Minor proportions of *G. Bulloides* before 8.5 Ma might rather reflect the abyssal depth of the sediments drilled at DSDP-ODP sites, and poor preservation of Foraminifera because of strong dissolution below the lysocline. Similarly, the general increase in carbonate preservation in the Indian Ocean (Peterson et al., 1992) may be the result of the 8-9 Ma-old episode of intra-plate deformation rather than the expression of a climatic or deep-sea circulation change. The latter confirms that the monsoon might have already been strong before 8.5 Ma (Clift et al., 2008; Prasanta and Sinha, 2010). Contouritic drifts lay on the Late Miocene reliefs (Fig. 7), leading to the hypothesis that the uplift of the Owen Ridge also changed the conditions of record of deep-sea current activity.

Similarly to the role played by the East African Rift over the climatic evolution of Africa (DeMenocal, 2004; Sepulchre et al., 2006), a Late Miocene episode of continental uplift over the Arabian Sea coasts might have acted as a topographic barrier for atmospheric circulation, leading to increased seasonal aridity over Pakistan and hence, selection of $C_4$ plants. This environmental change is supposed to have influenced the evolution of mammals in the Late Miocene (Elton, 2008). Of particular interest is *Sivapithecus*, considered as a likely ancestor of *Pongo pygmae* (Andrews and Cronin, 1982), who disappeared in Pakistan following the ~8-Ma ecological change. The Late Miocene avulsion of the Indus river in response to surface uplift together with the isolation of Pakistan climate from oceanic influence, might account for the fragmentation of habitats in Pakistan, changes in ecological relationships between mammals (Barry et al., 2002), and the first stages of migration of *Sivapithecus* towards eastern Asia (Begun, 2004).

**Acknowledgements**

We are grateful to Captain Rémi De Monteville, officers and crew members of the BHO Beautemps-Beaupré, and to the GENAVIR team and the hydrographer D. Levieuge for their help in data acquisition. Processing of the Owen-2 dataset was carried out using the Geocluster 5000 software from CGGVeritas.We thank A. Rabaute who helped the organization of the Owen-2 cruise. We thank P. Dubernet and N. Bacha for technical assistance. This study was supported by SHOM, IFREMER, INSU-CNRS, and CEA (LRC Yves-Rocard).

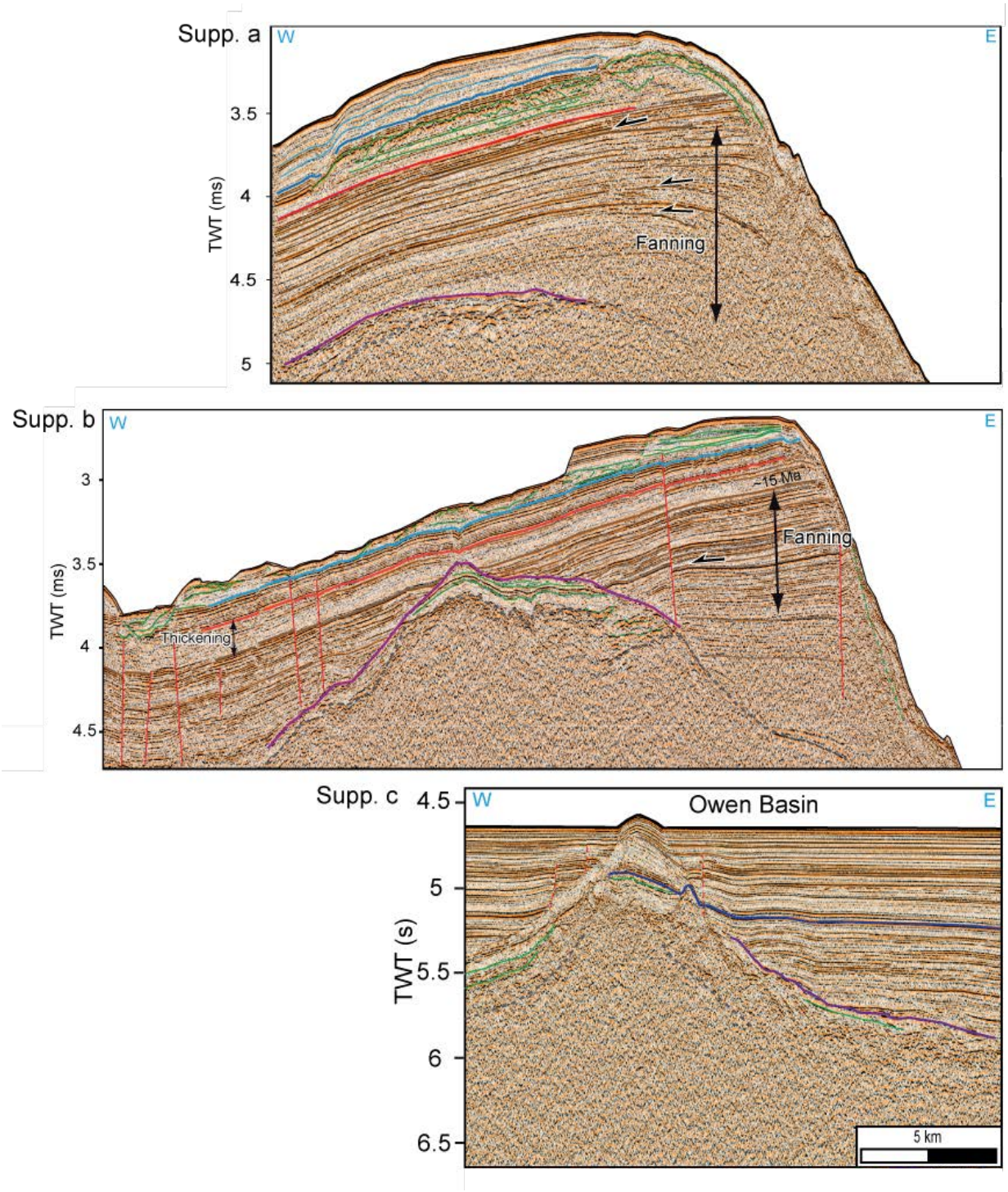


***Supplementary material** : a) and b) Seismic profiles crossing the top of the Owen Ridge, highlighting the fanning pattern of early Miocene turbidites (see Figure 2 for location). c) Seismic profile crossing partly buried reliefs in the middle of the Owen Basin (See Fig. 2b for location). It displays an unconformity draped by 0.3s TWT of pelagic sediments, similarly to the Late Miocene unconformity observed on the Central Owen Ridge.*

**References**

An, Z., Kutzbach, J.E., Prell, W.L., Porter, S.C., 2001.Evolution of Asian monsoons and phased uplift of the Himalaya–Tibetan plateau since Late Miocene times. Nature 411, 62–66.

Andrews, P., and Cronin, J. E., 1982. The relationships of Sivapithecus and Ramapithecus and the evolution of the orang-utan. Nature 297, 541-546.

Bache, F., Leroy, S., Baurion, C., Robinet, J., Gorini, C., Lucazeau, F., Razin, P., d'Acremont, E., Al-Toubi, K., 2010. Post-rift uplift of the Dhofar margin (Gulf of Aden).Terra nova 23, 11-18, DOI: 10.1111/j.1365-3121.2010.00975.x, 2010.

Barnes, P., Pondard, N., 2010. Derivation of direct on-fault submarine paleoearthquake records from high-resolution seismic reflection profiles: Example from the Wairau Fault, New Zealand, Geochem. Geophys. Geosyst. 11, Q11013, doi:10.1029/2010GC003254.

Barry, J., Morgan, M. E., Flynn, L. J., Pilbeam, D., Behrensmeyer, A. K., Raza, S. M., Khan, I. A., Bagdley, C., Hicks, J., Kelley, J., 2002. Faunal and environmental change in the late Miocene Siwaliks of northern Pakistan. Paleobiology 28, 1-71, http://dx.doi.org/10.1666/0094-8373(2002)28[1:FAECIT]2.0.CO;2

Begun, D. R., 2004. Sivapithecus is east and Dryopithecus is west, and never the twain shall meet. Anthropological science 113, 53-64.

Bonatti, E., Ligi, M., Gasperini, L., Peyve, A., Raznitsin, Y., Chen, Y. J., 1994. Transform migration and vertical tectonics at the Romanche fracture zone, equatorial Atlantic. J. Geophys. Res. 99, 21779-802.

Bonatti, E., Brunelli, D., Buck, W. R., Cipriani, A., Fabretti, P., Ferrante, V., Gasperini, L., Ligi, M., 2005. Flexural uplift of a lithospheric slab near the Vema transform (Central Atlantic) : timing and mechanisms. Earth. Planet. Sci. Lett. 240, 642-655.

Bourget, J., Zaragosi, S., Mulder, T., Schneider, J.-L., Garlan, T., Van Toer, A., Mas, V., Ellouz-Zimmermann, N., 2010. Hyperpycnal-fed turbidite lobe architecture and recent sedimentary processes: A case study from the Al Bathaturbidite system, Oman margin. Sedimentary Geology 229, 144-159.

Bourget, J., Zaragosi, S., Rodriguez, M., Fournier, M., Garlan, T., Chamot-Rooke, N., 2013. Late Quaternary megaturbidites of the Indus Fan : origin and stratigraphic significance. Mar. Geol. 336, 10-23, doi:10.1016/j.margeo.2012.11.011.2013

Buck., W. R., 1993. Effect of lithospheric thickness on the formation of high- and low-angle normal faults. Geology 21, 933-936.

Bull, J. M., DeMets, C., Krishna, K. S., Sanderson, D. J., Merkouriev, S., 2010. Reconciling plate kinematic and seismic estimates of lithospheric convergence in the central Indian Ocean. Geology 38, 307-310, doi: 10.1130/G30521.1

Burg, J.P., Bernoulli, D., Smit, J., Dolati, A., Bahroudi, A., 2008. A giant catastrophic mud-and-debris flow in the Miocene Makran. Terra Nova 20, 188–193, doi: 10.1111/j.1365-3121.2008.00804.x

Calvès, G., 2008.Tectonostratigraphic and climatic record of the NE Arabian Sea, Ph.D. thesis, 305 pp., Univ. of Aberdeen, Aberdeen U. K.

Cerling, T.E., Harris, J.M., MacFadden, B.J., Leakey, M.G., Quade, J., Eisenmann, V.,Ehleringer, J.R., 1997.Global vegetation change through the Miocene/Pliocene boundary. Nature 389, 153-158.

Chamot-Rooke, N., Jestin, F., DeVoogd, B., 1993. Intraplate shortening in the central Indian-ocean determined from a 2100-km-long north-south deep seismic-reflection profile. Geology 21(11), 1043–1046.

Cochran, J. R., 1981. The Gulf of Aden: structure and evolution of a young ocean basin and continental margin. J. Geophys. Res. 86, 263-287.

Clift, P. D., Shimizu, N., Layne, G. D., Blusztain, J. S., Gaedicke, C., Schluter, H.-U., Clark,M. K., Amjad, S., 2001.Development of the Indus Fan and its significance for the erosional history of the Western Himalaya and Karakoram.Geol. Soc. Am. Bull. 113, 1039–1051.

Clift, P. D., Gaedicke, C., 2002. Accelerated mass flux to the Arabian Sea during the middle to late Miocene. Geology 30, 207-210, doi:10.1130/0091-13(2002)030<0207:AMFTTA>2.0.CO;2

Clift, P. D., Hodges, K. V., Heslop, D., Hannigan, R., Van Long, H., Calvès, G., 2008.Correlation of Himalayan exhumation rates and Asian monsoon intensity. Nat. Geosci. 1, 875-880, doi:10.1038/ngeo351

Clift, P. D., 2010. Enhanced global continental erosion and exhumation driven by Oligo-Miocene climate change. Geophys. Res. Lett. 37, L09402, doi:10.1029/2010GL043067

Cloething, S., Beekman, F., Ziegler, P. A., van Wees, J-D., Sokoutis, D., 2008. Post-rift compressional reactivation potential of passive margins and extensional basins. Geol. Soc. London Spec. Publ. 306, 27-70.

Delescluse, M., Chamot-Rooke, N., 2007.Instantaneous deformation and kinematics of the India-Australia Plate. Geophys. J. Int. 168, 818-842, doi: 10.1111/j.1365-246X.2006.03181.x

Delescluse, M., Montési, L. G. J., Chamot-Rooke, N., 2008. Fault reactivation and selective abandonment in the oceanic lithosphere. Geophys. Res. Lett. 35, L16312, doi:10.1029/2008GL035066.

deMenocal, P., 2004. African climate change and faunal evolution during the Pliocene-Pleistocene. Earth Planet. Sci. Lett. 220, 3-24.

DeMets, C., Gordon, R., Royer, J-Y., 2005. Motion between the Indian, Capricorn and Somalian plates since 20 Ma : implications for the timing and magnitude of distributed lithospheric deformation in the equatorial Indian Ocean. Geophys. J. Int. 161, 445-468, doi: 10.1111/j.1365-246X.2005.02598.x

DeMets C., Gordon, R. G., Argus, D.F., 2010.Geologically current plate motions. Geophys. J. Int. 181, 1-80, doi: 10.1111/j.1365-246X.2009.04491.x.

Dupont-Nivet, G., Hoorn, C., Konert, M., 2008. Tibetan uplift prior to the Eocene-Oligocene climate transition : Evidence from pollen analysis of the Xining Basin. Geology 36, 987-990, doi: 10.1130/G25063A.1

Edwards, R.A., Minshull, T. A., White, R. S., 2000. Extension across the Indian–Arabian plate boundary: the Murray Ridge. Geophys. J. Int. 142, 461-477.

Edwards, R. A.,Minshull, T. A., Flueh, E. R., Kopp, C., 2008. Dalrymple Trough: An active oblique-slip ocean-continent boundary in the northwest Indian Ocean. Earth Planet. Sci. Lett. 272, 437-445.

Ellouz Zimmermann, N., Deville, E., Müller, C., Lallemant, S., Subhani, A. B., Tabreez, A. R., 2007. Impact of sedimentation on convergent margin tectonics : example of the Makran Accretionary prism (Pakistan). Thrust Belts and Foreland Basins: From Fold Kinematics to Hydrocarbon Systems, edited by O. L. Lacombe et al., pp. 327–350, Springer, Berlin.

Ellouz Zimmermann, N. et al., 2007. Offshore frontal part of the Makranaccretionary prism (Pakistan) the Chamak Survey. Thrust Belts and Foreland Basins: From Fold Kinematics to Hydrocarbon Systems, edited by O. L. Lacombe et al., pp. 349–364, Springer, Berlin.

Elton, S., 2008. The environmental context of human evolutionary history in Eurasia and Africa. J. Anat. 212, 377–393, doi: 10.1111/j.1469-7580.2008.00872.x

Faugères, J.C., Stow, D.A.V., Imbert, P., Viana, A., 1999.Seismic features diagnostic of contourite drifts. Mar. Geol. 162, 1-38.

Fournier, M., Chamot-Rooke N., Petit C., Fabbri O., Huchon P., Maillot B., Lepvrier C., 2008a. In-situ evidence for dextral active motion at the Arabia-India plate boundary. Nat. Geosci. 1, 54-58, doi:10.1038/ngeo.2007.24.

Fournier, M., Petit C., Chamot-Rooke N., Fabbri O., Huchon P., Maillot B., Lepvrier, C., 2008b) Do ridge-ridge-fault triple junctions exist on Earth? Evidence from the Aden-Owen-Carlsberg junction in the NW Indian Ocean. Basin Research 20, 575-590.doi: 10.1111/j.1365-2117.2008.00356.x

Fournier, M., Chamot-Rooke, N., Petit, C., Huchon, P., Al-Kathiri, A., Audin, L., Beslier, M.-O., d'Acremont, E., Fabbri, O., Fleury, J.-M., Khanbari, K., Lepvrier, C., Leroy, S., Maillot B., Merkouriev, S., 2010.Arabia-Somalia plate kinematics, evolution of the Aden-Owen-Carlsberg triple junction, and opening of the Gulf of Aden. J. Geophys. Res. 115, B04102, doi:10.1029/2008JB006257

Fournier, M., Chamot-Rooke N., Rodriguez, M., Huchon, P., Petit, C., Beslier, M.-O., Zaragosi S., 2011. Owen Fracture Zone: the Arabia-India plate boundary unveiled. Earth Planet. Sci. Lett. 302, 247-252, doi:10.1016/j.epsl.2010.12.027.

Gaedicke, C., Prexl, A., Schlüter, H.U., Roeser, H., Clift, P., 2002. Seismic stratigraphy and correlation of major regional unconformities in the northern Arabia Sea.The Tectonic and Climatic Evolution of the Arabian Sea Region, edited by Clift, P. D., Kroon, D., Gaedicke, C., & Craig, J., Geol. Soc. Spec. Publ. 195, 25-36.

Gourlan, A.T., Meynadier, L., Allègre, C. J., 2008. Tectonically driven changes in the Indian Ocean circulation over the last 25 Ma: Neodymium isotope evidence. Earth. Planet. Sci. Lett., 267, 353-364.

Harrison, T.M., Copeland, P., Kidd, W.S.F., Yin, A., 1992. Raising Tibet. Science 255, 1663-1670.

Henstock, T. J.,Minshull, T. A., 2004. Localized rifting at Chagos bank in the India-Capricorn plate boundary zone. Geology 32, 237–240.

Hiscott, R. N., Pickering, K. T.,Bouma, A. H., Hand, B. M., Kneller, B. C.,Postma, G.,Soh, W.,1997.Basin-Floor Fans in the North Sea: Sequence Stratigraphic Models vs. Sedimentary Facies: Discussion. AAPG bull. 81, 662-665

Huang, Y., Clemens, S. C., Liu, W., Wang, L., Prell, W. L., 2007. Large-scale hydrological change drove the Late Miocene C4 plant expansion in the Himalayan foreland and Arabian Peninsula. Geology 35, 531-534.

Kolla, V., Bé, A. W. H., Biscaye, P. E., 1976. Calcium Carbonate distribution in the surface sediments of the Indian Ocean. J. Geophys. Res. 81, 2605-2616.

Krishna, K. S., Bull, J. M., Scrutton, R. A., 2009. Early (pre-8 Ma) fault activity and temporal strain accumulation in the central Indian Ocean. Geology 37, 227-230, doi: 10.1130/G25265A.1

Kroon, D., Steens, T.,Troelstra, S.R., 1991. Onset of monsoonal related upwelling in the western Arabian Sea as revealed by planktonic foraminifers. In Prell, W.L., Niitsuma, N., et al., Proceedings of the Ocean Drilling Project, Sci. Results, 117, 257- 263 College Station, Texas (Ocean Drilling Program).

Leroy, S. et al., 2010. From rifting to oceanic spreading in the Gulf of Aden: a synthesis. Arab.J.Geosci. doi 10.1007/s12517-011-0475-4

Marches E., Mulder T., Gonthier E., Hanquiez V., Cremer M., Garlan T., Lecroart P., 2010. Perched lobes formation induced by contourite construction in the Gulf of Cadiz: Interactions between gravity processes and contour currents (Algarve Margin, South Portugal), Sedimentary Geology 229, 81-94.

McCall, G.J.H., 1997. The geotectonic history of the Makran and adjacent areas of southern Iran. J. Asian Earth Sci., 15, 517-531.

Mercuriev, S., DeMets, C., 2006.Constraints on Indianplate motion since 20 Ma from dense Russian magnetic data:Implications for Indian plate dynamics. Geochem. Geophys.Geosyst. 7, Q02002, doi:10.1029/2005GC001079.

Molnar, P., England, P., 1990. Late Cenozoic uplift of mountain ranges and global climatic change: chicken or egg? Nature 346, 29-34.

Molnar, P., England, P., Martinod, J., 1993. Mantle dynamics, uplift of the Tibetan Plateau, and the Indian monsoon. Rev. Geophys. 31, 357–396.

Molnar, P., 2005. Mio-Pliocene Growth of the Tibetan Plateau and Evolution of East Asian Climate. Palaeontologia Electronica 8, 1-23.

Molnar, P., Stock, J., 2009. Slowing of India's convergence with Eurasia since 20 Ma and its implications for Tibetan mantle dynamics. Tectonics, 28, TC3001, doi:10.1029/2008TC002271

Molnar, P., Boos, W. R., Battisti, D. S., 2010. Orographic controls on climate and paleoclimate of Asia: thermal and mechanical role of the Tibetan Plateau. Annu. Rev. Earth Planet. Sci. 38, 77-102.

Mountain, G. S.,Prell, W.L., 1990.A multiphase plate tectonic history of the southeast continental margin of Oman. The Geology and Tectonics of the Oman Region, edited by Robertson, A. H. F., Searle, M. P. and Ries, A. C., Geol. Soc. Spec. Publ., 49, 725-743.

Mouthereau, F., Lacombe, O., Vergés, J., 2012.Building the Zagros collisional orogen: Timing, strain distribution and the dynamics of Arabia/Eurasia plate convergence. Tectonophysics 532–535, 27–60.

Nelson, S., 2006. Isotopic reconstructions of habitat change surrounding the extinction of Sivapithecus, a Miocene hominoid, in the Siwalik Group of Pakistan. Paleaogeo., Paleaoclim., Palaeoeco. 243, 204-222.

Peterson, L. C., Murray, D. W., Ehrmann, W. U., Hempel, P., 1992.Cenozoic carbonate accumulation and compensation depth changes in the Indian Ocean. In Synthesis of results from scientific drilling in the Indian Ocean, ed. RA Duncan, DK., Rea, R. B. Kidd, U. von Rad, J. K., Weissel, Geophys. Monogr. 70, 311-333. Am. Geophys. Union, Washington, D. C.

Petit, C., Fournier, M., Gunnell, Y., 2007.Tectonic and climatic controls on rift escarpments: Erosion and flexural rebound of the Dhofar passive margin (Gulf ofAden, Oman), J. Geophys. Res., 112, B03406, doi:10.1029/2006JB004554

Pichot, T., Patriat, M., Westbrook, G.K., Nalpas, T., Gutscher, M. A., Roest, W. R., Deville, E., Moulin, M., Aslanian, D., Rabineau, M., 2012. The Cenozoic tectonostratigraphic evolution of the Barracuda Ridge and Tiburon Rise, at the western end of the North America-South America plate boundary zone. Mar. Geol. 303-306, 154-171, doi: 10.1016/j.margeo.2012.02.001

Piper, D. J. W., Normark, W. R., 1983.Turbidite depositional patterns and flow characteristics, Navy Submarine Fan, California Borderland. Sedimentology 30, 681-694.DOI: 10.1111/j.1365-3091.1983.tb00702.x

Platel, J.P., Roger, J., 1989. Evolution géodynamique du Dhofar (Sultanatd'Oman) pendant le Crétacé et le Tertiaire en relation avec l'ouverture du golfe d'Aden, Bull. Soc. Géol. France 2, 253-263.

Prasanta, S., Sinha, R., 2010.Evolution of the Indian summer monsoon: synthesis of continental records. From: Clift, P. D., Tada, R. & Zheng, H. (eds) Monsoon Evolution and Tectonics–Climate Linkage in Asia. Geological Soc. London, Spec. Publ., 342, 153–183.

Quade, J., Cerling, T.E., Bowman, J.R., 1989. Development of Asian monsoon revealed by marked ecological shift during the latest Miocene in northern Pakistan. Nature 342, 163-166.

Qayyum, M., Lawrence, R. D., Niem, A. R., 1997. Discovery of the palaeo-Indus delta-fan complex. Journal of the Geological Society 154, 753-756, doi:10.1144/gsjgs.154.5.0753

Rodriguez, M., Fournier, M., Chamot-Rooke, N., Huchon, P., Bourget, J., Sorbier, M., Zaragosi, S., Rabaute, A., 2011.Neotectonics of the Owen Fracture Zone (NW Indian Ocean): structural evolution of an oceanic strike-slip plate boundary. Geochem., Geophys., Geosyst. 12, doi:10.1029/2011GC003731.

Rodriguez, M., Fournier, M., Chamot-Rooke, N., Huchon, P., Zaragosi, S., Rabaute, A., 2012. Mass wasting processes along the Owen Ridge (NW Indian Ocean). Mar. Geol. 326-328, 80-100, doi: 10.1016/j.margeo.2012.08.008

Royer, J. Y., Chaubey, A. K., Dyment, J., Bhattacharya, G. C., Srinivas, K., Yateesh, V., Ramprasad,T., 2002.Paelogene plate tectonic evolution of the Arabian and Eastern Somali basins.in The Tectonic and Climatic Evolution of the Arabian Sea Region, edited by P. D. Clift et al., Geol. Soc. Spec. Publ., 195, 7–23

Schlüter, H. U., Prexl, A., Gaedicke, C., Roeser, H., Reichert, C., Meyer, H., von Daniels C., 2002.The Makran accretionary wedge: sediment thicknesses and ages and the origin of mud volcanoes, Mar. geol. 185, 219-232.

Sepulchre, P., Ramstein, G., Fluteau, F., Schuster, M., 2006.Tectonic uplift and Eastern Africa aridification. Science 313, 1419-1423.

Sakai, T., Saneyoshi, M., Sawada, Y., Nakatsukasa, M., Mbua, E., Ishida, H., 2010. Climate shift recorded at around 10 Ma in Miocene succession of Samburu Hills, northern Kenya Rift, and its significance. From: Clift, P. D., Tada, R. &Zheng, H. (eds) Monsoon Evolution and Tectonics–Climate Linkage in Asia. Geol. Soc., London, Spec. Publ. 342,109-127, doi:10.1144/SP342.9

Waheed, A., Wells, N. A., 1990. Changes in paleocurrents during the development of an obliquely convergent plate boundary (Sulaiman fold-belt, southwestern Himalayas, west-central Pakistan). Sedimentary Geology 67, 237-261.

Waheed, A., Wells, N. A., 1992. Fluvial history of late Cenozoic molasse, Sulaiman range, Pakistan. Geol. Bull. Univ. Peshawar 25, 1-15.

Wang, P., Steven Clemens, S., Beaufort, L., Braconnot, P., Ganssene, G., Jiana, Z., Kershawf, P., Sarntheing, M., 2005. Evolution and variability of the Asian monsoon system: state of the art and outstanding issues. Quaternary Sci. Rev. 24, 595–629.

Wang, E., Kirby, E., Furlong, K. P., van Soest, M., Xu, G., Shi, X., Kamp, P. J. J., Hodges, K. V., 2012. Two-phase growth of high topography in eastern Tibet during Cenozoic. Nat. Geosci. 5, 640–645, doi:10.1038/ngeo1538

Weissel, J.K., Childers, V.A., Karner, G.D., 1992. Extensional and Compressional Deformationof the Lithosphere in the Light of ODP Drilling in the Indian Ocean.Synthesisof Results from

Scientific Drilling in the Indian Ocean. : Geophysical Monograph70, American Geophysical Union.

White, R. S., Klitgord, K., 1976. Sediment deformation and plate tectonics in the Gulf of Oman. Earth. Planet. Sci. Lett. 32, 199-209.

Whitmarsh, R.B., 1979. The Owen Basin off the south-east margin of Arabia and the evolution of the Owen Fracture Zone. Geophysical Journal of the Royal Astronomical Society 58, 441-470.

Wiens, D. A., Demets, C., Gordon, R. G., Stein, S., Argus, D., Engeln, J. F., Lundgren, P., Quible, D., Stein, C.,Weinstein, S., Woods,D. F., 1985. A diffuse plate boundary model for Indian ocean tectonics. Geophys. Res.Lett. 12, 429–432.

## Conclusions de l'article "The Owen Ridge uplift and the record of Asian paleo-climate"

*Les corps contouritiques de la marge est-omanaise et la circulation océanique depuis le Miocène terminal*

L'identification de corps contouritiques tout le long de la marge est-omanaise dès la phase de déformation à 8-9 Ma ouvre une perspective intéressante : les discontinuités dans la géométrie des corps contouritiques peuvent correspondre à des changements dans l'intensité des courants, qui dans la région est en partie contrôlée par le régime des moussons. Les forages situés dans la baie de Sauquarah peuvent fournir un contrôle temporel partiel sur la succession de ces discontinuités. Cependant, au vu de la complexité de l'architecture des corps contouritiques sur la marge, ce contrôle stratigraphique pourrait s'avérer insuffisant pour la compréhension du système sédimentaire... Les corps sédimentaires d'origine gravitaire (formés par les courants de turbidité) sont très souvent difficiles à différencier des corps formés par les courants de contour : comment courants de contour et courants de turbidité interagissent le long d'une marge est une question très complexe. Mais cette approche mérite d'être au moins tentée ! Déterminer l'origine du courant formant ces dépôts serait également d'un grand intérêt pour les reconstitutions de la paléo-circulation des courants de l'océan Indien au Miocène, période marquée par plusieurs évènements tel que la fermeture de la Parathétys.

*Le soulèvement de la Ride d'Owen et la relocalisation de la limite de plaque Inde-Arabie Fini-Miocène.*

Le fait que la ZFO semble se localiser et recouper la Ride d'Owen indépendamment de son relief est surprenant au premier abord (il est *a priori* plus facile d'imaginer que la faille passe au pied du relief). Ce type de configuration est cependant chose commune au niveau des transformantes océaniques (Figure 4), dont les rides transverses sont souvent recoupés par la transformante principale, souvent après un processus de migration de quelques kilomètres (*Bonatti et al., 1994; Sclater et al., 2005*). Dans la note précédente j'identifie la trace de la limite de plaque Inde-Arabie miocène au pied de la Ride d'Owen, enfouie à seulement quelques kilomètres de la trace de la ZFO actuelle. Le soulèvement de la Ride d'Owen à la fin du Miocène est probablement responsable de la relocalisation de la limite au niveau de l'OFZ actuelle. Un mécanisme, inspiré de travaux sur les failles normales (*Forsyth, 1992; Buck., 1993; Bonatti et al., 2005*) peut expliquer le rôle du soulèvement de la ride sur la

relocalisation de la faille. Il a été montré que la croissance du rejet d'une faille normale modifie le champ de contrainte autour de la faille. L'évolution du champ de contraintes au cours du jeu de la faille fait qu'il devient de plus en plus difficile pour la faille de continuer à se développer au cours du temps. Il se peut alors qu'une nouvelle faille se forme, alors que la faille initiale s'inactive. Moins le plan de faille initial est résistant, et plus le rejet développé sur ce plan sera important avant que le développement d'une nouvelle faille ne devienne nécessaire. *Buck (1993)* a montré que plus l'épaisseur élastique de la lithosphère est importante, plus la résistance au rejet est forte. *Buck (1993)* montre également que la topographie formée au cours du rejet sur la faille est fonction de l'épaisseur élastique de la lithosphère, i.e. de son âge dans le cas de la lithosphère océanique.

Appliqués à la limite de plaque Inde-Arabie, ces travaux pourraient fournir la clé de la compréhension de son évolution structurale au Miocène. Du fait de contraintes probablement transpressives (selon les plis identifiés au pied de la ride) appliquées dès le changement cinématique initié à 11 Ma, la transformante miocène aurait accumulé les contraintes nécessaires au soulèvement de la ride; puis se serait inactivée une fois son rejet critique atteint, ce dernier étant déterminé par l'épaisseur élastique de la lithosphère. Une nouvelle transformante se localise alors à proximité : la Zone de Fracture d'Owen. La ZFO a fonctionné majoritairement de façon purement dextre depuis sa mise en place (du moins au niveau des segments sud et central), mais les quelques plis identifiés sur la bathymétrie (*Fournier et al., 2011; Rodriguez et al., 2011*) suggèrent qu'un peu de transpression s'accumulerait au niveau de la ZFO. Ce scénario doit être précisé par l'étude de la cinématique de la limite de plaque Inde-Arabie à partir des anomalies magnétiques, travaux en cours de réalisation par N. Chamot-Rooke. Il a été montré pour la transformante de la Romanche que des mécanismes similaires à ceux exposés ci-dessus pouvaient expliquer la surrection de rides transverses de plusieurs milliers de mètres de haut en seulement un ou deux millions d'années (*Bonatti et al., 2005*).

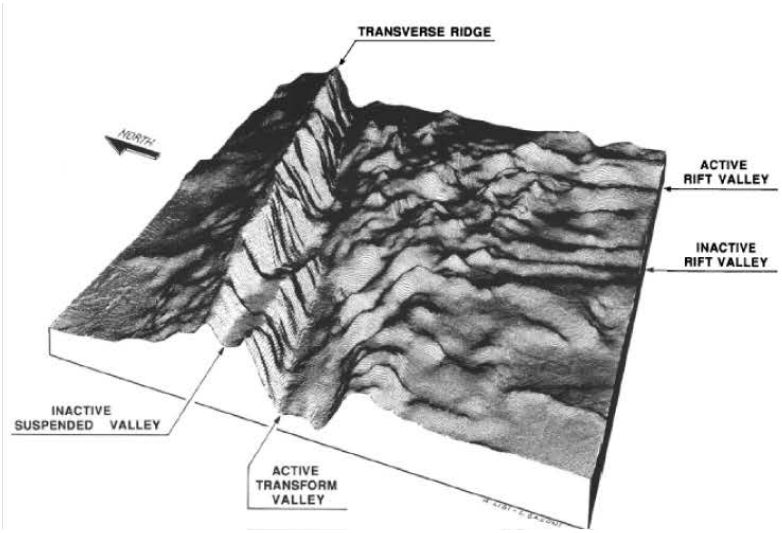


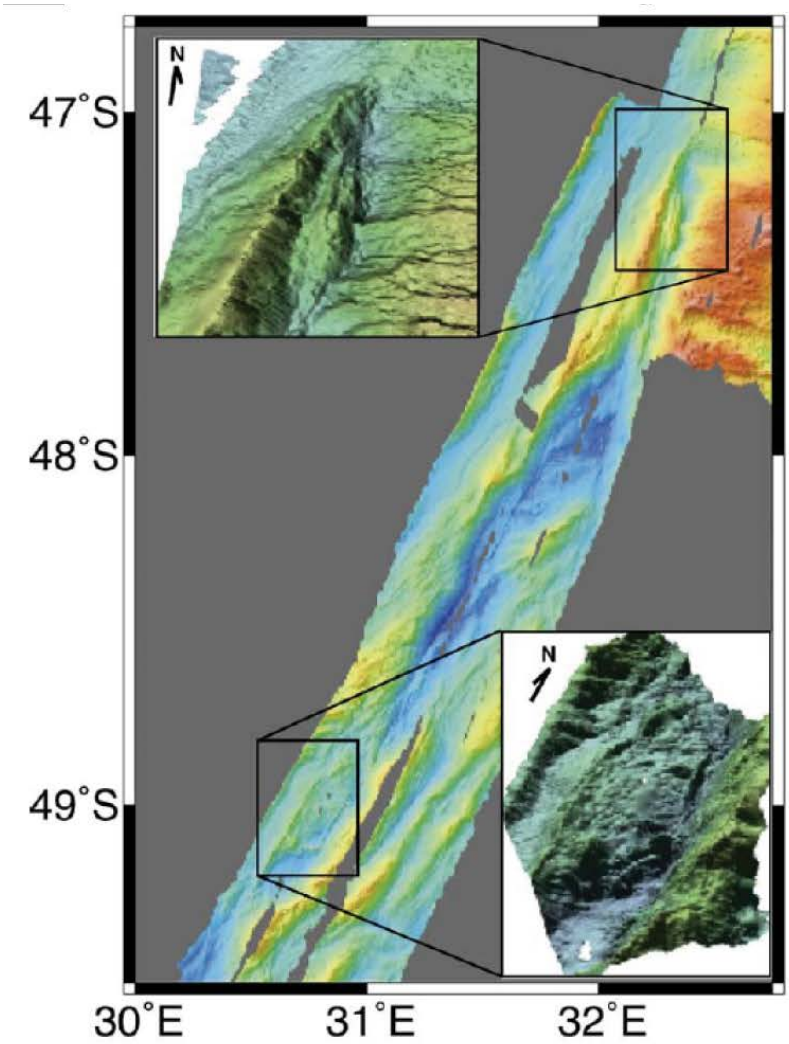


*Figure 4 : Vues 3D de rides transverses associées à la transformante de la Romanche (Atlantique) (Haut, Bonatti et al., 1994) et à la transformante d'Andrews-Bain (Océan Indien) (Bas; Sclater et al., 2005). Ces deux rides sont recoupées par la faille transformante principale.*


*Planche IV : Dessin à l'encre de chine de la place de Salalah, au sud de l'Oman ; où nous nous étions arrêtés prendre le thé quelques heures avant d'embarquer à bord du Beautemps-Beaupré.*

# Chapitre 5 : A la recherche de la limite de plaque Inde-Arabie au cours du Paléogène

Ce chapitre est principalement basé sur un article en préparation pour la revue Tectonics. Il s'intitule "*Tracking the India-Arabia Plate boundary since Paleocene to Early Miocene times*", et s'attaque à la question de la localisation de la limite de plaque Inde-Arabie avant le Miocène, détaillée en chapitre 1. Du fait de l'arrivée tardive des données d'Owen 2 et des contraintes de temps liées à la thèse, je n'ai pu finaliser comme je l'aurais souhaité cette étude, qui mérite encore quelques mois de réflexion. Néanmoins, en l'état actuel, cette étude présente déjà quelques résultats intéressants, qui je pense suffisent à alimenter une première discussion. Les profils sismiques présentés dans cette étude permettent d'établir un premier cadre stratigraphique du Bassin d'Owen, révèlent plusieurs traces potentielles d'activité de failles transformantes, ainsi que des lambeaux de l'ophiolite de Masirah gisant sur le socle du bassin. La morphologie du socle du bassin est aussi révélée, et présente plusieurs similitudes avec la morphologie de systèmes transformants et de zone de fracture actuels. Cependant, les traces de déformation ne peuvent pas toujours être corrélées à des forages, et les directions des déformations observées sont difficiles à déterminer, ce qui complique les reconstitutions de l'histoire de la limite de plaque. Le cadre chronologique est basé sur les anomalies magnétiques de la région (non identifiées dans le Bassin d'Owen), et les âges des principaux évènements géodynamiques. Le résultat principal de ce projet de note est l'identification d'une réorganisation structurale majeure de la marge omanaise vers la fin de l'Eocène (marquée par la formation de rides marginales), probablement en lien avec la formation du Zagros et l'ouverture du golfe d'Aden, et ayant probablement impliqué le transfert d'un large segment de la plaque Inde à la plaque Arabie. La réorganisation de la limite de plaque Inde-Arabie semble fortement associée à la phase d'accrétion ultra-lente de la dorsale de Carlsberg reconnue entre 25 et 40 Ma.

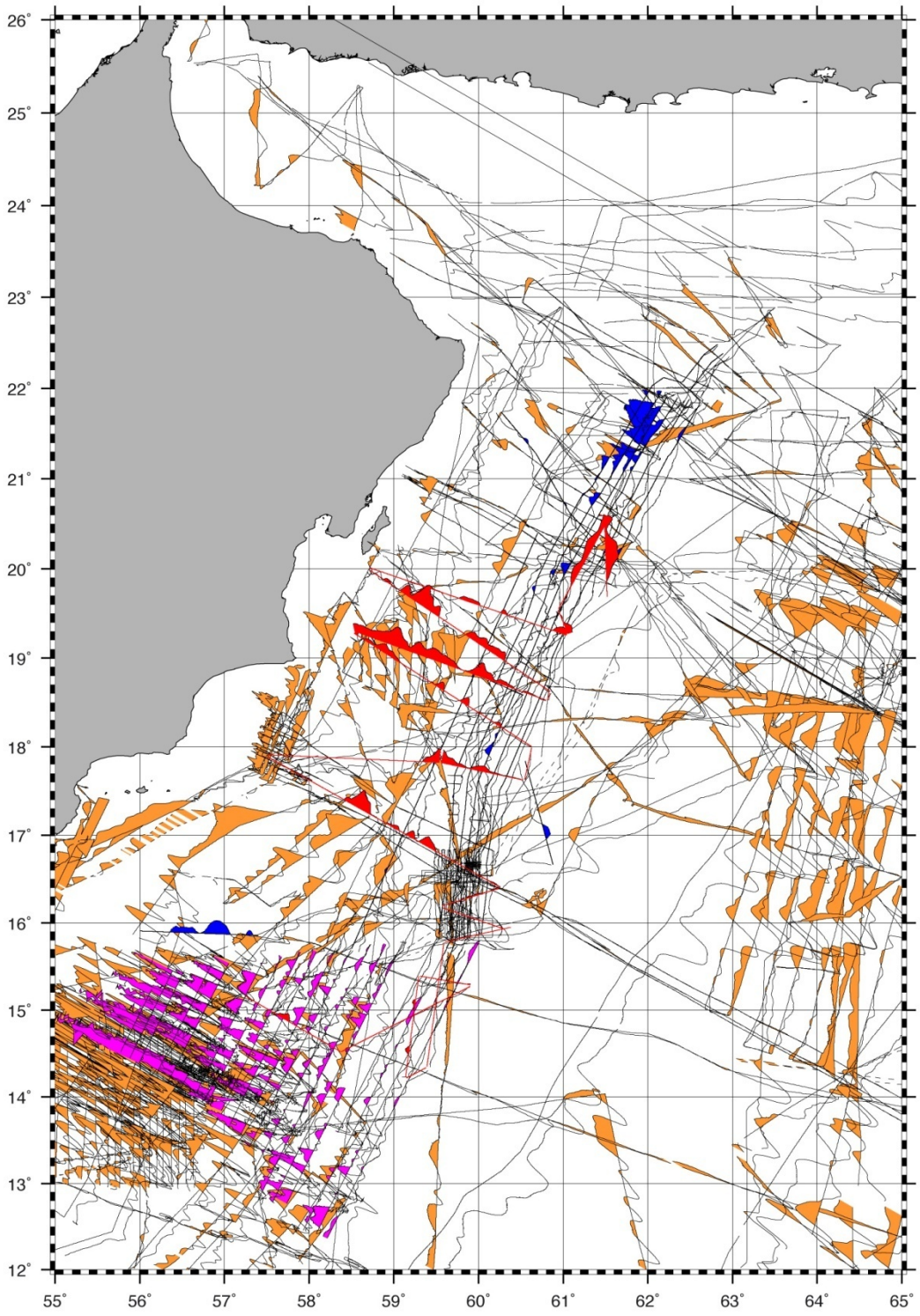


*Figure 1 : Compilation des mesures du champ magnétique dans la région du Bassin d'Owen (Fournier, com. pers.). Le bassin d'Owen est riche en anomalies magnétiques, ce qui indique très probablement une nature océanique. Il demeure toutefois difficile d'identifier les anomalies dans ce bassin : quelques indices sont présentés dans le projet d'article qui suit.*

**Tracking the India-Arabia Plate boundary since Paleocene to Early Miocene times : implications for the origin of the Owen Basin off Oman**

Mathieu Rodriguez[1,2,3*], Nicolas Chamot-Rooke[3], Marc Fournier[1,2], Philippe Huchon[1,2], Matthias Delescluse[3], Thomas François[1,2]

(1) Institut des Sciences de la Terre de Paris, CNRS UMR 7193, Université Pierre & Marie Curie, case 129, 4 place Jussieu, 75005 Paris, France

(2) iSTeP, UMR 7193, CNRS, F-75005 Paris, France

(3) Laboratoire de Géologie de l'Ecole normale supérieure de Paris; CNRS UMR 8538, 24 rue Lhomond, 75005 Paris, France

**Corresponding author*: rodriguez@geologie.ens.fr

*in prep. for TECTONICS*

**Abstract**

**The location of the India-Arabia plate boundary prior to the formation of the Sheba ridge in the Gulf of Aden is a matter of debate. A seismic dataset crossing the Owen Fracture Zone, the Owen Basin, and the Oman Margin was acquired to track the past locations of the India-Arabia plate boundary. We highlight the composite age of the Owen Basin basement, made of Paleocene crust drilled on its eastern part, and composed of pre-Maastrichtian crust overlaid by Early Paleocene ophiolites on its western side. A major transform fault crossing the Owen Basin juxtaposed these two slivers of lithosphere of different ages. This transform system inactivated in response to a kinematic change in Late Eocene-Early Oligocene times, evidenced by the uplift of marginal ridges along the Oman Margin. The transform system then shifted to the edge of the present-day Owen Ridge during the Oligocene, before seafloor spreading began at the Sheba Ridge. This migration of the plate boundary involved the transfer of a part of the oceanic lithosphere accreted at the Carlsberg Ridge to the Arabian plate. Consequently, the lithosphere subducting beneath the Makran derived from the Late Cretaceous Indian Ocean (and not the Neotethys). The episode of plate transfer at the India-Arabia plate boundary relates in time with the 25-40 Ma ultra-slow spreading episode at the Carlsberg Ridge, and with major geological events at the Zagros belt. The Owen Ridge uplifted in Late Miocene times, and was not associated to the Oligocene kinematic change.**

## 1. Introduction

The Zagros and Himalaya mountain belts are the most prominent reliefs built by continental collision. They respectively result from Arabia and India collision with Eurasia. Convergence motions at the origin of the Zagros and Himalaya mountains have been responsible of most of plate reorganization events in the Indian Ocean during the Cenozoic [*Molnar et al.*, 1993; *Patriat et al.*, 2008; *Hatzfeld and*

*Molnar*, 2010]. Although critical for paleogeographic reconstitutions [*Cande et al*., 2010; *Gibbons et al.*, 2013], the way relative motion between Arabia and India was accommodated since its inception ~90 Ma ago remains poorly understood. The India-Arabia plate-boundary belongs to the category of long-lived (~100-Ma) oceanic transform boundaries, including the Romanche (central Atlantic Ocean) or the Andrew-Bain (SW Indian Ocean) transforms [*Ligi et al*., 2002]. The India-Arabia plate-boundary provides a good case study to investigate the role of kinematic events over the structural evolution of a long-lived transform system.

The present-day India-Arabia plate boundary is a 800-km-long strike-slip fault known as the Owen Fracture Zone (OFZ hereafter) (Figure 1).The OFZ runs along the Owen-Murray Ridge system, a series of prominent oceanic reliefs that currently isolate the Owen Basin to the west from the Indus turbiditic system to the east. The general trend of the OFZ (8°NE) differs from the trend of the Owen Transform (30°NE), which offsets the Carlsberg and Sheba Ridges over 250-km (Figure 1). Morphological offsets of the Owen Ridge indicate a finite dextral displacement of 10-12 km along the active trace of the OFZ [*Fournier et al*., 2011]. Assuming a steady-state motion for the recent times ($3 \pm 1$ mm.a$^{-1}$), the present-day trace of the OFZ is Pliocene in age (3-6 Ma) [*Fournier et al*., 2008; 2011]. This age drastically contrasts with the age estimated for the onset of the India-Arabia relative motion, assumed to begin at ~90 Ma in reconstitutions (formation of Chain Ridge [*Bunce et al*., 1967; *Cochran*, 1988] and opening of the Mascarene Basin [*Besse and Courtillot*, 1988], and raises the question of the location and the structure of the pre-Pliocene plate-boundary.

According to magnetic anomalies recorded in the Arabian Sea, the India-Arabia plate boundary is supposed to run along the Owen Ridge during the Miocene [*Chamot-Rooke et al.*, 2009], but no clear structural evidence of the fault has been provided up to now. On the other hand, conflicting views have been proposed with regards to the location of the India-Arabia boundary prior to the beginning of seafloor spreading in the Gulf of Aden (Figure 2) [*Whitmarsh*, 1979; *Mountain and Prell*, 1990; *Edwards et al.*, 2000; *Royer et al*., 2002]. Whereas *Whitmarsh* [1979] postulated that the India-Arabia plate boundary has still close to its present-day location since Late Cretaceous times, *Mountain and Prell* [1990] proposed that Paleogene strike-slip motion took place at the edge of the Oman margin. Paleogeographic reconstitutions based on magnetic anomalies also suggest the plate-boundary was located in the Owen Basin during those times [*Royer et al.*, 2002], and may have undergone at least one significant reorganization event. Although critical to unravel the past locations of the India-Arabia plate boundary, the structure of the Owen Basin has never been documented with the exception of preliminary works by *Mountain and Prell* [1990] and *Barton et al.* [1990] (Figure 1c).

In March 2012, we surveyed the Owen Basin onboard the French R/V *Beautemps-Beaupré* in order to track the pre-Pliocene traces of the India-Arabia plate boundary. About 5000-km of seismic lines crossing the Owen Basin, the Owen Ridge, and the OFZ were acquired. Seismic lines are calibrated with the DSDP and ODP drillings available in the area to define the stratigraphic framework of the basin and the age of the deformation episodes. The objective of this study is to locate and describe the

structure of the India-Arabia plate boundary prior to the activation of the OFZ, with a peculiar emphasis over the Paleogene period, i.e. the period of separation of Arabia from Africa. We then discuss the implications for the origin of the lithosphere subducting beneath the Makran.

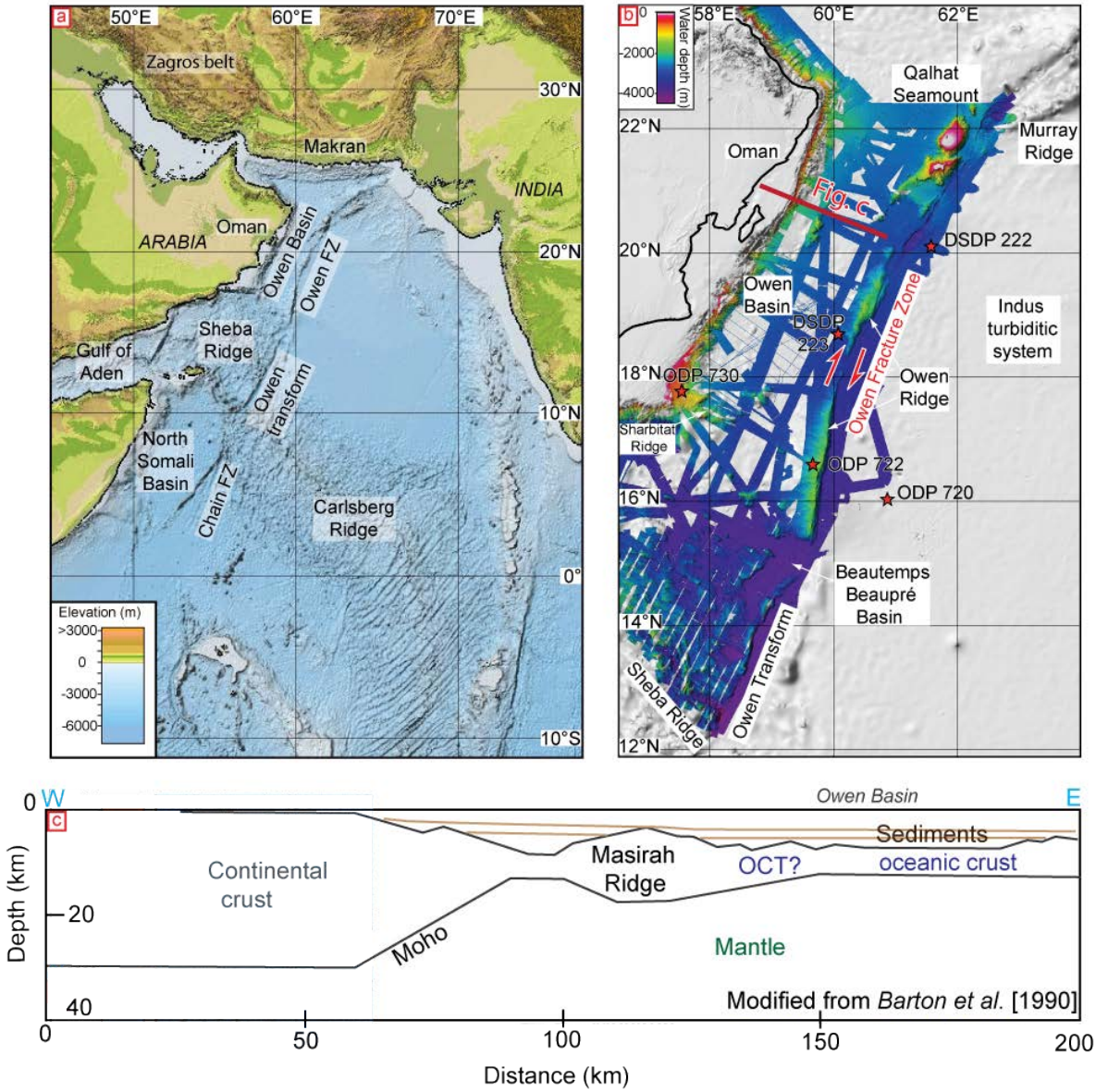


***Figure 1 :*** *a) General map of the western Indian Ocean (FZ : Fracture Zone); b) Multibeam bathymetry of the Owen Basin, compiled with SRTM topography at 30". c) Deep-structure of the Owen Basin deduced from wide-angle seismic data [Barton et al., 1990]. OCT: inferred ocean-continent transition.*

## 2. Geological background

### *2.1. Geological history of the Arabian Sea and the India-Arabia plate boundary*

The record of magnetic anomalies related to the onset of oceanic spreading at the Carlsberg Ridge began about 63 Ma ago (A28), in response to a transition in the Deccan hotspot activity following the episode of Seychelles-India breakup and the formation of the Gop Basin [*Minshull et al.*, 2008; *Yateesh et al.*, 2009; *Calvès et al.*, 2011]. A continuous record of magnetic field inversion revealing paleo-propagators is available from chrons 27 to 20 (i.e. from 60 to 40 Ma) (Figure 3) [*Chaubey et al.*, 1998; *Dyment*, 1998; *Chaubey et al.*, 2002; *Royer et al.*, 2002]. An episode of slowing-down of seafloor spreading at the Carlsberg Ridge (chrons 25-26) documents India's collision with Eurasia around 50-40 Ma (between chrons 24n and 18) [*Patriat and Achache*, 1984; *Hatzfeld and Molnar*, 2010]. From chrons18 to 7 (i.e. from ~40 to 24Ma), a period of ultra-slow spreading probably involving propagators occurred at the Carlsberg Ridge (Figure 3) [*Mercuriev et al.*, 1996]. The onset and the termination of this ultra-slow spreading episode induced drastic changes in the mean spreading direction of the Carlsberg Ridge [*Mercuriev et al.,* 1996]. The rifting of the Gulf of Aden [*Bosworth et al.*, 2005; *Leroy et al.*, 2010] and the episode of ultra-slow spreading at the Carlsberg Ridge followed the onset of continental underthrusting at the Zagros belt between ~36-40 and 25 Ma (Figure 2) [*Agard et al.*, 2011; *Mouthereau et al.*, 2012]. The separation of Arabia from Africa was enhanced by the development of the Afar hotspot about 30 Ma ago [*Bosworth et al.*, 2005].

The magnetic anomaly record suggests useful hypothesis about the past locations of the India-Arabia plate boundary (Figure 3). Because the magnetic anomalies recorded over the Owen Basin and the North Somali Basin have never been related to the magnetic time-scale, the age of the crust in the Owen Basin and the Makran subduction Zone, together with the amount of relative motion accommodated by the India-Arabia boundary, remains a matter of debate [*Edwards et al.*, 2000]. In spite of these drawbacks, the magnetic anomaly record at the Carlsberg Ridge documents at least 1000-km of left-lateral relative motion somewhere east of Oman prior to the Himalayan collision [*Royer et al.*, 2002]. Subsequently to the Himalayan collision, the India-Arabia relative motion remained sinistral prior to the opening of the Gulf of Aden, India travelling fast towards Eurasia while Arabia was still attached to Africa (Figure 2) [*Besse and Courtillot*, 1988].The amount of relative motion accommodated during the Oligocene is unknown. The reconstitution of the India-Arabia motion since 20 Ma based on magnetic anomalies recognized at both the Sheba [*Fournier et al.*, 2010] and Carlsberg [*Mercuriev and DeMets*, 2006] ridges suggests that dextral strike-slip motion remained located along the present-day Owen Ridge since the first stages of seafloor spreading in the Gulf of Aden 20 Ma ago, accommodating 70-km of relative motion between 17 Ma and the emplacement of the OFZ [*Chamot-Rooke et al.*, 2009]. The present-day trace of the OFZ observed on the seafloor would then be the latest stage of structural evolution of this strike-slip system, older traces being buried under the Indus fan [*Rodriguez et al.*, 2011].

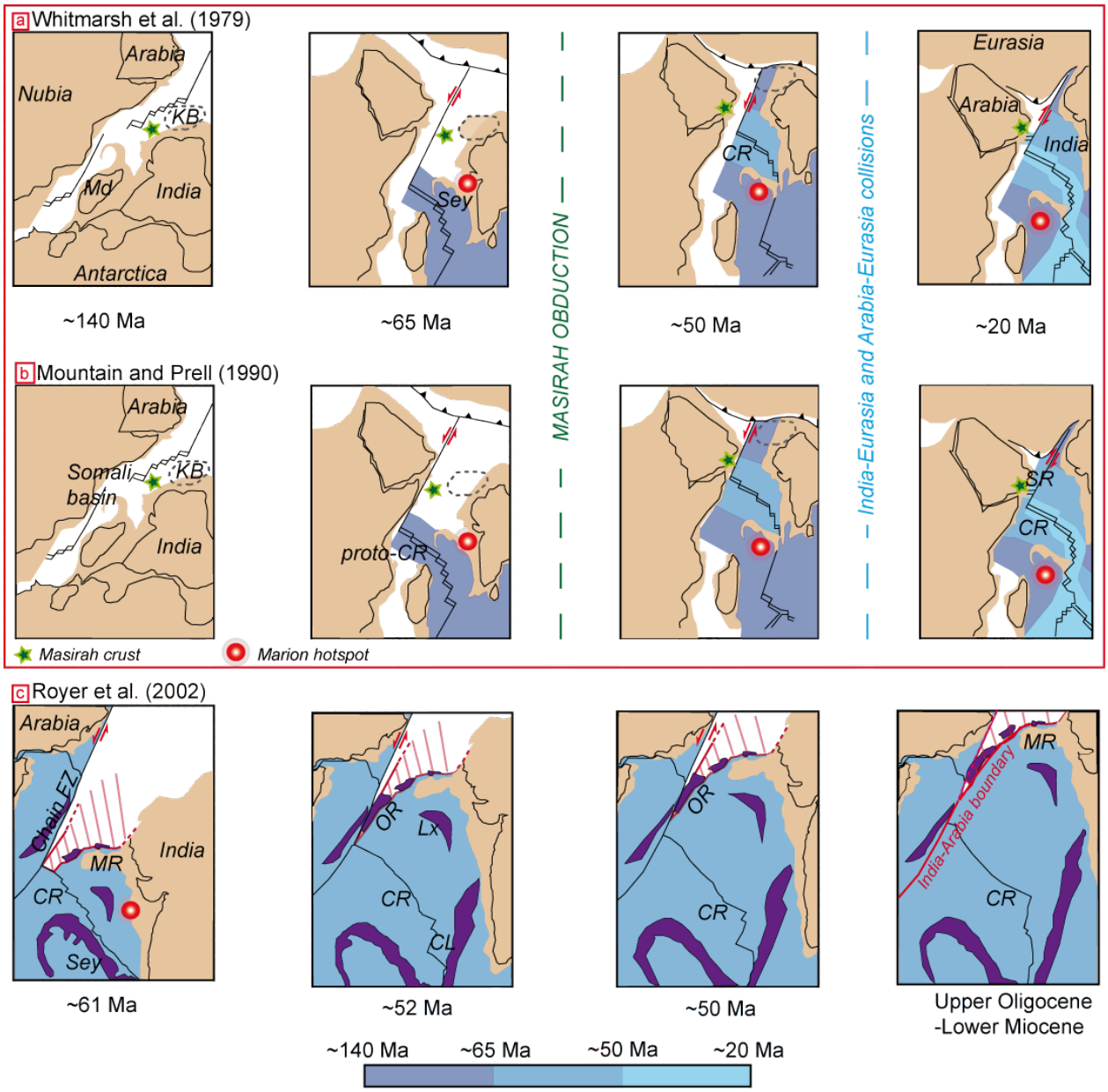


***Figure 2 :*** *Reconstitutions of the India-Arabia relative motion since Tithonian times according to a) Whitmarsh et al. [1979] and b) Mountain and Prell [1990]. The first reconstitution assumes that the India-Arabia plate boundary stayed close to its present-day location since Late Cretaceous times, while the second one hypothesizes that the plate-boundary was located further west along the Oman margin during Paleogene times, and then moved to its present-day location at the Early Miocene. c) Paleogeographic reconstitutions from Paleocene to Oligocene based on magnetic studies [Royer et al., 2002] also imply a location of the Paleogene India-Arabia plate boundary in the Owen Basin. Hatched areas represent the piece of Indian plate transferred in Oligocene times. CL :Chagos Lacadive Ridge; CR : Carlsberg Ridge; KB : Kabul Bloc; Lx : Laxmi Ridge; Md : Madagascar; MR : Murray Ridge; OR : Owen Ridge; Sey : Seychelles; SR : Sheba Ridge.*

*2.2. Previous reconstitutions of the India-Arabia relative motion*

2.2.1. Reconstitutions from *Whitmarsh* [1979]

First paleogeographic reconstitutions from *Whitmarsh et al.* [1979] suggests that the India-Arabia plate boundary has still at its present-day location since India started to move northwards at ~90 Ma (Figure 2). This reconstitution considers that the OFZ is the conjugate of the Chain Fracture Zone, which marks the present-day India-Somalia plate-boundary (Figure 1). This reconstitution implies a Jurassic-Early Cretaceous age of the Owen Basin basement, which is considered as a remnant of the Gondwanaland break-up.

2.2.2. Reconstitutions from *Mountain and Prell* [1990]

In this second model, the India-Arabia plate-boundary initially laid along the East Oman margin (forming its abrupt slope typical of a transform margin), while the Mascarene Basin opened and when the Carlsberg Ridge developed (Figure 2) [*Mountain and Prell*, 1990].The India-Arabia plate boundary then switched to its present-day position about 20 Ma ago, when seafloor spreading started at the Sheba Ridge. This inferred jump of the India-Arabia plate-boundary marks the inactivation of strike-slip motion along the Oman margin, and may be responsible for the Owen Ridge uplift. This model implies an Upper Cretaceous- Early Paleocene age for the Owen Basin, which was formed by a spreading center subsequently subducted in the Makran subduction zone. The latter is in good agreement with the oldest rocks drilled in the Owen Basin, which are trachybasalt overlaid by sediments of Paleocene age (Figure 4) [*Shipboard Scientific Party*, 1974, 1989]. The reconstitution of *Mountain and Prell* [1990] implies that the crust of the Masirah Ophiolites located on the Oman Margin is Upper-Cretaceous.

2. 2. 3. Reconstitutions from *Royer et al.* [2002]

The last reconstitution to date is supported by the record of magnetic anomalies over the Arabian Sea(*Royer et al.* [2002]) (Figure 2).In contrast with *Whitmarsh* [1979], these reconstitutions show that the present-day OFZ cannot be the conjugate of the Chain Fracture Zone prior to the opening of the Gulf of Aden. The latter is consistent with the Pliocene age of the OFZ estimated by *Fournier et al*. [2008, 2011]. According to *Royer et al*. [2002], the conjugate of the Chain Fracture Zone must cut obliquely through the Owen Basin, and therefore constitutes a good candidate as a fossil plate-boundary. Considering the India-Arabia plate-boundary at its present-day location for the entire Cenozoic time span would imply a major subduction zone in the area of the Murray Ridge complex between chrons 27 and 20, which is not observed.

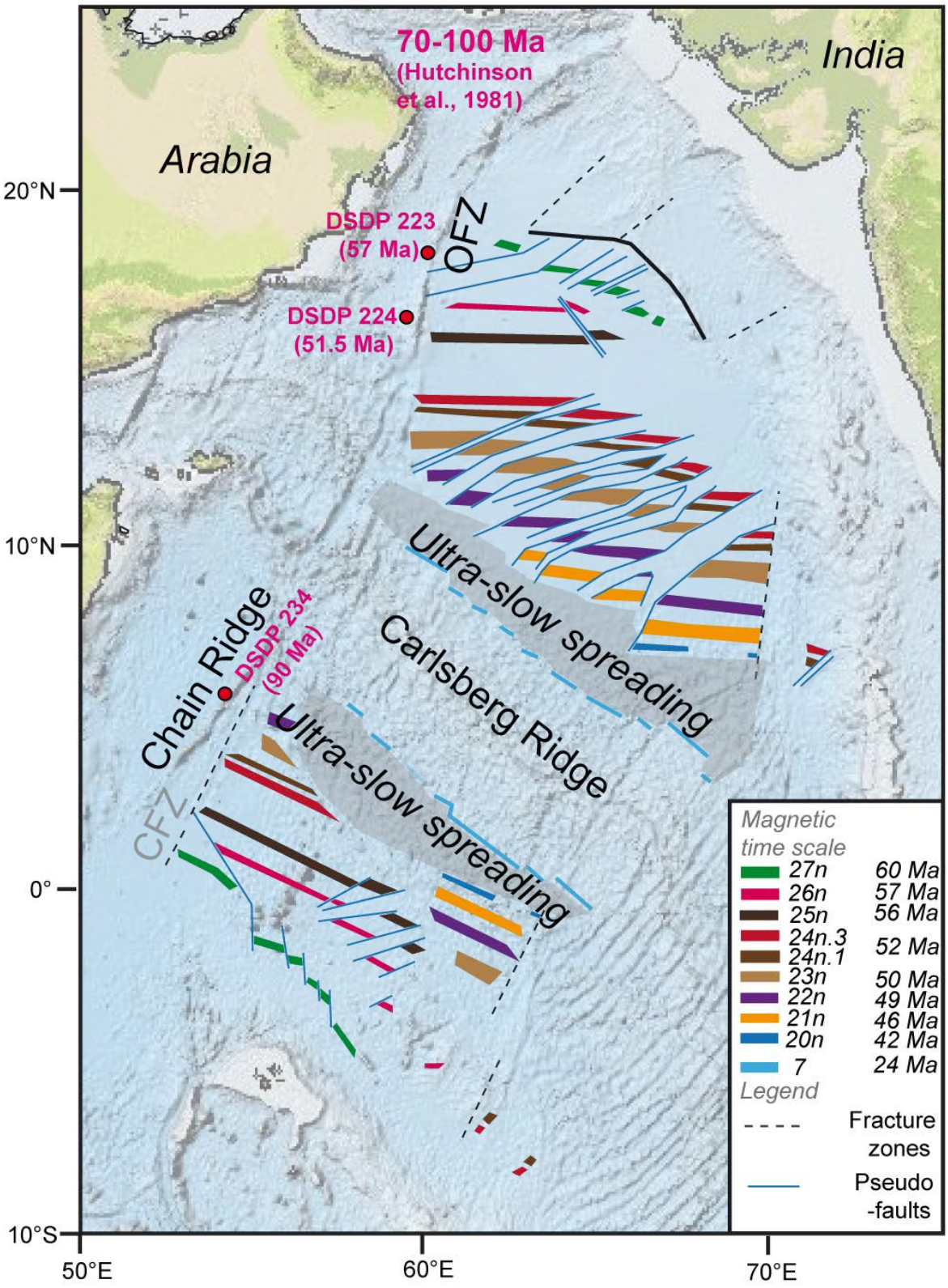


***Figure 3 :*** *Magnetic anomalies map over the Arabian Sea, modified from Mercuriev et al. [1996] and Chaubey et al. [2002], and ages of basement from deep-sea drillings. Note that the distance between 51.5 and 57 Ma-old basements in the Owen Basin is roughly the same as the distance between anomalies 24n3 and 25n in the Arabian Sea. CFZ : Chain Fracture Zone.*

*2. 3. The Oman margin during Mesozoic times*

2. 3. 1. The Masirah obduction

A critical point of the model exposed by *Mountain and Prell* [1990] is the age of the Masirah Ophiolitic body, which is expected to be Late Cretaceous in age. Parts of the Masirah ophiolitic body are observed along the Oman margin at the location of Ras Madraka, Ras Jib'sch, and the Island of Masirah. Eocene limestone deposits overly unconformably the Masirah ophiolites [*Immenhauser et al.*, 1996], whereas Upper-Cretaceous (Maastrichtian) formations are folded in the Batain Plain to the North-East of Oman [*Schreurs and Immenhauser*, 1999].This set of evidences indicates an Upper Cretaceous-Early Paleocene age of the obduction [*Immenhauser*, 2000], distinct from the obduction of the Semail ophiolites in Campanian times. Paleomagnetic studies show that the accretion of the Masirah oceanic crust occurred at the latitude of ~30-50°S (Figure 2) [*Gnos and Perrin*, 1997]. Radiometric ages documents a Tithonian age for the accretion [*Peters and Mercolli*, 1998]. The oceanic lithosphere exposed at the Masirah Island thus corresponds to a piece of the Indian Ocean formed during the earlystages of Gondwanaland break-up and the opening of the Somali Basin (Figure 2) [*Peters and Mercolli*, 1998]. An important northwards motion of the initial oceanic crust is necessary to the Masirah obduction, which lead *Gnos and Perrin* [1997] to assume that the Masirah ophiolitic body used to be a part of the Indian plate (Figure 2). These results do not fit the reconstitution of *Mountain and Prell* [1990].

2. 3. 2. Evidences of Cretaceous strike-slip motion

A past location of the India-Arabia plate-boundary close to the Oman Margin would have implied the record of significant strike-slip motion during Cretaceous (Figure 4). Several strike-slip features are observed, including the Sawain-Nafun Fault System in the Huqf desert [*Ries and Shackleton*, 1990], the Maradi Fault Zone [*Filbrandt et al.*, 2006] and the Jebel Ja'alan-Qalhat Fault System in the North-East of Oman [*Filbrandt et al.*, 1990]. *Ries and Shackleton* [1990] noticed a Santonian-Campanian phase of activity of the Sawain-Nafun system. Northwards, seismic lines crossing the Maradi Fault Zone display flower structures that indicate a coeval strike-slip activity (with evidences of Late Cretaceous pull-apart and sinistral motion) [*Filbrandt et al.*, 2006]. Morphological offsets of the Khufai, Shuram, Anquau, and Mahatta Humaid folds also indicate a left-lateral activity of the Sawain-Nafun System during the Upper Cretaceous-Paleocene interval [*Pilcher et al.*, 1996]. A Cretaceous activity of strike-slip faults is also reported on the Somali margin [*Bosselini*, 1986].

### 2. 3. 3. Age of the Owen Basin and comparison with East-Africa Basins

A part of the Owen Basin may have an origin similar to its North Somali conjugate (Figure 1). The North Somali Basin used to be connected with the West Somali Basin by a set of transform faults referred as the Dhow-VLCC-ARS complex [*Cochran*, 1988]. According to paleogeographic reconstitutions, the North Somali Basin appears to be the third of a series of oceanic basins separated by long transform faults (>2000 km for the Davie transform) created during Mesozoic relative motion between West and East Gondwanaland [*Cochran*, 1988]. However, the Paleocene age of the oldest sediments drilled at the Owen Ridge (Figure 4) [*Shipboard Scientific Party*, 1989; *Mountain and Prell*, 1990] does not support the Jurassic-Early Cretaceous age inferred by comparison with the East-African margin [*Whitmarsh*, 1979]. On the other hand, thermal flux analysis in the Gulf of Oman suggests an Upper Cretaceous age of the northernmost part of the Owen Basin [*Hutchison et al.*, 1981].

## 2. 4.*The Oman margin during Cenozoic times*

### 2. 4. 1. Evidences of Cenozoic strike-slip motion

Some workers suggested that the Masirah Ophiolites have been affected by strike-slip faults [*Moseley and Abbotts*, 1979], but others interpreted the same structures as thrust faults [*Peters and Mercoli*, 1998]. Offshore, *Mountain and Prell* [1990] hypothesized the presence of flower-structures on low-quality seismic lines collected on the Oman Platform (Sauquara Bay), subsequently referred as the Masirah Transform in the literature [*Loosveld et al*., 1996]. The deep structure of the Owen Basin basement revealed by seismic refraction data [*Barton et al.*, 1990] displays juxtaposed blocs with large and abrupt changes in crustal thickness (Figure 1c), a feature commonly observed along transform margins as strike-slip motion favors the juxtaposition of individual blocs at different stages of isostatic compensation. *Barton et al*. [1990] proposed that a paleo-transform boundary might have helped the Masirah obduction.

### 2. 4. 2. The Owen-Murray Ridge uplift

The uplift of the Owen Ridge was first related to an angular unconformity between Oligocene pelagic chalk and Early Miocene turbidites drilled at DSDP site 223 at the western side of the central Owen Ridge (Figures 4, 5) [*Whitmarsh et al*., 1974, 1979]. The same unconformity is observed on seismic profiles crossing the southern Owen Ridge, showing the onlap of Early Miocene turbidites over the Oligocene deposits (the turbidite immediately overlying Oligocene chalks being biostratigraphically dated at 19.6 Ma) (Figure 5). ODP reporters of Leg 117 subsequently suggested a depositional origin for this angular unconformity, i.e. a simple transition from Oligocene pelagites to Early Miocene

turbidites as the reliefs formed by the substratum of the Owen Basin gets progressively buried under the Indus deep-sea fan [*Mountain and Prell*, 1990]. ODP reporters interpreted a 14-15 Ma-old mixed pelagic-turbiditic sequence, as the uppermost part of the turbiditic plume being deposited during the first stages of ridge uplift. However, this transitional facies has been drilled on the levee of a fossil turbiditic channel (Figure 5b) and simply indicates a process of channel over-spilling. The uplift of the Owen-Murray Ridge system is therefore much younger than 15 Ma, but predates the onset of the present-day OFZ in the Pliocene [*Fournier et al.*, 2008]. In spite of these strong limitations, the age of uplift of the Owen Ridge (and, by extrapolation, the age of the Murray Ridge) is generally assumed as a proof of a migration of the India-Arabia plate boundary at ~20 Ma, i.e. coeval with the beginning of oceanic accretion at the Sheba Ridge [*Whitmarsh*, 1979; *Mountain and Prell*, 1990; *Edwards et al.*, 2000; *Gaedicke et al.*, 2002].

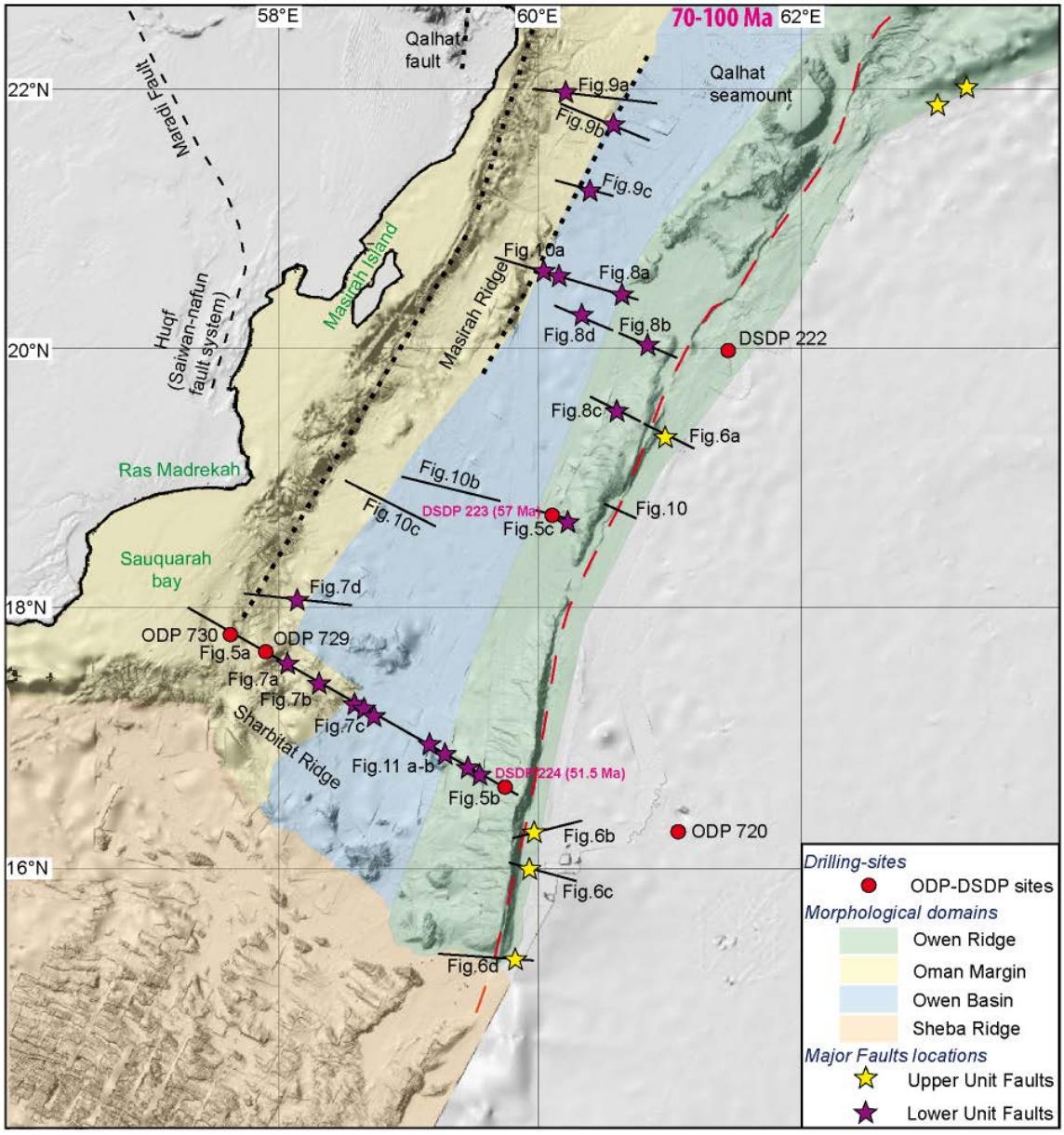

***Figure 4*** *:Bathymetric map of the Owen Basin. The Owen Basin area is divided in three morphological domains : the Oman margin, the Owen Basin, and the Owen Ridge. Stars represent the location of the major faults identified in this study; yellow stars represent faults active during the deposition of the Upper Unit, and purple stars represent faults active during the deposition of the Lower Unit. Location of seismic profiles presented in this study. Same horizontal scale for all profiles.*

## 3. Material and Methods

### 3. 1.Dataset

The dataset presented in this study was acquired onboard the French vessel *Beautemps-Beaupré* during the Owen-1 (2009), and Owen-2 (2012) surveys. Multi-beam bathymetry was collected using a Kongsberg-Simrad EM 120, which provides a DEM at 80 m grid interval, missing areas being filled-in by the SRTM 30" bathymetry. The Owen-2 seismic reflection dataset was acquired using two GI air-guns and a 600 m-long streamer. The common mid-point (CDP) spacing was 6.25 m. The high speed acquisition has a limited subsurface penetration of ~2s TWT. The processing consisted in geometry setting, water-velocity normal move-out, stacking, water-velocity F-K domain post-stack time migration, bandpass filtering, and automatic gain control (AGC). All the profiles are displayed with a vertical exaggeration of 8 at the seafloor. The reflectors picked on seismic profiles have been selected upon the base of seismic discontinuities that either reflect lithological changes, stratigraphic hiatuses or tectonic deformation.

### 3.2. Calibration with ODP and DSDP drillings

The Arabian Sea was the subject of drilling legs DSDP and ODP (Figure 3) [*Shipboard Scientific Party*, 1974, 1989]. Only one drilling (DSDP site 223) is available in the Owen Basin at the latitude of the central segment of the Owen Ridge, and penetrates the sedimentary cover down to its basement. Four drilling sites are located on the southern segment of the Owen Ridge (sites ODP 721, 722, 731, site DSDP 224, the latter penetrating down to the basement). Unfortunately, the western flank of the southern ridge is dissected by numerous and voluminous landslides [*Rodriguez et al.*, 2012; 2013a] that preclude any reliable detailed correlation with the Owen Basin. Eight ODP drillings sites are available on the Oman Margin at the latitude of the Sharbitat Ridge, the deepest reaching the middle Miocene (ODP site 730). ODP Site 729 is located in a horst structure (hereafter defined as the Sauquarah Ridge) and sampled a major unconformity between Eocene and Pleistocene sediments. Stratigraphic correlations with the Owen Basin are difficult because of abrupt faults dissecting the margin, however some events can be clearly recognized upon the base of an erosion surface that can be correlated from the margin to the basin.

## 4. Stratigraphic framework

The Indus abyssal plain mainly consists in turbidites alternating with pelagic deposits, with well-developed channel-levee systems since the Middle Miocene (Figure 6) [ODP site 720 and DSDP site 222; *Shipboard Scientific Party*, 1974; 1989; *Clift et al.*; 2001; 2002; *Clift and Gaedicke*, 2002].The stratigraphic framework of the Owen Basin is divided in two major units according to differences in their seismic character and a regional unconformity. The determination of the nature of sedimentary deposits is based upon calibration with DSDP and ODP deep-sea drillings and their seismic facies.

### *4. 1. Lower Unit (Paleocene to Late Oligocene)*

A Paleocene to Oligocene unit, composed of nanno-chalk and claystone, was drilled at DSDP sites 223 and 224 at the Owen Ridge (Figure 5c) [*Shipboard Scientific Party*, 1974]. The very slow sedimentation rates calculated at drilling sites (in the order of 5-20 m. $Ma^{-1}$) [*Shipboard Scientific Party*, 1974], together with the configuration of sedimentary deposits of the Lower Unit (Figures 5, 7-10) indicate a pelagic blanket over the basement. At DSDP site 223 on the flank of the central Owen Ridge (Figure 5), the thickness of the Lower Unit is ~220 m, the Oligocene section representing only ~50 m of sediments [*Shipboard Scientific Party*, 1974].

Numerous Mass Transport Deposits (MTD hereafter), characterized by a typical chaotic to transparent facies on seismic data and locally sampled at site DSDP 224, are observed at the edge of basement flanks (especially at the latitude of the Southern Owen Ridge) (Figures 5b, 11), and introduce large thickness variations within the Lower Unit.

The thickness of the Lower Unit is larger in the vicinity of the Oman margin ( Figure 7), which probably reflects the terrigenous input from the margin. On the platform, Eocene limestones drilled at site 729 (Figures 4, 5a) indicate a shallow-water context of deposition and are very similar in nature with the limestones overlying the Masirah Ophiolites on land [*Peters et al.*, 1995]. An angular unconformity (picked in dark purple) is identified all along the east Oman margin within the Lower Unit, and laterally merges with a younger diachronous unconformity in the Owen Basin (Figures7b, 9, 10).

### *4. 2. A regional diachronous angular unconformity (Late Oligocene-Early Miocene)*

The Lower Unit is sealed by a regional angular unconformity (picked in light purple), marked by onlap terminations of turbidites from the Upper Unit (Figures7 to 11). Late Oligocene turbiditic deposits from the Indus fan drilled between two basement highs at the southern ridge indicates when the Indus deposits started to flood the Owen Basin [site DSDP 224, *Shipboard Scientific Party*, 1974]. The foraminifera found in the turbiditic layer immediately overlying the unconformity at site DSDP

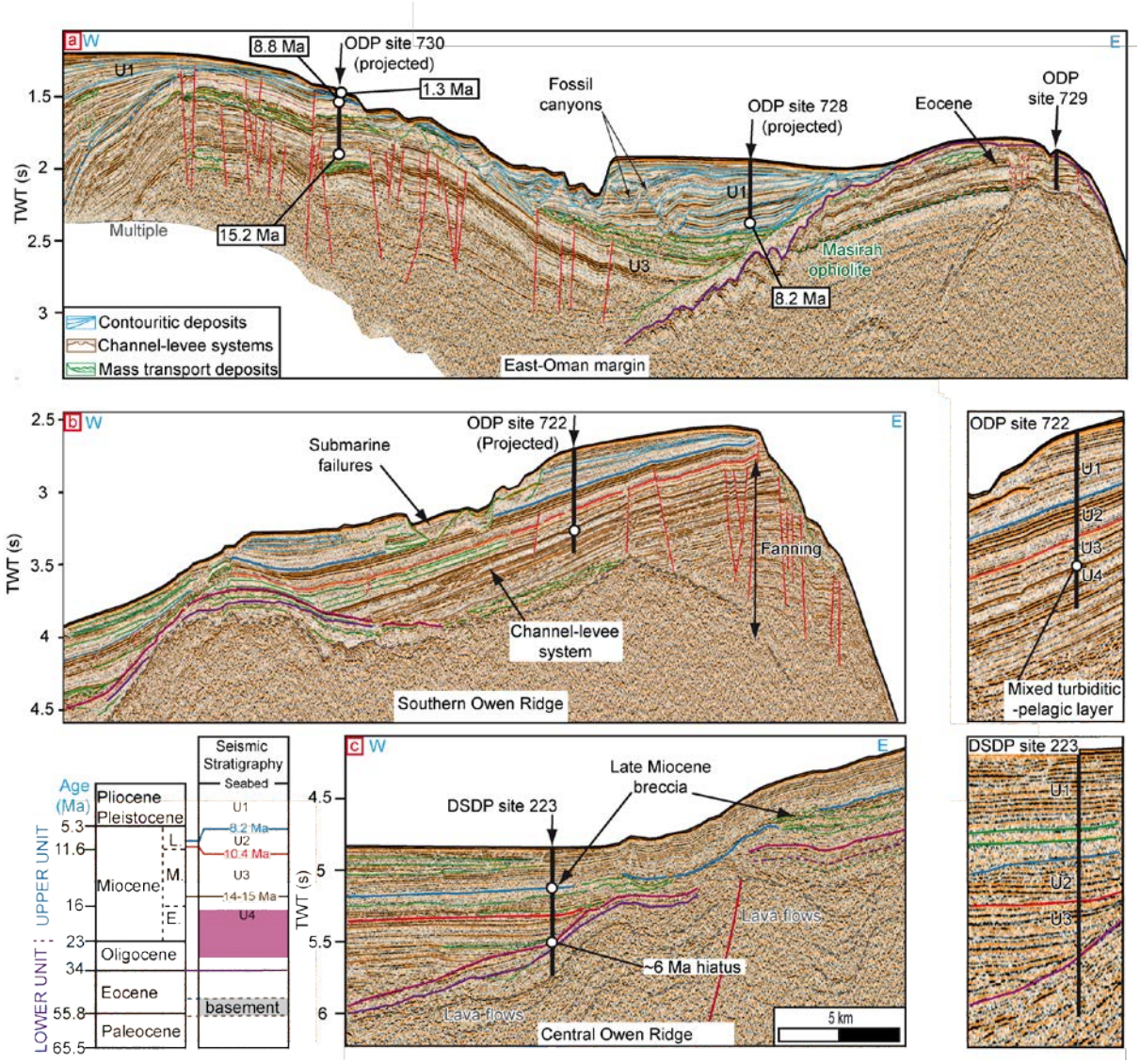


***Figure 5 :****Seismic profiles crossing a) the Oman Margin, b) the Southern Owen Ridge, c) the Central Owen Ridge (see Fig. 4 for location). Insets show close-views of the seismic profiles in the area of deep-sea drilling (ODP and DSDP) locations. The stratigraphic framework is summarized on the lower left hand corner. Profile a) displays a Late Miocene anticline that is overlapped by an 8 Ma-old contouritic drift. An upper Eocene unconformity and Masirah Ophiolites are also observed. Profile b) shows a W-E seismic profile crossing the Southern Owen Ridge at the location of ODP site 722. The basement, drilled at DSDP sites, consists of 51-57 Ma-old basaltic lamprophyres. A major unconformity is observed on the western side of the ridge, where Early Miocene turbiditic deposits (Unit 4) onlap Oligocene deposits drilled at DSDP site 224. The top of Unit 4 corresponds to a pelagic layer previously interpreted as the facies transition related to the ridge uplift and ends at 14 Ma. The overlying Unit 2 and 3are composed of pelagic chalk and ends at 8.2 Ma. Unit 1 is composed of pelagic ooze and chalk, and dissected by landslide failures. c) shows an W-E seismic profile crossing the Central Owen Ridge. A major unconformity, corresponding to a hiatus of 6 Ma, has been drilled at DSDP site 223, together with Late Miocene mass transport deposits. Same horizontal scale for all profiles.*

224 on the southern ridge is 19.6 Ma old (Figure 5b) [*Shipboard Scientific Party*, 1974]. The first turbidite to onlap the unconformity at site DSDP 223 west to the central ridge is 6-Ma younger according to biostratigraphic dating(Figure 5c) [*Shipboard Scientific Party*, 1974]. The age of the first turbidite overlying the unconformity marks the time at which the turbiditic system was developed enough to bury the pre-existing relief at the site of drilling. The 6-Ma misfit between the age of the first turbidite at site DSDP 223 and DSDP 224 simply indicates that site DSDP 223 used to be shallower than site DSDP 224 (Figures4, 5).The upper limit of the Lower Unit is thus highly diachronous over the Owen Basin (Upper Late Oligocene to Early Middle Miocene according to the area) and does not relate to a diachronous uplift of the Owen Ridge [*Mountain and Prell*, 1990].

Along the Oman margin, the Lower Unit is sealed by an erosion surface, characterized by truncated reflectors, and V-shaped incisions typical of erosion by turbiditic canyons (Figure 7). Downslope, the erosion surface merges laterally with the angular unconformity described above (light purple). This surface of erosion was drilled at sites ODP 726 and 729, where it cuts into Eocene limestones and is sealed by Pleistocene deposits (Figure 5a). The seismic profile displayed in Figure 5a crossing the Oman platform shows that reflectors much older than 15-Ma (according to correlation with site ODP 730) terminate as onlaps on the erosion surface. These observations indicate an Oligocene age of the erosive surface.

Because of the highly diachronous character of the unconformity sealing the Lower Unit, it is difficult to correlate this erosion surface to stratigraphic events described on land in absence of drillings. The Upper Late Oligocene-Early Miocene age associated to the unconformity suggests that the erosion surface may correspond to the major emersion of the Arabian continent recorded at the end of the Dhofar group (Mughsayl Fm., ~19 Ma), that marks the end of the synrift phase in the Gulf of Aden [*Carbon*, 1996; *Leroy et al.*, 2012].

### *4. 3. Upper Unit (Upper Late Oligocene to Present)*

Well-developed channel-levee systems, typical of turbiditic sedimentation, are observed within the Upper Unit around the latitude of 20°N in the Owen Basin (Figures 8a). As evidenced by channel-levee systems that are still well expressed on the seafloor of the Owen Basin, the topographic low at the latitude of 20°N used to be a major gateway with the Indus deep-sea fan, which was cut off in the Pliocene (~3 Ma) as the OFZ settled as a topographic barrier, forming a major pull-apart basin [*Fournier et al.*, 2011; *Rodriguez et al.*, 2011; 2013b].Most of the channel-levee complexes observed in the Owen Basin can be correlated to channel-levee complexes drilled at site DSDP 222 in the Indus fan (Figure 8a).The connection between the Indus Fan and the Owen Basin was enhanced by the increase in the Indus sedimentation since the Early-Middle Miocene observed by *Clift et al.* [2001] and *Clift* [2002] in response to the coeval episode of Himalayan uplift and the onset of the Asian Monsoon. It is consistent with previous observations of Indus turbiditic deposits in the Oman abyssal

plain that highlight an episode of basin connection during the Miocene prior to the uplift of the Murray Ridge [*Gaedicke et al.*, 2002; *Ellouz-Zimmerman et al*., 2007]. The identification of Indus deposits within the Owen Basin implies that wherever the India-Arabia plate-boundary was located, it did not act as a topographic barrier for the Indus sediments during most of the Miocene. Turbiditic deposits from the Indus fan encountered in the Upper Unit were emplaced at very high sedimentation rates during the Middle-Late Miocene (up to 600 $m.Ma^{-1}$ according to DSDP site 222 [*Shipboard Scientific Party*, 1974]), which could have buried the topography associated with strike-slip activity.

On the other hand, drillings of the Miocene interval at the Oman margin (Figure 4a) (OPD sites 728, 730) documents mainly pelagic chalk sequences separated by slump deposits and thin (<10 m) calcareous turbidites [*Shipboard Scientific Party*, 1989]. Since the Early Miocene, the Owen Basin has therefore been dominantly filled-in by turbiditic deposits coming from the Indus deep-sea fan, although a component of the Upper Unit turbidites may come from the Oman Margin.

The Upper Unit is also characterized by large MTDs inter-fingered between turbiditic and pelagic deposits (Figures 5, 7, 11). The distribution of MTDs within the Upper Unit in the Owen Basin varies according to the source of the sedimentary material, namely the Oman Margin or the Owen Ridge, the most voluminous MTDs coming from the southern segment of the Owen Ridge (Figure 11) [*Rodriguez et al*., 2012]. Large MTDs coming from the Oman Margin are largely distributed in the Owen Basin (Fig. 7), excepted at the latitude of the Masirah Ridge, where they are trapped in the Masirah Basin (Figure 10).

Contouritic drift architectures, indicating interaction between sediment and deep-sea currents [*Faugères et al*., 1999; *Faugères and Mulder*, 2011], are commonly observed within the Upper Unit all along the Oman Margin and display a large variety of configurations (e.g. Figure 5a). Contouritic bodies emplaced at 8.2 Ma according to calibration with ODP site 728 (Figure 5a).

***Figure 6 :****a) Seismic profile crossing the central segment of the Owen Ridge, showing the active OFZ and an extinct transform fault to the east, buried under Indus turbidites.* ***b****-d )Seismic profiles crossing the southern segment of the Owen Ridge (see Figure 4 for location). Profile b) shows an abrupt and sharp vertical offset of the basement of the Owen Ridge interpreted as a transform fault. Profile c) shows folds and vertical faults buried under the Indus deposits. Profile d) shows the vertical truncature of the series of sediments composing the Owen Ridge to the East (interpreted as the remnant of a former India-Arabia plate boundary)and the present-day boundary to the West. MTDs : mass transport deposits. Same horizontal scale for all profiles.*

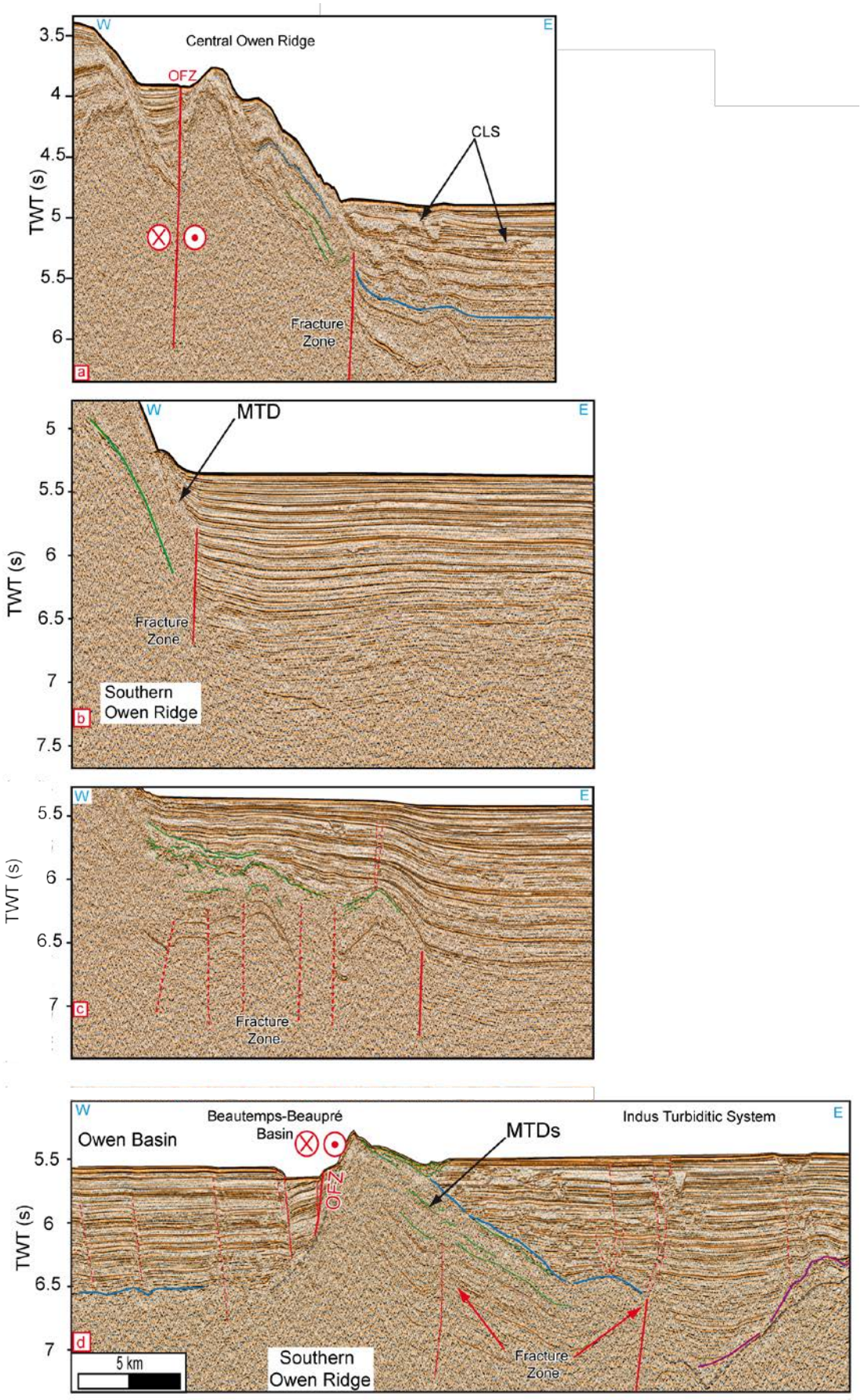
W
E
Central Owen Ridge
OFZ
CLS
TWT (s)
3.5
4
4.5
5
5.5
6
Fracture Zone
a
W
E
MTD
5
5.5
6
6.5
7
7.5
TWT (s)
Fracture Zone
Southern Owen Ridge
b
W
E
5.5
6
6.5
7
TWT (s)
c
Fracture Zone
W
Owen Basin
Beautemps-Beaupré Basin
Indus Turbiditic System
E
MTDs
OFZ
5.5
6
6.5
7
TWT (s)
d
5 km
Southern Owen Ridge
Fracture Zone

## 5. Structure of the Owen Basin and its borders

### *5. 1. Structure of the Owen Ridge*

The basement of the Owen Ridge displays strong reflectors on the seismic data set, with chaotic hyperbolae, corresponding to trachybasalts of Late Paleocene age [*Shipboard Scientific Party*, 1974].The basement of the southern, central, and buried segments of the Owen Ridge displays on its western side strong offsets, with apparent dip ranging between 20 and 45°, delineating 5-20 km-wide areas (Figures 5c, 8, 11). These basements offsets are commonly associated with large MTDs at their edge (Figures 5, 8, 11), which removed either the basement rocks or its pelagic cover, and smoothed fault escarpments. Because pelagic sedimentation rates are too slow and MTDs smooth fault scarps, the Lower Unit sedimentation does not provide good conditions for the record of the deformation. Nevertheless, fanning configurations are evidenced at the southern ridge (Figure 11) and at the central ridge (Figures 5c, 8b).The fanning configurations evidenced at the transition between the basement and the sedimentary cover corresponds to the succession of lavas flows that recorded the tectonic activity of half-grabens (the last flow dated at DSDP site 224 (Southern Owen Ridge) and DSDP site 223 (Central Owen Ridge) being 51.5 Ma-old and 57 Ma-old, respectively [*Shipboard Scientific Party*, 1974]).MTD observed within the Lower Unit and trapped at the edge of half graben structures also display a fanning configuration (Figure 8b).

On their eastern, Indus-facing side, the basement of the southern and central segments of the Owen Ridge display sharp vertical contacts with Indus sediments, interpreted as buried and extinct tectonic structures (Figure 6). Below ~6 s (TWT) the Indus sediments are folded or tilted (Figure 6) on the eastern side of these faults. An angular unconformity (picked in blue) underlines the tilt of the Indus deposits in the vicinity of the fault, and marks its inactivation (Figure 6).The sedimentary sequence at the top of the southern Owen Ridge, composed of Early Miocene turbidites [*Shipboard Scientific Party*, 1989], displays a fanning configuration (Figure 5b), which indicates tectonic activity east of the southern ridge before its uplift. The fanning pattern is Early Miocene according to calibration with ODP site 722.

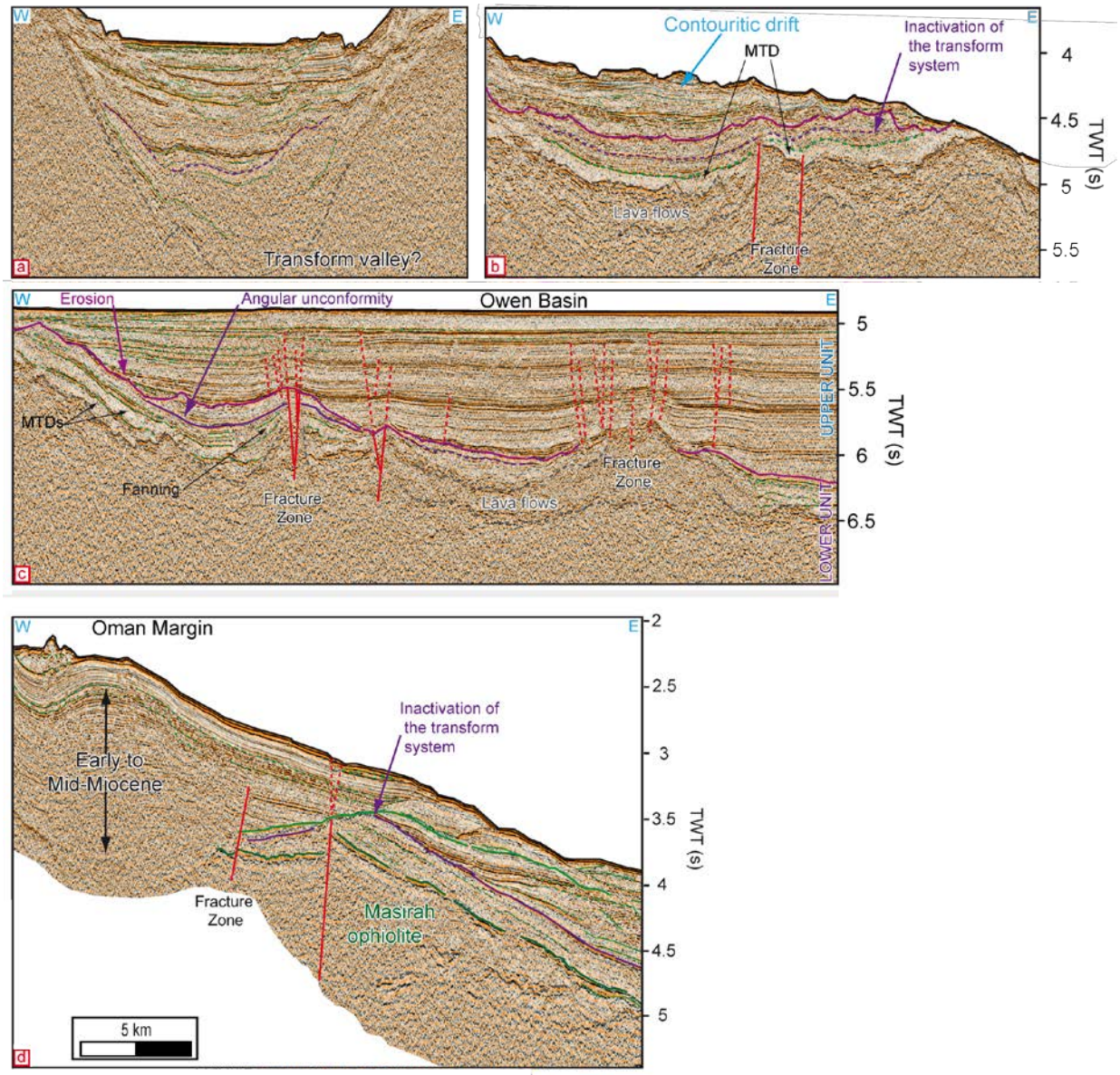


***Figure 7 :****a-d) Seismic profiles acquired in the southern part of the Oman margin (see figure 4 for location). Seismic profile a) shows the structure of the edge of the Sauquarah Ridge, which looks similar to a transform valley. Seismic profile b) shows abrupt and sharp offsets of sediments composing the Lower Unit interpreted as fossil transform traces. The erosive surface sealing the Lower Unit is also evidenced. Seismic profile c) shows traces of extinct transform fault activity within the Lower Unit, together with an angular unconformity (picked in dark purple) that could correspond to the end of their activity. The erosive surface separating the Lower and the Upper Unit is well observed. The Upper Unit is composed of turbidites and MTDs and is affected by differential subsidence structures localized at the edge of fossil transforms. Seismic profile c) shows the Masirahophiolitic body offset by an extinct transform; and the Late Miocene episode of folding. Same horizontal scale for all profiles.*

*5. 2. Structure of the Oman Margin*

Between 20°N and 21°N, the morphology of the Oman continental slope is characterized by the Masirah Ridge (Figure 4) [*Barton et al*., 1990], which forms a horst structure up to ~1500 m-high with respect to the Owen Basin seafloor and oriented ~25-30°NE. The basement of the Masirah Ridge is partly buried under sediments, and extends between 19°N and 21°50'N on seismic lines. A similar prominent horst is observed at the latitude of Ras Sharbitat on Figure 5a, although its bathymetric expression has been smoothed by subsequent sedimentation trapped on its western side. Because located of the Sauquarah bay, this ridge is hereafter referred as the "Sauquarah Ridge". Conspicuous graben structures, bordered by abrupt basement highs, are observed down the Masirah (Figure 10) and the Sauquarah Ridges (Figure 7a). They are filled in by voluminous and folded MTDs.

A peculiar, acoustically chaotic body with an irregular thickness lies on the western flank of the Sauquarah Ridge (Figure 5a), and is overlaid by the same Eocene limestones observed on Masirah Island (ODP site 729). The same chaotic body is observed at the foot of the continental slope (Figure 7d). This acoustically chaotic body is therefore interpreted as the offshore prolongation of the Masirah ophiolitic body [*Mountain and Prell*, 1990]. Considering that the obduction occurred in Late Cretaceous-Early Paleocene times [*Immenhauser*, 2000], the identification of off-shore pieces of the Masirah Ophiolites implies that the basement at the edge of the Oman margin is at least Cretaceous in age (and probably older), in agreement with seismic studies of *Beauchamp et al.* [1995] showing tilted blocs under the Masirah Ophiolites.

West to the Masirah-Sauquarah ridges, the structure of the Upper Unit is mainly characterized by a large anticline (Figures 5a, 7d) at the edge of the platform affecting Early to Late Miocene sediments according to calibration with the nearby ODP sites [*Shipboard Scientific Party*, 1989]. The youngest turbidites affected by the deformation are ~8.8 Ma old, whereas the overlying, undeformed sediments are ~8.2 Ma-old [*Shipboard Scientific Party*, 1989].

Traces of extinct tectonic activity in the Lower Unit are further evidenced downslope, east of the ridges. Down the Masirah Ridge, the basement exhibits a strong offset (~0.4 s TWT) facing the Masirah Ridge, possibly indicating extinct tectonic activity.

At the foot of the Sharbitat Ridge, the basement and the overlying sediments are tilted and offset by two vertical faults (Figure 7). These faults are outlined by a 0.2 s-thick MTD offset vertically by 0.3 s (TWT) (Figure 7), which may indicate the activity of the faults (Figure 4). No trace of activity is evidenced in the uppermost 0.2-0.3 s (TWT) of the Lower Unit (Figures 7b and c), indicating either an inactivation during the end of the Lower Unit in this area, or a shift to pelagic deposition that precluded a good record of the deformation. Similar vertical faults are evidenced at the latitude of 17°50'N, where the chaotic body interpreted as the offshore continuation of the Masirah Ophiolite, together with the overlying MTD, is offset by 0.2 s (TWT) (Figure 7), and tilted in direction of the Owen Basin. Compressive deformation is observed within the Lower Unit between latitudes 21°30’N

and 22°30'N, where the Oman Margin trends ~15°NE (Figure 9). The anticline structure probably roots on a reverse fault within the basement and is sealed by the angular unconformity shown in dark purple on Figure 9.

Some relative chronology arguments constrain the age of uplift of the marginal ridges. The Masirah ophiolitic body lying on the Sauquarah Ridge and the associated Eocene sedimentary cover are tilted westward (Figure 5), and unconformably overlain by the miocene turbiditic sediments (Figure 5). The post-Eocene erosive surface cutting through the sedimentary cover of the Masirah ophiolite involved turbiditic canyons, suggesting the development of an abrupt topography associated to the rise of the Sauquarah Ridge. On the other hand, the transform system cuts both the ophiolitic body and its Eocene cover (Figure 7d). The angular unconformity observed within the Lower Unit (picked in dark purple in Figures 7-10) seals the deformation associated to this tectonic episode. According to the diachronous character of the light-purple unconformity that separates the Lower and the Upper Unit, and taking into account the very thin (50 m) layer of Oligocene sediments drilled at site DSDP 223, the dark purple unconformity is probably Late Eocene-Early Oligocene in age. The uplift of the marginal ridges thus occurred in post-Late Eocene times, probably in response to compression as suggested by the folds observed on Figure 9. Consistently, transpression is also recorded on land along the Qalhat Fault between Late Eocene (Jafnayn Fm.) and Burdigalian times (Thawah Fm.) [*Carbon*, 1996].

*5. 3. Structure of the Owen Basin*

The basement of the Owen Basin displays buried reliefs up to 1.5 s (TWT) high with respect to the surrounding basement, associated with abrupt sub-vertical fault offsets. The deformation affects the sediments of the Lower Unit (Figures 7, 8, 10) that are tilted on the flanks of the sub-vertical faults (with apparent dip locally in the order of 70° on figure 8d). The basement of the Owen Basin also forms several symmetric and narrow buried reliefs up to ~0.5 s TWT high (with respect to the surrounding substratum) (Figures 7, 8a, 10). In some places, vertical offsets and upward tilt of MTDs coming from the Oman margin (Figure 7) or slightly expressed fanning configurations (Figures 8, 11) underline the tectonic activity of these structures. The dark-purple angular unconformity indicates the top of the fanning (for example on Figure 8b), and therefore may indicate the end of the tectonic activity, consistently with what observed along the margin. Elsewhere, the poor conditions of record of deformation in the Lower Unit do not allow us to provide an exhaustive map of active structures during Paleogene. Conspicuous structures, composed of multiple and steep fault strands merging in one single fault at depth, are characteristic of the Upper Unit in the Owen Basin (and the Oman margin) (Figures7-10). These set of faults individualize narrow and tilted blocs. The throw at individual faults increases at depth, which indicates long-lived structures. Their location systematically coincides with abrupt and sharp basement offsets described above.

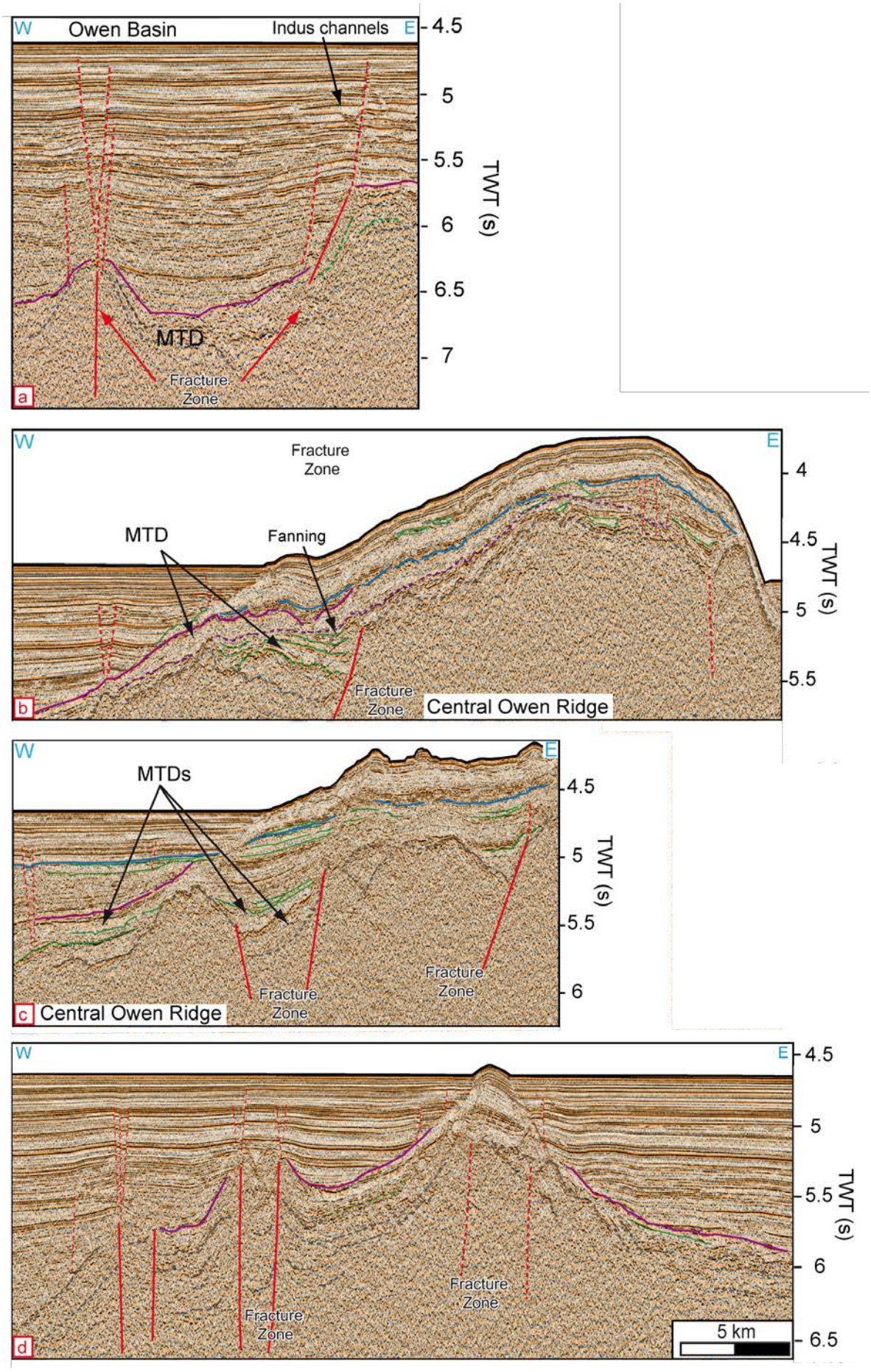
W
Owen Basin
Indus channels
E
4.5
5
5.5
6
6.5
7
TWT (s)
MTD
Fracture Zone
a
W
Fracture Zone
E
MTD
Fanning
4
4.5
5
5.5
TWT (s)
Fracture Zone
Central Owen Ridge
b
W
MTDs
E
4.5
5
5.5
6
TWT (s)
Fracture Zone
Fracture Zone
c Central Owen Ridge
W
E
4.5
5
5.5
6
6.5
TWT (s)
Fracture Zone
Fracture Zone
5 km
d

***Figure 8 :****Seismic profiles a) to c) show abrupt and sharp sub-vertical offsets interpreted as traces of a fossil Paleogenetransform activity close to the present-day central Owen Ridge. Profile a) also shows differential compaction structures, and turbiditic channel levees coming from the Indus Fan. Profile b) highlights a particular fanning configuration in the MTDs coming from the central ridge. Profile d) shows the uneven basement of the Owen Basin, associated with sharp sub-vertical offsets of the Lower Unit interpreted as extinct transforms. See Figure 4 for location. Same horizontal scale for all profiles.*

## 6. Discussion

### *6.1. Diagnostic features of fracture zones*

Tracking the fossil locations of the India-Arabia plate boundary implies to discriminate whether inactive structures identified on seismic profiles result from strike-slip activity or other processes. At the lithospheric scale, transform boundaries form vertical planes juxtaposing two lithospheric plates with more or less pronounced rheological contrasts. They are commonly localized within narrow and elongated valleys, bounded on at least one side by an asymmetric ridge of flexural origin, with a steep slope facing the valley and a more gentle slope outwards (Figure 12). Although the slopes created by transform reliefs are the steepest encountered in the world, they are far from strictly vertical because of erosion [*Basile and Lallemand,* 2002] related to submarine landslides. Continent-ocean transforms commonly displays uplifted reliefs referred as marginal ridges (Figure 12). In areas of turbiditic sedimentation, strike-slip faults generally produce flower-structures. However, the diagnostic of buried and inactive strike-slip structure needs some precautions as several non-tectonic processes can produce seismic features that mimic flower structures on 2D seismic profiles (i.e. fluid escapes or differential compaction).

### *6. 2. Structure of the India-Arabia plate-boundary during Paleogene times*

*Owen Ridge and Owen Basin*

The pattern of the basement offsets observed on the western side of the Owen Ridge, together with the lava flows located at their edge, strongly looks like fracture zone offsets of the Carlsberg Ridge previously imaged by seismic profiles [*Gaedicke et al*., 2002]. The apparent dip of basement offsets ranges in the commonly observed dip values for transforms and fracture zones [*Basile and Lallemand,* 2002]. The lava flows observed at the Owen Ridge (Figure 11) may be the result of magma trapped along transforms faults in the vicinity of a spreading center. The structure of the basement and the presence of Eocene lavas (51-57 Ma according to DSDP sites) thus suggest that the pre-existing Owen Ridge used to be a relief associated to a fracture zone system. The less pronounced basement offsets associated to Paleogene strike-slip deformation in the Owen Basin (Figures 7, 10) may correspond to

secondary fracture zones. Defining the basement of the Owen Basin from the foot of the Masirah-Sauquarah Ridges to the Owen Ridge as an oceanic crust affected by fracture zones is in good agreement with the crustal structure of the Owen Basin (Figure 1c) deduced by *Barton et al.* [1990].
Because of the scarcity of Paleogene sediments along the Owen Ridge and the fact that transform activity does not necessary produce important tilt of sediments (see for example the active OFZ on Figure 7a), the period of activity of this potential transform system is difficult to assess. The fanning configuration of lava flows observed along the southern Owen Ridge underlines the activity of these structures up to at least 51.5 Ma. It is difficult to assess if the MTDs of the Lower Unit recorded tectonic activity. The fanning configuration of MTDs on the Central Owen Ridge points out activity up to a level that appears to correspond to the beginning of Oligocene times (Figure 8b), but we acknowledge that correlations with DSDP site 223 are complicated by the numerous MTDs encountered in this area.

*Oman margin*

The Oman margin displays several features characteristic of a transform margin. First, the horst-pattern of the Masirah and Sauqaurah Ridges (Figures 5, 7, 10) is similar to the marginal ridge observed along the Ghana-Ivory coast margin [*Mascle et al.*, 1988; *Basile et al.*, 1993; *Lamarche et al.*, 1997]. The marginal ridges correspond to continental lithosphere according to seismic refraction data [*Barton et al*., 1990]. Additionally, the pattern of basement offsets at the edge of the Masirah-Sauquarah ridges strongly looks like the transform valley identified along the Ghana-Ivory margin [*Basile et al.*, 1993]. Second, sub-vertical faults cut through the ophiolites and the Lower Unit sediments, and are responsible of their tilt (Figures 7b, 9). This set of evidences confirms that a major transform system used to mark the ocean-continent transition at the edge of the Oman Margin, and gave birth to a marginal ridge system in post-Late Eocene times, namely the Masirah and Sauquarah Ridges.

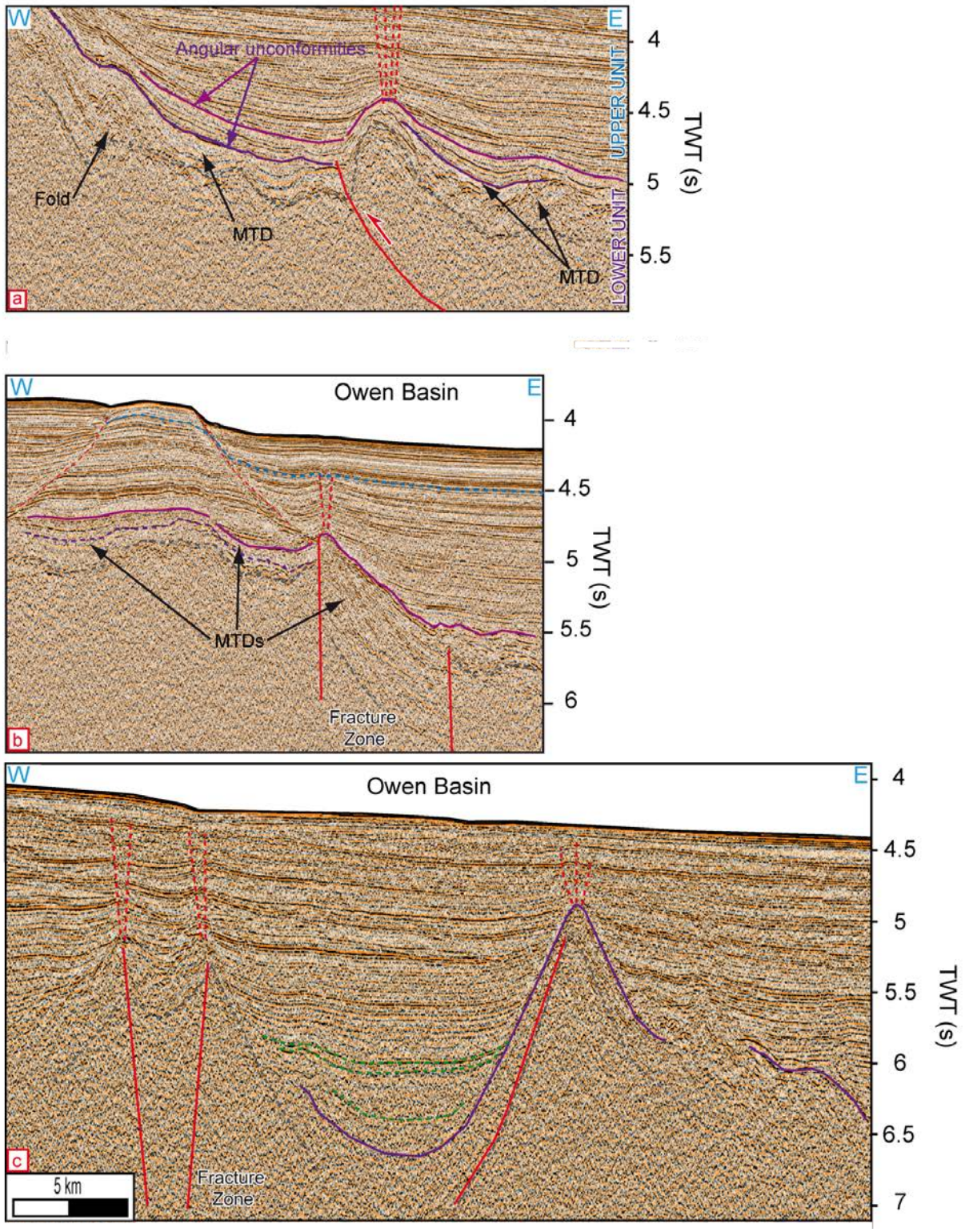


***Figure 9 :****Seismic profiles crossing the edge of the section of the Oman margin oriented 15°NE (see Figure 4 for location). Profile a) shows a fold rooted on a reverse fault, indicating an Oligocene episode of compression. Profile b) shows the abrupt tilt of the Lower Unit sediments towards the Owen Basin, along a vertical fault interpreted as a trace of transform activity. Profile c) shows two basement highs that could correspond to a fossil transform valley. Same horizontal scale for all profiles.*

*6. 3. Structure of the India-Arabia plate-boundary during Late Oligocene-Middle Miocene times*

The vertical faults evidenced on the eastern side of the Owen Ridge (Figure 6) are associated with the deformation of the miocene Indus sediments. These faults correspond to fracture zone segments that may represent good candidates for a narrow Miocene India-Arabia Plate-boundary (Figure 6). Moreover, tectonic activity is evidenced close to the Owen-Murray Ridge since about 20 Ma by the fanning configuration of Indus deposits on the top of the Owen Ridge (Figure 5b). Transform motion may have thus existed at this location prior to the Early Miocene, but it could not be detected due to the limited penetration of the seismic profiles.

The structures identified in the Upper Unit on the Oman margin and in the Owen Basin do not represent fracture zones. First, the Masirah Transform previously defined by *Mountain and Prell* [1990] is not recognized, and actually corresponds to canyon incisions cutting through the Oman platform filled-in by a contouritic drift (Figure 5a). In contrast, the structure of the Upper Unit of the Oman margin is characterized by a large anticline, emplaced 8.2 to 8.8 Ma ago (Figures 5a, 7d), indicating a compressive event in Late Miocene times.

On the other hand, the structures identified within the Upper Unit in the Owen Basin (Figures 7-10) may be confused with the flower-structure typically identified along currently active strike-slip faults. A tectonic origin of these structures would imply the activity of a distributed plate boundary in the Owen Basin and on the Oman Margin from the Early Miocene to the Early Pliocene, which is inconsistent with the coeval seafloor spreading at the Sheba Ridge [*Fournier et al.,* 2010]. Deep-sea sediments can undergo processes of differential subsidence and compaction according to the distribution of irregularities in the basement topography [*Wilson,* 2000]. Differential compaction creates growth faults unrelated to any tectonic process commonly referred to as polygonal faults [e.g. *Shoulders et al*., 2007; *Qiliang et al*., 2009]. Because of the progressive cooling of the oceanic lithosphere that progressively smooth their vertical offsets, extinct transform faults are likely to promote differential subsidence in the sediments above. The "polygonal-structures" in the Upper Unit coincide with fracture zone offsets and thus underline their location, but does not reflect tectonic activity during the Miocene (Figures 7-10).

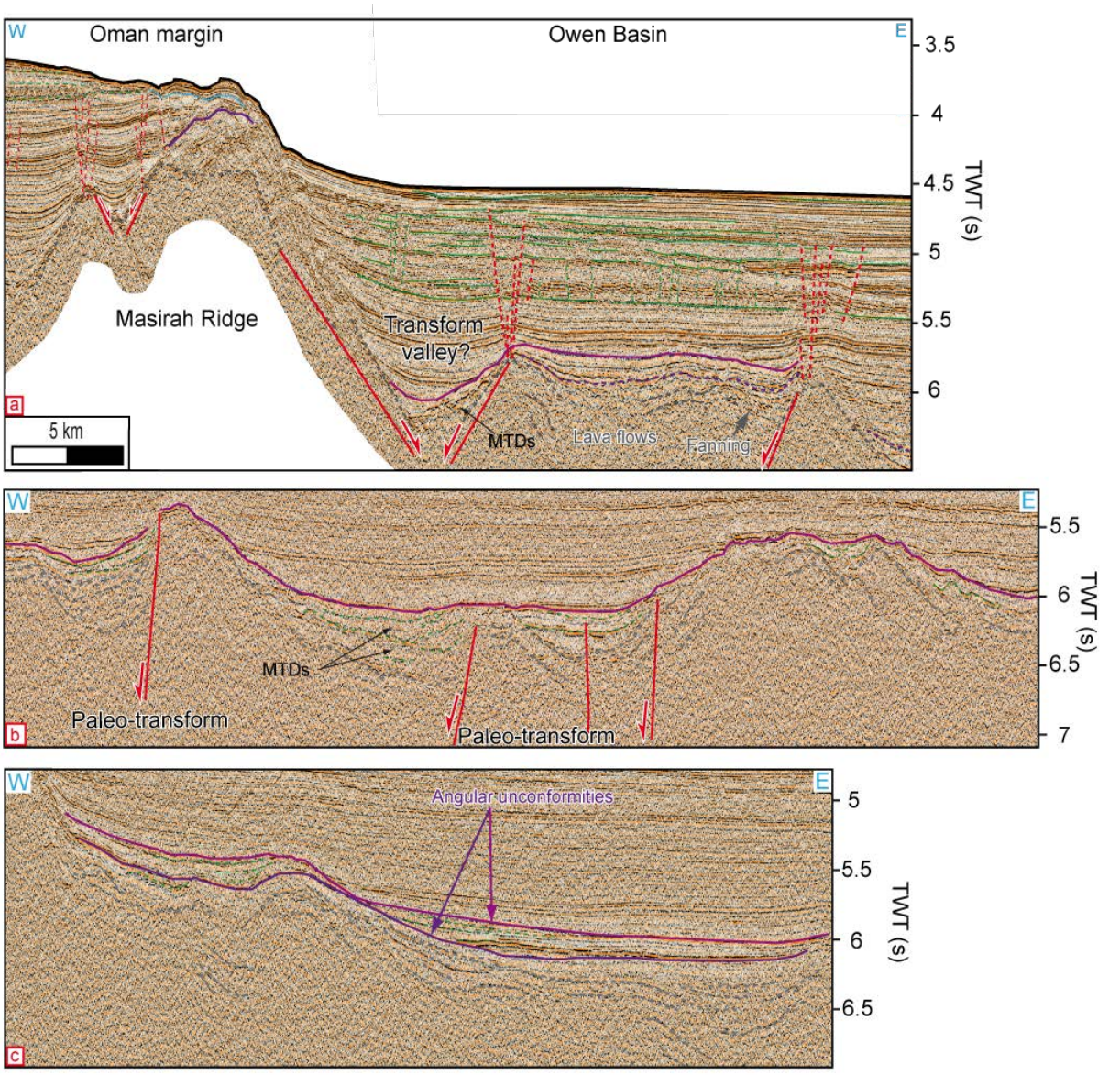


***Figure 10 :****Seismic profile a) shows the Masirah Ridge and differential compaction structures. A graben, corresponding to a potential transform valley, is evidenced at the foot of the Masirah Ridge. Seismic profile b) highlights the uneven character of the basement. Potential transforms are underlined by the fanning configuration of MTDs. Seismic profile c) shows the regional angular unconformity separating the Lower Unit from the Upper one, and the regional unconformity corresponding to the inactivation of the Paleocene-Eocene transform systems.See Figure 4 for location. Same horizontal scale for all profiles.*

*6. 4. Revised geological history of the India-Arabia plate-boundary (Paleocene-Miocene)*

We provided geological evidences for a system composed of several oceanic fracture zones active in the eastern Owen Basin up to Late Eocene times. The east Oman margin displays the characteristics of a fossil transform margin, with the Ocean-Continent transition lying at the edge of the Masirah-Sauquarah Ridges.

We also evidenced a transpressive event marked by a regional angular unconformity (dark purple) that raised the Sauquarah-Masirah marginal ridges and probably induced the inactivation of the Paleocene-Eocene oceanic fracture zones. The first observed trace of transform activity on the eastern side of the Owen Ridge is about 20 Ma-old, and indicates a narrow strike-slip boundary. The trend of these fracture zone systems remain difficult to determine because of the scarcity of the seismic and magnetic anomalies coverage in the Owen Basin. The most probable trend of the fracture zone systems is thus identified from the magnetic anomalies associated to the Carlsberg Ridge (we use the picking of *Royer et al*. [2002], which is the most recent for the area; although recent works by *Cande et al*. [2010] suggest that slight adjustments should be done). Critical points to investigate with regards to the past locations of the India-Arabia plate boundary are the composite age of the Owen Basin (pre-Maastrichtian to the West, Paleocene-Eocene to the East) and the identification of the spreading center at the origin of the basin (subducted beneath the Makran [*Mountain and Prell*, 1990] or located elsewhere?). Whether the uplift of the Owen Ridge reflects a migration of the India-Arabia plate boundary is also critical to the validation of the scenario proposed by *Mountain and Prell* [1990]. The geological reconstitution of the India-Arabia relative motion must also fit the Tithonian age of the oceanic crust exposed at Masirah.

***Figure 11*** *:Seismic Profiles a) and b) show the western side of the Owen Ridge, and abrupt basement offsets representing potential remnants of a Paleocene-Eocene transform activity (recorded by the fanning configuration of lavas).MTDs: mass transport deposits. See Figure 4 for location. Same horizontal scale for all profiles.*

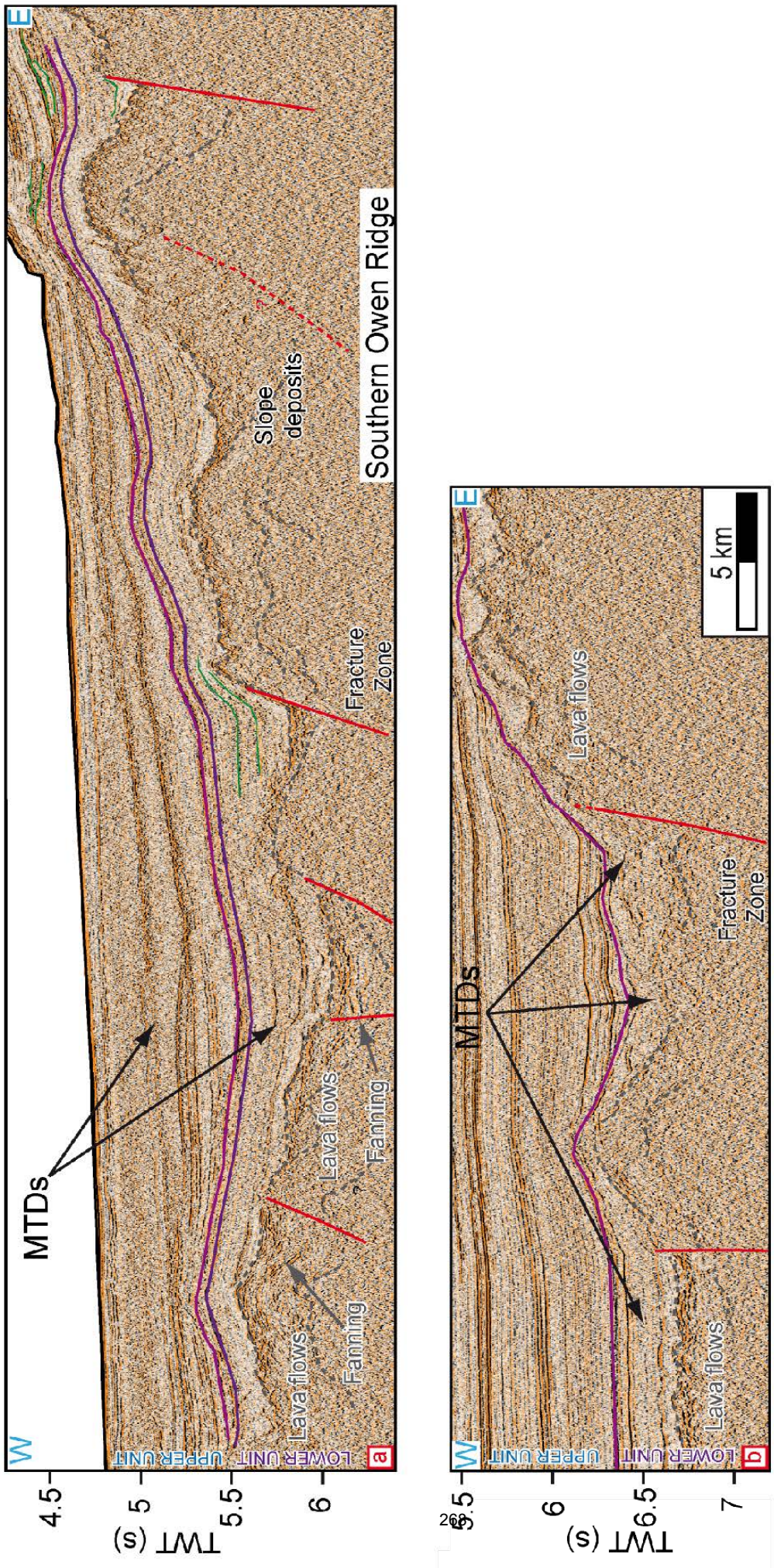
W
E
MTDs
Lava flows
Fanning
Lava flows
Fanning
Slope deposits
Southern Owen Ridge
Fracture Zone
LOWER UNIT
UPPER UNIT
a
TWT (s)
4.5
5
5.5
6
W
E
MTDs
Lava flows
Fracture Zone
5 km
LOWER UNIT
UPPER UNIT
b
TWT (s)
5.5
6
6.5
7

*6. 4. 1. Paleocene-Eocene*

A way to solve the paradox of the composite age of the Owen Basin is to consider that it reflects the juxtaposition of oceanic silvers of different ages by a transform system inactivated in post-Eocene times (uplift of the marginal ridges and transpression). The transform system running at the edge of the marginal ridges and marking the Ocean-Continent transition is the best candidate (Figures 8d, 9c).
The structures identified at the edge of the marginal ridges roughly fit the location of the conjugate of the Chain Fracture Zone during Paleocene-Eocene times deduced from reconstitutions of *Royer et al.* [2002]. The predicted trend of the conjugate of the Chain Fracture Zone is also in good agreement with the ~15-20°NE trend of the Oman margin between latitudes 21°30'N and 22°30'N. The trend of the Sauquarah-Masirah marginal ridges is ~25-30°NE, which represents a difference of ~15° with the inferred direction of the Paleocene-Eocene boundary. The trend of marginal ridges does not necessary follow the trend of the transform motion, as exemplified along the Ghana-Ivory coast margin [*Antobreh et al.*, 2009], and may alternatively indicate a shear-influenced rifted margin. However, this direction is in good agreement with the direction of the 20-30°NE extensive stress field affecting the entire Arabian plate since the emplacement of the Afar hotspot [*Lepvrier et al.*, 2002; *Fournier et al.*, 2004]. The extensive stress field related to the first stages of rifting of the Gulf of Aden might have interacted with the Paleocene-Eocene India-Arabia transform boundary, and favored a context of rifted-influenced sheared margin, similarly to what occurred at the Ghana or the Barents Sea transform margins [*Antobreh et al*., 2009]. Whether the shearing of the Oman margin during Eocene times reactivated inherited structures, and isolated a continental sliver that was later uplifted as the Sauquarah-Masirah marginal ridge, needs to be further investigated.
The post-Eocene relocation of the India-Arabia boundary in the vicinity of the Owen Ridge would imply an episode of transfer of a large piece of the Indian oceanic crust to the Arabian Plate (Figure 13) in Late Eocene- Oligocene times. According to the reconstitutions of *Royer et al*. [2002] (Figure 2), the amount of Indian oceanic crust accreted at the Carlsberg Ridge was sufficient at the end of the Paleocene to support the 51-57 Ma-old basement of the Owen Ridge (Figure 4) [*Shipboard Scientific Party*, 1974]. Moreover, the distance between drilling sites DSDP 223 and 224, where basement of 57 and 51.5 Ma have been respectively drilled, is roughly the same as the distance (i.e. ~250 km) between the magnetic anomalies 24 (52 Ma) and 25 (56 Ma) recorded in the Arabian Sea further east (Figure 3). The main implication of the plate transfer is that the Owen Basin was mostly formed by the Carlsberg Ridge, which rules out an origin from a now subducted spreading center as previously proposed by *Mountain and Prell* [1990].

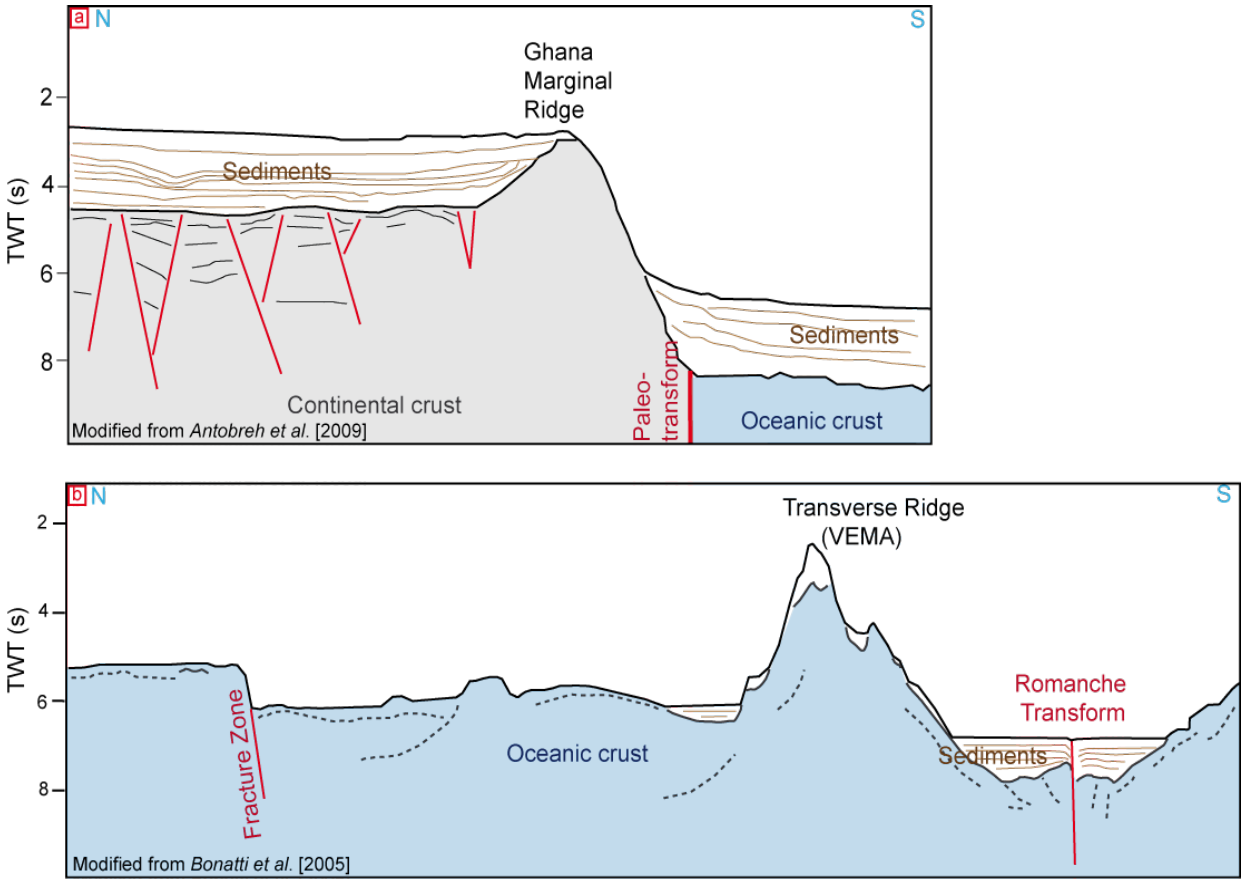


***Figure 12 :****Examples of the diagnostic features of a transform plate boundary on seismic profiles. a) Simplified line-drawing of a seismic line crossing the Ghana-Ivory Coast Marginal Ridge and b) of a seismic line crossing the RomancheTransform. The topography associated to the uplifted shoulder of the transform valley is dependent upon the physical properties of the juxtaposed lithospheres, including their nature (continental or oceanic), their elastic thickness (which controls their flexural behaviour), and their thermal structure (related to their age). The erosion enhances the flexural uplift of the transform shoulder by isostatic compensation. End-members reliefs associated to transform boundaries encompass several thousands of meters reliefs (such as the transverse ridges of the Romanche Transform [Bonatti et al., 1994; Gasperini et al., 1997; 2001], the Shakleton Transform [Livermore et al., 2004], or the Barracuda Ridge [Pichot et al., 2012] in the Atlantic Ocean) or relatively modest reliefs (in the order of tens or hundreds meters) commonly observed at fracture zones. Sub-vertical offsets related to transform faults may disappear with time when the transform becomes inactive and when thermal equilibrium between the juxtaposed lithospheres is reached.*

### *6.4.2. Oligocene*

The onset of ultra-slow spreading at the Carlsberg Ridge ~40 Ma ago (chron 18) was accompanied by a drastic change in the spreading direction (~30°) with regards to the direction of the Paleocene-Eocene Chain Fracture Zone [*Mercuriev et al*., 1996], which is compatible with the hypothesis of a transfer of a large piece of the Indian plate to the nascent Arabian plate since the end of Eocene times (Figure 13). The 50-55°NE spreading direction [*Mercuriev et al*., 1996] implies a relocation 30°E of the conjugate of the Chain Fracture Zone that fits with a relocation of the India-Arabia boundary in the vicinity of the present-day Owen Ridge. The magnetic anomaly 7 (24 Ma) marks not only a change in the spreading direction of the Carlsberg Ridge, but also a global kinematic change recognized at the Southwest Indian Ridge, in the Atlantic, and the Pacific oceans [*Patriat et al.*, 2008]. It indicates the minimal age of the Owen Transform and of the episode of transfer of plate. In this framework, the formation of the Sharbitat Ridge and its conjugate, the Error Ridge, may be linked to a magmatic pulse before the beginning of seafloor spreading at the Sheba Ridge ~20 Ma ago [*Stein and Cochran*, 1985], which could explain why no clear strike-slip offset is evidenced at these reliefs.

The location of the India-Arabia plate boundary during Oligocene times remains a major gap. The Owen Basin does not display any trace of Late Oligocene activity of transform faults, and we do not evidence any trace of transform activity older than Early Miocene at the Owen Ridge, but it may be due to the limited penetration of our seismic lines. Because the Oligocene is thin (<50 m) or absent in most places of the Owen Basin, it is possible that the tectonic activity of the India-Arabia boundary was not recorded. It is even possible that the rate of rifting was similar to the rate of spreading at the Carlsberg Ridge, which would imply that Arabia and India were coupled during most of Oligocene times, prior to the clear separation of Arabia from Nubia.

However, recent stratigraphic works along the Oman margin document an uplift up to the Lutetian-Bartonian boundary (~40.4 Ma) [*Robinet et al.*, 2013], an age that is strikingly coeval with the onset of ultra-slow spreading at the Carlsberg Ridge and may marks the inactivation of the boundary. Distances between DSDP site 223 and magnetic anomaly 25 on one's hand, and between DSDP site 224 and magnetic anomaly 24 on the other hand, are in the order of 140 km, which corresponds to the total amount of dextral relative motion along the India-Arabia boundary. Considering that the India-Arabia plate boundary accommodated ~80 km of relative motion since ~20 Ma [*Chamot-Rooke et al.*, 2009] makes likely the existence of an Oligocene plate boundary nearby the present-day Owen Ridge, accommodating about 70 km of relative motion (with a mean rate of 3-4 $mm.yr^{-1}$ similar to the Neogene rate).

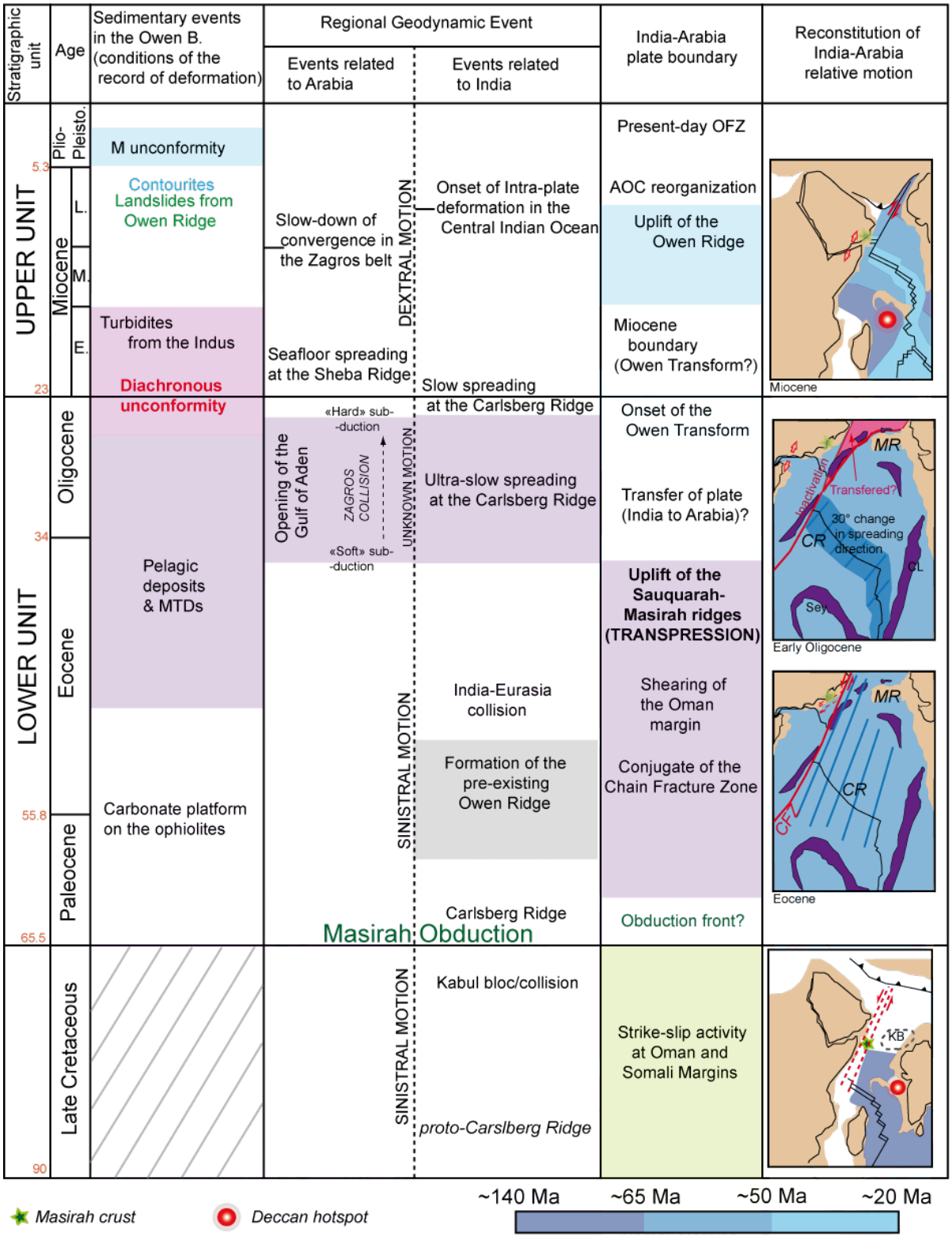


***Figure 13 :****Synthesis of the India-Arabia relative motion geological history since Late Cretaceous Times, and summary of the new geological framework proposed in this study, involving a transfer of a part of the Indian plate to the Arabian plate in Oligocene.CFZ : Chain fracture zone; CL : ChagosLacadive Ridge; CR : Carlsberg Ridge; KB : Kabul Bloc; Lx : Laxmi Ridge; Md : Madagascar; MR : Murray Ridge; OR : Owen Ridge; Sey : Seychelles; SR : Sheba Ridge.*

*6. 4. 3. Early Miocene to present-day*

The simplest explanation with regards to the origin of the transform segments identified on the western side of the Owen Ridge is to consider they used to be the continuation of the Owen Transform during Miocene times, prior to the structural reorganization of the Aden-Owen-Carlsberg triple junction that separated the Owen Transform from the OFZ in Late Miocene-Pliocene times [*Fournier et al.,* 2008a, b]. The uplift of the Owen Ridge is unrelated to an Early Miocene migration of the India-Arabia plate boundary corresponding to the onset of the Sheba Ridge 20 Ma ago. If the uplift was synchronous with the emplacement of the plate boundary, then the fault cannot have produced the fanning configuration of the Late Miocene turbidites (15-20 Ma) lying on the Owen Ridge (Figure 5b). The ~8.5 Ma compressive deformation observed along the Oman Margin may correspond to the tectonic episode at the origin of the uplift of the Owen Ridge. We propose as a working hypothesis that the western part of the Indian Ocean also reacted to the kinematic change at the origin of intra-plate deformation in the Central Indian Ocean [*Wiens et al*., 1985; *Chamot-Rooke et al*., 1993; *Henstock et al*., 2004; *DeMets et al*., 2005; *Mercuriev and DeMets*, 2006; *Delescluse and Chamot-Rooke*, 2007] dated at about 8-9 Ma [*Delescluse et al*., 2008] (Figure 13).

*6. 5.Regional implications*

*6. 5.1. Age and origin of the oceanic crust in the Makran subduction zone*

Heat-flow measurements show that the lithosphere north of the Qalhat Seamount is 70 to 100 Ma-old [*Hutchison et al*., 1982], and implies that the first stages of spreading at the Carlsberg Ridge occurred in a Late Cretaceous oceanic lithosphere west of the Indian continent. The age of the basement of Chain Ridge east of the North Somali Basin is ~90 Ma [*Bunce et al*., 1967]. The age of the Chain Ridge basement contrasts with the inferred Late Jurassic-Early Cretaceous age of the western part of the North Somali Basin [*Cochran*, 1988]. On the other hand, the trend of Chain Ridge is the same as the trend of magnetic lineations in the Mascarene Basin [*Bernard and Munschy*, 2000], which suggests Chain Ridge as a relic of the Late Cretaceous India-Africa boundary, prior to the emplacement of the Carlsberg Ridge and the coeval formation of the Chain Fracture Zone. The fossil Upper Cretaceous boundary is clearly evidenced on the few available seismic lines [*Bunce et al.,* 1967] by a strong vertical offset on the western side of Chain Ridge. Considering that the Owen Basin was formed by the Carlsberg Ridge implies that the lithosphere in the Gulf of Oman was facing Chain Ridge in Late Cretaceous, and was probably formed by the Mascarene spreading center shortly before Madagascar-Seychelles break-up at ~84 Ma. The Tithonian lithosphere, which was at the latitude of the Masirah Island ~60 Ma ago, has been subducted beneath the proto-Makran during the Cenozoic, the Late Cretaceous lithosphere currently in the eastern Gulf of Oman being a remnant of the lithosphere

formed by the Mascarene spreading center. Thus, the oceanic lithosphere subducting beneath the Makran is a remnant of the proto-Indian Ocean formed by the successive stages of Gondwanaland break-up, and does not constitute an arm of the Neotethys Ocean. The suture marking the full subduction of the Neotethys Ocean may be located further north, a good candidate being the front of the Sirjan-Sanandaj domain in Iran and Pakistan [*McCall*, 1997; *Agard et al*., 2005; 2011].

*6. 5. 2. Origin of the plate reorganization during Oligocene times*

Along the east Oman Margin, the rise of the Sauquarah-Masirah marginal ridges in Late Eocene times, associated with the compressive deformation recorded to the North of the basin (Figure 9), are likely to mark the inactivation of the Paleocene-Eocene fracture zone systems in response to a kinematic change recorded by the ultra-slow spreading episode in the Arabian Sea [*Mercuriev et al.*, 1996]. The onset of ultra-slow spreading at the Carlsberg Ridge was first interpreted as a consequence of the India-Eurasia collision [*Patriat and Achache*, 1984] following the initial slowing-down ~50 Ma ago. However, a second episode of slowing-down at 40 Ma is difficult to reconcile with the post collisional history of the Himalaya [*van Hinsbergen et al*., 2012; *Clark*, 2012], and it remained difficult to identify which event associated to the Himalaya triggered the 30° change in spreading direction at ~40 Ma. On the other hand, the timing of the ultra-slow spreading episode strikingly fit the age of major geological events at the Zagros belt. First clues of collision are evidenced since the Late Eocene [*Agard et al.,* 2011]. The definitive suture between the Arabian and Eurasia plates is thought to occur shortly after 25 Ma, following the separation of Arabia from Africa (marked by a 30% decrease in Africa's velocity [*McQuarrie et al*., 2003]).

The commonly accepted scenario relates the entire history of the Zagros building to the Neotethys subduction [*Agard et al.,* 2011; *Mouthereau et al*., 2012]. Two alternative views are discussed. The first one [*Agard et al*., 2011] invokes an episode of slab break-off of the steep Neotethys lithosphere in the Late Eocene to explain the transition towards a relatively flat subduction during the Oligocene, the end of the calc-alkaline activity of the Urumieh-Dokhtar arc on the Eurasian plate, and moderate surface uplift. The second scheme [*Ballato et al*., 2011; *Mouthereau et al.,* 2012] relates the Oligocene change in slab dip to a change in the nature of the subducting lithosphere, from the oceanic Neotethys in Eocene to the stretched Arabian continental margin during Oligocene ("soft-collision"). The definitive collision corresponds to the arrival of the unstretched Arabian continental lithosphere into the subduction zone some 25 Ma ago ("hard-collision") [*Ballato et al*., 2011]. However, the latter framework would require a 400 to 600-km-long stretched Arabian margin to explain the "soft-collision" episode, whereas the North Oman margin is at the most 200-km-long [*MacQuarrie and van Hinsbergen*, 2013] implying a collision around 25-27 Ma.

The identification of Late Cretaceous Indian Ocean subducting beneath the Makran has strong implications over the understanding over the Zagros collision. Indeed, it becomes likely that the Late

Eocene-Early Oligocene change in slab dip reflects the end of the subduction of the Neotethys and the beginning of the subduction of a piece of Indian Ocean of Late Jurassic-Cretaceous age. This piece of Indian Ocean must have been at least 400 to 600 km-wide to fit paleogeographic reconstitutions [*MacQuarrie et al.,* 2003]. Invoking the subduction of a piece of the Indian Ocean under Eurasia since ~40 Ma does not preclude an episode of slab break-off related to the definitive suture of the Neotethys. The suture of the Neotethys in Late Eocene times, accompanied by the accretion of micro-blocks in the Sistan area to the Eurasian plate [*McCall,* 1997], together with the initiation of the subduction of the Indian Ocean during Oligocene, provide a consistent origin for the major geodynamic change recorded at the Carlsberg Ridge by the ultra-slow spreading episode at 40 Ma (Figure 3). The end of the ultra-slow episode kinematic change probably marks the first stages of Arabia-Eurasia collision following the diachronous subduction of the Indian Ocean that is still undergoing in the Makran. Similarly, a two stages convergence, involving the subduction of a ~2000 km-long ocean located north of India and delineated to the north by a continental terrane, has been proposed to explain the timing and the amount of shortening of the India-Eurasia collision [*van Hinsbergen et al*., 2012].

### *6. 5. 3. Indian, Somali, North Arabian margins*

Considering that the eastern Owen Basin was formed by the Carlsberg Ridge has also implications over the understanding of the surrounding margins. First, the distance between the magnetic anomalies 25 and 28 (64 Ma) in the Arabian Sea is about 380 km, which corresponds to the distance between site DSDP 223 and the northern extremity of the Qalhat Seamount on the Arabian plate. Therefore, the Qalhat Seamount lies on an Upper Maastrichtian-Early Paleocene lithosphere, and used to be a part of the Indian plate. This volcano may be an indicator of the late activity of the Deccan Hotspot, or associated with the Gop rift history. On the other hand, the Carlsberg origin of the Owen Basin implies that the North Somali Basin is not its conjugate, but a Mesozoic basin that used to lie west of the Chain Fracture Zone, accordingly with reconstitutions from *Cochran* [1988] and the pre-Maastrichtian age of the basement at the edge of the Oman margin. Finally, the identification of Indian Ocean at the Makran casts doubt on the Neotethys origin of the Semail ophiolites to the North of Oman. Indeed, the North Arabian margin is Triassic to Jurassic in age, and the spreading center at the origin of the Semail body emplaced in Late Cretaceous (~95 Ma) in a Jurassic oceanic lithosphere [Searle and Cox, 1999]. It is possible that the Jurassic oceanic lithosphere was formed during the earliest stages of Gondwanaland break-up, and that a piece of proto-Indian Ocean laid north of East Africa during Mesozoic times. We propose as a working hypothesis that the spreading center at the origin of the Semail body, emplaced in a Late Jurassic-Early Cretaceous ocean, might have been connected to the Mascarene spreading center via the Late Cretaceous India-Arabia plate boundary.

## 7. Conclusions and perspectives

Since Paleocene times, the India-Arabia plate-boundary principally reacted to the major plate reorganization event in the Oligocene related to the formation of the Zagros mountain belts, that inactivated the Paleocene-Eocene boundary and probably controlled its migration ~200-km east. The Miocene trace of the boundary is identified close to the present-day Owen ridge, but the migration of the India-Arabia plate boundary is unrelated with the uplift of the Owen Ridge. The latter most probably occurred in Late Miocene, which implies that the Owen Ridge did not act as a topographic barrier for Indus sedimentation during most of the Miocene period. The composite nature of the Owen Basin results from the juxtaposition by a major transform boundary of a part of the Paleocene-Eocene oceanic lithosphere formed at the Carlsberg Ridge with the mesozoic margin of Arabia affected by the Masirah obduction. The transform boundary was probably the conjugate of the Chain Fracture Zone. The Oligocene plate boundary reorganization involved the transfer of a piece of the Paleocene-Eocene oceanic lithosphere of the Indian Plate to the Arabian Plate. The transfer of a piece of the Paleogene Indian plate resolves the inconsistencies of the previous reconstitutions [*Whitmarsh*, 1979; *Mountain and Prell*, 1990]. Prior to the Masirah obduction, the India-Arabia transform system could have juxtaposed the Tithonic oceanic basement at the origin of the Masirah ophiolites with the Oman margin. The Carlsberg Ridge emplaced farther south, and the Late Jurassic-Early Cretaceous proto-Indian ocean subducted under Eurasia.

A dense magnetic survey over the Owen Basin would be helpful to the validation of this reconstitution. The drilling of the angular unconformity observed within the Lower Unit and the drilling of the basement of the Sharbitat Ridge could also provide useful time constrains. The identification of a piece of Indian Ocean at the front of the Makran accretionnary wedge contrasts with previous interpretations highlighting a Neotethys origin. This has potentially strong implications over the understanding of the Zagros orogeny and its link with break-up events between Arabia and Africa, but also over the history of the Makran wedge, the origin of the Semail Ophiolites, and finally the geological history of Mediterranean Sea [*Jolivet and Faccenna*, 2000].

Moreover, this study highlights the Masirah obduction as a unique case of obduction occurring at a large age-offset transform system. The Masirah Ophiolitic body is of limited extend with regards to the Semail ophiolites and no major subduction zone existed off the east Oman coasts in the Late Cretaceous. Prior to the Masirah obduction, the India-Arabia transform system juxtaposed the Tithonic oceanic basement at the origin of the Masirah ophiolites with the older oceanic crust that was attached to the Oman Margin since the initial stages of continental break-up of the Gondwana. Strong contrasts of density on both sides of a transform (resulting from large age offsets) could favor the initiation of intra-oceanic subduction in response to transpressive stresses, as observed along the Romanche Transform [*Bonatti et al*., 1994]. In the case of the Masirah Ophiolite, the plate reorganization related to the formation of the Carlsberg Ridge, and possibly, the collision of the Kabul bloc [*Gnos et al*., 1997], could account for the transpressive stresses necessary to trigger the obduction. A transform

India-Arabia plate boundary in Late Cretaceous time juxtaposing oceanic silvers of different ages and thicknesses could also explain why two oceanic lithospheres of different thicknesses (~500 and 1500-m) are in contact at the Masirah Island [*Marquer et al*., 1995; *Peters and Mercolli*, 1998].

**Acknowledgements**

We are grateful to Commandant Rémi De Monteville, officers and crew members of the BHO Beautemps-Beaupré, and to the team GENAVIR and the hydrographer D. Levieuge for their help in data acquisition. Processing of the Owen-2 dataset was carried out using the Geocluster 5000 software from CGGVeritas. We thank J. Dyment and J. Robinet for scientific discussions. We thank A. Rabaute who helped the organization of the Owen-2 cruise, and P. Dubernet and N. Bacha for technical assistance. This study was supported by SHOM, IFREMER, INSU-CNRS, and CEA (LRC Yves-Rocard).

**References**

Agard, P., J. Omrani, L. Jolivet, and F. Mouthereau (2005), Convergence history across Zagros (Iran): constraints from collisional and earlier deformation, *Int. J. Earth Sci*., 94, 401–419, DOI 10.1007/s00531-005-0481-4

Agard, P., J. Omrani, L. Jolivet, H.Whitechurch, B.Vrielynck, W.Spakman, P.Monié, B. Meyer, and R.Wortel (2011), Zagros orogeny: a subduction-dominated process, In: Lacombe, O., Grasemann, B., Simpson, G. (Eds.), Geodynamic Evolution of the Zagros. *Geological Magazine*, 692–725.

Ballato, P., C. E. Uba, A. Landgraf, M. R. Strecker, M. Sudo, D. F. Stockli, A. Friedrich and S. Tabatabaei (2011), Geol. Soc. of AM. Bull., 123, 106-131, doi:10.1130/B30091.1

Barton, P.J.,T.R.E. Owen, and R.S. White (1990), The deep structure of the east Oman continental margin : preliminary result and interpretation,*Tectonophysics*, 173, 319-331.

Basile, C., J. Mascle, M. Popoff, J.P. Bouillin, and G. Mascle (1993), The Ivory-Coaqt Ghana transform margin -a marginal ridge structure deduced from seismic data, *Tectonophysics*, 222, 1-19.

Basile, C. and P.Lallemand (2002), Erosion and flexural uplift along transform faults, *Geophys. J. Int*., 151, 646-653.

Beauchamp, W. H., A. C.Ries, M. P.Coward, and J.A. Miles (1995),MasirahGraben, Oman : a hidden Cretaceous rift basin?, American Association of Petroleum Geologists' Bulletin 79, 864-79.

Bernard, A., M. Munschy (2000), Le bassin des Mascareignes et le bassin de Laxmi (océan Indien occidental) se sont-ils formés à l'axe d'un même centre d'expansion ?, *C. R. Acad. Sci. Paris*, 330, 777–783

Besse, J., and V. Courtillot, 1988. Paleogeographic maps of the continents bordering the Indian Ocean since the Early Jurassic,*J. Geophys.Res*., 93, 11791-808.

Bonatti, E., and K. Krane (1982), Oscillatory spreading explanation of anomalously old uplifted crust near oceanic transform, *Nature*, 300, 343-345.

Bonatti, E., M. Ligi, L.Gasperini, A.Peyve, Y.Raznitsin,and Y.J. Chen(1994), Transform migration and vertical tectonics at the Romanche fracture zone, equatorial Atlantic,*J. Geophys. Res*., 99, 21779-802.

Bonatti, E., D. Brunelli, W.R. Buck, A. Cipriani, P. Fabretti, V. Ferrante, L. Gasperini, and M. Ligi (2005). Flexural uplift of a lithospheric slab near the Vema transform (Central Atlantic) : Timing and mechanisms,*Earth. Planet. Sci. Lett.*, 240, 642-655.

Bosselini, A.(1986), East Africa continental margins, *Geology*, 14, 76-78.

Bosworth W., P. Huchon, K. McClay, E. Abbate (2005), The Red Sea and Gulf of Aden basins, *J. Afr. Earth Sc.*, "Phanerozoic evolution of Africa" sp. issue, 43,344-378.

Bunce, E. T., M. G. Langseth, R. L. Chase, and M. Ewing (1967), Structure of the western Somali Basin, *J. Geophys. Res.*, 72, 25477–2555, doi:10.1029/JZ072i010p02547

Cande, S., P. Patriat, and J. Dyment (2010), Motion between the Indian, Antarctic and African plates in the early Cenozoic, Geophys. J. Int., 183, 127-149, doi: 10.1111/j.1365-246X.2010.04737.x

.Carbon, D. (1996),Tectonique post-obduction des montagnes d'Oman dans le cadre de la convergence Arabie - Iran, PhDthesis, University of Montpellier II, 408 pp.

Calvès, G., A. M. Schwab, M. Huuse, P. D. Clift, C. Gaina, D. Jolley, A. R. Tabrez, and A. Inam (2011), Seismicvolcanostratigraphy of the western Indian rifted margin: The pre-Deccan igneous province, *J. Geophys. Res*., 116, B01101,doi:10.1029/2010JB000862.

Chamot-Rooke, N., M. Fournier, Scientific Team of AOC and OWEN cruises (2009), Tracking Arabia-India motion from Miocene to Present, American Geophysical Union, Fall Meeting 2009.

Chaubey, A. K., G. C. Bhattacharya, G. P. S. Murty, K. Srinivas, T. Ramprasad, and D. GopalaRao (1998), Early Tertiary seafloor spreading magnetic anomalies and paleo-propagators in the northern Arabian Sea, *Earth. Planet. Sci. Lett*., 154, 41-52.

Chaubey, A. K., J. Dyment, G. C. Bhatthacharya, J-Y. Royer, K. Srinivas, and V. Yateesh (2002).Paleogene magnetic isochrons and palaeo -propagators in the Arabian and Eastern Somali Basins, NW Indian Ocean, in The Tectonic and Climatic Evolution of the Arabian Sea Region, edited by P. D. Clift et al., *Geol. Soc. Spec. Publ.*, 195,71-85.

Clark, M. K. (2012), Continental collision slowing due to viscous mantle lithosphere rather than topography, *Nature*, 483, 74–77, doi:10.1038/nature10848

Clift, P. D., N. Shimizu, G. D. Layne, J. S. Blusztain, C. Gaedicke, H. U. Schluter, M. K. Clark, and S. Amjad(2001), Development of the Indus Fan and its significance for the erosional history of the Western Himalaya and Karakoram, *Geol. Soc. Am. Bull*.,113, 1039–1051.

Clift, P. D., and C.Gaedicke (2002). Accelerated mass flux to the Arabian Sea during the middle to late Miocene,*Geology*, **30**, 207-210, doi:10.1130/0091-13(2002)030<0207:AMFTTA>2.0.CO;2

Clift, P.D., C. Gaedicke, R. Edwards, J.I. Lee, P. Hildebrand, S.Amjad, R.S. White, and H. U. Schülter, (2002), The stratigraphic evolution of the Indus Fan and the history of sedimentation in the Arabian Sea. *Marine Geophysical Researches*, 23, 223–245.

Cochran, J. R. (1988), Somali Basin, Chain Ridge, and origin of the northern Somali Basin gravity and geoid low,*J.Geophys.Res*., 93, 11985-12008.

Delescluse, M., L. G. J. Montési, N. Chamot-Rooke(2008),Fault reactivation and selective abandonment in the oceanic lithosphere,*Geophys. Res. Lett.*, 35, L16312, doi:10.1029/2008GL035066.

DeMets C., R. G. Gordon, and D.F. Argus (2010), Geologically current plate motions, *Geophys. J. Int.*,*181*, 1-80, doi: 10.1111/j.1365-246X.2009.04491.x

Dyment, J.(1998), Evolution of the Carlsberg Ridge between 60 and 45 Ma: Ridge propagation, spreading asymmetry, and the Deccan-Reunion hotspot,*J. Geophys. Res.*, 103, 24067–24084 DOI: 10.1029/98JB01759.

Edwards R.A., T. A. Minshull, and R. S. White (2000), Extension across the Indian–Arabian plate boundary: the Murray Ridge, *Geophys. J. Int., 142*, 461–477

Edwards, R. A., T. A. Minshull, E. R. Flueh and C. Kopp (2008), Dalrymple Trough: An active oblique-slip ocean-continent boundary in the northwest Indian Ocean, *Earth Planet. Sci. Lett*.,*272*, 437-445.

Faugères, J.C., D.A.V. Stow, P. Imbert, and A. Viana (1999), Seismic features diagnostic of contourite drifts, *Mar. Geol., 162*, 1-38.

Faugeres J.C., and T. Mulder (2011), Contour Currents and Contourite Drifts, *In: HeikoHuneke and Thierry Mulder, Editor(s), Developments in Sedimentology, Elsevier, 2011, Volume 63, Deep-Sea Sediments*, 149-214.

Filbrandt, J. B., S.C. Nolan, and A. C.Ries(1990), Late Cretaceous and Early Tertiary evolution of Jebel Ja'alan and adjacent areas, NE Oman. In The Geology and Tectonics of the Oman Region. *Geological Society Special Publication* (eds A. H. F. Robertson, M. P. searle, and A. C. Ries), 49, 697-714.

Filbrandt, J. B., S. Al-Dhahab, A. Al-Habsy, K. Harris, J. Keating, S. Al-Mahruqi, S. I. Ozkaya, P. D. Richard and T. Robertson(2006),Kinematic interpretation and structural evolution of North Oman, Block 6, since the Late Cretaceous and implications for timing of hydrocarbon migration into Cretaceous reservoirs,*GeoArabia*, 11, 97-140.

Fournier, M., N. Bellahsen, O. Fabbri, and Y. Gunnell (2004), Oblique rifting and segmentation of the NE Gulf of Aden passive margin, *Geochem. Geophys. Geosyst., 5*, Q11005, doi:10.1029/2004GC000731.

Fournier, M., C. Petit, N. Chamot-Rooke, O. Fabbri, P. Huchon, B. Maillot, and C. Lepvrier (2008a), Do ridge-ridge-fault triple junctions exist on Earth? Evidence from the Aden-Owen-Carlsberg junction in the NW Indian Ocean, *Basin Research*, *20*, 575-590, doi: 10.1111/j.1365-2117.2008.00356.x

Fournier, M., N. Chamot-Rooke, C. Petit, O. Fabbri, P. Huchon, B. Maillot, and C. Lepvrier (2008b), In-situ evidence for dextral active motion at the Arabia-India plate boundary, *Nat. Geosci., 1*, 54-58, doi:10.1038/ngeo.2007.24.

Fournier, M., N. Chamot-Rooke, C. Petit, P. Huchon, A. Al-Kathiri, L. Audin, M.-O. Beslier, E. d'Acremont, O. Fabbri, J.-M. Fleury, K. Khanbari, C. Lepvrier, S. Leroy, B. Maillot, and S. Merkouriev (2010), Arabia-Somalia plate kinematics, evolution of the Aden-Owen-Carlsberg triple junction, and opening of the Gulf of Aden, *J. Geophys. Res., 115*, B04102, doi:10.1029/2008JB006257.

Fournier, M., N. Chamot-Rooke, M. Rodriguez, P. Huchon, C. Petit, M.-O. Beslier, and S. Zaragosi (2011), Owen Fracture Zone: the Arabia-India plate boundary unveiled, *Earth Planet. Sci. Lett., 302*, 247-252, doi:10.1016/j.epsl.2010.12.027

Gaedicke, C., H. U. Schlüter, H. A. Roeser, A. Prexl, B. Schreckenberger, H. Meyer, C. Reichert, P. Clift, and S.Amjad (2002), Origin of the northern Indus Fan and Murray Ridge, Northern Arabian Sea: interpretation from seismic and magnetic imaging, *Tectonophysics*, 355,127–143, http://dx.doi.org/10.1016/S0040-1951(02)00137-3

Gaedicke, C., A. Prexl, H.U. Schlüter, H. Roeser and P. Clift (2002), Seismic stratigraphy and correlation of major regional unconformities in the northern Arabia Sea, in *The Tectonic and Climatic Evolution of the Arabian Sea Region*, edited by P. Clift, D. Kroon, C. Gaedicke and J. Craig, *Geol. Soc. Spec. Publ*., 195, 25-36.

Gasperini L., E. Bonatti, M. Ligi, R. Sartori, A.M. Borsetti, A.Negri, A. Ferrari, and S. Sokolov (1997), Stratigraphic numerical modelling of a carbonate platform on the Romanche transverse ridge, Equatorial Atlantic, *Mar. Geol*., 136, 245-257.

Gasperini L., D. Bernoulli, E. Bonatti, A.M. Borsetti, M. Ligi, A. Negri, R. Sartori and K. von Salis,(2001), Lower Cretaceous to Eocene sedimentary transverse ridge at the Romanche fracture zone and the opening of the Equatorial Atlantic, *Mar. Geol.*, 176, 101-119.

Gibbons, A. D., J. M. Whittaker, and R. D. Müller (2013), The breakup of East Gondwana: Assimilating constraints from Cretaceous ocean basins around India into a best-fit tectonic model, *J. Geophys. Res. Solid Earth*, 118, doi:10.1002/jgrb.50079.

Gnos, E., A. Immenhauser, and Tj. Peters (1997), Late Cretaceous/early tertiary convergence between the Indian and Arabian plates recorded in ophiolites and related sediments,*Tectonophysics*, 271, 1-19.

Hatzfeld, D., and P. Molnar (2010), Comparisons of the kinematics and deep structures of the Zagros and Himalaya and of the Iranian and Tibetan plateaus and geodynamic implications, *Rev. Geophys.*, 48, RG2005, doi:10.1029/2009RG000304.

Hutchison I., K. E. Louden, R.S. White, and R. P. von Herzen (1981), Heat flow and age of the Gulf of Oman, *Earth. Planet. Sci. Lett*., 56, 252-262.

Immenhauser A. (1996),Cretaceous sedimentary rocks on the MasirahOphiolite (Sultanate of Oman): evidence for an unusual bathymetric history,*J. of the Geol. Soc. of London*, 153, 539-551.

Immenhauser A., G. Schreurs, E.Gnos, H. W.Oterdoom, and B. Hartmann(2000), Late Palaeozoic to Neogene geodynamic evolution of the northeastern Oman margin,*Geol. Mag.* 137, 1-18.

Jolivet, L. and C. Faccenna (2000), Mediterranean extension and the Africa-Eurasia collision, Tectonics, 19, 1095-1106

Lamarche, G., C. Basile, J. Mascle, and F. Sage (1997), The Côte d'Ivoire-Ghana transform margin : sedimentary and tectonic structure from multichannel seismic data, *GeomarineLett.*, 17, 62-69.

Lepvrier, C., M. Fournier, T. Bérard, and J. Roger (2002),Cenozoic extension in coastal Dhofar (southern Oman):Implications on the oblique rifting of the Gulf of Aden,*Tectonophysics*, 357, 279–293, doi:10.1016/S0040-1951 (02)00372-4.

Leroy, S. et al., 2012. From rifting to oceanic spreading in the Gulf of Aden: a synthesis. Arab.J.Geosci. doi 10.1007/s12517-011-0475-4

Ligi, M., E. Bonatti, L.Gasperini, and A.N.B.Poliakov(2002), Oceanic broad multifault transform plate boundaries. *Geology*,30;11-14 doi: 10.1130/0091-7613(2002)030<0011:OBMTPB>2.0.CO;2

Livermore, R., G. Eagles, P. Morris, and A. Maldonado (2004),Shackleton Fracture Zone: No barrier to early circumpolar ocean circulation, *Geology*, 32;797-800 doi: 10.1130/G20537.1

Loosveld, R. J. H., A. Bell, and J. J. M. Terken(1996), The tectonic evolution of interior Oman, *Geoarabia*, 1, 28-51.

Marquer, D., T. Peters, and E. Gnos(1995),A new structural interpretation for the emplacement of the Masirahophiolites (Oman) : a main Paleocene intra-oceanic thrust,*GeodinamicaActa*, 8, 13-19.

Mascle, J., E. Blarez, and M. Marinho (1988), The shallow structure of the Guinea and Cote d'Ivoire - Ghana transform margins: their bearing on the equatorial Atlantic Mesozoic evolution, *Tectonophysics*, 155, 193-209.

Massell, C., M. F. Coffin, P. Mann,S. Mosher, C. Frohlich, C. S. Duncan, G. Karner, D. Ramsay, and J.-F. Lebrun(2000),Neotectonics of the Macquarie ridge complex, Australia-Pacific plate boundary, *J. Geophys. Res.*, 105, 13457-13480.

McCall, G.J.H. (1997), The geotectonic history of the Makran and adjacent areas of southern Iran, *J. Asian Earth Sci*., 15, 517-531.

McQuarrie, N, J. M. Stock, C. Verdel, and B. P. Wernicke (2003), Cenozoic evolution of Neotethys and implications for the causes of plate motions, *Geophys. Res. Lett*., 30, 2036, doi:10.1029/2003GL017992.

McQuarrie, N., and D. J. J. van Hingsbergen (2013), Retrodeforming the Arabia-Eurasia collision zone : age of collision versus magnitude of continental subduction, *Geology*, 41, 315-318.

Menard, H. W., and T. Atwater(1968), Changes in direction of sea floor spreading,*Nature*, 219, 463-467.

Mercuriev, S., P. Patriat, and N. Sochevanova(1996), Evolution de la dorsale de Carlsberg: Evidence pour une phase d'expansion très lente entre 40 et 25 Ma (A18 à A7), *Oceanol. Acta*, 19, 1–13.

Merkouriev, S., and C. DeMets(2006), Constraints on Indianplate motion since 20 Ma from dense Russianmagneticdata:Implications for Indian plate dynamics.*Geochem. Geophys.Geosyst.*, 7, Q02002, doi:10.1029/2005GC001079.

Minshull, T., C. Lane, J. S. Collier, and R. Whitmarsh(2008), The relationship between rifting and magmatism in the northeastern Arabian Sea, *NaureGeosci*., 1, 463-467, doi:10.1038/ngeo228.

Molnar, P., P. England, and J. Martinod (1993), Mantle dynamics, uplift of the Tibetan Plateau, and the Indian monsoon,*Rev. Geophys.*,31, 357–396.

Mountain, G. S. and W. L. Prell(1990), A multiphase plate tectonic history of the southeast continental margin of Oman, *The Geology and Tectonics of the Oman Region*, edited by Robertson, A. H. F., Searle, M. P. and Ries, A. C., *Geol. Soc. Spec. Publ.*, 49, 725-743.

Mouthereau, F., O. Lacombe, J.Vergés(2012), Building the Zagros collisional orogen: Timing, strain distribution and the dynamics of Arabia/Eurasia plate convergence, *Tectonophysics*,532–535, 27–60.

Patriat, P. and J. Achache(1984), India-Eurasia collision chronology has implications for crustal shortening and driving mechanism of plate, *Nature*, 311, 615-621.

Patriat, P., H. Sloan and D. Sauter (2008), From slow to ultraslow : a previously undetected event at the Soutwest Indian Ridge at ca. 24 Ma, *Geology*, 36;207-210, doi: 10.1130/G24270A.1

Peters et al. (1995), Geological map of Masirah north and Masirah South

Peters, Tj. and I. Mercolli(1998), Extremely thin oceanic crust in the Proto-Indian Ocean : Evidence from the MasirahOphiolte, Sultanate of Oman. *J. Geophys.Res.*, 103, 677-689.

Pichot, T., M. Patriat, G. K. Westbrook, T. Nalpas, M. A. Gutscher, W. R. Roest, E. Deville, M. Moulin, D. Aslanian, and M. Rabineau (2012), The Cenozoictectonostratigraphic evolution of the Barracuda Ridge and Tiburon Rise, at the western end of the North America-South America plate boundary zone, *Mar. Geol*., 303-306, 154-171.

Pilcher R., R. Roberts, R., Buckley, and N.Harbury(1996), Structures within the MahattaHumaid area, Huqf Uplift : implications for the tectonics of eastern Oman,*Journal of African Earth Sciences*, 22, 311-321.

Ries A. C., and R.M. Shackleton(1990), Structures in the Huqf-Haushi Uplift, east Central Oman. In Robertson, A.H.F., Searle, M.P. and Ries, A.C. (eds), The Geology and Tectonics of the Oman Region,*Geol. Soc. Spec. Pub*.,49, 653-664.

Robinet, J., P. Razin, J. Serra-Kiel, A. Gallardo-Garcia, S., Leroy, J. Roger, C. Grelaud (2013), The Paleogene pre-rift to syn-rift succession in the Dhofar margin (northeastern gulf of Aden): stratigraphy and depositional environments, *Tectonophysics*, in press.

Rodriguez, M., M. Fournier, N. Chamot-Rooke, P. Huchon, J. Bourget, M. Sorbier, S. Zaragosi, and A. Rabaute (2011), Neotectonics of the Owen Fracture Zone (NW Indian Ocean): Structural evolution of an oceanic strike-slip plate boundary, *Geochem. Geophys. Geosyst*.,12, Q12006, doi:10.1029/2011GC003731

Rodriguez, M., M. Fournier, N. Chamot-Rooke, P. Huchon, S. Zaragosi, and A. Rabaute (2012), Mass wasting processes along the Owen Ridge (Northwest Indian Ocean), *Mar. Geol.*, 326-328, 80-100, doi:10.1016/j.margeo.2012.08.008.

Royer, J. Y., A. K. Chaubey, J. Dyment, G. C. Bhattacharya, K. Srinivas, V. Yateesh, and T. Ramprasad (2002), Paelogene plate tectonic evolution of the Arabian and Eastern Somali basins, in The Tectonic and Climatic Evolution of the Arabian Sea Region, edited by P. D. Clift et al., *Geol. Soc. Spec. Publ.*, 195, 7-23

Sclater, J. G., N. R. Grindlay, J. A. Madsen, and C. Rommevaux-Jestin (2005), Tectonic interpretation of the Andrew Baintransform fault: Southwest Indian Ocean, *Geochem. Geophys. Geosyst*., 6, Q09K10, doi:10.1029/2005GC000951.

Searle, M., and J. Cox (1999), Tectonic setting, origin, and obduction of the Oman ophiolite, *GSA bull*., 111, 104-122.

Shackleton R. M., and A. C. Ries(1990), Tectonics of the Masirah fault zone and eastern Oman. In The Geology and Tectonics of the Oman Region,*Geol. Soc. Spec. Pub*. (eds A. H. F. Robertson, M. P. searle, and A. C. Ries) 49, 715-24.

Schreurs, G., and A. Immenhauser(1999), West-northwest-directed obduction of the Batain group on the eastern Oman continental margin at the Cretaceous-Tertiary boundary,*Tectonics*, 18, 148-60.

Shipboard Scientific Party(1974), Site 222. In: Whitmarsh, R.B., Weser, O.E., Ross, D.A. (Eds.), DSDP Init.Repts, leg 23 http://dx.doi.org/10.2973/dsdp.proc.23.106.

Shipboard Scientific Party (1989),Site 731. In: Prell, W.L., Niitsuma, N., et al. (Eds.), Proc. ODP, Init.Repts., 117. College Station, TX (Ocean Drilling Program).

Stein, C. A., and J. Cochran (1985), The transition between the Sheba Ridge and the Owen Basin: rifting of an old oceanic lithosphere, *Geophys. J. R. Astr. Soc*., 81, 47-74.

Taylor, B., A. Goodliffe, and F. Martinez (2009), Initiation of transforms faults at rifted continental margins, *Comptes rendus Geosci*., 341, 428-438.

van Hinsbergen, D. J. J., P. C. Lippert, G. Dupont-Nivet, N. McQuarrie, P. V. Doubrovine, W. Spakman, and T. H. Torsvik (2012), Greater India Basin hypothesis and a two-stage Cenozoic collision between India and Asia, *PNAS*, 109, 7659-7664.

Whitmarsh, R.B. (1979), The Owen Basin off the south-east margin of Arabia and the evolution of the Owen Fracture Zone. *Geophysical Journal of the Royal Astronomical Society* 58, 441-470.

Wilson, T.(2000), Seismic evaluation of differential tectonic subsidence, compaction, and loading in an interior basin, *AAPG bulletin*, 84, 376-398.

Yatheesh, V., G. C. Bhattacharya, and J. Dyment (2009), Early oceanic opening off Western India-Pakistan margin : the Gop Basin revisited, *Earth. Planet. Sci. Lett*., 284, 399-408.

## Conclusions de l'article "Tracking the India-Arabia Plate boundary since Paleocene to Early Miocene times" : éléments de réflexion sur la marge omanaise à terre

L'évolution tectonique de l'Oman est marquée par quatre évènements géodynamiques majeurs depuis le Crétacé : l'obduction des ophiolites de Semail au Campanien, l'obduction des ophiolites de Masirah à la fin du Maastrichtien (caractérisée par une direction E-W), l'ouverture du Golfe d'Aden à l'Oligocène (caractérisée par des directions N150°E et N20°E; *Lepvrier et al., 2002; Huchon et Khanbari, 2003; Fournier et al., 2004*), et la collision entre l'Arabie et l'Eurasie (à l'origine des montagnes du Zagros) à la fin de l'Oligocène (caractérisée par une direction N-S).

Cependant, certaines traces de déformations, orientées E-W à NNW-SSE et affectant la couverture sédimentaire Crétacé sup./ Paléogène de la marge Est-Omanaise restent difficiles à relier aux grands évènements géologiques de l'Oman mentionnés ci-dessus. Ces traces de déformation pourraient être associées à l'évolution structurale de la limite de plaque Inde-Arabie et à l'histoire géologique de la marge omanaise.

Nous présentons ici une analyse préliminaire des données microtectoniques (analyse de fractures, voir *Angelier 1984* pour le principe de la méthode) recueillies au cours de missions de terrain réalisées en 2004 (MEBEE, *Fournier et al., 2004*) et en 2009, dans le but de reconstituer les paléo-champs de contraintes associés aux évènements tectoniques du Tertiaire. Ces analyses de fractures sont interprétées à la lumière des principales découvertes issues de la campagne Owen 2. Les formations sédimentaires ciblées au cours de ces missions reposent principalement sur le dôme du Huqf et sur les ophiolites associées à la phase d'obduction Masirah (l'île de Masirah et Ras Madrekah essentiellement). Un bref descriptif de la stratigraphie de la marge est fourni sous forme d'encart hors-texte en fin de chapitre.

Trois stades de déformation, caractérisées par des directions distinctes sont identifiées. La première, présentant des directions (N-S à N170°E) semblables aux directions ( N150°E et N20°E) identifiées dans le golfe d'Aden; correspond à la déformation associée à l'ouverture du golfe d'Aden, déjà pleinement discutée dans des études précédentes (*Lepvrier et al., 2002; Fournier et al., 2004*).

Un second stade d'extension, E-W à N70°E, est identifié. Les fractures étudiées dans les formations Crétacé sup. proches du Huqf (sites 72, 73) révèlent une phase d'extension grossièrement E-W (Fig. 2), qui est enregistrée également au niveau des formations Oligo-

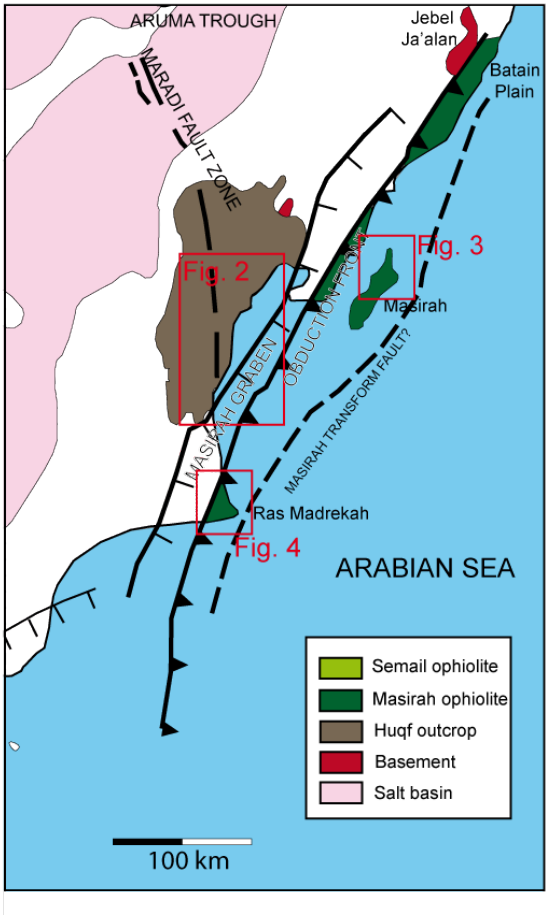


*Figure 1 : Schéma structural simplifié de la marge est-omanaise*

Miocène de Ras Madrekah (Fig. 4). Les directions d'extension N160°E obtenues sur les sites Madrak1A, 5, 6 (Fig 4) pourraient être l'effet d'une permutation des contraintes σ2-σ3 lors de l'extension. Ce stade d'extension n'est pas observé sur l'île de Masirah (Fig. 3).

Le troisième stade témoigne d'un régime décrochant à transpressif orienté E-W à NE-SW. Cette phase de déformation est révélée au niveau de la marge Est Omanaise par des plissements dans la couverture tertiaire (synforme de Naft sur l'île de Masirah, antiforme au sein de la formation de Shuwayr sur Ras Madreka). L'antiforme affectant la formation de Shuwayr sur Ras Madrekah est recoupé par une faille décrochante dextre. Les sites établis sur les formations d'Aydim (île de Masirah) et de Shuwayr (Ras Madrekah) documentent des mouvements décrochants à transpressifs correspondant à une compression orientée E-W à NE-SW (Fig. 5). Des fractures ayant joué initialement en faille normale ont été réactivées en décrochement suggérant que la phase compressive est postérieure aux stades extensifs 1 et 2 (*Fournier et al., 2004*). Les mêmes directions ont été identifiées par *Fournier et al. (2004)* au niveau de la marge omanaise du golfe d'Aden. A l'échelle de la plaque Arabie, le régime de contrainte transpressif dans le Nord de l'Oman devient purement décrochant dans le Sud au niveau du golfe d'Aden.

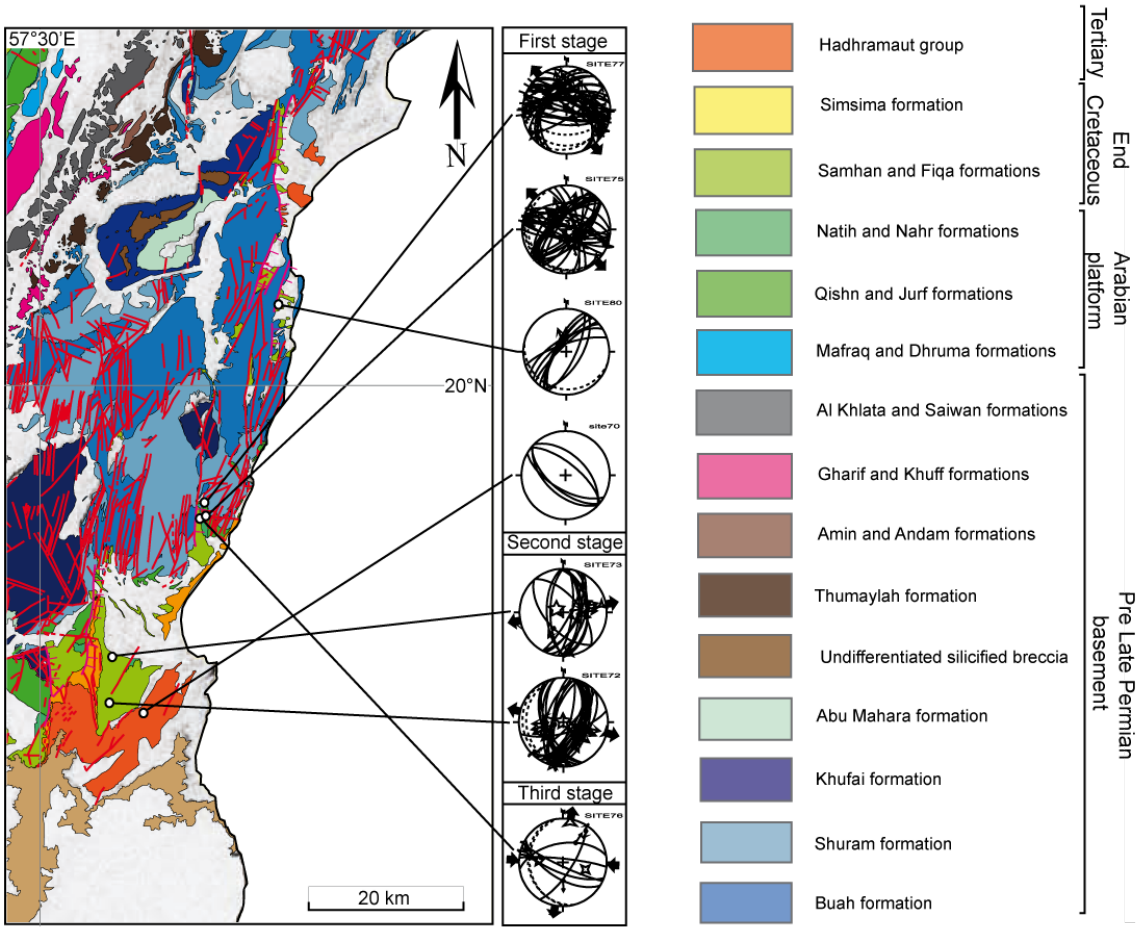


*Figure 2 : Champs de contrainte enregistrés dans les formations Crétacé sup./ Paléogène dans la région du Huqf. Trois stades principaux sont identifiés : un stade d'extension N170°E, un stade d'extension E-W, et un stade compressif E-W.*

*Interprétation :*

Les arguments disponibles pour interpréter ces champs de contraintes sont encore faibles, « la fente demeurant à la faille ce que le merle est à la grive (Huchon, very pers. com., 2009) ». Cependant, les résultats obtenus en mer grâce à la campagne Owen 2 autorisent quelques spéculations, présentées ici à titre d'hypothèses de travail. Le troisième stade pourrait être lié à la déformation Miocène supérieur identifiée en mer et décrite dans les chapitres 4-5. La déformation a été reconnue jusque dans la formation de Shuwayr (Miocène inférieur), mais un examen plus approfondi des quelques affleurements appartenant à la formation de Warak (Miocène moyen) pourrait aussi en révéler les traces. La direction de la déformation E-W/NE-SW est plutôt compatible avec l'hypothèse selon laquelle la plaque Arabie aurait été déformée en réponse au changement cinématique daté entre 11 et 9 Ma dans l'océan Indien, un processus de déformation intra-plaque associé à la croissance du

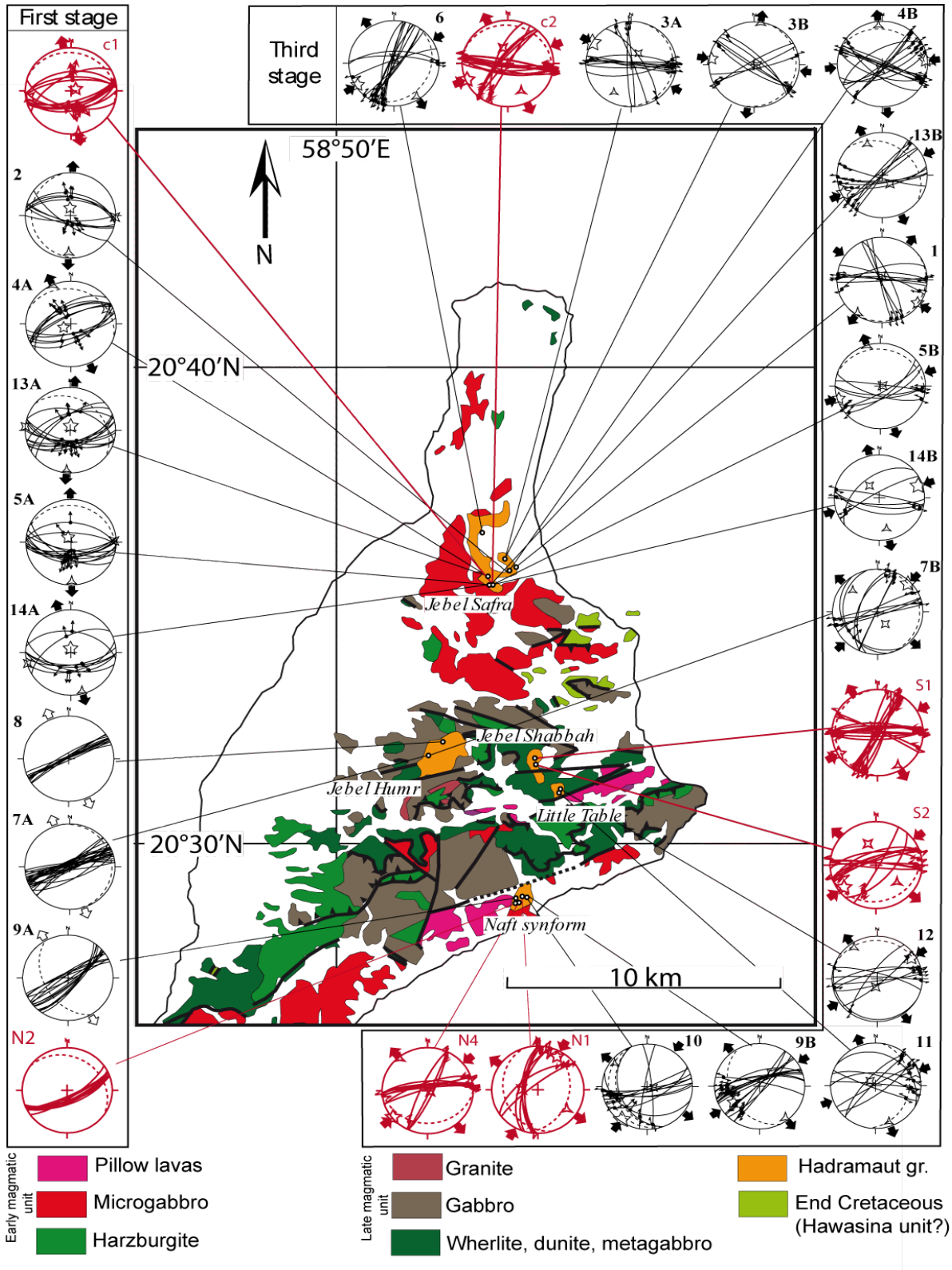


*Figure 3 : Champs de contrainte enregistrés dans les formations Paléogène de l'île de Masirah. Deux stades principaux sont identifiés : un stade d'extension N-S à N170°E et un stade compressif N20°E à E-W.*

Zagros étant supposé générer un champ de contrainte plutôt N-S. Ce régime de contrainte aurait pu réactiver ponctuellement certaines failles en jeu dextre.

Le second stade pourrait indiquer le champ de contrainte associé à la subsidence du Bassin d'Owen et l'étalement gravitaire de la marge. En effet, des études sur la marge du Ghana (*Antobreh et al., 2009*) montrent que les blocs initialement individualisés par les failles transformantes subissent des rotations en direction du bassin océanique après que le mouvement transformant ait cessé. Pour être validée, cette hypothèse nécessiterait de mieux imager la structure du système de Saiwan-Nafun par sismique réflexion.

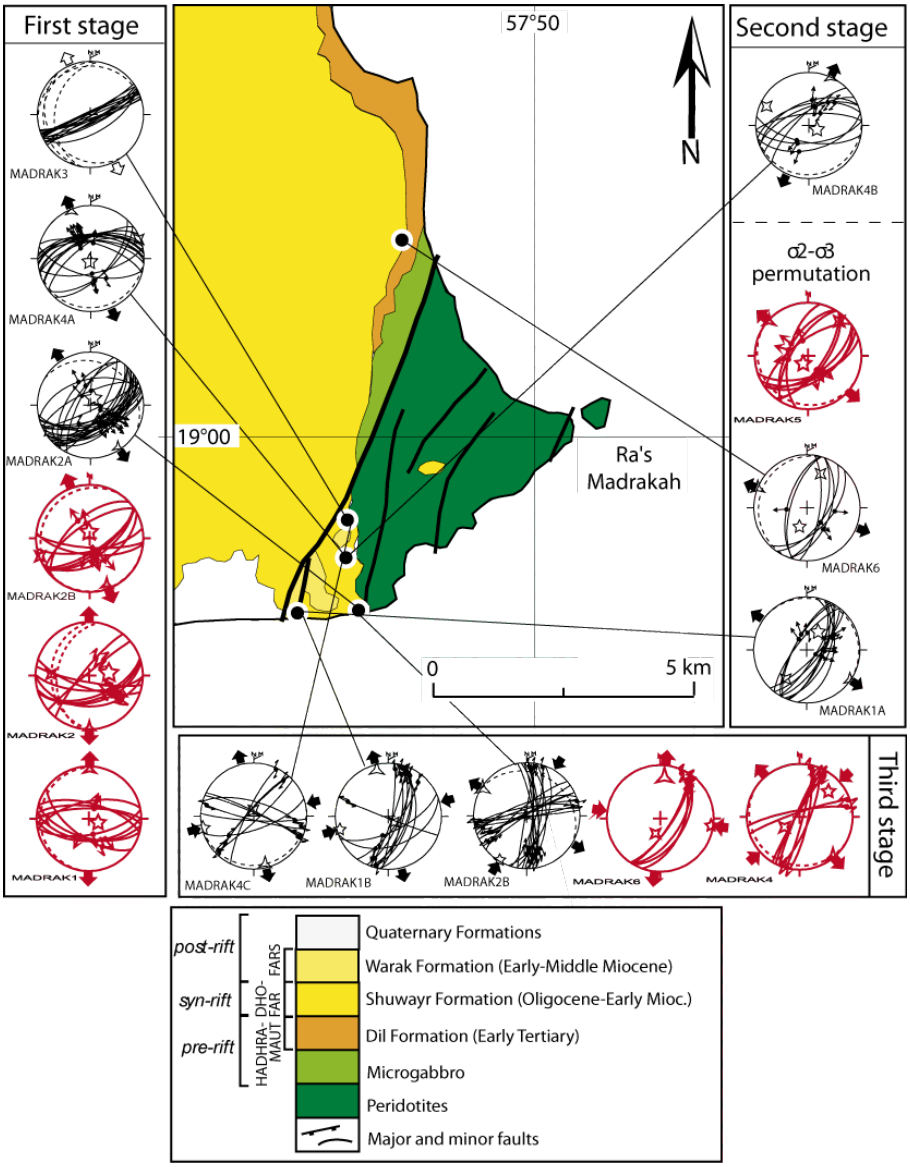


*Figure 4 : Champs de contrainte enregistrés dans les formations Paléogène de Ras Madrekah. Trois stades principaux sont identifiés : un stade d'extension N-S à N170°E, un stade d'extension N20°E à E-W, un stade compressif N20°E à E-W.*

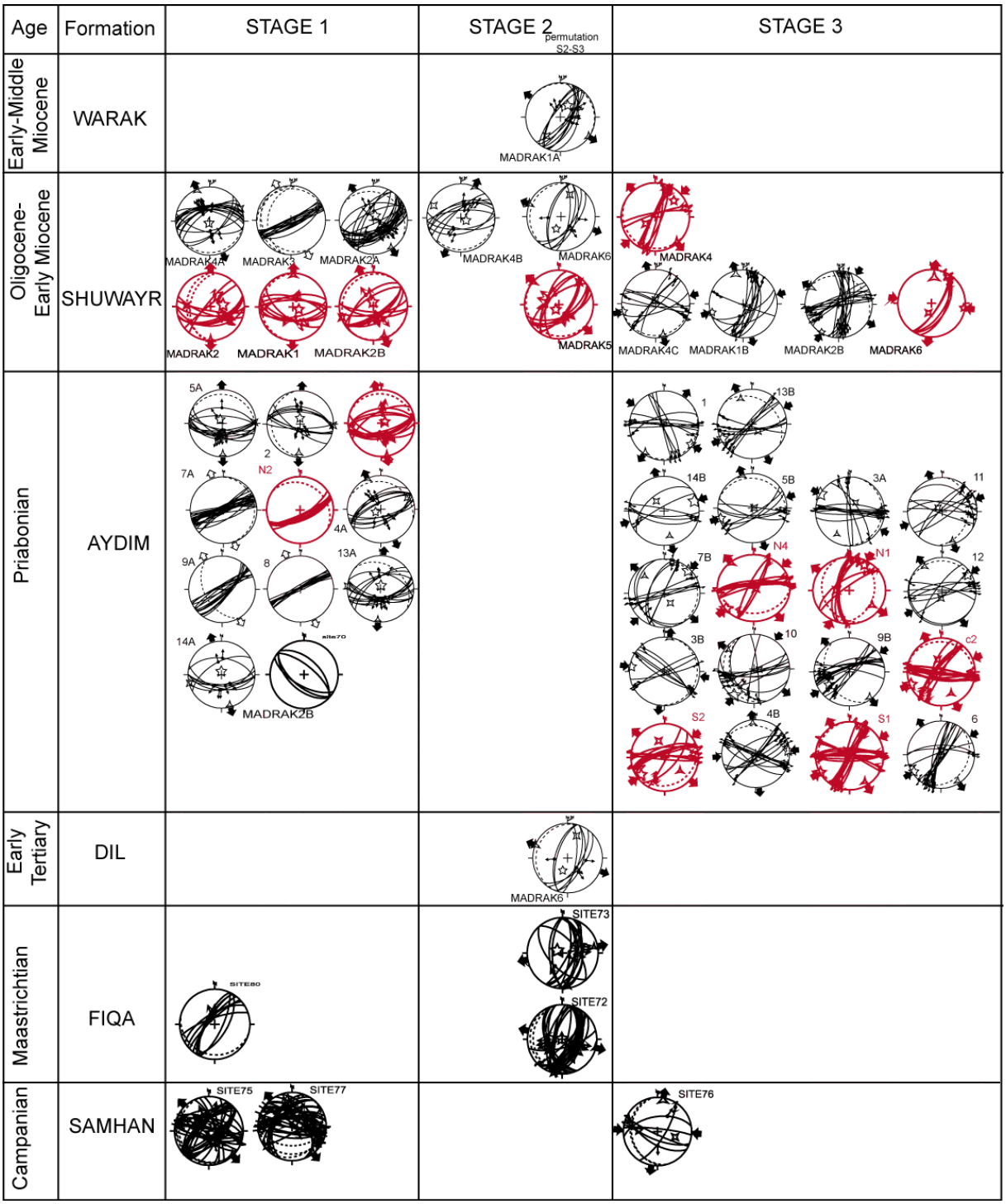


*Figure 5 : Synthèse de la déformation sur la marge Est-Omanaise. Trois stades de déformation sont identifiés : un stade d'extension N-S à N170°E, un stade d'extension E-W à N20°E, et stade de compression N20°E à E- W.*

**La stratigraphie de la marge Est-Omanaise du Campanien au Miocène.**

Suite à l'obduction des ophiolites du Semail, la sédimentation sur l'ensemble de l'Oman est composée d'une succession de formations carbonatées (Samhan et Filim fm.), marno-calcaire (Fiqa fm.) et gréso-calcaire (Simsima fm.), qui composent le groupe d'Aruma (Campanien-Maastrichtien), discordant sur les formations antérieures. Ce groupe est scellé par une surface d'érosion régionale qui entaille la formation de Simsima (d'âge Maastrichtien) dans la couverture post-nappe du Semail (*Nolan et al., 1990*) et dans le Huqf (*Immenhauser et al., 2000*). Une surface d'érosion comparable est observée dans le sud de l'Oman au sommet de la formation de Samhan (*Platel et Roger, 1990*). *Carbon (1996)* suggère que cette surface d'érosion ferait suite à la surrection des reliefs associée à l'obduction Masirah. Le groupe d'Aruma constitue d'importantes formations tabulaires à l'Ouest du Huqf. Son extension est plus réduite à l'Est du dôme, où on le rencontre préférentiellement en bordure de failles normales et dans le Nord Est du Huqf, en bordure de la péninsule d'Hikman. Une formation détritique caractéristique d'un milieu de dépôt profond et contemporaine du groupe d'Aruma (*LeMétour et al., 1992*) a été identifiée : il s'agit de la formation de Fayah, décrite dans la plaine du Batain et sur l'île de Masirah (*Immenhauser, 1996*), et interprétée comme le dernier stade de sédimentation marine profonde avant la phase d'obduction Masirah. Un âge antérieur (Coniacien à Santonien) a toutefois également été avancé pour cette formation (*Immenhauser, 1996*). Les formations sédimentaires déposées depuis le Paléocène reposent en discordance sur la plaine du Batain, le Huqf et les ophiolites de la phase Masirah. La couverture Tertiaire se divise en trois groupes : le groupe d'Hadramaut (Paléocène à Eocène); le groupe du Dhofar (Eocène sup. à Miocène Moyen), et le groupe de Fars (Miocène Moyen à Pliocène). Ces groupes correspondent aux séries pré-, syn- et post-rifting du Golfe d'Aden, respectivement. Les ophiolites de Masirah sont recouvertes par les formations calcaire d'Aydim (Eocène sup., Hadramaut gr.) et de Shuwayr (Oligocène, Dhofar gr.). Les ophiolites de Ras Madrekah sont recouvertes par les formations calcaires de Shuwayr et Warak (Fars gr.), d'âge Oligocène à Miocène Moyen. Cette couverture sédimentaire a été affectée par l'ouverture du Golfe d'Aden et la collision du Zagros (*Fournier et al., 2004*). De façon plus locale, on note la réactivation des blocs basculés de la marge Est-Omanaise dès les premiers stades de l'ouverture du Golfe d'Aden à l'Oligocène (*Filbrandt et al., 1990; LeMétour et al., 1992; Beauchamp et al., 1995*).


*Planche V: Dessin à l'encre de Chine de l'île de Masirah (Oman), vue depuis le sommet des formations calcaires Eocène.*

## Chapitre 6 : Aléa tsunami associé aux glissements de terrain de la Ride d'Owen

Ce chapitre s'articule autour de deux articles publiés. Le premier article est publié à la revue *Marine Geology* sous la référence suivante : *Rodriguez, M., M. Fournier, N. Chamot-Rooke, P. Huchon, S. Zaragosi, and A. Rabaute (2012), Mass wasting processes along the Owen Ridge (Northwest Indian Ocean), Mar. Geol., 326-328, 80-100, doi: 10.1016/j.margeo.2012.08.008.*

Le second article est publié à la revue *Natural Hazards and Earth System Sciences* sous la référence suivante : *Rodriguez, M., N. Chamot-Rooke, H. Hébert , M. Fournier, P. Huchon (2013), Owen Ridge deep-water submarine landslides : implications for tsunami hazard along the Oman coast, NHESS,*13, 417-424.

La morphologie des marges est façonnée par les processus d'instabilités gravitaires, qui remobilisent les sédiments précédemment déposés sur la plate-forme et réalisent l'essentiel du transfert de matière vers l'océan profond. Ces processus peuvent être de grande ampleur en milieu marin ; le plus grand glissement sous-marin connu à ce jour, celui des Agulhas au large de l'Afrique du sud, ayant mobilisé près de 20 000 $km^3$ de sédiment *(Dingle, 1977).* Le terme d'instabilité gravitaire regroupe les glissements de terrain, les coulées de débris, les écoulements (granulaires, liquéfiés), et les courants de turbidité *(Mulder et Cochonat, 1996*). L'évolution de la masse déstabilisée dépend du comportement mécanique du matériel mobilisé, de ses propriétés de cohésion, mais aussi des processus qui entretiennent le déplacement : la turbulence du fluide, les pressions exercées lors des collisions des grains qu'elle contient, la rigidité de la matrice et la flottabilité des clastes qui en sont prisonniers. Lors de leur passage, les masses déstabilisées peuvent éroder et "cannibaliser" le matériel sur lequel elles se déplacent. Un tri des particules sédimentaires s'opère selon le mode de transport impliqué. L'analyse des séquences de dépôt permet donc de déterminer le processus de transport à l'origine du dépôt et est à l'origine des principales classifications des dépôts gravitaires (*Mulder et Cochonat, 1996*). La notion d'instabilité gravitaire dérive de la géotechnique : la stabilité d'une zone se caractérise par son facteur de sécurité (*FOS, pour Factor Of Safety*), qui est le rapport des forces de résistance du sédiment sur les forces motrices :

$$FOS = c' + \gamma' . z . \cos^2 \alpha . \tan \varphi / \gamma' . z . \sin \alpha . \cos \alpha$$

*Avec c'= cohésion ; γ' = densité sèche ; z= épaisseur des glissements; α= pente ; φ=coefficient de frottement interne.*

Lorsque ce rapport est inférieur à 1, la zone est considérée instable et peut être déstabilisée à tout moment. La stabilité des couches sédimentaires est gouvernée par les variations de pression effective. De façon générale, tout processus susceptible d'induire un excès de pression interstitielle est capable de réduire la résistance du sédiment au niveau d'un plan de cisaillement, d'initier la rupture et de générer un glissement de terrain.

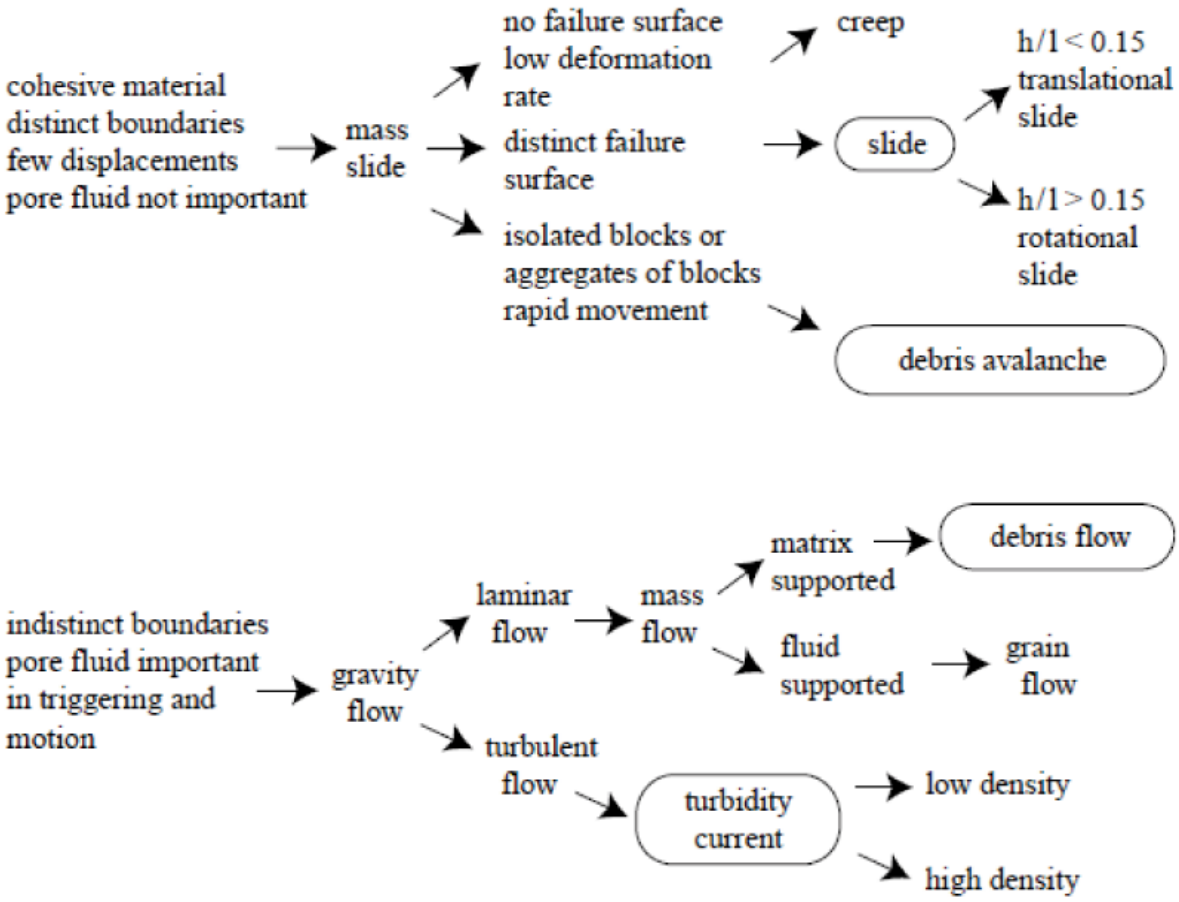


*Figure 1 : classification des processus d'instabilités gravitaires, d'après Mulder et Cochonat (1996).*

*Les facteurs de distribution des glissements de terrain sous-marins et l'originalité de la Ride d'Owen :*

Les sondeurs multifaisceaux, ainsi que l'étude de la réflectivité acoustique des fonds marins, permettent de cartographier, à l'échelle d'une marge entière, la distribution des diverses figures sédimentaires associées aux instabilités gravitaires. La couverture multi-faisceaux des marges continentales est encore lacunaire, mais l'étude de la distribution des glissements est en cours de généralisation, les marges les plus étudiées à l'heure actuelle étant les marges européennes (*Canals et al., 2004*) et nord-américaines (*McAdoo et al., 2000; Chaytor et al., 2009; ten Brink et al., 2009; Twitchell et al., 2009*). L'intérêt premier de cette approche est d'identifier les contextes géologiques qui favorisent la formation des glissements de terrain, en terme de fréquence mais aussi de volume.

Les facteurs de contrôle des processus d'instabilité gravitaire sont nombreux sur les marges continentales : séismes, échappement de fluides (gaz, sédiments liquéfiés), diapirisme, valeur de la pente... L'un des principaux facteurs de répartition des glissements de terrain est le taux de sédimentation sur la plate-forme continentale, qui conditionne la quantité de matériel susceptible d'être déstabilisé. Les taux de sédimentation sont actuellement fonction de la physiographie des continents (la répartition des fleuves et des chaînes de montagne), les grandes accumulations sédimentaires prenant place préférentiellement au niveau des deltas fluviatiles. La distribution des taux de sédimentation actuels est aussi fonction des ceintures climatiques, qui conditionnent la quantité de sédiments charriés par les fleuves via la pluviométrie, l'étendue des glaciers, la nature des sols, ainsi que l'étendue et la nature du couvert végétal. A l'échelle des temps géologiques, l'accumulation des sédiments sur la plate-forme continentale est surtout fonction des variations du niveau marin relatif. Selon le modèle de la stratigraphie séquentielle proposé par *Vail et Mitchum (1977),* les bas niveaux marins relatifs sont associés à l’incision de la plate-forme continentale par un canyon et le développement des systèmes turbiditiques dans le bassin, tandis que les hauts niveaux marins relatifs sont caractérisés par l'accumulation des sédiments sur la plate-forme et l’arrêt progressif de l’alimentation du bassin. Ainsi, dans l'exemple d'une période de bas niveau marin relatif, il y aura moins de sédiments disponibles sur la plate-forme pour alimenter les systèmes gravitaires localisés en dehors des canyons. En revanche, avec le retrait de la ligne de rivage vers le large, des sédiments situés en bordure de plate-forme peuvent se retrouver dans la zone d'action des tempêtes (~<100m de profondeur) et être déstabilisés en conséquence. Les périodes de haut niveau marin relatif semblent favoriser les processus

d'instabilité gravitaire, les plus grands glissements observés sur les fonds marins ayant majoritairement été déposés au cours des dix derniers milliers d'années (ex. des glissements de la marge norvégienne).

Des travaux de géotechnique récents (*Viesca et Rice, 2011*) ont cherché à modéliser l'évolution de la pression interstitielle d'une couche soumise à une charge sédimentaire croissante. Ces travaux montrent que, pour une pente continentale de 4°, l'épaisseur de sédiments nécessaire pour déclencher la rupture est largement supérieure à la centaine de mètres, même en prenant en compte la circulation de fluides. Le déclenchement d'un glissement de terrain par la seule action des taux de sédimentation semble donc peu réaliste, les plans de rupture (identifiés par sismique réflexion) s'initiant le plus souvent dans la première centaine de mètres de la colonne de sédiment. Nous considérons donc ici les taux de sédimentation comme un facteur prédisposant (ou limitant) les déstabilisations gravitaires : plus une marge est riche en sédiments, plus elle dispose de matériel susceptible d'être déstabilisé par un facteur déclenchant. Au contraire, une marge appauvrie en sédiments est relativement moins affectée par des glissements de terrain. Du fait d'interactions complexes entre les nombreux facteurs de contrôle des instabilités gravitaires, les études menées sur les marges continentales se limitent souvent à l'inventaire des facteurs potentiellement impliqués dans la déstabilisation des sédiments, sans réussir à déterminer lequel (lesquels) prédomine(nt). La difficulté vient du fait que la diversité des morphologies associées aux dépôts gravitaires ne dépend pas du processus à l'origine de la déstabilisation, mais du mode de transport (slide, slump, avalanche de débris, courant de turbidité) qui efface les structures formées dans le sédiment par les premiers stades de la déformation.

Considérant le rôle important des taux de sédimentation dans la distribution des glissements de terrain sur les marges continentales, la présence de glissements de terrain sur la Ride d'Owen était inattendue : isolée de tout apport continental (si ce n'est une fraction minime de sédiments transportés par les vents et les courants océaniques), la Ride d'Owen se situe en contexte de sédimentation pélagique, caractérisé par de très faibles taux de sédimentation (de l'ordre de 30-40 m/Ma) (*Shipboard Scientific Party, 1989*). Le sommet de la Ride d'Owen est à 2000 m de fond (400 m pour le Mont Qalhat), au delà de toute influence des variations du niveau marin. La Ride d'Owen présente donc un contexte géologique simplifié par rapport aux marges continentales, les facteurs susceptibles de contrôler les processus gravitaires étant les suivants : la sismicité de la mer d'Arabie (activité de la Zone de Fracture d'Owen, du prisme du Makran, et de la dorsale de Sheba), les faibles

taux de sédimentation pélagique, et la topographie de la Ride d'Owen. Par endroits nous avons identifié quelques figures d'échappement de fluides, susceptibles de localiser la déstabilisation des sédiments.

*Les questions posées par les glissements de terrain de la Ride d'Owen*

Les faibles taux de sédimentation pélagique excluent *a priori* l'occurrence de glissement de terrain sur la Ride d'Owen. A cela s'ajoutent la compaction des sédiments, ainsi que le drainage des eaux interstitielles lors du passage des ondes sismiques, qui consolident la couverture pélagique au cours du temps (*Locat and Lee, 2002; Lee et al., 2007*). Cependant, les vases pélagiques de la Ride d'Owen sont gorgées d'eau (40 à 50%) et peu perméables. Dans certains cas, l'eau interstitielle peut supporter une part de la charge sédimentaire, et empêcher les pores de la roche d'être comprimés sous le poids de la colonne de sédiments. Ce mécanisme peut maintenir les couches sédimentaires à un état sous-consolidé, et prédisposer des plans de faiblesse lors de la rupture des sédiments. Les séismes générés par la Zone de Fracture d'Owen et les régions actives de la mer d'Arabie peuvent également générer des surpressions interstitielles dans les sédiments et déclencher leur rupture. Les séismes sont-ils le facteur déclenchant des glissements de terrain sur la Ride d'Owen ? Un moyen de répondre à cette question est de comparer la fréquence des séismes avec la fréquence des glissements de terrain. S'il y a une bonne corrélation entre les fréquences des deux phénomènes, alors il est raisonnable de penser que les séismes sont à l'origine des glissements de terrain. Cependant, pour qu'un séisme soit enregistré par un glissement de terrain, il faut qu'il y ait du matériel sédimentaire susceptible d'être déstabilisé. Ainsi la démarche de la stratigraphie évènementielle est-elle limitée dans le cas de la Ride d'Owen, où le renouvèlement du matériel sédimentaire - dépendant des taux de sédimentation - est très lent.

L'autre particularité du système sédimentaire de la Ride d'Owen est la diversité des figures sédimentaires associées aux processus d'instabilité gravitaire, et la variabilité des volumes impliqués selon la région de la ride considérée. Comment se fait-il que des régions adjacentes soient disséquées par des modes de déstabilisation différents ? Pour expliquer cela, nous avons procédé à la cartographie détaillée des figures sédimentaires observées sur la Ride d'Owen, dans le but d'identifier les facteurs géologiques à l'origine de cette diversité. A ce titre, l'étude des paramètres morphométriques des glissements de terrain permet de comparer différentes régions entre elles, et de poser des hypothèses sur le mode de rupture et sur les facteurs de contrôle de la distribution des glissements (*McAdoo et al., 2000*).

L'exercice comporte quelques difficultés dans le cas de la Ride d'Owen. Les classifications des processus d'instabilités gravitaires sont principalement basées sur l'analyse détaillée de carottages (*Mulder et al., 1996*) et sont toutes génétiques (c'est-à-dire basées sur le mode de transport des sédiments). Il est difficile d'appliquer ces classifications seulement à partir des données d'imagerie acoustique ou de sismique réflexion, les slumps et les avalanches de débris ayant souvent la même signature sur ce type de données. Les glissements de terrains sont alors classés en glissement "cohésifs" ou "désintégrés" selon la présence ou l'absence de dépôt à la base de la cicatrice d'arrachement, respectivement. De plus, il est parfois difficile de dire si une morphologie est le résultat d'un processus d'instabilité gravitaire, une même morphologie pouvant être le résultat de différents processus (*Faugères et al., 1999*). Dans le cas de la Ride d'Owen, deux types de morphologies posent ce problème: les dépressions circulaires observées sur le sommet de la ride, et les ondulations sédimentaires. Des dépressions sédimentaires semblables à celles observées sur la Ride d'Owen ont été précédemment observées par *Michaud et al*. (2005) sur la ride de Carnegie dans l'océan Pacifique (Figure 2). Ces morphologies peuvent être le résultat de la dissolution des carbonates, de l'échappement de fluides, comme de la déformation de la colonne de sédiments sous l'effet de la gravité (déformation plastique). Des ondulations sédimentaires semblables à celles observées sur la Ride d'Owen ont été identifiées dans plusieurs endroits (Figure 2). Dans le cas de la région de l'Humboldt (marge Nord-est américaine), cette morphologie a été soit rattachée à un glissement de terrain, soit à des dunes sous-marines formées par les courants (*Lee et al., 2002*). Cependant, *Sultan et al. (2008)* ont montré que des ondulations comparables (observées dans l'Adriatique) pouvaient être le fait d'une déformation des sédiments suivi d'un recouvrement par d'autres dépôts (Figure 2). Sur le plateau landais, la genèse de ce type d'ondulations a été rattachée à plusieurs processus dont les instabilités gravitaires (*Faugères et al., 2002*). Il nous est impossible de discriminer, dans l'état actuel des données dont nous disposons, si ces figures sédimentaires sont le résultat d'instabilités gravitaires ou d'autres processus sur la Ride d'Owen.

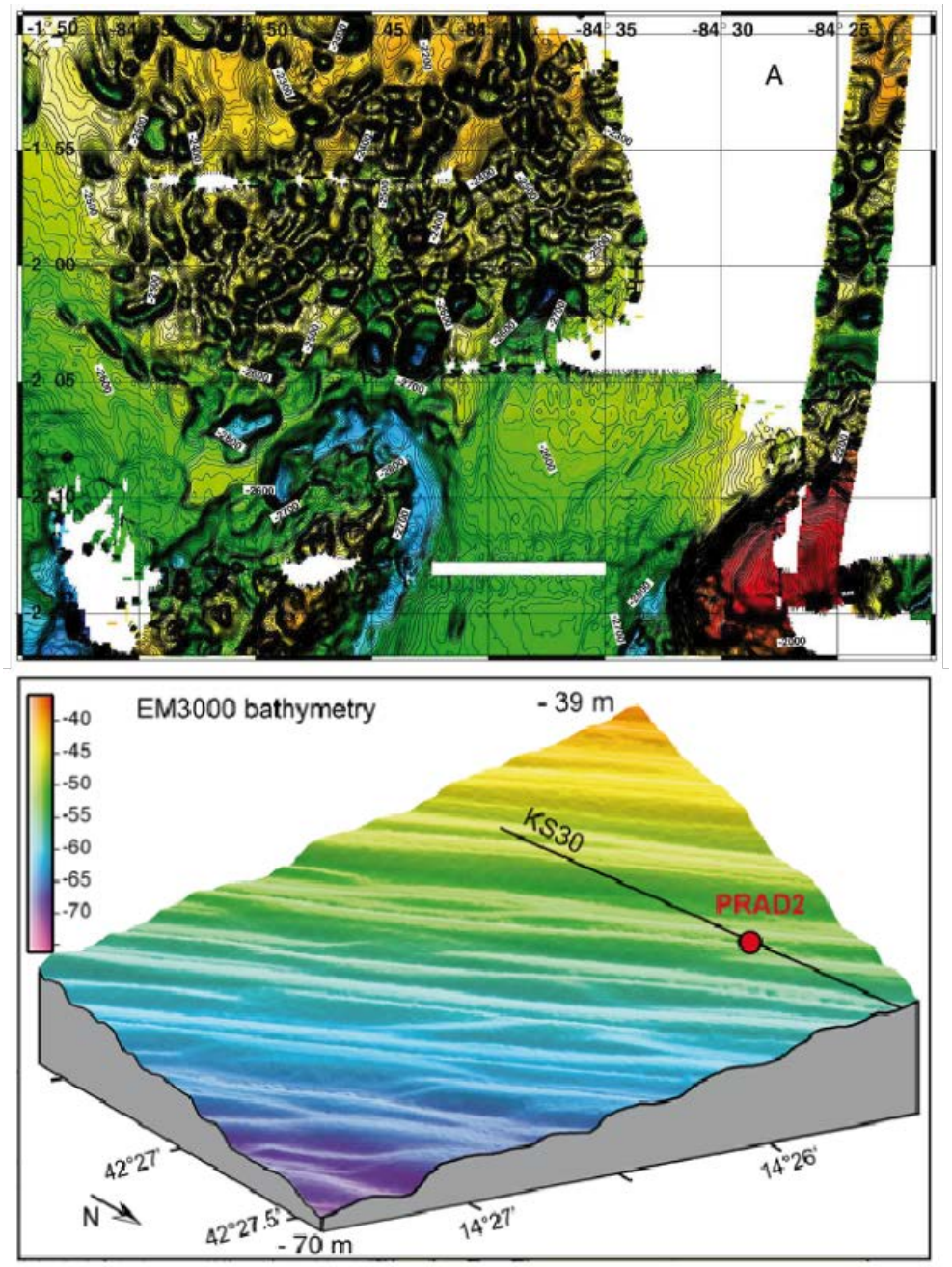


*Figure 2 : Exemples de convergence de faciès morphologiques. En haut : Dépressions circulaires observées sur la Ride de Carnegie, interprétée comme le résultat de processus de dissolution des carbonates (Michaud et al., 2005). Cette morphologie peut aussi être créée par des échappements de fluides (pockmarks) ou des instabilités gravitaires. En bas : ondulations sédimentaires observées dans l'Adriatique (Sultan et al., 2008), interprétée comme le résultat d'interactions complexes entre la déformation des sédiments sous l'effet de la gravité et le dépôt contemporain de sédiments.*

La mise en évidence de glissements de terrain sous-marins au niveau de la Ride d'Owen, située à ~200 km des côtes omanaises, nécessite de ré-évaluer l'aléa tsunami de la région. Les tsunamis sont générés par la mise en oscillation de la colonne d'eau suite à la rupture d'un plan de faille ou à un glissement de terrain. La genèse d'un tsunami dépend du volume de sédiment mobilisé mais aussi des paramètres physiques qui en gouvernent le mouvement. La Ride d'Owen étant disséquée par plusieurs cicatrices d'arrachement distinctes, il est nécessaire de déterminer - par l'étude de l'arrangement relatif des dépôts sédimentaires - si les différents glissements de terrain sont synchrones d'un même évènement déclenchant, afin d'évaluer le volume de sédiments potentiellement impliqué dans la genèse d'un tsunami. Le contexte sédimentaire des glissements de la Ride d'Owen est proche de celui du Banc de Gorringe au large du Portugal, lui aussi disséqué par des glissements. Le comportement des sources gravitaires est comparé pour les deux cas.

Le premier article publié à *Marine Geology* expose une étude complète des glissements de terrains affectant la Ride d'Owen, principalement à l'échelle du sondeur de sédiment (SBP). Selon nos conclusions, les séismes de la ZFO sont le processus déclenchant les glissements de terrain. La récurrence estimée des séismes de magnitude >6 est de l'ordre d'un évènement tous les 1000 ans environ (détail dans l'article qui suit). Cependant, la récurrence des glissements de terrain est de l'ordre de $10^5$ à $10^6$ Ma selon le segment de la Ride d'Owen considéré. Le temps nécessaire pour que la charge sédimentaire soit suffisamment importante pour être déstabilisée lors d'un séisme semble fortement contraint par les faibles taux de sédimentation pélagique. La conclusion principale de cet article est donc que les faibles taux de sédimentation pélagique limitent la fréquence des glissements de terrain, en dépit d'une sismicité pouvant être élevée au niveau de l'OFZ. En raison de la ré-évaluation de l'âge du soulèvement de la Ride d'Owen à ~8-9 Ma au lieu de 20 Ma réalisée après la publication de cet article, il est possible que la fréquence des glissements au niveau de la ride sud soit un peu plus élevée que ce qui était suggéré par les seules données ODP (j'ai probablement pris en compte des glissements déclenchés sur la proto-ride d'Owen dans mes estimations des fréquences). Mes études préliminaires des données de la campagne Owen 2 suggèrent une récurrence plutôt de l'ordre de 2 Ma selon l'endroit considéré (au lieu des 4 Ma précédemment déterminés à certains endroits).

A partir de simulations numériques réalisées à partir du code avalanche (*Heinrich et al., 2001*), le second article publié à *NHESS* présente la propagation d'un tsunami potentiellement généré par le glissement de terrain le plus volumineux identifié au niveau du segment sud de

la Ride d'Owen. La ville de Salalah, 190 000 habitants, serait potentiellement affectée par une source qui aurait les mêmes dimensions que celle simulée.

Marine Geology 326–328 (2012) 80–100

Contents lists available at SciVerse ScienceDirect

Marine Geology

journal homepage: www.elsevier.com/locate/margeo

# Mass wasting processes along the Owen Ridge (Northwest Indian Ocean)

Mathieu Rodriguez [a,b,c,*], Marc Fournier [a,b], Nicolas Chamot-Rooke [c], Philippe Huchon [a,b], Sébastien Zaragosi [d], Alain Rabaute [a,b]

[a] Institut des Sciences de la Terre de Paris, CNRS UMR 7193, Université Pierre & Marie Curie, case 129, 4 place Jussieu, 75005 Paris, France
[b] iSTeP, UMR 7193, CNRS, F-75005 Paris, France
[c] Laboratoire de Géologie de l'Ecole normale supérieure de Paris; CNRS UMR 8538, 24 rue Lhomond, 75005 Paris, France
[d] EPOC Université Bordeaux1, UMR 5805, avenue des facultés, 33405 Talence, France

ARTICLE INFO

*Article history:*
Received 21 November 2011
Received in revised form 13 June 2012
Accepted 3 August 2012
Available online 25 August 2012

Communicated by: D.J.W. Piper

*Keywords:*
submarine landslides
Owen Ridge
Owen Fracture Zone
Indian Ocean
Arabian Sea
strike–slip fault

ABSTRACT

The Owen Ridge is a prominent relief that runs parallel to the coast of Oman in the NW Indian Ocean and is closely linked to the Owen Fracture Zone, an 800-km-long active fault system that accommodates today the Arabia–India strike–slip motion. Several types of mass failures mobilizing the pelagic cover have been mapped in details along the ridge using multibeam bathymetry and sediment echosounder. Here we present a synthetic map of the different types of mass wasting features observed along the ridge and we further establish a morphometric analysis of submarine landslides. The spatial variation of failure morphology is strongly related to the topography of the basement. The highest volumes of multi-events generated slides are mobilized along the southern portion of the ridge. There, the estimated volume of evacuated material during a slide is up to 45 $km^3$. Combining these new observations with re-interpreted ODP seismic lines (Leg 117) documents sporadic mass wasting events through time along the southern segment of the ridge since its uplift in the Early Miocene, with a typical recurrence rate of the order of $10^5$–$10^6$ years. Although seismicity may still be the final triggering process, mass wasting frequency is mainly controlled by the slow pelagic sedimentation rates and hence, time needed to build up the 40–80 m thick pelagic cover required to return to a mechanically unstable pelagic cover.



## 1. Introduction

The study of mass wasting processes on continental margin has become a major topic of research during the last decades, since it plays a key role in sediment transportation to the deep ocean (Masson et al., 2006 and references herein). Mass wasting encompasses all gravity-driven mass movement processes. Failures affect the seabed morphology and its subsequent evolution in a variety of ways, in relation with the mechanical properties of the mobilized sediments and the large variation in volume, frequently less than one $km^3$ but exceptionally over 20,000 $km^3$ (Agulhas slump in SE Africa; Dingle, 1977). Although well described at continental margins (Prior, 1999; Canals et al., 2004), mass wasting along the slopes of oceanic highs standing in deep water remains poorly investigated, with the exception of the Lomonosov Ridge in the Arctic Ocean (Kristoffersen et al., 2007), the Macquarie Ridge in the South Pacific (Massel et al., 2000), and Chain Ridge off the Horn of Africa (Pimm et al., 1972). Unlike continental margins, sedimentation on these remote oceanic ridges is generally characterized by low rates of pelagic sedimentation, not directly controlled by relative sea level variations or clastic continental input. Rapid sedimentation has commonly been invoked as an important pre-conditioning factor for slope instability (Hampton et al., 1996; Lee et al., 2007), even though slope failure as a result of sedimentation alone seems unlikely based on theoretical grounds (Viesca and Rice, 2012). Other non-gravitational triggering factors invoked in deep-sea environments include earthquakes (Almagor and Wisenam, 1982; Hampton et al., 1996; Mulder et al., 2009), internal waves and/or fluid (including gas) escapes (Mienert and Posewang, 1999). To avoid any confusion, the term "failure" is hereafter used for ruptures related to mass wasting processes, and the term "fault" is used for ruptures related to tectonic processes, although both terms refer to a mechanical discontinuity in rocks.

The ~2000-m deep Owen Ridge in the NW Indian Ocean is one of these deep-water sites of widespread mass wasting where links with active tectonics can be tested. The India–Arabia plate boundary — known as the Owen Fracture Zone — runs along the ridge for more than 800 km, where it accommodates 3 mm $a^{-1}$ of dextral relative motion generating moderate seismicity (Fig. 1; Fournier et al., 2008a, 2011). Both the Owen Ridge and Owen Fracture Zone were extensively surveyed during the OWEN and FANINDIEN 2009 cruises (Fig. 1) aboard the BHO Beautemps-Beaupré of the French Navy. Between 15°N (Beautemps-Beaupré Basin; Fournier et al., 2008b) and 22°30'N (Dalrymple Trough; Edwards et al., 2000; Gaedicke et al., 2002; Edwards et al., 2008), the Owen Ridge is composed of three distinct bathymetric highs covered by a ~500 m thick pelagic drape (Shipboard

* Corresponding author at: Institut des Sciences de la Terre de Paris, CNRS UMR 7193, Université Pierre & Marie Curie, case 129, 4 place Jussieu, 75005 Paris, France. Tel.: +33 1 44 27 59 43.
*E-mail address:* rodriguez@geologie.ens.fr (M. Rodriguez).

0025-3227/$ – see front matter © 2012 Elsevier B.V. All rights reserved.
http://dx.doi.org/10.1016/j.margeo.2012.08.008

Scientific Party, 1989) affected by numerous submarine landslides displaying a large variety of morphological features. Here we use these newly acquired multibeam bathymetry and SBP120 (Sub-Bottom Profiler) data, together with data collected during the DSDP (Shipboard Scientific Party, 1974) and the ODP Leg 117 (Shipboard Scientific Party, 1989), to give a detailed description of mass wasting along the Owen Ridge.

The first topic of this paper is the study of spatial variations of the mass wasting process along the three segments of the Owen Ridge. The relative arrangement of slope failures and their deposits is first described to determine the variety of mass movement types. The evolution of the material during failure and transport is then investigated for each ridge segment. Using the method established by McAdoo et al. (2000) for bathymetric data, the volume of material mobilized at the initial stage of slope failure is estimated for each event, allowing a quantitative comparison of the erosive pattern along each of the ridge segments as well as on both sides of it. A statistical analysis of the morphological parameters of landslide scars is also performed to establish simple hypotheses regarding the origin and behaviour of failure along the Owen Ridge.

The second topic of this paper is to assess factors that control mass wasting processes through time, including triggering factors of submarine landslides. Such approach is limited to the southern Owen Ridge for which ODP data are available and allow us to date the mass transport deposits (MTDs hereafter) back to Early Miocene (Fig. 2). Whether the multi-failures landslides currently displayed on the seafloor are the product of one single catastrophic event destabilizing the entire southern ridge segment or the product of distinct and sporadic events destabilizing only limited areas is resolved by studying the relative arrangement of MTDs displayed on ODP seismic lines. The time recurrence of mass wasting events is compared with a model of earthquake recurrence along the southernmost segment of the Owen Fracture Zone to identify whether seismicity is a potential triggering factor of slope failure and MTDs a paleo-seismicity record. Slope failure frequency, together with the spatial distribution of volumes of sediment involved for each failure, allow us to discuss the preservation of submarine relief through time.

## 2. Geological background

### 2.1. Geodynamic setting

The present-day India–Arabia plate boundary in the NW Indian Ocean is located along the Owen Fracture Zone, which is an 800-km-long strike–slip fault system (Fig. 1; Rodriguez et al., 2011). This fault system connects the Sheba and Carlsberg ridges to the eastern end of the Makran subduction zone. Northward migration of the Arabian plate with respect to Eurasia being slightly faster than the Indian plate at this longitude, the relative plate motion is accommodated by a $3 \pm 1$ mm $a^{-1}$ dextral component (Fournier et al., 2008a; DeMets et al., 2010). The present-day fault system has led to a finite displacement of about 10 to 12 km measured by morphologic offsets in the seafloor, which would indicate, at a constant rate of 3 mm $a^{-1}$, a Pliocene age for the youngest fault system expressed today at the seafloor (Fournier et al., 2011). Dextral motion, however, may have started as early as the Miocene (magnetic anomaly An 6, 19.7 Ma), as soon as spreading in the Gulf of Aden became effective (Chamot-Rooke et al., 2009; Fournier et al., 2010). The seismicity along the fault is rather low and scattered (Fig. 1), so that only few focal mechanisms are available (Quittmeyer and Kafka, 1984; Gordon and DeMets, 1989; Fournier et al., 2001). They consistently indicate pure strike–slip motion. The maximum magnitude recorded to date is a $M_w$ 5.3 earthquake (Harvard CMT, 7 April 1985). However infrequent but large earthquake may be expected as at other fracture zones (Antolik et al., 2006; Robinson, 2011).

### 2.2. Morphology of the Owen Ridge and sedimentary setting

The Owen Fracture Zone follows a major morphological feature, the Owen Ridge, which is a SSW-NNE trending ridge-and-through system that may be divided — starting from the Beautemps-Beaupré Basin in the south — into five geographic provinces (Fig. 1): the southern ridge, which consists of a 300 km-long, 50 km-wide, up to 2000 m-high relief (Fig. 3); the central ridge, which is a 220 km-long, 50 km-wide, and up to 1700 m-high relief (Fig. 4); the 20°N pull apart basin; the Qalhat Seamount (or northern ridge) which is a 210 km-long, more than 55 km-wide, and up to 2700 m-high relief (Fig. 5); and the Dalrymple Trough. The Owen Ridge topographic highs act as a barrier for the Indus turbiditic sedimentation and isolate the Owen Basin, located west of the Owen Ridge, from any sediment supply from the east (Whitmarsh, 1979; Mountain et al., 1990). Since its uplift in the Early Miocene (Shipboard Scientific Party, 1989), the ridge has mainly supported the deposition of a ~500 m thick chalk and ooze pelagic blanket, and minor terrestrial input from monsoonal eddies (Clemens and Prell, 2006) and oceanic jet (Ras al Hadd jet; Böhm et al., 1999; Fig. 6). The establishment of an upwelling zone in the Late Miocene induced an increase in sedimentation rates (from 8–15 m $Ma^{-1}$ to 54 m $Ma^{-1}$) (Mountain and Prell, 1989). Since the Pliocene, the sedimentation is mainly oozy in composition, with sedimentation rates typical of pelagic deposition (30 to 40 m $Ma^{-1}$) (Mountain and Prell, 1989; Shipboard Scientific Party, 1989), and is controlled by seasonal monsoon (Clemens and Prell, 2006).

### 2.3. Geological and tectonic history of the Owen Ridge

The present-day morphology of the Owen Ridge results from successive tectonic and volcanic events. The southern and central segments of the Owen Ridge were uplifted ~19 Ma ago, as attested by the rapid transition from turbiditic to pelagic deposits in DSDP and ODP cores (Whitmarsh et al., 1974; Shipboard Scientific Party, 1989; Weissel et al., 1992). The southern ridge appears as a large-scale tilted and relatively flat slab, interpreted as flexural response to compression (Weissel et al., 1992). Several seismic lines run as pre-site surveys for ODP reached the basement of the southern ridge, and show an uneven paleo-topography (Fig. 2). The substratum is basaltic in composition and of Paleocene age (Shipboard Scientific Party, 1974, 1989). Both the southern and the central ridges may have stand as positive basement features being progressively buried under turbiditic deposits during the Paleogene to Early Miocene interval, as suggested by the Oligocene turbiditic deposits drilled between two basement highs on the southern ridge (Fig. 2) (Shipboard Scientific Party, 1989; Clift et al., 2001; Gaedicke et al., 2002). The southern and central segments rose significantly above the level of the Indus fan to their present-day configuration following the 19 Ma uplift episode (Fig. 6).

At the northern end of the OFZ, the history of the Qalhat Seamount is not clearly established. The nature of the underlying basement remains unknown since it has never been directly sampled. The nearby presence of the Little Murray Ridge volcanic seamounts buried under the Oman basin (Gaedicke et al., 2002; Mouchot, 2009), coupled with the existence of a strong magnetic anomaly in the vicinity of the seamount and a typical flat top morphology, strongly suggest that the Qalhat Seamount is a volcanic guyot (Edwards et al., 2000; Fournier et al., 2011). Onlap of Paleocene sediments onto the Qalhat Seamount (Edwards et al., 2000; Gaedicke et al., 2002; Edwards et al., 2008) demonstrates that the seamount is Cretaceous in age or older.

## 3. Materials and methods

### 3.1. Bathymetry and sub-bottom profiles

Swath bathymetry and backscatter data were collected using a hull-mounted Kongsberg-Simrad EM120 multibeam echosounder

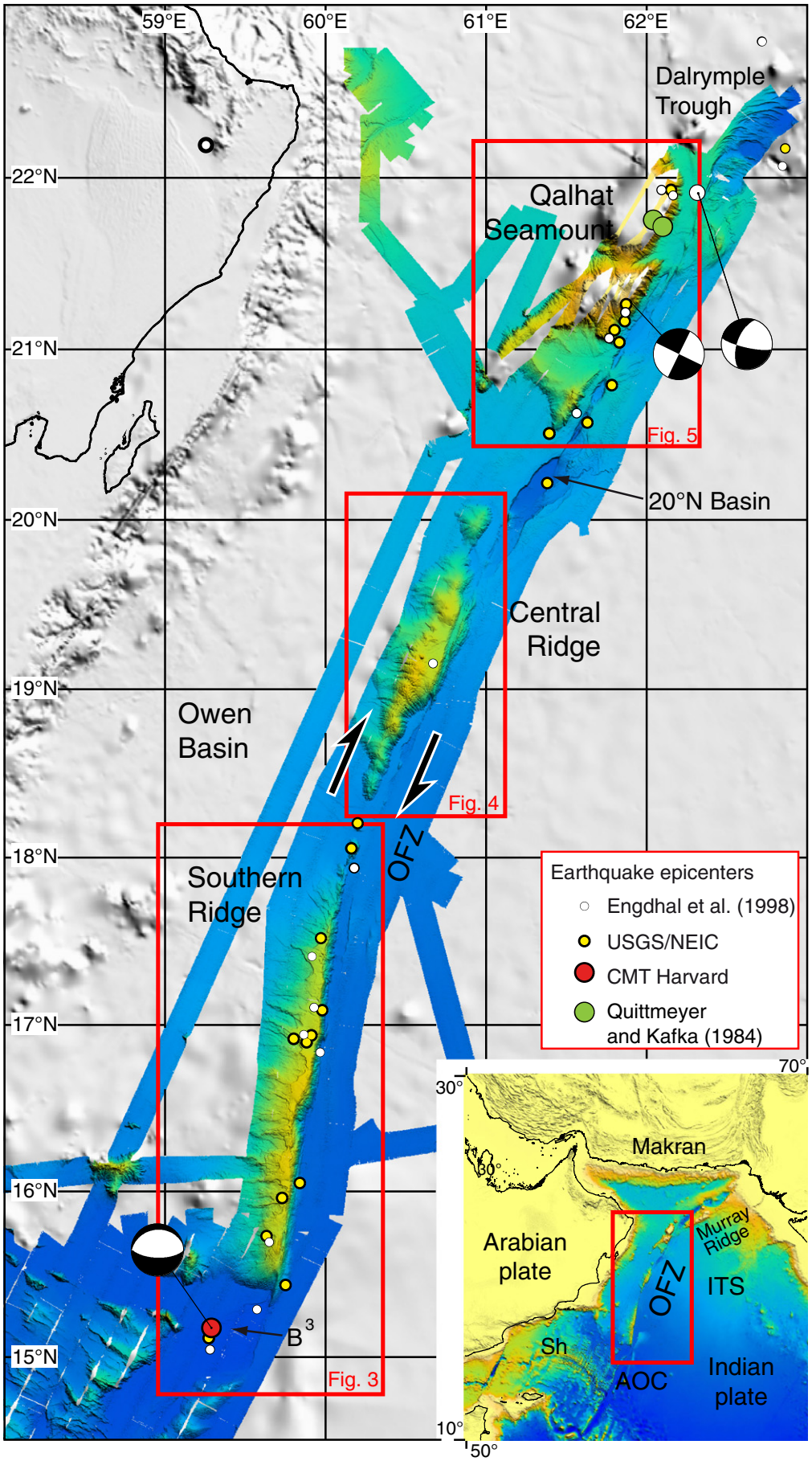
59°E
60°E
61°E
62°E
22°N
21°N
20°N
19°N
18°N
17°N
16°N
15°N
Dalrymple Trough
Qalhat Seamount
Fig. 5
20°N Basin
Central Ridge
Owen Basin
Fig. 4
OFZ
Southern Ridge
B3
Fig. 3
Earthquake epicenters
Engdhal et al. (1998)
USGS/NEIC
CMT Harvard
Quittmeyer and Kafka (1984)
70°
30°
30°
10°
50°
Makran
Arabian plate
Murray Ridge
OFZ
ITS
Sh
AOC
Indian plate

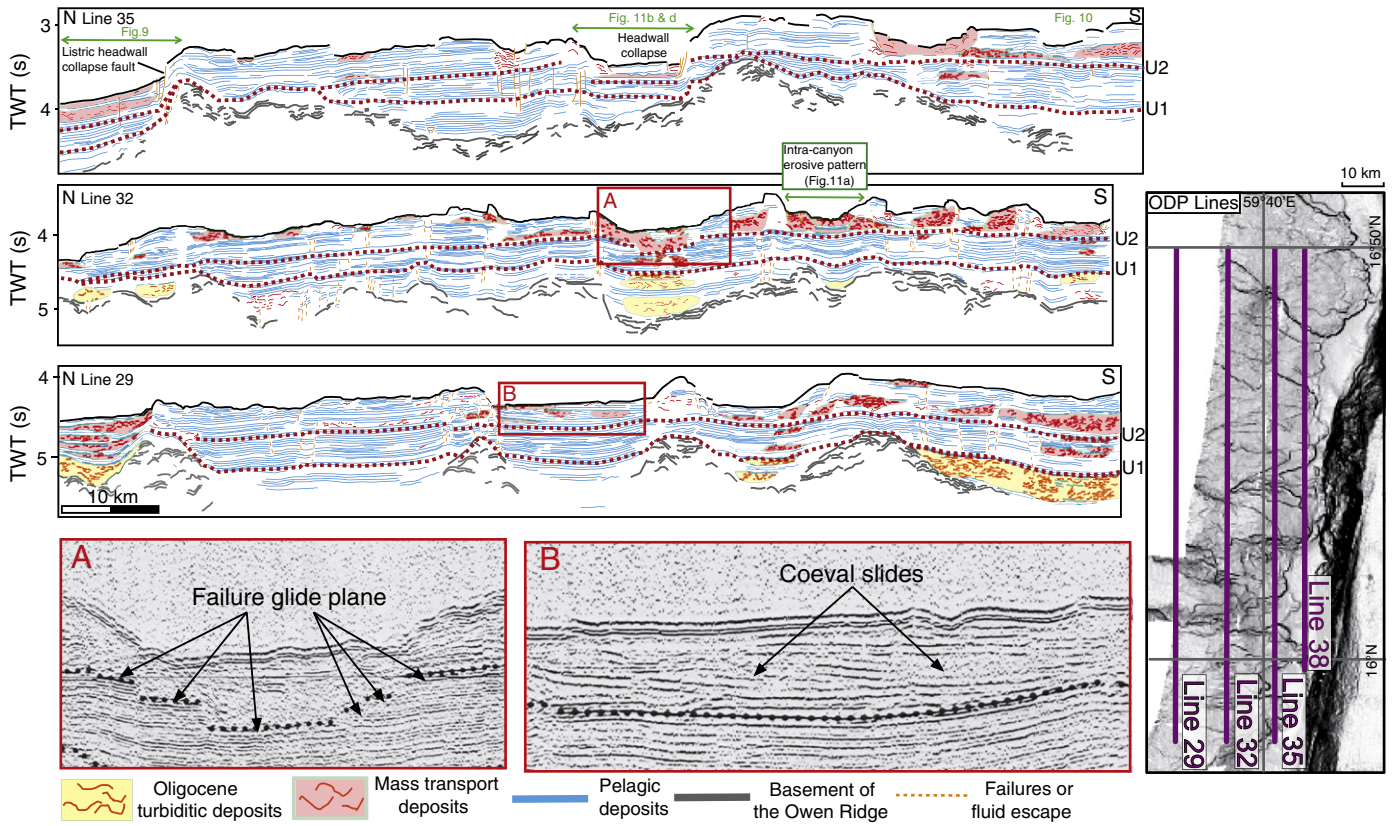


**Fig. 2.** Seismic lines collected during the ODP Leg 117 (Shipboard Scientific Party, 1989) and their new interpretation, with special emphasises on mass wasting events. Dotted line U1 marks the earliest uplift of the Owen Ridge in Early Miocene (ca. 19 Ma) and images the pre-uplift topography of the southern ridge. Dotted line U2 marks the facies change from turbidites to pelagic sediments at about 15 Ma. Inset on the right hand corner shows the location of ODP seismic profiles. Insets A and B are close-up of portions of seismic lines 32 and 29, respectively.

during the OWEN and FANINDIEN surveys (2009). Final maps were produced at an 80-m-grid interval. The vertical resolution of the swath bathymetric data is of the order of 10 m, higher resolution being reached for vertical beams and lower resolution for far-angle lateral beams. SBP120 sub-bottom profiles were acquired along with bathymetry and reflectivity, providing a set of high frequency (3.5 kHz) high-resolution profiles with penetration down to 100 m in fine-grained sediments and about 25 m in sand-rich floor. The subsurface geology is complementary documented by ODP seismic lines along the southern Owen Ridge (Shipboard Scientific Party, 1989). This dataset is used to identify and map the different mass wasting types along the Owen Ridge.

### 3.2. Statistical analysis of morphological parameters

Numerous slope failures are imprinted in the present-day morphology and can directly be studied from multibeam mapping. A statistical analysis of morphometric parameters of submarine landslides was performed following the method described by McAdoo et al. (2000), which considers only multi-failures events, i.e. large failures composed of several individual failures that occurred as one single event. As an improvement of the method of McAdoo et al. (2000), we also analyze morphometric parameters of individual failures, which can be good proxies for the rheology of the mobilized material. The statistical analysis of morphometric parameters will be further used to discuss the variability of failure processes along the three segments of the Owen Ridge.

Forty-six multi-failure events have been recognized along the Owen Ridge, and almost 400 individual slope failures have been studied. A set of morphological parameters have been systematically measured: headscarp water depth, headscarp height, total area of seafloor affected by the failure, unfailed adjacent slope, runout slope, headscarp slope, and finally slide volume (Table 1). The headscarp region is the steepest slope in the eroded scar zone. The failure area is defined either as the portion of seafloor with a hummocky facies enclosed by a scar (in case of cohesive failure), or as the portion of seafloor enclosed by a scar (in case of disintegrative failure). Runout distances cannot be fully addressed because of the narrow swath available around the Owen Ridge. Table 1 summarizes correlations (covariance) between all those morphological parameters.

Following McAdoo et al. (2000), we estimated the volume mobilized in the initial stage of multi-failures events (see Table 1 for the details of the method). This volume estimation does not take into account the volume mobilized during mass motion. The estimation of the volume of multi-failure event is dependent on the interpretation of the timing of slope failure (see Section 4).

**Fig. 1.** Multibeam bathymetry of the study area acquired during the AOC 2006, OWEN and FANINDIEN 2009 cruises, with location of Figs. 3, 4 and 5. Inset shows the regional setting of the India–Arabia plate boundary. Crustal seismicity since 1973 (focal depth < 50 km, magnitude $M_w > 2$) is from the USGS/NEIC database (yellow dot), Engdhal et al. (1998, white dot), CMT Harvard database (red dot), and Quittmeyer and Kafka (1984; green dot). AOC: Aden–Owen–Carlsberg triple junction, $B^3$: Beautemps-Beaupré Basin, ITS: Indus turbiditic system, OFZ: Owen Fracture Zone, Sh: Sheba Ridge. The three boxes correspond to the segmentation of the Owen Ridge (southern, central, and northern segments) used throughout the text.

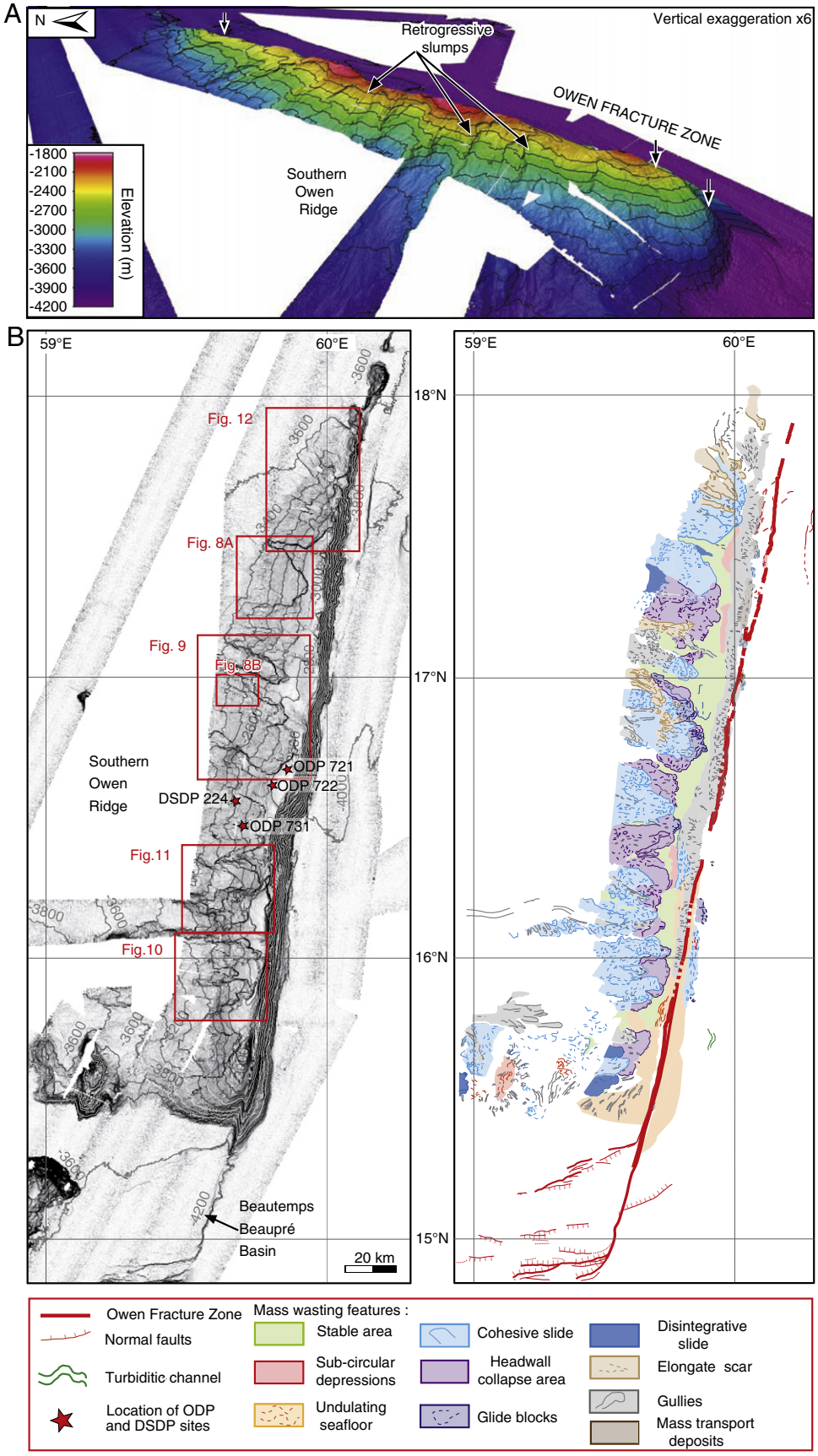


**Fig. 3.** A) Bird's eye view of the southern ridge with 200-m interval bathymetric contours, and main seabed features. B) Slope map of the southern Owen Ridge with location of Figs. 8A and B, and 9 to 12, and synthetic map of the different types of mass wasting observed.

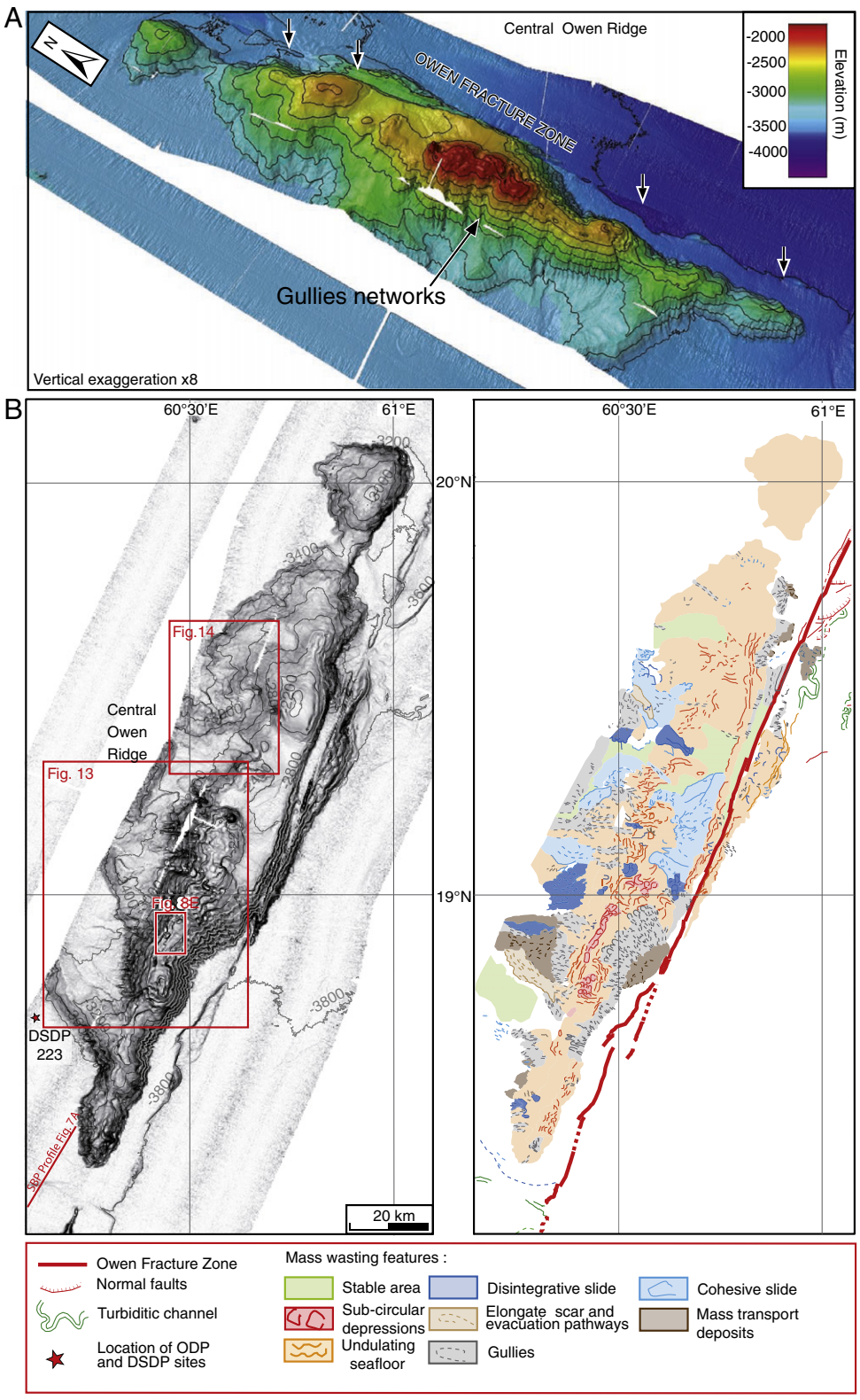


**Fig. 4.** A) Bird's eye view of the central ridge with 200-m interval bathymetric contours, and main seabed features. B) Slope map of the central Owen Ridge with location of Figs. 7A, 8E, 13 and 14, and synthetic map of the different types of mass wasting mode observed.

### 3.3. Estimation of mass transport deposits recurrence

The vertical distribution of MTDs can be observed on ODP seismic lines on the southern ridge (Fig. 2) and SBP profiles on the central and the northern ridges (Fig. 7). ODP seismic lines reach the Early Miocene, whereas the penetration of SBP profiles is limited to the last 3 Ma. Age estimates used in this study are based upon ODP Leg 117, and DSDP Leg 222 bio-stratigraphic dating and sedimentation rate estimates. Sedimentation rates were used on sub-bottom profiles and on ODP seismic lines to estimate the time recorded by pelagic

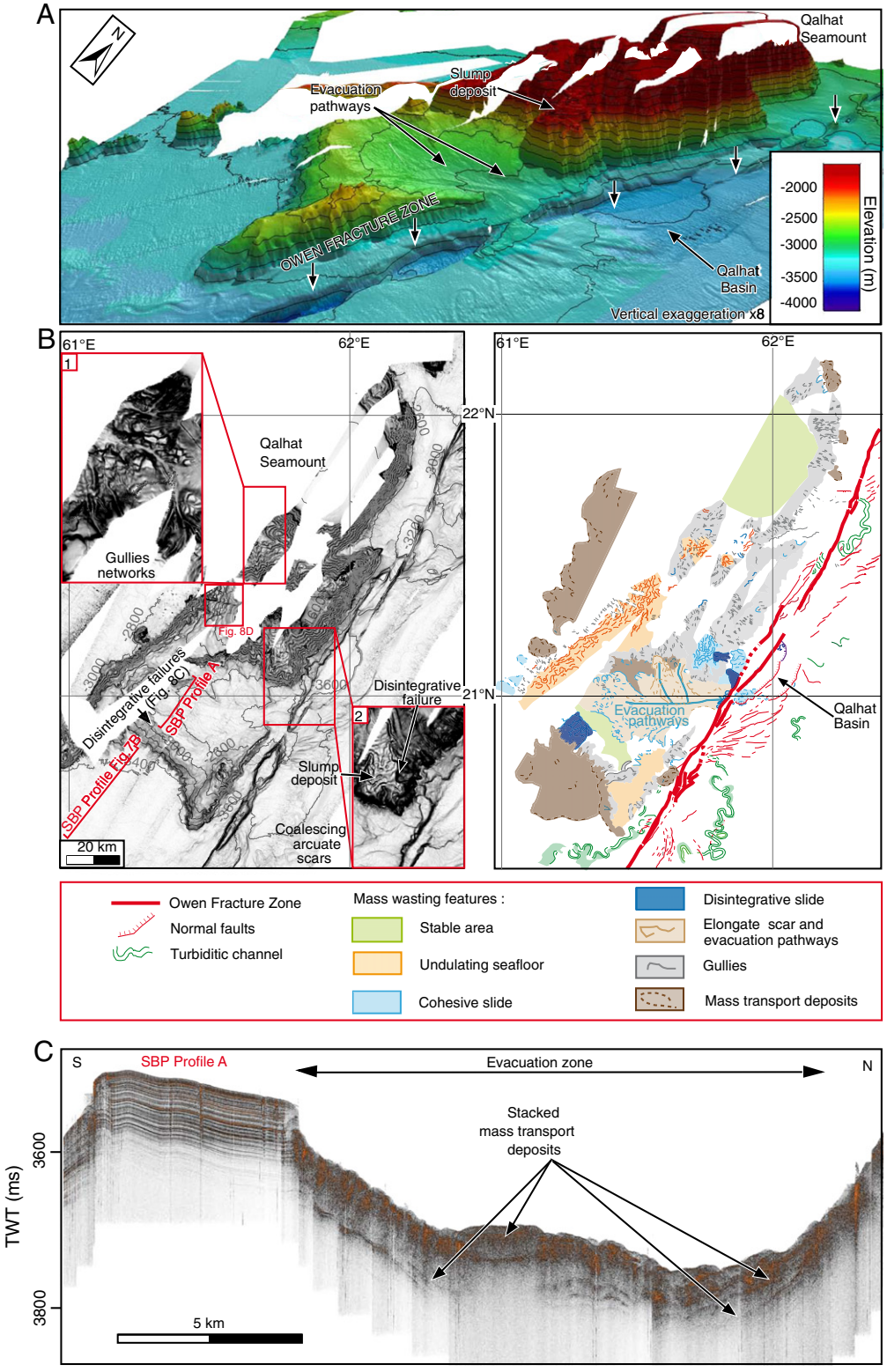


**Fig. 5.** A) Bird's eye view of the Qalhat seamount with 200-m interval bathymetric contours, and main seabed features. B). Slope map of the Qalhat Seamount with location of Figs. 7B and 8D, and synthetic map of the different types of mass wasting mode observed. Inset 1 shows networks of gullies, which display short dendritic network at its head, that rapidly merge into rectilinear evacuation pathways. Inset 2 shows gullies locally cutting into a slump deposit, which shows an undulated seafloor evolving down-slope into an irregular morphology, composed of coalescing and irregular circular depressions. C) 3.5 kHz profiles showing several generations of MTDs merging in the evacuation zone (see B for location).

deposits that lie between two MTDs. Although the deposition of a MTD implies the removal of a part of the underlying pelagic cover, the time recorded by pelagic deposits is assumed to give an estimation of the time period between two MTDs. Sedimentation rates are in the range of 20–44 m $Ma^{-1}$ for the southern ridge from Early Miocene to Early Pliocene. From Pliocene to present, sedimentation rates for the

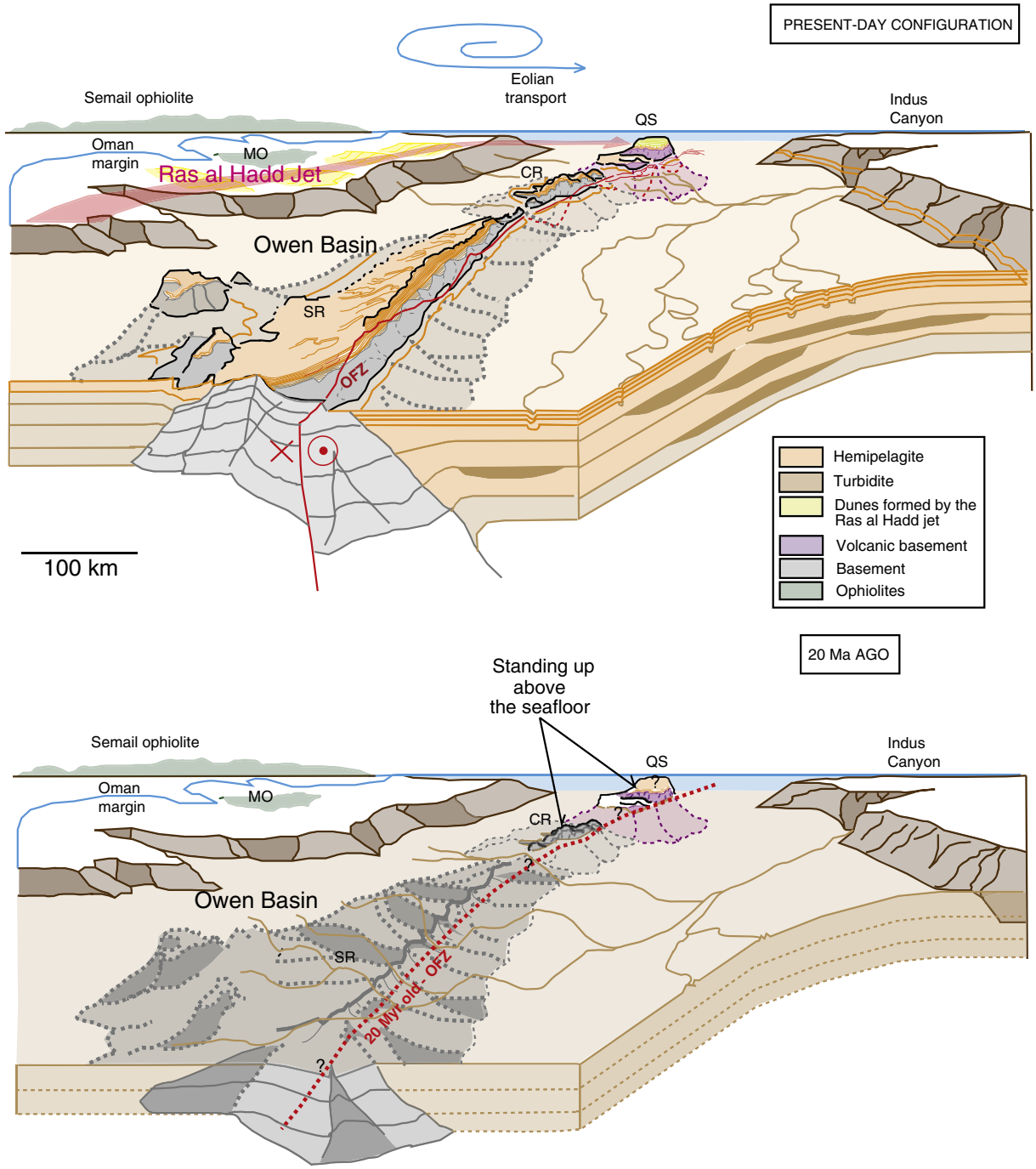


**Fig. 6.** Perspective views of the sedimentary system of the Owen Ridge before the uplift (bottom) and at present (top). Both the Qalhat Seamount and the Central Ridge stood above the Indus abyssal plain 20 Ma ago. Sediment waves on the Oman continental shelf are generated by the Ras al Hadd Jet. CR: Central Ridge, MO: Masirah Ophiolites, OFZ: Owen Fracture Zone, QS: Qalhat Seamount, SR: Southern Ridge.

central and northern ridges are of the order of 60 m $Ma^{-1}$ (DSDP site 223), and 42–53 m $Ma^{-1}$ (DSDP site 222), respectively. A P-wave velocity of 1500 m $s^{-1}$ is used for SBP profiles to convert two-way travel time to depth. Depth dependent P-wave velocities curves from Shipboard Scientific Party (1989) are used to calibrate the thickness of sedimentary layers on ODP seismic lines.

## 4. Nomenclature of mass wasting features

Submarine landslide nomenclatures are mainly based on detailed core analyses, which reveal the large variety of mass wasting processes (Hampton et al., 1996; Mulder and Cochonat, 1996; Mulder and Alexander, 2002; Canals et al., 2004). In these nomenclatures, each term is related to a depositional mode. Based only on multibeam bathymetry and SBP120 data, it is difficult to determine whether a mass movement is a slump, a slide, or a debris flow, and these nomenclatures are inappropriate for these types of data (McAdoo et al., 2000; Tripsanas et al., 2008). The use of genetic nomenclatures is still more difficult in the case of multi-processes generated morphology. Indeed, different genetic processes, such as gravity instability, deformation, or sedimentary construction, may lead to quite similar sea-bottom morphology and echo-facies (see discussion for the Humboldt slide in Lee

**Table 1**
Correlation coefficients (covariance) for the morphometric parameters of slope failures along the Owen Ridge. All of the measured and calculated variables are correlated to explore possible relationships. Coefficients greater than or equal to 0.5 are highlighted in bold and yellow. Coefficients used to discuss failure mechanisms are highlighted in green.

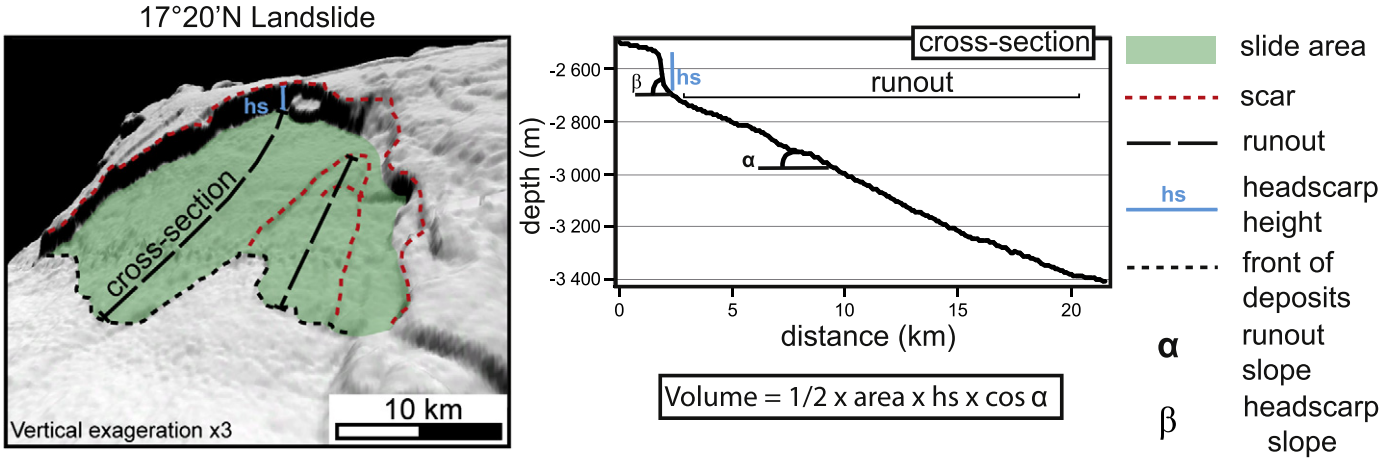


| correlations (covariance) Southern ridge (western slope) | area | water depth of failure initiation | headscarp height | scar length | headscarp slope | runout slope | volume |
|---|---|---|---|---|---|---|---|
| area | 1 | | | | | | |
| water depth of failure initiation | 0.10 | 1 | | | | | |
| headscarp height | -0.02 | -0.32 | 1 | | | | |
| scar length | 0.93 | 0.15 | 0.02 | 1 | | | |
| headscarp slope | -0.19 | -0.34 | 0.19 | -0.25 | 1 | | |
| runout slope | -0.17 | -0.18 | 0.37 | -0.16 | 0.39 | 1 | |
| volume | 0.69 | -0.06 | 0.56 | 0.69 | -0.09 | 0.15 | 1 |

| Central ridge | area | water depth of failure initiation | headscarp height | scar length | headscarp slope | runout slope | volume |
|---|---|---|---|---|---|---|---|
| area | 1 | | | | | | |
| water depth of failure initiation | -0.20 | 1 | | | | | |
| headscarp height | 0.03 | -0.55 | 1 | | | | |
| scar length | 0.87 | -0.12 | 0.01 | 1 | | | |
| headscarp slope | -0.08 | -0.41 | 0.73 | -0.07 | 1 | | |
| runout slope | -0.07 | 0.14 | -0.17 | 0.10 | 0.15 | 1 | |
| volume | 0.89 | -0.41 | 0.29 | 0.70 | 0.09 | -0.10 | 1 |

| Northern ridge | area | water depth of failure initiation | headscarp height | scar length | headscarp slope | runout slope | volume |
|---|---|---|---|---|---|---|---|
| area | 1 | | | | | | |
| water depth of failure initiation | 0.05 | 1 | | | | | |
| headscarp height | -0.17 | -0.06 | 1 | | | | |
| scar length | 0.94 | 0.03 | -0.10 | 1 | | | |
| headscarp slope | -0.18 | 0.09 | 0.65 | -0.07 | 1 | | |
| runout slope | -0.20 | -0.41 | -0.10 | -0.05 | 0.32 | 1 | |
| volume | 0.66 | 0.13 | 0.25 | 0.78 | 0.37 | -0.08 | 1 |

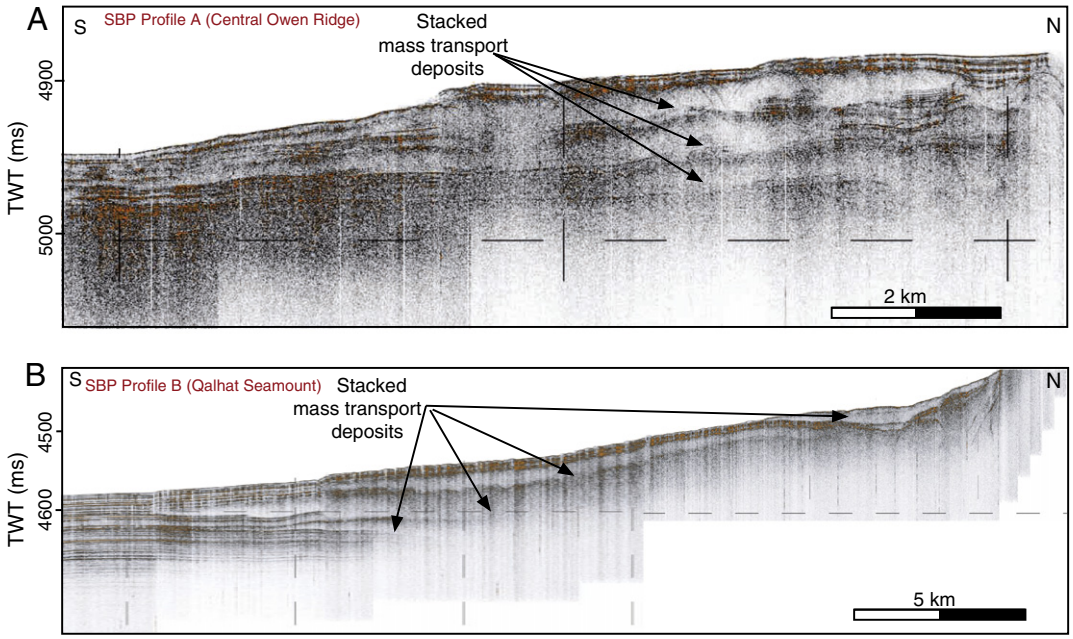


**Fig. 7.** 3.5 kHz profiles showing A) several lenses of MTDs related to the erosion of the southern flank of the central Owen Ridge by disintegrative failures and B) MTDs related to the erosion of the southern flank of the Qalhat Seamount by disintegrative failures (see Figs. 4 and 5 for location, respectively).

et al., 2002). Complex interaction between these processes may also be misleading (Faugères et al., 2002). Despite these drawbacks, bathymetry, sub-bottom and seismic profiles are still powerful tools to study mass wasting processes at the scale of an entire margin. Based on observations of failure geometry on bathymetry and SBP profiles, we describe the mode of slope failure development of representative field examples of each mass wasting type that we observe and map (Fig. 8), and link them to previously published nomenclatures. In absence of core analysis, the understanding of the timing of slope failure from the interpretation of SBP profiles somehow provides arguments relative to the failure processes involved.

### 4.1. Cohesive failures and retrogressive slumps

Where deposits lie at the edge of the headwall scar, the failure is mapped as "cohesive". In this case, slope deposits are enclosed by the headwall scar and display a hummocky seafloor or scattered blocks on bathymetry (Figs. 8, 10). Such deposits display chaotic and hyperbolic reflections or a transparent facies on SBP profiles (Fig. 8, see also Figs. 5, 9, 10 for similar examples). They show as disturbed, chaotic or transparent reflectors on ODP seismic lines (Figs. 2, 9, 11). Such a description could correspond to slide, slump, debris avalanche, or rock fall deposits of mass wasting classifications (Mulder and Cochonat, 1996; McAdoo et al., 2000), i.e., all deposits related to the movement of a coherent mass of sediment bounded by distinct failures planes. Scattered glide blocks observed on bathymetry (Figs. 9, 10) might result from a partial disintegration of the sediment mass, but as they remain generally enclosed by the failure scar, they are included in the "cohesive" category. A particular case of "bottleneck failure" (Fig. 10) is observed along the southern Owen Ridge. Because the SBP profile shows MTD enclosed in the scar (Fig. 10), this type of failure is considered as cohesive. The term of "bottleneck failure" refers to a type of failure already defined by Prior and Coleman (1980) in the Gulf of Mexico.

Overlapping sub-parallel scars at headwall escarpments are commonly observed at the rear of a main failure scar that accommodated cohesive removal (Figs. 9, 10, 11). Such scars delineate areas of smooth or hummocky seafloor (Figs. 9, 10, 11) named hereafter as headwall collapse areas. The folded aspect of headwall collapse areas on SBP profiles can be either the result of gravitational deformation (linked to mass wasting processes) (Fig. 9) or the pelagic cover of an older irregular MTD surface at the limit of the SBP120 penetration, as seen on Fig. 11. The deep geometry of headwall collapse areas is observed on ODP seismic lines (Figs. 2, 9), which show blocks with limited down-slope total displacement along shallow listric faulting, and little internal remoulding near the headwall (Figs. 2, 9, 11).

Headwall collapse failures might either be fossil scars of previous landslides, or failures triggered subsequently to the cohesive departure of sediment, such as in retrogressive slumping events (Piper et al., 1999). In some areas (Fig. 9), the failure at the front of the headwall collapse area clearly offsets MTDs on SBP profile. The headwall collapse failure thus occurred both down and up-slope the main cohesive failure plane, affecting MTD and pelagic deposits, respectively (Fig. 9). Such a relative chronological constrain strongly suggests that headwall collapse motion and related failures are a subsequent response to the steep slope created by the cohesive mass departure.

An other interpretation is suggested by the failure exposed in Fig. 11. The ODP seismic line shows two distinct MTDs, the older one being covered by thicker pelagic deposits. The younger scar is located downslope the older one, suggesting a progressive erosion of the slope in this area.

Where cohesive failures are closely related to headwall collapse areas, they are thus interpreted as occurring as one single retrogressive slump event, consistently with previous works on similar failures (Grand Banks (Piper et al., 1999), Cretan margin (Strozyk et al., 2010), Storegga slide (Kvalstad et al., 2005)), excepted in the area illustrated in Fig. 11.

### 4.2. Disintegrative failure features

Where there are no obvious landslide deposits at the base of the scar or in the area enclosed by the scar, the failure is mapped as "disintegrative." The seafloor enclosed by the scar is smooth on bathymetry (Fig. 8). Reflectors display a rough facies on SBP profiles, as the result of the erosion related to the motion of the destabilized mass (Figs. 8, 12). The sediment mass could have lost its cohesion either during failure, or by incorporating fluids during the down-slope movement of the mass.

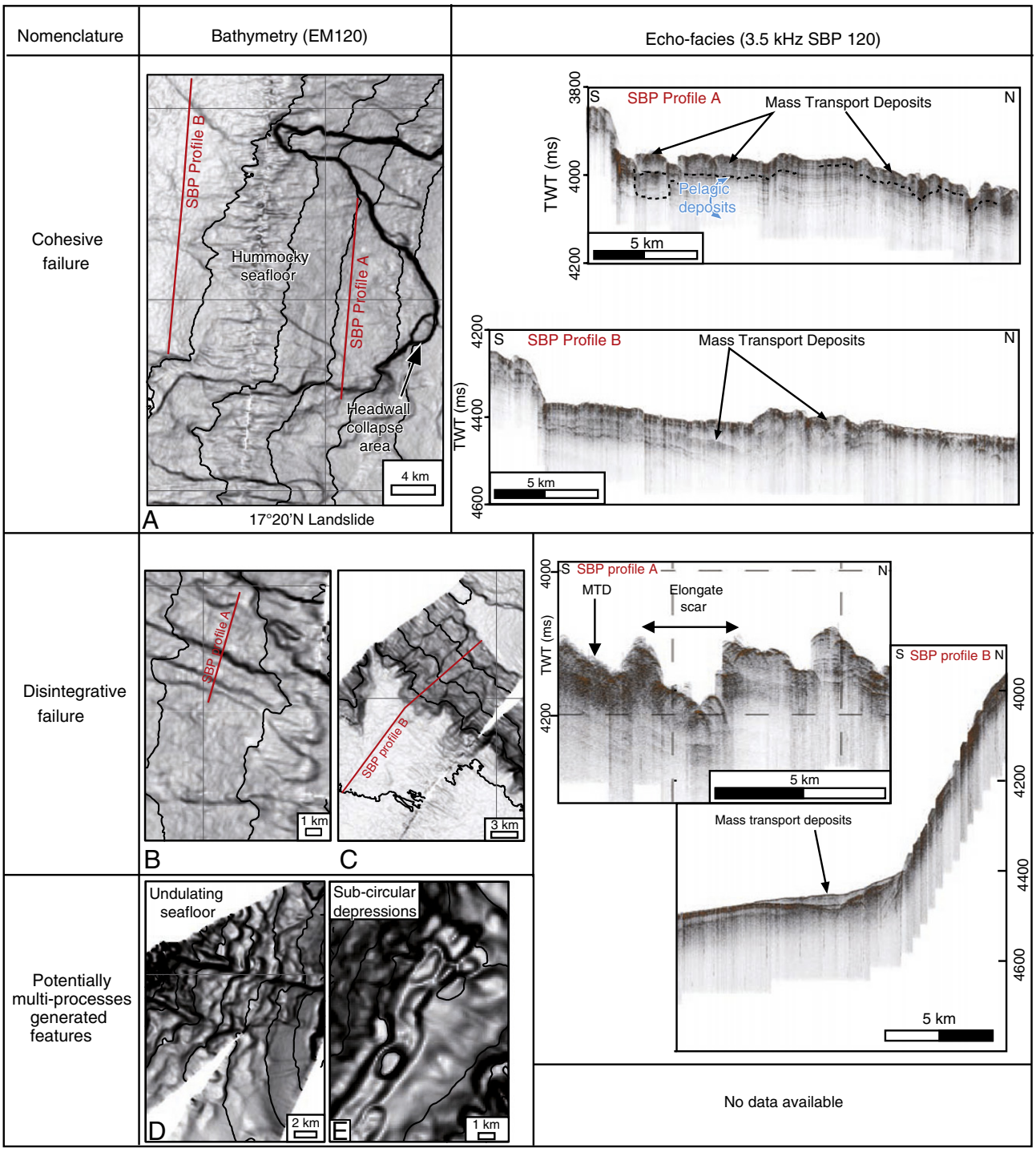


**Fig. 8.** Synthesis of EM120 swath bathymetry (slope map) features, 3.5 kHz echo-facies and their interpretation. The cohesive failure category is illustrated by the landslide located at 17°20'N on the southern ridge (see Fig. 3 for location). A hummocky seafloor area is enclosed in a failure scar. SBP profiles crossing the hummocky seafloor area shows chaotic to transparent reflections, which relates hummocky seafloor to areas of MTDs. This category of failure is complementary illustrated in Figs. 9 to 13. The disintegrative failure category is illustrated by two field examples. Elongate failures displayed on example A are located down-slope the western flank of the southern ridge (see Fig. 9). The SBP profile shows an elongate scar that eroded previously deposed MTDs. Arcuate failures displayed on example B are located on the southern flank of the Qalhat seamount (see Fig. 5 for location). MTDs are not observed in areas enclosed by a scar, but down-slope. This category is further illustrated in Figs. 5, 9, 12 and 13. The "multi-processes generated features" category is illustrated by two field examples. The undulating seafloor area displayed on example A is located on the western flank of the Qalhat Seamount (Fig. 5). It could be either the result of slump processes, or the result of bottom currents, or both of these processes. The sub-circular features displayed on example B are located on the top of the central ridge (Fig. 4). They could be either the result of fluid escape, carbonate dissolution, or early stages of slope destabilisation. See Section 4 in text for detailed explanations.

This second category relates to debris flow and grain flow in the classification of Mulder and Cochonat (1996).

Disintegrative failures observed along the Owen Ridge include arcuate failures (Fig. 8), evacuation pathways (Fig. 8, see also Figs. 5, 12, 13, 14 for other examples), and gullies (Fig. 13). Arcuate failures show a semi-circular, concave-upward shape (Fig. 8). The term of evacuation pathway refers to very elongate, rectilinear scars that erode previously deposed MTDs located down-slope, as shown on several SBP profiles (Fig. 8).

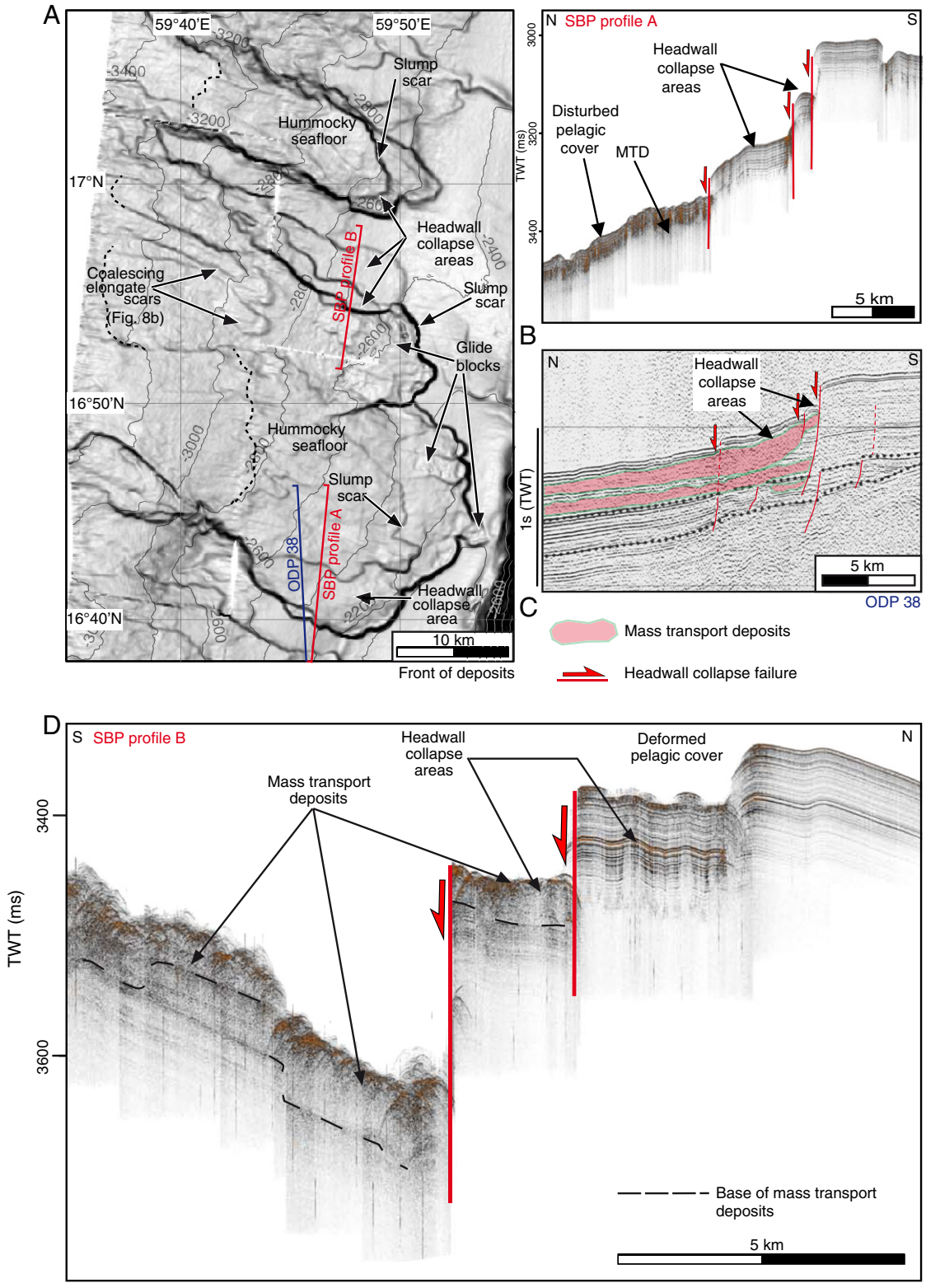


**Fig. 9.** A) Slope map of a multi-event generated scar on the southern Owen Ridge, showing the main slump scar and the related headwall collapse at the rear, with some block fall associated to the headwall collapse (see Fig. 3 for location). B) SBP profile crossing a headwall collapse area, and C) the related ODP seismic line (see Fig. A for location). D) 3.5 kHz profile showing MTD faulted by headwall collapse fault, and gently disturbed pelagic drape within the headwall collapse area (see Fig. A for location).

Gullies are forming by multiple small-scale episodes of retrogressive sedimentary removal (Fig. 13) and can be considered as a particular case of disintegrative failure, as no MTD lie in the area enclosed by the scar. Where deposits are identified outside of the area enclosed by the scar, they are mapped under the general term of MTDs.

### 4.3. Potentially multi-processes generated features

Two morphological features that could be the result of the interaction of slope instability with other processes (such as bottom currents or fluid escapes) were further identified along the Owen Ridge: undulating

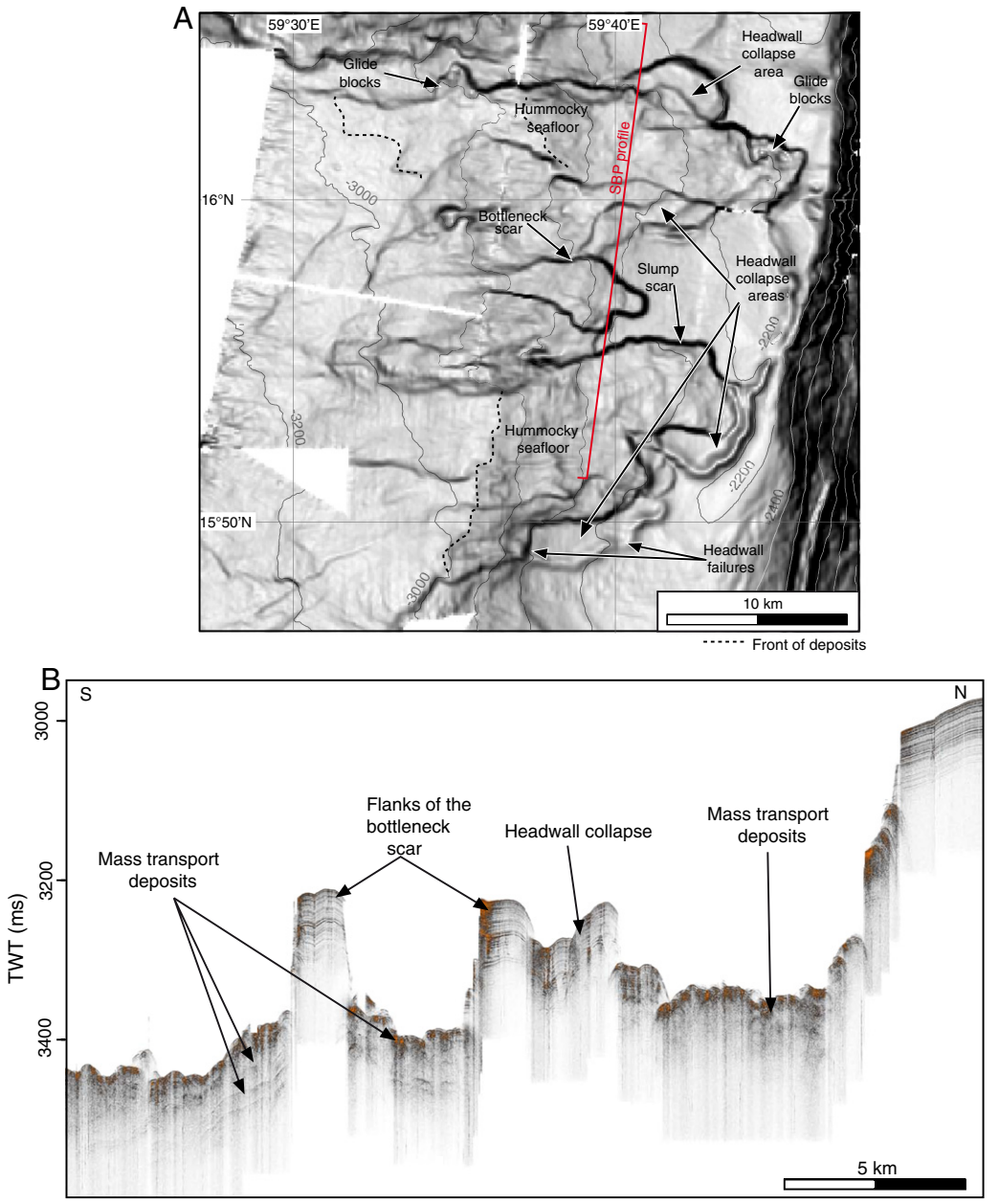


**Fig. 10.** A) Slope map of a multi-event generated scar on the southern Owen Ridge, showing a bottleneck scar (see Fig. 3 for location). Bottleneck scars are characterized by narrow opening (1000 m to 2760 m) at their mouth, through which a part of the cohesive flow is discharged. B) 3.5 kHz profile crossing the bottleneck scar and adjacent mass transport deposits (see A for location).

seafloor (Figs. 3, 4, 5, 8) and sub-circular depressions (Figs. 5, 8). Some authors identify undulating seafloor features as deformation structures, creep and/or early indication of slope instability (Lee et al., 1981; Field and Barber, 1993; Baraza and Ercilla, 1996; Gardner et al., 1999; Corregiari et al., 2001; Lee et al., 2002), or as the result of a combination of deformation and depositional processes (Faugères et al., 2002; Gonthier et al., 2002; Shillington et al., 2012). Sub-circular depressions similar to the ones observed along the Owen Ridge are described on the Malpelo Ridge (Lonsdale and Fornari, 1980) and on the Carnegie Ridge (Michaud et al., 2005) in the Pacific Ocean. Various origins have been proposed by Michaud et al. (2005), including underwater dissolution, submarine currents, fluid escape (such as in pockmarks features) and creeping. However, it is not possible to discriminate if slope instability is the dominant genetic process for the formation of these seafloor undulations and sub-circular depressions without geotechnical data (Sultan et al., 2008). Therefore, these two features are mapped but not discussed.

## 5. Results

Mass wasting affects the three topographic highs of the Owen Ridge in different ways and to different degrees. For each ridge segment, we first describe the large-scale morphology of the Owen Ridge and the distribution of failure volumes. We then describe the distribution of each mass movement type on both sides of each segment. Stratigraphic data from ODP Leg 117 are also used to assess the vertical distribution of MTDs. The tectonics of the Owen Fracture Zone is detailed in Rodriguez et al. (2011), but where necessary we describe the relationship between the MTDs and the surface traces of the active faults. In the following, the term of open-slope type means that no topographic barrier obstructs

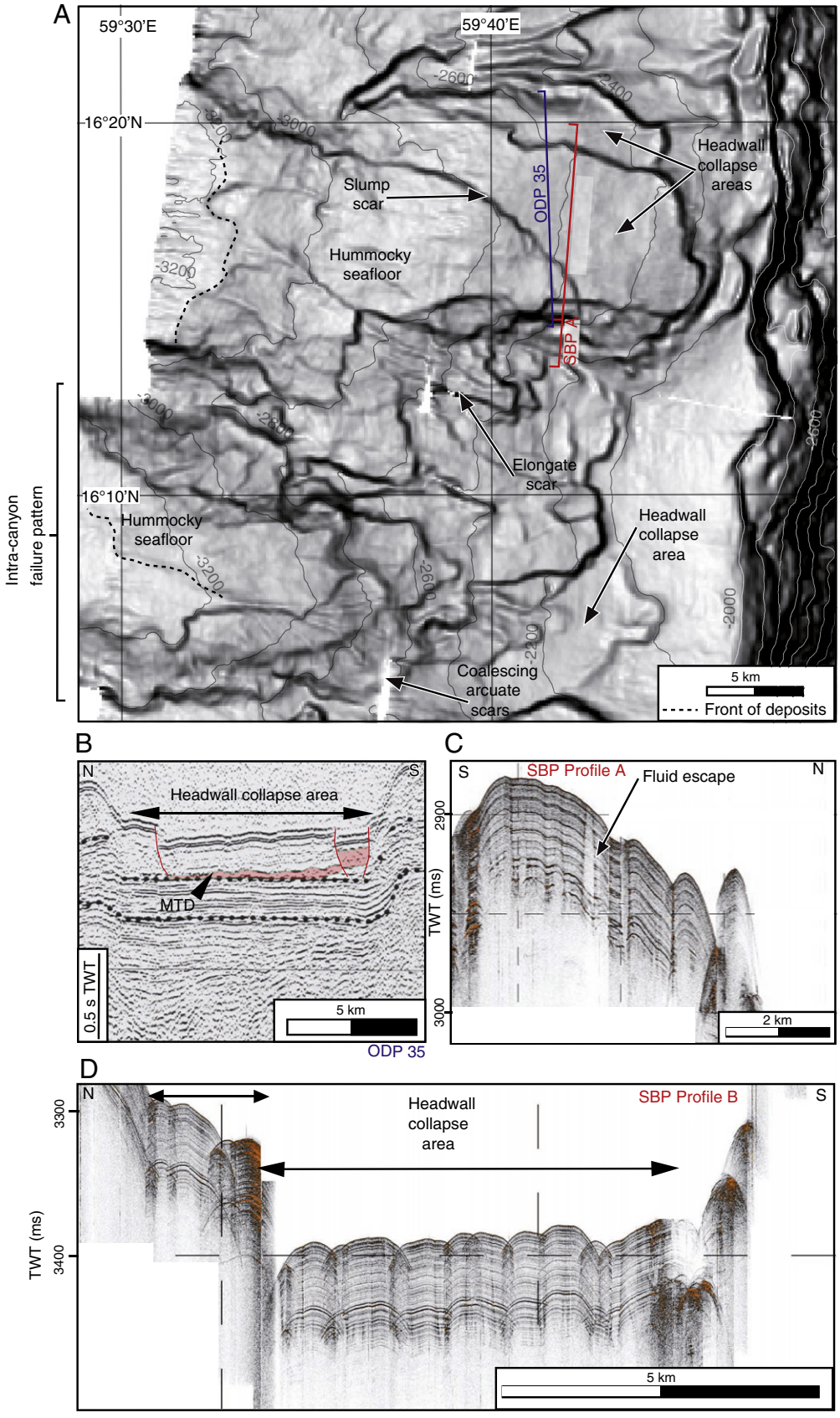


**Fig. 11.** A) Slope map of a multi-event generated scar on the southern Owen Ridge, showing the main slump scar and the related headwall collapse at the rear; and an area of "intra-canyon" failure pattern (see Fig. 3 for location). B) ODP seismic line crossing headwall collapse area (see Fig. A for location). 3.5 kHz profiles showing C) fluid escape features and D) folded reflectors in the headwall collapse area, similarly to the ODP seismic line in B) (see A for location).

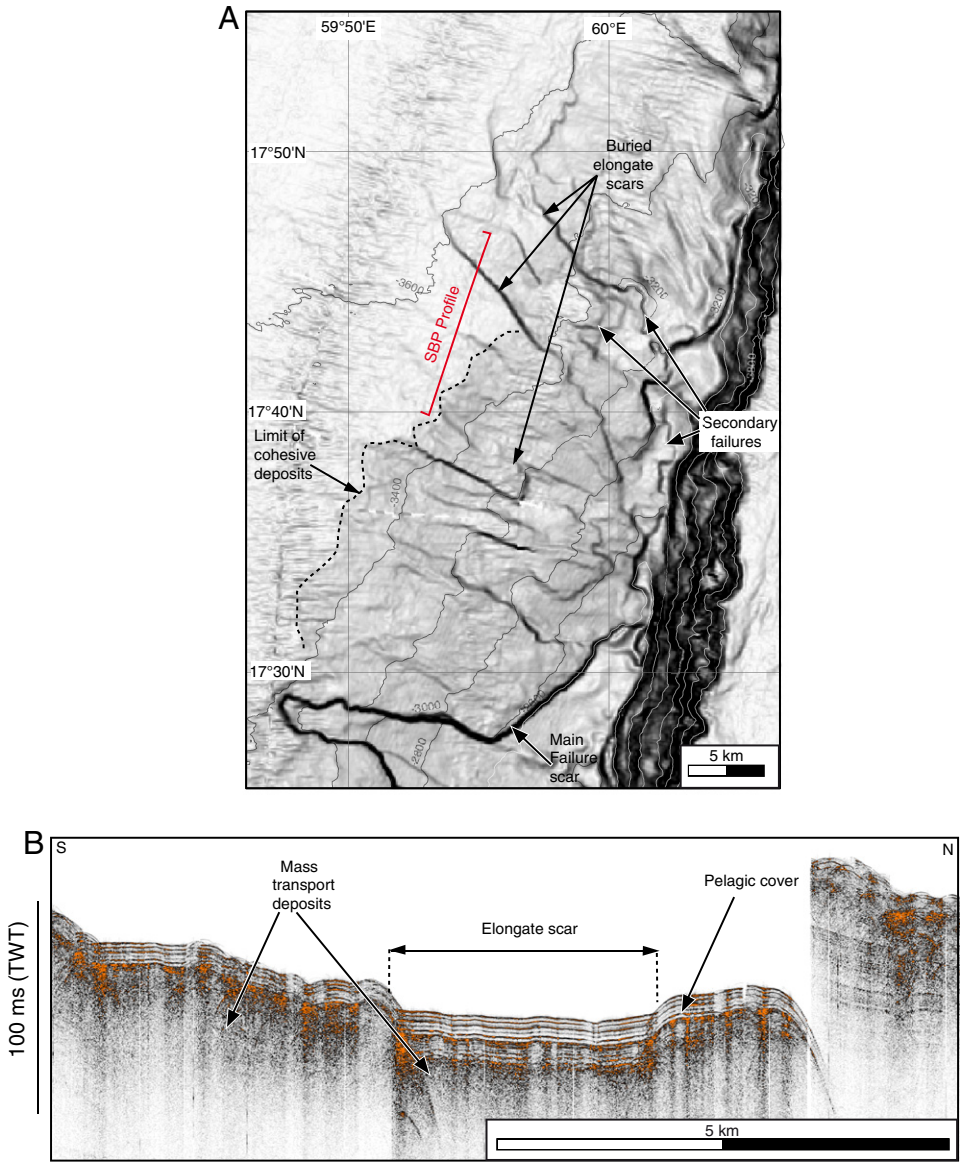


**Fig. 12.** A) Slope map of the largest multi-event generated scar on the southern Owen Ridge, with elongate scars buried under MTDs (see Fig. 3 for location). B) 3.5 kHz profile crossing a disintegrative elongate failure buried under a thicker pelagic cover than the surrounding MTDs (see A for location).

mass movement once initiated. The term of "intra-canyon" erosive pattern means that the local topography influences the evolution of mass movements, similarly to canyons that dissect passive margins.

### 5.1. Mass wasting along the southern Owen Ridge

The southern ridge is an asymmetric relief, with a steep east-facing scarp associated with the Owen Fracture Zone and a regular western slope corresponding to sedimentary beds gently tilted 3° to the west (Fig. 3; Shipboard Scientific Party, 1989). The environment is thus of open-slope type. However, the contrast in slopes correlates with a contrast in types of mass wasting found on both sides of the ridge. The morphology of the western slope generally favors retrogressive slumps, with large volume failures (up to ~40 $km^3$, Fig. 15), and long transport distances (up to 40 km). On the other hand, gullies dominantly erode the steeper and shorter flank to the east (Arabian Sea side), although block falls and cohesive deposits are locally observed at the foot of the main slope and locally beyond the active fault trace (Fig. 3).

With regards to the volumes of a multi-failure generated event, the western slope of the southern ridge is characterized by the highest number of events ($n=25$) involving more than 1 $km^3$ of material (Fig. 15). The southern ridge also displays the largest landslides, with 9 events extending over 100 $km^2$ or more. Retrogressive slumps are the dominant mode of mass wasting on the western slope (40 % of the southern ridge area). Cohesive failures are mostly arcuate, with various length comprised between 7.9 km and 41.4 km, and large runout

**Fig. 13.** A) Slope map of the central Owen Ridge, showing "intra-canyon" failure pattern on the western side and complex networks of gullies (see Fig. 5 for location). B) and C) Bird's eye views failure A and B, respectively, with 200-m interval bathymetric contours (vertical exaggeration ×6). D) 3.5 kHz profile showing slump deposits remobilized by disintegrative failures. E) 3.5 kHz profile crossing the curved scar (see Fig. A for location). Failure A results from the coalescence of three slides with volume ranging from 0.15 $km^3$ to 0.8 $km^3$. These slides are characterized by an indented shape, which results from the merging of several 840 to 1620 m wide half-rounded scars, mobilizing volumes between 0.006 and 0.013 $km^3$. Failure B is also the result of three overlapping scars. A smooth seafloor aspect characterizes the first scar, whereas the 3.5 kHz profile reveals the presence of a 30 m thick MTD buried underneath a thin pelagic cover enclosed by the scar. The second scar is curved and encloses MTDs. Three generations of nearly 10 m-thick MTDs are inserted within the pelagic cover. Downslope, the third failure is disintegrative and is composed of small coalescing gullies.

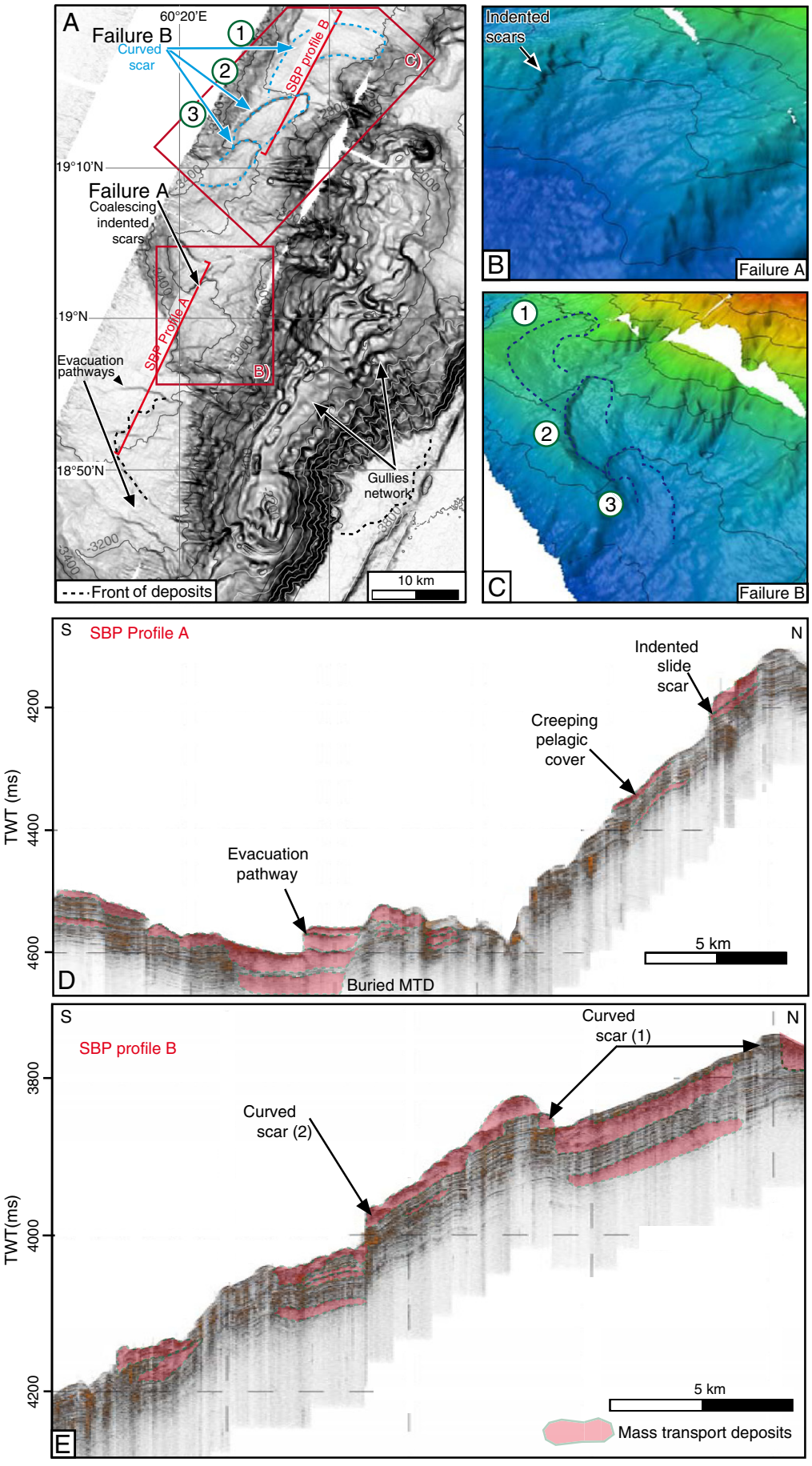
A
60°20'E
Failure B
Curved scar
1
2
3
SBP profile B
C)
19°10'N
Failure A
Coalescing indented scars
19°N
SBP Profile A
B)
Evacuation pathways
18°50'N
Gullies network
10 km
Front of deposits
Indented scars
B
Failure A
1
2
3
C
Failure B
S
SBP Profile A
N
Indented slide scar
Creeping pelagic cover
Evacuation pathway
TWT (ms)
4200
4400
4600
5 km
D
Buried MTD
S
SBP profile B
N
Curved scar (1)
Curved scar (2)
TWT(ms)
3800
4000
4200
5 km
E
Mass transport deposits

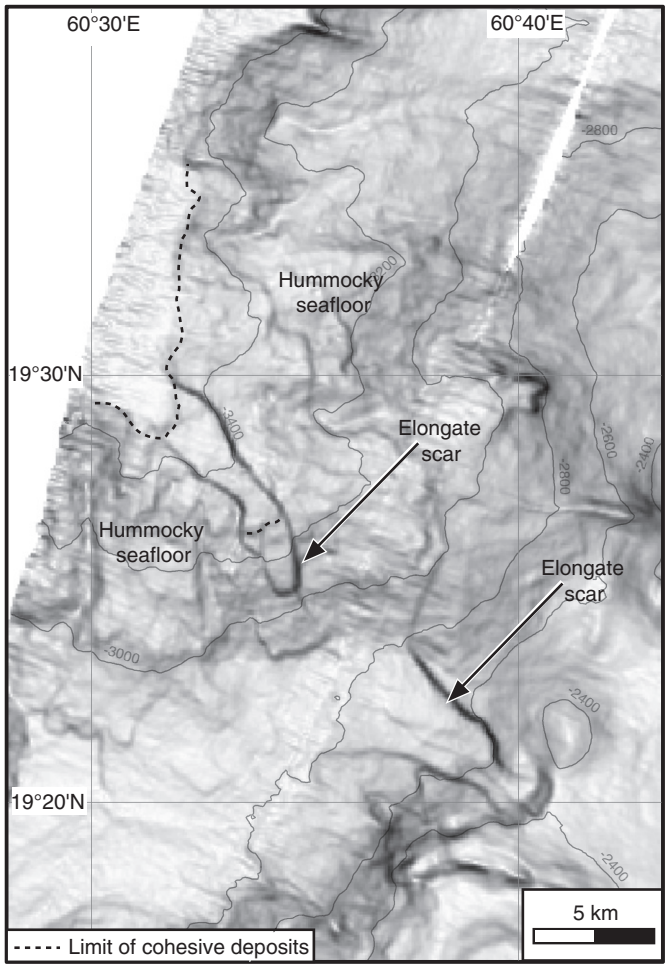


**Fig. 14.** Slope map of the central Owen Ridge, showing elongate disintegrative failures (see Fig. 5 for location).

distances (>30 km) (Fig. 3). The associated headwall collapse areas range from 3 to 240 km$^2$ (Figs. 3, 9, 10, 11). Several glide blocks, with sizes varying between $10^4$ and $1.5\times10^7$ m$^3$, have been identified close to headwall collapse failures (Figs. 9, 10). In some areas, the scar related to the glide blocks is meshed in the headwall collapse failure, suggesting that those block falls could have been triggered by the headwall collapse motion after the mass departure (Fig. 9). Scarps heights created by headwall collapse motion cluster between 20 m and 90 m, but can locally reach 140 m when associated with glide blocks (Figs. 9, 10). One particular case of bottleneck slide is observed around 16°N (Fig. 10).

Disintegrative failures show arcuate (Fig. 3), and elongate scars (Figs. 9, 10, 12). Arcuate disintegrative scars are isolated along the southern ridge, and occur mainly at the edge of headwall collapse areas (Fig. 3), whereas elongate scars occur preferentially down-slope (between 2600 and 3400 m depth) in areas of hummocky seafloor (Figs. 3, 8, 9, 12), where they form coalescing failures (Figs. 8, 9, 12). They accommodate superficial erosion, with base of the failure rooted between 20 and 40 meters below sea-floor. Elongate scars mobilize volumes ranging between 0.07 to 3 km$^3$.

The northern end of the southern ridge displays a particular mode of slope failure, with the two largest failures of the Owen Ridge, which are located between 17°20'N (Fig. 8) and 17°40'N (Fig. 12). In the area of the 17°20'N landslide, a 400 km$^2$ area of hummocky seafloor, characterized by a chaotic facies on echo-sounder profiles (SBP120), is partly enclosed by a 35 km-long arcuate failure scar (Fig. 8), suggesting a cohesive motion of the transported mass. The 17°20'N landslide may have mobilized 40 km$^3$ of pelagic material during the initial stage of failure.

The landslide located between 17°30'N and 17°45'N is more complex and shows multiple and sinuous failure scars (Fig. 12). The main failure encloses a ~430 km$^2$ area of hummocky seafloor. It is unclear if the hummocky area is the product of a single multi-failure event covering older elongate scars, or if it is the product of several generations of elongate failures. According to the first hypothesis, the failure may have mobilized 45 km$^3$ of pelagic material during the initial stage of failure. The hummocky area partially covers the proximal part of elongate scars A and B located down-slope (Fig. 12). Thus, elongate scars observed down-slope predate the cohesive failure that was triggered up-slope. The SBP profile shown in Fig. 12 shows that the pelagic layer that covers the area enclosed by the elongate scar B is thicker than for the area enclosed by elongate scar A (Fig. 12). This is consistent with several generations of elongate failures dissecting the slope.

The "open-slope" erosive pattern described above vanishes at the latitude of 16°10'N, where an "intra-canyon" erosive pattern is observed (Fig. 11). The slope displays an amphitheatre shape dissected by complex network of coalescing arcuate scars and headwall collapse up-slope (Figs. 3 and 11). Fluid outlets are locally observed on SBP120 profiles (Fig. 11). In this area, gliding planes are parallel to the stratigraphic bedding, and sometimes seem to jump between different stratigraphic levels when approaching the headwall of the slides (Fig. 2).

In addition to subsurface analysis, ODP data highlights the stratigraphy of mass transport deposits since the Early Miocene. The extension of ODP seismic lines does not cover the entire southern segment, and does not allow the estimate of volumes of buried MTDs. However, ODP and DSDP reporters noticed several hiatuses along the ridge that they interpreted as consecutive to slump removals (Shipboard Scientific Party, 1989). Missing thicknesses of material range from 50 to 150 m, and locally removed up to 5 Ma of sedimentation history. Over 60 MTDs facies are evidenced on ODP seismic data, which may represent ~30 failures events that have affected the pelagic cover. (Fig. 2; Shipboard Scientific Party, 1989). This is a minimum number, since only major MTDs are identified because of the low resolution of the ODP seismic lines. Truncated reflectors allow us to identify erosive surfaces due to mass departures. These MTDs are difficult to date using seismic correlation with ODP cores, due to faulting above substratum highs. However, mass wasting events along the southern ridge are mainly asynchronous, since they are covered by pelagic reflectors of various ages (Fig. 2). Only two coeval events are observed on seismic line 29 (Fig. 2). In some places, the same glide plane is associated with several MTDs (Fig. 2). Those deep failure glide planes are located above basement highs and delineate major mass wasting areas (Fig. 2). Thicknesses of MTDs measured from ODP seismic since Early Miocene range from 30 m to 220 m, which is consistent with thicknesses measured on SBP profiles for the most recent MTDs. Thicknesses of MTDs increase downward the slope, suggesting the erosion and the capture of superficial material (Fig. 2).

The crude frequency of major mass wasting events can be estimated from the study of the pelagic interval between two superposed MTDs. The thickness of pelagic interval ranges between 25 to 170 m, which would correspond to a periodicity of 0.6 to 4.2 Ma for the very large events over the unstable areas (using a standard sedimentation rate of 40 m Ma$^{-1}$). In contrast, some areas along the southern ridge seem to be totally devoid of large MTDs since the Early Miocene (Fig. 2).

### 5.2. Mass wasting along the central Owen Ridge

The central ridge displays an irregular morphology, with a 2400 m-deep plateau spreading over 485 km$^2$ (Fig. 4). The irregular morphology is mainly associated with an "intra-canyon" pattern of slope failure. Complex networks of gullies dissect both the western and the eastern side of the ridge. They locally merge down-slope into evacuation pathways on the western side (Fig. 13). This failure pattern is characterized by a strong correlation between headscarp height and headscarp slope

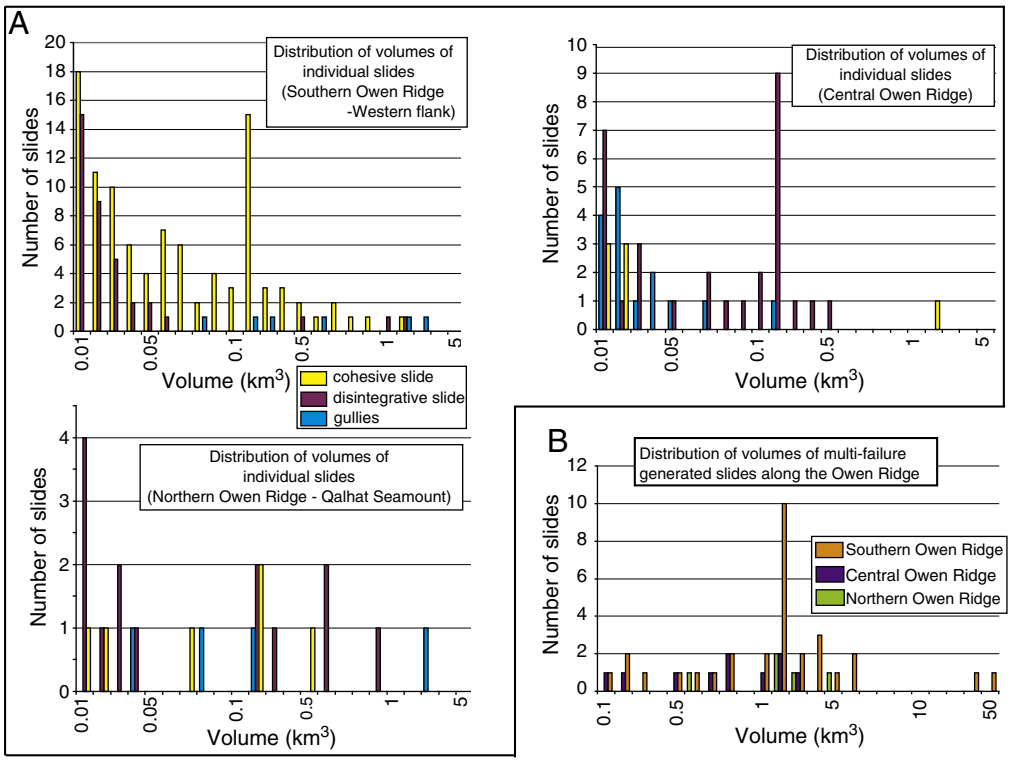


**Fig. 15.** A) Distribution of the volumes of individual failure according to the mode of failure (gullies, cohesive and disintegrative) for each segment of the Owen Ridge. B) Volumes distribution for multi-failures events along the Owen Ridge.

and an anti-correlation between the headscarp height and its depth of initiation (Table 1).

Some conspicuous failures are observed on the western flank of the central ridge. One of them is the disintegrative failure located at 19°N (Fig. 13, failure A), which is composed of three main coalescing and indented scars. Another particular failure is the curved and cohesive slide observed northward, at the latitude of 19°15'N (Fig. 13, failure B). Its seafloor signature is composed of three overlapping major scars. Initially E-W oriented, the slump course bends southwards when moving downslope. A last example of conspicuous erosive network extends in the area between 19°20'N and 19°35'N. Superficial disintegrative flows mainly dissect this area, mobilizing 0.003 to 0.03 km$^3$ of sediments. The most noticeable feature is a 2530 m wide (at the mouth), 9630 m-long elongate scar which removed 0.39 km$^3$ of material (Fig. 14).

Three stacked MTDs are observed on SBP profile at the southern foot of the central ridge (Fig. 7). The thickness of pelagic intervals gives return periods of 64 to 108 ka.

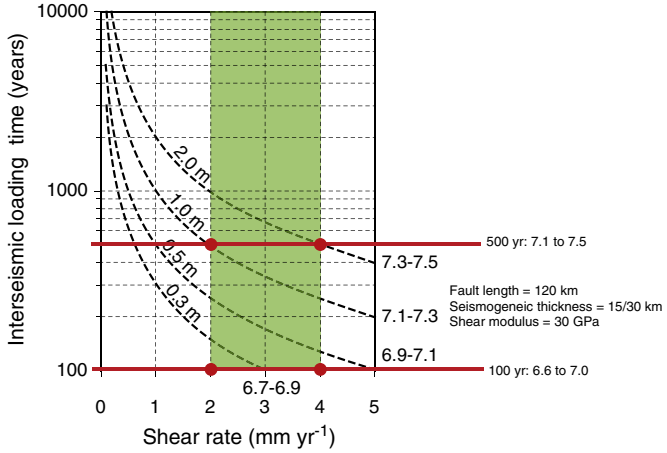


**Fig. 16.** Estimation of earthquake recurrence along the segment of the OFZ crossing the southern ridge. Co-seismic slips along the OFZ and expected earthquake magnitude are expressed according to the shear rate ($x$ axis) and the interseismic loading time ($y$ axis). The domain of shear rate estimated for the OFZ ($3\pm1$ mm a$^{-1}$) is outlined by the green area. See text for detailed explanations.

### 5.3. Mass wasting along the northern Owen Ridge (Qalhat Seamount)

The top region of the Qalhat Seamount is flat and stable over an area of 1210 km$^2$. Between 20°30'N and 21°30'N, the northern ridge displays an irregular morphology being eroded on its flank by complex networks of gullies, and evacuation pathways (Fig. 5). Similarly to the central ridge, morphological parameters of failure show a strong correlation between the headscarp height and the headscarp slope (Table 1).

Gullies networks are complex on the Qalhat Seamount. They initiate at different water depths (between −400 and −1800 m), and display short dendritic network at their head, that rapidly merge into rectilinear evacuation pathways (Fig. 5). Disintegrative failure events within gullies networks removed up to 3.72 km$^3$ of sediments. Between 20°50'N and 21°10'N, gullies merge into a semi-circular (amphitheatre shape) evacuation pathways system that extends over a 1730 km$^2$ area (Fig. 5). All evacuation pathways initiated by mass wasting processes in the amphitheatre merge in a single one at 3000 m water depth. This gathering evacuation pathway is 8.5 km wide at its mouth, and connected to the east with the Qalhat pull-apart Basin along the Owen Fracture Zone. A complex multi-retrogressive failure composed of coalescing scars is located where the major evacuation pathways of the northern ridge merge with the Qalhat Basin (Fig. 5). Volumes of sediment mobilized by these failures range from 0.03 to 0.86 km$^3$.

Two major disintegrative failures are observed on the 2.5° steep southern flank of the Qalhat Seamount (Figs. 5 and 8). They mobilized 0.5 and 0.17 km$^3$ of material. Four related MTDs are stacked on SBP profile (Fig. 7) at the foot of the Qalhat Seamount (Fig. 7). The thickness

of pelagic intervals between MTDs gives return periods ranging between 29 and 178 ka.

## 6. Discussion

### 6.1. Modes of slope failure along the Owen Ridge

The location of the largest failures is not controlled by the trace of the Owen Fracture Zone. The modal value of the volumes mobilized by individual slides is quite similar for the three ridges (0.05 $km^3$; Fig. 15), which is consistent with the fact that failures affect the same pelagic material along the entire ridge. However, the southern ridge displays the largest failure areas and the most voluminous landslides. This means that the "open slope" setting, due to the tilted pelagic banks configuration, allows the mobilization of large slope areas by the same failure plane and favors the evolution of slope failure into large landslides. This configuration also favors the departure of large cohesive masses necessary to trigger headwall collapse motion, and therefore retrogressive slumping. On the other hand, the "intra-canyon" pattern of the central ridge prevents the evolution of large slope failures. The "open slope" pattern of mass wasting along the southern ridge thus contrasts with the "intra-canyon" pattern displayed by the central and northern ridges.

Correlative relationships of the morphological parameters of slope failure give indications about the failure mechanism. Correlations between the morphological parameters do not reveal peculiar failure behaviour on the western side of the southern Owen Ridge (Table 1). Both the central and the northern ridges show a good correlation (>0.6) between headscarp height and headscarp slope (Table 1). McAdoo et al. (2000) suggested that headscarp height and slope may be used as a proxies for sediment strength, steeper and higher scarps indicating sediment overconsolidation and higher dynamic strengths. On the central ridge, there is an anti-correlation between the headscarp height and its depth of initiation, hence suggesting a lower cohesion of the material removed downslope. This is consistent with observations of MTDs being removed by an elongate disintegrative failure on SBP profile (Fig. 13). Evacuation pathways on the western side of the central ridge are likely to remobilize MTDs from the gullies network above (Figs. 4, 13). On the northern ridge, the semi-circular evacuation zone cuts into several generations of stacked MTDs (Fig. 5), suggesting it removes previously unconsolidated deposits too. Moreover, slope failures display irregular morphology, such as the curved scars observed on the central ridge (Fig. 13). Thus, steep slopes created by the uneven topography of the basement favors irregular-shaped, frequent and small-scale failures, whose deposits are remobilized downslope by larger, and more elongate failures, which compose evacuation pathways.

### 6.2. Influence of the pre-uplift topography of the Owen Ridge

The topography of the southern Owen Ridge before its uplift is identified on ODP seismic lines (Fig. 2). During the Paleocene to Early Miocene interval, the Indus turbiditic system progressively smoothed the uneven topography of the southern ridge (Fig. 2) (Shipboard Scientific Party, 1989), and predisposed a relatively flat substratum for the subsequent pelagic cover. The small areas of basement features that used to stand above the seafloor before the uplift define and isolate several areas of "open slope" failure, which do not fail synchronously, and where the recurrence of MTDs is different (Fig. 2). The only area where mass wasting processes display an "intra-canyon" pattern (Fig. 11) is located where the distance between two basement highs is the smallest (Fig. 2). Moreover, the pre-uplift topography strongly controls the location of failure glide planes, which are reactivated through time (Figs. 2, 9). In areas delimitated by basement highs, fluid escape may also act as a pre-conditioning factor of slope instability and play a role in the difference in failure distribution between two areas.

On the other hand, the guyot morphology of the Qalhat Seamount indicates that its paleo-topography was close to the sea level, thus preserved from turbiditic burial. Similarly, the pre-20 Ma uplift topography of the central ridge was probably higher than the southern segment during the same period and has been partly preserved from turbiditic burial (Fig. 6). This configuration thus predisposed an "intra-canyon" pattern for the erosion of the pelagic cover of the central and northern ridges. The variation in the topography of the Owen Ridge before its uplift is thus partly responsible for the variety of mass wasting features observed.

### 6.3. Recurrence interval and triggering mechanisms of slope failure

Seismicity is frequently invoked as a triggering factor for slope failures in deep-sea environments. Earthquakes add to ambient gravitational forces by generating horizontal and vertical ground accelerations, while simultaneously increasing pore fluid pressure (Almagor and Wisenam, 1982; Hampton et al., 1996). The seismicity along the Owen Fracture Zone might be the triggering process of slope instability. However, the seismicity reported for the last 40 years is negligible: the total seismic moment release sums to 1.5 $10^{18}$ N.m for the entire strike–slip portion of the fault (more than 700 km), which is equivalent to the seismic release of a single $M_w$ 6 earthquake. Rupturing the southern segment of the fault (120-km-long; Fournier et al., 2011) would require a $M_w > 6.5$ earthquake if the recurrence time is $10^2$ years, and several earthquakes of that size would be required to break the entire fault system (Fig. 16). Yet, the centennial earthquake catalogue (Engdahl et al., 1998) (supposed to be complete down to magnitude 7 earthquakes) does not report any significant event along the Owen Fracture Zone. One possibility is that the recurrence time is significantly longer, and that the Owen Fracture Zone is presently in an interseismic loading stage. If the recurrence time is $10^3$ years or greater, then earthquakes with $M_w > 7.7$ would be expected. Although the structure of the Owen Fracture Zone was probably not the same as in present day during the Early Miocene to Late Pliocene period, we hypothesize that fault segments of similar lengths could have ruptured. The estimate of earthquake recurrence (Fig. 16) shows that rupturing the southern fragment of the fault (120-km-long) would require an $M_w > 7$ earthquake for recurrence intervals ranging between $10^2$ and $10^3$ years. This earthquake recurrence estimate does not fit with the observed landslide frequency, of the order of $10^5$–$10^6$ years.

Since the Early Miocene, the modal thickness of removed material on the southern ridge is 80 m, and it is rare that more than two slides occurred at the same location at different times (Fig. 2). In spite of the slow pelagic deposition (2 to 2.5 Ma are necessary to accumulate 80 m of sediments), the scarcity of mass wasting events at a given location, together with dominantly cohesive motion and short transport distances (an important fraction of MTDs remains on the ridge and does not reach the Owen Basin (Fig. 2)), provides the durability of the sedimentary system. If slides of these magnitudes occurred after each earthquake, there would be very little pelagic cover remaining after a few events. As a result, large magnitude earthquakes may still be the dominant triggering process, but slow sedimentation rates restrict landslide frequency. If the pelagic sedimentary load is not sufficient, then it could not be mobilized during an earthquake. With regards to the central and the northern ridges, the failure at a given location seems to be more frequent, but involves smaller volumes than on the southern ridge (Fig. 15). Steep slopes may reduce the accumulation of sediments, and increase mass wasting frequency. This erosive pattern seems to preserve the pelagic cover too.

### 6.4. Comparison with continental margins

Volumes of landslides over the Owen Ridge compare closely to continental margins. The largest landslides on the Owen Ridge occur in areas where the slope gradient is low (2–3°), which is consistent with other observations of large landslides occurring on low mean seafloor slope angles (Canals et al., 2004). Similarly to the Owen Ridge, landslides

volumes estimated over the US continental slope range between less than 0.1 km$^3$ to 42.5 km$^3$, except in the Gulf of Mexico where volumes reach 150 km$^3$ (McAdoo et al., 2000, 2004; Chaytor et al., 2009; Twichell et al., 2009).

The comparison with landslides at convergent margins, which are frequently affected by high magnitude earthquakes and supplied by important sedimentation rates (>100 m/Ma), offers an interesting perspective. The Algerian margin, which undergoes frequent earthquakes, displays small landslides (with a maximal volume of 0.20 km$^3$) (Dan et al., 2010) compared to the Owen Ridge. On the other hand, volumes of landslides in the Cascadia area, which is supplied by abundant sedimentary material and submitted to infrequent but high magnitude earthquakes, compare closely with volumes estimated along the Owen Ridge, with volumes up to 42.5 km$^3$ according to McAdoo et al. (2000, 2004). Recent studies in the area of the $M_w = 8.8$ Maule earthquake of the 27 February 2010 offshore Chile shows that only small scale slides where produced by the earthquake and its aftershocks (Völker et al., 2011). Similar conclusions have been proposed for the Hellenic arc (Strozyk et al., 2010) or Sumatra (Tappin et al., 2007). It thus appears that areas with frequent shaking and important sedimentation rates (>100 m/Ma) do not provide the most voluminous landslides.

In the case of the Southern Owen Ridge, the restriction imposed on landslide frequency by slow pelagic sedimentation rates favors the mobilization of quite large volumes, and limits the occurrence of small-scale landslides. The poor sedimentary supply to the Owen Ridge, together with the low rate (~1 event/ka) of strong magnitude earthquakes ($M_w > 6$) that could shake hard enough the seafloor to trigger mass wasting, probably explain why large failure scars are preserved on the seafloor.

## 7. Conclusions

The three segments of the Owen Ridge display a large variety of mass wasting features strongly constrained by the basement topography. The uneven topography of the basement of the southern ridge has been partly smoothed by turbiditic deposits. This allowed the deposition of horizontal and parallel pelagic beds over wide areas. As a result the southern Owen Ridge displays an "open-slope" pattern, which favors the development of large but infrequent landslides. The landslide morphology on the southern ridge is the result of distinct and sporadic events, and not of a giant failure mobilizing the pelagic cover over the entire length of the southern ridge. In this area, slope failures remove up to ~40–45 km$^3$ of pelagic material, which compare closely to the volume estimated for some continental margins (McAdoo et al., 2000), but these events are far less frequent on the Owen Ridge. On the other hand, the steeper slopes of the central and northern ridges favor smaller but more frequent slides. In spite of different mass wasting pattern in space and in time, the pelagic cover over the three segments of the Owen Ridge is preserved. Our study demonstrates that earthquakes are more frequent than landslides, leading to the interpretation that mass-wasting frequency is strongly limited by sedimentation rates. It remains unknown how the volumes of buried MTDs observed on ODP seismic lines compare with the volumes of the initial stages of failures estimated from the morphology imprinted on the seafloor.

## Acknowledgements

We are indebted to the Captain Geoffroy de Kersauson, officers and crewmembers of the BHO Beautemps-Beaupré, and to the French Navy hydrographers Vincent Lamarre and Yves-Marie Tanguy, and the hydrographic team of the 'Groupe Océanographique de l'Atlantique', for their assistance in data acquisition. We greatly acknowledge the editor D.J.W. Piper, D. R. Tappin, and three anonymous reviewers for their helpful and constructive comments. We thank Patrick Meunier, Siegfried Lallemant, and Rob Viesca for their interest in our work and their suggestions, and Baptiste Mulot and Pierpaolo Dubernet for their technical assistance. We acknowledge the support of SHOM, IFREMER, CEA and INSU-CNRS for the Owen cruise.

## References

Almagor, G., Wisenam, G.H., 1982. Submarine slumping in the continental slope of Israel. In: Saxov, S., Nieuwenhuis, J.K. (Eds.), Marine Slides and other mass movements: Proc of a NATO Workshop on Marine Slides and Other Mass Movements, Algarve, Portugal,15-21 dec. 1980, ser. 4, vol. 6, pp. 95–128.

Antolik, M., Abercrombie, R.E., Pan, J., Ekström, G., 2006. Rupture characteristics of the 2003 Mw 7.6 mid-Indian Ocean earthquake: Implications for seismic properties of young oceanic lithosphere. Journal of Geophysical Research 111, B04302 http://dx.doi.org/10.1029/2005JB003785.

Baraza, J., Ercilla, G., 1996. Gas charged sediments and large pockmark-like features on the Gulf of Cadiz slope (SW Spain). Marine and Petroleum Geology 13, 253–261.

Böhm, E., Morrison, J.M., Manghnani, V., Kim, H.-S., Flagget, C.N., 1999. The Ras al Hadd Jet: remotely sensed and acoustic Doppler current profiler observations in 1994–1995. Deep-Sea Research II 46, 1531–1549.

Canals, M., Lastras, G., Urgeles, R., Casamor, J.L., Mienert, J., Cattaneo, A., De Batist, M., Haflidason, H., Imbo, Y., Laberg, J.S., Locat, J., Long, D., Longva, O., Masson, D.G., Sultan, N., Trincardi, F., Bryn, P., 2004. Slope failure dynamics and impacts from seafloor and shallow sub-seafloor geophysical data: case studies from the COSTA project. Marine Geology 213, 9–72.

Chamot-Rooke, N., Fournier, M., Scientific Team of AOC and OWEN cruises, 2009. Tracking Arabia–India motion from Miocene to Present. American Geophysical Union, Fall Meeting 2009.

Chaytor, J.D., Ten Brink, U.S., Solow, A.R., Andrews, B.D., 2009. Size distribution of submarine landslides along the U.S. Atlantic margin. Marine Geology 264, 16–27.

Clemens, S.C., Prell, W.L., 2006. Viewpoint: the timing of orbital-scale Indian monsoon changes. Quaternary Science Reviews 25, 658–662.

Clift, P.D., Shimizu, N., Layne, G.D., Blusztain, J.S., Gaedicke, C., Schluter, H.-U., Clark, M.K., Amjad, S., 2001. Development of the Indus Fan and its significance for the erosional history of the Western Himalaya and Karakoram. Geological Society of America Bulletin 113 (8), 1039–1051.

Corregiari, A., Trincardi, F., Langone, L., Roveri, M., 2001. Styles of failure in late Holocene highstand prodelta wedges on the Adriatic shelf. Journal of Sedimentary Research 71, 218–236.

Dan, G., Sultan, N., Cattaneo, A., Deverchere, J., Yelles, K., 2010. In: Mosher, D.C., Ship, C., Moscardelli, L., Chaytor, J., Baxter, C., Lee, H., Urgeles, R. (Eds.), Mass-transport deposits on the Algerian Margin (Algiers Area): morphology, Lithology and Sedimentary Processes, Advances in Natural and Technological Hazards Research: Submarine Mass Movements and Their Consequences, 28, pp. 527–539.

DeMets, C., Gordon, R.G., Argus, D.F., 2010. Geologically current plate motions. Geophysical Journal International 181, 1–80 http://dx.doi.org/10.1111/j.1365-246X.2009.04491.x.

Dingle, R.V., 1977. The anatomy of a large submarine slump on a sheared continental margin (SE Africa). Journal of the Geological Society of London 134 (3), 293–310.

Edwards, R.A., Minshull, T.A., White, R.S., 2000. Extension across the Indian–Arabian plate boundary: the Murray Ridge. Journal Geophysical International 142, 461–477.

Edwards, R.A., Minshull, T.A., Flueh, E.R., Kopp, C., 2008. Dalrymple Trough: an active oblique-slip ocean–continent boundary in the northwest Indian Ocean. Earth and Planetary Science Letters 272, 437–445.

Engdahl, E.R., van der Hilst, R., Buland, R., 1998. Global teleseismic earthquake relocation with improved travel times and procedures for depth determination. Bulletin of the Seismological Society of America 88, 722–743.

Faugères, J.C., Gonthier, E., Mulder, T., Kenyon, N., Cirac, P., Griboulard, R., Berné, S., Lesuavé, R., 2002. Multi-process generated sediment waves on the Landes Plateau (Bay of Biscay, North Atlantic). Marine Geology 182, 279–302.

Field, M.E., Barber, J.H., 1993. A submarine landslide associated with shallow seafloor gas and gas hydrates off northern California. In: Schwab, W.C., et al. (Ed.), Submarine landslides: selected studies in the U.S. Exclusive Economic Zone: US Geological Survey Bulletin, pp. 151–157. 2002.

Fournier, M., Patriat, P., Leroy, S., 2001. Reappraisal of the Arabia–India–Somalia triple junction kinematics. Earth and Planetary Science Letters 189, 103–114.

Fournier, M., Chamot-Rooke, N., Petit, C., Fabbri, O., Huchon, P., Maillot, B., Lepvrier, C., 2008a. In-situ evidence for dextral active motion at the Arabia–India plate boundary. Nature Geoscience 1, 54–58 http://dx.doi.org/10.1038/ngeo.2007.24.

Fournier, M., Petit, C., Chamot-Rooke, N., Fabbri, O., Huchon, P., Maillot, B., Lepvrier, C., 2008b. Do ridge-ridge-fault triple junctions exist on Earth? Evidence from the Aden–Owen–Carlsberg junction in the NW Indian Ocean. Basin Research 20, 575–590 http://dx.doi.org/10.1111/j.1365-2117.2008.00356.x.

Fournier, M., Chamot-Rooke, N., Petit, C., Huchon, P., Al-Kathiri, A., Audin, L., Beslier, M.-O., d'Acremont, E., Fabbri, O., Fleury, J.-M., Khanbari, K., Lepvrier, C., Leroy, S., Maillot, B., Merkouriev, S., 2010. Arabia–Somalia plate kinematics, evolution of the Aden–Owen–Carlsberg triple junction, and opening of the Gulf of Aden. Journal of Geophysical Research 115, B04102 http://dx.doi.org/10.1029/2008JB006257.

Fournier, M., Chamot-Rooke, N., Rodriguez, M., Huchon, P., Petit, C., Beslier, M.-O., Zaragosi, S., 2011. Owen Fracture Zone: the Arabia–India plate boundary unveiled. Earth and Planetary Science Letters 302, 247–252 http://dx.doi.org/10.1016/j.epsl.2010.12.027.

Gaedicke, C., Prexl, A., Schlüter, H.-U., Roeser, H., Clift, P., 2002. Seismic stratigraphy and correlation of major regional unconformities in the northern Arabina Sea. In: Clift, P., Kroon, D., Gaedicke, C., Craig, J. (Eds.), The tectonic and climatic evolution of the Arabian Sea Region: Geological Society of London, Special Publication, 195, pp. 25–36.

Gardner, J.V., Prior, D.B., Field, M.E., 1999. Humboldt slide: a large shear-dominated retrogressive slope failure. Marine Geology 154, 323–338.
Gonthier, E., Faugères, J.C., Gervais, A., Ercilla, G., Alonso, B., Baraza, J., 2002. Quaternary sedimentation and origin of the Orinoco sediment wave field on the Demerara continental rise (NE margin of South Amercia). Marine Geology 192, 189–214.
Gordon, R.G., DeMets, C., 1989. Present-day motion along the Owen fracture zone and Dalrymple trough in the Arabian Sea. Journal of Geophysical Research 94, 5560–5570.
Hampton, M.A., Lee, H.J., Locat, J., 1996. Submarine landslides. Review of Geophysics 34, 33–59.
Kristoffersen, Y., Coakley, B.J., Hall, J.K., Edwards, M., 2007. Mass wasting on the submarine Lomonosov Ridge, central Arctic Ocean. Marine Geology 243, 132–142.
Kvalstad, T.J., Andresen, L., Forsberg, C.F., Kjell Berg, K., Bryn, P., Wangen, M., 2005. The Storegga slide: evaluation of triggering sources and slide mechanics. Marine and Petroleum Geology 22, 245–256.
Lee, H., Edwards, B.D., Field, M.E., 1981. Geotechnical analysis of a submarine slump, Eureka, California, paper presented at Offshore Technology Conference. American Association of Petroleum Geology, Houston, Tex.
Lee, H.J., Syvitski, P.M., Parker, G., Orange, D., Locat, J., Hutton, J.H.W., Imran, J., 2002. Distinguishing sediment waves from slope failure deposits: field examples, including the Humboldt slide and modelling results. Marine Geology 192, 79–104.
Lee, H.J., Locat, J., Desgagnes, P., Parsons, J.D., McAdoo, B.G., Orange, D.L., Puig, P., Wong, F.L., Dartnell, P., Boulanger, E., 2007. Submarine mass movements on continental margins. In: Nittrouer, C.A. (Ed.), Continental Margin Sedimentation. Blackwell, U.K., pp. 213–274 http://dx.doi.org/10.1002/9781444304398.ch5.
Lonsdale, P., Fornari, D., 1980. Submarine geology of Malpelo ridge, Panama basin. Marine Geology 36, 65–83.
Massel, C., Coffin, M.F., Mann, P., Mosher, S., Frohlich, C., Duncan, C.S., Karner, G., Ramsay, D., Lebrun, J.-F., 2000. Neotectonics of the Macquarie Ridge Complex, Australia–Pacific plate boundary. Journal of Geophysical Research 105, 13457–13480.
Masson, D.G., Harbitz, C.B., Wynn, R.B., Pedersen, G., Løvholt, F., 2006. Submarine landslides: processes, triggers and hazard prediction. Philosophical Transaction of the Royal Society A 364, 2009–2039.
McAdoo, B.G., Pratson, L.F., Orange, D.L., 2000. Submarine landslide morphology, US continental slope. Marine geology 169, 103–136.
McAdoo, B.G., Capone, M.K., Minder, J., 2004. Seafloor morphology of convergent margins: implications for Cascadia seismic hazard. Tectonics 23, TC 6008 http://dx.doi.org/10.1029/2003TC001570.
Michaud, F., Chabert, A., Collot, J.-Y., Sallarès, V., Flueh, E.R., Charvis, P., Graindorge, D., Gustcher, M.A., Bialas, J., 2005. Fields of multi-kilometer scale sub-circular depressions in the Carnegie Ridge sedimentary blanket: effect of underwater carbonate dissolution? Marine Geology 216, 205–219.
Mienert, J., Posewang, J., 1999. Evidence of shallow- and deep-water gas hydrate destabilizations in North Atlantic polar continental margin sediments. Geo-Marine Letters 19, 143–149.
Mouchot, N., 2009. Tectonique et sédimentation sur le complexe de subduction du Makran pakistanais. Unpublished PhD thesis, Cergy Univ., France, 364 pp.
Mountain, G.S., Prell, W.L., 1989. Geophysical Reconnaissance Survey for ODP Leg 117 in the Northwest Indian Ocean. Proc. ODP, Init. Repts. (Ocean Drilling Program), 117. College Station, TX, pp. 51–64.
Mountain, G.S., Prell, W.L., 725–743, 1990. A multiphase plate tectonic history of the southeast continental margin of Oman. In: Robertson, A.H.F., Searle, M.P., Ries, A.C. (Eds.), The Geology and Tectonics of the Oman Region: 1990, 49, pp. 725–743.
Mulder, T., Alexander, J., 2002. Abrupt change in slope causes variation in the deposit thickness of concentrated particle-driven density currents. Marine Geology 175, 221–235.
Mulder, T., Cochonat, P., 1996. Classification of offshore mass movements. Journal of Sedimentary Research 66, 43–57.
Mulder, T., Gonthier, E., Lecroart, P., Hanquiez, V., Marches, E., Voisset, M., 2009. In: Gaullier et Vendeville, V. (Ed.), Sediment failures and flows in the Gulf of Cadiz (western Atlantic): Marine and Petroleum Geology, Spec. Issue, 26, pp. 660–672.
Pimm, A.C., Burroughs, R.H., Bunce, E.T., 1972. Oligocene sediments near Chain Ridge, northwest Indian Ocean: structural implications. Marine Geology 13, 14–18.
Piper, D.J.W., Cochonat, P., Morrison, M., 1999. The sequence of events around the epicenter of the 1929 Grand Bank earthquake: initiation of debris flows and turbidity current inferred from sidescan sonar. Sedimentology 46, 79–97.
Prior, D.B., 1999. Sea floor engineering geomorphology: recent achievements and future directions. Geomorphology 31, 411–439.
Prior, D.B., Coleman, J., 1980. Sonograph mosaics of submarine slope instabilities, Mississippi River delta. Marine Geology 36, 226–239.
Quittmeyer, R.C., Kafka, A.L., 1984. Constraints on plate motions in southern Pakistan and the northern Arabian Sea from the focal mechanisms of small earthquakes. Journal of Geophysical Research 89, 2444–2458.
Robinson, D.P., 2011. A rare great earthquake on a oceanic fossil fracture zone. Geophysical Journal International 186, 1121–1134 http://dx.doi.org/10.1111/j.1365-246X.2011.05092.x.
Rodriguez, M., Fournier, M., Chamot-Rooke, N., Huchon, P., Bourget, J., Sorbier, M., Zaragosi, S., Rabaute, A., 2011. Neotectonics of the Owen Fracture Zone (NW Indian Ocean): structural evolution of an oceanic strike–slip plate boundary (2011). Geochemistry, Geophysics, Geosystems 12, Q12006 http://dx.doi.org/10.1029/2011GC003731.
Shillington, D.J., Seeber, L., Sorlien, C.C., Steckler, M.S., Kurt, H., Dondurur, D., Çifçi, G., İmren, C., Cormier, M.H., McHugh, C.M.G., Gürçay, S., Poyraz, D., Okay, S., Atgın, O., Diebold, J.B., 2012. Evidence of widespread creep on the flanks of the Sea of Marmara transform basin from marine geophysical data. Geology 40, 439–442 http://dx.doi.org/10.1130/G32652.1.
Shipboard Scientific Party, 1974. Site 222. In: Whitmarsh, R.B., Weser, O.E., Ross, D.A. (Eds.), DSDP Init. Repts, leg 23 http://dx.doi.org/10.2973/dsdp.proc.23.106.
Shipboard Scientific Party, 1989. Site 731. In: Prell, W.L., Niitsuma, N., et al. (Eds.), Proc. ODP, Init. Repts., 117. College Station, TX (Ocean Drilling Program).
Strozyk, F., Strasser, M., Krastel, S., Meyer, M., Huhn, K., 2010. Reconstruction of retreating mass wasting in response to progressive slope steepening of the northeastern Cretan margin, eastern Mediterranean. Marine Geology 271, 44–54.
Sultan, N., Cattaneo, A., Urgeles, R., Lee, H., Locat, J., Trincardi, F., Berne, S., Canals, M., Lafuerza, S., 2008. A geomechanical approach for the genesis of sediment undulations on the Adriatic shelf. Geochemistry, Geophysics, Geosystems 9, Q04R03 http://dx.doi.org/10.1029/2007GC001822.
Tappin, D.R., McNeil, L.C., Henstock, T., Mosher, D., 2007. Mass wasting processes — offshore Sumatra. In: Lykousis, V., Sakellariou, D., Locat, J. (Eds.), Submarine Mass Movements and Their Consequences, pp. 327–336.
Tripsanas, E.K., Piper, D.J.W., Jenner, K.A., Bryant, W.R., 2008. Submarine mass-transport facies: new perspectives on flow processes from cores on the eastern North American margin. Sedimentology 55, 97–136.
Twichell, D.C., Chaytor, J.D., ten Brink, U.S., Buczkowski, B., 2009. Morphology of late Quaternary submarine landslides along the U.S. Atlantic continental margin. Marine Geology 264, 4–15.
Viesca, R.C., Rice, J., 2012. Nucleation of sleep-weakening rupture instability in landslides by localized increase in pore pressure. Journal of Geophysical Research 117, B03104 http://dx.doi.org/10.1029/2011JB008866.
Völker, D., Scholz, F., Geersen, J., 2011. Analysis of submarine landsliding in the rupture area of the 27 February 2010 Maule earthquake, Central Chile. Marine Geology 288, 79–89.
Weissel, J.K., Childers, V.A., Karner, G.D., 1992. Extensional and Compressional Deformation of the Lithosphere in the Light of ODP Drilling in the Indian Ocean. Synthesis of Results from Scientific Drilling in the Indian Ocean. : Geophysical Monography 70American Geophysical Union.
Whitmarsh, R.B., 1979. The Owen Basin off the south-east margin of Arabia and the evolution of the Owen Fracture Zone. Geophysical Journal of the Royal Astronomical Society 58, 441–470.
Whitmarsh, R.B., Weser, O.E., Ross, D.A., 1974. Initial Report DSDP, U.S., v. 23. Government Printing Office, Washington, D.C., p. 1180.

## Etude préliminaire de la stabilité des pentes au niveau de la Ride d'Owen

L'hypothèse selon laquelle les taux de sédimentation limitent la fréquence des glissements de terrain sur le segment sud de la Ride d'Owen peut être confirmée par une analyse rudimentaire de la stabilité des pentes. Un glissement de terrain est déclenché lorsque la contrainte cisaillante $\tau$ devient supérieure à la résistance au cisaillement *Su* du sédiment (*Morgenstern, 1967*). On considère ici que la surpression interstitielle développée en réponse au passage de l'onde sismique n'a pas le temps de se dissiper (modèle non drainé). Ceci s'exprime sous la forme :

$$F = Su/\tau \leq 1$$

où F est le facteur de sécurité.

Dans ces conditions, $\tau$ s'exprime de la façon suivante :

$$\tau = \gamma' z \sin\beta \cos\beta + k \gamma z \cos^2\beta$$

où $\gamma'$ est la densité du sédiment gorgé d'eau, $\gamma$ la densité sèche, z l'épaisseur du glissement (ou la profondeur du plan de rupture), $\beta$ la pente, et k l'accélération horizontale du sédiment lors du passage de l'onde sismique.

De cette équation, il est possible d'extraire l'accélération horizontale critique *ky* pour laquelle le facteur de sécurité devient égal à 1 et la pente instable :

$$ky = (Su/\gamma z)/\cos^2\beta - \gamma'/\gamma \tan\beta$$

Ceci signifie que l'accélération horizontale doit devenir supérieure ou égale à *ky* pour surmonter l'effet stabilisateur de la résistance au cisaillement du sédiment. Cependant, ces équations ne tiennent pas en compte de la durée de l'oscillation subie par le sédiment : des modélisations (*Newmark, 1965*) ont montré que l'accélération nécessaire pour causer la rupture de la pile sédimentaire doit être bien plus importante que la résistance de cette dernière au cisaillement. Les valeurs de *ky* calculées par la suite sont donc des valeurs minimales.

Les valeurs des paramètres *Su*, $\gamma'$, $\gamma$, sélectionnées sont extraites des forages ODP des sites 721, 722, et 731 (Shipboard Scientific Party, 1989), localisés sur le segment sud de la Ride d'Owen, dont la pente moyenne $\beta$ est de 2°. Les sites ODP sont suffisamment dispersés sur la Ride Sud pour prendre en compte de la variabilité spatiale des propriétés physiques du sédiment. Les valeurs et les résultats sont consignés dans la table 1.

Il est difficile de relier les accélérations critiques calculées à une magnitude de séisme donnée, en raison de l'importance des effets de sites. Les relations entre accélérations critiques et magnitude sismique existantes sont établies de façon empirique sur les continents, et ne sont

valables que pour une région donnée. Ces relations empiriques sont basées sur l'analyse de dizaines de sismogrammes obtenus sur des dizaines de stations dans la zone d'étude considérée : de telles relations ne peuvent évidemment pas être établies dans le milieu océanique. Cependant, d'après l'ensemble des études réalisées à terre, nous obtenons l'ordre de grandeur suivant : il est rare qu'un séisme Mw =7 - similaire à ceux potentiellement générés par la ZFO- soit associé à des PGA (Peak Ground Acceleration) supérieures à 0,5 (une PGA à 0,5 étant déjà une valeur très élevée pour un séisme de Mw =7 ). Les glissements étant proches de la ZFO (distance <20 km), il n'est pas nécessaire de prendre en compte l'atténuation de l'accélération horizontale *k* avec la distance à la faille.

Les résultats obtenus sont cohérents avec notre hypothèse initiale : la rupture se déclenche pour des valeurs de *ky* cohérentes (≤0,5 ) avec la sismicité de l'OFZ à partir d'une épaisseur de sédiment comprise entre 40 et 100 m (Figure 3). Si l'on assimile la hauteur d'une cicatrice d'arrachement à la profondeur du plan de rupture, on observe que la distribution des hauteurs des cicatrices sur la Ride Sud est cohérente avec les épaisseurs de sédiments critiques déduites des calculs de stabilité. A un taux de sédimentation moyen de 40 m/ Ma (*Shipboard scientific party, 1989*), il faut donc accumuler des sédiments pendant 0,75 à 2,5 Ma pour que les séismes générés par la ZFO soient susceptibles de déclencher la rupture. Ces résultats sont du même ordre de grandeur que la fréquence des glissements de terrains estimée pour la Ride Sud à partir de l'étude stratigraphique exposée dans l'article publié à *Marine Geology* (la valeur de 4 Ma étant surestimée du fait de l'erreur initiale sur l'âge du soulèvement de la ride).

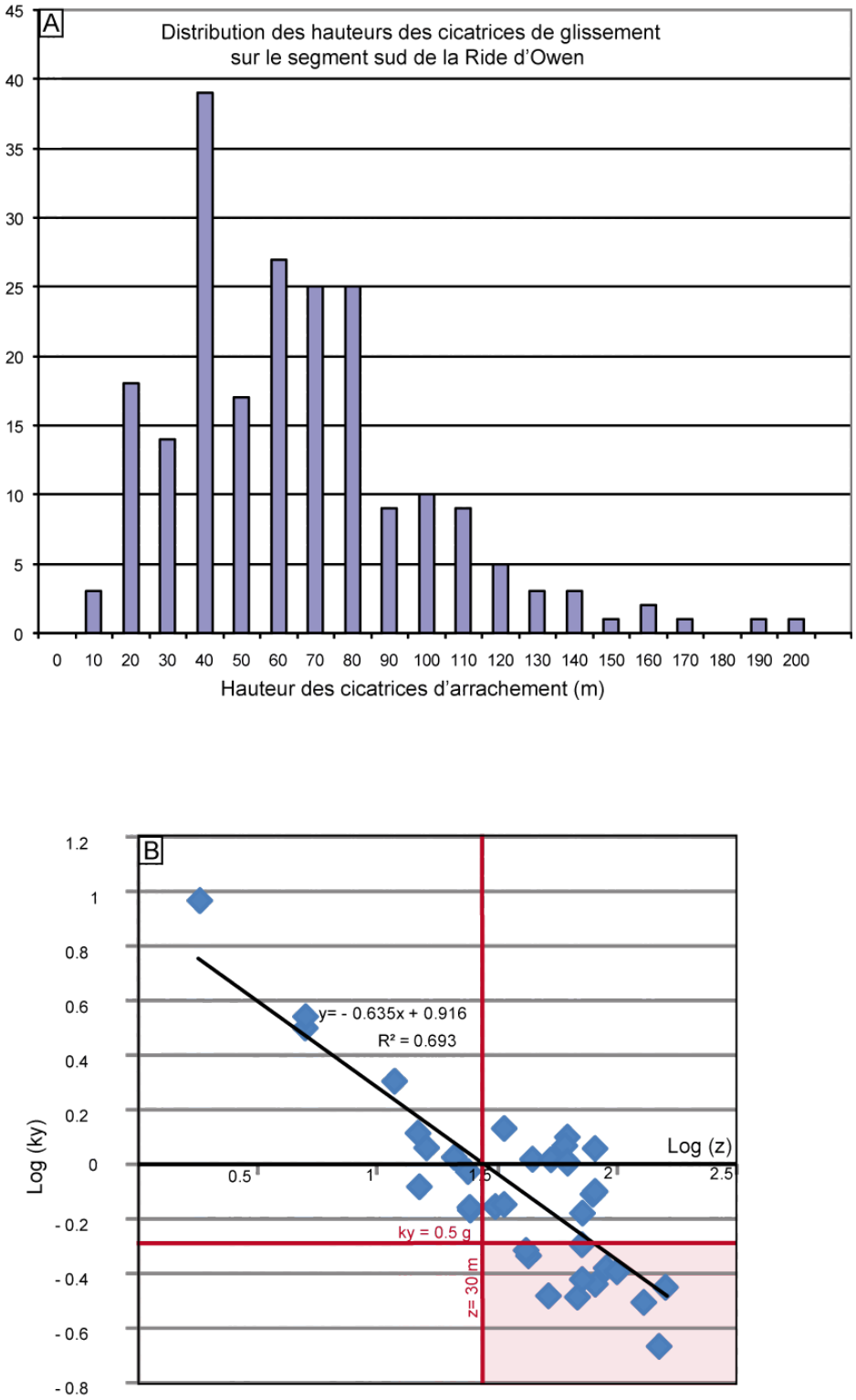


*Figure 3 : A. Distribution des hauteurs des cicatrices des glissements de terrains sous-marins du segment sud de la Ride d'Owen. B. Relation entre l'accélération horizontale critique (ky) et la profondeur du sédiment (z). Le domaine encadré en rouge correspond au domaine d'instabilité sur le segment sud de la Ride d'Owen.*

| Site 731 | | | | | | | |
|---|---|---|---|---|---|---|---|
| | z | Su | γ | γ' | γ'/γ | Su/(γ''z) | ky |
| | 15 | 12900 | 977 | 1658 | 1.69 | 0.518 | 0.82 |
| | 24 | 18500 | 770 | 1480 | 1.92 | 0.520 | 0.93 |
| | 34 | 36100 | 751 | 1497 | 1.99 | 0.709 | 1.34 |
| | 43 | 22300 | 1007 | 1655 | 1.64 | 0.313 | 0.46 |
| | 62.6 | 68400 | 832 | 1532 | 1.84 | 0.713 | 1.25 |
| | 69 | 27600 | 1057 | 1694 | 1.60 | 0.236 | 0.32 |
| | 82 | 37200 | 1095 | 1712 | 1.56 | 0.264 | 0.3 |
| | 91 | 42000 | 982 | 1623 | 1.65 | 0.284 | 0.41 |
| | 101 | 49300 | 1074 | 1683 | 1.56 | 0.2 | 0.40 |
| Site 721 | | | | | | | |
| Core A | z | Su | γ | γ' | γ'/γ | Su/(γ''z) | ky |
| | 1.8 | 14600 | 873 | 1553 | 1.77 | 5.22 | 9.24 |
| | 11.8 | 23800 | 978 | 1624 | 1.6 | 1.24 | 2.00 |
| | 24.5 | 17600 | 983 | 1590 | 1.61 | 0.45 | 0.67 |
| | 31.2 | 23600 | 1006 | 1665 | 1.65 | 0.45 | 0.69 |
| | 44.7 | 44700 | 912 | 1587 | 1.74 | 0.63 | 1.03 |
| | 53.45 | 62300 | 1072 | 1688 | 1.57 | 0.6 | 1.03 |
| | 62.75 | 72300 | 1090 | 1698 | 1.55 | 0.67 | 1.00 |
| | 72.4 | 56100 | 1090 | 1693 | 1.55 | 0.45 | 0.6 |
| | 81.75 | 97700 | 1003 | 1643 | 1.63 | 0.7 | 1.13 |
| Core B | z | Su | γ | γ' | γ'/γ | Su/(γ''z) | ky |
| | 4.98 | 15000 | 940 | 1578 | 1.6 | 1.90 | 3.15 |
| | 16.08 | 19500 | 1012 | 1648 | 1.6 | 0.7 | 1.14 |
| | 21 | 25200 | 1082 | 1714 | 1.58 | 0.70 | 1.05 |
| | 42 | 22300 | 988 | 1654 | 1.67 | 0.32 | 0.48 |
| | 52.14 | 20000 | 1001 | 1649 | 1.64 | 0.23 | 0.32 |
| | 61.1 | 70800 | 950 | 1599 | 1.68 | 0.72 | 1.16 |
| | 72 | 43800 | 1092 | 1694 | 1.55 | 0.35 | 0.50 |
| | 80.1 | 67300 | 1015 | 1663 | 1.63 | 0.50 | 0.77 |
| | 130.8 | 51700 | 1088 | 1720 | 1.58 | 0.22 | 0.31 |
| | 151.7 | 42000 | 1030 | 1680 | 1.63 | 0.16 | 0.21 |
| | 161.4 | 63700 | 965 | 1629 | 1.6 | 0.24 | 0.35 |
| Site 722 | | | | | | | |
| | z | Su | γ | γ' | γ'/γ | Su/(γ''z) | ky |
| | 5 | 19100 | 1086 | 1725 | 1.58 | 2.21 | 3.47 |
| | 14.8 | 20400 | 1022 | 1674 | 1.63 | 0.82 | 1.29 |
| | 24.4 | 18100 | 993 | 1643 | 1.65 | 0.45 | 0.69 |
| | 34 | 28500 | 1101 | 1717 | 1.55 | 0.48 | 0.70 |
| | 62.5 | 73100 | 1094 | 1723 | 1.5 | 0.67 | 1.01 |
| | 72.2 | 33800 | 1093 | 1701 | 1.55 | 0.27 | 0.37 |
| | 81.8 | 65400 | 945 | 1559 | 1.64 | 0.51 | 0.79 |

*Table 1 : Paramètres de l'analyse de stabilité, d'après Shipboard scientific party, 1989. Su : résistance au cisaillement, en Pa; γ : densité sèche du sédiment (kg/m$^3$); γ': densité du sédiment chargé en eau (kg/m$^3$), ky: accélération horizontale critique, en g (1g = 9,82 m.s$^{-2}$).*

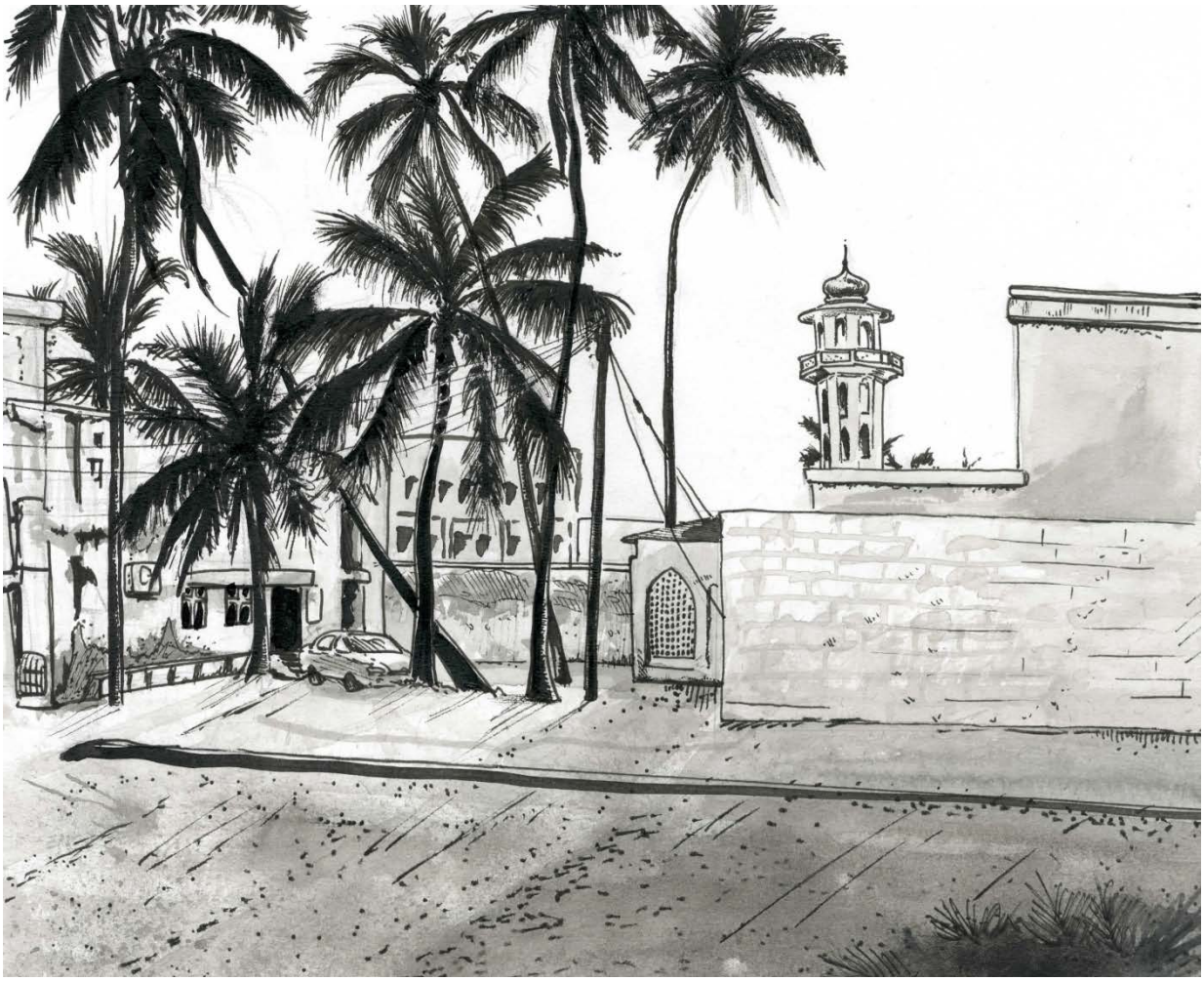

*Planche VI : Dessin à l'encre de chine d'une rue de Salalah, au sud de l'Oman.*

Nat. Hazards Earth Syst. Sci., 13, 417–424, 2013
www.nat-hazards-earth-syst-sci.net/13/417/2013/
doi:10.5194/nhess-13-417-2013


Natural Hazards and Earth System Sciences
Open Access

# Owen Ridge deep-water submarine landslides: implications for tsunami hazard along the Oman coast

**M. Rodriguez[1,2,3], N. Chamot-Rooke[3], H. Hébert[4], M. Fournier[1,2], and P. Huchon[1,2]**

[1]Institut des Sciences de la Terre de Paris, UMR7193, Université Pierre et Marie Curie, case 129, 4 place Jussieu, 75252 Paris cedex 05, France
[2]iSTeP, UMR7193, CNRS, 75005 Paris, France
[3]Laboratoire de Géologie, Ecole normale supérieure, 24 rue Lhomond, 75231 Paris cedex 05, France
[4]CEA, DAM, DIF, 91297 Arpajon, France

*Correspondence to:* M. Rodriguez (rodriguez@geologie.ens.fr)

Received: 25 September 2012 – Published in Nat. Hazards Earth Syst. Sci. Discuss.: –
Revised: 15 January 2013 – Accepted: 19 January 2013 – Published: 15 February 2013

**Abstract.** The recent discovery of voluminous submarine landslides along the Owen Ridge may represent a source of tsunami hazard for the nearby Oman coast. We assess the severity of this potential hazard by performing numerical simulations of tsunami generation and propagation from the biggest landslide (40 km$^3$ in volume) observed along the Owen Ridge. A finite-difference model, assimilating the landslide to a visco-plastic flow, simulates tsunami generation. Computation results show that Salalah city (190 000 inhabitants) is impacted by 2.5 m-high tsunami waves one hour after sediment failure. Higher wave elevation values (4 m) are reached in the low populated Sawqara Bay over 80 min after slide initiation. Although large submarine failures along remote oceanic ridges are infrequent, this study reveals an underestimated source of tsunami hazard in the Arabian Sea.

## 1 Introduction

Arabian Sea coasts have been affected by numerous and disastrous tsunamis in the past (Jourdan, 2008; Heidarzadeh et al., 2008; Donato et al., 2008, 2009; Jaiswal et al., 2009; Pilarczyk et al., 2011; Pilarczyk and Reinhardt, 2012) and storm waves from cyclones (Fritz et al., 2010). The main tsunami source in the Arabian Sea is the seismic activity of the Makran subduction zone, which caused the 1945 event ($M_w = 8.1$) and the subsequent 4000 human fatalities. Other far field sources, such as the seismic activity of the Indonesian subduction zone, may generate modest tsunamis on Arabian Sea coastlines (Okal et al., 2006). Although previous studies have identified submarine landslides as the source of some of the deadliest tsunamis over the last decades (for instance the 1998 Papua New Guinea event (Heinrich et al., 2000; Tappin et al., 2001, 2008)), the severity of such hazard remains unknown in the Arabian Sea.

Tsunamis are dispersive gravity water waves with a phase velocity $c = \sqrt{gh}$ at long period, where $h$ is the bathymetry and $g$ the gravitational acceleration. Submarine landslide-generated tsunamis display distinct differences compared to earthquake-generated tsunamis (Trifunac and Todorovska, 2002): because of their smaller source dimensions, landslide-generated tsunamis are more affected by frequency dispersion, resulting in shorter wavelength and faster wave amplitude attenuation. However, vertical displacements at the source can be larger in comparison to earthquake source, and lead to potentially higher amplitude waves, which requires the consideration of non-linearity of the propagating waves.

The recent discovery of voluminous submarine landslides along the Owen Ridge may represent an under-estimated source of tsunami hazard in the Arabian Sea (Fournier et al., 2011). The Owen Ridge is a prominent submarine relief located 300 to 400 km away from the coast of Oman and is closely linked to the Owen Fracture Zone, a 800 km-long active strike-slip fault system (Rodriguez et al., 2011; Bourget et al., 2013) (Fig. 1). Several types of mass failures have been mapped in details along the ridge using multibeam bathymetry and sediment echo-sounder (Rodriguez et

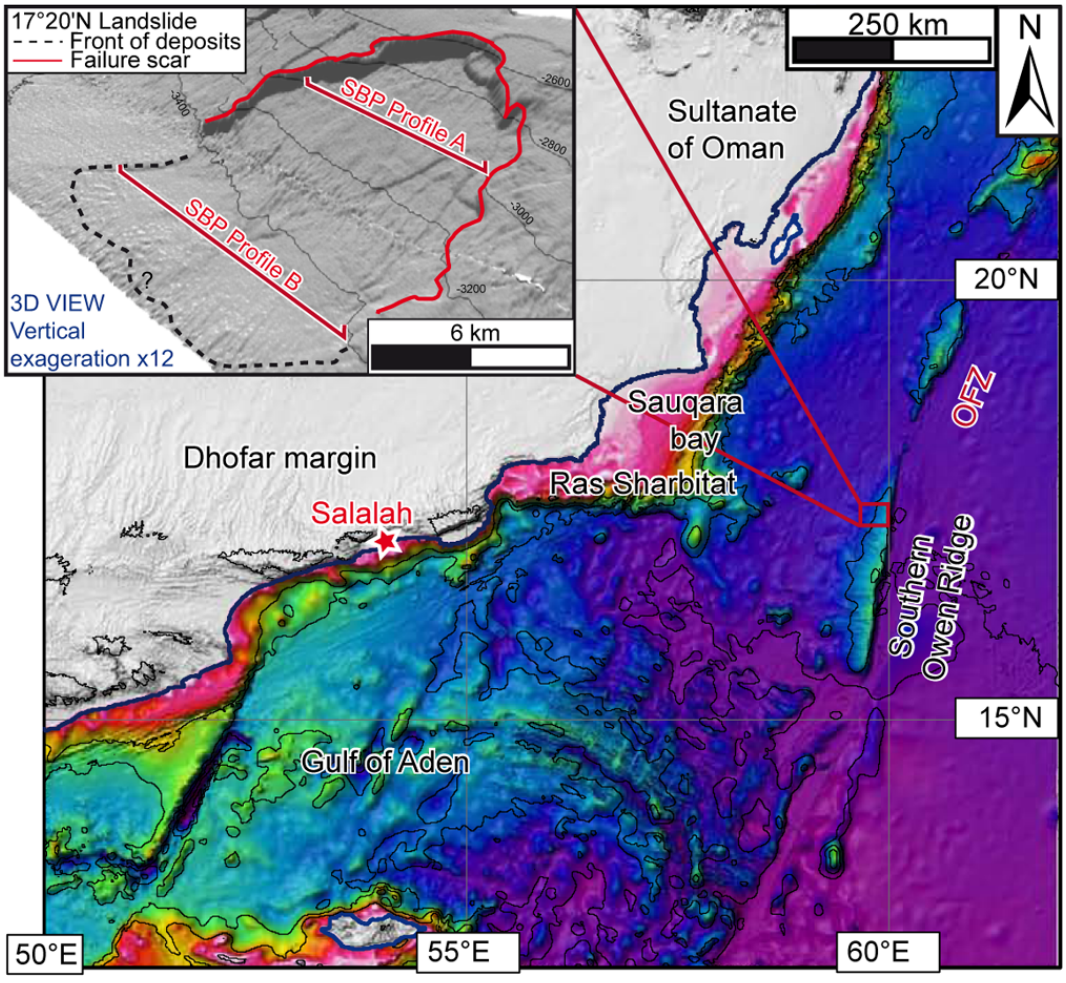


**Fig. 1.** Regional topographic map of the Sultanate of Oman and the offshore Owen Fracture Zone. Inset shows a 3-D view of the 17°20′N landslide located on the Owen Ridge. OFZ: Owen Fracture Zone.

al., 2012). The southern segment of the Owen Ridge displays the most voluminous landslides, including two landslides that removed up to 40–45 km$^3$ of sediment according to their failure morphology (Rodriguez et al., 2012). To date, there are neither historical witnesses of a tsunami nor tsunami deposits on the Oman coast that can be related to a mass-wasting episode over the Owen Ridge (Pilarczyk et al., 2011; Hoffman et al., 2013). In contrast with subaerial or shallow landslides (Fritz et al., 2009; Mohammed and Fritz, 2012), the tsunami hazard associated with deep-sea (> 2000 m) landslides remains poorly investigated (Lo Iacono et al., 2012). The objective of this paper is to assess the severity of this potential source of tsunami hazard along the nearby Oman coasts, by modelling the generation, propagation, and heights from tsunamis triggered by the biggest submarine landslide (located at the latitude of 17°20′N) on the southern segment of the Owen Ridge.

## 2 Geological background and description of the 17°20′N submarine landslide

The Owen Ridge is composed of three distinct bathymetric highs running parallel to the Owen Fracture Zone, including the 300 km-long, 50 km-wide, and 2000 m-high asymmetric southern Owen Ridge (Fig. 1). The southern Owen Ridge is covered by a ∼ 500 m thick pelagic drape, mainly made up of nanno-fossil ooze and clays (Shipboard scientific party, 1989). The regular western slope of the Owen Ridge, corresponding to sedimentary beds gently tilted 2–3° to the west, favours the occurrence of large retrogressive slumps with 25 events mobilizing more than 1 km$^3$ of sediments observed on the seafloor (Rodriguez et al., 2012). The relative arrangement of slope failures and mass transport deposits along the southern ridge reveals that each slide occurred as a distinct event. Stratigraphic studies document sporadic mass wasting events through time since the uplift of the Owen Ridge in the Miocene, with a typical recurrence rate of the

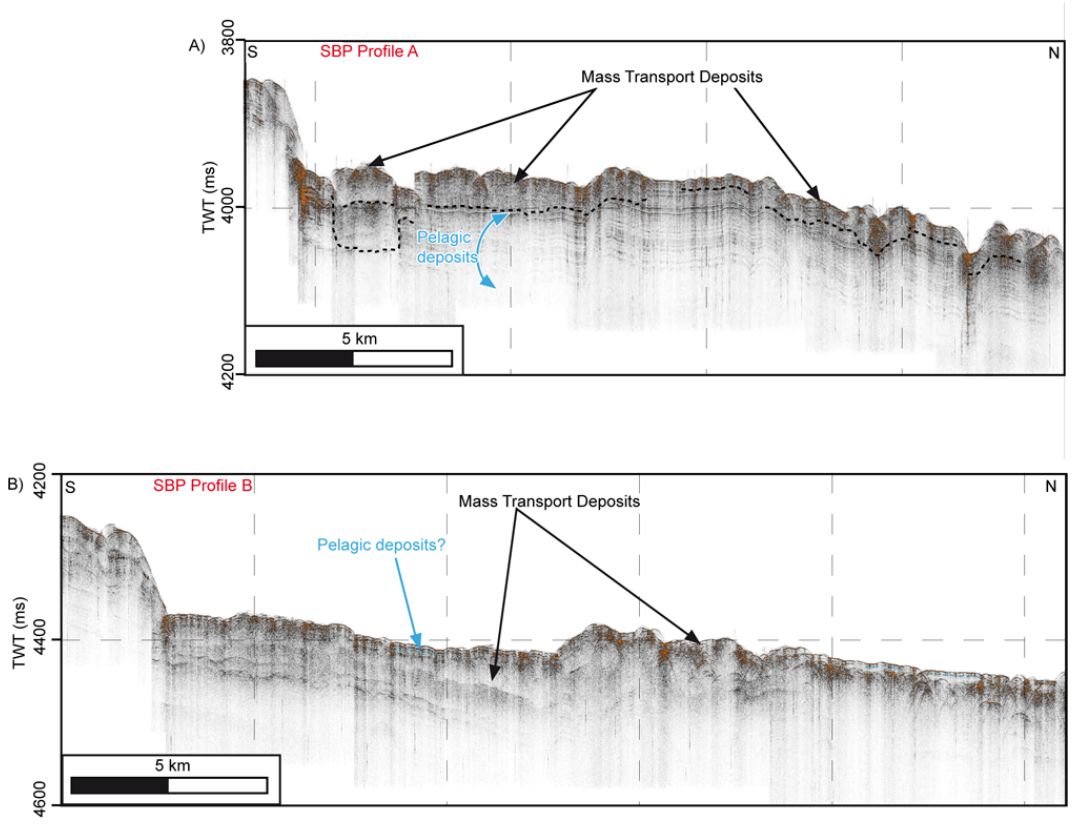


**Fig. 2.** 3.5 kHz echo-sounder profiles (SBP 120) across the 17°20′N landslide. See Fig. 1 for location. Vertical exaggeration x28.

order of $10^5$–$10^6$ yr (Rodriguez et al., 2012). The recurrence rate is determined by converting into time the thickness of pelagic deposits lying between successive mass transport deposits according to sedimentation rates calculated at ODP sites (Shipboard Scientific Party, 1989; Rodriguez et al., 2012). The seismicity along the Owen Fracture Zone is rather low and scattered (Quittmeyer and Kafka, 1984; Gordon and DeMets, 1989; Fournier et al., 2001), the maximum magnitude recorded to date being a $M_w = 5.3$ earthquake (Harvard CMT, 7 April 1985). However, millennial large earthquakes ($M_w \sim 7$) are expected (Fournier et al., 2008; Rodriguez et al., 2012) as reported at other oceanic fracture zones. Although earthquakes are the most likely triggering factor of slope failure, the apparent discrepancy between earthquake frequency and mass wasting frequency highlights the dominant control of slow pelagic sedimentation rates and hence, time needed to return to a mechanically unstable pelagic cover (Rodriguez et al., 2012).

Because the speed of the failed mass strongly affects the amplitude of the out-going wave (Trifunac and Todorovska, 2002), it is important to determine the kinematics of the landslide, i.e., whether the mass movement is a slump or a debris flow. Based solely on multibeam bathymetry and echo-sounder data, it is ambiguous to solve the latter problem as mass movement type is usually assessed by rigorous core analyses (Mulder and Cochonat, 1996; McAdoo et al., 2000; Tripsanas et al., 2008). Nevertheless, mapping the architecture of sediment failures using subsurface data provides fundamental constraints on numerical models of tsunami generation (Tappin, 2010).

The landslide located at 17°20′N is the biggest landslide (volume = 40 km$^3$) that occurred along the southern Owen Ridge (Fig. 1) (Rodriguez et al., 2012). In this area, the failure initiates at 2000 m water depth, and a 400 km$^2$ area of hummocky seafloor, characterised by a chaotic facies on echo-sounder profiles (SBP120), is partly enclosed by a 35 km-long arcuate failure scar (Figs. 1, 2). This description of the 17°20′N failure suggests a sedimentary material remaining close to the slide scar and hence a cohesive motion of the transported mass (such as in slump processes) rather than a disintegrative motion (such as in debris flow processes). Consequently, we modelled the 17°20′N landslide as a homogeneous visco-plastic flow subjected to gravity. The age of the 17°20′N landslide can be roughly inferred by converting into time the thickness of pelagic deposits that blankets mass transport deposits downslope (Fig. 2). By taking into account sedimentation rates of the order of 40 m Myr$^{-1}$ (Shipboard scientific party, 1989), the ∼5.4 m thick pelagic cover indicates an age for the 17°20′N deposits around 130 kyr.

## 3 Methods

### 3.1 Multi-beam bathymetry

Multi-beam bathymetry was collected using a hull-mounted Kongsberg-Simrad EM120 multi-beam echosounder during the OWEN 2009 survey onboard the French R/V *Beautemps-Beaupré* (Fournier et al., 2011). The vertical resolution of the swath bathymetric data is of the order of 10 m. The dataset allows the production of maps at a 80 m grid interval. It was combined with the SRTM grid at 30″ to produce a uniform digital elevation model (DEM) at 1km grid spacing (datum:WGS 84). The DEM was then used for the source sensitivity studies and to investigate the impact of landslide-generated tsunami on the Arabian Sea coasts. Although the DEM includes the coastline, it is however not refined in its shallowest bathymetric part and in the first emerged meters. Thus the only estimations provided in the following consist of maximum water heights close to the coast, but do not provide any detailed mappings of flooding.

### 3.2 Landslide modelling

We use the AVALANCHE code that has been described in details and successfully tested for the 1998 Papua New Guinea event (Heinrich et al., 2001) and the 1979 Nice event (Labbé et al., 2012). The model is based on the shallow water assumption, with slide thickness much smaller than its length and width. This approach allows us to ignore the exact mechanical behaviour within the flow (Savage and Hutter, 1989). The mechanism initiating the landslide is not investigated in this study and it is assumed that the whole mass suddenly loses its equilibrium and begins to flow down the slope. Modelling the 17°20′N landslide as a viscous flow requires a parabolic profile of the slope-parallel velocity of the sedimentary mass, with a no-slip condition at the sea bottom (Jiang and Leblond, 1992). The shear stress $\tau_{xz(z=0)}$ at the sea bottom is expressed as

$$\boldsymbol{\tau}_{xz(z=0)} = -3\mu\,\boldsymbol{u}/h\rho_s$$

where μ is the dynamic viscosity, $\boldsymbol{u}$ the slide velocity, h the slide thickness perpendicular to the slope, and $\rho_s$ the sediment density.

As viscous flows never stop on the sea bottom whatever the viscosity coefficient, it is necessary to model the 17°20′N landslide as a visco-plastic fluid (also called a Bingham plastic fluid). In a visco-plastic fluid, no deformation takes place until a specified shear stress, called the yield stress, is applied to the fluid. Above the yield stress, the material flows like a viscous fluid (Jiang and Leblond, 1993). By considering that equations are averaged through the thickness of the slide, the Bingham model requires two systems of equations to be solved, corresponding to two distinct zones in the flow, a shear flow driven by viscosity and a plug flow above it with a uniform velocity profile (Jiang and Leblond, 1993). Since the slide thickness (140 m at the initiation) is much smaller than the slide length in the case study, the Bingham model can be simplified by considering a single layer whose motion is initiated and driven by viscosity when the shear stress exceeds a given yield stress (Norem et al., 1991; McEwen and Malin, 1989). The resulting equations of mass and momentum conservation, written in a coordinate system linked to the topography, read (see Heinrich et al., 2001)

$$\begin{aligned}
&\tfrac{\partial h}{\partial t} + \tfrac{\partial}{\partial x}(h\boldsymbol{u}) + \tfrac{\partial}{\partial y}(hv) = 0\\
&\tfrac{\partial}{\partial t}(h\boldsymbol{u}) + \alpha\,\tfrac{\partial}{\partial x}(h\boldsymbol{u}.\boldsymbol{u}) + \alpha\,\tfrac{\partial}{\partial y}(h\boldsymbol{u}.v)\\
&= -\tfrac{1}{2}\boldsymbol{\kappa}\,\tfrac{\partial}{\partial x}(gh^2\cos\theta) + \boldsymbol{\kappa} gh\sin\theta_x - \boldsymbol{\tau}_{xz(z=0)}\\
&\tfrac{\partial}{\partial t}(hv) + \alpha\,\tfrac{\partial}{\partial x}(hv.\boldsymbol{u}) + \alpha\,\tfrac{\partial}{\partial y}(hv.v)\\
&= -\tfrac{1}{2}\boldsymbol{\kappa}\,\tfrac{\partial}{\partial y}(gh^2\cos\theta)\\
&+\boldsymbol{\kappa} gh\sin\theta_y - \boldsymbol{\tau}_{yz(z=0)},
\end{aligned}$$

where $\boldsymbol{\kappa} = 1-\rho_w/\rho_s$, $\tau_{xz\,(z=0)}$ and $\tau_{xy\,(z=0)}$ are the shear stresses at the bed surface, $\boldsymbol{u}$ =($\boldsymbol{u}$,v) is the depth-averaged velocity vector parallel to the bed, h is the slide thickness perpendicular to the slope, $\rho_w$ and $\rho_s$ are the water and sediments densities with a ratio $\rho_w/\rho_s$ =2, θ(x,y) is the local steepest slope angle, $\theta_x$ and $\theta_y$ are the slope angles along x- and y-axes, respectively. Values of α that deviate from unity provide information about the deviation of the slope normal profile of (u, v) from uniformity. These hyperbolic equations are solved in the same numerical scheme as the one used in the tsunami model.

### 3.3 Tsunami modelling

Simulations of the tsunami waves are based on the shallow-water approximation, which deals with the full interaction of landslide and water, including the deformation of the sediment body. Equations governing the landslide and the tsunami propagation are similar and non-dispersive. They are thus solved using the same Godunov-type scheme, extended to second order by using the concept of Vanleer (Alcrudo and Garcia-Navarro, 1993; Mangeney et al., 2000), which is based on a shock-capturing method originally derived from gas dynamics models (Heinrich et al., 2001). This model is particularly adapted to deal with nonlinear waves. The sea bottom deformation through time resulting from the landslide motion is introduced as a known forcing term $(\cos\theta)^{-1}\partial h/\partial t$ in the mass conservation equation of the tsunami model. Finally, our model also allows the computation of inundation (run-up) heights at the receiving shore.

## 4 Results

Several sensitivity tests of parameters were performed. The major parameter controlling tsunami generation is the cohesion of sediment within the flow, tsunami being generated

for cohesion less than $40\,g\,m^{-3}$. Simulations have been carried out for dynamic viscosity values ranging between 25 and $500\,m\,s^{-2}$, consistent with observations of subaerial debris avalanches (Sousa and Voight, 1991, 1995). For a fixed cohesion value, the dynamic viscosity of the flow has no significant impact on the slide motion and therefore on the wave field pattern. Values of dynamic viscosity ranging between 250 and $500\,m\,s^{-2}$ better reproduced the observed extension of mass transport deposits. About 400 s after slide initiation, the resulting average velocities of the landslide reach $\sim 40 \pm 3\,m\,s^{-1}$.

At the source location, the original radiated wave is formed of two peaks and one trough. The water ahead of the front face of the slide is pushed away, creating a leading positive wave in the slide direction. The trough following the crest is simultaneously created by the slide excavation, and is followed by a large second positive peak created by the infilling of the trough (Fig. 3). In spite of the $\sim 2000$ m water depth of slide initiation, water heights at the source can reach 4.8 m in elevation, the highest waves being formed in the out-going direction of the slide, thus towards the Oman coast. Amplitudes of the back-going waves are reduced and significantly attenuated only 8 km east from the source. The three out-going waves spread away from the source as cylindrical waves (Fig. 3). The tsunami wave field mainly affects Oman coasts, other areas being too far from the source. The time for the first leading wave to reach the Oman coastline at Ras (cape) Madrakah is 35 min (Fig. 3). The complex bathymetric pattern related to the transition between the Oman transform margin (between 18°′N and 22°30′N) and the rifted margins of the Gulf of Aden strongly influences the propagation of the tsunami wave field (Figs. 1, 3). Indeed, Hasik town and Salalah city are impacted by the tsunami 43 and 60 min after the submarine failure, respectively, whereas Ras Sharbitat, closer to the tsunami source, is impacted after 80 min of tsunami propagation (Fig. 3). This delay is due to the $\sim 120$ km wide continental shelf at the latitude of Ras Sharbitat, which slows down the propagation of the tsunami. Because of reduced continental shelves, the coastlines of the eastern Gulf of Aden are impacted earlier.

In order to investigate the behaviour of tsunami waves obtained for the maximum scenario, we plot the maximal water heights reached after a 2 h propagation time in the whole computational domain (Fig. 4). This map indicates the spatial distribution of the tsunami energy along Oman coastlines and reveals additional bathymetric forcing. First, numerous canyons that dissect the slope between 18° and 20° N locally amplify the wave elevation up to 2 m. Second, the Sharbitat Ridge, which is an E–W rectilinear, $\sim 140$ km-long submarine extension of the Oman margin located at the entrance of the Gulf of Aden, strongly influences the tsunami propagation and amplifies wave elevation up to 6 m (Fig. 4). The most affected area is the Sauqara Bay (between 18° and 19° N) with water heights reaching 2.5 m at the coastline, locally 4 m in the vicinity of Ras Sharbitat. Locally, tsunami waves

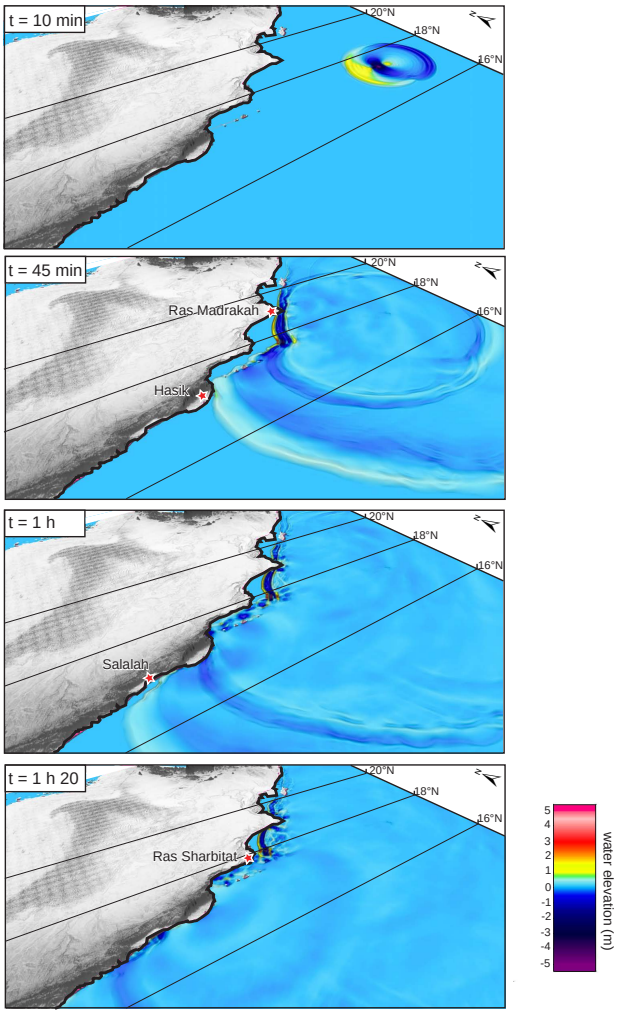


**Fig. 3.** Snapshots of the computed water surface for a dynamic viscosity value at $500\,m\,s^{-2}$. Vertical scale is exaggerated by a factor of 20 with respect to horizontal scale.

on the order of 1 m impact the coastline of the Masirah Bay. Run-up values of $\sim 2$ m are calculated at Salalah, the most populated city of the area.

## 5 Discussion and conclusions

Numerical results show that a submarine landslide similar to the one that occurred at 17°20′N on the Owen Ridge can produce moderate tsunamis along the Oman east coast. Such tsunamis would impact industrialised but low populated areas, except for the city of Salalah (190 000 inhabitants) in the Gulf of Aden and the newly built Port of Duqm on the east Oman coasts. Maximum calculated wave height values along the east Oman coasts would be of the same order as run-up values reported for the 2004 Indonesian transoceanic event for the same coasts (0.7 to 3.3 m) (Okal et al., 2006; Okal and

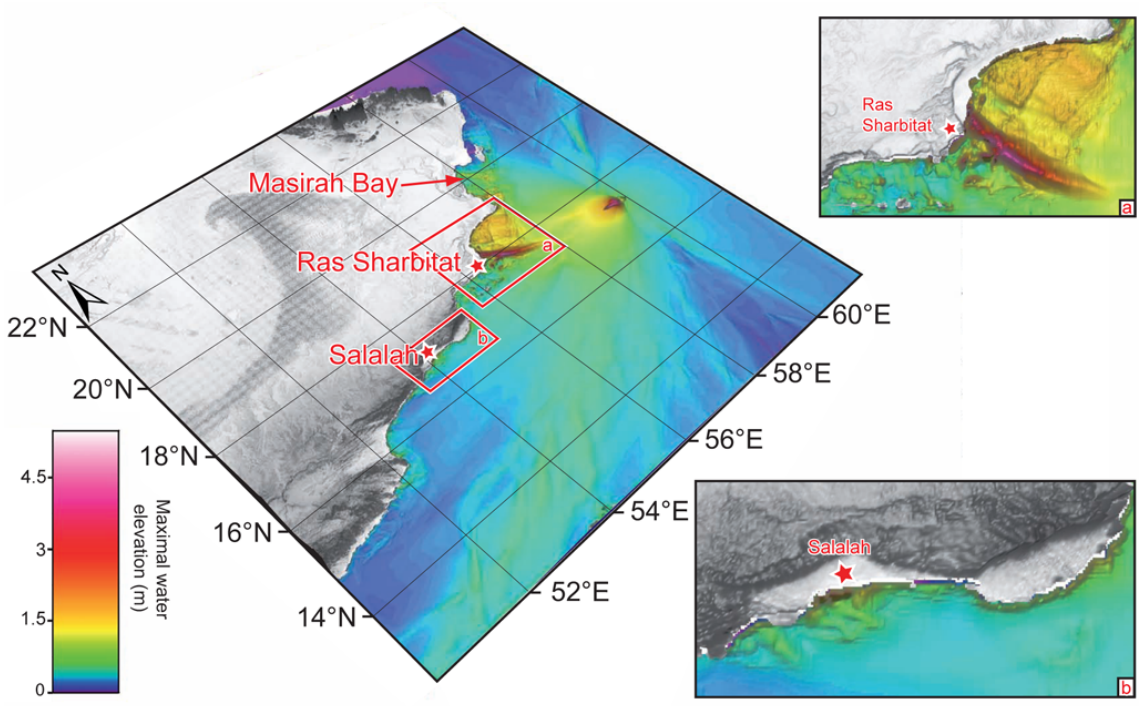


**Fig. 4.** Maximum water elevations computed after a 8000 s simulation for a dynamic viscosity value at 500 m s$^{-2}$. Insets show the maximum water elevations computed around Ras Sharbitat (inset **a**) and Salalah (inset **b**).

Synolakis, 2008), and stronger than amplitude values calculated for the 1945 Makran event (< 0.4 m) (Okal and Synolakis, 2008).

As already explained earlier, the modeled tsunami height values obtained with a 1 km cell size are not strictly run-up values since the flooding is not modeled, and they would be probably amplified using refined bathymetric grids close to the coast due to the tsunami shoaling effect which is all the more well accounted for as the grid spacing is lower. Depending on the local bathymetric slopes and configuration, these waves may locally be greatly amplified and yield amplitudes above 3 m at least. Another source of uncertainty is the non-dispersive numerical model that is not able to account for frequency dispersion inherent in tsunamis with short wavelengths, thus especially for landslide triggering. However the large extent of the 17°20′N landslide probably precludes a strong influence of frequency dispersion, specially because the wavelengths considered here are not so short with respect to the water depth, and also because the distance of propagation is not large enough to offer a significant effect of this dispersion. On the other hand, amplitude dispersion may locally occur on the continental shelf (Geist et al., 2009) and especially near Ras Sharbitat, leading to relatively attenuated wave heights in this area.

Other submarine landslides identified off Salalah on the Dhofar margin (Fig. 1) (Bache et al., 2010) may potentially be a more important source of tsunami hazard in the area. This study further demonstrates that submarine landslides occurring along remote and deep oceanic ridges (only blanketed by pelagic material) can be a source of infrequent but quite significant tsunamis. The present-day state of slope stability along the Owen Ridge remains unknown, and it is difficult to assess if a voluminous landslide is bound to occur in the near future. Other places in the world are potentially vulnerable to this type of tsunami sources. For instance, in the Atlantic Ocean, the Gorringe Bank rock avalanche (Zitellini et al., 2009), which is 60–80 km$^3$ in volume and 26–30 kyr old, could have generated a potentially destructive tsunami on densely populated Portuguese, Spanish (Lo Iacono et al., 2012) and Moroccan coastlines. In contrast with the numerous large landslides observed along the Owen Ridge, the Gorringe Bank rock avalanche is the only large landslide (> 1 km$^3$) observed along the Gorringe Bank since its Miocene uplift (Jiménez-Munt et al., 2010), which is conspicuous with regards to the high frequency of large magnitude earthquakes ($M_w > 6$) in the area (Baptista and Miranda, 2009). This contrasts with slope failures on the nearby Portuguese margin that produced turbiditic deposits whose estimated ages correlate well with the most important historic earthquakes and tsunamis (Gràcia et al., 2010). This comparison suggests that conditions for a large slope failure to occur along the Gorringe Bank might bring together a sufficient volume of sediment (limited by slow pelagic sedimentation rates) and a favourable state of consolidation. The

state of slope stability of remote oceanic ridges similar to the Owen Ridge or the Gorringe Bank needs to be further investigated, but the overall return periods of such deep-sea seated tsunamigenic instabilities are not expected to be less than several thousands of years.

*Acknowledgements.* We are indebted to the Captain Geoffroy de Kersauson, officers, and crew members of the BHO *Beautemps-Beaupré*, and to the French Navy hydrographs Vincent Lamarre and Yves-Marie Tanguy, and the hydrographic team of the 'Groupe Océanographique de l'Atlantique', for their assistance in data acquisition. The manuscript benefits from helpful and constructive comments from H. Fritz and an anonymous reviewer. We warmly thank Matthias Delescluse, Pierpaolo Dubernet and Nasser Bacha for their help and their technical assistance. We acknowledge the support of SHOM, IFREMER, CEA (LRC Yves Rocard), UPMC and INSU-CNRS for this study.

Edited by: I. Didenkulova
Reviewed by: H. M. Fritz and one anonymous referee


The publication of this article is financed by CNRS-INSU.

## References

Alcrudo, F. and Garcia-Navarro, P.: A high-resolution Godunov-type scheme in finite volumes for the 2D shallow water equations, Int. J. for. Num. Meth. Fluids, 16, 489–505, 1993.

Bache, F., Leroy, S., Baurion, C., Robinet, J., Gorini, C., Lucazeau, F., Razin, P., d'Acremont, E., and Al-Toubi, K.: Post-rift uplift of the Dhofar margin (Gulf of Aden), Terra nova, 23, 11–18, doi:10.1111/j.1365-3121.2010.00975.x, 2010.

Baptista, M. A. and Miranda, J. M.: Revision of the Portuguese catalog of tsunamis, Nat. Hazards Earth Syst. Sci., 9, 25–42, doi:10.5194/nhess-9-25-2009, 2009.

Bourget, J., Zaragosi, S., Rodriguez, M., Fournier, M., Garlan, T., and Chamot-Rooke, N.: Late Quaternary megaturbidites of the Indus Fan: Origin and stratigraphic significance, Mar. Geol., 336, 10–23, doi:10.1016/j.margeo.2012.11.011, 2013.

Donato, S. V., Reinhardt, E. G., Boyce, J. I., Rothaus, R., and Vosmer, T.: Identifying tsunami deposits using bivalve shell taphonomy, Geology, 36, 199–202, 2008.

Donato, S. V., Reinhardt, E. G., Boyce J. I., Pilarczyk, J. E., and Jupp, B. P.: Particle-size distribution of inferred tsunami deposits in Sur Lagoon, Sultanate of Oman. Mar. Geol., 257, 54–64, 2009.

Fournier, M., Patriat, P., and Leroy, S.: Reappraisal of the Arabia-India-Somalia triple junction kinematics, Earth Planet. Sci. Lett., 189, 103–114, 2001.

Fournier, M., Chamot-Rooke, N., Petit, C., Fabbri, O., Huchon, P., Maillot, B., and Lepvrier, C.: In-situ evidence for dextral active motion at the Arabia-India plate boundary, Nat. Geosci., 1, 54–58, doi:10.1038/ngeo.2007.24, 2008.

Fournier, M., Chamot-Rooke, N., Rodriguez, M., Huchon, P., Petit, C., Beslier, M.-O., and Zaragosi, Z.: Owen Fracture Zone: the Arabia-India plate boundary unveiled, Earth Planet. Sci. Lett., 302, 247–252, doi:10.1016/j.epsl.2010.12.027, 2011.

Fritz, H. M., Mohammed, F., and Yoo, J.: Lituya Bay Landslide Impact Generated Mega-Tsunami 50th Anniversary, Pure Appl. Geophys., 166, 153–175, doi:10.1007/s00024-008-0435-4, 2009.

Fritz, H. M, Blount, C. D., Albusaidi, F. B., and Al-Harthy, A. H. M.: Cyclone Gonu Storm Surge in Oman, Estuar. Coast. Shelf Sci., 86, 102–106, doi:10.1016/j.ecss.2009.10.019, 2010.

Gràcia, E., Vizcaino, A., Escutia, C., Asioli, A., Rodés, A., Pallàs, R., Garcia-Orellana, J., Lebreiro, S., and Goldfinger, C.: Holocene earthquake record offshore Portugal (SW Iberia): testing turbidite paleoseismology in a slow-convergence margin, Quaternary Sci. Rev., 29, 1156–1172, 2010.

Geist, E. L., Lynett,P. J., and Chaytor,J. D.: Hydrodynamic modeling of tsunamis from the Currituck landslide, Mar. Geol., 264, 41–52, 2012.

Gordon, R. G. and DeMets, C.: Present-day motion along the Owen fracture zone and Dalrymple trough in the Arabian Sea, J. Geophys. Res., 94, 5560–5570, 1989.

Heidarzadeh, M., Pirooz, M. D., Zaker, N. H., Yalciner, A. C., Mokhtari, M., and Esmaeily, A.: Historical tsunami in the Makran Subduction Zone off the southern coasts of Iran and Pakistan and results of numerical modeling, Ocean Eng., 35, 774–786, 2008.

Heinrich, P., Piatanesi, A., Okal, E. A., and Hébert, H.: Near-field modeling of the July 17, 1998 tsunami in Papua New Guinea, Geophys. Res. Lett., 27, 3037–3040, 2000.

Heinrich, P., Piatanesi, A., and Hébert, H.: Numerical modelling of tsunami generation and propagation from submarine slumps: the 1998 Papua New Guinea event, Geophys. J. Int., 145, 97–111, 2001.

Hoffman, G., Reicherter, K., Wiatr, T., Grützner, C., and Rausch, T.: Block and boulder accumulations along the coastline between Fins and Sur (Sultanate of Oman): tsunamigenic remains?, Nat. Hazards, 65, 851–873, 2013.

Jaiswal, R. K., Singh, A. P., and Rastogi, B. K.: Simulation of the Arabian Sea Tsunami propagation generated due to 1945 Makran Earthquake and its effect on western parts of Gujarat (India) Nat. Hazards, 48, 245–258, doi:10.1007/s11069-008-9261-3, 2009.

Jiang, L. and Leblond, P.: The coupling of a submarine slide and the surface waves which it generates, J. Geophys. Res., 97, 731–744, 1992.

Jiang, L. and Leblond, P.: Numerical modelling of an underwater Bingham plastic mudslide and the waves which it generates, J. Geophys. Res., 98, 304–317, 1993.

Jiménez-Munt, I., Fernàndez, M., Vergés, J., Afonso, J. C., Garcia-Castellanos, D., and Fullea, J.: Lithospheric structure of the Gorringe Bank: Insights into its origin and tectonic evolution, Tectonics, 29, TC5019, doi:10.1029/2009TC002458, 2010.

Jourdan, B.: Tsunamis of the Arabian peninsula : a guide of historic events, Sci. Tsunami Hazards, 27, No. 1, 31–46, 2008.

Labbé, M., Donnadieu, C., Daubord, C., and Hébert, H.: Refined numerical modeling of the 1979 tsunami in Nice (French Riviera): Comparison with coastal data, J. Geophys. Res., 117, F01008,

doi:10.1029/2011JF001964, 2012.

Lo Iacono, C., Gràcia, E., Zaniboni, F., Pagnoni, G., Tinti, S., Bartolomé, R., Masson, D. G., Wynn, R. B., Lourenço, N., Pinto de Abreu, M., Danobeitia, J., and Zitellini, N.: Large, deepwater slope failures : implications for landslide-generated tsunamis, Geology, 40, 931–934, doi:10.1130/G33446.1, 2012.

Mangeney, A., Heinrich, V., and Roche, V.: Analytical and numerical solutions of dam-break problem for application to water floods, debris and dense snow avalanche, Pure Appl. Geophys., 157, 1081–1096, 2000.

McAdoo, B. G., Pratson, L. F., and Orange, D. L.: Submarine landslide morphology, US continental slope, Mar. Geol., 169, 103–136, 2000.

McEwen, A. and Malin, M.: Dynamics of Mount St Helens'1980 pyroclastic flows, rockslide-avalanche, lahars and blast, J. Volc. Geotherm. Res., 37, 205–231, 1989.

Mohammed, F. and Fritz, H. M.: Physical modeling of tsunamis generated by three-dimensional deformable granular landslides, J. Geophys. Res. Oceans, 117, C11015, doi:10.1029/2011JC007850, 2012.

Mulder, T. and Cochonat, P.: Classification of offshore mass movements, J. Sediment. Res., 66, 43–57, 1996.

Norem, H., Locat, J., and Schieldrop, B.: An approach to the physics and the modelling of submarine flowslides, Mar. Geotech., 9, 93–111, 1991.

Okal, E. A. and Synolakis, C. E.: Far-field tsunami hazard from mega-thrust earthquakes in the Indian Ocean, Geophys. J. Int., 172, 995–1015, doi:10.1111/j.1365-246X.2007.03674.x, 2008.

Okal, E. A., Fritz, H. M., Synolakis, C. E., Raad, P. E., Al-Shijbi, Y., and Al-Saifi, M.: Field Survey of the 2004 Indonesian Tsunami in Oman, Earthq. Spectra, 22, S203–S218, 2006.

Pilarczyk, J. E. and Reinhardt, E. G.: Testing foraminiferal taphonomy as a tsunami indicator in a shallow arid system lagoon: Sur, Sultanate of Oman. Mar. Geol., 295–298, 128–136, doi:10.1016/j.margeo.2011.12.002, 2012.

Pilarczyk, J. E., Reinhardt, E. G., Boyce, I. J., Schwarcz, H. P., and Donato, S. V.: Assessing surficial foraminiferal distributions as an overwash indicator in Sur Lagoon, Sultanate of Oman, Mar. Micropaleontol., 80, 62–73, 2011.

Quittmeyer, R. C. and Kafka, A. L.: Constraints on plate motions in southern Pakistan and the northern Arabian Sea from the focal mechanisms of small earthquakes, J. Geophys. Res., 89, 2444–2458, 1984.

Rodriguez, M., Fournier, M., Chamot-Rooke, N., Huchon, P., Bourget, J., Sorbier, M., Zaragosi, S., and Rabaute, A.: Neotectonics of the Owen Fracture Zone (NW Indian Ocean): structural evolution of an oceanic strike-slip plate boundary, Geochem. Geophys. Geosyst., 12, Q12006, doi:10.1029/2011GC003731, 2011.

Rodriguez, M., Fournier, M., Chamot-Rooke, N., Huchon, P., Zaragosi, S., and Rabaute, A.: Mass wasting processes along the Owen Ridge (NW Indian Ocean), Mar. Geol., 326–328, 80–100, doi:10.1016/j.margeo.2012.08.008, 2012.

Savage, S. and Hutter, K.: The motion of a finite mass of granular material down a rough incline, J. Fluid. Mech., 199, 177–215, 1989.

Shipboard Scientific Party: Site 731, in: Proc. ODP, Init. Repts., edited by: Prell, W. L., Niitsuma, N., Emeis, K. C., Al-Sulaiman, Z. K., Al-Tobbah, A. N. K., Anderson, D. M., Barnes, R. O., Bilak, R. A., Bloemendal, J., Bray, C. J., Busch, W., Clemans, S. C., de Menocal, P., Debrabant, P., Hayashida, A., Hermelin, O. J. R., Jarrad, R. D., Krissek, L. A., Kroon, D., Murray, D. W., Nigrini, C.A. , Pedersen, T. F., Ricken, W, Shimmield, G. B., Spaulding, S. A., Takayama, T., Lo ten Haven, H., and Weedon, G. P., Leg 117, College Station, TX (Ocean Drilling Program), 585–652, 1989.

Sousa, J. and Voight, B.: Continuum simulation of flow failures, Geotechnique, 41, 515–538, 1991.

Sousa, J. and Voight, B.: Multiple pulsed debris avalanche emplacement at Mount St Helens in 1980: Evidence from numerical continuum flow simulations, J. Volc. Geotherm. Res., 66, 227–250, 1995.

Tappin, D. R.: Digital elevation models in the marine domain: investigating the offshore tsunami hazard from submarine landslides, Geol. Soc. London, spec. pub., 345, 81–101, 2010.

Tappin, D. R., Watts, P., McMurtry, G. M., Laffoy, Y., and Matsumoto, T.: The Sissano, Papua New Guinea tsunami of July 1998 – offshore evidence on the source, Mar. Geol., 175, 1–23, 2001.

Tappin, D. R., Watts, P., and Grilli, S. T.: The Papua New Guinea tsunami of 17 July 1998: anatomy of a catastrophic event, Nat. Hazards Earth Syst. Sci., 8, 243–266, doi:10.5194/nhess-8-243-2008, 2008.

Trifunac, M. D. and Todorovska, M. I.: A note on differences in tsunami source parameters for submarine slides and earthquakes, Soil Dynam. Earthq. Eng., 22, 143–155, 2002.

Tripsanas, E. K., Piper, D. J. W., Jenner, K. A., and Bryant, W. R.: Submarine mass-transport facies: new perspectives on flow processes from cores on the eastern North American margin, Sedimentology, 55, 97–136, 2008.

Zitellini, N., Gràcia, E., Matias, L., Terrinha, P., Abreu, M. A., DeAlteriis, G., Henriet, J. P., Dañobeitia, J. J., Masson, D. G., Mulder, T., Ramella, R., Somoza, L., and Diez, S.: The quest for the Africa–Eurasia plate boundary west of the Strait of Gibraltar, Earth Planet. Sci. Lett., 280, 13–50, doi:10.1016/j.epsl.2008.12.005, 2009.

## Conclusions générales et perspectives

L'histoire géologique de la limite de plaque Inde-Arabie exposée dans le chapitre 1 a été profondément remaniée à la lumière des données acquises lors des campagnes Owen 1 & 2. Cette nouvelle histoire géologique permet d'illustrer le rôle des changements cinématiques sur l'évolution structurale d'une limite de plaque décrochante sur une échelle de temps d'environ 60 Ma. Une comparaison entre le cadre géologique admis en début de thèse, et le nouveau cadre proposé à son issue, est proposée sous la forme d'un tableau bilan à la fin de ce dernier chapitre (Figure 1).

*Conclusions régionales : révision de l'histoire géologique de la limite de plaque Inde-Arabie (du Paléocène à l'actuel)*

*La Zone de Fracture d'Owen, limite de plaque Plio-Pléistocène*

D'après les 10-12 km de rejet mesurés, et considérant son taux de mouvement actuel de 3 ±1mm/an constant au cours du temps, la ZFO a un âge compris entre 3 et 6 Ma. Ceci est confirmé par les estimations des âges des principales structures découvertes au niveau de la ZFO : le bassin pull-apart 20°N est âgé d'environ 2.5±1 Ma et la fosse de Dalrymple d'environ 2±1 Ma. La formation de la fosse de Dalrymple est contemporaine de la discordance M, dont l'âge a été révisé de ~6 Ma à ~2 Ma. La Ride Nord de Murray, dont la topographie est localement élevée (1500 m par rapport au fond), a été formée par la flexure des flancs de la fosse de Dalrymple. Bien que l'âge du bassin de Qalhat demeure encore inconnu, il semble avoir subi une réorganisation structurale vers 0.8 Ma. L'âge des autres structures observées le long de l'OFZ doit encore être précisé à partir des données de sismique réflexion de la campagne Owen 2. A terme, nous espérons pouvoir décrire en détail l'évolution structurale de l'OFZ au cours du Pliocène.

Du fait des incertitudes sur l'âge exact de la ZFO, il est difficile de savoir si le bassin 20°N et la fosse de Dalrymple sont contemporains de son activation, ou se sont mis en place quelques millions d'années plus tard. La structure de la ZFO a été définie comme celle d'un décrochement purement dextre. Cependant, le modèle cinématique MORVEL (*DeMets et al., 2010*) suggère de la transtension à partir de la latitude 18°N, ce qui correspond à la zone d'apparition des bassins pull-apart. Est-ce que l'activation de la ZFO actuelle et la formation des bassins pull-aparts correspondent à un changement cinématique récent (autour de 3 Ma) et non détecté jusqu'à présent? Ou est-ce qu'ils correspondent à une réorganisation structurale de

la limite de plaque indépendante de tout changement cinématique (simple évolution du système en fonction de la redistribution des contraintes au cours du temps)?

*La limite de plaque Inde-Arabie au Miocène et le soulèvement de la Ride d'Owen*

La trace de la limite de plaque Miocène a été identifiée sous les sédiments de l'Indus au pied est de l'actuelle Ride d'Owen, enfouie à seulement quelques kilomètres de distance de la ZFO actuelle. Ceci confirme l'hypothèse des travaux cinématiques basés sur les anomalies magnétiques des dorsales de Sheba et de Carlsberg (*Chamot-Rooke et al., 2009*) qui indiquent un fonctionnement depuis au moins 20 Ma (mais avec de grandes incertitudes pour les mouvements pré-Pliocène). L'âge du soulèvement de la Ride d'Owen et de la Ride Sud de Murray a été révisé de ~20 Ma à ~8-10 Ma sur la base d'une phase de déformation compressive identifiée sur tout le Bassin d'Owen, de discordances angulaires identifiées à l'Est de la Ride d'Owen, et de l'apparition de glissements de terrains volumineux à cette période. Contrairement à ce qui était établi avant cette thèse, la limite de plaque Miocène ne semble pas avoir joué un rôle de barrière topographique majeure entre la plaine de l'Indus et le Bassin d'Owen : la barrière topographique n'est effective que depuis le soulèvement de la Ride d'Owen et l'activation de l'OFZ à la fin du Miocène.

La phase de déformation compressive tortonienne a été identifiée plus particulièrement au niveau de la marge omanaise et de la zone de connexion entre l'OFZ et la fosse de Dalrymple-Ride de Murray. Cette phase de déformation est probablement associée au changement cinématique à l'origine de la déformation intra-plaque dans l'Océan Indien Central. L'origine de ce changement cinématique pourrait être l'importante croissance de l'Himalaya à la fin du Miocène, qui a modifié le champ des contraintes à l'intérieur de la plaque Indienne (*Molnar et Stock*, 2009). Il est possible que le soulèvement post-rift de la marge du Dhofar (au nord du golfe d'Aden), dont l'origine est débattue (*Leroy et al., 2012*), soit aussi le résultat de cet épisode de déformation, les marges passives ayant tendance à localiser les phénomènes de déformation intra-plaque (*Cloething et al., 2008*). Le soulèvement de la Ride d'Owen est-il à l'origine de la transition entre la limite de plaque Miocène et l'OFZ (indépendamment de tout changement cinématique autour de 3 Ma) ? Cela impliquerait que la limite de plaque Miocène ait accompagné l'essentiel du soulèvement de la ride avant d'être inactivée. Il demeure inconnu à quel moment précis s'est fait cette transition structurale : entre 8 et 6 Ma ? Autour de 3 Ma ?

Un pointé précis des anomalies magnétiques des dorsales de Sheba et Carlsberg permettrait peut-être de mettre en évidence un changement cinématique jusqu'ici inconnu au niveau de la limite de plaque Inde-Arabie entre 3 et 6 Ma. Il permettrait aussi de savoir si la limite de plaque Inde-Arabie a bien subi une compression (ou une transpression) autour de 8-10 Ma. Cependant, vu la lenteur du mouvement relatif Inde-Arabie, de fortes incertitudes sur les prévisions du mouvement au cours du Miocène et du Pliocène seront à considérer. Ces travaux sont en cours (*Chamot-Rooke et al., 2009*).

*La limite de plaque Inde-Arabie au Paléogène*

L'histoire de la limite de plaque Inde-Arabie au Paléogène demeure encore spéculative du fait de la difficulté d'établir un cadre stratigraphique précis, et des mauvaises conditions de l'enregistrement sédimentaire de la déformation à l'Oligocène (seulement 50 m de sédiments au maximum pour environ 10 Ma !). Plusieurs résultats importants ont été néanmoins établis. L'identification de lambeaux de l'ophiolite de Masirah sur le socle du Bassin d'Owen aux abords de la marge est-omanaise indique que le socle est à cet endroit d'âge Crétacé (au minimum). Cela contraste avec l'âge paléocène des roches forées au niveau de la Ride d'Owen. Ces observations indiquent que le socle du Bassin d'Owen est d'âge mixte, et que des portions de lithosphère d'âge différent ont été mises en contact par une faille transformante majeure. Cela peut s'expliquer par un épisode de transfert d'une portion de plaque Inde à la plaque Arabie avant l'ouverture du golfe d'Aden. Ce phénomène de transfert de plaque est en accord avec les reconstitutions cinématiques proposées pour le Paléogène (*Royer et al., 2002*). Des indices de failles transformantes autrefois associées au centre d'accrétion de Carlsberg ont été mis en évidence dans la partie est du Bassin d'Owen. Une phase de création de rides marginales est identifiée au niveau de la marge omanaise à la fin de l'Eocène. Elle correspond à un régime transpressif le long de la limite de plaque Paléocène-Eocène, en accord avec les reconstitutions de *Royer et al*. (2002) (transpression prédite à partir des chrons 21-22). La relocalisation de la limite de plaque Inde-Arabie au niveau de la Ride d'Owen actuelle s'est faîte probablement autour de 25 Ma. Une différence majeure avec les reconstitutions de *Mountain et Prell* (1990) est que le soulèvement de la Ride d'Owen ne marque pas une migration majeure de la limite de plaque Inde-Arabie au Burdigalien. L'histoire de la limite de plaque à l'Oligocène demeure inconnue, en raison de l'impossibilité d'estimer le taux de rifting du golfe d'Aden, et de la trop faible épaisseur de sédiments pour enregistrer une hypothétique déformation décrochante. Par conséquent il est difficile de savoir si la limite de plaque était

sénestre, dextre... ou même si elle existait! Afin de déterminer le mouvement Inde-Arabie à l'Oligocène, il est nécessaire de reprendre le circuit des plaques global à cette période.

L'histoire de la limite de plaque Inde-Arabie semble fortement liée à l'histoire de la séparation de la plaque Arabe du reste de l'Afrique en réponse aux collisions en Méditerranée Orientale et à l'apparition du point chaud des Afars, le ralentissement absolu de l'Afrique étant daté entre 30 et 40 Ma (Jolivet et Faccenna, 2000). Pendant la même période, la marge Arabe très étirée (400-600 km selon les estimations, *MacQuarrie et al., 2003*) commence à entrer en subduction. Il est donc possible que les changements cinématiques peu avant 40 Ma aient provoqué un régime transpressif à l'origine de l'inactivation de la limite de plaque Inde-Arabie qui à cette époque était localisée au pied de la marge omanaise, sans ralentir la migration de la proto-plaque Arabe vers le Nord (*MacQuarrie et al., 2003*). Suite à ces évènements, le golfe d'Aden a commencé à s'ouvrir autour de 30 Ma (âge du point chaud des Afars). Du côté du Zagros, la subduction de la lithosphère continentale Arabe (très épaisse, la plaque Arabe étant un craton) ne commence qu'à 25 Ma. Cet évènement est probablement responsable de l'individualisation de la plaque Arabe à 25 Ma, avec les premiers stades de formation de la mer Rouge, et probablement l'activation de la limite de plaque Inde-Arabie au niveau de la Ride d'Owen actuelle.

La phase d'expansion ultra-lente au niveau de la dorsale de Carlsberg (entre 40 et 25 Ma) a été précédemment reliée à la formation de l'Himalaya (Patriat et Achache, 1984), dont les premiers stades de collision sont détectables dans les anomalies magnétiques dès 50 Ma environ. La limite de plaque Inde-Arabie à l'Oligocène n'étant pas identifiée, il se pourrait que les plaques Inde et Arabie aient été couplées à l'Oligocène, et que la phase d'expansion ultra-lente de la dorsale de Carlsberg corresponde en réalité à la séparation de l'Arabie du reste de l'Afrique. Les distances entre les sites où le socle du Bassin d'Owen a été foré et les anomalies magnétiques correspondantes sur la plaque Inde sont plutôt de l'ordre de 200 km, ce qui suggère que la limite de plaque a été relocalisée dès le début de l'Oligocène, mais ceci doit être confirmé par l'identification précise des anomalies magnétiques du Bassin d'Owen. L'anomalie 7 (24 Ma) correspond à une réorganisation globale du circuit des plaques composant l'Océan Indien, dont l'origine est attribuée à la formation du Zagros (*Patriat et al., 2008*), mais encore difficile à démontrer (*Cande et al., 2010*). Cette anomalie pourrait correspondre à l'individualisation définitive de la plaque Arabie du reste de l'Afrique. Ainsi l'Afrique n'est plus soumise à la traction exercée par le Zagros à 25 Ma. Cela pourrait aussi

marquer la séparation entre l'Inde et l'Arabie dans le cas où elles aient été couplées à l'Oligocène.

Une des implications de ces reconstitutions est que la lithosphère océanique actuellement en subduction sous le Makran ne serait pas un vestige de la Téthys, mais un vestige de l'océan Indien formé autour de 90 Ma, par un centre d'accrétion probablement connecté à celui des Mascareignes. Quelle est-donc l'origine de la lithosphère ayant été subduite lors de la formation du Zagros ? Etait-ce entièrement de la Néotéthys, ou alors est-ce qu'une partie d'océan indien (d'âge crétacé sup.) est entrée en subduction à l'Oligocène ? Autrement dit, est-il possible qu'un océan étroit, d'environ 1000 à 2000 km de large, ait existé au sud des blocs de Bisotoun/Pichakun, au nord de la marge Arabe ? Certaines études suggèrent l'existence d'un tel domaine (Wrobel-Daveau et al., 2011), mais la signification des nappes de l'Hawasina en Oman reste énigmatique dans ce cadre conceptuel. Le fait qu'un centre d'accrétion se soit mis en place au nord de la plaque Arabie dans un domaine océanique Jurassique autour de 90 Ma, pour former la lithosphère qui a été ensuite obductée au niveau du Semail, est intriguant. Comment se fait-il qu'un centre d'accrétion se mette en place à l'extrémité sud de l'océan téthysien ? Quel évènement serait responsable de la localisation de ce nouveau bras de la Téthys ? Une alternative, proposée ici à titre d'hypothèse de travail, serait qu'il s'agisse plutôt d'un bras de l'océan indien, qui subissait une profonde réorganisation autour de 90 Ma, avec le développement de centres d'accrétion bien identifiés (par ex. celui des Mascareignes).

Cette proposition de reconstitution a le mérite d'être cohérente avec toutes les observations géologiques connues. Cependant, une telle hypothèse ne peut être validée tant que les anomalies magnétiques du Bassin d'Owen n'ont pas été identifiées. Les quelques forages du socle permettent de calibrer l'âge de certaines anomalies. L'acquisition d'un relevé magnétique dense sur l'ensemble du bassin d'Owen permettrait certainement de confirmer ou réfuter les hypothèses exposées dans cette thèse. Le navire Beautemps-Beaupré dispose du matériel nécessaire, ainsi que d'une mobilité suffisante pour échapper aux attaques pirates. D'autre part, le Bassin Nord Somalien, conjugué du Bassin d'Owen, est une région sous-étudiée. Son histoire géologique est liée à celle du Bassin d'Owen, et a probablement enregistré les évènements géologiques associés à l'histoire de la limite de plaque Inde-Afrique (avant l'ouverture du golfe d'Aden). Par exemple, il existe un fort contraste entre l'âge estimé de la partie ouest du bassin (Jurassique sup.-Crétacé inf.) et la partie est, avec un forage indiquant un socle à 90 Ma (Bunce et al., 1967). A l'ouest de la ride de Chain est clairement

identifiée, sur l'un des rares profils disponibles, la trace d'une zone de fracture majeure (figure 2). Il est donc possible que cette zone de fracture marque l'ancienne limite de plaque Inde-Afrique du Crétacé sup., et qu'un épisode de migration de la limite de plaque vers la Zone de Fracture de Chain, associé à un transfert de plaque, ait eu lieu lors de la formation de la dorsale de Carlsberg et de l'obduction Masirah. Comme pour le Bassin d'Owen, le Beautemps-Beaupré serait capable d'assurer des campagnes de géophysique dont les objectifs seraient de déterminer la structure superficielle (2 premiers km) du Bassin Nord Somalien et de traquer les anomalies magnétiques (avec cependant le risque de tomber dans la période calme du Crétacé). A terme, l'objectif est de fournir une synthèse des évènements géodynamiques ayant affecté les plaques Afrique et Inde du Crétacé sup. à l'Oligocène.

*Conclusions thématiques : évolution structurale d'une limite de plaque décrochante en domaine océanique conséquences en termes d'aléas naturels et de changements environnementaux*

L'enjeu thématique principal de cette thèse était de comprendre la géométrie, la localisation et l'évolution structurale des frontières de plaques décrochantes en fonction des conditions aux limites (cinématique des plaques) et de la rhéologie de la lithosphère océanique. La séparation de la plaque Arabie du reste de l'Afrique à l'Oligocène accompagnée par la capture d'un fragment de la plaque indienne par la plaque Arabie semble avoir été à l'origine de la migration de la limite de plaque entre la marge omanaise et la Ride d'Owen actuelle. Ces phénomènes semblent étroitement associés à la nature de la croûte qui entre en subduction au niveau du Zagros : est-ce que la subduction des blocs de Bisotun/Pichakun a entraîné la première phase, modeste, de croissance du Zagros à l'Eocène ; suivie par un épisode de subduction océanique (Téthys ou océan indien ?) aboutissant à la collision véritable du craton Arabe avec l'Eurasie autour de 25 Ma ?

La transpression fini-Eocène au niveau de la limite de plaque Inde-Arabie correspond peut-être aux phénomènes de collision en Méditerranée Orientale ou aux premiers stades (énigmatiques) de formation du Zagros autour de 40 Ma. Le changement de contrainte associé au début de la subduction de la lithosphère arabe (épaisse) à 25 Ma aurait quant à lui initié l'ouverture de la Mer Rouge, et la réactivation de la limite de plaque Inde-Arabie au niveau de la Ride d'Owen, dont le socle a été structuré par le système transformant Paléocène-Eocène associé à la dorsale de Carlsberg. Est-ce que la limite de plaque s'est relocalisée à 25 Ma au niveau de la transformante montrant les décalages d'âge (et donc les contrastes rhéologiques)

les plus importants, ou dès le début de l'Oligocène avec le début de la phase d'accrétion ultra-lente au niveau de Carlsberg ? Il est pour l'instant impossible de conclure. La localisation de la frontière de plaque semble en revanche avoir été stable du Burdigalien au Tortonien, en dépit de données encore lacunaires pour proposer une carte structurale complète de cette limite de plaque. Le changement cinématique associé à la croissance du Tibet à la fin du Miocène a déclenché le soulèvement de la Ride d'Owen, et probablement la relocalisation de la limite de plaque au niveau de l'OFZ actuelle, après un délai de quelques millions d'années, défini par le comportement flexural de la lithosphère du Bassin d'Owen et la capacité de la limite de plaque au Miocène à permettre le soulèvement de la ride. Le soulèvement de rides transverses le long des transformantes océaniques en réponse aux changements cinématiques est une caractéristique commune à de nombreuses transformantes, comme la Romanche (*Bonatti et al., 2005*).

D'autre part, la caractéristique la plus surprenante de la ZFO est la dimension de certains de ces bassins pull-apart ( bassin 20°N et fosse de Dalrymple), de l'ordre de la centaine de km de long en dépit du faible rejet accumulé depuis l'activation de la faille. Des réorganisations structurales du système décrochant, isolant des micro-blocs structuraux lors de la formation des relais, sont probablement à l'origine de ces bassins de grandes dimensions, la dizaine de km d'extension étant par la suite distribuée sur l'ensemble du bassin. Comment la rhéologie de la lithosphère océanique a pu contrôler l'ouverture de ces bassins pull-apart offre une perspective intéressante au regard des nombreuses études réalisées sur les bassins pull-apart continentaux (notamment la mer Morte). Des campagnes d'OBS (Ocean Bottom Sismometer) permettraient de mieux contraindre la structure profonde de ces bassins, reconstituer l'histoire de la subsidence de ce bassin, et servir de base à des travaux de modélisation thermo-mécanique. Des forages permettraient également de mieux contraindre dans le détail l'évolution structurale des bassins principaux. Malheureusement, de telles campagnes sont difficiles à organiser dans un futur proche du fait des nombreux actes de piraterie reportés dans la région.

Le soulèvement de la Ride d'Owen a eu plusieurs conséquences. Tout d'abord, il a favorisé le déclenchement de volumineux glissements de terrain, probablement tsunamigéniques, en direction des côtes de l'Oman. Il s'agit d'une des rares cas connus de glissement de terrains sur un relief associé à une faille transformante, mais d'autres reliefs comme la Ride de Chain, ou la Ride du Mozambique pourraient être le siège d'une source d'aléa similaire. Ces glissements de terrain ont permis d'étudier le comportement d'un système

sédimentaire pélagique soumis à des déstabilisations gravitaires répétées. Heureusement, la fréquence de tels glissements de terrain (et des tsunamis associés) semble limitée fortement par les faibles taux de sédimentation pélagique, qui limitent le renouvellement du volume sédimentaire nécessaire au déclenchement des glissements. Les glissements de terrain de la Ride d'Owen ne sont donc pas des bons marqueurs stratigraphiques de la sismicité de l'OFZ. Le contexte pélagique de ces glissements offre des perspectives intéressantes sur la compréhension du rôle des taux de sédimentation en tant que facteur prédisposant ou limitant les glissements. Le soulèvement de la Ride d'Owen a également modifié les conditions de l'enregistrement sédimentaire des variations climatiques au cours du Miocène, et en particulier l'enregistrement des variations de l'intensité de la mousson asiatique. L'apparition de dépôts contouritiques immédiatement après la phase de déformation tortonienne indique potentiellement une réorganisation de la circulation océanique, ou du moins un changement des conditions de son enregistrement sédimentaire. Ces découvertes donnent naissance à de nouvelles hypothèses sur la compréhension des changements environnementaux survenus sur les côtes de la mer d'Arabie à la fin du Miocène. Une étude détaillée de la géométrie des corps contouritiques pourrait aider à la compréhension de l'évolution de la circulation océanique dans la région (dominés par des courants parmi les plus rapides au monde), et son lien avec l'évolution climatique.

*Figure 1 : Comparaison de l'histoire géologique de la limite de plaque Inde-Arabie telle que définie au début de cette thèse, puis de celle établie à son terme. Les évènements surlignés en rouge correspondent aux points de l'histoire qui ont été revisités.*

## Previous geological framework

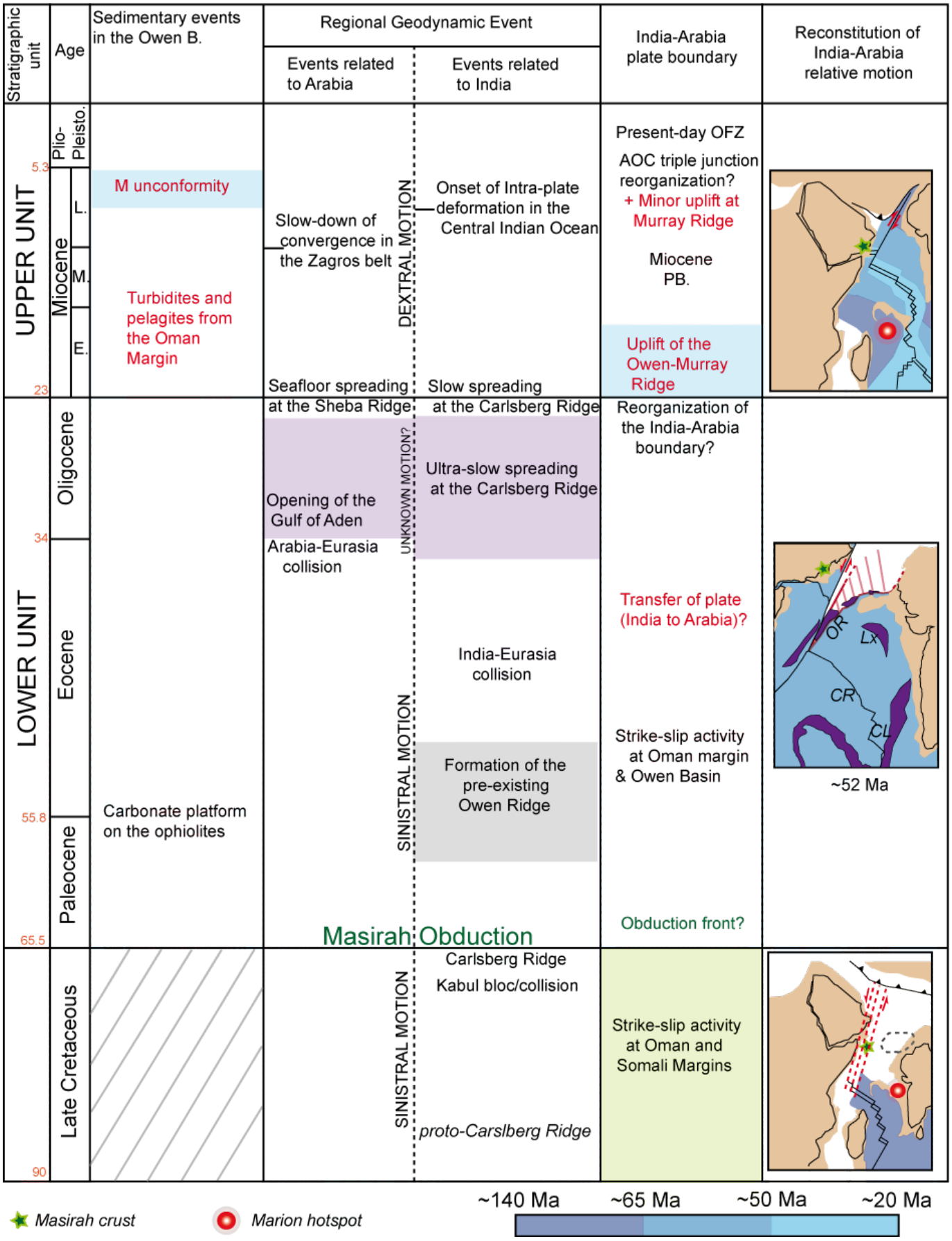

## New geological framework

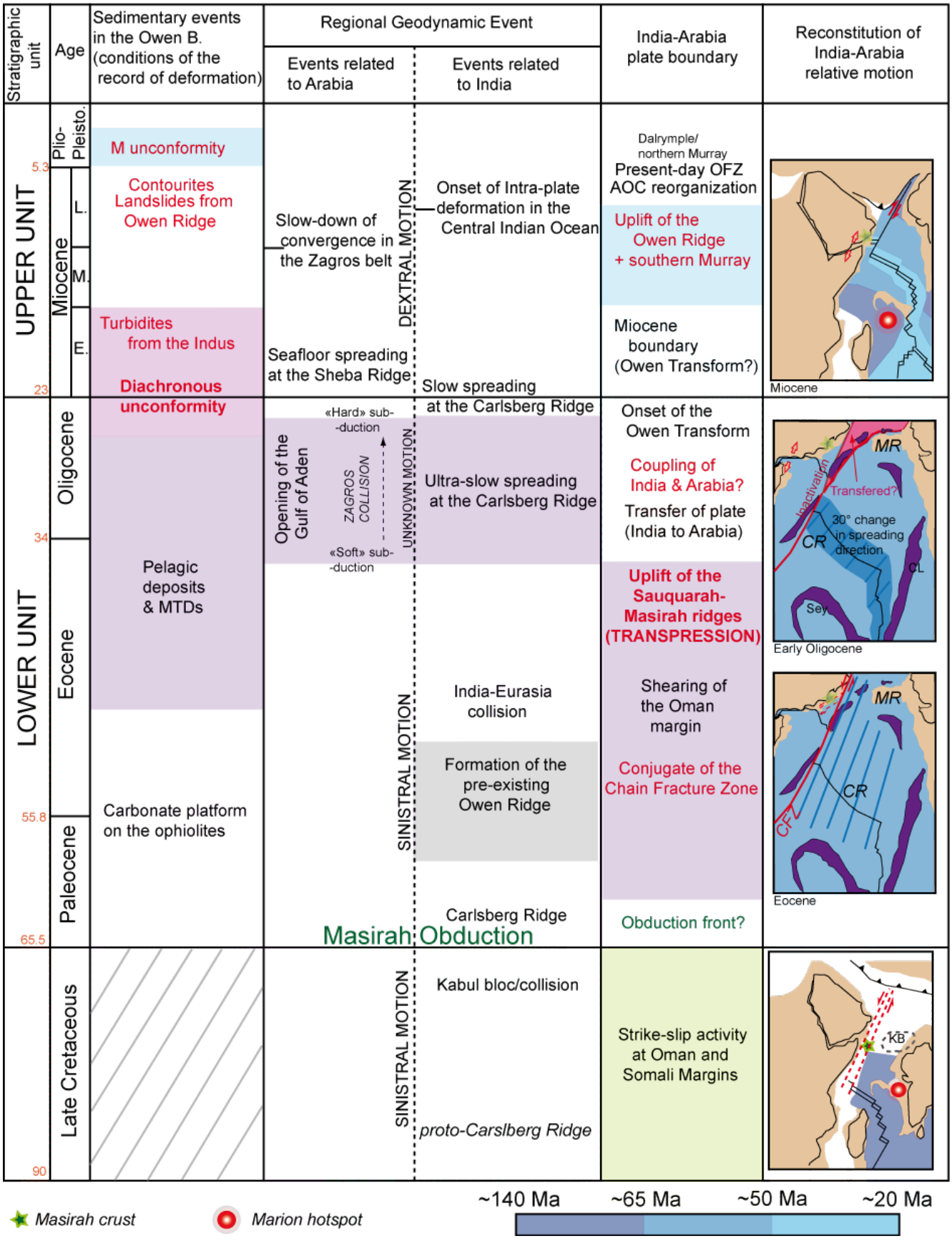

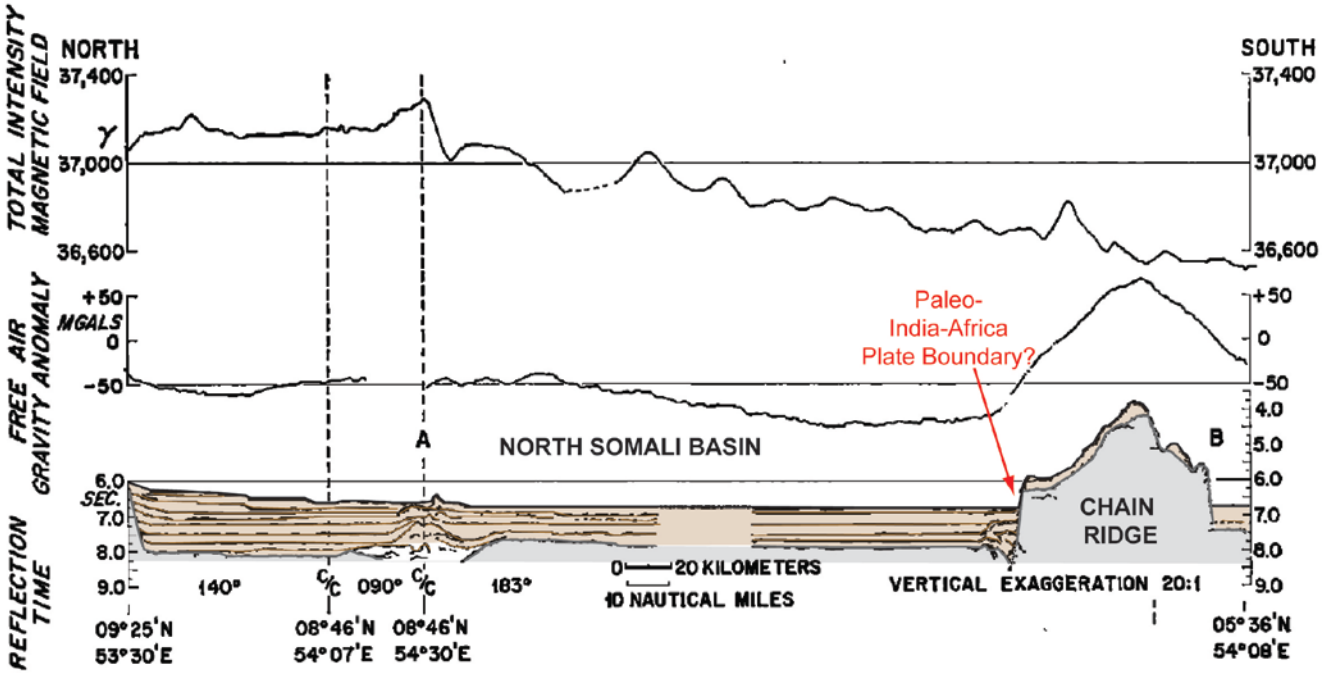


*Figure 2 : Profils magnétiques, gravimétrique, et sismique du bassin Nord Somalien : est-ce que le décalage sub-vertical observé au Nord ouest de la Ride de Chain marque la trace de l'ancienne limite de plaque Inde-Afrique au Crétacé supérieur ?*

*Planche VII : Dessin à l'encre de Chine du port de l'île de Masirah, Oman.*

*Remerciements*

Voici venu le temps de clore cette thèse, et d'abandonner la limite de plaque Inde-Arabie à ses mystères. Je remercie mes directeurs de thèse pour m'avoir permis de travailler sur un jeu de données aussi riche, prodigué des conseils bien utiles, et pour avoir enduré quasi-quotidiennement mes élucubrations parfois d'ordre psychiatrique. Je leur suis reconnaissant d'avoir accepté la surcharge de travail que mes travaux, s'avérant plus riches en résultats que prévu, ont entraîné. Travailler quotidiennement sur un objet aussi beau que le bassin 20°N a été un privilège que je n'oublierai pas. Tout comme ces nuits magnifiques sur la proue du Beautemps-Beaupré, au milieu de la Mer d'Arabie, à la seule lueur des étoiles et du plancton phosphorescent. Se promener sur le plancher du proto-océan Indien à Masirah et Madraka reste une grande émotion, qui n'a cessé de m'inspirer tout au long de cette thèse. Cette thèse a été grandement facilitée par la qualité des moyens mis à ma disposition par le laboratoire de géologie de l'école normale supérieure, et l'aide toujours irréprochable du staff informatique (notre P. Dubernet international-dont l'humour si léger et délicat anime le vol des colombes dans l'azur, mais aussi B. Mulot puis N. Bacha). Je remercie Hélène Hébert et le laboratoire du CEA pour avoir financé certains de mes travaux, et fourni le code numérique de modélisation de tsunami.

Plusieurs rencontres et discussions ont enrichie cette thèse. Merci à Jean-Paul Breton pour son accueil chaleureux en Oman, et pour m'avoir fait partager sa connaissance inestimable de la géologie de l'Oman dans les premiers temps de ma thèse. Ma reconnaissance éternelle à celui que l'on nomme El gringo, El Mariachi, El sombrero, descendant direct de la plus grande lignée de torero du royaume d'Espagne, le Don Diego de la Vega des temps modernes : l'inénarrable Alaing Rabaute, dont le soutien a été très précieux au cours de ces années de thèse. Un big-up intersidéral à Matthias Delescluse pour m'avoir

aidé à lever le pied (et le coude!) dans les moments de surmenage, et m'avoir enseigné (avec une efficacité salvatrice) les rudiments informatiques qui me manquaient pour le traitement de la sismique. Merci à Michaël Jentzer et Marc Fournier (euguaine) pour m'avoir accompagné dans mes débuts d'enseignant.

Je remercie le jury qui m'a fait l'honneur d'évaluer cette thèse, et de s'être levé très tôt pour assister à ma soutenance ! Merci à Jean-Luc Schneider et Jean-Yves Royer pour avoir assumé la tâche difficile et chronophage de rapporteur ; et merci à Tim Minshull et Michel Sébrier pour avoir accepté d'examiner mon travail. Merci pour la grande qualité du travail effectué, et pour la richesse des corrections et des pistes de recherche suggérées lors des questions (même s'il reste probablement un ou deux « mouvements accommodés » dans le texte…).

A titre plus personnel, je tiens à dédier ces travaux à mes amis d'enfance (Anaïs V., Andréa F., Clément D., Nicolas G. & M., Taran L.), qui ont nourri ma volonté de devenir scientifique; ainsi qu'à mes amis des bancs de la faculté, en particulier mes camarades de la préparation à l'agrégation de Bordeaux (Hélène B., Cédric G., Nicolas L., Sophie L., & Sophie-Emilie N.), qui à travers leur écoute, leur soutien, et les discussions scientifiques échangées, ont inspiré l'essentiel des découvertes exposées dans cette thèse et m'ont aidé à ne pas m'éloigner de moi-même dans les moments où la solitude devenait trop violente. Les moments difficiles révèlent les personnes sur qui compter : je sais désormais que vous serez là. Je remercie aussi ma famille, avec une pensée particulière pour mes grands parents, dont j'espère faire la fierté avec ces travaux de thèse.

Les fou-rires désormais légendaires du triumvirat des Badass ont porté le quotidien de cette thèse : merci à Grand Thomas, le boss des slabs qui pendouillent, avec qui j'ai retrouvé la bonne humeur du sud et bâché les vilaines aux cheveux rêches à coup de galactiques gifles (entre deux petites anecdotes sur la Motown). Merci d'avoir eu une thèse encore plus galère que la mienne et de m'avoir servi de souffre-douleur avec tant de gentillesse et d'abnégation. Merci à Grand Nicolas, la relève du comique troupier français. Je n'arrive peut-être pas (encore) à faire fondre le fromage à raclette à mains nues, mais si aujourd'hui je ris tout seul dans la rue, c'est grâce à vous (et un peu à Doudou Delerm). Une pensée pour la Team Chamot-Rooke/Pubellier : Dimitri, Choupette, Stavros, Flo, Kenny… Merci à Jean-Marc et Jean-Michel, mes amis imaginaires, pour leur fidèle accompagnement et leurs nombreuses suggestions scientifiques.

L'amitié de Fatima E., Kristell L., Anne V., Nafi T. et mes autres camarades de thèse a été très précieuse lors de la rédaction des derniers articles de cette thèse, et aussi lors de l'annulation (heureusement temporaire) de la campagne Owen 2. Une attention particulière pour les petits nouveaux (Félicie K., Alex B., Xavier D., Arnaud V., Leïla-diladada (un p'tit steack ?), Jordane ( hum hum ha…ouuuuu), le jeune Plunder (plus si jeune que ça, t'es le prochain mec !)) dont la fraîcheur et la bonne humeur m'ont fait beaucoup de bien. Merci à Marco pour m'avoir fait partager les trésors de sa collection de bande-dessinées, merci à Dovy Tristani et Françoise Larincq pour m'avoir guidé dans les méandres opaques de l'administration.

J'ai enfin une pensée pour les enseignants de l'université de Pau (Y. Hervouët & B. Rodaz) puis de Bordeaux (C. Langlois, P. Lecroart, et encore J.L. Schneider), qui ont su me transmettre leur passion pour la géologie (me détournant de mes ambitions initiales de biochimiste!), et dont le souvenir a constitué un profond soutien aux cours de ces années de thèse. Cet enthousiasme est aujourd'hui renouvelé à travers mes élèves, dont la curiosité a entretenu ma passion pour la géologie entre deux crises de nerfs sur Arcgis… et inspiré bien des hypothèses, notamment au sujet de la queue de cheval de Dalrymple et les changements environnementaux tardi-Miocène du Moyen-Orient.

*« Ah, l'homme est un dieu quand il rêve, et un mendiant quand il réfléchit, et quand l'enthousiasme ne l'inspire plus, il est là comme un fils raté que le père a chassé de la demeure, contemplant les misérables pièces de monnaie que la pitié lui a values tout au long du chemin. ».*

*F. Hölderlin*

*Hypérion, 1797.*

## Références bibliographiques

### A

Abbotts, I.L. (1978), High-potassium granites in the Masirah ophiolite of Oman: Geological Magazine, 115, p. 415-425.

Agard, P., J. Omrani, L. Jolivet, H. Whitechurch, B. Vrielynck, W. Spakman, P. Monié, B. Meyer, and R. Wortel (2011), Zagros orogeny: a subduction-dominated process, In: Lacombe, O., Grasemann, B., Simpson, G. (Eds.), Geodynamic Evolution of the Zagros. Geological Magazine, 692–725.

Alcrudo, F., and P. Garcia-Navarro (1993), A high-resolution Godunov-type scheme in finite volumes for the 2D shallow water equations, Int. J. for. Num. Meth. in Fluids, 16, 489-505.

Allen, M., J. Jackson, R. Walker (2004), Late Cenozoic reorganization of the Arabia-Eurasia collision and the comparison of short term and long term deformation rates, Tectonics, 23, TC2008, doi:10.1029/2003TC001530.

Almagor, G., and G. H.,Wisenam (1982), Submarine slumping in the continental slope of Israel, In: Saxov, S., Nieuwenhuis, J.K. (Eds.), Marine Slides and other mass movements, Proc of a NATO Workshop on Marine Slides and Other Mass Movements, Algarve, Portugal,15-21 dec. 1980, ser. 4, vol. 6, pp. 95–128.

An, Z., J. E. Kutzbach, W.L. Prell, S.C. Porter (2001), Evolution of Asian monsoons and phased uplift of the Himalaya–Tibetan plateau since Late Miocene times, Nature, 411, 62–66.

Andrews, P., and Cronin, J. E. (1982), The relationships of Sivapithecus and Ramapithecus and the evolution of the orang-utan. Nature 297, 541-546.

Angelier, J. (1984), Tectonic analysis of fault slip data sets, J. Geophys. Res., 89, 5835-5848.

Antolik M., R.E. Abercrombie, J. Pan, G. Ekström (2006), Rupture characteristics of the 2003 Mw 7.6 mid-Indian Ocean earthquake: Implications for seismic properties of young oceanic lithosphere, J. Geophys. Res., 111, B04302, doi:10.1029/2005JB003785

Armijo, R., B. Meyer, S. Navarro, G. King, A. Barka (2002), Asymmetric slip partitioning in the Sea of Marmara pull-apart : a clue to propagation processes of the North Anatolian Fault?, Terra Nova, 14, 80-86.

Armijo et al., 2005 (2005), submarine fault scarps in the Sea of Marmara pull-apart (North Anatolian Fault) : Implications for seismic hazard in Istanbul, Geochem. Geophys. Geosyst., 6, Q06009.

Aydin, A. and A. Nur (1982), Evolution of pull-apart basins and their scale independence, Tectonics, 1, 91-105, doi:1029/TC001i001p00091.

### B

Babonneau, N., B. Savoye, M. Cremer, and B. Klein **(**2002), Morphology and architecture of the present canyon and channel system of the Zaire deep-sea fan, Mar. Pet. Geol., 19, 445-467.

Bache, F., S. Leroy, C. Baurion, J. Robinet, C. Gorini, F. Lucazeau, P. Razin, E. d'Acremont, K. Al-Toubi (2010), Post-rift uplift of the Dhofar margin (Gulf of Aden), Terra nova, 23, 11-18, DOI: 10.1111/j.1365-3121.2010.00975.x.

Baptista, M. A., and J. M. Miranda (2009), Revision of the Portuguese catalog of tsunamis, Nat. Hazards Earth Syst. Sci., 9, 25–42, 2009.

Baraza, J., and G. Ercilla (1996), Gas charged sediments and large pockmark-like features on the Gulf of Cadiz slope (SW Spain), Mar. Petr. Geol., 13, 253-261.

Barnes, P. M., R. Sutherland, B. Davy, J. Delteil (2001), Rapid creation and destruction of sedimentary basins on mature strike-slip faults: an example from the offshore Alpine Fault, New Zealand, J. Struct. Geol., 23, 1727-1739.

Barnes, P., and N. Pondard (2010), Derivation of direct on-fault submarine paleoearthquake records from high-resolution seismic reflection profiles: Example from the Wairau Fault, New Zealand, Geochem. Geophys. Geosyst.,11, Q11013, doi:10.1029/2010GC003254.

Barton, P.J., T.R.E. Owen, and R.S. White (1990), The deep structure of the east Oman continental margin : preliminary result and interpretation, Tectonophysics, 173, 319-331.

Barry, J., Morgan, M. E., Flynn, L. J., Pilbeam, D., Behrensmeyer, A. K., Raza, S. M., Khan, I. A., Bagdley, C., Hicks, J., Kelley, J. (2002), Faunal and environmental change in the late Miocene Siwaliks of northern Pakistan. Paleobiology 28, 1-71, http://dx.doi.org/10.1666/0094-8373(2002)28[1:FAECIT]2.0.CO;2

Basile, C., J. Mascle, M. Popoff, J.P. Bouillin, and G. Mascle (1993), The Ivory-Coaqt Ghana transform margin - a marginal ridge structure deduced from seismic data, Tectonophysics, 222, 1-19.

Basile, C. and J.P. Brun (1999), Transtensional faulting patterns ranging from pull-apart basins to transform continental margins: an experimental investigation, J. Struct. Geol., 21, 23–37.

Beauchamp, W. H., A. C. Ries, M. P. Coward, and J.A. Miles (1995), Masirah Graben, Oman : a hidden Cretaceous rift basin?, American Association of Petroleum Geologists' Bulletin 79, 864-79.

Beck, C., et al. (2007), Late Quaternary co-seismic sedimentation in the Sea of Marmara's deep basins, Sediment. Geol., 199, 65-89.

Begun, D. R. (2004), Sivapithecus is east and Dryopithecus is west, and never the twain shall meet. Anthropological science 113, 53-64.

Ben Avraham, Z. and U. S. Ten Brink (1989), Transverse faults and segmentation of basins within the Dead Sea Rift, J. African Earth Sci., 8, 603-616.

Ben-Avraham, Z. and M.D. Zoback (1992), Transform normal extension and Asymmetric basins: an alternative to pull-apart models, Geology, 20, 423–426.

Ben Avraham, Z., T. M., Niemi, C. J. H., Hartnady (1994), Mid Tertiary changes in deep ocean circulation patterns in the Natal Valley and Transkei Basin, Southwest Indian Ocean, Earth. Planet. Sci. Lett., 121, 639-646.

Ben Avraham Z and G. Schubert (2006), Deep "drop down "basin in the southern Dead Sea, Earth Planet. Sci. Lett., 251, 254-63.

Ben Avraham Z., Z. Garfunkel, M. Lazar (2008), Geology and evolution of the southern Dead Sea Fault with emphasis on subsurface structure, Annu. Rev. Earth Planet. Sci., 36, 357-87

Ben-Zion, Y., and C. G. Sammis (2003), Characterization of fault zones, Pure Appl. Geophys.,160, 677–715.

Besse, J., and V. Courtillot, 1988. Paleogeographic maps of the continents bordering the Indian Ocean since the Early Jurassic, J. Geophys. Res., 93, 11791-808.

Böhm, E., J. M. Morrison, V. Manghnani, H-S. Kim, C. N. Flagget (1999), The Ras al Hadd Jet: Remotely sensed and acoustic Doppler current profiler observations in 1994-1995, Deep-Sea Research II, 46, 1531-1549.

Bonatti, E., and K. Krane (1982), Oscillatory spreading explanation of anomalously old uplifted crust near oceanic transform, Nature, 300, 343-345.

Bonatti, E., M. Ligi, L. Gasperini, A. Peyve, Y. Raznitsin, and Y.J. Chen (1994), Transform migration and vertical tectonics at the Romanche fracture zone, equatorial Atlantic, J. Geophys. Res., 99, 21779-802.

Bonatti, E., D. Brunelli, W.R. Buck, A. Cipriani, P. Fabretti, V. Ferrante, L. Gasperini, and M. Ligi (2005). Flexural uplift of a lithospheric slab near the Vema transform (Central Atlantic) : Timing and mechanisms, Earth. Planet. Sci. Lett., 240, 642-655.

Bosselini, A. (1986), East Africa continental margins, Geology, 14, 76-78.

Bourget, J. (2009) Les systèmes turbiditiques du golfe d'Oman et de la marge Est-africaine: architecture, évolution des apports au quaternaire terminal, et impact de la distribution sédimentaire sur les propriétés géoacoustiques des fonds, PhD thesis, 404 pp., Univ. Bordeaux 1, France.

Bourget, J., S. Zaragosi, T. Mulder, J.-L. Schneider, T. Garlan, A. Van Toer, V. Mas, N. Ellouz-Zimmermann (2010), Hyperpycnal-fed turbidite lobe architecture and recent sedimentaryprocesses: A case study, Sediment. Geol. 229, 144-159 doi:10.1016/j.sedgeo.2009.03.009

Bourget, J., S. Zaragosi, N. Ellouz-Zimermann, N. Mouchot, T. Garlan, J-L Schneider, V. Lanfumey, S. Lallemant (2010), Turbidite system architecture and sedimentary processes along topographically complex slopes: the Makran convergent margin, Sedimentology, 58, 376-406, doi: 10.1111/j.1365-3091.2010.01168.

Bourget, J., S. Zaragosi, M. Rodriguez, M. Fournier, T. Garland, and N. Chamot-Rooke (2013), Late quaternary megaturbidites from the Indus fan : origin and stratigraphic significance, Mar. Geol., 336, 10-23,doi: 10.1016/j.margeo.2012.11.011

Breton, J. P., F. Béchennec, J. Le Métour, L. Moen-Maurel, and P. Razin (2004), Eoalpine (Cretaceous) evolution of the Oman Tethyan continental margin: insights from a structural field study in Jabal Akhdar (Oman Mountains), GeoArabia, 9, 1-18.

Brothers, D.S., N.W. Driscoll, G.M. Kent, A.J. Harding, J.M. Babcock, R.L. Baskin (2009), Tectonic evolution of the Salton Sea inferred from seismic reflection data, Nature Geoscience, 2, 581-584, doi: 10.1038/ngeo590.

Brun, J.-P., and O. Mauduit (2008), Rollovers in salt tectonics: the inadequacy of the listric fault model, Tectonophysics, 457, 1-11.

Buck., W. R. (1993), Effect of lithospheric thickness on the formation of high- and low-angle normal faults, Geology, 21, 933-936.

Bunce, E. T., M. G. Langseth, R. L. Chase, and M. Ewing (1967), Structure of the western Somali Basin, J. Geophys. Res., 72, 25477–2555, doi:10.1029/JZ072i010p02547

Burg, J.P., D. Bernoulli, J. Smit, A. Dolati, A. Bahroudi (2008), A giant catastrophic mud-and-debris flow in the Miocene Makran, Terra Nova, 20, 188–193, doi: 10.1111/j.1365-3121.2008.00804.x

Burgath, K. P., U. Von Rad, W. Van der Linden, M. Block, A. Ali Khan, H. A. Roeser, W. Weiss, (2002), Basalt and peridotites from Murray Ridge: are they of supra-subduction origin? in The Tectonic and Climatic Evolution of the Arabian Sea Region, edited by P. D. Clift et al., Geol. Soc. Spec. Publ., 195, 117-135

**C**

Calvès, G. (2008), Tectonostratigraphic and climatic record of the NE Arabian Sea, PhD thesis, 305 pp., Univ. Aberdeen, U.K.

Calvès, G., A. M. Schwab, M. Huuse, P. D. Clift, C. Gaina, D. Jolley, A. R. Tabrez, and A. Inam (2011), Seismic volcanostratigraphy of the western Indian rifted margin: The pre-Deccan igneous province, J. Geophys. Res., 116, B01101, doi:10.1029/2010JB000862.

Canals, M., G. Lastras, U. Urgeles, J. L. Casamor, J. Mienert, A. Cattaneo, M. De Batist, H. Haflidason, Y. Imbo, J. S. Laberg, J. Locat, D. Long, O. Longva, D. G. Masson, N. Sultan, F. Trincardi, P. Bryn (2004), Slope failure dynamics and impacts from seafloor and shallow sub-seafloor geophysical data: case studies from the COSTA project, Mar. Geol., 213, 9-72.

Cande, S. C., P. Patriat, and J. Dyment (2010), Motion between the Indian, Antarctic and African plates in the early Cenozoic, Geophys. J. Int, 183, 127-149.

Cane, M. A., and P. Molnar (2001), Closing of the Indonesian seaway as a precursor to east African aridification around 3-4 million years ago, Nature, 411, 157-162.

Carbon, D. (1996), Tectonique post-obduction des montagnes d'Oman dans le cadre de la convergence Arabie - Iran, PhD thesis, University of Montpellier II, 408 pp.

Carmichael, S.M., S. Akhter, J. K. Bennett, M. A., Fatimi, K., Hosein, R. W., Jones et al. (2009), Geology and hydrocarbon potential of the offshore Indus Basin, Pakistan, Petroleum Geoscience, 15, 107–116.

Carton, H., et al. (2007), Seismic imaging of the three-dimensional architecture of the Cinarcık Basin along the North Anatolian Fault, J. Geophys. Res., 112, B06101, doi:10.1029/2006JB004548.

Cattin, R., N. Chamot-Rooke, M. Pubellier, A. Rabaute, M. Delescluse, C. Vigny, L. Fleitout, P. Dubernet, (2009), Stress change and effective friction coefficient along the Sumatra-Andaman-Sagaing fault system after the 26 December 2004 (Mw=9.2) and the 28 March 2005 (Mw=8.7) earthquakes, Geochem.Geophys.Geosyst., v. 10, doi:10.1029/2008GC002167.

Catuneanu, O., et al. (2009), Towards the standardization of sequence stratigraphy, Earth-Sci Rev, 92, 1-33.

Cerling, T.E., J. M Harris, B. J. MacFadden, M. G. Leakey, J. Quade, V. Eisenmann, J. R. Ehleringer (1997), Global vegetation change through the Miocene/Pliocene boundary, Nature, 389, 153-158.

Chamot-Rooke, N., F. Jestin, B. DeVoogd (1993), Intraplate shortening in the central Indian-ocean determined from a 2100-km-long north-south deep seismic-reflection profile, Geology, 21(11), 1043–1046.

Chamot-Rooke, N., M. Fournier, Scientific Team of AOC and OWEN cruises (2009), Tracking Arabia-India motion from Miocene to Present, American Geophysical Union, Fall Meeting 2009.

Chaubey, A. K., G. C. Bhattacharya, G. P. S. Murty, K. Srinivas, T. Ramprasad, and D. Gopala Rao (1998), Early Tertiary seafloor spreading magnetic anomalies and paleo-propagators in the northern Arabian Sea, Earth. Planet. Sci. Lett., 154, 41-52.

Chaubey, A. K., J. Dyment, G. C. Bhatthacharya, J-Y. Royer, K. Srinivas, and V. Yateesh (2002). Paleogene magnetic isochrons and palaeo -propagators in the Arabian and Eastern Somali Basins, NW Indian Ocean, in The Tectonic and Climatic Evolution of the Arabian Sea Region, edited by P. D. Clift et al., Geol. Soc. Spec. Publ., 195, 71-85.

Chaytor, J. D., U. S. Ten Brink, A. R. Solow, B. D. Andrews (2009), Size distribution of submarine landslides along the U.S. Atlantic margin, Mar. Geol., 264, 16-27.

Christie-Blick, N., and K.T. Biddle (1985), Deformation and basin formation along strike-slip faults, in Strike-slip Deformation, Basin Formation, and Sedimentation, edited by K. T. Biddle and N. Christie-Blick, Society of Economic Paleontologists and Mineralogists, Spec. Publ., 37, 1–35.

Clemens, S.C., and W. L. Prell (2006), Viewpoint: The timing of orbital-scale Indian monsoon changes. Quaternary Science Reviews 25, 658-662.

Clift, P. D., N. Shimizu, G. D. Layne, J. S. Blusztain, C. Gaedicke, H. U. Schluter, M. K. Clark, and S. Amjad (2001), Development of the Indus Fan and its significance for the erosional history of the Western Himalaya and Karakoram, Geol. Soc. Am. Bull., 113, 1039-1051.

Clift, P. D., and C. Gaedicke (2002). Accelerated mass flux to the Arabian Sea during the middle to late Miocene, Geology, 30, 207-210, doi:10.1130/0091-13(2002)030<0207:AMFTTA>2.0.CO;2

Clift, P. D., K. V. Hodges, D. Heslop, R. Hannigan, H. Van Long, G. Calvès (2008), Correlation of Himalayan exhumation rates and Asian monsoon intensity, Nature Geoscience,1, 875-880, doi:10.1038/ngeo351

Clift, P. D. (2010), Enhanced global continental erosion and exhumation driven by Oligo-Miocene climate change, Geophys. Res. Lett. 37, L09402, doi:10.1029/2010GL043067

Cloething, S., F. Beekman, P. A. Ziegler, J-D. van Wees, D. Sokoutis (2008), Post-rift compressional reactivation potential of passive margins and extensional basins, Geol. Soc. London Spec. Publ., 306, 27-70.

Cloos, E. (1998), Experimental analysis of Gulf Coast fracture patterns. Am. Assoc. Pet. Geol. Bull., 52, 420-444.

Cochran, J. R. (1981), The Gulf of Aden : structure and evolution of a young ocean basin and continental margin, J. Geophys. Res., 86, 263-287.

Cochran, J. R. (1988), Somali Basin, Chain Ridge, and origin of the northern Somali Basin gravity and geoid low, J. Geophys. Res., 93, 11985-12008.

Corregiari, A., F. Trincardi, L. Langone, M. Roveri (2001), Styles of failure in late Holocene highstand prodelta wedges on the Adriatic shelf, J. Sedim. Res., 71, 218-236.

Coumes, F., and V. Kolla (1984), Indus Fan: seismic structure, channel migration and sediment thickness in the upper fan. in: Haq, B.U., J.D., M. (Eds.), Marine Geology and Oceanography of Arabian Sea and coastal Pakistan. Van Nostrand Reinhold Comp., New York, pp. 101-110.

Cunningham, W. D. and P. Mann, (2007), Tectonics of strike-slip restraining and releasing bends, in Tectonics of Strike-Slip Restraining and Releasing Bends, edited by W.D. Cunningham and P. Mann, Geol. Soc. Spec. Publ., 290, 1–12.

**D**

Dan G., N. Sultan, A. Cattaneo, J. Deverchère, K. Yelles (2009), Mass transport deposits on the Algerian margin (Algiers area): morphology, lithology and sedimentary processes. 4th international symposium, Austin (United states).

Delescluse, M. and N. Chamot-Rooke (2007), Instantaneous deformation and kinematics of the India-Australia Plate, Geophys. J. Int., 168, 818-842, doi: 10.1111/j.1365-246X.2006.03181.x

Delescluse, M., L. G. J. Montési, N. Chamot-Rooke (2008), Fault reactivation and selective abandonment in the oceanic lithosphere, Geophys. Res. Lett., 35, L16312, doi:10.1029/2008GL035066.

Delescluse, M. (2008), Déformation intraplaque de la lithosphère océanique indo-australienne: cinématique, réactivation et serpentinisation, Thèse de doctorat Paris XI, 249p.

Delescluse, M., N. Chamot-Rooke, R. Cattin, L. Fleitout, O. Trubienko, C. Vigny (2012), April 2012 intraoceanic seismicity off Sumatra boosted by the Banda-Aceh megathrust, Nature, doi: 10.1038/nature11520

deMenocal, P. (2004), African climate change and faunal evolution during the Pliocene-Pleistocene, Earth Planet. Sci. Lett.,220, 3-24.

DeMets, C., R.G. Gordon, D.F. Argus and S. Stein (1990), Current plate motions, Geophys. J. Int., 101, 425-478.

DeMets, C., R.G. Gordon, D.F. Argus and S. Stein (1994), Effect of recent revisions of the geomagnetic reversal time scale on estimates of current plate motions, Geophys. Res. Lett. 21, 2191-2194

DeMets, C., R. Gordon, J-Y. Royer (2005), Motion between the Indian, Capricorn and Somalian plates since 20 Ma: implications for the timing and magnitude of distributed lithospheric deformation in the equatorial Indian Ocean, Geophys. J. Int., 161, 445-468, doi: 10.1111/j.1365-246X.2005.02598.x

DeMets C., R. G. Gordon and D.F. Argus (2010), Geologically current plate motions, Geophys. J. Int., 181, 1-80, doi: 10.1111/j.1365-246X.2009.04491.x,.

Dingle, R.V. ( 1977), The anatomy of a large submarine slump on a sheared continental margin (SE Africa). Journal of the Geological Society of London, 134, 293-310.

Donato, S.V., E. G. Reinhardt, J.I. Boyce, R. Rothaus, T. Vosmer (2008), Identifying tsunami deposits using bivalve shell taphonomy, Geology 36, 199–202.

Donato, S.V., E. G. Reinhardt, J. I. Boyce, J.E. Pilarczyk, B. P. Jupp (2009), Particle-size distribution of inferred tsunami deposits in Sur Lagoon, Sultanate of Oman, Mar. Geol., 257, 54–64.

Dooley, T. and G. Schreurs (2012), Analogue modelling of intraplate strike-slip tectonics: a review and new experimental results, Tectonophysics, 574-575, 1-71.

Dupont-Nivet, G., C. Hoorn, M. Konert (2008), Tibetan uplift prior to the Eocene-Oligocene climate transition : Evidence from pollen analysis of the Xining Basin, Geology, 36, 987-990, doi: 10.1130/G25063A.1

Dyment, J. (1998), Evolution of the Carlsberg Ridge between 60 and 45 Ma: Ridge propagation, spreading asymmetry, and the Deccan-Reunion hotspot, J. Geophys. Res., 103, 24067–24084 DOI: 10.1029/98JB01759.

**E**

Edwards R.A., T. A. Minshull and R. S. White (2000), Extension across the Indian–Arabian plate boundary: the Murray Ridge, Geophys. J. Int., 142, 461-477.

Edwards, R. A., T. A. Minshull, E. R. Flueh and C. Kopp (2008), Dalrymple Trough: An active oblique-slip ocean-continent boundary in the northwest Indian Ocean, Earth Planet. Sci. Lett., 272, 437-445.

Ellouz Zimmermann, N., Deville, E., Müller, C., Lallemant, S., Subhani, A. B., Tabreez, A. R., 2007. Impact of sedimentation on convergent margin tectonics : example of the Makran Accretionary prism (Pakistan). Thrust Belts and Foreland Basins: From Fold Kinematics to Hydrocarbon Systems, edited by O. L. Lacombe et al., pp. 327–350, Springer, Berlin.

Ellouz Zimmermann, N. et al. (2007b), Offshore frontal part of the Makran accretionary prism (Pakistan) the Chamak Survey, in Thrust Belts and Foreland Basins: From Fold Kinematics to Hydrocarbon Systems, edited by O. L. Lacombe et al., pp. 349–364, Springer, Berlin.

Elton, S. (2008), The environmental context of human evolutionary history in Eurasia and Africa, J. Anat., 212, 377–393, doi: 10.1111/j.1469-7580.2008.00872.x

Engdahl, E.R., R. van der Hilst and R. Buland (1998), Global teleseismic earthquake relocation with improved travel times and procedures for depth determination, Bull. Seism. Soc.Am., 88, 722-743.

Ewing, M. and B. C. Heezen (1960), Continuity of mid-oceanic ridge and rift valley in the southwestern Indian Ocean confirmed, Science, 131, 1677-1679.

**F**

Farquharson, W. I. (1936), John Murray expedition 1933-34, Topography, Edited by British Museum of Natural History, London, 18p.

Faugères, J.C., D.A.V. Stow, P. Imbert, and A. Viana (1999), Seismic features diagnostic of contourite drifts, Mar. Geol., 162, 1-38.

Faugères J.C., E. Gonthier T. Mulder, N. Kenyon, P. Cirac, R. Griboulard, S. Berné, R. Lesuavé (2002), Multi-process generated sediment waves on the Landes Plateau (Bay of Biscay, North Atlantic), Mar. Geol., 182, 279-302.

Faugeres J.C., and T. Mulder (2011), Contour Currents and Contourite Drifts, In: HeikoHuneke and Thierry Mulder, Editor(s), Developments in Sedimentology, Elsevier, 2011, Volume 63, Deep-Sea Sediments, 149-214.

Field, M. E., and J. H. Barber (1993), A submarine landslide associated with shallow seafloor gas and gas hydrates off northern California, in Submarine landslides: selected studies in the U.S. Exclusive Economic Zone, W.C. Schwab et al (eds), US Geological Survey Bulletin, 2002, 151-157.

Filbrandt, J. B., S.C. Nolan, and A. C. Ries (1990), Late Cretaceous and Early Tertiary evolution of Jebel Ja'alan and adjacent areas, NE Oman. In The Geology and Tectonics of the Oman Region. Geological Society Special Publication (eds A. H. F. Robertson, M. P. searle, and A. C. Ries), 49, 697-714.

Filbrandt, J. B., S. Al-Dhahab, A. Al-Habsy, K. Harris, J. Keating, S. Al-Mahruqi, S. I. Ozkaya, P. D. Richard and T. Robertson (2006), Kinematic interpretation and structural evolution of North Oman, Block 6, since the Late Cretaceous and implications for timing of hydrocarbon migration into Cretaceous reservoirs, GeoArabia, 11, 97-140.

Forsyth, D. W. (1992), Finite extension and low-angle normal faulting, Geology, 20, 27–30.

Fournier, M., P. Patriat, S. Leroy (2001), Reappraisal of the Arabia-India-Somalia triple junction kinematics. Earth Planet. Sci. Lett., 189, 103-114.

Fournier, M., N. Bellahsen, O. Fabbri, and Y. Gunnell (2004), Oblique rifting and segmentation of the NE Gulf of Aden passive margin, Geochem. Geophys. Geosyst., 5, Q11005, doi:10.1029/2004GC000731.

Fournier, M., C. Lepvrier, P. Razin and L. Jolivet (2006), Late Cretaceous to Paleogene post-obduction extension and subsequent Neogene compression in the Oman Mountains, GeoArabia, 11, 17-40.

Fournier, M., C. Petit, N. Chamot-Rooke, O. Fabbri, P. Huchon, B. Maillot, and C. Lepvrier (2008a), Do ridge-ridge-fault triple junctions exist on Earth? Evidence from the Aden-Owen-Carlsberg junction in the NW Indian Ocean, Basin Research, 20, 575-590, doi: 10.1111/j.1365-2117.2008.00356.x

Fournier, M., N. Chamot-Rooke, C. Petit, O. Fabbri, P. Huchon, B. Maillot, and C. Lepvrier (2008b), In-situ evidence for dextral active motion at the Arabia-India plate boundary, Nature Geoscience, 1, 54-58, doi:10.1038/ngeo.2007.24.

Fournier M. (2009), Cinématique et déformation associées à l'extension continentale et l'accrétion océanique : à l'Est d'Aden, Habilitation à diriger des recherches, Univ. Pierre & Marie Curie, 127p.

Fournier, M., N. Chamot-Rooke, C. Petit, P. Huchon, A. Al-Kathiri, L. Audin, M.-O. Beslier, E. d'Acremont, O. Fabbri, J.-M. Fleury, K. Khanbari, C. Lepvrier, S. Leroy, B. Maillot, and S. Merkouriev (2010), Arabia-Somalia plate kinematics, evolution of the Aden-Owen-Carlsberg triple junction, and opening of the Gulf of Aden, J. Geophys. Res., 115, B04102, doi:10.1029/2008JB006257.

Fournier, M., N. Chamot-Rooke, M. Rodriguez, P. Huchon, C. Petit, M.-O. Beslier, and S. Zaragosi (2011), Owen Fracture Zone: the Arabia-India plate boundary unveiled, Earth Planet. Sci. Lett., 302, 247-252, doi:10.1016/j.epsl.2010.12.027.

Fournier, M., P. Patriat and S. Leroy (2001), Reappraisal of the Arabia-India-Somalia triple junction kinematics, Earth Planet. Sci. Lett., 189, 103-114.

Frieslander, U. (2000), The structure of the Dead Sea transform emphasizing the Arava using new geophysical data, Ph.D. thesis, 204 pp., Hebrew University of Jerusalem, Israel.

Fritz, H.M., F. Mohammed, J. Yoo (2009), Lituya Bay Landslide Impact Generated Mega-Tsunami 50th Anniversary, Pure Appl. Geophys., 166, 153-175, doi:10.1007/s00024-008-0435-4.

Fritz, H.M, C. D. Blount, F. B. Albusaidi, A. H. M. Al-Harthy (2010), Cyclone Gonu Storm Surge in Oman, Estuarine Coastal and Shelf Sciences, 86, 102–106, doi:10.1016/j.ecss.2009.10.019.

**G**

Gaedicke, C., A. Prexl, H.U. Schlüter, H. Roeser and P. Clift (2002), Seismic stratigraphy and correlation of major regional unconformities in the northern Arabia Sea, in The Tectonic and Climatic Evolution of the Arabian Sea Region, edited by P. Clift, D. Kroon, C. Gaedicke and J. Craig, Geol. Soc. Spec. Publ., 195, 25-36.

Garcia Moreno, D., A. Hubert Ferrari, J. Moernaut, J.G. Fraser, X. Boes, M. Van Daele, U. Avsar, N. Cagatay and M. De Batist (2010), Structure and recent evolution of the Hazar Basin: a strike slip basin on the East Anatolian Fault, Eastern Turkey, Basin Research, 23, 191-207, doi: 10.1111/j.1365-2117.2010.00476.

Gardner, J.V., D. B., Prior, M. E., Field (1999), Humboldt slide: A large shear-dominated retrogressive slope failure, Mar. Geol., 154, 323-338.

Garfunkel, Z. (1981), Internal structure of the Dead Sea leaky transform (Rift) in relation to plate kinematics, Tectonophysics, 80, 81-108.

Garfunkel, Z. and Z. Ben-Avraham (1996), The structure of the Dead Sea basin, Tectonophysics, 266, 155–176.

Garfunkel, Z. and Z. Ben-Avraham (2001), Basins along the Dead Sea transform, in Peri-Tethys Memoir 6: Peri-Tethyan Rift/Wrench Basins and Passive Margins, edited by P.A. Ziegler, W. Cavazza, A.H.F. Robertson, and S. Crasquin-Soleau, Mémoires Museum National d'Histoire Naturelle de Paris, 186, 607–627.

Gasperini L., E. Bonatti, M. Ligi, R. Sartori, A.M. Borsetti, A. Negri, A. Ferrari, and S. Sokolov (1997), Stratigraphic numerical modelling of a carbonate platform on the Romanche transverse ridge, Equatorial Atlantic, Mar. Geol., 136, 245-257.

Gasperini L., D. Bernoulli, E. Bonatti, A.M. Borsetti, M. Ligi, A. Negri, R. Sartori and K. von Salis, (2001), Lower Cretaceous to Eocene sedimentary transverse ridge at the Romanche fracture zone and the opening of the Equatorial Atlantic, Mar. Geol., 176, 101-119.

Geist, E. L., P. J. Lynett, and J. D. Chaytor (2012), Hydrodynamic modeling of tsunamis from the Currituck landslide, Mar. Geol., 264, 41-52.

Ginat, H., Y. Enzel, Y. Avni (1998), Translocated Plio-Pleistocene drainage systems along the Arava fault of the Dead Sea transform, Tectonophysics, 284, 151-160.

Gnos, E., A. Immenhauser, and Tj. Peters (1997), Late Cretaceous/early tertiary convergence between the Indian and Arabian plates recorded in ophiolites and related sediments, Tectonophysics, 271, 1-19.

Gonthier E., J. C. Faugères, A. Gervais, G. Ercilla, B. Alonso, J. Baraza (2002), Quaternary sedimentation and origin of the Orinoco sediment wave field on the Demerara continental rise (NE margin of South Amercia), Mar. Geol., 192, 189-214.

Gordon, R.G. and C. DeMets (1989), Present-day motion along the Owen fracture zone and Dalrymple trough in the Arabian Sea, J. Geophys. Res. 94, 5560-5570.

Gourlan, A.T., Meynadier, L., Allègre, C. J. (2008), Tectonically driven changes in the Indian Ocean circulation over the last 25 Ma: Neodymium isotope evidence. Earth. Planet. Sci. Lett., 267, 353-364.

Govil, P. and P. D. Naidu (2008), Late Quaternary changes in depositional processes along the western margin of the Indus Fan, Geo-Marine Letters, 28**,** 1-6.

Gràcia E., A. Vizcaino, C. Escutia, A. Asioli, A. Rodés, R. Pallàs, J. Garcia-Orellana, S. Lebreiro, C. Goldfinger (2010), Holocene earthquake record offshore Portugal (SW Iberia) : testing turbidite paleoseismology in a slow-convergence margin, Quaternary Sci. Rev., 29, 1156-1172.

**H**

Hampton, M.A., H. .J., Lee, J., Locat (1996), Submarine landslides, Rev. Geophys., 34, 33-59.

Harrison, T.M., P., Copeland, W.S.F., Kidd, A., Yin (1992), Raising Tibet, Science, 255, 1663-1670.

Hatzfeld, D., and P. Molnar (2010), Comparisons of the kinematics and deep structures of the Zagros and Himalaya and of the Iranian and Tibetan plateaus and geodynamic implications, Rev. Geophys., 48, RG2005, doi:10.1029/2009RG000304.

Heidarzadeh, M., M. D. Pirooz, N. H. Zaker, A. C.,Yalciner, M. Mokhtari, A. Esmaeily (2008), Historical tsunami in the Makran Subduction Zone off the southern coasts of Iran and Pakistan and results of numerical modeling, Ocean Engineering 35, 774-786.

Heinrich, P., A. Piatanesi, E. A., Okal, H., Hébert (2000), Near-field modeling of the July 17, 1998 tsunami in Papua New Guinea, Geophys. Res. Lett., 27, 3037-3040.

Heinrich, P., A. Piatanesi, H. Hébert (2001), Numerical modelling of tsunami generation and propagation from submarine slumps: the 1998 Papua New Guinea event, Geophys. J. Int., 145, 97-111.

Henstock, T. J., and T. A. Minshull (2004), Localized rifting at Chagos bank in the India-Capricorn plate boundary zone, Geology, 32, 237–240.

Hoffman, G., K. Reicherter, T. Wiatr, C. Grützner, T. Rausch (2013), block and boulder accumulations along the coastline between Fins and Sur (Sultanate of Oman) : tsunamigenic remains? Nat. Hazards, 65, 851-873.

Huang, Y., S. C. Clemens, W. Liu, L. Wang, W. L. Prell (2007), Large-scale hydrological change drove the Late Miocene C4 plant expansion in the Himalayan foreland and Arabian Peninsula, Geology, 35, 531-534.

Huchon, P. et K. Khanbari (2003), Rotation of the syn-rift stress field of the northern Gulf of Aden margin, Yemen, Tectonophysics, 364, 147-166.

Hutchison I., K. E. Louden, R.S. White, and R. P. von Herzen (1981), Heat flow and age of the Gulf of Oman, Earth. Planet. Sci. Lett., 56, 252-262.

**I**

Immenhauser A. (1996), Cretaceous sedimentary rocks on the Masirah Ophiolite (Sultanate of Oman): evidence for an unusual bathymetric history, J. of the Geol. Soc. of London, 153, 539-551.

Immenhauser A., G. Schreurs, E. Gnos, H. W. Oterdoom, and B. Hartmann (2000), Late Palaeozoic to Neogene geodynamic evolution of the northeastern Oman margin, Geol. Mag. 137, 1-18.

**J**

Jaiswal, R.K., A. P. Singh, B. K. Rastogi (2009), Simulation of the Arabian Sea Tsunami propagation generated due to 1945 Makran Earthquake and its effect on western parts of Gujarat (India), Nat. Hazards, 48, 245–258, DOI 10.1007/s11069-008-9261-3.

Jiang, L. and P., Leblond (1992), The coupling of a submarine slide and the surface waves which it generates. J. Geophys. Res., 97, 731-744.

Jiang, L. and P., Leblond (1993), Numerical modelling of an underwater Bingham plastic mudslide and the waves which it generates, J. Geophys. Res., 98, 304-317.

Jiménez-Munt, I., M. Fernàndez, J. Vergés, J. C. Afonso, D. Garcia-Castellanos, J. Fullea : Lithospheric structure of the Gorringe Bank (2010) : Insights into its origin and tectonic evolution, Tectonics, 29, TC5019, doi:10.1029/2009TC002458.

Jourdan, B. (2008), Tsunamis of the Arabian peninsula : a guide of historic events. Science of Tsunami Hazards, 27, 31-46.

**K**

Kashai, EL. and P. F. Croker (1987), Structural geometry and evolution of the Dead Sea-Jordan rift system as deduced from new subsurface data, Tectonophysics, 141, 33-60.

Kenyon, N.H., A. Amir, and A. Cramp (1995), Geometry of the younger sediment bodies of the Indus Fan, in Atlas of deep water environments: architectural style in turbidite systems, edited by Pickering, K.T., Hiscott, R.N., Kenyon, N.H., Ricci Lucchi, F., Smith, R.D.A., Chapman & Hall, London, pp. 89-90.

Kolla, V., A. W. H. Bé, P.E. Biscaye (1976), Calcium Carbonate distribution in the surface sediments of the Indian Ocean, J. Geophys. Res., 81, 2605-2616.

Kolla, V., and F., Coumes (1987), Morphology, internal structure, seismic stratigraphy, and sedimentation of Indus Fan, The American Association of Petroleum Geologists Bulletin, 650-677.

Kremeer, C., W. E. Holt, and A. J. Haines (2003), An integrated global model of present-day plate motions and plate boundary deformation, Geophys. J. Int, 154, 8-34.

Kroon, D., T. Steens, S. R. Troelstra (1991), Onset of monsoonal related upwelling in the western Arabian Sea as revealed by planktonic foraminifers, In Prell, W.L., Niitsuma, N., et al., Proceedings of the Ocean Drilling Project, Sci. Results, 117, 257- 263 College Station, Texas (Ocean Drilling Program).

Kvalstad T.J., L. Andresen, C. F. Forsberg, K. Berg, P. Bryn, M. Wangen (2005), The Storegga slide: evaluation of triggering sources and slide mechanics; Mar. Petr. Geol., 22, 245–256.

Kristoffersen, Y., B. J. Coakley, J. K. Hall, M. Edwards (2007), Mass wasting on the submarine Lomonosov Ridge, central Arctic Ocean, Mar. Geol., 243, 132–142.

**L**

Labbé, M., C. Donnadieu, C. Daubord, H. Hébert (2012), Refined numerical modeling of the 1979 tsunami in Nice (French Riviera): Comparison with coastal data, J. Geophys. Res., 117, F01008, doi:10.1029/2011JF001964.

Lamarche, G., C. Basile, J. Mascle, and F. Sage (1997), The Côte d'Ivoire-Ghana transform margin : sedimentary and tectonic structure from multichannel seismic data, Geomarine Lett., 17, 62-69.

Larroque C. and J. Virieux (2001), Physique de la terre solide : observations et théories, Gordon and Breach Science Publisher, 359 p.

Laughton, A. S. (1966), The Gulf of Aden, Phil. Trans. Roy. Soc. London, A259, 150-171.

Lazar, M., Z. Ben-Avraham and U. Schattner (2006), Formation of sequential basins along a strike-slip fault - geophysical observations from the Dead Sea basin, Tectonophysics, 421, 53–69.

Le Beon, M., Y. Klinger, A. Q. Amrat, A. Agnon, L. Dorbath, G. Baer, J.-C. Ruegg, O. Charade, and O. Mayyas (2008), Slip rate and locking depth from GPS profiles across the southern Dead Sea Transform, J. Geophys. Res., 113, B11403,doi:10.1029/2007JB005280.

Lee, H., B. D. Edwards, M. E.Field (1981), Geotechnical analysis of a submarine slump, Eureka, California, paper presented at Offshore Technology Conference, American Association of Petroleum Geology, Houston, Tex.

Lee, H.J., P. M. Syvitski, G. Parker, D. Orange, J. Locat, J.H.W. Hutton, J. Imran (2002), Distinguishing sediment waves from slope failure deposits : Field examples, including the Humboldt slide and modelling results, Mar. Geol., 192, 79-104.

Lee, H. J., J. Locat, P. Desgagnes, J.D. Parsons, B.G. McAdoo, D.L. Orange, P. Puig, F.L. Wong, P. Dartnell, E. Boulanger (2007), Submarine mass movements on continental margins, in Continental Margin Sedimentation, edited by C. A. Nittrouer, pp. 213–274, doi:10.1002/9781444304398.ch5, Blackwell, U. K.

Le Pichon X., and J.M. Gaulier (1988), The rotation of Arabia and the Levant fault system, Tectonophysics, 153, 271-94

Le Pichon X., A.M.C. Sengor, E. Demirbag, C. Rangin, C. Imren, R. Armijo, N. Gorue, N. Cagatay, B. Mercier de Lepinay, B. Meyer, R. Saatcilar and B. Tok (2001), The active main Marmara fault, Earth Planet. Sci. Lett., 192, 595 – 616.

Lepvrier, C., M. Fournier, T. Bérard, and J. Roger (2002), Cenozoic extension in coastal Dhofar (southern Oman): Implications on the oblique rifting of the Gulf of Aden, Tectonophysics, 357, 279-293.

Leroy S., E. d'Acremont, C. Tiberi, C. Basuyau, J. Autin, F. Lucazeau, H. Sloan (2010), Recent off-axis volcanism in the eastern Gulf of Aden : Implications for plume-ridge interaction, Earth Planet. Sci. Lett., 293, 140-153.

Leroy, S. et al., 2012. From rifting to oceanic spreading in the Gulf of Aden: a synthesis. Arab.J.Geosci. doi 10.1007/s12517-011-0475-4

Ligi, M., E. Bonatti, L. Gasperini, and A.N.B. Poliakov (2002), Oceanic broad multifault transform plate boundaries. Geology, 30;11-14 doi: 10.1130/0091-7613(2002)030<0011:OBMTPB>2.0.CO;2

Livermore, R., G. Eagles, P. Morris, and A. Maldonado (2004), Shackleton Fracture Zone: No barrier to early circumpolar ocean circulation, Geology, 32;797-800 doi: 10.1130/G20537.1

Locat, J. and H. J. Lee (2002), Submarine landslides: advances and challenges, Can. Geotech. J., 39, 193-212.

Lo lacono, C., E. Gràcia, F. Zaniboni, G. Pagnoni, S. Tinti, R. Bartolomé, D. G. Masson, R. B. Wynn, N. Lourenço, N. M. Pinto de Abreu, J. Danobeitia, N. Zitellini, N. (2012), Large, deepwater slope failures : implications for landslide-generated tsunamis, Geology, 40, 931-934, doi: 10.1130/G33446.1, 2012

Lonsdale, P., and D. Fornari (1980), Submarine geology of Malpelo ridge, Panama basin, Mar. Geol., 36, 65-83.

Loosveld, R. J. H., A. Bell, and J. J. M. Terken (1996), The tectonic evolution of interior Oman, Geoarabia, 1, 28-51.

**M**

Mangeney, A., V., Heinrich, V., Roche (2000), Analytical and numerical solutions of dam-break problem for application to water floods, debris and dense snow avalanche, Pure Appl. Geophys. 157, 1081-1096.

Mann, P., M. R. Hempton, D.C. Badley, and K. Burke (1983), Development of pull-apart basins, Journal of Geology, 91, 529–554.

Mann, P. (2007), Global catalogue, classification and tectonic origins of restraining- and releasing bends on active and ancient strike-slip fault systems, Geol. Soc. Spec. Publ., 290, 13-142.

Marches E., T. Mulder, E., Gonthier, V., Hanquiez, M., Cremer, T., Garlan, P., Lecroart (2010), Perched lobes formation induced by contourite construction in the Gulf of Cadiz: Interactions between gravity processes and contour currents (Algarve Margin, South Portugal), Sedimentary Geology, 229, 81-94.

Marquer, D., T. Peters, and E. Gnos (1995), A new structural interpretation for the emplacement of the Masirah ophiolites (Oman) : a main Paleocene intra-oceanic thrust, Geodinamica Acta, 8, 13-19.

Mascle, J., E. Blarez, and M. Marinho (1988), The shallow structure of the Guinea and Cote d'Ivoire -Ghana transform margins : their bearing on the equatorial Atlantic Mesozoic evolution, Tectonophysics, 155, 193-209.

Massell, C., M. F. Coffin, P. Mann,S. Mosher, C. Frohlich, C. S. Duncan, G. Karner, D. Ramsay, and J.-F. Lebrun (2000), Neotectonics of the Macquarie ridge complex, Australia-Pacific plate boundary, J. Geophys. Res., 105, 13457-13480.

Masson, D.G., C. B. Harbitz, R.B. Wynn, G. Pedersen, F. Løvholt (2006), Submarine landslides: processes, triggers and hazard prediction, Philosophical Transaction of the Royal Society A. 364, 2009-2039.

Matthews D. H. (1966), The Owen Fracture Zone and the northern end of the Carlsberg Ridge, Phil. Trans. Royal Soc., A, 259, 172-186.

Matthews D. H., C. Williams, and A. S. Laughton (1967), Mid-ocean ridge in the mouth of the Gulf of Aden, Nature, 215, 1052-1053.

Mauduit, T., and J.-P. Brun (1998), Development of growth fault/ rollover systems, J. Geophys. Res., 103, 18119-18130

Mc Adoo, B.G., L. F. Pratson, D. L. Orange (2000), Submarine landslide morphology, US continental slope. Mar. Geol.169, 103-136.

Mc Adoo B.G., M. K. Capone, J. Minder (2004), Seafloor morphology of convergent margins: implications for Cascadia seismic hazard, Tectonics 23, TC 6008, doi: 10. 1029/2003TC001570.

McCall, G.J.H., 1997. The geotectonic history of the Makran and adjacent areas of southern Iran. J. Asian Earth Sci., 15, 517-531.

Mc Ewen, A. and M. Malin (1989), Dynamics of Mount St Helens'1980 pyroclastic flows, rockslide-avalanche, lahars and blast, J. Volc. Geotherm. Res., 37, 205-231.

McHugh, C.M.G., L. Seeber, M-H. Cormier, J., Dutton, N., Cagatay, A., Polonia, A., W.B.F. Ryan, and N. Gorur (2006), Submarine earthquake geology along the North Anatolia Fault in the Marmara Sea, Turkey: A model for transform basin sedimentation, Earth Planet. Sci. Lett.,248, 661-684, doi:10.1016/j.epsl.2006.05.038

McKenzie, D. P., and J. G. Sclater (1971), The evolution of the Indian Ocean since the Late Cretaceous, Geophys. J. R. Astron. Soc., 25, 437–528.

McQuarrie, N, J. M. Stock, C. Verdel, and B. P. Wernicke (2003), Cenozoic evolution of Neotethys and implications for the causes of plate motions, Geophys. Res. Lett., 30, 2036, doi:10.1029/2003GL017992.

McQuarrie, N., and D. J. J. van Hingsbergen (2013), Retrodeforming the Arabia-Eurasia collision zone : age of collision versus magnitude of continental subduction, Geology, 41, 315-318.

Menard, H. W., and T. Atwater (1968), Changes in direction of sea floor spreading, Nature, 219, 463-467.

Merkouriev, S. and C. DeMets (2006), Constraints on Indian plate motion since 20 Ma from dense Russian magnetic data: Implications for Indian plate dynamics, Geochem. Geophys. Geosyst., 7, Q02002, doi:10.1029/2005GC001079.

Michaud, F., A. Chabert, J-Y. Collot, V Sallarès, E. R. Flueh, P. Charvis, D. Graindorge, M. A. Gustcher, M.A. J. Bialas (2005), Fields of multi-kilometer scale sub-circular depressions in the Carnegie Ridge sedimentary blanket: Effect of underwater carbonate dissolution? Mar. Geol., 216, 205-219.

Mienert, J., and J., Posewang (1999), Evidence of shallow- and deep-water gas hydrate destabilizations in North Atlantic polar continental margin sediments, Geo-marine letters, 19, 143-149.

Migeon, S. (2000), Dunes géantes et levées sédimentaires en domaine marin profond : approche morphologique, sismique et sédimentologique. Unpublished Ph. D. thesis, Univ. Bordeaux 1, 288 pp.

Milliman, J.D., G. S. Quraishee, M.A.A., Beg (1984), Sediment discharge from the Indus River to the ocean: past, present and future. In: Haq, B.U., Milliman, J.D. (Eds.),Marine Geology and Oceanography of Arabian Sea and Coastal Pakistan. Van Nostrand Reinhold, New York, pp. 65–70.

Minshull, T., C. Lane, J. S. Collier, and R. Whitmarsh (2008), The relationship between rifting and magmatism in the northeastern Arabian Sea, Nat. Geosci., 1, 463-467, doi:10.1038/ngeo228.

Mohammed, F., and H. M. Fritz (2012), Physical modeling of tsunamis generated by three-dimensional deformable granular landslides, J. Geophys. Res. Oceans, 117, C11015, doi:10.1029/2011JC007850.

Molnar, P., England, P. (1990), Late Cenozoic uplift of mountain ranges and global climatic change: chicken or egg? Nature, 346, 29-34.

Molnar, P., P. England, and J. Martinod (1993), Mantle dynamics, uplift of the Tibetan Plateau, and the Indian monsoon, Rev. Geophys.,31, 357–396.

Molnar, P. (2005), Mio-Pliocene Growth of the Tibetan Plateau and Evolution of East Asian Climate, Palaeontologia Electronica, 8, 1-23.

Molnar, P., and J. Stock (2009), Slowing of India's convergence with Eurasia since 20 Ma and its implications for Tibetan mantle dynamics, Tectonics, 28, TC3001, doi:10.1029/2008TC002271

Molnar, P., W. R. Boos, D. Battisti (2010), Orographic controls on climate and paleoclimate of Asia: thermal and mechanical role r the Tibetan Plateau, Annu. Rev. Earth Planet. Sci., 38, 77-102.

Morgenstern, N. R. (1967), Submarine slumping and the initiation of turbidity currents, A.F. Richards (Ed.), Marine Geotechnique, University of Illinois Press, Urbana, IL, pp. 189–210

Morton, D.M. (1959), The geology of Oman: Proceedings, 5th World Petroleum Congress, New York, p. 227-280.

Moseley, F. (1969), The Upper Cretaceous ophiolite complex of Masirah Island, Oman: Geological Journal, 6, 293-306.

Moseley, F. and I. L. Abbotts (1979), The ophiolite mélange of Masirah, Oman, Geol. Soc. London, 136, 713-724.

Mouchot, N. (2009), Tectonique et sédimentation sur le complexe de subduction du Makran pakistanais. PhD thesis, 364 pp., Univ. Cergy-Pontoise, France.

Mouchot, N, L. Loncke, G. Mahieux, J. Bourget, S. Lallemant, N. Ellouz-Zimmermann, P. Leturmy (2010), Recent sedimentary processes along the Makran trench (Makran active margin, off Pakistan), Mar. Geol., 271, 17-31.

Mouchot, N, S. Lallemant, L. Loncke, P. Leturmy, G. Mahieux, F. Chanier, N. Ellouz-Zimmermann (2008), Vertical movements and recent sedimentary processes on the Makranaccretionary prism off Pakistan, EGU General Assembly, Vienna

Mountain, G.S. and W. L. Prell (1989), Geophysical Reconnaissance Survey for ODP Leg 117 in the Northwest Indian Ocean, in Proc. ODP, Init. Repts., Leg 117, edited by W.L. Prell and N. Niitsuma, 117, pp. 51-64, College Station, TX.

Mountain, G. S. and W. L. Prell (1990), A multiphase plate tectonic history of the southeast continental margin of Oman, The Geology and Tectonics of the Oman Region, edited by Robertson, A. H. F., Searle, M. P. and Ries, A. C., Geol. Soc. Spec. Publ., 49, 725-743.

Mouthereau, F., O. Lacombe, J. Vergés (2012), Building the Zagros collisional orogen: Timing, strain distribution and the dynamics of Arabia/Eurasia plate convergence, Tectonophysics,532–535, 27–60.

Mulder, T., and Cochonat, P. (1996), Classification of offshore mass movements. J. Sediment. Res. 66, 43-57.

Mulder, T., and J., Alexander (2002), Abrupt change in slope causes variation in the deposit thickness of concentrated particle-driven density currents, Mar. Geol., 175, 221-235.

Mulder, T., E. Gonthier, P. Lecroart, V. Hanquiez, E. Marches, M. Voisset (2009), Sediment failures and flows in the Gulf of Cadiz (western Atlantic), Mar. Petr. Geol., Spec. Issue, V. Gaullier et Vendeville (eds), 26, 660-672.

**N**

Nelson, S. (2006), Isotopic reconstructions of habitat change surrounding the extinction of Sivapithecus, a Miocene hominoid, in the Siwalik Group of Pakistan. Paleaogeo., Paleaoclim., Palaeoeco. 243, 204-222.

Newmark, N. M. (1965), Effects of earthquakes on dams and embankments, Geotechnique, 15, 139–159.

Nolan, S. C., P. W. Skelton, B. P. Clissod, J. D. Sweming (1990), Maastrichtian to Early Tertiary stratigraphy and paleogeography of the Central and Northern Oman mountains. In: Robertson, A.H.F., Searle M. P. & Ries A.C. (eds), The Geology and Tectonics of the Oman Region. Geol. Soc. London Spec. Pub., 49, 495-520.

Norem, H., J. Locat, B. Schieldrop (1991), An approach to the physics and the modelling of submarine flowslides, Mar. Geotech., 9, 93-111.

**O**

Okal E.A., H. M. Fritz, C. E. Synolakis, P.E. Raad, Y. Al-Shijbi, M. Al-Saifi (2006), Field Survey of the 2004 Indonesian Tsunami in Oman, Earthquake Spectra, 22, 203–218.

Okal E.A. and C. E., Synolakis (2008), Far-field tsunami hazard from mega-thrust earthquakes in the Indian Ocean, Geophys. J. Int., 172**,** 995–1015, DOI: 10.1111/j.1365-246X.2007.03674.x.

**P**

Pacault, A., J. C. Le Gac, B. Langli (2004), Sondeur de sédiments multifaisceaux : présentation du SBP 120 (Kongsberg) et premiers résultats, Seatech Week 2004, In-Situ Seabed Characterization, Brest 21-22 Ocotber 2004.

Patriat, P. and J. Achache (1984), India-Eurasia collision chronology has implications for crustal shortening and driving mechanism of plate, Nature, 311, 615-621.

Patriat, P., H. Sloan and D. Sauter (2008), From slow to ultraslow : a previously undetected event at the Soutwest Indian Ridge at ca. 24 Ma, Geology, 36;207-210, doi: 10.1130/G24270A.1

Peters, Tj. and I. Mercolli (1998), Extremely thin oceanic crust in the Proto-Indian Ocean : Evidence from the Masirah Ophiolte, Sultanate of Oman. J. Geophys. Res., 103, 677-689.

Peterson, L. C., D. W. Murray, W. U. Ehrmann, P. Hempel (1992), Cenozoic carbonate accumulation and compensation depth changes in the Indian Ocean. In Synthesis of results from scientific drilling in the Indian Ocean, ed. RA Duncan, DK., Rea, R. B. Kidd, U. von Rad, J. K., Weissel, Geophys. Monogr. 70, 311-333. Am. Geophys. Union, Washington, D. C.

Petit, C., M. Fournier, Y. Gunnell (2007), Tectonic and climatic controls on riftescarpments: Erosion and flexural rebound of the Dhofar passive margin (Gulf ofAden, Oman), J. Geophys. Res., 112, B03406, doi:10.1029/2006JB004554

Petrunin, A. and S. Sobolev (2006), What controls thickness of sediments and lithospheric deformation at a pull-apart basin?,Geology, 34, 389-392. doi: 10.1130/G22158.1

Pilarczyk J.E., E. G. Reinhardt, I. J. Boyce, H. P. Schwarcz, S.V. Donato (2011), Assessing surficial foraminiferal distributions as an overwash indicator in Sur Lagoon, Sultanate of Oman. Marine Micropaleontology, 80, 62–73.

Pilarczyk, J.E., and E. G., Reinhardt (2012), Testing foraminiferal taphonomy as a tsunami indicator in a shallow arid system lagoon: Sur, Sultanate of Oman. Mar. Geol., 295-298, 128-136, doi:10.1016/j.margeo.2011.12.002.

Pilcher R., R. Roberts, R. Buckley, and N. Harbury (1996), Structures within the Mahatta Humaid area, Huqf Uplift : implications for the tectonics of eastern Oman, Journal of African Earth Sciences, 22, 311-321.

Pimm, A. C., R. H. Burroughs, E. T. Bunce (1972), Oligocene sediments near Chain Ridge, northwest Indian Ocean: structural implications. Mar. Geol., 13, 14-18.

Piper, D. J. W., and W. R. Normark (1983), Turbidite depositional patterns and flow characteristics, Navy Submarine Fan, California Borderland. Sedimentology, 30, 681-694.DOI: 10.1111/j.1365-3091.1983.tb00702.x

Piper, D.J.W., P. Cochonat, M. Morrison (1999), The sequence of events around the epicenter of the 1929 Grand Bank earthquake: initiation of debris flows and turbidity current inferred from sidescan sonar, Sedimentology, 46, 79-97.

Platel, J.P., and J. Roger (1989), Evolution géodynamique du Dhofar (Sultanatd'Oman) pendant le Crétacé et le Tertiaire en relation avec l'ouverture du golfe d'Aden, Bull. Soc. Géol. France, 2, 253-263.

Platel, J. P., A. Berthiaux, J. Le Métour, M. Beurrier, J. Roger (1992), Geological map of Duqm and Madraka, Sultanate of Oman, sheet NE 40-03/07, scale 1: 250000, Oman Minist. of Pet. and Miner., Dir. Gen. of Miner., Muscat.

Pondard, N., and P. M. Barnes (2010), Structure and paleoearthquake records of active submarine faults, Cook Strait, New Zealand: Implications for fault interactions, stress loading, and seismic hazard, J. Geophys. Res., 115, B12320, doi:10.1029/2010JB007781.

Posamentier, H.W., M.T. Jervey, and P.R. Vail (1989), Eustatic controls on clastic deposition I - conceptual framework, in: Wilgus, al., e. (Eds.), Sea-level changes: an integrated approach. SEPM Special Publication, Tulsa, pp. 110-124.

Posamentier, H.W., and V. Kolla (2003), Seismic Geomorphology and Stratigraphy of Depositional Elements in Deep-Water Settings, J. Sediment. Res., 73, 367-388.

Prasanta, S., and R. Sinha (2010), Evolution of the Indian summer monsoon: synthesis of continental records. From: Clift, P. D., Tada, R. & Zheng, H. (eds) Monsoon Evolution and Tectonics–Climate Linkage in Asia. Geological Soc. London, Spec. Publ., 342, 153–183.

Prins, M.A., and G. Postma (2000), Effects of climate, sea level, and tectonics unraveled for last deglaciation turbidite records of the Arabian Sea, Geology, 375-378.

Prins, M.A., G. Postma, J. Cleveringa, A. Cramp, and N.H. Kenyon (2000), Controls on terrigenous sediment supply to the Arabian Sea during the late Quaternary: the Indus Fan, Mar. Geol.,169, 327-349.

Prior, D.B., and J., Coleman (1980), Sonograph mosaics of submarine slope instabilities, Mississippi River delta, Mar. Geol., 36, 226-239.

Prior, D.B. (1999), Sea floor engineering geomorphology: recent achievements and future directions. Geomorphology, 31, 411-439.

**Q**

Qayyum M, R. A. Lawrence and A. R. Niem (1997), Molasse-Delta-Flysch continuum of the Himalayan orogeny and closure of the Paleogene Katawaz remnant ocean, Pakistan, Int. Geol. Rev., 39, 861–875.

Quade, J., T. E., Cerling, J. R., Bowman (1989), Development of Asian monsoon revealed by marked ecological shift during the latest Miocene in northern Pakistan, Nature, 342, 163-166.

Quittmeyer, R. C. and A. L. Kafka (1984), Constraints on plate motions in southern Pakistan and the northern Arabian Sea from the focal mechanisms of small earthquakes, J. Geophys. Res., 89, 2444-2458.

**R**

Rabu, D., J. LeMétour, F. Béchennec, M. Beurrier, M. Villey and C. H. de Grissic (1990), Sedimentary aspects of the Eo Alpine cycle on the northeast edge of the Arabian platform, In : Robertson, A.H.F., Searle M. P. & Ries A.C. (eds), The Geology and Tectonics of the Oman Region. Geol. Soc. London Spec. Pub. 49, 49-68.

Rabinowitz, P. D., M. F. Coffin, and D. Falvey (1983), The separation of Madagascar and Africa, Science, 220, 67-69.

Rahe, B., D. Ferrill and A. Morris (1998), Physical analog modeling of pull-apart basin evolution, Tectonophysics, 285, 21–40.

Rangin C. and X. Le Pichon, Strain localization in the Sea of Marmara: Propagation of the North Anatolian Fault in a now inactive pull-apart, Tectonics, 23, TC2014, doi:10.1029/2002TC001437, 2004

Reading, H.G., and M. Richards (1994), Turbidites systems in deep-water basin margins classified by grain size and feeder system, Am. Assoc. Petrol. Geol. Bull., 792-822.

Reilinger R., et al. (2006), GPS constraints on continental deformation in the Africa – Arabia – Eurasia continental collision zone and implications for the dynamics of plate interactions, J. Geophys. Res., 111, B05411, doi:10.1029/2005JB004051.

Ries A. C., and R.M. Shackleton (1990), Structures in the Huqf-Haushi Uplift, east Central Oman. In Robertson, A.H.F., Searle, M.P. and Ries, A.C. (eds), The Geology and Tectonics of the Oman Region, Geol. Soc. Spec. Pub., 49, 653-664.

Robinet, J., P. Razin, J. Serra-Kiel, A. Gallardo-Garcia, S., Leroy, J. Roger, C. Grelaud (2013), The Paleogene pre-rift to syn-rift succession in the Dhofar margin (northeastern gulf of Aden): stratigraphy and depositional environments, Tectonophysics, in press.

Robinson, D. P. (2011), A rare great earthquake on a oceanic fossil fracture zone. Geophysical Journal International, 186, 1121-1134. doi:10.1111/j.1365-246X.2011.05092.x

Rodriguez, M., M. Fournier, N. Chamot-Rooke, P. Huchon, J. Bourget, M. Sorbier, S. Zaragosi, and A. Rabaute (2011), Neotectonics of the Owen Fracture Zone (NW Indian Ocean): Structural evolution of an oceanic strike-slip plate boundary, Geochem. Geophys. Geosyst.,12, Q12006, doi:10.1029/2011GC003731

Rodriguez, M., M. Fournier, N. Chamot-Rooke, P. Huchon, S. Zaragosi, and A. Rabaute (2012), Mass wasting processes along the Owen Ridge (Northwest Indian Ocean), Mar. Geol., 326-328, 80-100, doi: 10.1016/j.margeo.2012.08.008.

Rodriguez, M., N. Chamot-Rooke, H. Hébert , M. Fournier, P. Huchon (2013), Owen Ridge deep-water submarine landslides : implications for tsunami hazard along the Oman coast, NHESS,13, 417-424.

Roger, J., F. Béchennec, D. Janjou, J. LeMétour, R. Wyns, M. Beurrier (1991), Geological map of Ja'alan, Sheet NF 40-08E, scale 1: 100000, with explanatory notes. Directorate General of Minerals, Ministry of Petroleum and Minerals.

Ross, D. A., E., Uchupi, R., White (1986), The geology of the Persian-Gulf of Oman Region : a synthesis, Rev. Geophys., 24, 537-556.

Rothé, J. P. (1954), La zone sismique médiane Indo-Atlantique, Proc. Roy. Soc., A., 222, 387-397.

Royer J.Y., A.K. Chaubey, J. Dyment, G.C. Bhattacharya, K. Srinivas, V. Yateesh and T. Ramprasad (2002), Paelogene plate tectonic evolution of the Arabian and Eastern Somali basins, in The Tectonic and Climatic Evolution of the Arabian Sea Region, edited by P. Clift, D. Kroon, C. Gaedicke and J. Craig, Geol. Soc. Spec. Publ., 195, 7-23.

Ryan, W. B. F., et al. (2009), Global Multi-Resolution Topography synthesis, Geochem. Geophys. Geosyst.,10, Q03014,doi:10.1029/2008GC002332.

**S**

Sakai, T., M. Saneyoshi, Y. Sawada, M. Nakatsukasa, E. Mbua, H. Ishida (2010), Climate shift recorded at around 10 Ma in Miocene succession of Samburu Hills, northern Kenya Rift, and its significance. From: Clift, P. D., Tada, R. & Zheng, H. (eds) Monsoon Evolution and Tectonics–Climate Linkage in Asia. Geol. Soc., London, Spec. Publ., 342,109-127, doi:10.1144/SP342.9

Schattner, U. and R. Weinberger (2008), A mid-Pleistocene deformation transition in the Hula basin, northern Israel: Implications for the tectonic evolution of the Dead Sea Fault, Geochem. Geophys. Geosyst., 9, Q07009, doi:10.1029/2007GC001937.

Schattner, U. (2010), What triggered the early-to-mid Pleistocene tectonic transition across the entire eastern Meditterranean? Earth Planet. Sci. Lett., 289, 539-548.

Schlische, R. W., M. O. Withjack, and G. Eisenstadt (2002), An experimental study of the secondary deformation produced by oblique slip normal faulting, AAPG Bull., 86(5), 885-906.

Schlüter, H. U., A. Prexl, C. Gaedicke, H. Roeser, C. Reichert, H. Meyer, C. von Daniels (2002), The Makran accretionary wedge: sediment thicknesses and ages and the origin of mud volcanoes, Mar. geol., 185, 219-232.

Schulz, H., U. von Rad, H. Erlenkeuser (1998), Correlation between Arabian Sea and Greenland climate oscillations of the past 110 000 years, Nature, 393, 54-57.

Sclater, J. G., N. R. Grindlay, J. A. Madsen, and C. Rommevaux-Jestin (2005), Tectonic interpretation of the Andrew Bain transform fault: Southwest Indian Ocean, Geochem. Geophys. Geosyst., 6, Q09K10, doi:10.1029/2005GC000951.

Schmidt, J. (1932), Dana's Togt Omkring Jorden, 1928-1930, Gyldendal edn., Copenhagen, 269p.

Seeber, L., C. Sorlien, M. Steckler, and M.-H. Cormier (2010), Continental transform basins: Why are they asymmetric?, Eos Trans. AGU, 91(4), 29–30.

Ségoufin, J. and P. Patriat (1980), Existence d'anomalies mésozoïques dans le bassin de Somalie. Implications pour les relations Afrique-Antarctique-Madagascar, C. R. Acad. Sc. Paris, 291, Ser. B, 85-88.

Sepulchre, P., G. Ramstein, F. Fluteau, M. Schuster (2006), Tectonic uplift and Eastern Africa aridification, Science, 313, 1419-1423.

Shackleton R. M., and A. C. Ries (1990), Tectonics of the Masirah fault zone and eastern Oman. In The Geology and Tectonics of the Oman Region, Geol. Soc. Spec. Pub. (eds A. H. F. Robertson, M. P. searle, and A. C. Ries) 49, 715-24.

Schreurs, G., and A. Immenhauser (1999), West-northwest-directed obduction of the Batain group on the eastern Oman continental margin at the Cretaceous-Tertiary boundary, Tectonics, 18, 148-60.

Shipboard Scientific Party, Site 222 (1974), in DSDP Init. Repts, leg 23, edited by R.B. Whitmarsh, O.E. Weser and D.A. Ross, doi:10.2973/dsdp.proc.23.106.

Shipboard Scientific Party, Site 222 (1974), In R.B. Whitmarsh, O.E. Weser, and D.A. Ross, DSDP Init. Repts, 23, doi:10.2973/dsdp.proc.23.106.

Shipboard Scientific Party (1989), site 731 , in Proc. ODP, Init. Repts., leg 117, edited by Prell, W.L., N. Niitsuma et al., College Station, TX (Ocean Drilling Program), 585-652.

Smit J., J. P Brun, S. Cloetingh and Z. Ben-Avraham (2008), Pull-apart basin formation and development in narrow transform zones with application to the Dead Sea Basin, Tectonics, 27, TC6018, doi:10.1029/2007TC002119.

Smith, W. H. F., and D. T. Sandwell (1997), Global seafloor topography from satellite altimetry and ship depth soundings, Science, 277, 1957-1962.

Sousa, J and B. Voight (1991), Continuum simulation of flow failures, Geotechnique, 41, 515-538.

Sousa, J and B., Voight (1995), Multiple pulsed debris avalanche emplacement at Mount St Helens in 1980 : Evidence from numerical continuum flow simulations, J. Volc. Geotherm. Res., 66, 227-250.

Stein, C. A., and J. Cochran (1985), The transition between the Sheba Ridge and the Owen Basin : rifting of an old oceanic lithosphere, Geophys. J. R. Astr. Soc., 81, 47-74.

Stoneley, R. (1974), On the origin of ophiolite complexes in the southern Tethyan region: Tectonophysics, 25, 303-322.

Storti, F., F. Salvini, F. Rossetti, J. Phipps Morgan (2007), Intraplate termination of transform faulting within the Antarctic continent, Earth Planet. Sci. Lett., 260, 115-126.

Strozyk, F., M. Strasser, S. Krastel, M. Meyer, K. Huhn (2010), Reconstruction of retreating mass wasting in response to progressive slope steepening of the northeastern Cretan margin, eastern Mediterranean, Mar. Geol., 271, 44-54.

Sultan, N., A. Cattaneo, R. Urgeles, H. Lee, J. Locat, F. Trincardi, S. Berne, M. Canals, S. Lafuerza (2008), A geomechanical approach for the genesis of sediment undulations on the Adriatic shelf, Geochemistry, Geophysics, Geosystems 9, Q04R03, doi: 10.1029/2007GC001822.

Sweming, J. D., I. L. Abbots, L. A. Dune, D. C. Rex (1991), Formation and emplacement ages of the Masirah Ophiolite, Sultanate of Oman, Geology, 19, 453-456.

Sykes, L. R. (1968), Seismological evidence for transform faults, sea floor spreadig, and continental drift, History of the Earth's crust, A symposium, R. A. Phinney Ed. , 120-150.

Sylvester, A. G. (1988), Strike-slip faults, Geol. Soc. Am. Bull., 100, 1666–1703.

**T**

Tappin, D. R., P. Watts, G. M. McMurtry, Y. Laffoy, T. Matsumoto (2001) : The Sissano, Papua New Guinea tsunami of July 1998 – offshore evidence on the source, Mar. Geol., 175, 1-23.

Tappin, D.R., L. C. McNeil, T. Henstock, D. Mosher (2007), Mass wasting processes - offshore Sumatra**.** V. Lykousis, D. Sakellariou and J. Locat (eds.), Submarine Mass Movements and Their Consequences 327–336.

Tappin, D. R., P. Watts, S. Grilli (2008), The Papua New Guinea tsunami of 17 july 1998 : anatomy of a catastrophic event. Natural Hazard and Earth System Science, 8, 243-246.

Tappin, D. R. (2010), Digital elevation models in the marine domain : investigating the offshore tsunami hazard from submarine landslides, Geol. Soc. of London, spec. pub., 345, 81-101.

Taylor, B., A. Goodliffe, and F. Martinez (2009), Initiation of transforms faults at rifted continental margins, Comptes rendus Geosci., 341, 428-438.

Tchalenko, J. S. (1970), Similarities between shear zones of different magnitudes, Geol. Soc. Am. Bull.,81, 1625-1640.

Ten Brink, U. S. and Z. Ben-Avraham (1989), The anatomy of a pull-apart basin: seismic reflection observations of the Dead Sea, Tectonics, 8, 333-350.

Ten Brink, U. S. and M. Rybakov (1999), Anatomy of the Dead Sea transform; does it reflect continuous changes in plate motion? Geology, 27, 887-890.

ten Brink, U.S., Z. Ben-Avraham, R.E. Bell, M. Hassouneh, D.F. Coleman, G. Andreasen, G. Tibor, and B. Coakley (1993), Structure of the Dead Sea pull-apart basin from gravity analyses, J. Geophys. Res., 98, 877-21,894.

ten Brink, U. S., and C. H. Flores (2012), Geometry and subsidence history of the Dead Sea basin: A case for fluid induced mid-crustal shear zone?, J. Geophys. Res., 117, B01406, doi:10.1029/2011JB008711.

Trifunac M.D. and M. I., Todorovska (2002), A note on differences in tsunami source parameters for submarine slides and earthquakes, Soil Dynamics and Earthquake Engineering 22, 143-155.

Tripsanas, E.K., D. J. W. Piper, K. A. Jenner, W. R. Bryant (2008), Submarine mass-transport facies: new perspectives on flow processes from cores on the eastern North American margin, Sedimentology 55, 97-136.

Twichell, D.C., J. D. Chaytor, U.S. ten Brink, B. Buczkowski (2009), Morphology of late Quaternary submarine landslides along the U.S. Atlantic continental margin, Mar. Geol., 264, 4–15.

**V**

Vail, P.R., and R. M. Mitchum (1977), Seismic stratigraphy and global changes of sea-level, Part 1: overview. In: Payton, C.E. (Ed.), Seismic Stratigraphy — Applications to hydrocarbon exploration. AAPG Memoir, Tulsa

van Hinsbergen, D. J. J., P. C. Lippert, G. Dupont-Nivet, N. McQuarrie, P. V. Doubrovine, W. Spakman, and T. H. Torsvik (2012), Greater India Basin hypothesis and a two-stage Cenozoic collision between India and Asia, PNAS, 109, 7659-7664.

Vauchez, A., A. Tommasi, and M. Egydio-Silva (1994), Self-indentation of continental lithosphere. Geology, 22, 967-970

Viesca, R. C. (2011), The near and far of pore pressure during landslide and earthquake ruptures, Ph.D. thesis, Harvard University.

Viesca, R.C. and J. Rice (2012), Nucleation of sleep-weakening rupture instability in landslides by localized increase in pore pressure, J. Geophys. Res., 117, B03104, doi:10.1029/2011JB008866

Vine, F. J. and D. H. Matthews (1963), Magnetic anomalies over oceanic ridges, Nature, 199, 947-949.

Völker, D., F. Scholz, J. Geersen (2011), Analysis of submarine landsliding in the rupture area of the 27 February 2010 Maule earthquake, Central Chile, Mar. Geol., 288, 79-89.

von Rad, U., and M. Tahir (1997), Late Quaternary sedimentation on the outer Indus shelf and slope (Pakistan): evidence from high-resolution seismic data and coring, Mar. Geol.,138, 193-236.

Vrielynck, B. and P. Bouysse (2003), Le visage changeant de la Terre, CCGM, Unesco eds.

**W**

Waheed, A., Wells, N. A. (1990), Changes in paleocurrents during the development of an obliquely convergent plate boundary (Sulaiman fold-belt, southwestern Himalayas, west-central Pakistan). Sedimentary Geology 67, 237-261.

Waheed, A., Wells, N. A. (1992), Fluvial history of late Cenozoic molasse, Sulaiman range, Pakistan. Geol. Bull. Univ. Peshawar 25, 1-15.

Wang, P., S. Clemens, L. Beaufort, P. Braconnot, G. Ganssene, Z. Jiana, P., Kershawf, M. Sarntheing (2005), Evolution and variability of the Asian monsoon system: state of the art and outstanding issues, Quaternary Sci. Rev., 24, 595–629.

Wang, E., E. Kirby, K.P. Furlong, M. van Soest, G. Xu, X. Shi, P.J.J. Kamp, K. V. Hodges (2012), Two-phase growth of high topography in eastern Tibet during Cenozoic, Nature Geoscience 5, 640–645, doi:10.1038/ngeo1538

Wakabayashi, J., J. V. Hengesh and T. L. Sawyer (2004), Four-dimensional transform fault processes: progressive evolution of step-overs and bends, Tectonophysics, 392, 279–301.

Wakabayashi, J. (2007), Stepovers that migrate with respect to affected deposits: field characteristics and speculation on some details of their evolution, in Tectonics of Strike-Slip Restraining and Releasing Bends, edited by W.D. Cunningham and Paul Mann, Geol. Soc. Spec. Publ, 290, 169–188.

Weedon, G.P. and I.N. McCave (1991), Mud turbidites from the Oligocene and Miocene Indus Fan at sites 722 and 731 on the Owen Ridge, in ODP Proc. Scientific results, leg 116, edited by Prell, W.L., N. Niitsuma, K. Emeis et al., College Station, Texas, p. 215–220.

Weissel, J.K., V. A. Childers and G. D. Karner (1992), Extensional and Compressional Deformation of the Lithosphere in the Light of ODP Drilling in the Indian Ocean. Synthesis of Results from Scientific Drilling in the Indian Ocean, Geophysical Monography 70, American Geophysical Union.

Wesnousky, S. G. (1988), Seismological and structural evolution of strike-slip faults. Letters to Nature, 335, 340–343.

Wesnousky, S. G. (2005), The San Andreas and Walker Lane fault systems, western North America: transpression, transtension, cumulative slip and the structural evolution of a major transform plate boundary, J. Struct. Geol., 27, 1505–1512

White, R. S., and K. Klitgord (1976), Sediment deformation and plate tectonics in the Gulf of Oman, Earth. Planet. Sci. Lett., 32, 199-209.

Whitmarsh, R.B., O. E. Weser and D. A. Ross (1974), Initial report DSDP, U.S. Government Printing Office, Washington, D.C., v. 23, p. 1180.

Whitmarsh, R.B. (1979), The Owen Basin off the south-east margin of Arabia and the evolution of the Owen Fracture Zone, Geophys. J. Royal Astron. Soc., 58, 441-470.

Wiens, D. A., C. Demets, R.G. Gordon, S. Stein, D. Argus, J.F. Engeln, P. Lundgren, D. Quible, C. Stein, S.Weinstein, D.F. Woods (1985), A diffuse plate boundary model for Indian ocean tectonics, Geophys. Res.Lett.12, 429–432.

Wilson, J. T. (1965), A new class of faults and their bearing on continental drift, Nature, 207, 343-347.

Wilson, T. (2000), Seismic evaluation of differential tectonic subsidence, compaction, and loading in an interior basin, AAPG bulletin, 84, 376-398.

Woodcock, N. H., and M. C. Daly (1986), The role of strike-slip fault systems at plate boundaries, Phil. Trans. R. Soc. A, 317, 13-29.

Wu, J. E., K. McClay, P. Whitehouse and T. Dooley (2010), 4D analogue modelling of transtensional pull-apart basins, Mar. Petrol. Geol., 26, 1608-1623.

Y

Yatheesh, V., G. C. Bhattacharya, and J. Dyment (2009), Early oceanic opening off Western India-Pakistan margin : the Gop Basin revisited, Earth. Planet. Sci. Lett., 284, 399-408.

Z

Zhang, P.-Z., B. C. Burchfiel, S. Chen and Q. Deng (1989), Extinction of pull-apart basins. Geology, 17, 814–817.

Ziegler, M., L. J. Lourens, E. Tuenter, F. Hilgen, G-J. Reichart, N. Weber (2010). Precession phasing offset between Indian summer monsoon and Arabian Sea productivity linked to changes in Atlantic overturning circulation. Paleoceanography, 25, PA3213, doi:10.1029/2009PA001884.

Zitellini, N., E. Gràcia, L. Matias, P. Terrinha, M.A. Abreu, G. DeAlteriis, J.P. Henriet, J.J. Dañobeitia, D.G. Masson, T. Mulder, R. Ramella, L. Somoza, S. Diez (2009), The quest for the Africa–Eurasia plate boundary west of the Strait of Gibraltar, Earth Planet. Sci. Lett., 280, 13-50, doi:10.1016/j.epsl.2008.12.005.

# Liste des figures

Dans cet index, les légendes des figures sont ici simplifiées sous la forme d'un simple titre thématique afin de faciliter leur identification et la navigation d'une figure à l'autre. Les références des figures sont présentes dans le texte principal. Les figures propres à la thèse sont séparées des figures présentes dans les articles (publiés ou en préparation), pour des raisons de cohérence dans leur numérotation.

## Introduction

Figure 1 : Carte du second invariant de la déformation indiquant les frontières de plaque localisées et diffuses. **11**

Figure 2 : Définition des failles transformantes et décrochantes **13**

Figure 3 : Les différents contextes tectoniques favorables aux décrochements **15**

## Chapitre 1

Figure 4 : Cadre géodynamique de la plaque Arabie. **18**

Figure 5 : Carte physiographique de la Mer d'Arabie et des continents limitrophes,, avec la carte des anomalies magnétiques et les positions supposées des transitions continent-océan. **19**

Figure 6: Schéma structural simplifié du Sultanat d'Oman **21**

Figure 7 : Dessin de la physiographie du Nord Ouest de l'océan Indien, par Heezen et Tharp (1964). **23**

Figure 8 : Première carte bathymétrique de la Ride d'Owen et du point triple AOC (Aden-Owen-Carlsberg) établie par Matthews (1966). **24**

Figure 9 : La Zone de Fracture d'Owen est un des exemples choisis par Wilson (1965) pour définir les failles transformantes de type dorsale-fosse. **25**

Figure 10 : Sismicité et mécanismes au foyer des séismes dans la zone de la limite de plaque Inde-Arabie. **26**

Figure 11: Le Bassin Beautemps-Beaupré.
**28**

Figure 9: Reconstitution de l'évolution du point triple AOC, aux chrons 5C, 5, 3A et actuel (Fournier et al., 2010). **28**

Figure 10: Bathymétrie de la Fosse de Dalrymple (Edwards et al., 2008). **30**

Figure 11 : Profil sismique transverse au flanc du Fossé de Dalrymple et à la ride de Murray Sud **30**

Figure 12 : Profil sismique transverse à la Ride Sud d'Owen **31**

Figure 13 : Profil sismique transverse au Mont Qalhat **31**

Figure 14 : Bathymétrie multifaisceaux du canyon de l'Indus **34**

Figure 15 : Synthèse des âges des principaux évènements géologiques associés à l'activité de la limite de plaque Inde-Arabie depuis le Crétacé supérieur (cadre géologique communément admis avant cette thèse) **37**

Figure 16 : Reconstitution des principales étapes de l'ouverture de l'Océan Indien et de son évolution tectonique **40**

Figure 17 : Reconstitutions paléogéographiques de la Mer d'Arabie, modifié d'après Royer et al. (2002) pour les chrons 24n1y (52.4 Ma) et 23n1y (50.8 Ma). **42**

Figure 18 : Reconstitutions paléogéographiques de la Mer d'Arabie en considérant que la conjuguée de la Zone de Fracture de Chain était la limite de plaque Inde-Arabie entre le Crétacé sup. et le début du Miocène. **44**

Figure 19 : Reconstitutions paléogéographiques illustrant les deux principales hypothèses pour l'évolution tectonique de la Mer d'Arabie **45**

Figure 20 : schéma structural du Huqf, d'après la carte géologique du sultanat d'Oman au 1 : 1 000 000ème et coupe géologique de la région **47**

Figure 21 : Schéma structural de l'île de Masirah **49**

Figure 22 a : Carte des anomalies à l'air libre du Bassin d'Owen. **50**

Figure 22 b : Carte des anomalies de Bouguer de l'Oman. **51**

Figure 22c : Compilation des mesures du champ magnétique dans la région du Bassin d'Owen **52**

Figure 23 : Schéma structural du système décrochant de Haushi-Nafun (au centre du Huqf) **54**

Figure 24 : Schéma structural du système décrochant du dôme de Haushi (au NW du Huqf) **55**

Figure 25 : Schéma structural du système décrochant du Huqf NE **56**

Figure 26 : Schéma structural du secteur de la faille de Qalhat et du Jebel Ja'alan (haut) et coupe schématique entre Fita et la faille de Qalhat (bas) **57**

Figure 27 : Photographies de la faille décrochante dextre bordant les formations éocènes de Ras Madrekah. **58**

Figure 28 : Profil sismique montrant des structures en fleur potentielles dans la couverture sédimentaire de la marge Est-Omanaise selon Mountain et Prell, (1990). **59**

Figure 29 : Structure crustale du bassin d'Owen **61**

Figure 30 : Profil sismique transverse au bassin d'Owen **63**

Figure 31 : Reconstitution paléogéographique de la Mer d'Arabie et de la marge Est-Omanaise du Crétacé à l'actuel **68**

Figure 32 : carte des domaines géologiques du bassin d'Owen **72**

**Chapitre 2**

Figure 12 : Photo du Beautemps-Beaupré, le navire du SHOM (Cliché : M. Fournier). **75**

Figure 2 : Plan de position de la campagne Owen 1 **77**

Figure 3 : Plan de position de la campagne Owen 2 **78**

Figure 4: Gondole sous-coque du BHO Beautemps-Beaupré (sondeur EM 120) **80**

Figure 5 : bathymétrie multi-faisceaux recueillie lors de la campagne Owen **81**

Figure 6 : Exemples de profils de sondeur de sédiments. **84**

Figure **7** : Haut : Dispositif SISRAP à l'arrière du Beautemps Beaupré. Bas Gauche : Canon Sodera GI, source de la sismique. Bas droite : Mise à l'eau des canons Sodera GI. **86**

Figure 8 : exemple de profil SISRAP enregistré au cours de la campagne Owen 2, recoupant la marge omanaise et montrant une grande diversité de dépôts sédimentaires et de structures tectoniques. **87**

Figure **9** : magnétomètre de queue de flûte sismique utilisé à bord du BHO Beautemps-Beaupré **88**

Figure 10 : Carte des anomalies magnétiques recueillies lors des campagnes Owen et fanindien **89**

**Chapitre 3**

*Figures de la thèse* :

Figure 13 : a) Schéma structural du Danshui sur la faille de Haiyuan en Chine; b) Profil sismique transverse au bassin de Terkidag; c) Profil sismique transverse au bassin de Hazar, sur la Faille Est-Anatolienne **127**

Figure 14 : Schéma structural de la faille de San Andreas dans la région de la formation d'Olema's Creek **129**

Figure 15 : Profil sismique S-N recoupant la Mer Morte
**130**

Figure 16 : Blocs diagrammes synthétisant les différents scénarios possibles pour l'évolution structurale des relais le long d'un décrochement **131**

Figure 5 : Résultat des modèles analogiques de Smit et al. (2008) **133**

Figure 6 : Synthèse des modes d'ouverture proposés pour le bassin de la Mer Morte (faille du Levant).

**134**

*Figures des publications :*

***Fournier et al. 2011, EPSL***

Fig. 1. Active fault scarps of the OFZ mapped with a multibeam echo-sounder **96**

Fig. 2. Definition of the small circle of the OFZ. **97**

Fig. 3. The 20°N pull-apart basin **98**

Fig. 4. a) The horsetail splay of the Dalrymple Trough; b) Giant submarine landslides; c) Perspective view from the northwest of a multi-events generated landslide and related headwall collapses. **99**

***Rodriguez et al. 2011, G3***

Figure 1: Multibeam bathymetric map of the Owen Fracture Zone **103**

Figure 2: Slope map of the OFZ along the southern Owen Ridge. **105**

Figure 3: Slope map of the OFZ along the central Owen Ridge. **106**

Figure 4: Slope map of the asymmetric 20°N pull-apart basin, and interpretative structural scheme **107**

Figure 5: 3.5 kHz profiles oriented longitudinally along the 20°N basin **109**

Figure 6: 3.5 kHz profiles oriented transverse to the 20°N basin **110**

Figure 7: 3.5 kHz profiles across the turbiditic channels affected by the opening of the 20°N basin **111**

Figure 8: 3.5 kHz profile across the "en-échelon" fault system located at the southern end of the 20°N basin **112**

Figure 9: Slope map of the OFZ along the Qalhat Seamount, and interpretative structural scheme **113**

Figure 10: Seismic profile modified from Edwards et al. [2000], showing a negative flower structure buried under turbiditic deposits at the eastern foot of the Qalhat Seamount **114**

Figure 11: 3.5 kHz profile across the elevated graben of the Qalhat Basin **114**

Figure 12: Reflectivity map of the Qalhat Basin **115**

Figure 13: Measurements of the tilt of the turbiditic deposits within the 20°N Basin **116**

Figure 14: Chronology of the evolution of the Owen Fracture Zone (OFZ) in the vicinity of the Qalhat Seamount **117**

Figure 15: Chronology of the opening and the evolution of the 20°N basin **119**

***Rodriguez et al. submitted to Tectonics***

Figure 1 :Multibeam map of the 20°N pull-apart basin and interpretative structural scheme. **138**

Figure 2 :Longitudinal seismic line crossing the 20°N Basin **140**

Figure 3 :a) 3D bathymetric view of the en-échelon fault system near SB1 and SB2. b) 3.5 kHz profiles crossing the channel dissected by 20° Basin faults. 1.1 ±0.2 Ma-old turbiditic deposits overlying this channel comes from an adjacent, unfaulted channel. c) Seismic profile transverse to SB2 and d) the related interpretation. **143**

Figure 4 :a) 3D bathymetric view of SB3 and its arcuate normal fault system. b) 3.5 kHz profile crossing the arcuate normal fault system. c) Seismic line transverse to SB3 and d) the related interpretation. **145**

Figure 5 :a) 3.5 kHz profile showing the influence of bottom-current on sediment architecture on the western edge of the 20°N Basin. b) 3.5 kHz profile crossing the arcuate normal fault system. c) Seismic line transverse to SB3 and d) the related interpretation. **147**

Figure 6 : Close-view of the longitudinal seismic profile crossing the hinge zone between SB2 and SB3. **150**

Figure 7 :3.5 kHz profile crossing the en-échelon fault system. **151**

Figure 8 :Synthesis of the structural evolution of the 20°N Basin. **155**

Figure 9 : Schematic diagram showing subsidence in the 20°N Basin along the OFZ **157**

Table 1 : comparison of the thickness of pelagic deposits into time **147**

***Rodriguez et al. in prep.***

Figure 1 :a) Regional framework of the India-Arabia plate boundary. LMR : Little Murray Ridge. b) Simplified cross section of the Oman abyssal plain, modified from White and Klitgord ( 1976) (see a) for location). c) and d) : topographic profiles running transverse to the northern and southern Murray Ridge. **171**

Figure 2 : Multibeam imagery of the Dalrymple Trough (a), and interpretative morpho-structural scheme (b), with local crustal seismicity since 1973 **173**

Figure 3 :Line drawing of seismic profiles previously published in the Dalrymple Trough-Murray Ridge area **175**

Figure 4 : Seismic profile from the Chamak cruise (Ellouz-Zimmerman et al., 2007; Mouchot, 2009) crossing the Jinnah seamount, showing the M-unconformity **177**

Figure 5 : a) Bird eye view of the connection between the Owen Fracture Zone (OFZ) and the Dalrymple Trough, showing en-échelon faults evolving laterally into transverse faults within the trough. b) seismic profile crossing the synclinorium structure identified within the Dalrymple Trough and c) the related interpretation. **180**

Figure 6 : a) close view of the synclinorium structure identified within the Dalrymple Trough. b) Seismic profile transverse to the Dalrymple Trough **181**

Figure 7 : seismic profile crossing transverse faults **182**

Figure 8 : seismic profile crossing the Owen fracture Zone at the entrance of the Dalrymple Trough **183**

Figure 9 : Seismic profile crossing the Owen Fracture Zone (OFZ) and the en-échelon fault system 2 **184**

Figure 10 :Sketches of the geological history of the Dalrymple Trough and the Murray Ridge **190**

Table 1 : Age estimations of the different markers used in this study, from sedimentation rates calculated at the different drilling/coring sites available. See fig. 1 and 2 for sites locations. **187**

**Chapitre 4**

*Figures de la thèse:*

Figure 1 : Evolution des taux d'ouverture au niveau de la dorsale de Carlsberg au cours des 20 derniers Ma **200**

Figure 2 : profil sismique recoupant le segment sud de la Ride d'Owen. Une discordance angulaire observée à 10.4 Ma pourrait correspondre au début du soulèvement de la ride. **202**

Figure 3 : Profils sismiques recoupant la zone de déformation diffuse de l'Océan Central Indien (extraits de Delescluse (2008)) **204**

Figure 4 : Vues 3D de rides transverses associées à la transformante de la Romanche (Atlantique) et à la transformante d'Andrews-Bain (Océan Indien). **237**

*Figures des publications :*

***Rodriguez et al., in prep.***

Figure 1 :Bathymetric map of the Arabian Sea. Inset shows the regional tectonic setting of the India-Arabia plate boundary, and the position of the summer Inter-Tropical Convergence Zone (ITCZ). **207**

Figure 2 :Bathymetric maps of the southern (a) and central (b) portions of the Owen Basin, and location of the seismic lines. **209**

Figure 3 : Seismic profiles crossing a) the Oman Margin, b) the Southern Owen Ridge, c) the Central Owen Ridge (see Fig. 2 for location). Insets show close-views of the seismic profiles in the area of deep-sea drilling (ODP and DSDP) locations. **211**

Figure 4 : Seismic profile crossing the Oman margin, showing a major anticline affecting Miocene sediments. **213**

Figure 5 : Seismic profiles crossing the Southern Owen Ridge. **215**

Figure 6 :Seismic profiles crossing the eastern side of the Central Owen Ridge. **217**

Figure 7 : Anatomy of a canyon dissecting the Oman margin, with special emphasis over bottom-current deposits. a) Bird eye view of the canyon. b) Seismic profile crossing the uppermost flanks of the canyons, showing imbricated sigmoid bodies typical of contouritic drifts. c) Downslope seismic section of the canyon, showing typical plastered drifts **218**

Figure 9 :Map of the Indian Ocean compiling the different deformation areas related to the Late Miocene motion of the Indian Plate. **224**

**Chapitre 5**

*Figures de la thèse :*

*Introduction :*

Figure 17 : Compilation des mesures du champ magnétique dans la région du Bassin d'Owen (Fournier, com. pers.). Le bassin d'Owen est riche en anomalies magnétiques, ce qui indique une nature océanique. Il demeure toutefois difficile d'identifier les anomalies dans ce bassin. **240**

*Conclusions :*

Figure 1 : Schéma structural simplifié de la marge est-omanaise. **284**

Figure 2 : Champs de contrainte enregistrés dans les formations Crétacé sup./ Paléogène dans la région du Huqf. Trois stades principaux sont identifiés : un stade d'extension N170°E, un stade d'extension E-W, et un stade compressif E-W. **285**

Figure 3 : Champs de contrainte enregistrés dans les formations Paléogène de l'île de Masirah. Deux stades principaux sont identifiés : un stade d'extension N-S à N170°E et un stade compressif N20°E à E-W. **286**

Figure 4 : Champs de contrainte enregistrés dans les formations Paléogène de Ras Madrekah. Trois stades principaux sont identifiés : un stade d'extension N-S à N170°E, un stade d'extension N20°E à E-W, un stade compressif N20°E à E-W. **287**

Figure 5 : Synthèse de la déformation sur la marge Est-Omanaise. Trois stades de déformation sont identifiés : un stade d'extension N-S à N170°E, un stade d'extension E-W à N20°E, et stade de compression N20°E à E- W. **288**

*Figures des publications :*

***Rodriguez et al. in prep.***

Figure 1 : a) General map of the western Indian Ocean; b) Multibeam bathymetry of the Owen Basin, compiled with SRTM topography at 30''. c) Deep-structure of the Owen Basin deduced from wide-angle seismic data [Barton et al., 1990]. **243**

Figure 2 :Reconstitutions of the India-Arabia relative motion since Tithonian times according to a) Whitmarsh et al. [1979] and b) Mountain and Prell [1990]. c) Paleogeographic reconstitutions from Paleocene to Oligocene based on magnetic studies [Royer et al., 2002] also imply a location of the Paleogene India-Arabia plate boundary in the Owen Basin. **245**

Figure 3 :Magnetic anomalies map over the Arabian Sea, modified from Mercuriev et al. [1996] and Chaubey et al. [2002]. **247**

Figure 4 :Bathymetric map of the Owen Basin. The Owen Basin area is divided in three morphological domains : the Oman margin, the Owen Basin, and the Owen Ridge. **250**

Figure 5 :Seismic profiles crossing a) the Oman Margin, b) the Southern Owen Ridge, c) the Central Owen Ridge. **253**

Figure 6 :a) Seismic profile crossing the central segment of the Owen Ridge, showing the active OFZ and an extinct transform fault to the east, buried under Indus turbidites. b-d )Seismic profiles crossing the southern segment of the Owen Ridge. Profile b) shows an abrupt and sharp vertical offset of the basement of the Owen Ridge interpreted as a transform fault. Profile c) shows folds and vertical faults buried under the Indus deposits. Profile d) shows the vertical truncature of the series of sediments composing the Owen Ridge to the East (interpreted as the remnant of a former India-Arabia plate boundary)and the present-day boundary to the West. **256**

Figure 7 :a-d) Seismic profiles acquired in the southern part of the Oman margin. Seismic profile a) shows the structure of the edge of the Sauquarah Ridge, which looks similar to a transform valley. Seismic profile b) shows abrupt and sharp offsets of sediments composing the Lower Unit interpreted as fossil transform traces. The erosive surface sealing the Lower Unit is also evidenced. Seismic profile c) shows traces of extinct transform fault activity within the Lower Unit, together with an angular unconformity (picked in dark purple) that could correspond to the end of their activity. The erosive surface (light purple) separating the Lower and the Upper Unit is well observed. The Upper Unit is composed of turbidites and MTDs and is affected by differential compaction structures localized at the edge of fossil transforms. Seismic profile d) shows the Masirah ophiolitic body offset by an extinct transform; and the Late Miocene episode of folding. **258**

Figure 8 :Seismic profiles a) to c) show abrupt and sharp sub-vertical offsets interpreted as traces of a fossil Paleogene transform activity close to the present-day central Owen Ridge. Profile a) also shows differential compaction structures, and turbiditic channel levees coming from the Indus Fan. Profile b) highlights a particular fanning configuration in the MTDs coming from the central ridge. Profile d) shows the uneven basement of the Owen Basin, associated with sharp sub-vertical offsets of the Lower Unit interpreted as extinct transforms. **261**

Figure 9 :Seismic profiles crossing the edge of the section of the Oman margin oriented 15°NE. Profile a) shows a fold rooted on a reverse fault, indicating an Oligocene episode of compression.

Profile b) shows the abrupt tilt of the Lower Unit sediments towards the Owen Basin, along a vertical fault interpreted as a trace of transform activity. Profile c) shows two basement highs that could correspond to a fossil transform valley. **264**

Figure 10 :Seismic profile a) shows the Masirah Ridge and differential compaction structures. A graben, corresponding to a potential transform valley, is evidenced at the foot of the Masirah Ridge. Seismic profile b) highlights the uneven character of the basement. Potential transforms are underlined by the fanning configuration of MTDs. Seismic profile c) shows the regional angular unconformity separating the Lower Unit from the Upper one, and the regional unconformity corresponding to the inactivation of the Paleocene-Eocene transform systems. **266**

Figure 11 :Seismic Profiles a) and b) show the western side of the Owen Ridge, and abrupt basement offsets representing potential remnants of a Paleocene-Eocene transform activity (recorded by the fanning configuration of lavas). **268**

Figure 12 :Examples of the diagnostic features of a transform plate boundary on seismic profiles. **270**

Figure 13 :Synthesis of the India-Arabia relative motion geological history since Late Cretaceous Times, and summary of the new geological framework proposed in this study, involving a transfer of a part of the Indian plate to the Arabian plate in Oligocene. **272**

**Chapitre 6**

*Figures de la thèse :*

Figure 1 : classification des processus d'instabilités gravitaires, d'après Mulder et Cochonat (1996).**292**

Figure 2 : Exemples de convergence de faciès morphologiques. **297**

Figure 3 : A. Distribution des hauteurs des cicatrices des glissements de terrains sous-marins du segment sud de la Ride d'Owen. B. Relation entre l'accélération horizontale critique (ky) et la profondeur du sédiment (z). Le domaine encadré en rouge correspond au domaine d'instabilité sur le segment sud de la Ride d'Owen. **325**

Table 1 : Paramètres de l'analyse de stabilité, d'après Shipboard scientific party, 1989. Su : résistance au cisaillement, en Pa; γ : densité sèche du sédiment (kg/m$^3$); γ': densité du sédiment chargé en eau (kg/m$^3$), ky: accélération horizontale critique, en g (1g = 9,82 m.s$^{-2}$). **325**

*Figures des publications :*

***Rodriguez et al., 2012, Marine Geology***

Figure 1: Multibeam bathymetry of the study area **303**

Figure 2: Seismic lines collected during the ODP Leg 117 (Shipboard Scientific Party, 1989) and their new interpretation, with special emphasises on mass wasting events. **304**

Figure 3: A) Three-dimensional DEM of the southern ridge with 200-m interval bathymetric contours, and main seabed features. B) Slope map of the southern Owen Ridge with location of figures 8 to 12, and synthetic map of the different types of mass wasting observed. **305**

Figure 4: A) Three-dimensional DEM of the central ridge with 200-m interval bathymetric contours, and main seabed features. B) Slope map of the central Owen Ridge and synthetic map of the different types of mass wasting mode observed. **306**

Figure 5: A) Three-dimensional DEM of the Qalhat seamount with 200-m interval bathymetric contours, and main seabed features. B). Slope map of the Qalhat Seamount and synthetic map of the different types of mass wasting mode observed. C. 3.5 kHz profiles showing several generations of MTDs merging in the evacuation zone. **307**

Figure 6: Perspectives views of the sedimentary system of the Owen Ridge before and after the uplift. **308**

Figure 7: 3.5 kHz profiles showing A) several lenses of MTDs related to the erosion of the southern flank of the central Owen Ridge by disintegrative failures and B) MTDs related to the erosion of the southern flank of the Qalhat Seamount by disintegrative failures. **310**

Figure 8: Synthesis of EM120 swath bathymetry (slope map) features, 3.5 kHz echo-facies and their interpretation. **311**

Figure 9: A) Slope map of a multi-event generated scar on the southern Owen Ridge, showing the main slump scar and the related headwall collapse at the rear, with some block fall associated to the headwall collapse. B) SBP profile crossing an headwall collapse area, and C) the related ODP seismic line. D) 3.5 kHz profile showing MTD faulted by headwall collapse fault, and gently disturbed pelagic drape within the headwall collapse area **312**

Figure 10: A) Slope map of a multi-event generated scar on the southern Owen Ridge, showing a bottleneck scar. B) 3.5 kHz profile crossing the bottleneck scar and adjacent mass transport deposits

**313**

Figure 11: A) Slope map of a multi-event generated scar on the southern Owen Ridge, showing the main slump scar and the related headwall collapse at the rear; and an area of "intra-canyon" failure pattern. B) ODP seismic line crossing headwall collapse area. 3.5 kHz profiles showing C) fluid escape features and D) folded reflectors in the headwall collapse area, similarly to the ODP seismic line in B) **314**

Figure 12: A) Slope map of the largest multi-event generated scar on the southern Owen Ridge, with elongate scars buried under MTDs, B) 3.5 kHz profile crossing a disintegrative elongate failure buried under a thicker pelagic cover than the surrounding MTDs. **315**

Figure 13: "intra-canyon" failure pattern on the western side and complex networks of gullies. **316**

Figure 14: Slope map of the central Owen Ridge, showing elongate disintegrative failures **317**

Figure 15: A) Distribution of the volumes of individual failure according to the mode of failure (gullies, cohesive and disintegrative) for each segment of the Owen Ridge. B) Volumes distribution for multi- failures events along the Owen Ridge. **318**

Figure 16. Estimation of earthquake recurrence along the segment of the OFZ crossing the southern ridge. **318**

Table 1: Correlation coefficients (covariance) for the instability scar morphometric parameters. All of the measured and calculated variables are correlated to explore possible relationships. **309**

***Rodriguez et al., 2013, NHESS***

Figure 1: Regional topographic map of the Sultanate of Oman and the offshore Owen Fracture Zone. Inset shows a 3D view of the 17°20'N landslide located on the Owen Ridge. **330**

Figure 2: 3.5 kHz echo-sounder profiles (SBP 120) across the 17°20'N landslide. **331**

Figure 3: Snapshots of the computed water surface for a dynamic viscosity value at 500 $m.s^{-2}$. **333**

Figure 4: Maximum water elevations computed after a 8000 s simulation for a dynamic viscosity value at 500 $m.s^{-2}$. Insets show the maximum water elevations computed around Ras Sharbitat(inset a) and Salalah (inset b). **334**

**Conclusions**

Figure 1 : Comparaison de l'histoire géologique de la limite de plaque Inde-Arabie telle que définie au début de cette thèse, puis de celle établie à son terme. Les évènements surlignés en rouge correspondent aux points de l'histoire qui ont été revisités. **345**

Figure 2 : La ride de chain **347**

**ANNEXES**

Marine Geology 336 (2013) 10–23

Contents lists available at SciVerse ScienceDirect

Marine Geology

journal homepage: www.elsevier.com/locate/margeo

# Late Quaternary megaturbidites of the Indus Fan: Origin and stratigraphic significance

J. Bourget [a,*], S. Zaragosi [b], M. Rodriguez [c,d,e], M. Fournier [c,d], T. Garlan [f], N. Chamot-Rooke [e]

[a] Centre for Petroleum Geoscience and $CO_2$ Sequestration, School of Earth and Environment, University of Western Australia, 35 Stirling Hwy, Crawley, WA 6009, Australia
[b] Univ. Bordeaux, EPOC, UMR 5805, F-33400 Talence, France
[c] Institut des Sciences de la Terre de Paris, UMR 7193, Université Pierre et Marie Curie, case 129, place Jussieu, 75252 Paris cedex 05, France
[d] iSTeP, UMR 7193, CNRS, F-75005 Paris, France
[e] Laboratoire de Géologie, Ecole normale supérieure, 24 rue Lhomond, 75231 Paris cedex 05, France
[f] SHOM, Centre Hydrographie, BP146, F-29280 Brest, France

ARTICLE INFO

*Article history:*
Received 9 January 2012
Received in revised form 27 November 2012
Accepted 28 November 2012
Available online 7 December 2012

Communicated by D.J.W. Piper

*Keywords:*
Indus Fan
turbidite system
Quaternary
stratigraphy
sea-level
pull-apart basin
megaturbidite

ABSTRACT

The Indus sedimentary basin forms one of the largest "source-to-sink" systems of the Quaternary and extends over $10^6$ km$^2$ offshore. It is characterized by a complex tectonic setting marked by the Himalayan active orogenic belt in the source area, and the active strike-slip India-Arabia plate boundary (Owen Fracture Zone; OFZ) in its distal reaches. This paper focuses on a Late Quaternary channel–levee system from the Indus Fan captured by the recent opening of the 20°N pull-apart basin, located at 850 km off the present-day Indus Delta, along the OFZ. In this area the channel-mouth deposits consist of a set of up to 23 m thick megaturbidites trapped in the basin. These deposits form "ponded" lobe deposits in a tectonically-active confined basin. Age determination from radiocarbon dating and extrapolation of local deformation rates show that the older deposits observed on the seismic profiles are up to 358 ka BP old (MIS 10). The origin of these Late Quaternary deposits are investigated in the context of the Indus "source-to-sink" system and their significance is placed in a sequence stratigraphic framework. Integration of the stratigraphic architecture of the 20°N Basin megaturbidites with previous work in the area suggests that the Indus Fan evolved from a delta-fed turbidite system with several active canyons and channel–levee during the forced regressive conditions of the last falling stage of sea-level (122–25 ka BP), to a point source turbidite system during the sea-level lowstand (Last Glacial Maximum) and early transgressive stages (25–12 ka BP). This work sheds new light on the recent evolution of the Indus sedimentary system and illustrates the importance of the delta/river evolution during the fall of sea-level (e.g., incised valley formation) on the timing of sedimentary transfer and sediment distribution at the basin-scale.



## 1. Introduction

Large river-fed turbidite systems of the Quaternary (e.g. the Zaire, Amazon, Mississippi, Bengal, Indus, Zambezi or Tanzania deep-sea "fans") develop over distances exceeding 1000 km along continental slopes and abyssal plains (Kolla et al., 1980; Bouma, 1985; Droz and Mougenot, 1987; Kolla and Coumes, 1987; Savoye et al., 2000; Bourget et al., 2008). Intensive mapping of these deep-water giants during the last four decades led to the emergence of detailed architectural (e.g. Normark, 1978; Bouma et al., 1985; Piper and Normark, 2001) and stratigraphic (e.g., Posamentier et al., 1991; Posamentier and Kolla, 2003; Catuneanu et al., 2009) sedimentary models to predict their depositional patterns and their evolution through time. Large mud-rich fans are typically associated with the development of sinuous deep-water channels that extend over several hundreds of kilometers along very low-gradients (Pirmez and Flood, 1995; Peakall et al., 2000). In their distal areas, turbidite systems are associated with the transition between channel/levee systems and sand-rich channel-mouth lobes. On passive-margins, turbidite system growth is generally enhanced when rivers are directly connected to the canyon heads during periods of sea-level lowstands (Vail and Mitchum, 1977; Posamentier et al., 1991; Posamentier and Kolla, 2003; Catuneanu et al., 2009). Conversely periods of sea-level drop (falling-stage) and rise (transgressive) are thought to be dominated by mass-transport deposits and dominantly unconfined flows leading to poor turbidite system development (Posamentier and Kolla, 2003). However, recent studies show that active turbidite system growth in transgression and highstand is possible on tectonically active margins and/or along margins associated with narrow shelves (Goldfinger et al., 2003; Boyd et al., 2008; Bourget et al., 2010; Mas et al., 2010). This has been also observed on passive margins where highstand sediment supply is high enough to by-pass the continental shelves and is transferred basinward, either because of climate-induced high sediment discharges (Ducassou et al., 2009) or maintained river-canyon connection (Khripounoff et al.,

* Corresponding author. Tel.: +61 8 6488 2679.
*E-mail address:* julien.bourget@uwa.edu.au (J. Bourget).

0025-3227/$ – see front matter © 2012 Elsevier B.V. All rights reserved.
http://dx.doi.org/10.1016/j.margeo.2012.11.011

2003). Although the refinement of existing predictive models focusing on the stratigraphic organization of turbidite systems is partly driven by industrial needs, deep-water sedimentary record also constitutes a unique archive of the paleoenvironmental, paleoclimate and tectonic evolution of the source areas. Turbidite systems form the final end-members of the "sediment routing system" and therefore analysis of their stratigraphic evolution can unravel how the sedimentary basin responds to allogenic controls, in a "source-to-sink" perspective.

Here we use geophysical and sedimentary data acquired along the Indian-Arabian plate boundary to illustrate an atypical case of distal deep-water turbidite deposits fed by the Indus turbidite system, one of the largest marine sediment accumulation on earth. The dataset allows investigation of the sedimentary architecture of the 20°N pull-apart basin deposits and their mechanisms of deposition. The results are combined with the pre-existing mapping and dating of the Late Quaternary channel/levee systems from the Indus Fan (Coumes and Kolla, 1984; Kenyon et al., 1995; Prins et al., 2000; Carmichael et al., 2009) in order to examine their origin and their stratigraphic significance. The results highlight the sea-level control on the Late Quaternary evolution of the Indus sedimentary system.

## 2. Regional setting

### 2.1. The Indus turbidite system

The Indus "source-to-sink" system forms one of the most extensive and voluminous sedimentary basin around the world. Indus Fan sedimentation started during the Middle Eocene as the result of the onset of the India-Arabia collision and accelerated since the Early Miocene when uplift of the High Himalayas occurred (Clift et al., 2001, 2002). The Indus River currently drains an area of approximately $1.10^6$ km$^2$ in the Himalayan region, and its annual sediment discharge before damming was about $450.10^6$ T.yr$^{-1}$ (Milliman et al., 1984), representing the fifth largest sediment load in the world. This high sediment load is due to a poorly consolidated sediment source composed of glacial and fluvially-reworked detritus eroded from a high-relief, rapidly uplifting mountain ranges (Milliman et al., 1984; Giosan et al., 2006). Modern water discharge varies seasonally and generally peaks during the summer monsoon season reaching 30,000 m$^3$.s$^{-1}$ (Wells and Coleman, 1984) when the run-off increase due to the combination of snow melting and monsoonal rains (Milliman et al., 1984; Karim and Veizer, 2002). The Indus Delta forms a large sub-aerial delta extending over 750,000 km$^2$ (Fig. 1). The continental shelf develops on an average of 100 km off the present-day delta shoreline, and the shelf-break corresponds to the 135 m isobath (Giosan et al., 2006). Offshore, the Indus turbidite system (referred as "Indus Fan" hereafter) extends over $10^6$ km$^2$ in the Arabian Sea (Fig. 1), reaching 9 km thick at its thickest part (Coumes and Kolla, 1984; McHargue and Webb, 1986; Clift et al., 2001). Glacio-eustatic sea-level changes and subsequent position of the deltaic shoreline are thought to be the main factors that influenced the evolution of the Indus Fan during the Late Quaternary (Kenyon et al., 1995; von Rad and Tahir, 1997; Prins and Postma, 2000; Prins et al., 2000; Bourget et al., 2010). It forms a typical mud-rich, "passive margin fan" (*sensu* Reading and Richards, 1994). The Indus Fan architecture is characterized by numerous high-relief channel/levee systems and channel-mouth lobes (McHargue and Webb, 1986; Kolla and Coumes, 1987; Kenyon et al., 1995; Carmichael et al., 2009) that were fed by several canyon systems (McHargue and Webb, 1986; Kolla and Coumes, 1987). Three canyon complexes have been mapped in the shelf and upper slope areas near the Indus Delta, in an area referred as the Indus Trough (McHargue and Webb, 1986; Kolla and Coumes, 1987). Kolla and Coumes (1987) postulated that the eastern canyon system (Canyon system 3; Fig. 1) was the last active turbidity current pathway and was younger than the western canyon system (Canyon system 2; Fig. 1). However because this early work were based on seismic data and lacked stratigraphic data, the age of both canyon systems remain uncertain. The architectural evolution of the channel–levee systems of the Indus Fan is best constrained during the Late Quaternary and has been unraveled by side-scan sonar mapping and sediment core studies (Kenyon et al., 1995; von Rad and Tahir, 1997; Prins et al., 2000). Two main channel–levee complexes (CLC A and B; Fig. 1) successively formed through avulsion processes during the last sea-level cycle (Kenyon et al., 1995; Prins et al., 2000). The avulsion from CLC B to CLC A occurred at ca. 28 ka BP (Prins et al., 2000), i.e. close to the onset of the Last Glacial Maximum (LGM). The onset of the LGM at about 25 ka BP was characterized by a sea-level dropping from ~60 m to below 120 m in less than 10 ka (Lea et al., 2002; Waelbroeck et al., 2002; Clark et al., 2009). This enhanced rapid incision of the Indus River across the continental shelf, and headward erosion of the Indus Canyon. During the following sea-level lowstand and early rise, which lasted ca. 7500 years, the Indus River sediments were directly funnelled from the fluvial system into the canyon head and promoted the active growth of the CLC A (von Rad and Tahir, 1997; Prins and Postma, 2000; Prins et al., 2000), with reduced if not absent deposition onto the shelf. At present-day, the Indus Canyon is a 185 km long and up to 1.6 km-deep main feeder canyon (Kenyon et al., 1995; von Rad and Tahir, 1997; Prins et al., 2000). The canyon deeply incises the ~100 km-wide continental shelf, with the canyon head being at 20 m water depth, less than 4 km off the present day delta-mouth (Fig. 1). Another canyon system has also been mapped by Kolla and Coumes (1987) to the south-east (Saraswati canyon; Fig. 1). This canyon system would have been fed by the paleo-Saraswati river until the Holocene (Kolla and Coumes, 1987) and could have contributed to the development of the channel–levee complex B during the Late Quaternary (Kenyon et al., 1995).

### 2.2. The Owen Fracture Zone

The 20°N Basin forms a major releasing bend along the Owen Fracture Zone (OFZ) and started to develop about ~1.8–1.5 Ma (Rodriguez et al., 2011). The OFZ is an 800 km-long dextral strike-slip fault which forms the present-day, tectonically-active India-Arabian plate boundary (Fournier et al., 2008, 2011; Rodriguez et al., 2012). The active opening of the 20°N pull-apart basin from the onset of the Pleistocene has been associated with the capture of a distal channel–levee system thought to be part of the Indus Fan (Rodriguez et al., 2011). The present paper focus on the origin, mechanisms of formation and stratigraphic architecture of the 20°N Basin deposits (Fig. 1).

## 3. Material and methods

The bathymetry and acoustic imagery have been collected using the multibeam echosounder Kongsberg-SIMRAD EM120 during the Fanindien 2009 and Owen surveys (*R/V Beautemps-Beaupré*). More than 350 km of sub-bottom seismic profiles (SBP 120 profiler) were also acquired in the 20°N Basin area. Isopach thickness maps between interpreted horizons have been realized with The Kingdom © software. Two-way travel times (TWT) have been converted in m using an average seismic velocity of 1515 m.s$^{-1}$, corresponding to the typical internal acoustic velocity (*P* wave velocity) measured in the cores using a laboratory celerimeter during Fanindien 2009 cruise. Piston cores KS07 (60° 46.65 E; 19° 26.61 N), KS11 (61°18.48 E; 20°10.53 N) and KS12 (61°29.68 E; 20°11.53 N) were collected (using a Küllenberg corer). Thin slabs (15 mm-thick) were sampled and analyzed in the SCOPIX X-ray image processing tool. Grain size analyses were performed using a Malvern™ Supersizer 'S'. Nine AMS $^{14}$C dates have been obtained from mainly bulk planktonic foraminifer species sampled in hemipelagic clay intervals (Table 1). Radiocarbon dates have been corrected for a marine reservoir and calibrated to calendar years using the Calib 6.0.1 calibration program (Stuiver et al., 1998) with the Marine09 radiocarbon calibration curve (Reimer et al., 2009).

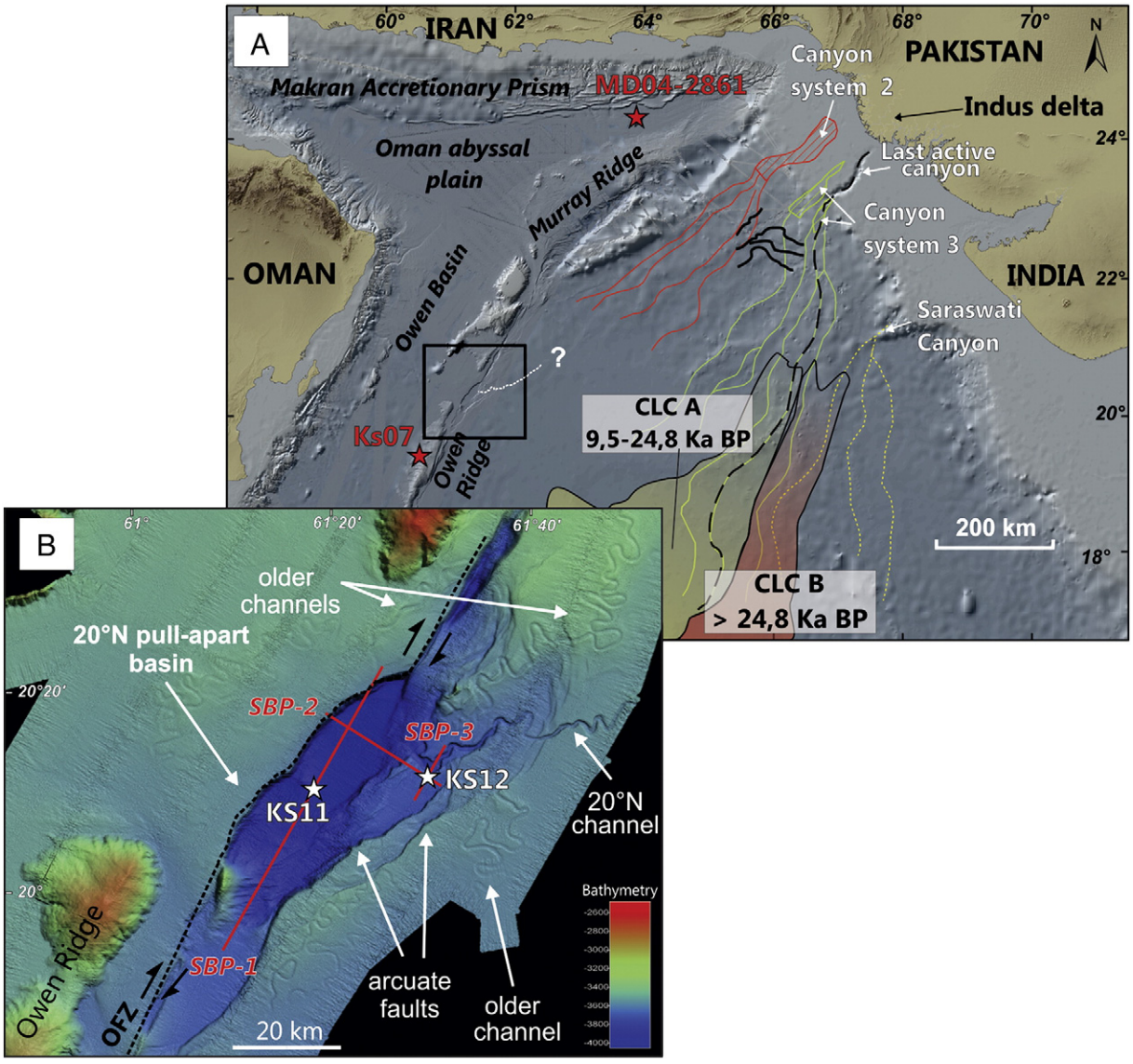


**Fig. 1.** (A) Physiography of the Arabian Sea, location of stratigraphic (hemipelagic) cores KS07 and MD04-2861 (Caley et al., 2011), distribution of Late Quaternary canyons and channel/levee systems of the Indus Fan. Canyon systems 2–3 and the Saraswati Canyon have been mapped by Kolla and Coumes (1987). The last active Indus canyon and the channel–levee complexes A and B were mapped by Kenyon et al. (1995) and Prins et al. (2000). Canyon-channels in black solid lines correspond to the upper Pleistocene Indus canyon/channels of Carmichael et al (2009). Age of the avulsion between CLC A and B is from Prins et al. (2000). (B) Multi-beam bathymetry of the 20°N pull-apart basin along the Owen Fracture Zone (OFZ). Location of the very-high resolution, sub-bottom seismic profiles (SBP-1 to SBP-3) and cores KS11 and KS12.

Radiocarbon ages of this study were performed at the "Laboratoire de Mesure du Carbone 14" in Saclay (SacA) through the "ARTEMIS" radiocarbon dating project. All the ages in the following text are given in calendar age (cal ka BP). Core stratigraphy and correlation have been also based on semi-quantitative geochemical element analyses performed at a cm-scale along the cores using an Avaatech © XRF "Core Scanner". We used the Bromine counts (associated with marine organic content (MOC) in the sediment of Arabian Sea; Ziegler et al., 2008) to correlate the cores KS11, KS12, and KS07 with the MD04-2861 (63° 54.79 E; 24° 7.99 N) stratigraphic reference (Caley et al., 2011). KS07 is located on the Owen Ridge and entirely composed of silt-mud sediments of hemipelagic origin. It therefore constitutes a good local stratigraphic reference that could be correlated to MD04-2861 (Fig. 1). Age model of the core MD04-2861 has been obtained through a combination of radiocarbon dates, biostratiographic correlations and oxygen isotope data (see Caley et al. (2011) for more details). More information about the XRF scanning technique and its relevance in paleo-environmental reconstructions can be found in Richter et al. (2006). Volume calculations of the turbidite events M1–M8 have been obtained through seismic interpretation of horizons across the 20°N Basin and creation of isopach maps using The Kingdom Software© (SMT). However, mapping extrapolation has been limited to a maximum distance of 2 km from the seismic profiles, resulting in a spatial coverage of only 66% of the total 20°N Basin surface. Hence in order to approach a more realistic volume value, estimation of the "total volume" deposited by each event has been calculated by applying a factor 1.5 (Table 2). However, these values are over-estimated as they encompass both turbiditic and hemipelagic deposits. In order to compare the volume of 20°N Basin deposits with previous studies, we therefore applied a correction factor based on the estimation of the proportion of hemipelagic deposits in the centre of the basin. We based our estimation on the depth correlation of the age of the M5 event, located at a maximum of 28 m deep in the basin centre (turbidites + hemipelagites) and corresponding to an age-equivalent depth of 3.5 m on KS07 (hemipelagic deposits only).

**Table 1**
Radiocarbon ages of cores used in this study, including source of the data if previously published.

| Core | Depth in core (cm) | Laboratory code | Material | $^{14}$C age (yr BP) | | | Calendar age (cal yr BP) | Source of data |
|---|---|---|---|---|---|---|---|---|
| MD042861 | 70 | SacA 19505 | Bulk. Pl. form. | 3905 | +/− | 30 | 3877 | Caley et al. (2011) |
| MD042861 | 140 | SacA 19506 | Bulk. Pl. form. | 6900 | +/− | 35 | 7416 | Caley et al. (2011) |
| MD042861 | 250 | SacA 17219 | *G. dutertrei* | 9845 | +/− | 45 | 10,757 | Caley et al. (2011) |
| MD042861 | 250 | SacA 17218 | *G. ruber* | 10,345 | +/− | 45 | 11,325 | Caley et al. (2011) |
| MD042861 | 180 | SacA 17216 | *G. ruber* | 12,170 | +/− | 50 | 13,635 | Caley et al. (2011) |
| MD042861 | 180 | SacA 17217 | *G. dutertrei* | 12,485 | +/− | 50 | 13,922 | Caley et al. (2011) |
| MD042861 | 339.5 | SacA 10439 | Bulk. Pl. form. | 14,160 | +/− | 60 | 16,866 | Bourget et al. (2011) |
| MD042861 | 450 | SacA 17220 | Bulk. Pl. form. | 17,470 | +/− | 70 | 20,268 | Caley et al. (2011) |
| MD042861 | 480 | SacA 22364 | Praeorbulina | 18,290 | +/− | 60 | 21,381 | Caley et al. (2011) |
| MD042861 | 500 | SacA 17221 | Bulk. Pl. form. | 19,850 | +/− | 70 | 23,310 | Caley et al. (2011) |
| MD042861 | 640 | SacA 17222 | Bulk. Pl. form. | 25,170 | +/− | 140 | 29,596 | Caley et al. (2011) |
| MD042861 | 810 | SacA 19507 | Bulk. Pl. form. | 34,170 | +/− | 260 | 38,711 | Caley et al. (2011) |
| KS11 | 178 | SacA 19504 | Bulk. Pl. form. | 18,140 | +/− | 70 | 21,245 | *This study* |
| KS11 | 462.5 | SacA 19499 | Bulk. Pl. form. | 23,850 | +/− | 90 | 28,236 | *This study* |
| KS11 | 512.5 | SacA 19501 | Bulk. Pl. form. | 25,970 | +/− | 130 | 30,409 | *This study* |
| KS11 | 606 | SacA 19503 | Bulk. Pl. form. | 28,480 | +/− | 160 | 32,271 | *This study* |
| KS11 | 733 | SacA 19500 | Bulk. Pl. form. | 31,430 | +/− | 220 | 35,330 | *This study* |
| KS12 | 136.5 | SacA 19502 | Bulk. Pl. form. | 21,750 | +/− | 100 | 25,493 | *This study* |
| KS07 | 0 | SacA 23237 | Bulk. Pl. form. | 2925 | +/− | 30 | 2713 | *This study* |
| KS07 | 20 | SacA 23238 | Bulk. Pl. form. | 8535 | +/− | 30 | 9177 | *This study* |
| KS07 | 40 | SacA 23239 | Bulk. Pl. form. | 12,405 | +/− | 40 | 13,849 | *This study* |
| KS07 | 55 | SacA 21240 | Bulk. Pl. form. | 13,620 | +/− | 50 | 16,209 | *This study* |
| KS07 | 60 | SacA 23240 | Bulk. Pl. form. | 14,710 | +/− | 50 | 17,384 | *This study* |
| KS07 | 150 | SacA 23241 | Bulk. Pl. form. | 20,970 | +/− | 80 | 24,560 | *This study* |
| KS07 | 329 | SacA 23242 | Bulk. Pl. form. | 34,800 | +/− | 290 | 39,292 | *This study* |
| KS07 | 376 | SacA 21241 | Bulk. Pl. form. | 35,130 | +/− | 300 | 39,759 | *This study* |

The latter result suggests that hemipelagic deposits contribute to 12.5% of the total deposit thickness in the basin centre. This factor has been applied to correct the volume calculations in Table 2.

## 4. Results

### 4.1. Sedimentary architecture of the 20°N Basin

The 20°N Basin forms a 90 km long and up to 35 km wide pull-apart basin, however restricted to less than 15 km wide off the mouth of an east-west trending channel–levee system (Figs. 1, 2). The basin is bounded by two major strike-slip faults (Fig. 1) trending N25°E to N30°E (Rodriguez et al., 2011). The western side of the basin is bounded by the OFZ as a steep master fault, and the structural pattern of the eastern basin boundary is more complex and consists of a single normal fault dividing into several arcuate splays (Figs. 2 and 3; Rodriguez et al., 2011). The eastern area is marked by the capture of a 1–3 km wide channel–levee system (Fig. 3). Its trajectory and sinuosity seem to be closely related to the propagation of the SW–NE trending arcuate active faults that are preserved on the bathymetry (Fig. 3). Levees relief varies between 30 and 115 m along the surveyed area and the sections marked by an increase in height correspond to the

**Table 2**
Measured characteristics of M1–M20 megaturbidite beds (thickness on Log Section 1 (S1), maximum thickness (*) measured in the centre of the 20°N basin, volume calculated from seismic interpretation and extrapolation, dip angles at S1 and S2, measured offset in caused by F1 fault) and chronostratigraphy from radiocarbon measurements, oxygen isotope correlation (**) from the core MD04-2861 (Caley et al., 2011), and interpolated ages (see text for explanation). *** Final megaturbidite ages correspond to chronostratigraphy results when available (M1–M9) then are based on extrapolation method (M9–M20). Ages from M14–M20 correspond to the average age obtained from S1 and S2 measurements. Uncertainty in age estimation is obtained from the calculated error in radiocarbon (M1–M5) and radioisotopic dating (M6–M8; Caley et al., 2011), and from the root mean square of the mean statistical variance for M9–M20 (see text for explanation).

| | Thickness S1 (m) | Thickness max. (m) * | Volume (km3) | $^{14}$C age KS11/KS12 | MD-61 age model** | Dip S1 (°) | Fault offset S1 (m) | Interpolated age S1 | Dip S2 (°) | Interpolated age S2 | Megaturbidites age *** | Uncertainty (yr) |
|---|---|---|---|---|---|---|---|---|---|---|---|---|
| Sea-floor | – | – | – | *0* | *0* | 0.190 | 3.540 | – | – | – | – | |
| M1 | 1.9 | 5.9 | 1.03 | *21,245* | – | 0.270 | 4.744 | – | – | – | *21,245* | *<260* |
| M2 | – | 1.3 | – | *25,155* | – | | – | – | – | – | *25,155* | *<260* |
| M3 | – | 1.5 | 0.40 | *28,237* | *29,597* | 0.280 | 6.390 | – | – | – | *28,237* | *<260* |
| M4 | 2.6 | 6.9 | 1.48 | *32,271* | – | 0.330 | 8.701 | – | – | – | *32,271* | *<260* |
| M5 | 4.7 | 8.0 | 1.87 | *35,331* | *38,711* | 0.380 | 9.837 | – | – | – | *35,331* | *<260* |
| M6 | 2.3 | 6.4 | 1.29 | – | *64,000* | 0.440 | 11.879 | – | – | – | *64,000* | *<1000* |
| M7 | 7.7 | 11.3 | 2.79 | – | *74,000* | 0.480 | 12.518 | – | – | – | *74,000* | *<1000* |
| M8 | 4.7 | 7.2 | 1.95 | – | *85,000* | 0.540 | 14.560 | – | – | – | *85,000* | *<1000* |
| M9 | 15.0 | 20.7 | – | – | – | 0.580 | 15.128 | *96,625* | – | – | *96,625* | *10,000* |
| M10 | 18.8 | 23.7 | – | – | – | 0.660 | – | *116,625* | – | – | *116,625* | *10,000* |
| M11 | 3.5 | 3.8 | – | – | – | 0.720 | – | *131,625* | – | – | *131,625* | *10,000* |
| M12 | 3.0 | 3.2 | – | – | – | 0.790 | – | *149,125* | – | – | *149,125* | *10,000* |
| M13 | 2.6 | 3.9 | – | – | – | 0.890 | – | *174,125* | – | – | *174,125* | *10,000* |
| M14 | 0.9 | – | – | – | – | 0.930 | – | *184,125* | 0.390 | *196,369* | *190,247* | *10,000* |
| M15 | 7.5 | – | – | – | – | 1.050 | – | *214,125* | 0.398 | *203,667* | *208,896* | *10,000* |
| M16 | 7.5 | – | – | – | – | 1.100 | – | *226,625* | 0.400 | *205,752* | *216,189* | *10,000* |
| M17 | 8.2 | – | – | – | – | 1.140 | – | *236,625* | 0.423 | *229,557* | *233,091* | *10,000* |
| M18 | 7.3 | – | – | – | – | 1.250 | – | *264,125* | 0.452 | *257,881* | *261,003* | *10,000* |
| M19 | 5.6 | – | – | – | – | 1.290 | – | *274,125* | 0.474 | *280,296* | *277,211* | *10,000* |
| M20 | 31.2 | – | – | – | – | – | – | – | 0.552 | *357,794* | *357,794* | *49,000* |

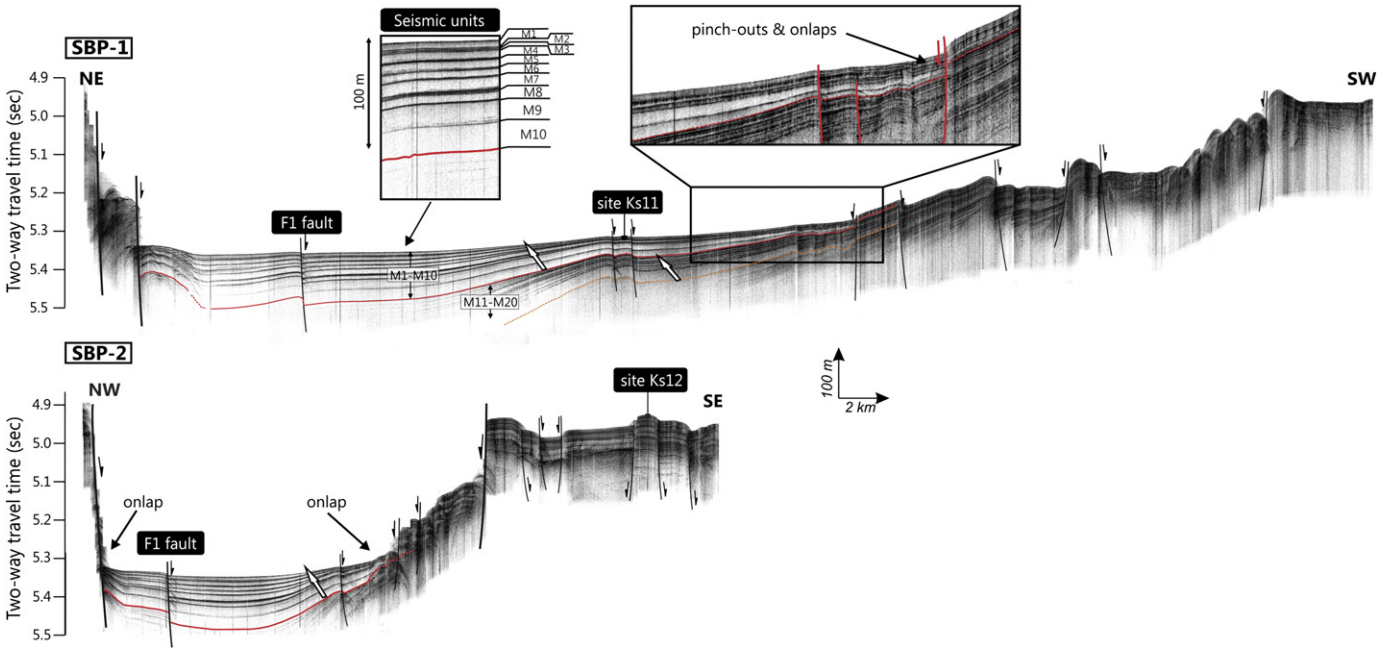


**Fig. 2.** Sub-bottom seismic profiles SBP-1 and SBP-2 (see location on Fig. 1) showing the internal architecture of the 20°N Basin deposits and the megaturbidites M1–M20. White arrows indicate thinning-upward sedimentary sequences.

locations where fault-induced knickpoint cause channel entrenchment. The channel course abruptly terminates into the 20°N Basin where a system of normal faults form a >120 m high knickpoint (Fig. 3) associated with an abrupt increase of slope gradient (from <1° to 3–5°). Lower relief sinuous channels are also observed within the study area and correspond to older, partly buried channel–levee systems (Fig. 3; Rodriguez et al., 2011). These channels are thought to be inactive since 1.32–0.95 Ma BP (Rodriguez et al., 2011). The edges of the 20°N Basin are generally sharp and despite the fact that its walls have slopes of 10–30° (particularly along its western edge), major slump scars are neither observed along the high-resolution bathymetry (Figs. 1, 3) nor on seismic profiles (Fig. 2). The basin fill is characterized by a vertical stacking of seismic units showing a dominant transparent acoustic echo-facies (Figs. 2, 4). These units considerably thicken in the centre of the basin where they reach more than 0.033 s TWT thick, i.e. up to 25 m (M10, Figs. 2, 4). The seismic units are associated with pinch-out geometry on the edges of the basin in both S–N and E–W directions (Fig. 2), where individual seismic units become considerably thinner (~70% thinner at site KS11, and about 95% twenty kilometers to the north on line SbP-2). The base of the seismic units is often characterized by higher seismic amplitudes (Figs. 2, 4). Twenty seismic units (named M1 to M20 hereafter) have been consistently recognized in the 20°N Basin (Figs. 2, 4). Below M20, sub-bottom profiler penetration decreases and interpretation is difficult. The vertical distribution of seismic units allows differentiating two thinning-upward sedimentary intervals (Figs. 2, 4). The upper ten seismic units (M1–M10) form a max. 0.132 s. TWT thick sequence in the center of the basin, i.e., about 100 m (Figs. 2, 4). Thickness of individual seismic units measured on Section 1 (Fig. 4) decreases from M10 (18.8 m thick) to M1 (1.9 m thick; Table 2). Seismic units M11 to M20 form a second thinning-upward sequence with a maximum thickness of 64 m on Section 1 (Fig. 4), and individual seismic units ranging from 31.2 m (M20) to 3.5 m thick (M11; Table 2). Although some seismic profiles suggest that this second thinning-upward sequence also includes deeper seismic units (Figs. 2, 4), these cannot be consistently mapped over the area and therefore are not considered in the following discussion. The 20°N Basin deposits are perturbed by a transverse fault system (F1) that offsets the M1–M20 seismic units in the north-western area (Fig. 4). It causes an offset of 3.5 to 16.3 m in the seismic units along the two measured sections shown in Fig. 4, the offset decreasing from the deeper seismic units (M9) to the shallower (M1; Table 2). Below M9 the fault offset cannot be calculated due to the lack of acoustic penetration in seismic profiles in the F1 fault area (Figs. 2, 4).

### 4.2. Sedimentary cores

Cores KS11 and KS12 were recovered on the southwestern edge of the 20°N Basin and on the left-hand levee of the channel–levee system, respectively (Fig. 1). Both cores are composed of fine-grained sediments, mostly clay to silty clay-sized particles (Fig. 5). Coarse silt layers are observed throughout the cores ($D_{50}$ = 11–40 μm; Figs. 5, 6). In both KS11 and KS12 they form thin (mm to dm-thick), fining-upward layers commonly associated with planar lamination, possible convolute bedding, and slightly erosional bases (Fig. 6). These coarse to fine silt layers grade up to structureless clays ($D_{50}$ = 4–11 μm). The upper, muddy unit is generally bioturbated and has variable planktonic foraminifer content. Thus, KS11 and KS12 deposits can be interpreted as fine-grained turbidites ("Tc "or "Td" of Bouma, 1962) capped by turbiditic muds ("Te") and hemipelagic sediments. Combination of AMS-$^{14}$C dating and XRF records enables correlations between the two cores (Fig. 5). Their Bromine (Br) record could also be correlated with cores KS07 and MD04-2861 (Fig. 1). These two cores are composed of hemipelagic sediments and are located away from any turbiditic input (Fig. 1; Caley et al., 2011). MD04-2861 is a regional stratigraphic reference providing a complete record of the paleo-environmental evolution of the Arabian Sea during the last 310 ka BP (Caley et al., 2011). Stratigraphic data show that turbidite activity in the 20°N Basin ceased after 25.4 and 21.2 ka BP at sites KS12 and KS11, respectively (Fig. 5), an age which roughly corresponds to the onset of the Last Glacial Maximum (LGM).

### 4.3. Nature and age of the 20°N Basin deposits

#### 4.3.1. Seismic-core correlation

As the seismic units pinch-out toward the edges of the basin (Fig. 2), the 9 m-long core KS11 potentially recovered much of the thick sedimentary succession in the centre of the 20°N Basin. Sand

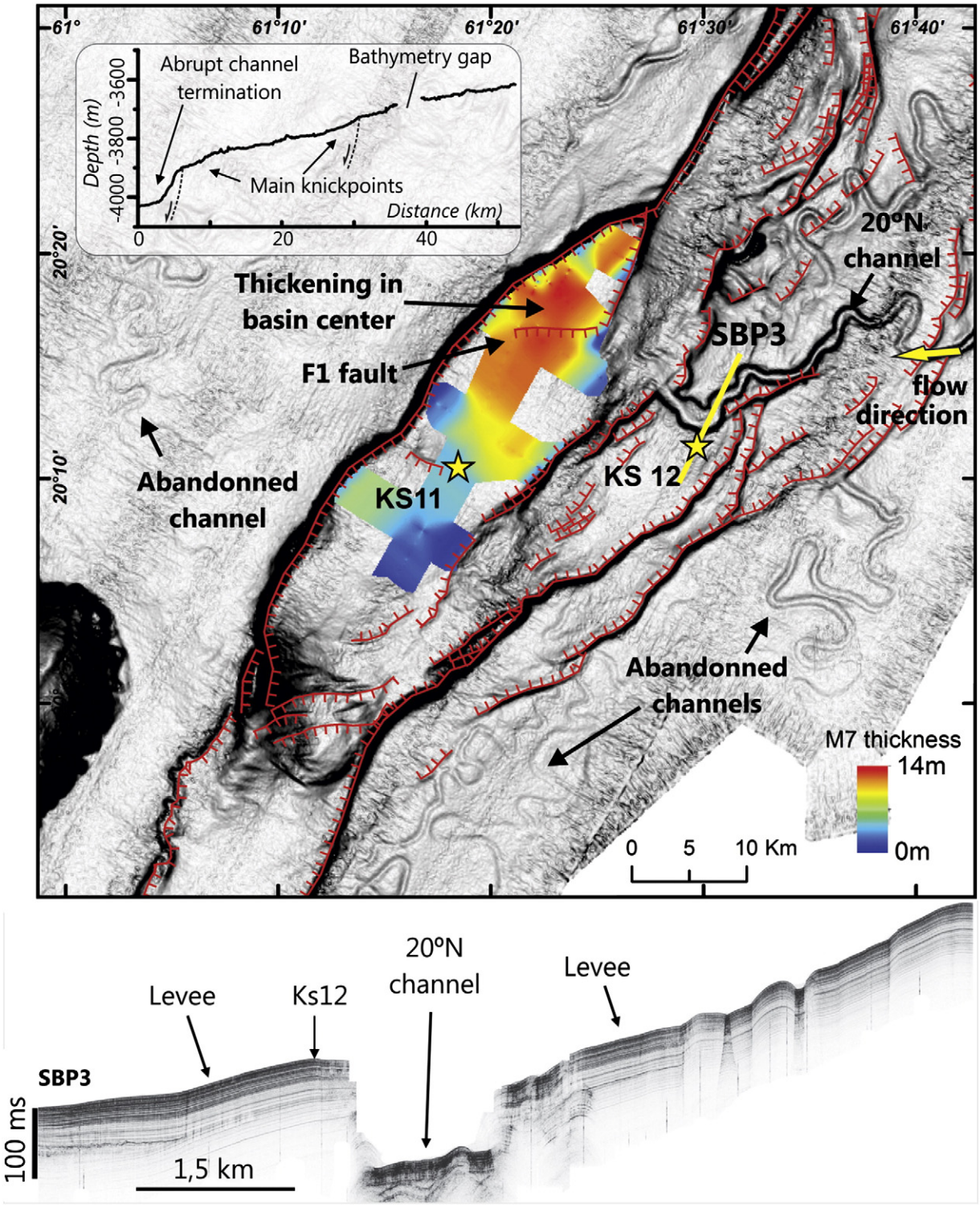


**Fig. 3.** Slope map of the 20°N Basin showing the distribution of the main structural elements (brown lines), the location of the cores KS11 and KS12, the last active Indus channel and the abandoned Indus channels (Rodriguez et al., 2011). SBP-3 sub-bottom seismic profile shows a cross-section of the last active Indus channel before it enters the 20°N Basin. Along-channel bathymetry profile highlights the location of main slope breaks along the last active Indus channel pathway including the >100 m high knickpoint at the 20°N Basin eastern edge. Thickness map of the megaturbidite M7 highlights megaturbidite deposition thickening in the basin centre and thinning on basin edges.

to silt turbidite bases typically produce strong contrast of impedance on sub-bottom, high-frequency seismic (Cita and Rimoldi, 1997; Rothwell et al., 2000). The key reflectors observed in the first 10 meters depth on seismic profiles at site KS11 can be correlated with the sand to silt turbidite bases observed in the core using a seismic velocity of 1515 $m.s^{-1}$ (Fig. 6). These reflectors define the base of the thick seismic units M1 to M5 observed in the centre of the basin centre (Fig. 6). Hence M1 to M5 units form a total thickness of about 26 m in the basin centre, corresponding to less than 9 m thick at site KS11 (Fig. 6). Older deposits (M6–20) are not recovered in KS11 (Figs. 5, 6) but show an acoustic facies similar to the M1–5 events, consisting of a thin high to moderate amplitude base capped by a thick transparent

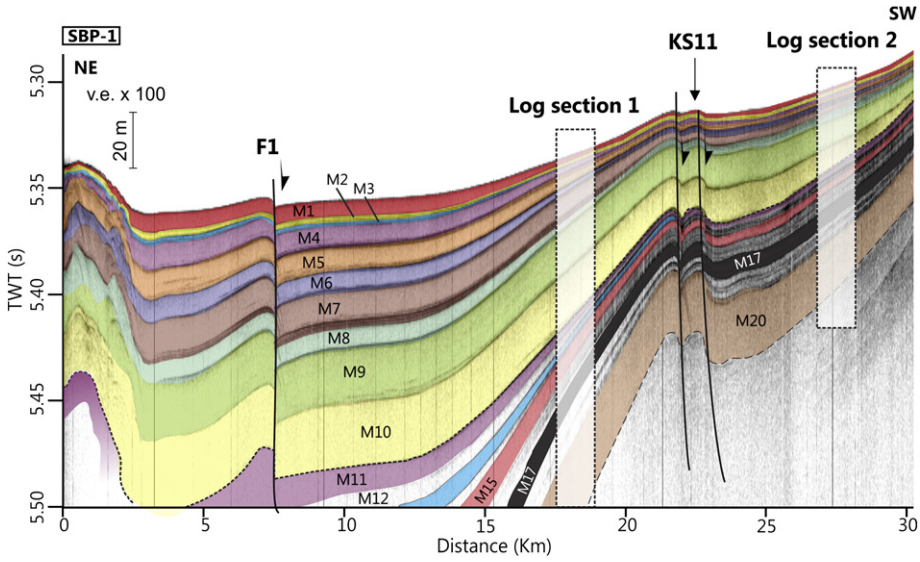


**Fig. 4.** Interpreted seismic profile SBP-1 showing the architecture of M20–M1 deposits, their offset at F1 fault location, and the location of log Sections 1 and 2 where dip angles have been measured.

echo-facies (Figs. 2, 4, 6). We interpret the basal strong reflections to be produced by sand to silt turbidite bases, which thicken in the basin centre, and the transparent eco-facies to be related to the thick Te-turbidite (clastic) and hemipelagic muds above (Fig. 4). This is consistent with previous studies that correlated similar thick acoustically-transparent layers in deep-water settings with thick turbidite deposits characterized by a thick upper clayey unit e.g., the Quaternary megaturbidites of the Mediterranean Sea (Cita et al., 1984; Cita and Rimoldi, 1997; Cita and Aloisi, 2000; Rebesco et al., 2000; Rothwell et al., 2000), the Marmara Sea (Beck et al., 2007), or the Gulf of Mexico (Tripsanas et al., 2004). The transparent echo-facies widely prevails in the centre of the basin (Figs. 2, 4). This suggests that the volume of turbidite mud is considerably more important than the volume of sand and silt in the 20°N Basin. Considering the seismic facies of M1–M20 units, their turbiditic origin (KS11) and their similarity with other deep water, Quaternary ponded deposits, the sedimentary deposits of the 20°N Basin are thus interpreted as mud-rich megaturbidites. The term "megaturbidite" is here used *sensu* the terminology of Bouma (1987), i.e. it describes exceptionally thick and/or laterally extensive layers of relatively homogeneous deposits consisting of material transported by gravity-driven density current or mass-flow.

*4.3.2. Age determination of the 20°N Basin megaturbidites*

Radiocarbon dates on cores KS11 and KS12 allows determining the age of the M1 to M5 megaturbidites (Fig. 5, Table 2), ranging from 21.2 ka BP (M1) to 35.3 ka BP (M5). Below M5, ages of M6, M7 and M8 have been obtained through correlation with the core MD04-2861 age model (Fig. 5; Caley et al., 2011). The results give an age of 85 ka BP for M8 (Table 2). Older megaturbidites could not be dated using the stratigraphic age model. However their ages can be estimated by using the evolution through time of the deformation rates on the edges of the basin. The angles of dip (in degrees) of the megaturbidite beds have been measured along the log Section 1 on the seismic profile SBP-1 (Fig. 4, Table 2). Dip values are regularly decreasing from the older megaturbidite beds (M20) to the younger (M1), suggesting constant rates of tilting on the edges of the 20°N Basin (Table 2). To test this hypothesis we measured the offset value (fault throw, in metres) of the megaturbidite beds at the location of the F1 normal fault on the seismic profile SBP-1 (Fig. 4). Results (Table 2) show that the fault throw also regularly decreases from M9 (15.1 m) to M1 (4.7 m). Linear regression between the age of megaturbidites and their offset at F1 gives an R-squared value of 0.93 (Fig. 7). These observations suggest that the subsidence (and tilting of sedimentary layers) occurred at a constant rate during the Late Quaternary. Considering a constant tilting rate, and hence dip values, increasing with time, the approximate age of pre-M8 deposits can be estimated (Fig. 7). We obtained the linear regression equation of relationship between the dipping of the megaturbidite beds and their age by using the eight dated (age model-based) deposits (M1–M8; Fig. 7). The obtained R-squared value is $>0.96$ (Fig. 7). The regression equation is then used to calculate the age of M9 to M19 deposits (Table 2). Dip values and age could not be estimated for M2 as it is too thin on the log section to be resolved with confidence at the scale of seismic data (Fig. 4). Penetration and quality of seismic signal decrease with depth hence measurement of seismic units dip angle is less accurate below M14–M15 on Section 1 (Fig. 4). Similarly, dip measurement and therefore age determination were impossible for M20 on Section 1 (Fig. 4). Thus similar measurements have been made along a second vertical log section (Section 2; Fig. 4) on the south-western edge of the profile SBP1 (Table 2). The linear regression equation of relationship between the dip of the megaturbidite beds and their age on Section 2 has been achieved by using the eight confidently dated (age model-based) deposits (M1–M8) as well as the M9–19 ages calculated from Section 1 (Table 2). The obtained R-squared value is $>0.95$ (Fig. 7). The regression equation has then been used to estimate the age of M14 to M20 deposits (Table 2), and the final age of these seismic units have been calculated as a mean of individual values obtained by the interpolation on both log sections (Table 2; Fig. 7). Using this technique, age estimation indicates that the oldest visible on the seismic data (megaturbidite event M20) is dated at 357.8 ka BP (MIS 10).

Uncertainties in age estimation increase from the youngest megaturbidites (M1–M8) to the oldest (M9–M20; Fig. 8; Table 2). M1 to M5 have been dated using radiocarbon data (Table 2). Their age uncertainty is thus given by the error in radiocarbon measurement (Table 1) and is less than 260 years. Megaturbidites 6 to 8 have been dated through core-to-core correlation with the stratigraphic reference MD04-2861 (Fig. 5). Chronostratigraphy of MD04-2861 was realized through biostratigraphy and correlation with U/Th dating in the Arabian Peninsula (Caley et al., 2011). This radioisotopic data is associated with error ranges of ca. 1 ka (Caley et al., 2011 and references therein). Age of the megaturbidites M9 to M19 were estimated at log Section 1 (Fig. 4). The uncertainty in the age determination was determined by calculating the standard deviation in the calculated ages, considering than more than 95% of the calculated error is contained within twice the standard deviation (Table 2). The mean statistical variance,

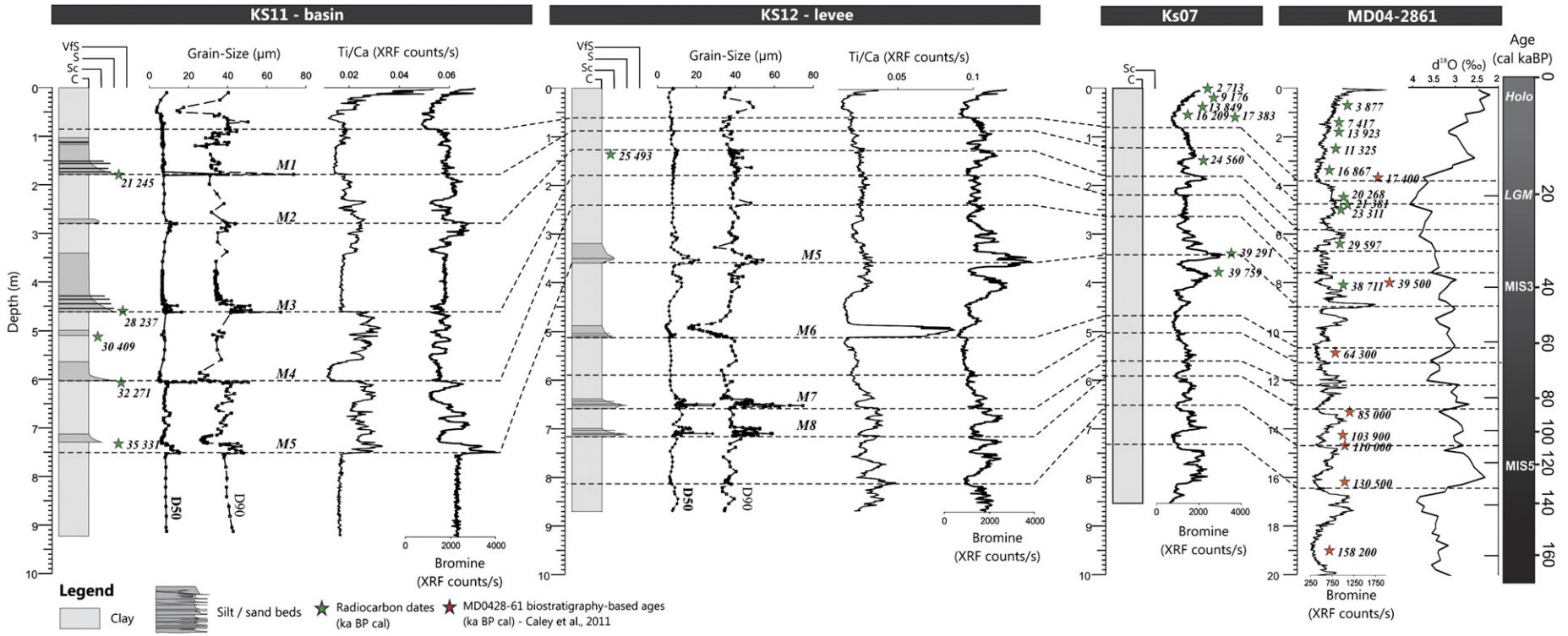


**Fig. 5.** Core correlation and stratigraphy based on grain-size measurement (D50, D90, µm), Bromine (Br) and Ti/Ca XRF measurement, radiocarbon dating and correlation with MD04-2861 regional stratigraphic reference (Caley et al., 2011).

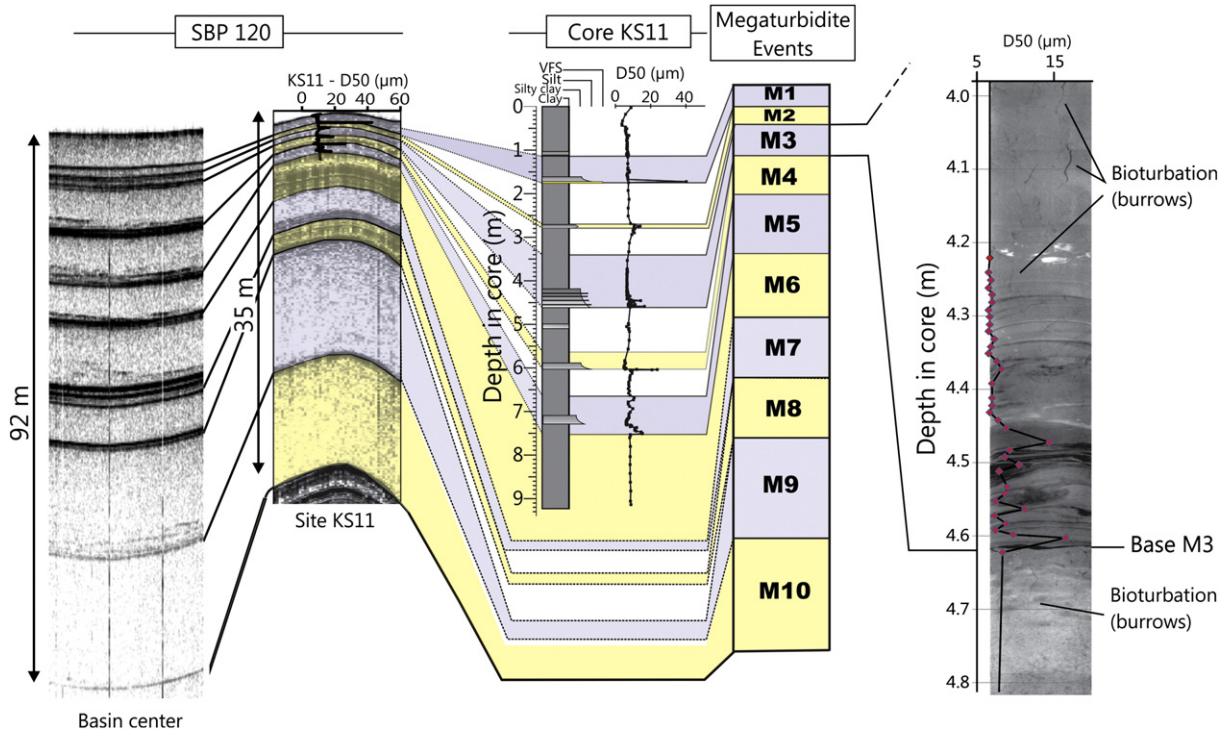


**Fig. 6.** Correlation between KS11 core data (lithology and grain-size measurement) and sub-bottom seismic reflections at site KS11 and in the centre of the 20°N Basin. Close-up on M3 megaturbidite bed showing X-ray core section and D50 (μm) grain-size measurement.

consisting of the mean of the squared differences between the estimated ages of M1–M8 at log Section 1 and their "core data" value, was first calculated. The standard deviation equals the root mean square of this value (Table 2). This provides an error range for the ages of M9–M19 of ca. 10 ka (Table 2). Uncertainty in the age of M20 was estimated by calculating the standard deviation at log Section 2 following the same method. Here the mean variance consists of the mean of the squared differences between the estimated ages of M1–M8 at log Section 2 and their "core data" value, and the estimated ages of M9–M19 at log Section 2 and their estimated age at log Section 1. Error range for M20 reaches 39 ka. However this value adds up to the error range associated with age estimation at log Section 1 (as these values were used to calculate the standard deviation at log Section 2), and the total error range for M20 is 49 ka (Table 2). These uncertainties in age determination are important when considering the timing of megaturbidite emplacement in the 20°N Basin and its relationship with sea-level or climate.

## 5. Discussion

### *5.1. Mechanisms of formation of the 20°N Basin megaturbidites: ponded lobes of the Indus Fan*

#### *5.1.1. Provenance of the turbidity currents*

The discovery of distal megaturbidite deposits at a deep-water plate boundary raises the question of the provenance of the turbidity currents at the origin of their formation. The 20°N Basin is fed by a

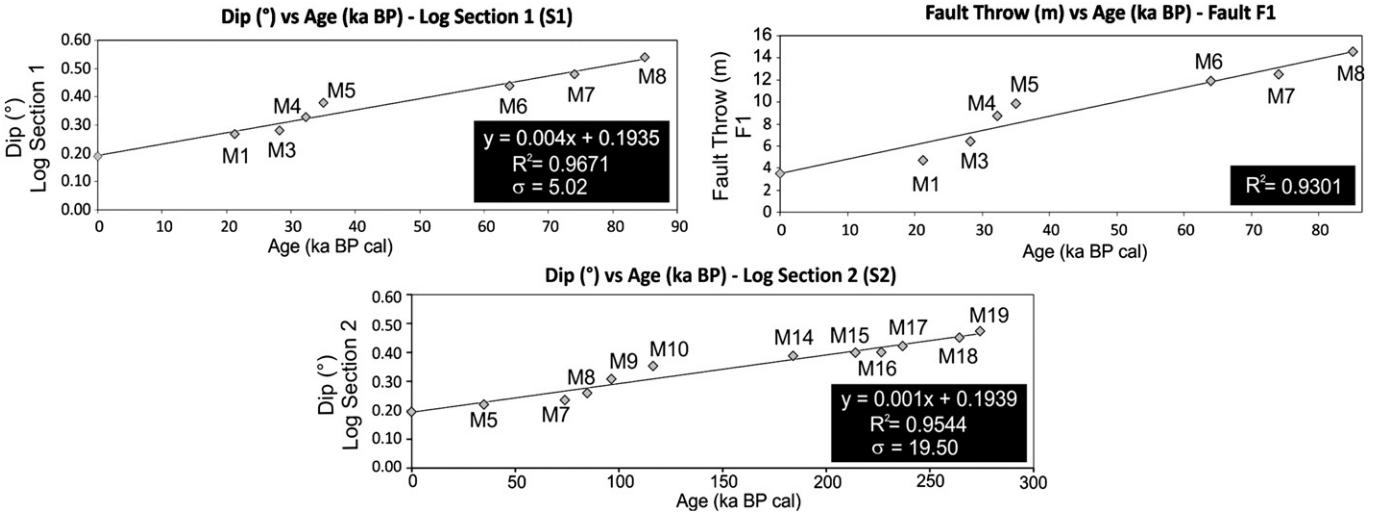


**Fig. 7.** Correlation between dip angle (°) and stratigraphic age at Log Sections 1 and 2 and between fault throw (m) and stratigraphic age at Log Section 1, showing linear regression equation and determination coefficient ($R^2$).

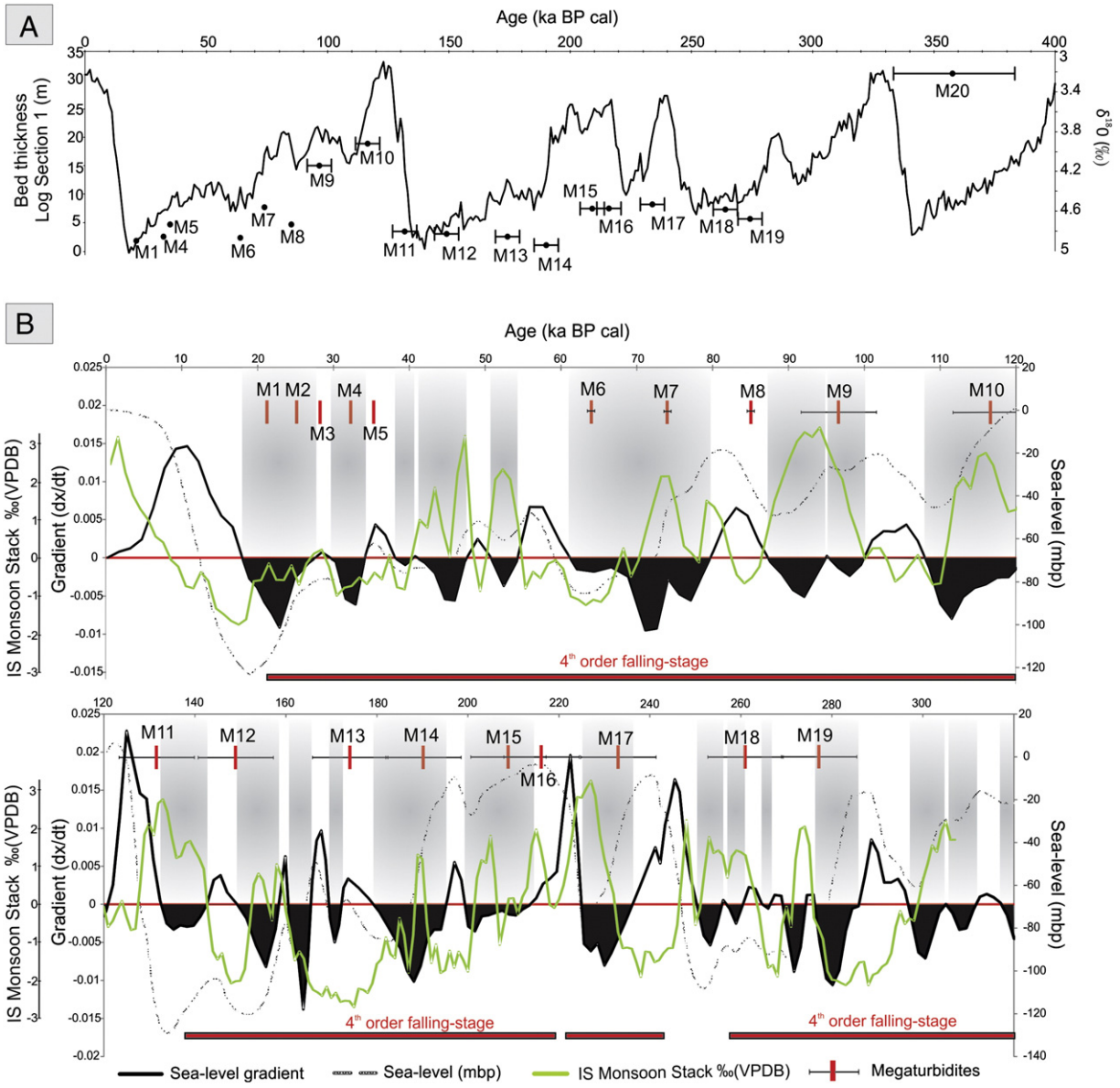


**Fig. 8.** (A) Age of 20°N Basin megaturbidites and LR04 benthic $\delta^{18}O$ stack constructed by the graphic correlation of 57 globally distributed benthic $\delta^{18}O$ records (Lisiecki and Raymo, 2005); (B) age of 20°N Basin megaturbidites and comparison with the global sea-level curve (in mbp – *metres below present* – from Waelbroeck et al., 2002), the sea-level gradient curve (showing periods of sea-level fall (shaded in black color), periods of sea-level rise, and still-stands), and the Indian Summer Monsoon stack from Caley et al (2011) based on core MD04-2861. Error bars on megaturbidites represent the uncertainty in age estimation (Table 2).

channel–levee system trending east to west (Fig. 3), thus indicating a possible connection with the turbidite system of the Indus Fan to the east (Fig. 1). A local origin for the 20°N Basin deposits can be ruled out as slump scars are not observed along the pull-apart basin walls and mass-transport deposits are not observed on seismic profiles (Rodriguez et al., 2011; Figs. 1, 2, 3). Bathymetry and shallow seismic data also show that there is no sediment supply from the Oman margin to the west (Rodriguez et al., 2011; Figs. 1, 3). The bathymetry data used in this study is incomplete but does not suggest a direct linkage with the main Indus canyon upslope (Fig. 1). Instead, the feeder channel of the 20°N Basin is located approximately 200 km downstream of the channel–levee systems of the Canyon system 2 mapped by Kolla and Coumes (1987) from bathymetry and sub-bottom seismic data (Fig. 1). The age of the canyon system 2 and its channel–levee systems is uncertain but the lack of channel-plug deposits on the published seismic data of Kolla and Coumes (1987) suggests that they were active recently and presumably during the Late Quaternary. This is also suggested by the more recent seismic profiles analysed by Carmichael et al. (2009) in the same area (western Indus Fan) that revealed several recent canyons and channel/levee complexes of latest Pleistocene in age (Fig. 1). Thus, it is possible that the 20°N channel was connected to distal channels from the canyon system 2 (Fig. 1) but this remains speculative due to the limitations of the data presently available and the lack of stratigraphic control in the original data of Kolla and Coumes (1987). However the data available suggest that the megaturbidites of the 20°N Basin are distal turbidite deposits of the Indus Fan.

### 5.1.2. Ponded lobe deposits

The distal parts of deep-water turbidite systems are often associated with the formation of channel-mouth lobe complexes. The latter form depositional areas where sands are generally concentrated as the gravity currents have been progressively depleted in fine-grained sediments through overbank processes along the channel–levee systems. Along mud-rich, passive margin turbidite systems such as the Indus Fan,

channel-mouth lobes develop across unconfined basin plains and generally extend over very large distances, exceeding 100 km on the Amazon, Nile, Zaire or Mississippi fans (Twichell et al., 1991; Savoye et al., 2000; Jegou et al., 2008; Migeon et al., 2010). These lobes typically form highly ramified, channelized and elongated depositional environments. In the Indus Fan, deep sea lobes from the last active channel/levee complexes (CLC A and B) also developed over very large distances across the very low gradient, eastern basin plain (Kenyon et al., 1995). Conversely the last active channel–levee system in the study area abruptly terminates its course in a very confined trough, less than 13 km-wide and up to 320 m-deep at this location (Fig. 1). Individual lobe deposits in mud-rich fans are dispersed over very large distances (>100 km) and form relatively thin (typically cm to dm-thick) deposits (Twichell et al., 1991; Bonnel, 2005; Migeon et al., 2010). However the range of thicknesses and volumes of individual lobe deposits in other mud-rich fans approaches the values obtained in the 20°N Basin. A 20 cm, 50 cm, or 1 m thick turbidite (e.g., range of lobe thickness deposits in mud-rich deep-sea lobes; Twichell et al., 1991; Bonnel, 2005; Migeon et al., 2010) deposited within a lobe area of 4800 km$^2$ (the size of the Nile deep-sea lobes off the Rosetta channel–levee complex; Migeon et al., 2010) represent a volume of 0.96, 2.4, and 4.8 km$^3$, respectively. This is of similar if not higher order of magnitude than the values calculated for M1–M8 megaturbidites in the 20°N Basin (0.4 to 2.79 km$^3$; Table 2), which is only 260 km$^2$ in area (Fig. 1). Thus the great thickness of each turbidite event in the 20°N Basin is more likely related to the confinement of the depositional area rather than to an exceptional volume of sediment transported by gravity currents. Therefore, the Indus megaturbidites differ from the previously described megaturbidites of the Quaternary that are usually thinner (7 m-thick deposit on average) but laterally extensive (51,000 km$^2$ on average) and are rather similar to ancient megaturbidites, generally thicker (average 40 m) but deposited in confined basins (435 km$^2$ on average; Reeder et al., 2000; Mulder et al., 2009). Considering the volume of individual turbidite deposits in the 20°N Basin, it is unlikely that turbidity currents at their origin were formed through local mass-reworking of levee deposits from the upper Indus Fan, although it is possible that downslope erosion along the turbidity current pathway may have contributed to the final turbiditic volumes observed in the 20°N Basin. The thick, acoustically-transparent seismic facies of the 20°N Basin megaturbidites is a characteristic often observed in ponded turbidites deposits (e.g., Cita and Aloisi, 2000; Tripsanas et al., 2004; Beck et al., 2007). Thick acoustically-transparent layers correspond to ungraded, often structureless clastic muds representing fallout from a suspension cloud produced by axial ponding of the muddy tail of turbidity currents (Pickering and Hiscott, 1985; Haughton, 1994; Mulder et al., 2009). Therefore, the capture of a distal Indus turbidite channel by the 20°N pull-apart basin resulted in the formation of the very thick (individually up to 20 m), mud-rich megaturbidite beds through flow ponding in a confined trough. These form unusual deposits equivalent to distal "lobe" deposits trapped at a transform (strike-slip) plate boundary.

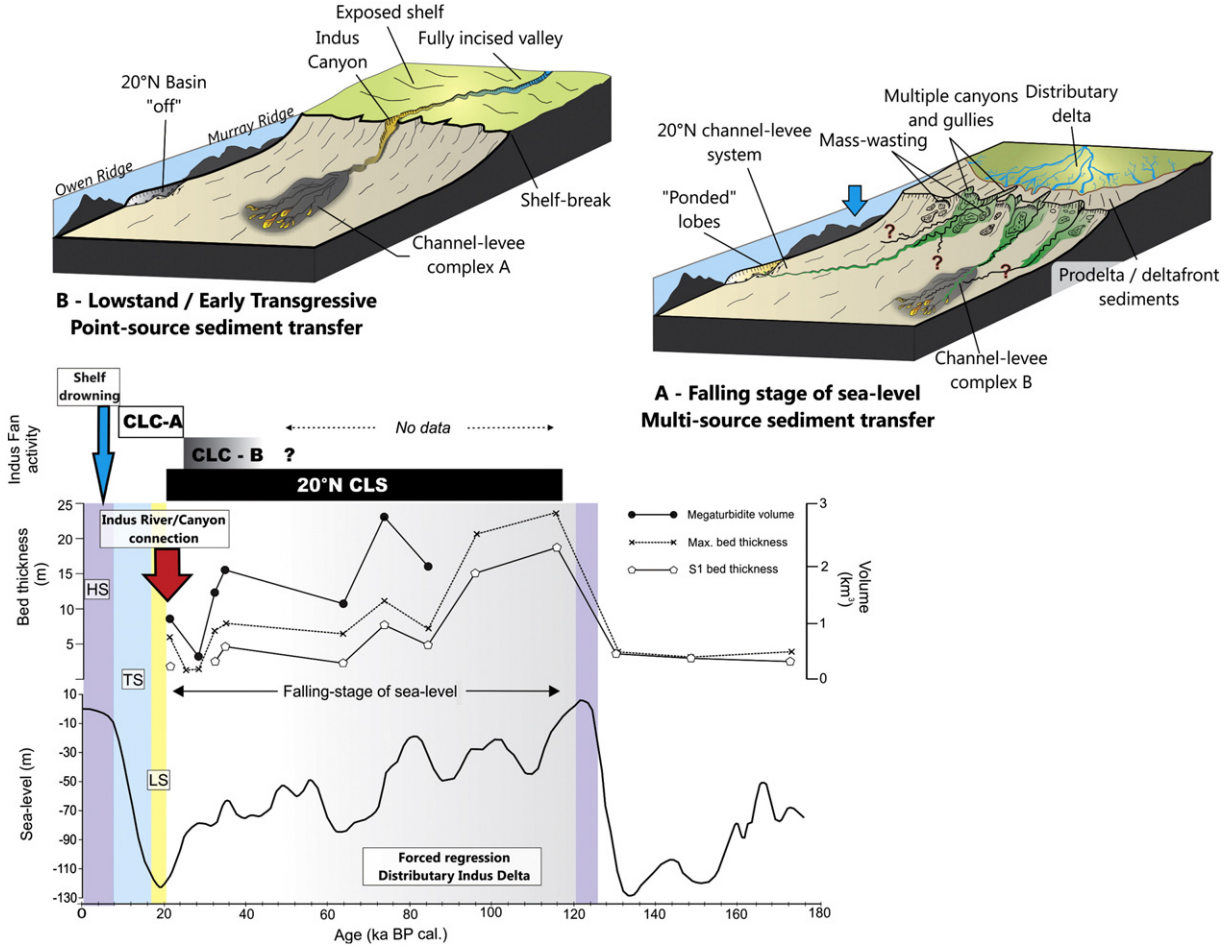


**Fig. 9.** Late Quaternary (last 122 ka BP) evolution of the Indus Delta and turbidite system: comparison between the measured thicknesses of 20°N megaturbidite deposits at Log Section 1 (S1, m) and in the basin centre (Max. bed thickness, m), their estimated volume (km$^3$) and the relative sea-level curve (m below its present-day position) from Waelbroeck et al. (2002). Periods of activity of the channel–levee complexes A and B (Kenyon et al., 1995; Prins and Postma, 2000; Prins et al., 2000) and 20°N Basin (this study) are indicated. LS = sea-level lowstand; TS = transgression; HS = sea-level highstand.

### 5.2. Late Quaternary evolution of the Indus Fan and stratigraphic significance of the 20°N Basin megaturbidites

#### 5.2.1. Link between the 20°N megaturbidites, sea-level and climate

The comparison of the age and thickness of the best dated sequence of megaturbidites of the 20°N Basin (M1–M10) with the oxygen isotope and sea-level record of the Late Quaternary primarily shows two main trends (Figs. 8 & 9). Firstly, the deposition of the megaturbidites occurred within the context of a 4th-order (ca. 100 ka-duration) falling-stage of sea-level period (Figs. 8 & 9). In addition, the maximum bed thickness of the megaturbidites (measured in the basin centre), their bed thickness measured at log Section 1, and their estimated volume all globally decrease with their age (Figs. 8 & 9). These observations suggest that the volume of sediments brought by individual turbidity current to the 20°N Basin decreased with time as the sea-level felt (i.e., in conditions of forced regression). These trends are less pronounced for older megaturbidites (M11–M20; Fig. 8). Measurements at log Section 1 show that within megaturbidites deposited during the previous sea-level fall period (ca. 216–128 ka BP), M15 and M16 are thicker (7.5 m) than M14–M11 (0.9–3.5 m). Megaturbidites M17–M20 were formed in different 4th-order falling sea-level periods, where the low number of megaturbidites recorded precludes drawing significant conclusions (Fig. 8). Whether the 20°N Basin megaturbidites were deposited in conditions of high-frequency sea-level fall, rise or stillstand is more difficult to apprehend considering the limitations of the dataset. In particular, the error ranges associated with the age calculations for megaturbidites M9 to M19 (10 ka) and M20 (49 ka) need to be taken in account (Fig. 8). A gradient curve was calculated from the sea-level curve of Waelbroeck et al. (2002) in order to identify periods and rates of sea-level changes at high-frequency (Fig. 8). The results show that the age of 5 out of 8 (62.5%) of the best dated sequences (M1–M8) corresponds to a period of sea-level fall (Fig. 8). Similarly, eight out of eleven (72%) megaturbidites with higher uncertainty in age estimation (M9–19) correspond to periods of sea-level fall (with more than 50% of their age range coinciding with falling-stage periods; Fig. 8). In conclusion, the comparison between megaturbidite emplacement in the 20°N Basin and sea-level changes suggest that megaturbidites were formed during 4th-order sea-level fall periods, but their link with high-frequency sea-level changes is difficult to establish, maybe due to the low number of events and the errors in age estimation (Figs. 8 & 9).

The possible linkage between the timing of megaturbidite emplacement and climate-induced periods of increased sediment discharge in the Indus catchment is another interesting parameter to investigate. Indeed, monsoon-induced humid periods directly influenced the Late Quaternary evolution of basinward sediment transfer along the nearby Makran margin, resulting in more frequent, finer-grained turbidite system growth (Bourget et al., 2010). Similar monsoon-induced control on turbidite system growth was observed in the Nile turbidite system (Ducassou et al., 2009). However, the Indus River catchment includes the western part of the Himalayan orogen where glaciers develop (Benn and Owen, 1998; Owen et al., 2008). Continental record shows that the timing of glaciation within the Indus River catchment during the Late Quaternary was not synchronous with the global ice-volume maximum (Benn and Owen, 1998). Instead, regional glacier expansion coincided with the Northern Hemisphere insolation maxima and periods of enhanced summer monsoon (Benn and Owen, 1998; Owen et al., 2008). The increase in precipitation rates in the very high altitude Indus River catchment was associated with snowing and glacial advance (Owen et al., 2008). Therefore, maximum river discharge at the Indus River mouth and periods of increased turbidite system growth would coincide with melt-water pulses in deglacial periods, as is commonly observed in glacial-influenced turbidite systems of the Northern Hemisphere (e.g., Zaragosi et al., 2006). However, the comparison of the megaturbidite stratigraphy with the Indian Summer Monsoon stack of Caley et al. (2011) does not show any significant relationship between summer monsoon intensity and the 20°N Basin megaturbidites (Fig. 8). The megaturbidites do not systematically form following a peak in summer monsoon intensity (i.e., a likely melt-water pulse event) and no clear trend can be observed (Fig. 8). However this apparent lack of correlation could be the result of the error ranges in age estimation, as well as the very distal location of the 20°N Basin with regards to the Indus Delta (Fig. 1).

#### 5.2.2. A progressive confinement of sediment supply to the basin during the last sea-level cycle?

The 20°N Basin megaturbidites have been deposited during 4th-order periods of falling sea-level (Figs. 8 & 9). The best dated sequence, which corresponds to the last ten events (M1–M10), shows a decrease in megaturbidite thickness and volumes during the last sea-level fall period of the Quaternary. This stratigraphic evolution forms two apparent paradoxes:(i) the presence of a thinning-upward deep-water sequence within a period of forced-regression and increase in source-to-sink sediment transfer (Posamentier and Kolla, 2003; Catuneanu et al., 2009), and (ii) the cessation of turbidite activity in the 20°N Basin at the onset of the LGM, whilst the Indus River directly discharged sediments into the Indus Canyon and led to maximum fan aggradation into the basin (Kenyon et al., 1995; Prins and Postma, 2000; Prins et al., 2000). To understand this phenomenon, the linkage between the 20°N Basin and the upstream part of the Indus Fan need to be investigated, and the megaturbidites need to be replaced in the context of global evolution of the Indus sedimentary system during the Late Quaternary (Fig. 9).

Recent evolution of the Indus Delta has been marked by basinward progradation with 98% of the Indus River pre-damming sediment load being deposited in delta front (86%) and prodelta (13%) clinoforms (Giosan et al., 2006). Thus Holocene sedimentation in the Indus Delta corresponds to typical conditions of stillstand normal regression (Posamentier et al., 1989; Posamentier and Kolla, 2003; Catuneanu et al., 2009). Sediments are temporarily stored along the continental shelf during this highstand period and deep-water sediment deposition is therefore very limited, and restricted to occasional flushing of delta-front and pro-delta sediments in the Indus Canyon (von Rad and Tahir, 1997; Prins et al., 2000). Indus Delta-basin configuration during the MIS 5 sea-level highstand was likely similar to the present day conditions. The following onset of sea-level drop at ~122 ka BP was associated with forced regression of the delta (von Rad and Tahir, 1997), where either multiple river distributaries and/or tidal reworking could have created multiple points of sediment entry in the outer shelf (Fig. 9). Indeed, von Rad and Tahir (1997) mapped numerous buried or semi-buried channels and gullies west and east of the main Indus Canyon. Their results showed that they were formed during the last ~122 ka BP, and prior to the Last Glacial Maximum lowstand, in conditions of high rates of delta front/prodelta progradation and high sediment supply. This period was also associated with widespread mass-wasting in the upper-slope area (von Rad and Tahir, 1997). High sediment supply rates were likely enhanced by both rapid progradation of the Indus Delta toward the shelf-break and remobilization of the large volumes of delta-front and pro-delta fine-grained sediments accumulated on the continental shelf during the preceding highstand. It is also possible that other canyon systems were active during this period (Fig. 9), including the canyon system 2 (Fig. 1) of Kolla and Coumes (1987), although this remains speculative due to the lack of age control. Basinward, both channel–levee complex B, to the east (Kenyon et al., 1995; Prins et al., 2000) and the 20°N channel–levee system, to the west (this study) were synchronously active (Fig. 9). Thus turbidity currents originated from the Indus Delta were transported through at least two different channel–levee systems to the south-east (CLC B) and west (20°N channel) prior to the Last Glacial Maximum, in addition to the multiple shelf-edge canyon and gullies mapped by von Rad and Tahir (1997). The combination of the results obtained in the present study with previously published data suggests that during the last

falling stage of sea-level period, the Indus Fan consisted of a delta-fed turbidite system with several active canyons-channels system (Fig. 9).

According to Prins et al. (2000), avulsion from CLC B to CLC A occurred at around 28 ka BP, i.e. during period of rapid sea-level fall of about 60 m (Lea et al., 2002; Waelbroeck et al., 2002; Clark et al., 2009) that likely promoted shelf incision and erosion. This age is also only slightly younger than the age of the last turbiditic deposit the 20°N Basin (21.2 ka BP; Fig. 9). During the following sea-level lowstand and early transgression periods, the channel–levee systems of CLC A are the only known active turbidity current pathways (Prins et al., 2000). This suggests that the Indus Fan ultimately evolved from a multiple-source, delta-fed turbidite system to a point source, "river-canyon" turbidite system following the abrupt drop in sea-level at MIS 3/2 transition (Fig. 9). We infer that the last thinning-upward sequence in the 20°N Basin reflects the local, progressive diminution of sediment supply at the source of the 20°N Basin channel, as the Indus Delta evolved from a distributary delta (multiple points of sediment entry) to a single-channelled, incised valley system (one unique point of sediment entry in the Indus Canyon). The observation of two vertically-stacked thinning-upward megaturbidite sequences on seismic profiles (M1–M10, M11–M20; Figs. 2 & 4) suggests that this sea-level controlled depositional evolution could have repeated during the Quaternary. However age estimation for megaturbidite M20 falls out of the 330–135 ka BP falling-stage of sea-level sequence (Fig. 8). This result could highlight a discontinuous sediment supply to the 20°N Basin between 357 and 277 ka BP (Fig. 8), but could also be related to an overestimated M20 age caused by non-steady-state local deformation rates.

The megaturbidite depositional history of the 20°N Basin generally reflects a diminution of local sediment supply through times, during periods of global increase in sediment supply in the basin (Fig. 8). This highlights the importance of delta evolution during forced regressions (river entrenchment) for the spatial and temporal distribution of deep-water sediments.

## 6. Conclusion

The formation of a pull-apart basin at the Arabian-Indian transform plate boundary led to the capture of a Late Quaternary channel–levee system from the Indus Fan. Architecture of the 20°N Basin consists of a vertical stack of up to 23 m thick megaturbidites laterally confined in a 260 km$^2$ basin. Each of these beds corresponds to the deposition from a single gravity current. Unlike most of the previously described megaturbidites of the Quaternary, 20°N Basin deposits do not result from exceptionally large volumes of sediment reworked through mass-wasting processes. Conversely, they are related to the ponding of "classical" turbidity currents transported along a sinuous channel–levee system that abruptly terminates in a distal, confined pull-apart basin. Therefore they form unusual, "ponded" lobe deposits from the Indus Fan. The ten most recent megaturbidites have been deposited during the last falling stage of sea-level cycle. Both thickness and volume of each individual megaturbidite is decreasing through the last 122 ka BP. Local turbidite deposition ceases after 21 ka, i.e. during the sea-level lowstand period, when the Indus River was directly connected to the Indus Canyon enhancing maximum sediment transfer to the deep basin. This apparent paradox is analyzed in terms of sea-level control on source-to-sink sediment dispersal modes in the Indus sedimentary system. At least two channel–levee systems were active during the last falling stage of sea-level period, and were fed by a prograding delta (forced regression) with multiple points of sediment entry distributed along the outer shelf and shelf-break. Turbidite transfer locally decreased within these systems as the Indus River became increasingly entrenched in an incised valley and progressively focused its sediment discharge into the Indus Canyon. This led to the disconnection of the older channel–levee systems and development of a point-source turbidite system that remained active throughout the lowstand and early transgressive stages. This work shed new light on the recent evolution of the Indus sedimentary system and illustrates the importance of sea-level control on the sedimentary transfer mechanisms during forced regressive periods.

## Acknowledgment

We are indebted to all the crew from the "Owen" and "FanIndien" surveys 2009 (*BHO Beautemps-Beaupré*) for their assistance in data acquisition. We thank Peter Talling, an anonymous reviewer and the editor D. J. W Piper for their insightful reviews that greatly improved the paper.

## References

Beck, C., Mercier de Lepinay, B., Schneider, J.-L., Cremer, M., Cagatay, N., Wendenbaum, E., et al., 2007. Late Quaternary co-seismic sedimentation in the Sea of Marmara's deep basins. Sedimentary Geology 199, 65–89.
Benn, D.I., Owen, L.A., 1998. The role of the Indian summer monsoon and the mid-latitude westerlies in Himalayan glaciation: review and speculative discussion. Journal of the Geological Society of London 155, 353–363.
Bonnel, C., 2005. Mise en place des lobes distaux dans les systèmes turbiditiques actuels: Analyse comparée des systèmes du Zaïre, Var et Rhône. Unpublished Ph.D Thesis, Université Bordeaux 1, p. 314.
Bouma, A.H., 1962. Sedimentology of Some Flysch Deposits: A Graphic Approach to Facies Interpretation. Elsevier, Amsterdam.
Bouma, A.H., 1985. Introduction of submarine fans and related Turbidite facies. In: Bouma, A.H., Barnes, N.E., Normark, W.R. (Eds.), Submarine Fans and Related Turbidite Sequences. SpringerVerlag, NewYork, pp. 3–5.
Bouma, A.H., 1987. Megaturbidite: an acceptable term? Geo-Marine Letters 7, 63–67.
Bouma, A.H., Stelting, C.E., Coleman, J.M., 1985. Mississippi fan: Gulf of Mexico. In: Bouma, A.H., Barnes, N.E., Normark, W.R. (Eds.), Submarine Fans and Related Turbidite Sequences. Springer-Verlag, NewYork, pp. 143–150.
Bourget, J., Zaragosi, S., Garlan, T., Gabelotaud, I., Guyomard, P., Dennielou, B., et al., 2008. Discovery of a giant deep-sea valley in the Indian Ocean, off eastern Africa: the Tanzania channel. Marine Geology 255, 179–185.
Bourget, J., Zaragosi, S., Ellouz-Zimmermann, S., Ducassou, E., Prins, M.A., Garlan, T., et al., 2010. Highstand vs. lowstand turbidite system growth in the Makran active margin: Imprints of high-frequency external controls on sediment delivery mechanisms to deep water systems. Marine Geology 274, 187–208.
Bourget, J., Mouchot, N., Zaragosi, S., Ellouz-Zimmermann, N., Garlan, T., Lanfumey, V., VanToer, A., Schneider, J.-L., 2011. Turbidite system architecture and sedimentary processes along topographically complex slopes: the Makran convergent margin. Sedimentology 58 (2), 376–406.
Boyd, R., Ruming, K., Goodwin, I., Sandstrom, M., Schröder-Adams, C., 2008. Highstand transport of coastal sand to the deep ocean: a case study from Fraser Island, southeast Australia. Geology 36, 15–18.
Caley, T., Malaizé, B., Zaragosi, S., Rossignol, L., Bourget, J., Eynaud, F., et al., 2011. New Arabian Sea records help decipher orbital timing of Indo-Asian monsoon. Earth and Planetary Science Letters 308, 433–444.
Carmichael, S.M., Akhter, S., Bennett, J.K., Fatimi, M.A., Hosein, K., Jones, R.W., et al., 2009. Geology and hydrocarbon potential of the offshore Indus Basin, Pakistan. Petroleum Geoscience 15, 107–116.
Catuneanu, O., Abreu, V., Bhattacharya, J.P., Blum, M.D., Dalrymple, R.W., Eriksson, P.G., et al., 2009. Towards the standardization of sequence stratigraphy. Earth-Science Reviews 92, 1–33.
Cita, M.B., Aloisi, G., 2000. Deep-sea tsunami deposits triggered by the explosion of Santorini (3500 y BP), eastern Mediterranean. Sedimentary Geology 135, 181–203.
Cita, M.B., Rimoldi, B., 1997. Geological and geophysical evidence for a holocene tsunami deposit in the astern Mediterranean deep-sea record. Journal of Geodynamics 24, 293–304.
Cita, M.B., Beghi, C., Camerlenghi, A., Kastens, K.A., McCoy, F.W., Nosetto, A., et al., 1984. Turbidites and megaturbidites from the Herodotus abyssal plain (eastern Mediterranean) unrelated to seismic events. Marine Geology 55, 79–101.
Clark, P.U., Dyke, A.S., Shakun, J.D., Carlson, A.E., Clark, J., Wohlfarth, B., et al., 2009. The Last Glacial Maximum. Science 325, 710–714.
Clift, P.D., Shimizu, N., Layne, G.D., Blusztajn, J.S., Gaedicke, C., Schluter, H.-U., et al., 2001. Development of the Indus Fan and its significance for the erosional history of the Western Himalaya and Karakoram. Geological Society of America Bulletin 113, 1039–1051.
Clift, P., Gaedicke, C., Edwards, R., Lee, J.I., Hildebrand, P., Amjad, S., et al., 2002. The stratigraphic evolution of the Indus fan and the history of sedimentation in the Arabian Sea. Marine Geophysical Researches 223–245.
Coumes, F., Kolla, V., 1984. Indus Fan: seismic structure, channel migration and sediment thickness in the upper fan. In: Haq, B.U., Milliman, J.D. (Eds.), Van Nostrand Reinhold Comp., New York, pp. 101–110.
Droz, L., Mougenot, D., 1987. Mozambique upper fan: origin of depositional units. AAPG Bulletin 71, 1355–1365.
Ducassou, E., Migeon, S., Mulder, T., Murat, A., Capotondi, L., Bernasconi, S.M., et al., 2009. Evolution of the Nile deep-sea turbidite system during the Late Quaternary: influence of climate change on fan sedimentation. Sedimentology 56, 2061–2090.

Fournier, M., Chamot-Rooke, N., Petit, C., Fabbri, O., Huchon, P., Maillot, B., et al., 2008. In situ evidence for dextral active motion at the Arabia–India plate boundary. Nature Geoscience 1, 54–58.
Fournier, M., Chamot-Rooke, N., Rodriguez, M., Huchon, P., Petit, C., Beslier, M.O., et al., 2011. Owen fracture zone: the Arabia–India plate boundary unveiled. Earth and Planetary Science Letters 302, 247–252.
Giosan, L., Constantinescu, S., Clift, P.D., Tabrez, A.R., Danish, M., Inam, A., 2006. Recent morphodynamics of the Indus delta shore and shelf. Continental Shelf Research 26, 1668–1684.
Goldfinger, C., Nelson, C.H., Johnson, J.E., Party, T.S.S., 2003. Holocene earthquake records from the Cascadia subduction zone and northern San Andreas fault based on precise dating of offshore turbidites. Annual Review of Earth and Planetary Sciences 31, 55–77.
Haughton, P., 1994. Deposits of deflected and ponded turbidity currents, Sorbas basin, southeast Spain. Journal of Sedimentary Research A64, 233–246.
Jegou, I., Savoye, B., Pirmez, C., Droz, L., 2008. Channel–mouth lobe complex of the recent Amazon Fan: the missing piece. Marine Geology 252, 62–77.
Karim, A., Veizer, J., 2002. Water balance of the Indus River Basin and moisture source in the Karakoram and western Himalayas: implications from hydrogen and oxygen isotopes in river water. Journal of Geophysical Research 107, 4362.
Kenyon, N.H., Amir, A., Cramp, A., 1995. Geometry of the younger sediment bodies of the Indus Fan. In: Pickering, K.T., Hiscott, R.N., Kenyon, N.H., Ricci Lucchi, F., Smith, R.D.A. (Eds.), Atlas of Deep Water Environments: Architectural Style in Turbidite Systems. Chapman & Hall, London, pp. 89–90.
Khripounoff, A., Vangriesheim, A., Babonneau, N., Crassous, P., Dennielou, B., Savoye, B., 2003. Direct observation of intense turbidity current activity in the Zaire submarine valley at 4000 m water depth. Marine Geology 194, 151–158.
Kolla, V., Coumes, F., 1987. Morphology, internal structure, seismic stratigraphy, and sedimentation of Indus Fan. AAPG Bulletin 650–677.
Kolla, V., Kostecki, J.A., Henderson, L., Hess, L., 1980. Morphology and Quaternary sedimentation of the Mozambique Fan and environs, southwestern Indian Ocean. Sedimentology 27, 357–378.
Lea, D.W., Martin, P.A., Pak, D.K., Spero, H.J., 2002. Reconstructing a 350 ky history of sea level using planktonic Mg/Ca and oxygen isotope records from a Cocos Ridge core. Quaternary Science Reviews 21, 283–293.
Lisiecki, L.E., Raymo, M.E., 2005. A Pliocene–Pleistocene stack of 57 globally distributed benthic $^{18}O$ records. Paleoceanography 20, 1–17.
Mas, V., Mulder, T., Dennielou, B., Schmidt, S., Khripounoff, A., Savoye, B., 2010. Multiscale spatio-temporal variability of sedimentary deposits in the Var turbidite system (North-Western Mediterranean Sea). Marine Geology 275, 37–52.
McHargue, T.R., Webb, J.E., 1986. Internal geometry, seismic facies, and petroleum potential of canyons and inner fan channels of the Indus submarine fan. AAPG Bulletin 161–180.
Migeon, S., Ducassou, E., Le Gonidec, Y., Rouillard, P., Mascle, J., Revel-Rolland, M., 2010. Lobe construction and sand/mud segregation by turbidity currents and debris flows on the western Nile deep-sea fan (Eastern Mediterranean). Sedimentary Geology 229, 124–143.
Milliman, J.D., Quraishee, G.S., Beg, M.A.A., 1984. Sediment discharge from the Indus River to the ocean: past, present and future. In: Haq, B.U., Milliman, J.D. (Eds.), Marine Geology and Oceanography of Arabian Sea and Coastal Pakistan. Van Nostrand Reinhold, New York, pp. 65–70.
Mulder, T., Zaragosi, S., Razin, P., Grelaud, C., Lanfumey, V., Bavoil, F., 2009. A new conceptual model for the deposition process of homogenite: application to a cretaceous megaturbidite of the western Pyrenees (Basque region, SW France). Sedimentary Geology 222, 263–273.
Normark, W.R., 1978. Fan valleys, channels, and depositional lobes on modern submarine fans: characters for recognition of sandy turbidites environments. AAPG Bulletin 62, 912–931.
Owen, L.A., Caffee, M.W., Finkel, R.C., Seong, Y.B., 2008. Quaternary glaciation of the Himalayan–Tibetan orogen. Journal of Quaternary Science 23, 513–531.
Peakall, J., McCaffrey, B., Kneller, B., 2000. A process model for the evolution, morphology, and architecture of sinuous submarine channels. Journal of Sedimentary Research 70, 434–448.
Pickering, K.T., Hiscott, R.N., 1985. Contained (reflected) turbidity currents from the Middle Ordovician Cloridorme Formation, Quebec, Canada: an alternative to the antidune hypothesis. Sedimentology 32, 373–394.
Piper, D.J.W., Normark, W.R., 2001. Sandy fans–from Amazon to Hueneme and beyond. AAPG Bulletin 85, 1407–1438.
Pirmez, C., Flood, R.D., 1995. Morphology and structure of Amazon Channel. In: Flood, R.D., Piper, D.J.W., Klaus, A., et al. (Eds.), Proceedings of the Ocean Drilling Program, Initial Reports. Ocean Drilling Program, College Station, TX, pp. 23–45.
Posamentier, H.W., Kolla, V., 2003. Seismic geomorphology and stratigraphy of depositional elements in deep-water settings. Journal of Sedimentary Research 73, 367–388.
Posamentier, H.W., Jervey, M.T., Vail, P.R., 1989. Eustatic controls on clastic deposition I — conceptual framework. In: Wilgus, C.K., et al. (Ed.), Sea-Level Changes: An Integrated Approach. SEPM Special Publication, Tulsa, pp. 110–124.
Posamentier, H.W., Erskine, R.D., Mitchum, R.M.J., 1991. Models for submarine-fan deposition within a sequence-stratigraphic framework. In: Weimer, P., Link, M.H. (Eds.), Seismic Facies and Sedimentary Processes of Submarine Fans and Turbidite Systems. Spring-Verlag, New York, pp. 127–136.
Prins, M.A., Postma, G., 2000. Effects of climate, sea level, and tectonics unraveled for last deglaciation turbidite records of the Arabian Sea. Geology 375–378.
Prins, M.A., Postma, G., Cleveringa, J., Cramp, A., Kenyon, N.H., 2000. Controls on terrigenous sediment supply to the Arabian Sea during the late Quaternary: the Indus Fan. Marine Geology 169, 327–349.
Reading, H.G., Richards, M., 1994. Turbidites systems in deep-water basin margins classified by grain size and feeder system. AAPG Bulletin 792–822.
Rebesco, M., Vedova, B.D., Cernobori, L., Aloisi, G., 2000. Acoustic facies of Holocene megaturbidites in the Eastern Mediterranean. Sedimentary Geology 135, 65–74.
Reeder, M.S., Rothwell, R.G., Stow, D.A.V., 2000. Influence of sea level and basin physiography on emplacement of the late Pleistocene Herodotus Basin Megaturbidite, SE Mediterranean Sea. Marine and Petroleum Geology 17, 199–218.
Reimer, P.J., Baillie, M.G.L., Bard, E., Bayliss, A., Beck, J.W., Blackwell, P.G., et al., 2009. IntCal09 and Marine09 radiocarbon age calibration curves, 0–50,000 years cal BP. Radiocarbon 51, 1111–1154.
Richter, T.O., Van der Gaast, S.J., Koster, B., Vaars, A.J., Gieles, R., De Stigter, H.C., et al., 2006. The Avaatech XRF Core Scanner: technical description and applications to NE Atlantic sediments. In: Rothwell, R.G. (Ed.), New Techniques in Sediment Core Analysis. Special Publications. Geological Society, London, pp. 39–50.
Rodriguez, M., Fournier, M., Chamot-Rooke, N., Huchon, P., Bourget, J., Sorbier, M., et al., 2011. Neotectonics of the Owen Fracture Zone (NW Indian Ocean): structural evolution of an oceanic strike-slip plate boundary. Geochemistry, Geophysics, Geosystems 12, 1–24.
Rodriguez, M., Fournier, M., Chamot-Rooke, N., Huchon, P., Zaragosi, S., Rabaute, A., 2012. Mass wasting processes along the Owen Ridge (Northwest Indian Ocean). Marine Geology 326–328, 80–100.
Rothwell, R.G., Reeder, M.S., Anastasakis, G., Stow, D.A.V., Thomson, J., Kahler, G., 2000. Low sea-level stand emplacement of megaturbidites in the western and eastern Mediterranean Sea. Sedimentary Geology 135, 75–88.
Savoye, B., Cochonat, P., Apprioual, R., Bain, O., Baltzer, A., Bellec, V., et al., 2000. Structure et evolution recente de l'eventail turbiditique du Zaire: premiers resultats scientifiques des missions d'exploration Zaiango1 & 2 (marge Congo-Angola) Structure and recent evolution of the Zaire deep-sea fan: preliminary results of the ZaiAngo 1 & 2 cruises (Angola-Congo margin). Comptes Rendus de l'Academie des Sciences – Series IIA – Earth and Planetary Science 331, 211–220.
Stuiver, M., Reimer, P.J., Bard, E., Beck, J.W., Burr, G.S., Hughen, K.A., et al., 1998. INTCAL98 radiocarbon age calibration, 24,000–0 cal BP. Radiocarbon 40, 1041–1083.
Tripsanas, E.K., Bryant, W.R., Phaneuf, B.A., 2004. Depositional processes of uniform mud deposits (unifites), Hedberg Basin, northwest Gulf of Mexico: New perspectives. AAPG Bulletin 88, 825–840.
Twichell, D.C., Kenyon, N., H., Parson, L.M., McGregor, B.A., 1991. Depositional patterns of the Mississippi Fan surface: evidence from GLORIA II and high-resolution seismic profiles. In: Weimer, P., Link, M.H. (Eds.), Seismic Facies and Sedimentary Processes of Submarine Fans. Springer-Verlag, New York, pp. 349–363.
Vail, P.R., Mitchum, R.M., 1977. Seismic stratigraphy and global changes of sea-level, Part 1: overview. In: Payton, C.E. (Ed.), Seismic Stratigraphy — Applications to hydrocarbon exploration. AAPG Memoir, Tulsa.
von Rad, U., Tahir, M., 1997. Late Quaternary sedimentation on the outer Indus shelf and slope (Pakistan): evidence from high-resolution seismic data and coring. Marine Geology 138, 193–236.
Waelbroeck, C., Labeyrie, L., Michel, E., Duplessy, J.C., McManus, J.F., Lambeck, K., et al., 2002. Sea-level and deep water temperature changes derived from benthic foraminifera isotopic records. Quaternary Science Reviews 21, 295–305.
Wells, J.T., Coleman, J.M., 1984. Deltaic morphology and sedimentology, with special reference to the Indus River delta. In: Haq, B.U., Milliman, J.D. (Eds.), Marine Geology and Oceanography of Arabian Sea and Coastal Pakistan. Van Nostrand Reinhold, New York, pp. 85–100.
Zaragosi, S., Bourillet, J.F., Eynaud, F., Toucanne, S., Denhard, B., Van Toer, A., et al., 2006. The impact of the last European deglaciation on the deep-sea turbidite systems of the Celtic–Armorican margin (Bay of Biscay). Geo-Marine Letters 26, 317–329.
Ziegler, M., Jilbert, T., de Lange, G.J., Lourens, L.J., Reichart, G.J., 2008. Bromine counts from XRF scanning as an estimate of the marine organic carbon content of sediment cores. Geochemistry, Geophysics, Geosystems 9, 212–234.

LA FAILLE DU LEVANT

*Contexte cinématique actuel*

La faille du Levant est remarquablement linéaire et se concentre sur un seul accident sur la majeure partie de sa longueur. La faille du Levant connecte le Golfe d'Elat et la Mer Rouge, au Sud, avec la terminaison Est de la faille Nord Anatolienne (Turquie). Il s'agit d'un décrochement sénestre, d'environ 800 km de long, ayant accommodé près de 110 km de décalage latéral depuis sa mise en place (*Freund et al., 1990 ; Hatcher et al., 1981*). Les études de GPS indiquent que le mouvement sénestre est de l'ordre de 5-8 mm/an, avec une composante convergente croissante le long du segment nord de la faille (*McClusky et al., 2003*). Les petits cercles prédits par les études GPS diffèrent significativement de ceux prédits par les études géologiques de *Le Pichon and Francheteau (1978) et Garfunkel (1981).*

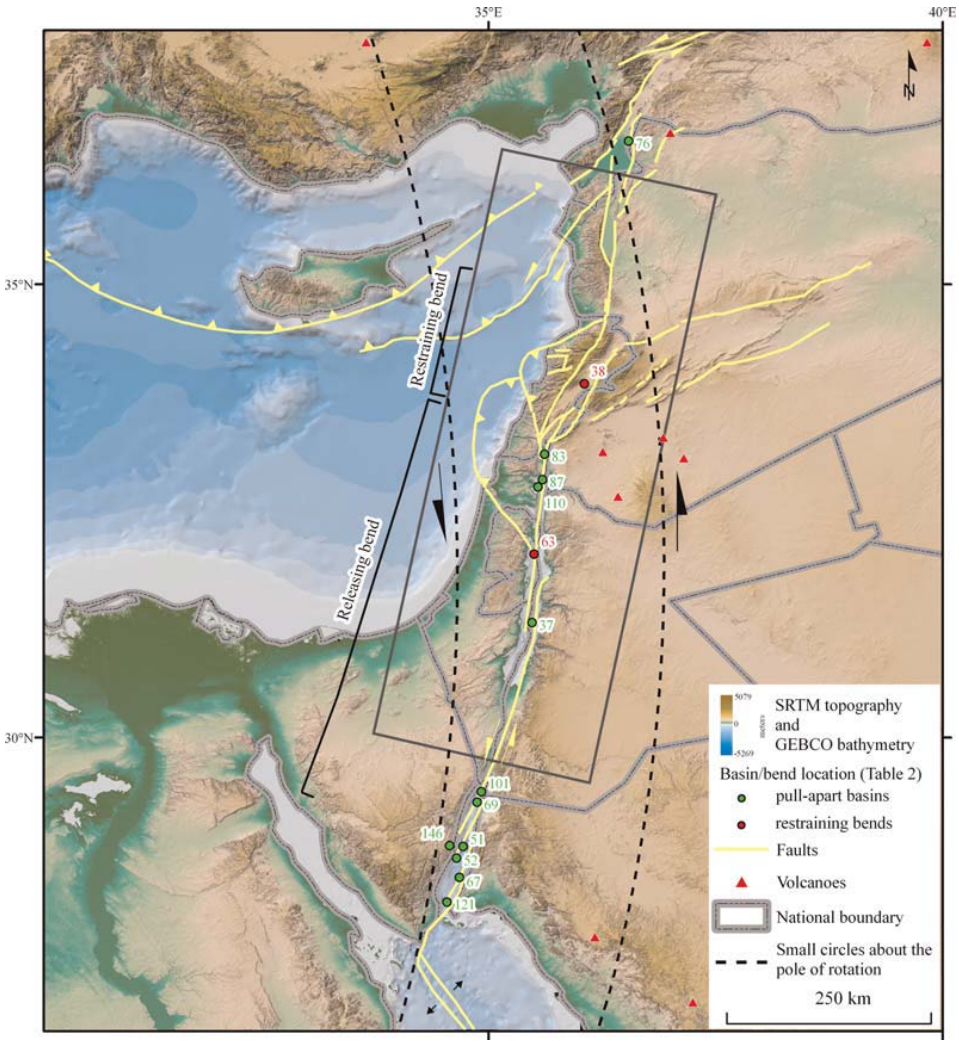


**Figure 1: structure générale et contexte cinématique de la Faille du Levant, d'après Mann, 2007**

*Schéma structural*

La structure générale de la faille du Levant se divise en trois domaines principaux (*Mann, 2007*):

_Un domaine long de 400 km, composé de bassins pull-apart, depuis le Golfe d'Elat jusqu'à la Mer de Galilée, en passant par la Mer Morte et la vallée du Jourdan. Cette section est parallèle aux petits cercles au niveau du Golfe d'Elat, mais devient oblique dans sa partie nord.

_Un domaine long de 200 km, composé du relai transpressif formé par les Monts Liban et Anti-Liban. Les failles sont orientées NE dans cette section, et sont très obliques par rapport à la direction du petit cercle. Le segment de faille actif de la région, la faille de Yammouneh connecte le segment sud et le segment nord de la faille du Levant.

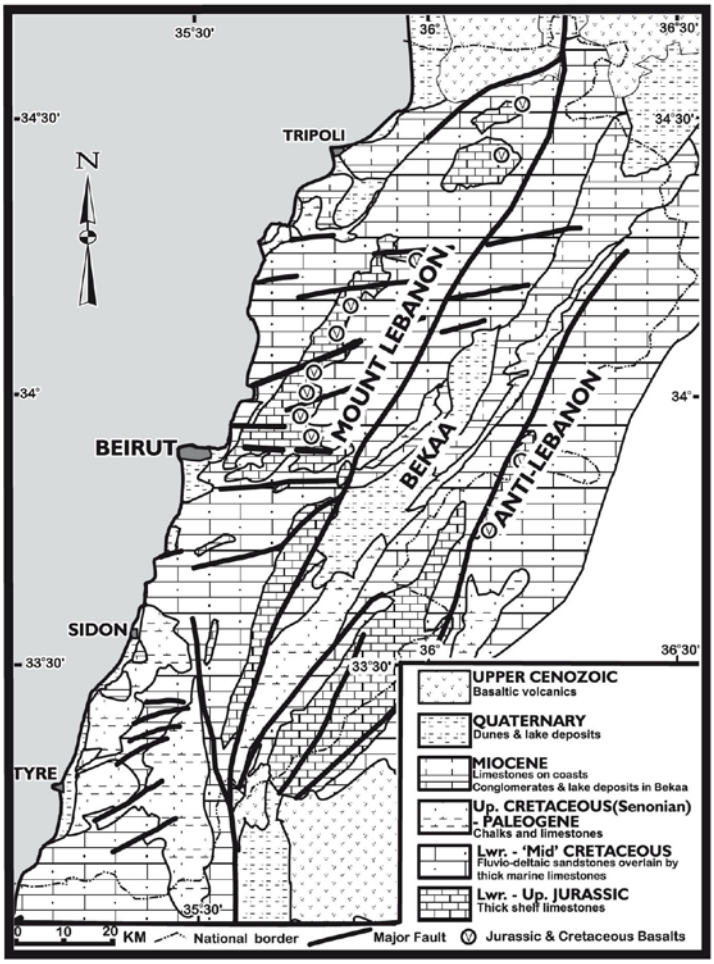


Fig. 2. Generalised geological map of Lebanon. From Dubertret (1955, 1975).

**Figure 2: Schéma structural de la Faille du Levant dans la région des monts du Liban (Dubertret 1955, 1975)**

_Un domaine long de 250 km, dans lequel les failles sont orientées N-S, et forment un bassin pull-apart (*Brew et al., 2001*). Ce domaine recouvre la Syrie et l'Est de la Turquie.

*Un exemple de relai transtensif majeur : la Mer Morte*

Le bassin le plus important est celui de *la Mer Morte*. Il s'agit d'un des plus grands bassins pull -apart actifs dans le monde, avec des dimensions de 110 x 16 km et une profondeur de 8-10 km (*Quennell, 1958, 1959; Aydin and Nur, 1982; Wdowinski and Zilberman, 1997*). Son ouverture s'est initiée entre deux grandes failles longitudinales, les failles de Jericho (à l'Ouest) et de l'Arava (à l'Est). La phase de subsidence principale a débuté il y a environ 3 Ma (*TenBrink et Flores, 2012*). Il est divisé en deux sous bassins : le bassin sud, sub -aérien; et le bassin nord, occupé par un lac qui culmine à -725 m en dessous du niveau de la mer (la différence topographique entre les deux bassins étant de 350 m). Le bassin nord, actif actuellement, est divisé en deux par un large diapir salifère, la péninsule de Lisan. Il s'agit d'un graben d'effondrement (*Ten Brink and Ben Avraham, 1989*), avec plusieurs blocs basculés sur le flanc Ouest du bassin. Les dépôts sédimentaires sont peu déformés à l'intérieur du bassin, sauf dans les endroits où ils sont recoupés par du diapirisme salifère (*Brun et Fort, 2009 + autres*). Ils sont également recoupés par des failles transverses formées lors des différentes migrations du dépôt centre depuis la formation du bassin, au Miocène (*Ten Brink and Ben Avraham, 1989*). Le mécanisme de l'ouverture de ce bassin fait encore l'objet de débats (*Lazar et al., 2006*).

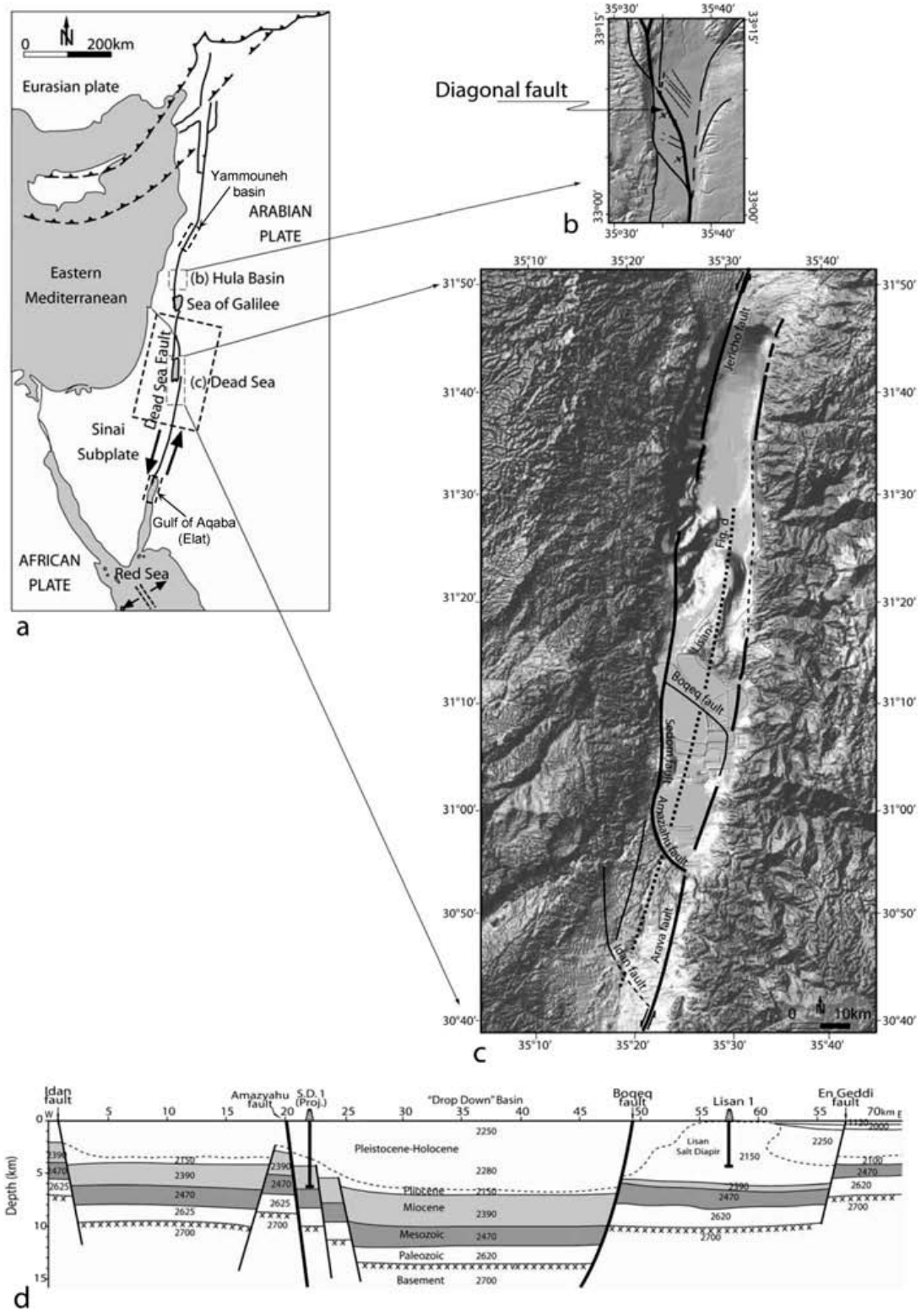


**Figure 3: Contexte géologique et structure des bassins de Hula et de la Mer Morte, d'après Smit et al. (2008)**

*Un exemple de relais transpressif majeur : les Monts du Liban et de l'anti-Liban*

La chaîne de montagne du Liban (point culminant : 3088 m), et ses annexes, l'anti-Liban (point culminant : 2814 m) et les monts des Palmyrides forment deux anticlinoria de socle, à coeur Jurassique, séparés par un synclinorium. Le segment principal de la faille du Levant dans la région, la faille de Yammouneh, est orientée NNE-SSW, et longe le flanc est du Mont Liban. Une série de failles auxiliaires vient se brancher sur cet accident principal et dissèque les plis d'échelle régionale *(Walley et al., 1998)*. La déformation transpressive est partitionnée (Gomez et al., 2007) (4mm/an le long de la faille de Yammouneh ; 2.8 mm/an de raccourcissement au niveau des plis).

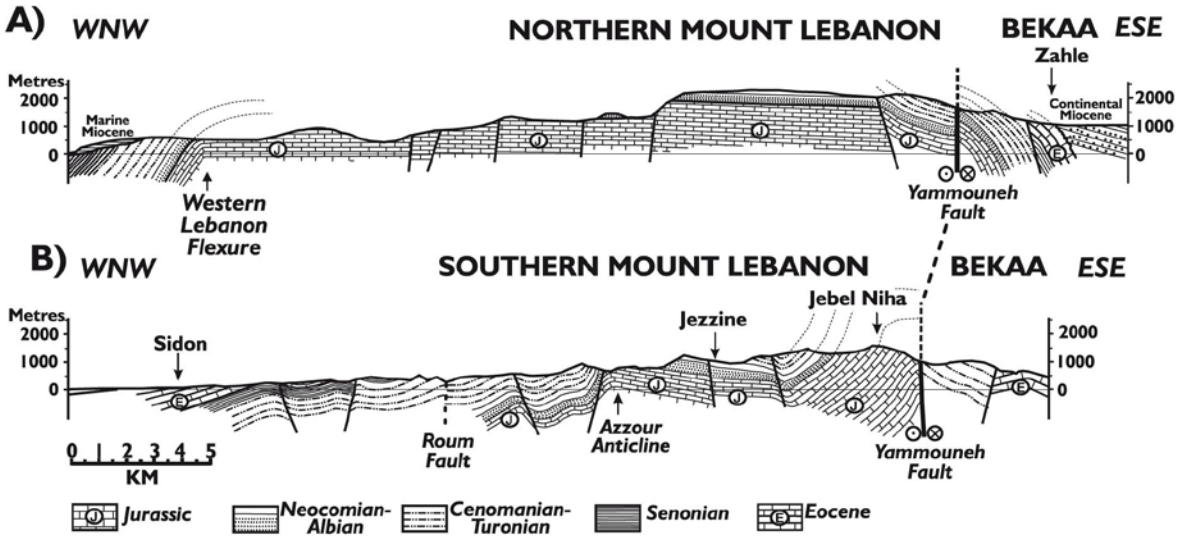

Fig. 4. Summary structural cross-sections of (A) Northern and (B) Southern Mount Lebanon showing differing structural style. Data from Dubertret (1951, 1955), and unpublished studies by G. Sabbagh and A. Guerre. Cross-section locations shown in Fig. 3.

**Figure 4: Coupes géologiques perpendiculaires aux Monts Liban et Anti-Liban, montrant les grands plis anticlinaux recoupés par la Faille du Levant**

*Histoire géologique*

*Mise en place de la faille et évolution structurale*

La faille du Levant s'est mise en place il y a environ 17 Ma (ref). Les 110 km de déplacement sénestre ont été accommodés au cours de deux phases distinctes. La première phase, correspondant à 60 km de déplacement, s'est déroulée au cours du Miocène moyen et tardif. La seconde phase a débuté au début du Pliocene et se poursuit actuellement. La mise en place de la faille du Levant est associée à l'ouverture de la Mer Rouge (Hempton, 1987). Parmi les évènements majeurs, nous noterons l'ouverture de la Mer Morte et du Golfe d'Elat il y a environ 5 Ma *(Ten Brink and Ben-Avraham, 1989 ; Ben-Avraham, 1985). Schattner et Weinberger (2008)* proposent une troisième phase, à ~1 Ma, principalement sur la base de la formation d'une faille diagonale au sein du bassin de Hula. Cette

phase est reliée à l'entrée en subduction du Mont Eratosthène en Méditerranée. Cependant, la mise en place de cette faille peut être simplement liée à l'évolution structurale du bassin au cours de son ouverture, sans lien avec la cinématique régionale.

matique

cette reconstitution ne résume pas à elle seule l'ensemble des évolutions récentes. L'hétérogénéité du réchauffement suivant les régions, la fonte de la banquise et des glaciers dans les régions polaires : tout cela est cohérent avec un rôle déjà manifeste de l'augmentation des émissions mondiales de gaz à effet de serre d'origine humaine. Cette reconstitution des températures durant l'Holocène reste toutefois un support de recherche indispensable pour mieux comprendre à quoi nous engage le changement climatique futur, au niveau global et local. Elle nous questionne aussi sur les processus à l'origine des variations naturelles du climat. Derrière un diagnostic de changement climatique qui tend à se confirmer chaque fois un peu plus, il y a encore beaucoup à apprendre et comprendre. ■ **Propos recueillis par Fabienne Lemarchand**

[1] S. Marcott *et al., Science, 339,* 1198, 2013.

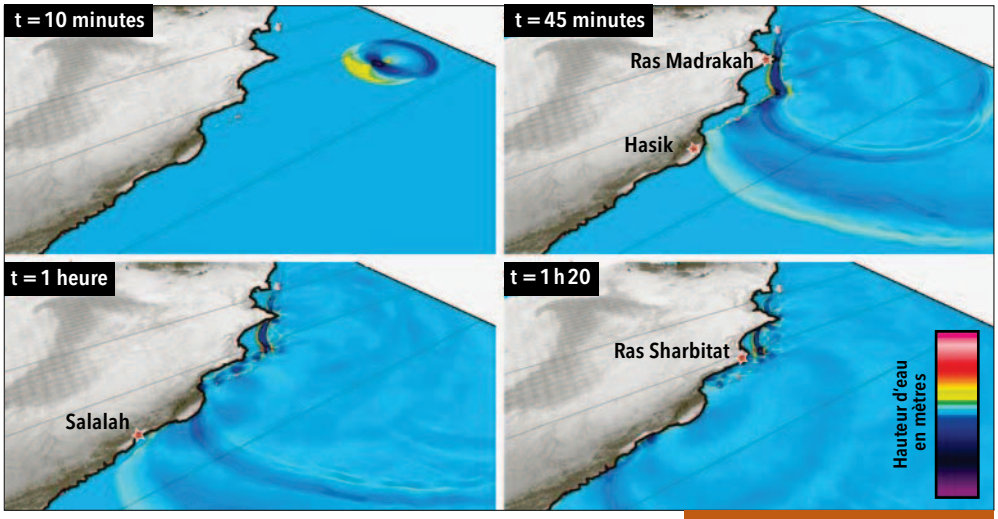


Cette simulation présente l'avancée d'un tsunami qui toucherait le sud-ouest du sultanat d'Oman en cas de glissement de terrain sous-marin à 300 ou 400 kilomètres plus à l'est. Des vagues de 1 à 4 mètres de hauteur atteindraient rapidement les villes côtières.
© RODRIGUEZ *ET AL., NHESS* 2013

# Risque de tsunami sur les côtes de l'Oman

**GÉOLOGIE**

**De brusques glissements de terrain sous-marins pourraient entraîner la formation en surface de vagues destructrices.**

Des vagues de 1 à 4 mètres de hauteur pourraient un jour déferler sur les côtes du sultanat d'Oman. Ce scénario ressort des travaux menés par des géologues français sur une zone située à 300 ou 400 kilomètres de là, au nord-ouest de l'océan Indien. C'est là que coulissent les plaques tectoniques de l'Arabie et de l'Inde, le long d'une faille. Cette frontière est matérialisée par un relief haut de plusieurs milliers de mètres, la « ride d'Owen ». En 2009, les géologues ont mis en évidence des cicatrices laissées par des glissements de terrain sous-marins, au cours desquels d'importants volumes de sédiments déposés sur la ride ont été déstabilisés. Grâce aux forages et aux enregistrements de sismique réflexion, ils viennent d'en préciser la distribution, l'ampleur et la fréquence [1].

**Seuil d'instabilité.** Ainsi, plusieurs centaines de glissements de terrain ont été identifiés sur les flancs de la ride d'Owen, dont vingt-cinq impliquent le déplacement de 1 à 40 kilomètres cubes de sédiments. « *Un nombre particulièrement important* », explique Mathieu Rodriguez, de l'École normale supérieure, premier auteur de l'étude. Leur origine ? Pas forcément des séismes. De fait, on compte dans cette zone un séisme de magnitude 6 à 7 tous les mille ans environ contre un glissement de terrain tous les 100 000 à 1 000 000 d'années selon les endroits.

Ces glissements se déclenchent lorsque l'épaisseur des sédiments atteint au moins une centaine de mètres. « *Il existe un seuil critique au-delà duquel le système devient instable. Tant qu'il n'est pas atteint, les séismes n'ont pas d'effet. Les faibles taux de sédimentation (de l'ordre de la dizaine de mètres par million d'années) limitent la fréquence des glissements. Mais ils font que les volumes mobilisés sont importants* », souligne Mathieu Rodriguez.

La probabilité qu'un tel événement se reproduise dans les décennies à venir reste à préciser. Mais il entraînerait la formation en surface de vagues potentiellement destructrices. Pour évaluer les risques encourus sur les côtes de l'Oman, les chercheurs ont utilisé les modèles numériques de genèse et de propagation des tsunamis développés par le CEA : un glissement de terrain de terrain au sud de la ride d'Owen, impliquant 40 kilomètres cubes de sédiment, engendrerait des vagues de 1 à 4 mètres de hauteur sur les côtes. ■ **F.L.**

[1] M. Rodriguez *et al., Nat. Hazards Earth Syst. Sci.* 13, 417, 2013.

## zoom Or et séismes

**L'or est le plus souvent concentré dans des veines de quartz (ci-contre). Celles-ci sont issues de la précipitation, dans des fractures de la croûte terrestre, de fluides chargés d'éléments métalliques, lorsque la pression change. Mais les processus à l'œuvre restent mal connus. Des géologues australiens affirment, simulations numériques à l'appui, que les précieux dépôts pourraient se former d'une façon quasi instantanée lors des séismes. Lorsque la terre tremble, l'ouverture de nouvelles fractures se traduit par une dépressurisation brutale de la roche. Les fluides subissent alors une vaporisation éclair : en une fraction de seconde, la silice cristallise, et les éléments métalliques se déposent. À chaque séisme, le phénomène se répète, et c'est ainsi que se formeraient nombre de gisements aurifères.**

D.K. Weatherley et R.W. Henley, *Nature Geoscience,* doi:10.1038/ngeo1759, 2013.